frontiers | Research Topics

Vaccine delivery and impact on kinetics of immune responses

Edited by
Gabriel Pedersen, Simon Daniel Van Haren and Ali M. Harandi

Published in
Frontiers in Immunology

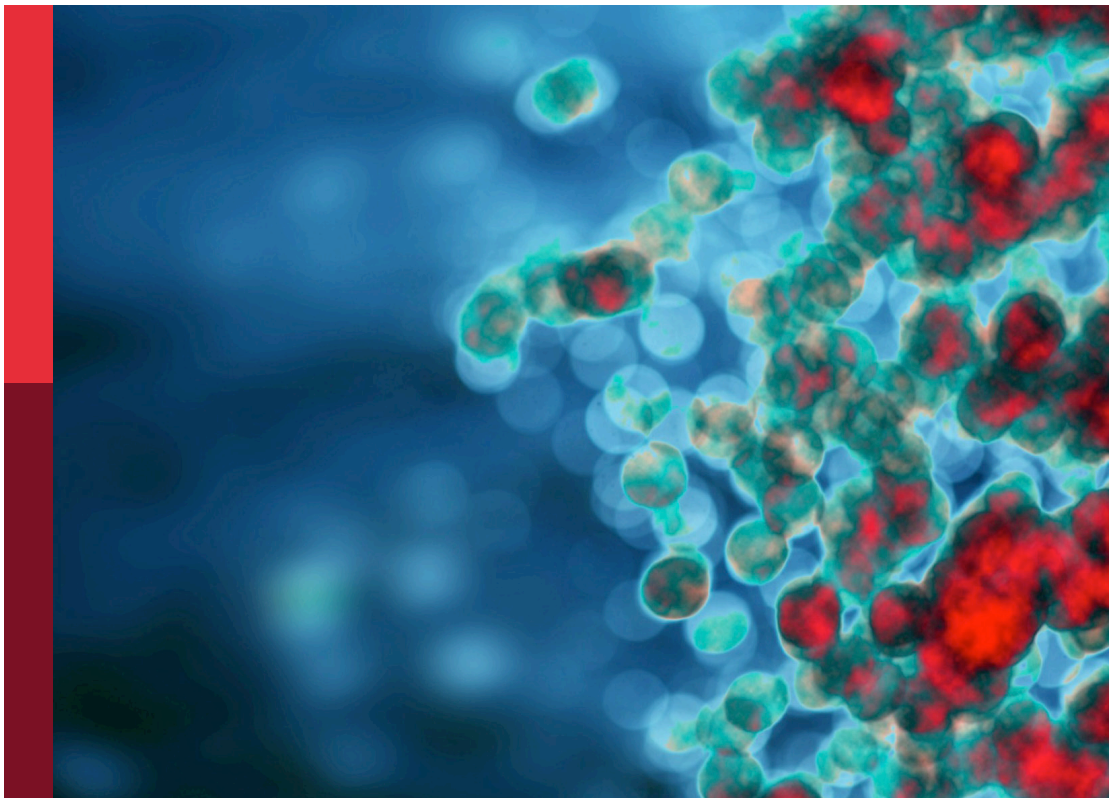

ISSN 1664-8714
ISBN 978-2-8325-2450-3
DOI 10.3389/978-2-8325-2450-3

About Frontiers

Frontiers is more than just an open access publisher of scholarly articles: it is a pioneering approach to the world of academia, radically improving the way scholarly research is managed. The grand vision of Frontiers is a world where all people have an equal opportunity to seek, share and generate knowledge. Frontiers provides immediate and permanent online open access to all its publications, but this alone is not enough to realize our grand goals.

Frontiers journal series

The Frontiers journal series is a multi-tier and interdisciplinary set of open-access, online journals, promising a paradigm shift from the current review, selection and dissemination processes in academic publishing. All Frontiers journals are driven by researchers for researchers; therefore, they constitute a service to the scholarly community. At the same time, the *Frontiers journal series* operates on a revolutionary invention, the tiered publishing system, initially addressing specific communities of scholars, and gradually climbing up to broader public understanding, thus serving the interests of the lay society, too.

Dedication to quality

Each Frontiers article is a landmark of the highest quality, thanks to genuinely collaborative interactions between authors and review editors, who include some of the world's best academicians. Research must be certified by peers before entering a stream of knowledge that may eventually reach the public - and shape society; therefore, Frontiers only applies the most rigorous and unbiased reviews. Frontiers revolutionizes research publishing by freely delivering the most outstanding research, evaluated with no bias from both the academic and social point of view. By applying the most advanced information technologies, Frontiers is catapulting scholarly publishing into a new generation.

What are Frontiers Research Topics?

Frontiers Research Topics are very popular trademarks of the *Frontiers journals series*: they are collections of at least ten articles, all centered on a particular subject. With their unique mix of varied contributions from Original Research to Review Articles, Frontiers Research Topics unify the most influential researchers, the latest key findings and historical advances in a hot research area.

Find out more on how to host your own Frontiers Research Topic or contribute to one as an author by contacting the Frontiers editorial office: frontiersin.org/about/contact

Vaccine delivery and impact on kinetics of immune responses

Topic editors

Gabriel Pedersen — Statens Serum Institut (SSI), Denmark

Simon Daniel Van Haren — Boston Children's Hospital, Harvard Medical School, United States

Ali M. Harandi — University of Gothenburg, Sweden

Citation

Pedersen, G., Van Haren, S. D., Harandi, A. M., eds. (2023). *Vaccine delivery and impact on kinetics of immune responses*. Lausanne: Frontiers Media SA.

doi: 10.3389/978-2-8325-2450-3

Table of contents

05 S-540956, a CpG Oligonucleotide Annealed to a Complementary Strand With an Amphiphilic Chain Unit, Acts as a Potent Cancer Vaccine Adjuvant by Targeting Draining Lymph Nodes
Takayuki Nakagawa, Tetsuya Tanino, Motoyasu Onishi, Soichi Tofukuji, Takayuki Kanazawa, Yukichi Ishioka, Takeshi Itoh, Akira Kugimiya, Kazufumi Katayama, Takuya Yamamoto, Morio Nagira and Ken J. Ishii

16 Deep Immune Phenotyping and Single-Cell Transcriptomics Allow Identification of Circulating TRM-Like Cells Which Correlate With Liver-Stage Immunity and Vaccine-Induced Protection From Malaria
Andrés Noé, Mehreen S. Datoo, Amy Flaxman, Mohammad Ali Husainy, Daniel Jenkin, Duncan Bellamy, Rebecca A. Makinson, Richard Morter, Fernando Ramos Lopez, Jonathan Sheridan, Dimitrios Voukantsis, Naveen Prasad, Adrian V. S. Hill, Katie J. Ewer and Alexandra J. Spencer

32 SARS-CoV-2 Spike Protein Expression *In Vitro* and Hematologic Effects in Mice Vaccinated With AZD1222 (ChAdOx1 nCoV-19)
Richard Stebbings, Christopher Jones, Peter Cotton, Gillian Armour, Shaun Maguire, Vicky Skellett, Chi-Man Tang, Joanne Goodman, Tyler Brady, Virginia Takahashi, Andrew Daunt, Jean-Martin Lapointe and Taylor S. Cohen

41 Intranasal Immunization With a c-di-GMP-Adjuvanted Acellular Pertussis Vaccine Provides Superior Immunity Against *Bordetella pertussis* in a Mouse Model
Wenwen Jiang, Xiaoyu Wang, Yuhao Su, Lukui Cai, Jingyan Li, Jiangli Liang, Qin Gu, Mingbo Sun and Li Shi

58 Oral mRNA Vaccines Against Infectious Diseases- A Bacterial Perspective [Invited]
Vijayakumar Jawalagatti, Perumalraja Kirthika and John Hwa Lee

66 Orf Virus-Based Vectors Preferentially Target Professional Antigen-Presenting Cells, Activate the STING Pathway and Induce Strong Antigen-Specific T Cell Responses
Melanie Müller, Alena Reguzova, Markus W. Löffler and Ralf Amann

79 Comparison of Immune Responses Elicited by SARS-CoV-2 mRNA and Recombinant Protein Vaccine Candidates
Yixin Wu, Huicong Zhang, Liuxian Meng, Fusheng Li and Changyuan Yu

87 Innate Immune Responses and *P. falciparum* CS Repeat-Specific Neutralizing Antibodies Following Vaccination by Skin Scarification
Robert A. Mitchell, Rita Altszuler, Sandra Gonzalez, Roshawn Johnson, Ute Frevert and Elizabeth Nardin

100 Differential Biodistribution of Adenoviral-Vectored Vaccine Following Intranasal and Endotracheal Deliveries Leads to Different Immune Outcomes
Vidthiya Jeyanathan, Sam Afkhami, Michael R. D'Agostino, Anna Zganiacz, Xueya Feng, Matthew S. Miller, Mangalakumari Jeyanathan, Michael R. Thompson and Zhou Xing

110 Induction of Mucosal IgA–Mediated Protective Immunity Against Nontypeable *Haemophilus influenzae* Infection by a Cationic Nanogel–Based P6 Nasal Vaccine
Rika Nakahashi-Ouchida, Hiromi Mori, Yoshikazu Yuki, Shingo Umemoto, Takashi Hirano, Yohei Uchida, Tomonori Machita, Tomoyuki Yamanoue, Shin-ichi Sawada, Masashi Suzuki, Kohtaro Fujihashi, Kazunari Akiyoshi, Yuichi Kurono and Hiroshi Kiyono

123 Analysis of immunization time, amplitude, and adverse events of seven different vaccines against SARS-CoV-2 across four different countries
Maria Elena Romero-Ibarguengoitia, Arnulfo González-Cantú, Chiara Pozzi, Riccardo Levi, Maximiliano Mollura, Riccardo Sarti, Miguel Ángel Sanz-Sánchez, Diego Rivera-Salinas, Yodira Guadalupe Hernández-Ruíz, Ana Gabriela Armendariz-Vázquez, Gerardo Francisco Del Rio-Parra, Irene Antonieta Barco-Flores, Rosalinda González-Facio, Elena Azzolini, Riccardo Barbieri, Alessandro Rodrigo de Azevedo Dias, Milton Henriques Guimarães Júnior, Alessandra Bastos-Borges, Cecilia Acciardi, Graciela Paez-Bo, Mauro Martins Teixeira and Maria Rescigno

135 A comparative study of adjuvants effects on neonatal plasma cell survival niche in bone marrow and persistence of humoral immune responses
Audur Anna Aradottir Pind, Sigrun Thorsdottir, Gudbjorg Julia Magnusdottir, Andreas Meinke, Giuseppe Del Giudice, Ingileif Jonsdottir and Stefania P. Bjarnarson

frontiers in Immunology

ORIGINAL RESEARCH
published: 23 December 2021
doi: 10.3389/fimmu.2021.803090

S-540956, a CpG Oligonucleotide Annealed to a Complementary Strand With an Amphiphilic Chain Unit, Acts as a Potent Cancer Vaccine Adjuvant by Targeting Draining Lymph Nodes

*Takayuki Nakagawa[1], Tetsuya Tanino[1], Motoyasu Onishi[1], Soichi Tofukuji[1], Takayuki Kanazawa[1], Yukichi Ishioka[1], Takeshi Itoh[1], Akira Kugimiya[1], Kazufumi Katayama[1], Takuya Yamamoto[2], Morio Nagira[1] and Ken J. Ishii[2,3,4]**

[1] Pharmaceutical Research Division, Shionogi & Co., Ltd., Osaka, Japan, [2] Laboratory of Adjuvant Innovation, Center for Vaccine and Adjuvant Research (CVAR), National Institute of Biomedical Innovation, Health and Nutrition (NIBIOHN), Osaka, Japan, [3] Laboratory of Mock-up Vaccine Project, Center for Vaccine and Adjuvant Research (CVAR), National Institute of Biomedical Innovation, Health and Nutrition (NIBIOHN), Osaka, Japan, [4] Division of Vaccine Science, Department of Microbiology and Immunology, The Institute of Medical Science, The University of Tokyo (IMSUT), Tokyo, Japan

OPEN ACCESS

Edited by:
Gabriel Pedersen, Statens Serum Institut (SSI), Denmark

Reviewed by:
Karl Kai McKinstry, University of Central Florida, United States
Floris Dammeijer, Erasmus Medical Center, Netherlands

***Correspondence:**
Ken J. Ishii
kenishii@ims.u-tokyo.ac.jp;
kenishii@biken.osaka-u.ac.jp

Specialty section:
This article was submitted to Vaccines and Molecular Therapeutics, a section of the journal Frontiers in Immunology

Received: *27 October 2021*
Accepted: *08 December 2021*
Published: *23 December 2021*

Citation:
Nakagawa T, Tanino T, Onishi M, Tofukuji S, Kanazawa T, Ishioka Y, Itoh T, Kugimiya A, Katayama K, Yamamoto T, Nagira M and Ishii KJ (2021) S-540956, a CpG Oligonucleotide Annealed to a Complementary Strand With an Amphiphilic Chain Unit, Acts as a Potent Cancer Vaccine Adjuvant by Targeting Draining Lymph Nodes. Front. Immunol. 12:803090. doi: 10.3389/fimmu.2021.803090

Robust induction of cancer-antigen-specific $CD8^+$ T cells is essential for the success of cancer peptide vaccines, which are composed of a peptide derived from a cancer-specific antigen and an immune-potentiating adjuvant, such as a Toll-like receptor (TLR) agonist. Efficient delivery of a vaccine antigen and an adjuvant to antigen-presenting cells in the draining lymph nodes (LNs) holds key to maximize vaccine efficacy. Here, we developed S-540956, a novel TLR9-agonistic adjuvant consisting of B-type CpG ODN2006 (also known as CpG7909), annealed to its complementary sequence oligodeoxynucleotide (ODN) conjugated to a lipid; it could target both a cancer peptide antigen and a CpG-adjuvant in the draining LNs. S-540956 accumulation in the draining LNs and activation of plasmacytoid dendritic cells (pDCs) were significantly higher than that of ODN2006. Mechanistic analysis revealed that S-540956 enhanced the induction of MHC class I peptide-specific $CD8^+$ T cell responses *via* TLR9 in a $CD4^+$ T cell-independent manner. In mice, the therapeutic effect of S-540956-adjuvanted with a human papillomavirus (HPV)-E7 peptide vaccine against HPV-E7-expressing TC-1 tumors was significantly better than that of an ODN2006-adjuvanted vaccine. Our findings demonstrate a novel adjuvant discovery with the complementary strand conjugated to a lipid, which enabled draining LN targeting and increased ODN2006 accumulation in draining LNs, thereby enhancing the adjuvant effect. Our findings imply that S-540956 is a promising adjuvant for cancer peptide vaccines and has a high potential for applications in various vaccines, including recombinant protein vaccines.

Keywords: cancer peptide vaccine, adjuvant, CpG oligonucleotide, delivery system, draining lymph node

INTRODUCTION

Despite the large number of clinical trials of cancer peptide vaccines, no human cancer peptide vaccine has been approved to date (1). To eliminate tumor cells, robust induction of prime and recall T cell-mediated immune responses is essential for cancer peptide vaccines, and secondary lymphoid organs are crucial for orchestrating immune responses (2). Typical components of cancer peptide vaccines include a major histocompatibility complex (MHC)-I-restricted peptide(s) and an adjuvant(s), where the adjuvants act as key players for enhancing $CD8^+$ T cell responses. Previous reports indicated that efficient delivery of adjuvants to draining lymph nodes (LNs) increased antigen-presenting cell (APC) activation and robust T cell responses, without increasing systemic toxicity (3, 4).

CpG oligodeoxynucleotides (ODNs) are synthetic single-stranded DNA fragments containing unmethylated CpG motifs that mimic bacterial DNA (5, 6). CpG ODNs can strongly activate plasmacytoid dendritic cells (pDCs) and B cells *via* the Toll-like receptor 9 (TLR9)-signaling pathway and promote the establishment of adaptive immunity (7). The efficacy and tolerability of CpG ODNs have been demonstrated in a large number of clinical trials (8); therefore, CpG ODN modification is a promising approach for developing effective and safe cancer peptide vaccines. Interestingly, a CpG ODN combined with an amphiphilic tail has been reported to enhance the accumulation of draining LNs *via* albumin-hitchhiking and increase $CD8^+$ T cell responses, which can maximize the anti-tumor effects of cancer peptide vaccines (3). In fact, the enhanced adjuvant effect provided by combining CpG ODN with amphiphilic tails has also been demonstrated when mixed with a severe acute respiratory syndrome coronavirus 2 (SARS-CoV-2) spike-2 receptor binding domain protein (9). Albumin is intrinsically transferred to draining LNs, and thus, molecules that bind albumin are effectively delivered to draining LNs (10). This albumin-hitchhiking strategy prompted us to further develop and characterize CpG ODNs capable of targeting draining LNs similar to a previous study that directly conjugated cholesterol, or a lipid, to the 5′ end of a CpG ODN and added an ODN to the 5′ end (3). Similarly, a mouse-specific CpG ODN has been evaluated in murine tumor model, however a similar human TLR9-selective CpG ODN has not been previously investigated for cancer peptide vaccines in mice. In addition, the immunological mechanisms have not been fully investigated to identify key players in the adjuvanticity of draining LN-targeting CpG ODNs. However, a previous structure–activity relationship study demonstrated that the agonistic activities of CpG ODNs for TLR9 were altered by modifying the 20-mer oligonucleotide sequence (11). Hence, the direct modification can potentially alter the immunostimulatory effects of CpG ODNs and may cause an unpredictable immunotoxicity.

Therefore, to develop a novel draining LN-targeting adjuvant, we synthetized modified CpG ODNs using different chemical approaches, based on a previous report (3). Specifically, we developed S-540956, which was synthesized by annealing a single complementary DNA strand with an amphiphilic chain unit to ODN2006 without modifying ODN2006 itself (12, 13). We then investigated the delivery and immunological characteristics of S-540956 as a potential cancer peptide vaccine adjuvant.

MATERIALS AND METHODS

Compounds

S-540956, a compound composed of a double-stranded oligodeoxynucleotide, was synthesized by solid-phase synthesis using a typical phosphoramidite method, as described previously (14). Briefly, CpG ODN2006 (5′-TCGTCGTTTTGTCGTTTTG TCGTT-3′) and complementary strands were synthesized using an automated nucleic acid synthesizer (ns-8-II; Ajinomoto-Biopharma Services, Osaka, Japan); lipid ligands were attached to the complementary strand. The complementary strand with the lipid ligands was named C-540956. The nucleotides of ODN2006 and C-540956 were linked *via* phosphorothioate and phosphodiester bonds, respectively. Individually purified ODN2006 and C-540956 were hybridized after briefly heating them to 65°C and subsequently cooling to 20-27°C. The purity of the hybridized oligonucleotides was analyzed using liquid chromatography-mass spectrometry. CpG1018 (B-type CpG) and ODN1826 (B-type CpG specific for murine TLR9) were also synthesized by the automated nucleic acid synthesizer (ns-8-II; Ajinomoto-Biopharma Services). ODN1826 was annealed with the complementary strand attached to the lipid ligands: these were synthesized using the same methods as that for S-540956. Alexa Fluor 647-labeled ODN2006 (ODN2006 AF647) was synthesized by Ajinomoto-Biopharma Services. Alexa Fluor 647-labeled S-540956 (S-540956 AF647) was composed of ODN2006 AF647 hybridized with C-540956. Polyinosinic-polycytidylic acid (polyI:C) was purchased from *In vivo*Gen (Toulouse, France).

Animals

Six-to eight-week-old female C57BL/6J mice were purchased from CLEA Japan, Inc. (Tokyo, Japan). *Tlr9*$^{-/-}$ mice were purchased from Oriental BioService, Inc. (Kyoto, Japan). *Tap1*$^{-/-}$ and *Cd4*$^{-/-}$ mice were obtained from The Jackson Laboratory (Bar Harbor, ME). All animal studies were conducted following appropriate guidelines and with the approval of the National Institutes of Biomedical Innovation, Health, and Nutrition, as well as the Shionogi Animal Care and Use Committee (Osaka, Japan).

TLR9 Reporter-Gene Assay

Secreted embryonic alkaline phosphatase (SEAP) reporter HEK-Blue™-hTLR9 cells (expressing human TLR9 and NF-κB-inducible SEAP) and HEK-Blue™-Null1 cells (expressing only NF-κB-inducible SEAP) were purchased from *In vivo*Gen. After activation by treatment with different compounds, secreted SEAP levels were measured using QUANTI-Blue medium (*In vivo*Gen), and the absorbance was measured at 540 nm using a Varioskan Flash multimode reader (Thermo Fisher Scientific, Waltham, MA).

Surface Plasmon Resonance Analysis

Interactions between S-540956 and human or mouse serum albumin (HSA or MSA, respectively) were analyzed using a BIACORE S51 system (GE Healthcare UK Ltd., Buckinghamshire, UK), according to a previously reported method (15). The sensorgrams for the S-540956 interaction with HSA or MSA were analyzed by curve fitting using numerical-integration analysis. The data were fitted globally by simultaneously fitting the S-540956 sensorgrams obtained at six different concentrations using BI evaluation software (version 4.1). The equilibrium dissociation constant (K_D) values were evaluated by applying linear or nonlinear fitting algorithms to the binding data using the 1:1 Langmuir binding model.

In Vivo Imaging System (IVIS)-Imaging Analysis

Mice were subcutaneously or intramuscularly injected with 5 nmol of S-540956 AF647 or ODN2006 AF647. After injection, the animals were sacrificed, and the draining LNs and spleens were collected at each sampling time. Fluorescence in the collected organs was analyzed using the IVIS imaging system (Perkin Elmer, Waltham, MA).

Immunofluorescence (IF) Imaging

Mice were intramuscularly injected with 5 nmol of S-540956 AF647, and then the draining LNs were excised after 24 h. The draining LNs were frozen in optimum cutting temperature compound (Sakura Finetek Japan Co., Ltd., Tokyo, Japan). Embedded 8 μm cryostat sections were fixed in cold acetone for 5 min. Anti-CD3 (clone SP7; Nichirei Corporation, Tokyo, Japan), anti-B220 (clone RA3-6B2; BioLegend, San Diego, CA), anti-CD169 (clone 3D6.112; BioLegend), and anti-plasmacytoid dendritic cell antigen-1 ([PDCA-1], JF05 1C2.4.1; Miltenyi Biotech Bergisch Gladbach, Germany) antibodies were used as primary antibodies. AF488-conjugated goat anti-rabbit IgG H&L (Abcam, Cambridge, UK) was used to detect the anti-CD3 antibody, and AF488-conjugated goat anti-rat IgG (minimal cross-reactivity; BioLegend) was used to detect the anti-B220, anti-CD169, and anti-PDCA1 antibodies. After staining the cells, the tissue sections were analyzed using a fluorescence microscope with 10 × and 60 × lenses (BX51; Olympus, Tokyo, Japan). Imaging data were processed using Adobe Photoshop CS2 (Adobe Systems Inc., San Jose, CA).

Imaging-Stream Analysis

To detect macrophages and pDCs, fluoresceine isothiocyanate (FITC)-conjugated anti-CD11b (cloneM1/70), and phycoerythrin (PE)-conjugated anti-Siglec-H (clone551) were purchased from BioLegend. Imaging-stream analysis was performed as previously described (16). Briefly, mice were intramuscularly injected with 5 nmol of S-540956 AF647 or ODN2006 AF647. Cells collected from draining LNs were stained with FITC anti-CD11b and PE anti-Siglec-H for 30 min at room temperature. Imaging data were obtained using Amnis™ ImageStreamX (Luminex, Austin, TX) and analyzed using IDEAS software (version 6.2; Luminex).

Splenomegaly Analysis

Mice were intramuscularly injected with 1, 2, or 4 nmol of S-540956 or ODN2006 on day 0, 2, and 4. Three days after the third injection, the mice were sacrificed, and the spleens were collected. The weight of each spleen was measured using an electronic balance.

Cytokine Measurements

Mice were intramuscularly injected with 5 nmol of S-540956 or ODN2006. Plasma samples were collected 3 and 24 h after injection. The plasma concentrations of TNF-α, IL-6, IFN-γ, and IP-10 were measured using a MILLIPLEX MAP Mouse Cytokine/Chemokine Magnetic Bead Panel-Immunology Multiplex Assay (Merck Millipore, Billerica, MA).

Immunization and Subsequent Evaluation of Cellular and Humoral Immune Responses

A $TRP2_{180\text{-}188}$ peptide (SVYDFFVWL-NH_2), an $OVA_{257\text{-}264}$ peptide (SIINFEKL-NH_2), and an $HPV16\text{-}E7_{49\text{-}57}$ peptide (RAHYNIVTF-NH_2) were synthesized by Sigma-Aldrich Japan K.K. (Tokyo, Japan). Montanide ISA-51 is an incomplete Freund's adjuvant (IFA) that was purchased from Seppic, Inc. (Fairfield, NJ). OVA protein with low endotoxin level was purchased from FUJIFILM Wako Pure Chemical Co., Ltd. (Osaka, Japan). To evaluate peptide-specific $CD8^+$ T cell responses, mice were subcutaneously immunized with 100 μg of TRP2, OVA, or HPV16-E7 peptide mixed with 5 nmol of S-540956 or ODN2006, or 50 μL of Montanide ISA51 on days 0 and 7. Peripheral blood mononuclear cells (PBMCs) were collected 14 days after the first immunization. To evaluate OVA protein-specific $CD8^+$ T cell and antibody responses, mice were subcutaneously immunized with 10 μg of OVA protein mixed with 5 nmol of S-540956 or ODN2006 on days 0 and 14. The PBMCs and plasma were collected 21 and 28 days after the first immunization, respectively.

Flow Cytometric Analysis

FITC-conjugated anti-CD86 (clone GL1, BD Pharmingen, San Diego, CA), brilliant violet (BV)-421-conjugated anti-F4/80 (clone T45-2342 BD Pharmingen), PE-conjugated anti-Siglec-H (clone 551 BL), and BV-605-conjugated anti-CD11b (clone M1/70, BioLegend) antibodies were used to detect CD86 expression in pDCs and macrophages. To analyze cytokine-expressing cells, allophycocyanin–cyanine (Cy)7-conjugated anti-CD-3ϵ (clone 2C11), BV-510-conjugated anti-CD4 (clone RM4-5), BV-570-conjugated anti-CD8α (clone 53-6.7), PE-conjugated anti-IL-2 (clone JES6-5H4), and PE-Cy7-conjugated anti-TNFα (clone MP6-XT22) antibodies were purchased from BioLegend, and an FITC-conjugated anti-IFN-γ (clone XMG1.2) antibody was purchased from BD Pharmingen. For peptide-specific T cell receptor detection, $TRP2_{180\text{-}188}$ peptide, $OVA_{257\text{-}264}$ peptide, or $HPV16\text{-}E7_{49\text{-}57}$ peptide loaded PE-labeled tetramers were purchased from Medical & Biological Laboratories, Co. Ltd. (Nagoya, Japan). To detect CD107a expression, BV786-conjugated anti-CD107a

antibody was used (clone 1D4B, BD Biosciences, Franklin Lakes, NJ). For tetramer staining, the collected PBMCs were incubated with PE-labeled tetramers and antibodies for 30 min at room temperature. For intracellular cytokine-staining assays, the collected PBMCs were stimulated with cognate peptides for 6 h; next, Golgi-Plug and Golgi-Stop were added, and the PBMCs were incubated for 30 min at room temperature. The cells were fixed and permeabilized using a Cytofix/Cytoperm Kit (BD Biosciences). Dead cells were excluded by LIVE/DEAD™ Fixable Aqua Dead Cell Stain Kit (Thermo Fisher). Data were collected using an LSRII flow cytometer (BD Biosciences) and analyzed using FlowJo software (version 9.8.2; Tree Star, Ashland, OR).

Measurement of Antibody Titers

Total plasma anti-OVA IgG, IgG1, and IgG2c titers were determined by performing enzyme-linked immunosorbent assays (ELISAs) as described previously (17), with the following modifications. Briefly, 384-well plates were coated with 10 μg/mL OVA antigen solution (FUJIFILM Wako Pure Chemical Co., Ltd, Osaka, Japan) overnight at 4°C. The plates were washed and incubated for 1 h with blocking buffer (phosphate-buffered saline [PBS] containing 1% bovine serum albumin). After blocking, the plates were washed and incubated with 5-fold serially diluted plasma for 2 h. To detect the bound antibodies, the plates were washed and incubated for 1 h with horseradish peroxidase-conjugated anti-mouse total IgG, IgG1, or IgG2c Ab (Bethyl Laboratories, Inc., Montgomery, TX). After the plates were washed, 1-Step Ultra TMB-ELISA solution (Thermo Fisher) was added to each well to initiate the color reaction. The reaction was stopped after 5 min by the addition of 1 M sulfuric acid, and the optical density at 450 nm (OD_{450}) was measured using SpectraMax® iD3 device (Molecular Devices, LLC, San Jose, CA). The titer was defined as the highest dilution factor with an OD value of > 0.1.

Depletion of pDCs, $CD4^+$ Cells, $CD8^+$ Cells, and Macrophages

An intraperitoneal injection with 500 μg of anti-PDCA1 (clone 927, BioLegend) or intravenous injection with 100 μg of anti-CD4 (clone GK1.5, BioLegend) was performed to deplete pDCs or $CD4^+$ cells 1 day before immunization with the vaccine. To deplete $CD8^+$ cells, an intraperitoneal injection with 100 μg of anti-CD8α (clone 2.43, Bio X cell, Lebanon, NH) was performed at 15, 17, 19, and 21 days after the inoculation of tumor. To deplete macrophages, 200 μL of clophosome-A (FormuMax Scientific, Inc., Sunnyvale, CA) was intravenously administered on days 1 and 6 before immunization with the vaccine.

Tumor Model

B16F10 melanoma cells expressing TRP2 (2×10^5 cells) or TC-1 tumorigenic cells expressing HPV16-E6 and E7 (3×10^5 cells) were subcutaneously inoculated into the flanks of mice. Tumor-bearing mice were subcutaneously immunized twice with 100 μg of $TRP2_{180\text{-}188}$ or $HPV16\text{-}E7_{49\text{-}57}$ peptide mixed with 5 nmol of S-540956 or ODN2006. Tumor sizes were measured using an electronic scale and calculated using the following formula: tumor size = tumor length × tumor width^2/2. Two-tailed Student's *t*-test was used for two-group comparisons. For groups of three or more, one-way analysis of variance (ANOVA) followed by Tukey's test was used. Statistical significance was set at a P value of < 0.05. Statistical analysis was performed using GraphPad Prism 9 (San Diego, CA).

RESULTS

The Complementary Strand With an Amphiphilic Chain Unit Increases ODN2006 Accumulation in the Draining LNs

Direct binding of the amphiphilic chain to CpG ODNs has been reported to enhance its accumulation in draining LNs by binding to albumin after injection, leading to APC activation and increased T cell responses in draining LNs (3). In this study, we designed an amphiphilic chain bound to the complementary strand of ODN2006 (B-type CpG ODN), and its efficacy and safety profiles have been confirmed in clinical trials (8). The ODN2006-annealed complementary strand with an amphiphilic chain unit was named S-540956 (**Figure 1A**). The *in vitro* effect of S-540956 on the activity of the TLR9 signaling pathway was compared with that of ODN2006 using HEK-Blue™ hTLR9 cells, which stably express the TLR9 gene. The half-maximal effective concentration values of S-540596 and ODN2006 were 300 and 180 nM, respectively (**Figure S1A**). C-540956, comprised of a complementary strand with an amphiphilic chain unit, did not activate the TLR9 signaling pathway (data not shown). TLR9-independent stimulation was not observed in HEK-Blue™-Null1 cells after incubation with S-540956, ODN2006, or C-540956 (**Figure S1B**). The mean at OD 620 nm of the positive control (tumor necrosis factor-α [TNF-α]) and negative control (buffer) samples were 2.60 and 0.11, respectively. These results suggest that the hybridization of the complementary strand with the amphiphilic chain to ODN2006 did not alter the *in vitro* effect of ODN2006 on TLR9 signaling. Interactions between S-540956 and HSA or MSA were analyzed by performing surface plasmon resonance (SPR) assays. The K_D values for the binding of S-540956 to HSA and MSA were 186 nM and 330 nM, respectively (**Figure 1B**). In contrast, a measurable K_D value could not be determined for the interactions between ODN2006 and HSA or MSA. The data from the SPR assays supported the concept of a delivery system for S-540956, based on the kinetics of albumin for efficient delivery to the draining LNs. To investigate the draining LN-targeting profile of S-540956, we examined S-540956 accumulation in the draining LNs using the IVIS imaging system. AF647-conjugated S-540956 or AF647-conjugated ODN2006 was injected *via* intramuscular, subcutaneous, or intravenous routes. S-540956–AF647 accumulated in the draining LNs at statistically higher levels than did ODN2006–AF647 following an intramuscular or subcutaneous injection, from 24 to 48 h post-injection ($P < 0.05$, **Figures 1C, D**). AF647 fluorescence was not detected in the draining LNs after

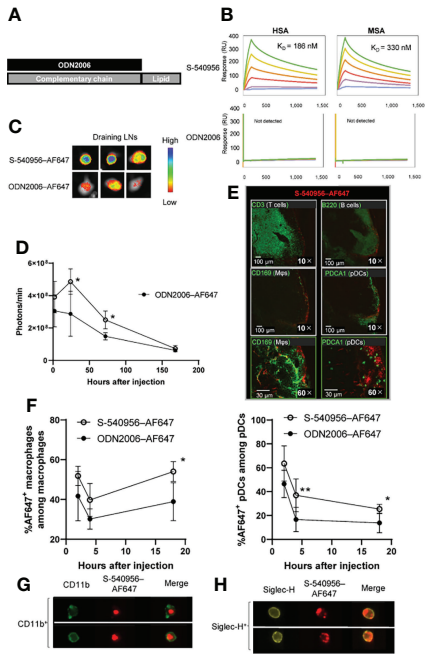

FIGURE 1 | Delivery of S-540956–AF647 to the draining LNs. **(A)** Schematic representation of S-540956. **(B)** Measurements of S-540956- and ODN2006-binding to immobilized HSA and MSA using the BIACORE S51 system. K_D values were calculated. **(C, D)** Mice were intramuscularly injected with S-540956–AF647 or ODN2006–AF647. Draining LNs were collected and analyzed at 2, 24, 72, and 168 h after injection (N = 3–5). The images shown represent draining LNs at 24 h after the intramuscular injection **(C)**. The fluorescence intensities of the draining LNs were measured using the IVIS spectrum system **(D)**. **(E)** T cells ($CD3^+$), B cells ($B220^+$), macrophages ($CD169^+$), and pDCs ($PDCA^+$) in the draining LNs were analyzed by immunofluorescence imaging at 24 h after the intramuscular injection of S-540956–AF647. **(F)** Incorporation of S-540956–AF647 or ODN2006–AF647 by $CD11b^+$ $F4/80^+$cells (macrophages) or Siglec-H^+ $CD11c^+$ cells (pDCs) in the draining LNs was analyzed by flow cytometric analysis at 2, 4, and 18 h after the intramuscular injection (N = 4–6). **(G, H)** Localization of S-540956–AF647 in $CD11b^+$ cells or Siglec-H^+ cells in draining LNs was imaged using ImageStreamX software at 4 h after the intramuscular injection of S-540956–AF647. **(D, F)** The data shown indicate the mean ± standard error (SE). $^*P < 0.05$ or $^{**}P < 0.01$, versus ODN2006–AF647; Student's *t*-test. Data are representative of two independent experiments.

intravenous injection of S-540956–AF647 or ODN2006–AF647 (data not shown). To examine the systemic distribution of S-540956, the accumulation of S-540956–AF647 in the spleen was also assessed after an intramuscular injection. S-540956–AF647 accumulation in the spleen was significantly lower than that of ODN2006–AF647 ($P < 0.01$, **Figures S2A, B**). The systemic distribution after a subcutaneous injection was consistent with that following an intramuscular injection (**Figures S2C, D**). A low systemic distribution profile is associated with reduced systemic toxicity (3). To assess the systemic toxicity of S-540956, splenomegaly was investigated after three repeated injections of S-540956 at 0, 2, and 4 days post-injection. The spleen weights of S-540956-injected mice were significantly lower than that of ODN2006-injected mice at a dose of 4 nmol ($P < 0.01$, **Figures S2E, F**). Systemic proinflammatory cytokine responses were measured in plasma samples after the intramuscular injection. The concentrations of TNF-α and IP-10 in S-54056-injected mice were significantly lower than those in ODN2006-injected mice at 3 h after injection ($P < 0.05$, **Figures S3A, D**). No statistical differences between S-540956- and ODN2006-injected mice were observed in terms of the TNF-α, IL-6, IFN-γ, and IP-10 concentrations at 24 h after injection (**Figures S3A–D**). The splenomegaly and cytokine-response data suggest that the draining LN-targeting profile of S-540956 did not increase the systemic toxicity of ODN2006 in mice.

TLR9 is expressed in DCs, macrophages, and B cells in mice, and these APCs orchestrate innate immune responses and contribute to the establishment of adaptive immunity (5, 7). Next, we focused on cells that incorporated S-540956 in the draining LNs. The distribution of S-540956 in the draining LNs was analyzed by IF imaging focusing on B cells ($B220^+$), macrophages ($CD169^+$), pDCs (Siglec-H^+), and T cells ($CD3^+$). The majority of S-540956–AF647 signal was detected on the surface of draining LNs and distributed to the B cell zone, localized to macrophages and pDCs (**Figure 1E**). We next examined the incorporation of S-540956–AF647 by macrophages or pDCs in the draining LNs by flow cytometry and ImageStreamX software. S-540956–AF647 was incorporated by pDCs and macrophages at higher levels, when compared to ODN2006 (**Figure 1F** and **Figure S4**), and S-540956–AF647 was detected in pDCs and macrophages, as determined by ImageStreamX software (**Figures 1G, H**). Taken together, the intrinsic property of albumin to translocate to the draining LNs (10) and our findings of the albumin binding and the enhanced accumulation of ODN2006 in the draining LNs by annealing the complementary strand with the amphiphilic chain unit suggest that S-540956 (injected into the muscle or subcutaneous tissue) translocated to the lymph vessels after binding albumin at the injection site and efficiently accumulated in the draining LNs.

The Draining LN-Targeting Profile Shows That ODN2006 Enhances pDC Activation in Draining LNs

Imaging analysis revealed that S-540956 was incorporated into macrophages and pDCs after an injection. Next, we focused on macrophages ($F4/80^+$, $CD11b^+$) and pDCs ($CD11c^+$, Siglec-H^+) in the draining LNs to further dissect the differences between S-540596 and ODN2006 in terms of their abilities to activate APCs. CD86 expression in both macrophages and pDCs was measured by flow cytometry to evaluate the effects of S-540956 on their maturation. The results showed that the number of macrophages in S-540956 injected mice was higher than that in ODN2006 at 18 h after injection (**Figure 2A**). The number of pDCs was not increased after injection of S-540956 (**Figure 2B**). S-540956 enhanced CD86 expression in both macrophages and pDCs (**Figures 2C, D**, **Figure S4**) and that CD86 expression in pDCs from S-540956-injected mice was significantly higher than that in ODN2006-injected mice ($P <$

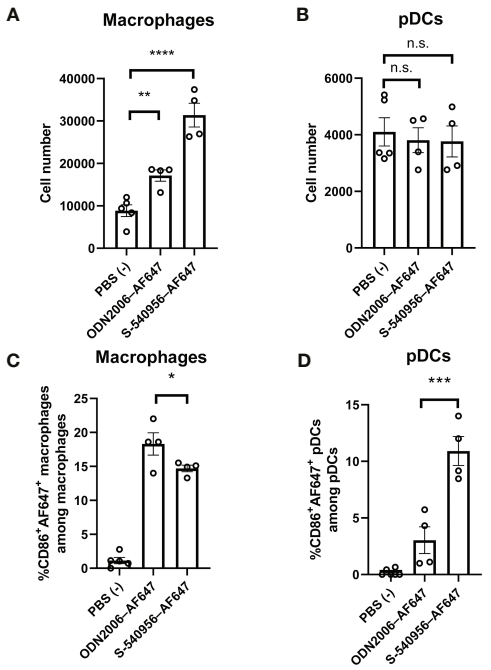

FIGURE 2 | S-540956 activated APCs in draining LNs. Mice were intramuscularly injected with S-540956–AF647 or ODN2006–AF647, and then draining LNs were collected at 18 h after an injection (N = 4–6). The numbers of **(A)** macrophages and **(B)** pDCs and **(C)** $CD86^+$ $AF647^+$ macrophages ($F4/80^+$, $CD11b^+$) or **(D)** $CD86^+$ $AF647^+$ pDCs ($CD11c^+$, $Siglec\text{-}H^+$) in the draining LNs were measured by flow cytometry. The data shown indicate the mean ± SE. $^*P < 0.05$, $^{**}P < 0.01$, $^{***}P < 0.005$, $^{****}P < 0.001$; one-way ANOVA. Data are representative of two independent experiments. not statistically significant (n.s.).

0.01, **Figure 2D**). These data suggest that S-540956 strongly promoted pDC activation (rather than macrophage activation) in draining LNs.

The Draining LN-Targeting Profile Reveals That ODN2006 Enhances the Induction of $CD8^+$ T Cell Responses to MHC Class I-Restricted Cancer Peptides

The complementary strand with an amphiphilic chain unit enhanced ODN2006 accumulation in the draining LNs and pDC activation. Activated pDCs carrying antigens can promote robust priming and T cell differentiation in LNs (18). This evidence prompted us to evaluate S-540956 as a vaccine adjuvant. Both humoral and cellular responses were investigated after immunization with a recombinant OVA antigen or peptide, mixed with S-540956. Both OVA-specific antibody levels (**Figures S5A–C**) and $CD8^+$ T cell responses (**Figure S5D**) were elevated after the addition of S-540956, and the adjuvanticity of S-540956 was statistically higher than that of ODN2006 (**Figures S5A, C, D**; $P < 0.01$, **Figure S5B**; $P < 0.05$). The adjuvant effect of S-540956 was also compared with that of CpG1018, which is contained in HEPLISAV-B launched as a hepatitis B vaccine (19). The OVA-specific $CD8^+$ T cell response enhanced by S-540956 was statistically higher than that by CpG1018 (**Figure S5E**; $P < 0.01$). Consistent with the results obtained with the recombinant OVA protein, S-540956 adjuvant enhanced the induction of $CD8^+$ T cell responses to TRP2 peptide (**Figure S6**, $P < 0.001$), and the adjuvanticity of S-540956 was statistically higher than that of ODN2006 ($P < 0.05$). Each TRP2, OVA, or HPV-E7 peptide-specific $CD8^+$ T cell responses induced by S-540956 was higher than that by IFA or ODN2006 (**Figures 3A, C, E**). To evaluate the versatility of our chemical approach, we synthesized ODN1826 annealed with the complementary strand with an amphiphilic chain unit (ODN1826-C1826). TRP2 peptide-specific $CD8^+$ T cell responses were measured after immunization with ODN1826-C1826-adjuvanted vaccine. The complementary strand with an amphiphilic chain unit enhanced the adjuvanticity of ODN1826 to induce TRP2 peptide-specific $CD8^+$ T cell responses (**Figure S7**). Polyfunctional effector $CD8^+$ T cells are thought to secrete multiple cytokines and cytotoxic markers and are associated with effective anti-tumor effects in humans (20, 21). To evaluate the quality of the $CD8^+$ T cells, the polyfunctionality of $CD8^+$ T cells was also investigated. The ratios of double- (IFN-γ/IL-2, IFN-γ/TNF-α, and IL-2/TNF-α) and triple- (IFN-γ/IL-2/TNF-α) positive $CD44^+$ $CD8^+$ T cells among cytokine-positive $CD44^+$ $CD8^+$ T cells specific to TRP2, OVA, and HPV-E7 peptides in the S-540956-adjuvanted vaccine groups were higher than those in the IFA-adjuvanted vaccine groups (**Figures 3B, D, F**). In addition, the peptide-specific $CD107a^+$ $CD8^+$ T cell responses in S-540956-adjuvanted vaccine groups were higher than those of ODN2006-adjuvanted vaccine groups (**Figures S8A–C**). No significant differences were observed in the ratios of double- and triple-positive $CD44^+$ $CD8^+$ T cells among cytokine-positive $CD44^+$ $CD8^+$ T cells between mice treated with S-540956 or ODN2006. These data suggest that draining LN targeting enhanced the adjuvant effect of ODN2006 to induce $CD8^+$ T cell responses but did not alter the quality of the $CD8^+$ T cells.

S-540956 Enhances $CD8^+$ T Cell Responses to the Cancer Peptide Vaccine in a pDC-Dependent Manner

Activation of the TLR9-signaling pathway by CpG ODNs can enhance the induction of antigen-specific $CD8^+$ T cell responses (22). To provide insights into how S-540956 strongly induced $CD8^+$ T cell responses, we next investigated the mechanisms involved in the adjuvanticity of S-540956. *Tlr9*$^{-/-}$ mice were immunized with a TRP2 peptide mixed with S-540956. $CD8^+$ T cell responses induced by S-540596 decreased in *Tlr9*$^{-/-}$ mice, suggesting that the mechanisms that induced $CD8^+$ T cell responses were not altered by the addition of complementary strands with amphiphilic chain units and that other signaling pathways were not involved in the induction of $CD8^+$ T cell responses (**Figure 4A**). To further understand which cells acted as key players in the adjuvanticity of S-540956, pDCs and $CD4^+$ T cells were depleted by injection of anti-PDCA-1 and anti-CD4 antibodies, respectively, and macrophages were depleted using clophosome-A (**Figures 4B–D** and **Figures S9A, B, D**). $CD8^+$ T cell responses were reduced by depleting pDCs (**Figure 4B**) or

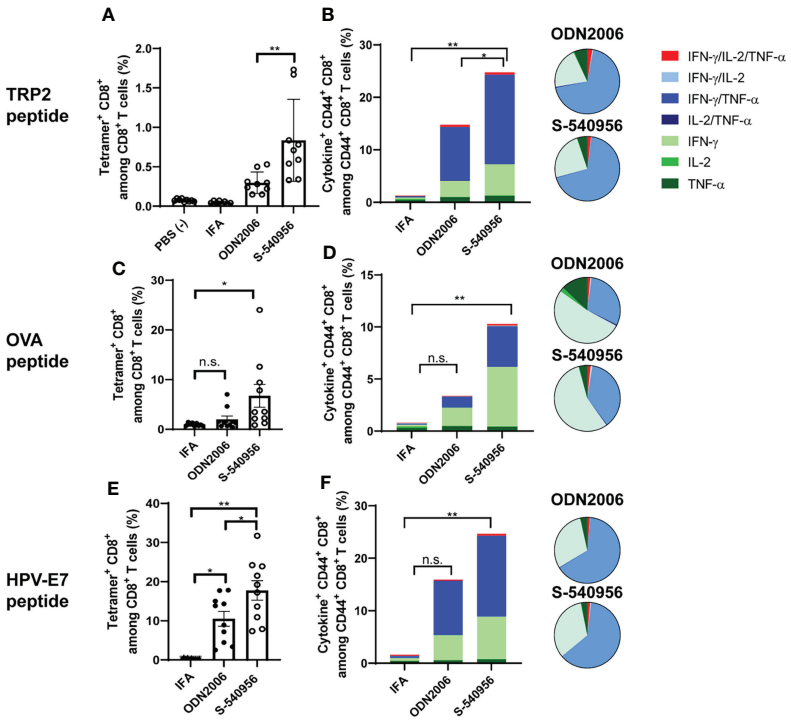

FIGURE 3 | S-540956 enhanced MHC class-I-restricted cancer peptide-specific $CD8^+$ T cell responses. Mice were intramuscularly immunized with peptide/S-540956, ODN2006, or Montanide ISA-51 on days 0 and 7 (N = 8–9). **(A, C, E)** TRP2, OVA, or HPV-E7 peptide-specific $CD8^+$ T cells among PBMCs and **(B, D, F)** polyfunctional $CD8^+$ cells in splenocytes were analyzed by flow cytometry on day 14. **(A, C, E)** The data shown indicate the mean ± SE. **(B, D, F)** The bar graphs indicate the mean, and the pie charts show the ratios of different cytokines expressed by $CD44^+$ $CD8^+$ cells. n.s., not statistically significant, $^*P < 0.05$, $^{**}P < 0.01$, as determined by one-way ANOVA. Data are representative of two independent experiments.

macrophages (**Figure 4D**). Depleting $CD4^+$ T cells did not affect $CD8^+$ T cell induction by S-540956 (**Figure 4C**). Collectively, these results suggest that the immunological mechanisms whereby S-540956 enhanced the induction of MHC class I-restricted peptide-specific $CD8^+$ T cell responses were not altered by the addition of complementary strands with amphiphilic chain units and that $CD4^+$ T cells were not required for inducing MHC class I-restricted peptide-specific $CD8^+$ T cell responses.

The Therapeutic Effect of the Cancer Peptide Vaccine Is Significantly Enhanced by S-540956 in a $CD4^+$ T Cell-Independent Manner

Our immunological analysis suggested that S-540956 strongly enhanced the anti-tumor effect of the MHC class I-restricted cancer peptide vaccine, when compared to ODN2006 (**Figures 3A–F**) and polyI:C (**Figure 4A**), which have been previously used as cancer peptide vaccines (8, 23). The anti-tumor effect of the S-540956-adjuvanted peptide vaccine was evaluated in TRP2-expressing B16F10 melanoma cell- or HPV-E7-expressing TC-1 tumor cell-grafted mice. The anti-tumor effect of the TRP2 peptide vaccine was significantly enhanced by the addition of S-540956, and the adjuvanticity of S-54095 was statistically higher than that of ODN2006 (**Figure 5A**, $P < 0.05$). S-540956 alone did not show anti-tumor effect in this model (**Figure 5B**). Consistent with the results in mice administered B16F10 melanoma cells, the anti-tumor effect of the HPV-E7 peptide vaccine was enhanced by S-540956, and the adjuvant effect of S-540956 was statistically higher than that of ODN2006 (**Figure 5C**, $P < 0.01$). The anti-tumor effect of the S-540956-adjuvanted vaccine was significantly reduced in *Tap1*$^{-/-}$ mice (**Figure 5D**). In addition, the depletion of $CD8^+$ T cells and not $CD4^+$ T cells reduced the anti-tumor effect of S-540956-adjuvanted vaccine (**Figures 5E** and **Figures S9C, D**). These results strongly suggest that the anti-tumor effect of the S-540956-adjuvanted vaccine depends on MHC class I peptide-specific $CD8^+$ T cells.

DISCUSSION

Cancer peptide vaccines represent one of the strategies used to control cancers by inducing robust MHC class I-restricted peptide-specific $CD8^+$ T cells with long-lasting responses to overcome the tumor-immunosuppressive environment. To eradicate tumor cells with high specificity, peptides are designed by exploring tumor-associated antigens, tumor-

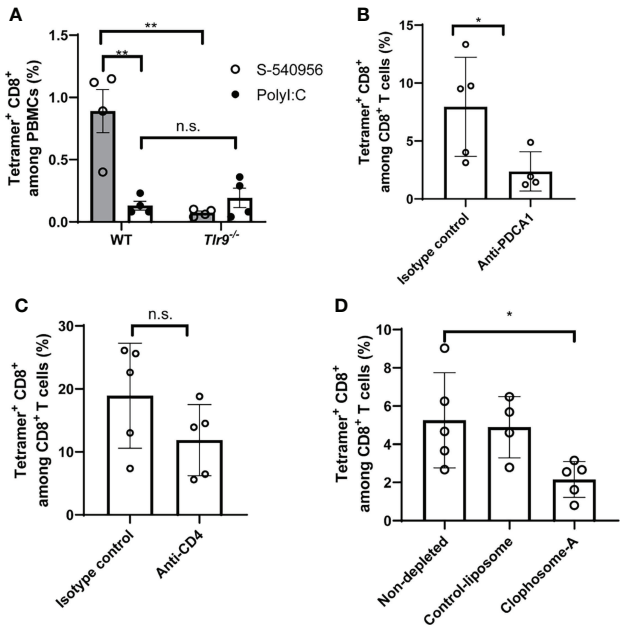

FIGURE 4 | S-540956 enhanced TRP2-specific $CD8^+$ T cell responses in TLR9- and pDC-dependent manners. **(A)** Wild-type (WT) or *Tlr9*$^{-/-}$ mice were subcutaneously immunized with TRP2 peptide/S-540956 or TRP2 peptide/Poly I:C on days 0 and 7 (N = 4). TRP2 peptide-specific $CD8^+$ T cells were measured by flow cytometry using a TRP2 tetramer, on day 14. **(B)** pDCs or **(C)** $CD4^+$ T cells were depleted by administering an anti-PDCA1 or anti-CD4 antibody (N = 4–5) to WT mice immunized with TRP2 peptide/S-540956, and TRP2 peptide-specific $CD8^+$ T cells were measured as described in **(A)**. **(D)** Macrophages were depleted by administering clophosome-A to WT mice immunized with TRP2 peptide/S-540956, and TRP2 peptide-specific $CD8^+$ T cells were measured as described in **(A)**. The data shown indicate the mean ± SE. n.s., not statistically significant, $^*P < 0.05$, $^{**}P < 0.01$, as determined by Student's *t*-test or one-way ANOVA. Data are representative of two independent experiments.

specific antigens, and neoantigens important for interactions between tumor cells and immune responses (2). Recently, in addition to monotherapy with cancer peptide vaccines, cancer peptide vaccines have been investigated for combination therapy with immune-checkpoint inhibitors (ICIs) with the objective of improving the clinical outcomes of ICIs (24). Adjuvants are crucial components of cancer peptide vaccines as they promote, prime, and recall peptide-specific $CD8^+$ T cell responses (25). To enhance the adjuvanticity, LN-targeting adjuvants have been explored by directly modifying TLR7/8 or TLR9 ligands (3, 26). These chemical modifications may alter the immunostimulatory effects of ligands, however, it is difficult to predict the immunotoxicity that may be attributable to the modified chemical structures in humans, based on pre-clinical research. Therefore, we elected to not modify the ligands and instead developed S-540596 by annealing complementary strands with amphiphilic chain units to ODN2006, one of the most commonly used adjuvants for cancer peptide vaccines in clinical trials (27, 28). Improved immunogenicity was confirmed; however, ODN2006-adjuvanted cancer peptide vaccines did not exhibit significant induction of cytotoxic T lymphocytes (CTLs) in patients, and no ODN2006 adjuvanted cancer peptide vaccine has been approved for clinical use till date. These clinical studies indicate the necessity of improving the adjuvanticity of ODN2006 for developing more effective cancer peptide vaccines. In this study, S-540956 exhibited more potent adjuvanticity than ODN2006 when evaluating the efficacies of cancer peptides against HPV-E7-expressing TC-1 tumors in mice. This promising result suggests that the S-540956-adjuvanted cancer peptide vaccine will show greater efficacy than ODN2006 against tumor cells in clinical settings.

TLR9 can recognize single-stranded DNA (ssDNA) and activate related signaling pathways originating from endosomes (6). Comparable stimulation of TLR9 signaling was observed between the double-stranded DNA (dsDNA) molecule, S-540956, and the ssDNA molecule, ODN2006, in HEK-Blue TLR9 cells. In this study, the nucleotides in ODN2006 are connected by a phosphorothioate linkage based on a previous report (29). The use of phosphorothioate nucleotides enhances the resistance of CpG ODNs to DNases when compared with the phosphodiester bond-linked nucleotides, which are components of native DNA (30). The nucleotides of the complementary strand (C-54056) for S-540956 were joined by phosphodiester linkage. A recent study indicated that DNase II in endosomes digests a phosphodiester linker of CpG ODN, in which the nucleotides at the center were joined by phosphodiester linkages with a phosphorothioated backbone at both ends, and the digested CpG ODN activates TLR9 (31). Hence, C-540956 is considered to be digested by DNase II in the endosomes, and the released ODN2006 stimulated TLR9 signaling pathway.

pDCs and conventional DCs are heterogeneous subsets of DCs that orchestrate innate and adaptive immune responses. pDCs can sense ssDNA *via* TLR9 and have diverse functions, which promote the establishment of optimal cellular immunity by presenting antigens to T cells (32). The delivery of antigen-targeting pDCs in combination with TLR agonists can enhance the induction of $CD8^+$ T cell responses (33). Our immunological analysis revealed differences between S-540956 and ODN2006 in terms of adjuvant incorporation by pDCs and activation of pDC, and the adjuvanticity of S-540956 diminished after the pDCs were depleted. A large number of DCs and $CD8^+$ T cells are considered to reside in LNs, when compared to those in peripheral tissues, and the transportation of antigens and adjuvants from the injection site to LNs is important for enhancing vaccine efficacy (34, 35). TLR9 is expressed in both mouse and human pDCs (36); therefore, we expect that S-540956 shows potent adjuvanticity in humans. Our immunological analysis indicated that the efficient activation of pDCs in LNs after the high accumulation of S-540956 is a critical innate immune response that enables S-540956 to induce more robust cellular-immune responses than ODN2006.

Some adjuvants can induce excessive proinflammatory cytokine responses related to cytokine storms and systemic inflammation (37). Excess systemic immune responses induced by frequent injections of CpG ODN cause splenomegaly, which

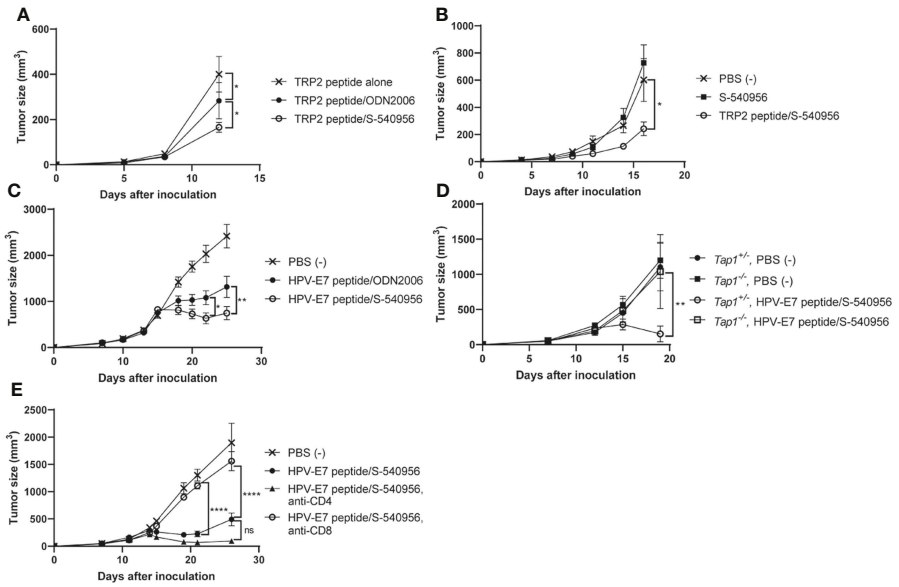

FIGURE 5 | Adjuvant effect of S-540956 with a cancer peptide vaccine against tumors in mice. **(A)** Mice were subcutaneously immunized with TRP2 peptide alone, TRP2 peptide/ODN2006, or TRP2/S-540956 on days 0 and 7 after the first immunization (N = 8). The mice were subcutaneously inoculated with TRP2-expressing B16F10 melanoma cells on day 14. **(B)** Mice were subcutaneously inoculated with TRP2-expressing B16F10 melanoma cells. The mice were subcutaneously immunized with PBS (–), S-540956, or TRP2/S-540956 at 7 and 14 days after inoculation (N = 9–10). **(C)** Mice were subcutaneously inoculated with HPV-E7-expressing TC-1 tumor cells. The mice were intramuscularly immunized with PBS (–) or HPV-E7 peptide mixed with S-540956 or ODN2006 at 9 and 16 days after inoculation (N = 8). **(D)** *Tap1*$^{+/-}$ or *Tap*$^{-/-}$ mice were subcutaneously inoculated with TC-1 tumor cells. The mice were subcutaneously immunized with PBS (–) or HPV-E7/S-540956 at 7 and 14 days after inoculation (N = 3–5). **(E)** Mice were subcutaneously inoculated with HPV-E7-expressing TC-1 tumor cells. The mice were intramuscularly immunized with PBS (–) or HPV-E7 peptide mixed with S-540956 at 7 and 14 days after inoculation. $CD4^+$ cells or $CD8^+$ cells were depleted by administrating anti-CD4 antibody or anti-CD8 antibody (N = 6–8). Tumor sizes were measured using a vernier caliper. The data shown indicate the mean ± SE. $^*P < 0.05$, $^{**}P < 0.01$, $^{****}P < 0.001$, as determined by one-way ANOVA. Data are representative of two independent experiments.

is mainly due to erythroid and myeloid expansion in the red pulp, and consequently lead to extramedullary hematopoiesis (38, 39). Although proinflammatory cytokine responses were observed in the blood after the S-540956 injection, each induction level was not statistically higher than that of ODN2006. In addition, splenomegaly induced by frequent injections of S-540956 was lower than that induced by ODN2006. ODN2006 is a well-known safe adjuvant that has been use in a large number of clinical trials (8). For instance, ODN2006 has been used as a vaccine adjuvant for the recombinant AMA1-C1/alhydrogel malaria vaccine. This addition of ODN2006 was found to significantly enhance the humoral immune responses; however, local and systemic adverse events were also increased (40). It is, therefore, necessary to reduce the number of adverse events induced by the adjuvant, particularly for preventive vaccines. The targeting of LNs by S-540956 might decrease the number of adverse events and thereby, regulate the severity of adverse event, especially systemic adverse effects. Therefore, we expect that S-540956 poses a low risk for inducing systemic inflammation and splenomegaly in humans.

Collectively, our data supports the conclusion that the targeting LN profile of S-540956 can elicit potent adjuvanticity without inducing excess systemic inflammation and immunotoxicity. However, future investigations into the safety profile of S-540956 *via* clinical trials are expected to further confirm the benefit of an LN-targeting profile as a vaccine adjuvant.

In conclusion, the results of this study demonstrated a chemical approach for discovering a novel adjuvant in which the complementary strand was conjugated to a lipid for draining LN targeting, which increased ODN2006 accumulation in the draining LNs and consequently enhanced the adjuvant effect, without elevating systemic inflammation.

DATA AVAILABILITY STATEMENT

The original contributions presented in the study are included in the article/**Supplementary Material**. Further inquiries can be directed to the corresponding author.

ETHICS STATEMENT

The animal study was reviewed and approved by National Institutes of Biomedical Innovation, Health, and Nutrition (NIBIOHN) and Shionogi Animal Care and Use Committee.

AUTHOR CONTRIBUTIONS

TN, TT, ST, TK, and YI designed and conducted the experiments, performed the data analysis, interpreted the results, and wrote the manuscript. TN and MO performed the data analysis, interpreted the results, and wrote the manuscript. TN, TI, AK, KK, TY, MN, and KI conceived the project, designed the experiments, interpreted the results, and revised the manuscript. All authors contributed to the manuscript and approved the submitted version.

FUNDING

This work was supported by Shionogi & Co., Ltd., and in part by NIBIOHN, Core Research for Evolutional Science and Technology (CREST)/Japan Science and Technology Agency (JST), and Japan Agency for Medical Research and Development (AMED).

ACKNOWLEDGMENTS

We thank Akiko Okabe, Mariko Nakamura, and Miyoko Kawatsu for their excellent technical assistance with animal husbandry and genotyping, as well as the members of K.J.I.'s laboratories for their valuable comments and help. We also thank Shinya Omoto, Masako Onishi, and Takeo Kamakura, scientists at Shionogi & Co., Ltd. for their expert comments about this study.

SUPPLEMENTARY MATERIAL

The Supplementary Material for this article can be found online at: https://www.frontiersin.org/articles/10.3389/fimmu.2021.803090/full#supplementary-material

REFERENCES

1. Bezu L, Kepp O, Cerrato G, Pol J, Fucikova J, Spisek R, et al. Trial Watch: Peptide-Based Vaccines in Anticancer Therapy. *Oncoimmunol* (2018) 4: e974411. doi: 10.1080/2162402X.2018.1511506
2. Hollingsworth RE, Jansen K. Turning the Corner on Therapeutic Cancer Vaccines. *NPJ Vaccines* (2019) 4:7. doi: 10.1038/s41541-019-0103-y
3. Liu H, Moynihan KD, Zheng Y, Szeto GL, Li AV, Huang B, et al. Structure-Based Programming of Lymph-Node Targeting in Molecular Vaccines. *Nature* (2014) 507:519–22. doi: 10.1038/nature12978
4. Hanson MC, Crespo MP, Abraham W, Moynihan KD, Szeto GL, Chen SH, et al. Nanoparticulate STING Agonists Are Potent Lymph Node-Targeted Vaccine Adjuvants. *J Clin Invest* (2015) 125:2532–46. doi: 10.1172/JCI79915
5. Klinman DM, Verthelyi D, Takeshita F, Ishii KJ. Immune Recognition of Foreign DNA. *Immunity* (1999) 11:123–9. doi: 10.1016/s1074-7613(00)80087-4
6. Klinman DM. Immunotherapeutic Uses of CpG Oligodeoxynucleotides. *Nat Rev Immunol* (2004) 4:249–58. doi: 10.1038/nri1329
7. Hemmi H, Takeuchi O, Kawai T, Kaisho T, Sato S, Sanjo H, et al. A Toll-Like Receptor Recognizes Bacterial DNA. *Nature* (2000) 408:740–5. doi: 10.1038/35047123
8. Karapetyan L, Luke JJ, Davar D. Toll-Like Receptor 9 Agonists in Cancer. *Oncol Targets Ther* (2020) 13:10039–60. doi: 10.2147/OTT.S247050
9. Steinbuck MP, Seenappa LM, Jakubowski A, McNeil LK, Haqq CM, DeMuth PC. A Lymph Node-Targeted Amphiphile Vaccine Induces Potent Cellular and Humoral Immunity to SARS-CoV-2. *Sci Adv* (2021) 7(6):eabe5819. doi: 10.1126/sciadv.abe5819
10. Faries MB, Bedrosian I, Reynolds C, Nguyen HQ, Alavi A, Czerniecki BJ. Active Macromolecule Uptake by Lymph Node Antigen-Presenting Cells: A Novel Mechanism in Determining Sentinel Lymph Node Status. *Ann Surg Oncol* (2000) 7:98–105. doi: 10.1007/s10434-000-0098-6
11. Jurk M, Kritzler A, Debelak H, Vollmer J, Krieg AM, Uhlmann E. Structure-Activity Relationship Studies on the Immune Stimulatory Effects of Base-Modified CpG Toll-Like Receptor 9 Agonists. *ChemMedChem* (2006) 1:1007–14. doi: 10.1002/cmdc.200600064
12. Cooper CL, Davis HL, Morris ML, Efler SM, Krieg AM, Li Y, et al. Safety and Immunogenicity of CPG 7909 Injection as an Adjuvant to Fluarix Influenza Vaccine. *Vaccine* (2004) 22:3136–43. doi: 10.1016/j.vaccine.2004.01.058
13. Krieg AM, Efler SM, Wittpoth M, Al Adhami MJ, Davis HL. Induction of Systemic TH1-Like Innate Immunity in Normal Volunteers Following Subcutaneous But Not Intravenous Administration of CPG 7909, a Synthetic B-Class CpG Oligodeoxynucleotide TLR9 Agonist. *J Immunother* (2004) 27:460–71. doi: 10.1097/00002371-200411000-00006
14. Akira K. *Nucleic Acid Derivative Having Immunostimulatory Activity*. Osaka, Japan. SHIONOGI & CO., LTD. Patent No WO2017/057540 Al. (2017).
15. Onishi R, Watanabe A, Nakajima M, Sekiguchi M, Kugimiya A, Kinouchi H, et al. Surface Plasmon Resonance Assay of Binding Properties of Antisense Oligonucleotides to Serum Albumins and Lipoproteins. *Anal Sci* (2015) 31:1255–60. doi: 10.2116/analsci.31.1255
16. Momota M, Lelliott P, Kubo A, Kusakabe T, Kobiyama K, Kuroda E, et al. ZBP1 Governs the Inflammasome-Independent IL-1α and Neutrophil Inflammation That Play a Dual Role in Anti-Influenza Virus Immunity. *Int Immunol* (2019) 32:203–12. doi: 10.1093/intimm/dxz070
17. Kobiyama K, Aoshi T, Narita H, Kuroda E, Hayashi M, Tetsutani K, et al. Nonagonistic Dectin-1 Ligand Transforms CpG Into a Multitask Nanoparticulate TLR9 Agonist. *Proc Natl Acad Sci USA* (2014) 111:3086–91. doi: 10.1073/pnas.1319268111
18. Eisenbarth SC. Dendritic Cell Subsets in T Cell Programming: Location Dictates Function. *Nat Rev Immunol* (2019) 19:89–103. doi: 10.1038/s41577-018-0088-1
19. Eng NF, Bhardwaj N, Mulligan R, Diaz-Mitoma F. The Potential of 1018 ISS Adjuvant in Hepatitis B Vaccines: HEPLISAV" Review. *Hum Vaccines Immunother* (2013) 9:1661–72. doi: 10.4161/hv.24715
20. Wimmers F, Aarntzen EHJG, Duiveman-deBoer T, Figdor CG, Jacobs JFM, Tel J, et al. Long-Lasting Multifunctional $CD8^+$ T Cell Responses in End-Stage Melanoma Patients can be Induced by Dendritic Cell Vaccination. *Oncoimmunology* (2016) 5:e1067745. doi: 10.1080/2162402X.2015.1067745
21. De Groot R, Van Loenen MM, Guislain A, Nicolet BP, Freen-Van Heeren JJ, Verhagen OJHM, et al. Polyfunctional Tumor-Reactive T Cells Are Effectively Expanded From Non-Small Cell Lung Cancers, and Correlate With an Immune-Engaged T Cell Profile. *Oncoimmunology* (2019) 8:e1648170. doi: 10.1080/2162402X.2019.1648170
22. Krieg AM. Therapeutic Potential of Toll-Like Receptor 9 Activation. *Nat Rev Drug Discovery* (2006) 5:471–84. doi: 10.1038/nrd2059
23. Ammi R, De Waele J, Willemen Y, Van Brussel I, Schrijvers DM, Lion E, et al. Poly(I:C) as Cancer Vaccine Adjuvant: Knocking on the Door of Medical Breakthroughs. *Pharmacol Ther* (2015) 146:120–31. doi: 10.1016/j.pharmthera.2014.09.010
24. Zhao J, Chen Y, Ding ZY, Liu JY. Safety and Efficacy of Therapeutic Cancer Vaccines Alone or in Combination With Immune Checkpoint Inhibitors in Cancer Treatment. *Front Pharmacol* (2019) 10:1184. doi: 10.3389/fphar.2019.01184
25. Khong H, Overwijk WW. Adjuvants for Peptide-Based Cancer Vaccines. *J Immunother Cancer* (2016) 4:56. doi: 10.1186/s40425-016-0160-y
26. Lynn GM, Sedlik C, Baharom F, Zhu Y, Ramirez-Valdez RA, Coble VL, et al. Peptide–TLR-7/8a Conjugate Vaccines Chemically Programmed for Nanoparticle Self-Assembly Enhance CD8 T-Cell Immunity to Tumor Antigens. *Nat Biotechnol* (2020) 38:320–32. doi: 10.1038/s41587-019-0390-x
27. Scheiermann J, Klinman DM. Clinical Evaluation of CpG Oligonucleotides as Adjuvants for Vaccines Targeting Infectious Diseases and Cancer. *Vaccine* (2014) 32:6377–89. doi: 10.1016/j.vaccine.2014.06.065

28. Krieg AM. Development of TLR9 Agonists for Cancer Therapy. *J Clin Invest* (2007) 117(5):1184–94. doi: 10.1172/JCI31414
29. Hartmann G, Weeratna RD, Ballas ZK, Payette P, Blackwell S, Suparto I, et al. Delineation of a CpG Phosphorothioate Oligodeoxynucleotide for Activating Primate Immune Responses. *In Vitro In Vivo J Immunol* (2000) 164:1617–24. doi: 10.4049/jimmunol.164.3.1617
30. Mutwiri GK, Nichani AK, Babiuk S, Babiuk LA. Strategies for Enhancing the Immunostimulatory Effects of CpG Oligodeoxynucleotides. *J Control Release* (2004) 97:1–17. doi: 10.1016/j.jconrel.2004.02.022
31. Chan MP, Onji M, Fukui R, Kawane K, Shibata T, Saitoh SI, et al. DNase II-Dependent DNA Digestion Is Required for DNA Sensing by TLR9. *Nat Commun* (2015) 6:4–6. doi: 10.1038/ncomms6853
32. Swiecki M, Colonna M. The Multifaceted Biology of Plasmacytoid Dendritic Cells. *Nat Rev Immunol* (2015) 15:471–85. doi: 10.1038/nri3865
33. Loschko J, Schlitzer A, Dudziak D, Drexler I, Sandholzer N, Bourquin C, et al. Antigen Delivery to Plasmacytoid Dendritic Cells *via* BST2 Induces Protective T Cell-Mediated Immunity. *J Immunol* (2011) 186:6718–25. doi: 10.4049/jimmunol.1004029
34. Thomas SN, Vokali E, Lund AW, Hubbell JA, Swartz MA. Targeting the Tumor-Draining Lymph Node With Adjuvanted Nanoparticles Reshapes the Anti-Tumor Immune Response. *Biomaterials* (2014) 35:814–24. doi: 10.1016/j.biomaterials.2013.10.003
35. Bachmann MF, Jennings GT. Vaccine Delivery: A Matter of Size, Geometry, Kinetics and Molecular Patterns. *Nat Rev Immunol* (2010) 10:787–96. doi: 10.1038/nri2868
36. Iwasaki A, Medzhitov R. Toll-Like Receptor Control of the Adaptive Immune Responses. *Nat Immunol* (2004) 5:987–95. doi: 10.1038/ni1112
37. Sauder DN, Smith MH, Senta-McMillian T, Soria I, Meng TC. Randomized, Single-Blind, Placebo-Controlled Study of Topical Application of the Immune Response Modulator Resiquimod in Healthy Adults. *Antimicrob Agents Chemother* (2003) 47:3846–52. doi: 10.1128/AAC.47.12.3846-3852.2003
38. Heikenwalder M, Polymenidou M, Junt T, Sigurdson C, Wagner H, Akira S, et al. Lymphoid Follicle Destruction and Immunosuppression After Repeated CpG Oligodeoxynucleotide Administration. *Nat Med* (2004) 10:187–92. doi: 10.1038/nm987
39. Sparwasser T, Hültner L, Koch ES, Luz A, Lipford GB, Wagner H. Immunostimulatory CpG-Oligodeoxynucleotides Cause Extramedullary Murine Hemopoiesis. *J Immunol* (1999) 162:2368–74.
40. Mullen GED, Ellis RD, Miura K, Malkin E, Nolan C, Hay M, et al. Phase 1 Trial of AMA1-C1/Alhydrogel Plus CPG 7909: An Asexual Blood-Stage Vaccine for Plasmodium Falciparum Malaria. *PloS One* (2008) 3(8):e2940. doi: 10.1371/journal.pone.0002940

Conflict of Interest: TN, TT, MO, ST, TK, YI, TI, AK, KK, and MN are employees of Shionogi & Co., Ltd.

The remaining authors declare that the research was conducted in the absence of any commercial or financial relationships that could be construed as a potential conflict of interest.

The authors declare that this study received funding from Shionogi & Co., Ltd. The funder had the following involvement in the study: study design, collection, analysis, interpretation of data, the writing of this article or the decision to submit it for publication.

frontiers in Immunology

ORIGINAL RESEARCH
published: 07 February 2022
doi: 10.3389/fimmu.2022.795463

Deep Immune Phenotyping and Single-Cell Transcriptomics Allow Identification of Circulating TRM-Like Cells Which Correlate With Liver-Stage Immunity and Vaccine-Induced Protection From Malaria

Andrés Noé[1†], Mehreen S. Datoo[1†], Amy Flaxman[1†], Mohammad Ali Husainy[2], Daniel Jenkin[1], Duncan Bellamy[1†], Rebecca A. Makinson[1†], Richard Morter[1†], Fernando Ramos Lopez[1†], Jonathan Sheridan[1†], Dimitrios Voukantsis[3†], Naveen Prasad[3], Adrian V. S. Hill[1†], Katie J. Ewer[1†] and Alexandra J. Spencer[1*†]*

[1] The Jenner Institute, University of Oxford, Oxford, United Kingdom, [2] Department of Radiology, John Radcliffe Hospital, Oxford, United Kingdom, [3] Bioinformatics Hub, Department of Oncology, University of Oxford, Oxford, United Kingdom

Protection from liver-stage malaria requires high numbers of CD8+ T cells to find and kill *Plasmodium*-infected cells. A new malaria vaccine strategy, prime-target vaccination, involves sequential viral-vectored vaccination by intramuscular and intravenous routes to target cellular immunity to the liver. Liver tissue-resident memory (TRM) CD8+ T cells have been shown to be necessary and sufficient for protection against rodent malaria by this vaccine regimen. Ultimately, to most faithfully assess immunotherapeutic responses by these local, specialised, hepatic T cells, periodic liver sampling is necessary, however this is not feasible at large scales in human trials. Here, as part of a phase I/II *P. falciparum* challenge study of prime-target vaccination, we performed deep immune phenotyping, single-cell RNA-sequencing and kinetics of hepatic fine needle aspirates and peripheral blood samples to study liver CD8+ TRM cells and circulating counterparts. We found that while these peripheral 'TRM-like' cells differed to TRM cells in terms of previously described characteristics, they are similar phenotypically and indistinguishable in terms of key T cell residency transcriptional signatures. By exploring the heterogeneity among liver CD8+ TRM cells at single cell resolution we found two main subpopulations that each share expression profiles with blood T cells. Lastly, our work points towards the potential for using TRM–like cells as a correlate of protection by liver-stage malaria vaccines and, in particular, those adopting a prime-target approach. A simple and reproducible correlate of protection would be particularly valuable in trials of liver-stage malaria vaccines as they progress to phase III, large-scale testing in African infants. We provide a blueprint for understanding and monitoring liver TRM cells induced by a prime-target malaria vaccine approach.

Keywords: malaria vaccine, malaria vaccine decelopment, correlates of protection (CoP), TRM, tissue resident memory CD8+ T cells, tissue resident memory T cell, scRNA seq

OPEN ACCESS

Edited by:
Gabriel Pedersen,
Statens Serum Institut (SSI), Denmark

Reviewed by:
Moriya Tsuji,
Columbia University Irving Medical Center, United States
Ian Andrew Cockburn,
Australian National University, Australia

****Correspondence:***
Andrés Noé
andres.noe@ndm.ox.ac.uk;
andres.noe@mcri.edu.au
Alexandra J. Spencer
alex.spencer@ndm.ox.ac.uk

†ORCID:
Andrés Noé
orcid.org/0000-0002-6408-7032
Mehreen S. Datoo
orcid.org/0000-0003-4968-2842
Amy Flaxman
orcid.org/0000-0001-6460-1372
Duncan Bellamy
orcid.org/0000-0003-3614-0032
Rebecca A. Makinson
orcid.org/0000-0001-7582-9073
Richard Morter
orcid.org/0000-0002-7005-1546
Fernando Ramos Lopez
orcid.org/0000-0002-9997-7879
Jonathan Sheridan
orcid.org/0000-0002-6806-2609
Dimitrios Voukantsis
orcid.org/0000-0002-7472-0794
Adrian V. S. Hill
orcid.org/0000-0003-0900-9629
Katie J. Ewer
orcid.org/0000-0001-9827-9836
Alexandra J. Spencer
orcid.org/0000-0001-7958-6961

Specialty section:
This article was submitted to Vaccines and Molecular Therapeutics, a section of the journal Frontiers in Immunology

Received: *15 October 2021*
Accepted: *10 January 2022*
Published: *07 February 2022*

INTRODUCTION

Malaria is the most problematic parasitic disease in human history. A highly efficacious vaccine could curb the hundreds of millions of cases and hundreds of thousands of deaths occurring each year. It has been over 30 years since Ruth and Victor Nussenzweig identified that protection from liver-stage malaria requires high numbers of CD8+ T cells to find and kill *Plasmodium*-infected cells (1). To this end, substantial effort has been invested in optimising viral vector strategies able to generate high frequencies of antigen-specific CD8+ T cells (2–7). A prominent approach entails vaccinating with heterologous viral vectors to induce CD8+ T cells and results in modest clinical efficacy in both malaria naïve and pre-exposed individuals (4, 8). CD8+ T cell numbers following vaccination correlate with efficacy, suggesting that increased numbers of circulating CD8+ T cells are associated with improved protection.

A new malaria vaccine strategy, prime-target vaccination (PTV), involves sequential viral-vectored vaccination by intramuscular and intravenous routes to target cellular immunity to the liver (9). The efficacy of leading liver-stage malaria vaccine candidates in mice can be enhanced with this approach from 0-30% to 100% efficacy. PTV substantially increases the number of antigen-specific tissue-resident memory (TRM) CD8+ T cells in the livers of mice (9). This and other studies have shown that this specialised subset of hepatic T cells can be induced by heterologous prime-boost vaccines and that they are necessary and sufficient for protection against liver-stage rodent malaria (9–11).

Relatively little is known about the human liver T cell population in health. It is now well established that TRM cells represent a functionally distinct compartment poised at portals of pathogen entry to provide local protection (12–15). Short of showing long-term residence in tissues and/or lack of recirculation, TRM cells can be identified by using a number of markers found on their cell surface. Identifying surface markers of human liver residency is an ongoing endeavour; CD69, CXCR3 and, to a lesser extent, CD103 are often used to distinguish TRM cells from other hepatic T cells (12, 16–18). PD-1, a marker of T cell hyporesponsiveness (19), and CXCR6, a chemokine that can mediate lymphocyte recruitment (20), are two other important markers of hepatic TRM cells (12, 21). Several reports have described core transcriptional signatures for TRM cells from multiple tissues identified by bulk (14), and single-cell RNA-sequencing (22–24).

The challenges associated with mapping hepatic immunological populations are threefold: i) access-related, ii) rare populations are thought to be critical mediators of immunity (such as TRM cells), and iii) highly specialised techniques are often required (ie. in sample collection and preparation, and analyses). The added complexity of trying to understand hepatic immunity in the context of malaria vaccine-induced immunity, at scale, makes for a seemingly insurmountable task. It is therefore critical to identify if inferences about the liver can be made by looking at the blood; that is, to identify correlates of hepatic immunity and of protection. Recently there have been reports that TRM cells from various sites can exit tissues in response to stimuli, re-enter the circulation and even contribute to the expansion of memory T cells (25–28). Indeed, small but significant proportions of circulating T cells have been demonstrated to express 'tissue-resident signature' genes at levels comparable to T cells in tissues (23). Therefore, we wanted to investigate the qualities of human hepatic TRM cells and determine whether there was a comparable or related subset of T cells in the blood.

Herein, we track the phenotype, transcriptomics and kinetics of blood-derived TRM-like cells with the aim of identifying a correlate of malaria vaccine-induced immunity against controlled human malaria infection (CHMI). A detailed understanding of TRM cells and any potential circulating counterpart in humans, as well as an appreciation of their relationship, will likely be critical in identifying correlates of liver-stage malaria protection and further vaccine development.

MATERIALS AND METHODS

Volunteers

As part of a phase I/IIa sporozoite challenge study to assess intravenous boosting (prime-target) with malaria vaccine candidates ChAd63 and MVA encoding ME−TRAP (**Supplementary Figure 1**, ClinicalTrials.gov Identifier: NCT03707353, Datoo et al. in preparation), T cells from the liver and blood were isolated and compared. An aim of this comparison was to investigate a translatable liver-stage malaria correlate of immunity, by using insights gained from studying liver TRM cells. All recruited volunteers were healthy, malaria naïve adults aged between 18 and 45 years with PBMCs isolated at multiple timepoints throughout the study. Fifteen of the thirty-nine participants were asked to participate in liver fine needle aspirate (FNA) sampling at a single timepoint after intravenous vaccine administration, with volunteers recruited equally across the four groups. The study protocol and associated documents were reviewed and approved by the UK National Research Ethics Service, Committee South Central–Oxford REC A (18/SC/0384) and the Medicines and Healthcare Products Regulatory Agency (EudraCT: 2017-001075-23). CHMI ("challenge") after vaccination and diagnosis of malaria was conducted as we previously described (5).

Sample Collection and Cell Isolation

Liver FNA was performed as previously described (29), with a few modifications. Briefly, under ultrasound guidance a 22-gauge spinal needle with an internal trocar was used to gain access, along an anaesthetised tract, to the edge of the liver capsule. The internal trocar was removed after a further 2-3cm insertion, into the parenchyma. Liver cells were collected into a 20mL syringe containing 3mL of cold sterile saline. Aspiration was performed as the needle was withdrawn 1-2cm, but while still remaining in the liver parenchyma using a 'fanning technique' (30, 31). Cells were transferred into a fresh 50mL tube containing 30ml catch media (RPMI supplemented with 25mM HEPES and 15IU/mL heparin) by flushing the syringe and needle with 3mL of media.

Two aspirates per volunteer were performed prior to transfer on ice for immediate processing. Any aspirate with frank blood were discarded.

Blood samples for PBMC separation were collected in heparinised tubes and separated on a centrifugation gradient using Lymphoprep (Axis Shield) within 4 hours of venepuncture. Liver samples were resuspended in RBC lysis solution (eBioscience) for less than five minutes, before counting and staining. FNA and PBMC sampling was performed 16-24 days after IV viral vector administration.

Flow Cytometry and Intracellular Cytokine Staining

For the characterisation of T cell kinetics after IV viral vector, freshly isolated PBMC were stimulated with anti-CD28 and anti-CD49d at 1μg/mL (Becton Dickinson), 200μg/mL of CD107a-PeCy5 (eBioscience) together with a pool of all 56 peptides of the T9/96 strain *P. falciparum* TRAP antigen (final concentration 5μg/mL) for 16-20 hours (32), 5μg/ml Staphylococcal enterotoxin B (SEB) (Sigma Aldrich) or media (unstimulated). Brefeldin A and monensin (eBioscience), both at 1 μg/mL, were added after two hours. For lymphocytes used in matched PBMC and FNA characterisation, no peptide stimulation was performed.

Following surface staining, fixation and intracellular staining (see **Supplementary Materials and Methods** for antibody list), acquisition was performed using an LSRII or LSRFortessa X-20 SORP (BD Biosciences). At least 500,000 events were acquired per sample, with data analysed on FlowJo version 10 (BD Biosciences). Lymphocytes were gated on live, size, and singlet (FSC-A vs FSC-H and FSC-A vs FSC-W) and dead cells (Live/Dead amine reactive+), monocytes (CD14+) and B cells (CD19+) were excluded. Cells were subsequently gated on CD45+ CD3+ CD8+ T cells.

RNA Sequencing

Cell sorting was conducted using a FACSAriaIII (BD Biosciences) using a 70μm nozzle and single cell purity. All mini-bulk samples consisted of 100 cells and were attained using a two-way sort based on CD69 status (positive or negative), pre-gated on live single CD20- CD45+ CD3+ CD4- CD8+ CD45RA- cells. All single cells were CD69+. Mini-bulk samples were collected into 0.2mL PCR tubes and single cells directly into RNAse free 96-well PCR plates with 4.01μL lysis catch buffer (0.4% (vol/vol) Triton X-100 and 2U/μl RNase inhibitor, $4x10^7$ dilution of ERCC spike-in RNA control, 2.5mM dNTPs (Thermo-Fisher), 2.5μM Oligo-dT30VN). Samples were vortexed, spun and placed on dry ice within 10 minutes. Smart-Seq2 libraries were generated following the established protocol (33).

Statistical and Bioinformatic Analyses

Prism version 8 (GraphPad) and/or RStudio (base R version 3.6.2) were used for analyses. Mean values with standard deviation are shown in all graphs, unless otherwise stated. Significance testing of differences between group means (for normally distributed data) used the two-tailed Student's t-test, or medians used the two-tailed Mann–Whitney U-test. Univariate immunological analysis compared time to malaria diagnosis between strata dichotomised by volunteer T cell proportions. Multiple regression Cox proportional hazards models were fitted to flow cytometry data with frequency of T cell populations as the independent variable and time to diagnosis as the dependent variable. Models were assessed as previously described (4); Akaike's information criterion (AIC) was used as an aid for choosing between competing nested models. Lower AIC values indicate a preferred model that maximises model parsimony. Immunological correlations with time to patent parasitaemia or other variables were pre-specified and prioritised analysis of T cell subsets based on observations from pre-clinical studies using prime-target vaccination. An alpha level of 0.05 was considered statistically significant.

Sequencing reads were aligned to the human genome using STAR (34). Ensembl gene counts were generated using featureCounts (35). DESeq2 v3.10 (36) was used for normalisation and feature selection in analysis of the mini-bulk experiment. The Wald test was the default used for hypothesis testing. Seurat (37, 38) was used for normalisation, variance stabilisation and feature selection in the single cell experiment. Differential expression was based on the non-parameteric Wilcoxon rank sum test (see **Supplementary Materials and Methods** for further information).

RESULTS

Hepatic T Cells Correlate Quantitatively to Matched Peripheral Blood T Cells

Following intravenous vaccination with a malaria vaccine candidate, the frequency and phenotype of TRM cells isolated from the liver by FNA sampling and peripheral blood were compared (**Figure 1A**). Using CD69 and CD11a positivity to identify TRM cells in the liver we observed an enrichment of these CD8+ T cells in the liver (**Table 1** and **Supplementary Figures 2**, **3**), consistent with previous reports (12, 30, 39). In contrast, memory CD8+ T cells expressing CD103 did not differentially populate the liver or blood (**Table 1**). Using an algorithm (30, 39) developed to determine the "liver–like" score of an FNA sample, showed that our sample quality was comparable with and, indeed, more representative of the liver (median liver-like score 78%, IQR 23.6%) than previously reported (39).

Cells with a TRM cell phenotype (ie. $CD69^+$ memory T cells) in the liver correlated significantly to a similar population observed in the blood (**Figure 1B**), present at a much lower frequency. The frequency of total CD8+ CD3+ CD56- T cells significantly positively correlated between PBMC and FNA samples. PBMC CD4+ CD3+ CD56- T cell frequency negatively correlated to matched FNA T cell frequencies (**Figure 1B**), but this was driven by one outlying volunteer. Consistent with previous reports, a higher frequency of both TRM cells and CD8+ T cells were observed in the liver compared to blood (39).

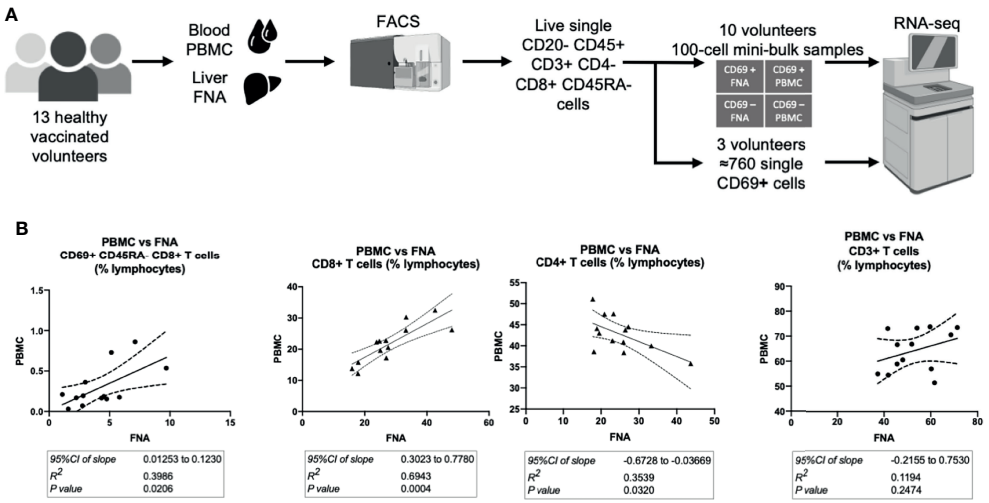

FIGURE 1 | Hepatic and circulating lymphocytes correlate numerically and phenotypically when analysed by flow cytometry. **(A)** Sampling workflow. 15 volunteers across all vaccination groups were recruited for liver FNA sampling. Two volunteers were unable to provide samples, due to logistical reasons, and withdrew on the sampling days. Hepatic fine needle aspirate and peripheral venesection were performed within one hour. Lymphocytes were isolated, stained for flow cytometry/cell sorting and sorted within three hours of sampling. Ten volunteers' FNA and PBMC samples were two-way sorted for 100-cell mini-bulk RNA-sequencing and three volunteer samples were sorted for single-cell RNA-sequencing. **(B)** Quantitative correlations between liver and blood samples. The 95%CI of linear regression slope, R2 value of goodness of fit and the p value that the slope is significantly non-zero are presented below the respective plots. The P values were calculated by F tests. All plots are derived from 13 matched FNA and PBMC samples. All values are presented as a proportion of single CD45+ lymphocytes in each sample. FNA, fine needle aspirate. PBMC, peripheral blood mononuclear cells. tSNE, t-distributed stochastic neighbour embedding. CI, confidence interval. FNA, fine needle aspirate. GMFI, geometric mean fluorescence intensity. PBMC, peripheral blood mononuclear cells. tSNE, t-distributed stochastic neighbour embedding.

Phenotypic characterisation of FNA and PBMC samples showed subsets of cells expressing TRM cell functional molecules. Regardless of tissue, CD69+ memory CD8+ T cells had on average a higher frequency of CXCR6+, CD103+, and PD−1+ cells and higher level of marker expression compared to CD8+ CD69- counterparts (**Supplementary Figure 4**). This was not evident in the CD103+ CD69+ cell proportion in PBMC, however, suggesting CD103 may be differentially expressed between liver and blood CD69+ memory T cells (**Supplementary Figure 4**, left panes). Using a t-distributed stochastic neighbour embedding algorithm to visualise and examine the co-expression of TRM cell markers on CD8+ memory T cells (**Supplementary Figure 5**), we identified three independent clusters, with little or no overlap between CD69+ and CD69- CD45RA- cells (**Supplementary Figures 5B, C**), signifying their relative enrichment in the CD69+ compartment. Differential expression of CXCR6, PD−1 and CD103 were the main drivers of cluster formation, with no substantial differences in the expression patterns of other markers (**Supplementary Figure 5D**). All three clusters co-occurred in FNA and PBMC samples, however Subset 2 appeared at a lower frequency in PBMC samples compared to FNA samples. The presence of circulating cells with established markers of tissue residency or 'circulating TRM cells' goes against the traditional definition of resident cells. We use "TRM-like cells" herein, instead of "circulating TRM cells", to indicate the (PBMC) circulating population of T cells that share phenotypic characteristics with bona fide (FNA) liver TRM cells.

The CD8+ Memory T Cell Transcriptome Can be Defined by CD69 Status

To determine whether surface expression of CD69 would also define TRM and TRM-like cells at the transcriptome level, we performed mini-bulk RNA sequencing on both CD69 positive and negative cells isolated from liver FNA and matched PBMC samples (**Figures 1A**, **2A**). CD69 status accounted for much of the variability found in the mini-bulk samples (**Figure 2B**). Differential gene expression between liver CD69+ and CD69- cells was consistent with previous resports (**Supplementary Data File 1**). The top 50 up-regulated genes included *IRF8*, *TOX2* and *CCL3* and down-regulated genes included *CCR4*, *IL23A* and *TSC2* (**Figure 2C**), as well as a large proportion of genes known to be important in T cell residency (14, 22, 40). Using a CD8+ TRM cell transcriptional signature generated by Kumar and colleagues (14), hierarchical clustering differentiated TRM and effector memory T (TEM) cells into independent populations (**Figure 2D**). Thirteen of the 25 most down-regulated genes and five of the 25 most up-regulated genes, between FNA CD69+ and CD69- cells, were present in the Kumar et al. signature. Gene set enrichment analysis (GSEA) of the genes upregulated in the Kumar et al. signature showed significant normalised enrichment in CD69+ cells from both FNA and PBMC comparisons (**Supplementary Data File 2**). Conversely, there was significant normalised enrichment of the downregulated Kumar et al. signature genes in FNA and PBMC CD69- cells (**Supplementary Data File 2**). Performing GSEA using other

TABLE 1 | Cells expressing TRM cell markers.

Population	FNA	PBMC	p value
CD8+ (%CD8+ T cells)	*Median (IQR)*	*Median (IQR)*	
CD69+ CD45RA-	13.80 (12.27)	0.380 (0.84)	0.0002
CD69+ CD11a hi CD45RA-	13.70 (12.26)	0.365 (0.83)	0.0002
CD103+ CD45RA-	1.280 (1.00)	1.29 (0.94)	0.4143
CD103+ CD11a hi CD45RA-	1.090 (0.87)	0.950 (0.75)	0.4143
CD69+ CD103+ CD11a hi CD45RA-	0.5200 (0.62)	0.00516 (0.01)	0.0002
CD4+ (%CD4+ T cells)			
CD69+ CD45RA-	4.55 (4.01)	0.15 (0.12)	0.0002
CD69+ CD11a hi CD45RA-	4.31 (4.03)	0.14 (0.12)	0.0002
CD103+ CD45RA-	ND	ND	NA
CD103+ CD11a hi CD45RA-	ND	ND	NA
CD69+ CD103+ CD11a hi CD45RA-	ND	ND	NA

Populations of CD8+ and CD4+ T cells expressing TRM cell markers. Representative flow cytometry plots from FNA and PBMC of the same donors is shown in ***Supplementary Figure 2****. The gating strategy for each of these populations is shown in* ***Supplementary Figure 3****. Wilcoxon matched pairs signed rank tests were used to check for significance of differences between FNA and PBMC samples. An exact p value is reported. Values reported are medians with interquartile ranges. Effective pairing, checked by Spearman correlation coefficient, was present for all samples (p<0.05). FNA, fine needle aspirate. IQR, interquartile range. NA, not applicable. ND, not detected. PBMC, peripheral blood mononuclear cells. TRM, tissue-resident memory T cells.*

gene sets relating to tissue residency further suggested FNA CD69+ cells as liver-resident T cells, however there was no significant enrichment in PBMC CD69+ cells. These data indicated that we were able to identify liver TRM cells transcriptionally, and differentiate them from liver TEM cells, using previously described residency signatures.

Gene Expression Differences Between Liver TRM and TRM-Like Cells

Having shown that CD69+ identifies liver TRM cells both phenotypically and transcriptionally, we next compared gene expression difference between liver TRM and TRM-like cells. Overall, genes upregulated in TRM-like cells were involved in glucose metabolism (*TKTL1*), zinc transport (*SLC39A7*) and *de novo* phospholipid synthesis (*AGPAT4*), suggesting that TRM-like cells are metabolically active (**Figure 3A** and **Supplementary Data File 3**). In contrast, genes upregulated in TRM cells included those of inter-cellular communication (*XCL1*) and interferon-induced proteins (*TRIM3*). These data support the notion that TRM cells are metabolically quiescent and ready for rapid effector function upon activation (14, 41–43). Interestingly, in this comparison between TRM and TRM–like cells there was no differential expression of a set of genes that has previously been shown to differ between tissue–derived TEM and blood-derived TEM (23). Clustering based on the 50 most variable genes was unable to separate TRM and TRM-like cells and indicated a volunteer-specific effect, for nine Y chromosome –associated genes (**Figure 3B**). The TRM cell core signature proposed by Kumar et al. co-clustered TRM-like and TRM cells (**Figure 3C**), suggesting these two cells populations are more similar, in terms of these core residency genes, than liver TEM and TRM cells, which were clearly separated into two independent clusters (**Figure 2D**). Given this, we explored gene expression differences between TRM-like and TRM cells.

Exploratory pathway analyses suggested differences between TRM and TRM–like cells. There was differential enrichment of genes involved in T cell differentiation, cell chemotaxis and interferon-gamma signalling (**Supplementary Figure 6A**). PBMC CD69+ T cells were enriched for gene sets related to GTPase activation, MHC protein complex binding, and ribosome structural component genes (**Supplementary Figure 6B**). Liver CD69+ T cells were enriched for genes involved in CD8+ T cell cytokine signalling (**Figure 4A**). There were no observed transcriptional differences in genes involved in cytotoxicity or a tissue-resident gene signature between liver CD69+ or PBMC CD69+ cells (**Figure 4B**). Other DGE analyses (**Figure 2A**) verified the uniqueness of TRM and TRM-like cells (**Supplementary Figures 6C–E**).

Single-Cell RNA-Sequencing Elucidates Liver TRM Cell Subpopulations

Using single-cell RNA-sequencing (scRNA-seq) we were able to dissect the heterogeneity of liver TRM cell transcriptomes (**Figure 2A**) and identifed three main clusters (**Figure 5A** and **Supplementary Figures 7A, B**). There were 142 genes differentially expressed between TRM cells in cluster (C)1 and C0 (**Figure 5B** and **Supplementary Data File 4**). Notable differential expression included *HLA-D* locus, chemokine receptor and ligand, and mucosal-associated invariant T (MAIT) cell receptor genes (**Figure 5B**).

Comparing DGE between TRM and TRM-like cells in C1, C0 and the mini-bulk analysis, we saw some agreement between the lists (**Figure 5C**). This may indicate the signature obtained from mini-bulk RNA-seq was an amalgam of several transcriptomic profiles. C0 showed a clear demarcation between TRM and TRM-like cells (**Figure 5A**). Differentially expressed genes included increased expression of *KLF2*, *RUNX3* and *S1PR1* in TRM-like cells compared to increased expression of *CXCR6* and *CD69* in TRM cells in C0, despite all cells exhibiting surface expression of CD69 by flow cytometry (**Supplementary Data File 5**). The distribution of hepatic and blood cells in C1 appeared more heterogeneous and there were less differentially expressed genes (**Figure 5C** and **Supplementary Data File 6**). Using gene signatures derived from liver-resident CD8+ T cells and MAIT cells described by Zhao et al. (22), qualitative signature enrichment scores for each cell were represented on

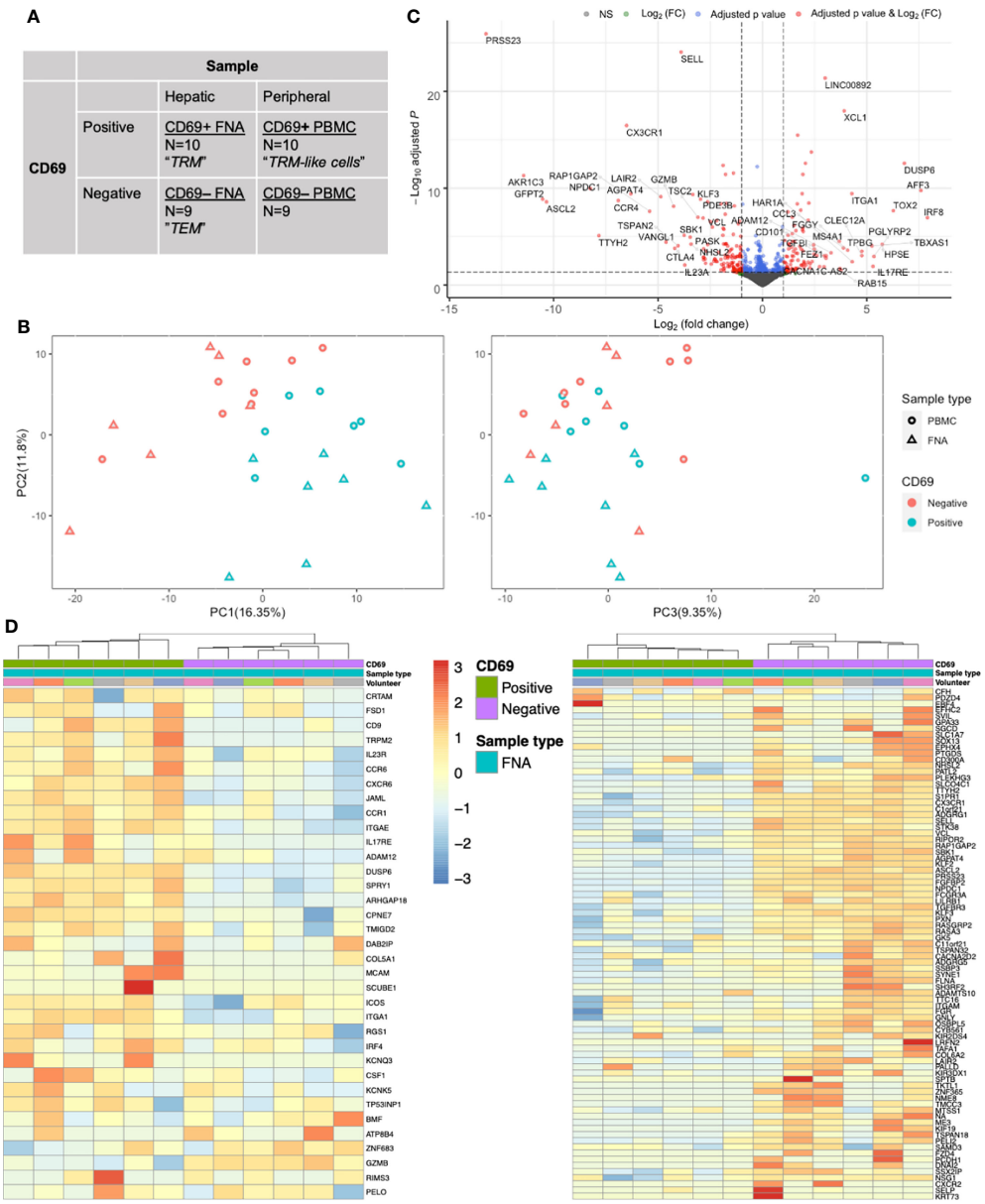

FIGURE 2 | CD69 status is a major driver of transcriptional differences in memory CD8+ T cells as assessed by mini-bulk RNA-seq. **(A)** Mini-bulk RNA-seq experimental design. Each category was composed of N number of 100-cell samples pre-gated on live single CD20- CD45+ CD3+ CD4- CD8+ CD45RA- cells sequenced in bulk by the SmartSeq2 protocol. Two volunteers' samples and one FNA paired (CD69+ and CD69-) samples were removed during QC. Non-normalised counts were input to DESeq2 and samples were paired according to volunteer and sample type. Differential expression analyses used a generalised linear model where counts were modelled using a negative binomial distribution. The Wald test was the default used for hypothesis testing when comparing gene expression between two sets of paired variables. See **Figure 1A** for sampling workflow. **(B)** PCA plots based on the 500 most variable genes by mini-bulk RNA sequencing. Plots of the first three PC, coloured according to CD69 status and sample type of the sequenced cells. Separation of CD69+ and CD69- cells was a composite of PC1 and PC2. PC3 does not distinguish CD69 status. Twenty-eight samples were analysed. **(C)** Volcano plot of up- and down-regulated genes between paired FNA CD69+ samples and CD69- samples. The top 50 up- and down-regulated genes have been annotated. Positive log(FC) values indicate greater gene expression in CD69+ samples, compared to CD69- samples. Negative log(FC) values indicate greater gene expression in CD69- samples. Differential expression of the 12,515 genes was tested for significance using the Wald test. P values were adjusted using the Benjamini-Hochberg (false discovery rate) correction. **(D)** Gene heatmap of FNA samples using the core TRM cell transcriptional signature described by Kumar et al. Left, heatmap of genes that are upregulated in the CD8+ Kumar et al. core transcriptional signature. Right, heatmap of genes that are downregulated in the CD8+ Kumar et al. core transcriptional signature. Columns are clustered based on Spearman's correlation of rlog normalised count values. Rows are clustered according to Pearson correlation of the rlog normalised gene counts. Gene count values are centred and scaled across rows. FACS, fluorescence-assisted cell sorting; FC, fold change; FNA, fine needle aspirate; PBMC, peripheral blood mononuclear cells; PC, principal component; PCA, principal component analysis; QC, quality control; TEM, effector memory T cell; TRM, tissue-resident memory T cell.

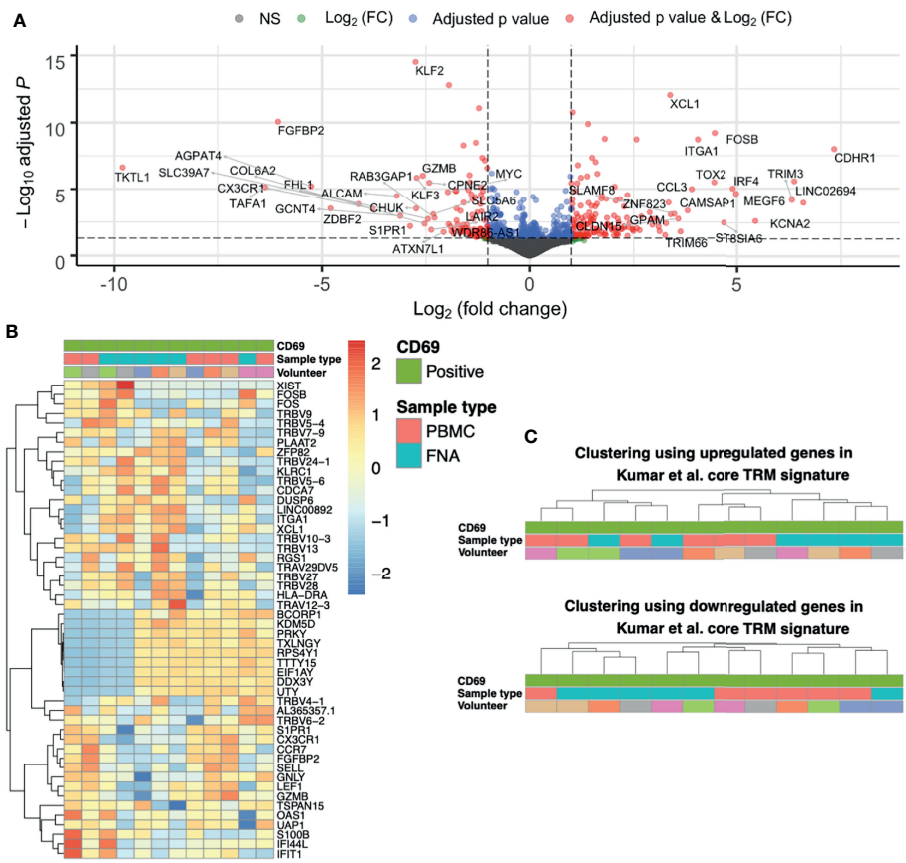

FIGURE 3 | The differences between CD69+ CD8+ T cells isolated from liver and blood are unique and not like those when comparing TRM and TEM cells. **(A)** Volcano plot of up- and down-regulated genes between paired FNA CD69+ and PBMC CD69+ samples. The top 50 up- and down-regulated genes have been annotated. Positive log(FC) values indicate greater gene expression in FNA CD69+ samples, compared to PBMC CD69+ samples. Negative log(FC) values indicate greater gene expression in PBMC CD69+ samples. DGE of 11,933 genes was tested for significance using the Wald test. P values were adjusted using the Benjamini-Hochberg correction (false discovery rate). **(B)** Heatmap of the most variable genes in the FNA CD69+ vs PBMC CD69+ comparison. Fifty most variable genes between FNA CD69+ and PBMC CD69+ samples. Yellow/red corresponds to increased counts compared to other samples and blue corresponds to decreased counts. Genes selected according to those with the greatest variance across samples. Columns are clustered based on Spearman's correlation of rlog normalised count values. Rows are clustered according to Pearson correlation of the rlog normalised gene counts. Gene count values are centred and scaled across rows. **(C)** Clustering of FNA and PBMC CD69+ samples using expression of TRM cell genes. Hierarchical clustering trees based on Spearman's correlation of sample rlog normalised count values considering up- and down-regulated genes in CD8+ Kumar et al. core TRM cell transcriptional signature. FC, fold change; FNA, fine needle aspirate; PBMC, peripheral blood mononuclear cells; rlog, regularised logarithm; TRM, tissue-resident memory T cell.

the UMAP (44). The liver TRM cell signature composed of 63 genes (such as *Gzmk*, *Cd160*, *Cxcr6* and *Eomes*) showed high enrichment scores in C1 FNA and PBMC-derived cells (**Figure 5D**). Both FNA and PBMC cells in C0 showed enrichment for the MAIT cell signature (**Figure 5D**). Interestingly, the circulating CD8+ memory T cell signature developed by Zhao et al. was highly enriched in C2 and, less so, in C1. Plausibly, C2 may have been composed of erroneously sorted CD69- cells or recently activated circulating CD69+ cells, particularly given the limited number of cells in this cluster. These signatures indicated C1 was comprised of cells resembling a conventional liver–resident T cell population and C0 was likely of MAIT or MAIT–like lineage cells.

TCR and CDR of the sequenced single cells were reconstructed using *in silico* techniques (45). There were several T cell clones that had frequencies of over 1% of reconstructed TCRs (**Supplementary Figure 8A**). Both FNA and PBMC samples exhibited substantial amounts of clonal and expanded clone T cells (**Supplementary Figures 8B, C**), as most expanded clones were present in both tissues. Similarly, almost all TCRα (TRAV & TRAJ) and TCRβ (TRBV & TRBJ) pairings in FNA samples were present in PBMC samples (**Supplementary Figure 8D**). Non-MAIT cell clones were present in both sample types, but no clones were shared between individuals (**Supplementary Figure 8E**). MAIT cells were present at considerable frequencies (**Figure 5E**). The proportion of MAIT cell recombinants did not vary greatly across volunteers or sample type (range 43-57%; **Figure 5E**). These analyses confirmed that most of C0 was composed of MAIT cells, with sparse contributions by MAIT cells to other clusters (**Figure 5F**). Importantly, MAIT cells were present in both sample types and in all three volunteers. On flow cytometry, the identified MAIT

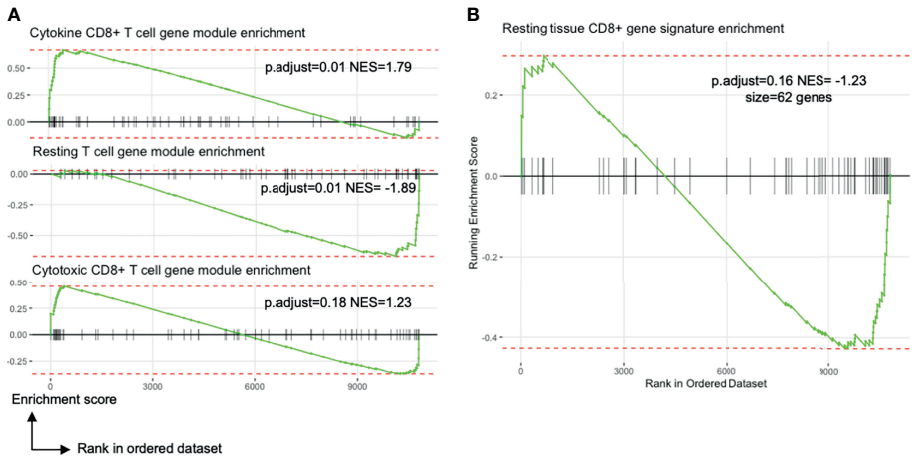

FIGURE 4 | Blood TRM-like cells may not be only activated memory T cells. All plots show the comparison of liver TRM and blood TRM-like cells (see **Figure 2A**). **(A)** Enrichment plots of gene expression modules related to T cell transcriptional states identified by Szabo and colleagues. The CD8+ cytokine module includes genes encoding chemokines and cytokines (CCL3, CCL4, CCL20) and inhibitory molecules (LAG3, CD226, HAVCR2). The resting T cell module involves genes important for CD4+ and CD8+ T cell survival in blood and in tissues. The CD8+ cytotoxic module includes genes associated with cytotoxicity (GNLY, GZMK) and transcription factors associated with effector/memory differentiation (ZEB2, EOMES, ZNF683). NES is the enrichment score normalised to the mean enrichment of random samples of the same size. **(B)** Enrichment plot of a tissue CD8+ T cell signature identified by Szabo and colleagues (23). The complement of genes is derived by differential expression analyses between resting CCL5++ CD8+ memory T cells from several tissues compared to blood. FDR, false discovery rate; FNA, fine needle aspirate; GSEA, gene set enrichment analysis; GTPase, guanosine triphosphate hydrolase; MHC, major histocompatibility complex; ORA, over-representation analysis; p.adjust, Benjamini-Hochberg adjusted p value; PBMC, peripheral blood mononuclear cells.

cells expressed higher quantities of CD69 and CD56, and lower CD11a and CD16 molecules, compared to non-MAIT cells (**Supplementary Figure 8F**). The TCR analyses suggested that there was shared clonality, TCRα and TCRβ chain usage, and MAIT cell frequencies between PBMC and FNA samples. Taken together, our transcriptomic analyses suggested a unique relationship between TRM and peripheral TRM-like cells.

Predicting Vaccine-Induced Protection From Malaria Using Circulating TRM-Like Cells

Having demonstrated a relationship between liver TRM and peripheral TRM-like cells, we investigated the kinetics of TRM-like cells and the frequency of these cells as markers of liver-stage immunity as a potential correlate of vaccine-induced protection from malaria challenge. We performed flow cytometry on blood samples taken before a controlled human malaria infection (CHMI) study (**Figure 6A** and **Supplementary Figure 1**). The frequency of cells within the CD69+ CD11a hi subset of CD45RA- T cells peaked at day (D)1 after IV viral vector (IV+1) and remained elevated at IV+3, compared to day of IV viral vector administration (**Figure 6B** and **Supplementary Figures 9**, **10**, **11A–C**). Viral vector administration led to increased expression of liver TRM cell functional markers (eg. CXCR6), which remained elevated for at least two weeks post–vaccination compared to pre-vaccination levels (**Figure 6C** and **Supplementary Figure 11D**).

We next investigated whether the frequency of TRM-like cells in the blood prior to CHMI could be used to estimate a volunteer's risk of malaria infection. Volunteers were stratified according to whether their IV+3 frequency of TRM-like cells was above or below the group median. Using this single parameter, we were able to separate volunteers who had a significantly greater rate of sterile protection (**Figure 6D**). IV+3 correlated with TRAP–specific T cells at several time points measured by flow cytometry or IFNγ ELISpot, with time to diagnosis and with mean parasites in the first three replication cycles (**Supplementary Figures 12A–E**). Only one other TRM-like cell parameter measured after IV vaccination, IV+1, had similar significance in estimating the risk of malaria diagnosis (**Supplementary Figure 12F**), but it did not correlate with IV+3 TRM-like cell frequency nor TRAP-specific T cells. Indeed, dichotomising volunteers according to TRAP-specific CD8+ T cells measured one day before CHMI did not separate volunteers with and without sterile protection (**Supplementary Figure 12F**).

Univariate and multivariate Cox models of TRM–like cells, and several other T cell populations, were generated to examine the effect of each predictor on the instantaneous risk of malaria diagnosis after CHMI. The two time points that were significantly associated with reduced hazard ratios (HR) were at IV vaccination (each $\log_{10}$ unit increase in TRM–like cells was associated with an 86% reduction in hazard of malaria diagnosis) and at IV+3 (each $\log_{10}$ unit increase in TRM–like cells was associated with a 75% reduction in hazard of malaria diagnosis; **Figure 6E**). Surprisingly, vaccine antigen-specific responses measured by ELISpot and ICS were not individually associated with a reduced hazard of malaria diagnosis, nor were other T cell subsets (**Supplementary Figure 13A**). The multivariate Cox model including TRM–like cells at IV and IV+3 was superior on $\Delta_?$ analysis (46) compared to univariate Cox models composed of each variable alone (**Figure 6F**; concordance

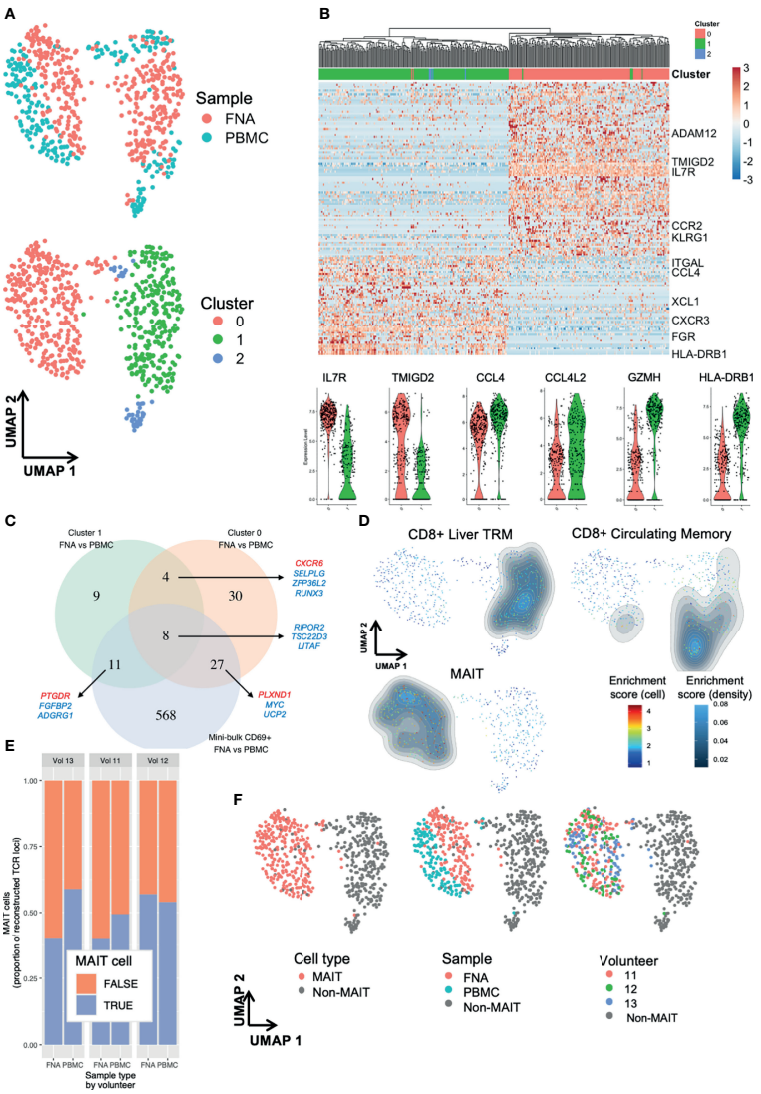

FIGURE 5 | Single-cell RNA-sequencing reveals subpopulations of liver TRM and blood TRM-like cells. Single cell differences between TRM and TRM-like cells depend on TRM cell cluster. **(A)** UMAP plots of 629 single cells. Plots according to sample type and Seurat cluster. Seurat FindClusters was run at 0.4 resolution. Each point represents one cell, either a PBMC or FNA live single CD20- CD3+ CD45+ CD8+ CD4- CD45RA- CD69+ lymphocyte FACS sorted and sequenced by the SmartSeq2 protocol. Six hundred and twenty-nine cells are presented in these plots. **(B)** Gene heatmap of the C1 TRM vs C0 TRM cell comparison. Cell gene count is centred and scaled across all row values. A sample of genes are shown, a full list of the 142 genes differentially expressed between C1 and C0 TRM cells is available in the source data file. All genes shown here were present in at least 50% of cells in each cluster, had |ln(FC)|>0.5 and an adjusted p value (Bonferroni correction)<0.05. The row hierarchical clustering dendrogram is based on Euclidean distances of cell gene count values considering all genes. Violin plots of gene expression of six selected genes are presented below. The violin colour corresponds to FNA cell cluster of origin, as seen in **(A, C)** Venn diagram of genes differentiating TRM and TRM-like cells. Venn diagram demonstrating the degree of convergence of cluster-level DGE and mini-bulk-level DGE. All included genes from single cell contrasts had a |ln(FC)|>0.25 and an adjusted p value (Bonferroni correction)<0.05 and the genes from mini-bulk contrasts had |log2(FC)|>1 and an FDR < 0.05. DGE, differential gene expression. The mini-bulk contrast refers to that which is presented in **Figures 3**, **4**. A sample of the genes that are shared among the datasets is illustrated; blue indicates the gene is down-regulated in FNA CD69+ cells and red indicates the gene is up-regulated in FNA CD69+ cells, compared to blood CD69+ cells. **(D)** UMAP plots with signature enrichment scores. The enrichment of three signatures was assessed for each of the 629 cells and visualised in the UMAP by Single-Cell Signature Explorer (44). The per-cell signature enrichment was plotted, and density distribution of scores was overlaid. The signature scores represent a qualitative measure for visualisation. The signatures were obtained from Zhao et al. (22). **(E)** Proportion of recombinants that were derived from MAIT cells. MAIT cells were defined based on TCR α locus: any cell that expressed TRAV1-2 paired with TRAJ33, TRAJ12 or TRAJ20 was defined as a MAIT cell, regardless of the TCR β locus recombinant, if present. Any recombinant derived from a MAIT cell was labelled as such and excluded from non-MAIT cell analyses. **(F)** UMAP of 629 single cells with plots according to cluster, MAIT cell TCR, sample type and volunteer. In all plots, grey points ("non-MAIT") represent cells that were either not classified as MAIT cells or cells for which TCR reconstruction could not be performed. Seurat FindClusters was run at 0.4 resolution, using a shared nearest neighbour clustering method. C, cluster; DGE, differential gene expression; FACS, fluorescence-assisted cell sorting; FDR, false discovery rate; FNA, fine needle aspirate; PBMC, peripheral blood mononuclear cells; MAIT, mucosal-associated invariant T cell; TRM, tissue-resident memory T cell; UMAP, uniform manifold approximation and projection.

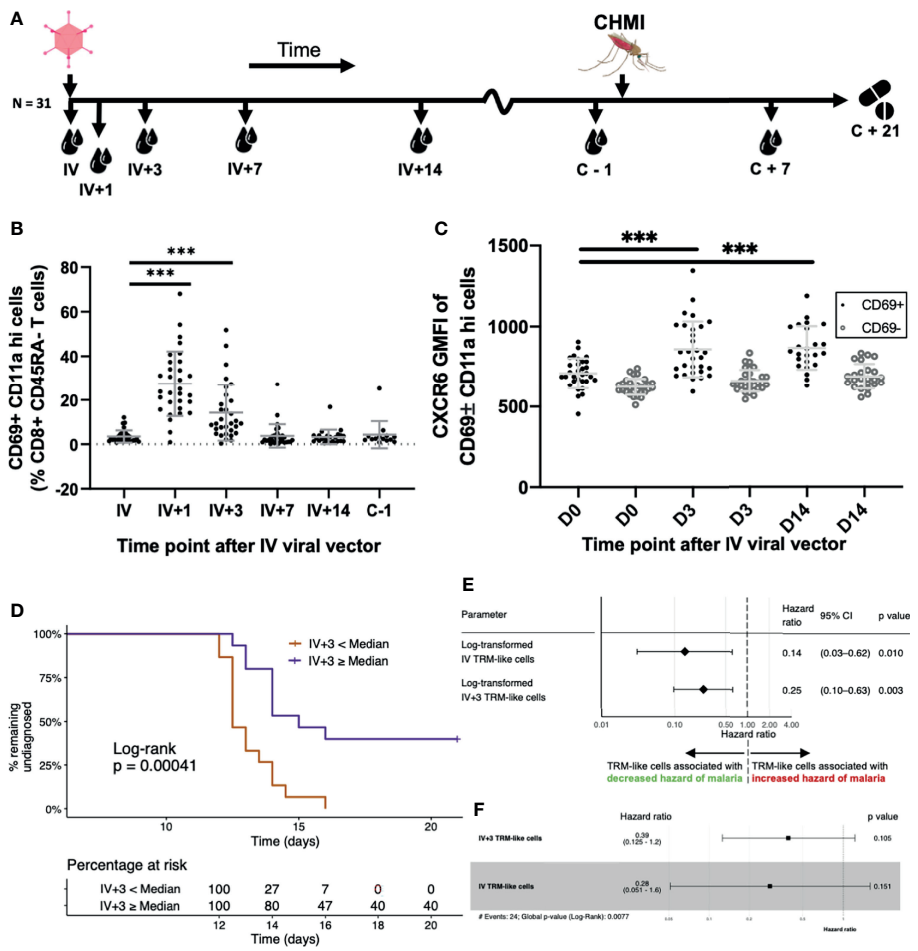

FIGURE 6 | Blood TRM-like cells can be used to estimate the hazard of malaria diagnosis after CHMI. **(A)** Sampling workflow. Thirty-one volunteers across all vaccination groups were sampled at several time points following IV viral vector (IV+ timepoints) and around controlled human malaria infection. One volunteer from this cohort was not challenged. Five more control (non-vaccinated) volunteers were challenged and followed up at pre- and post-challenge time points, only. All volunteers were treated with standard anti-malarial therapy at day 21 post-CHMI or, if earlier, when they met our diagnostic criteria for malaria (see methods). **(B)** TRM-like cells after IV administration of viral vector. Frequency of circulating CD69+CD11ahi cells (as a proportion of CD8+CD45RA- cells) by time point. Comparisons were assessed using ratio paired t tests. Lines represent significant differences between the bound groups; bars show mean and standard deviation. **(C)** The GMFI of TRM-like cell CXCR6 at three different time points following IV viral vector. Comparisons were assessed using ratio paired t tests. Lines represent significant differences between the bound groups; bars show mean and standard deviation. Matched GMFI values of CD69- cells are also presented for reference. *** represents a p value < 0.0001. **(D)** Kaplan Meier curve using TRM-like cells 3 days after IV viral vector to stratify volunteers. Volunteers were stratified according to whether their TRM-like cell fraction (as a proportion of CD8+ CD45RA- cells) at day 3 after IV viral vector was above or below the median of all values. A log-rank test was performed to test for difference in survival (delay/lack of malaria diagnosis). The risk table shows the percentage of volunteers, in each stratum, at risk of malaria diagnosis at five representative time points. Right censoring occurred at 21 days as all undiagnosed volunteers received antimalarial therapy at this time. **(E)** Univariate Cox regression models using TRM–like cells [CD69+ CD11a hi frequency (% CD45RA- CD8+ CD3+ T cells)] measured at two time points. Each regression model estimated the effect that the variable had on an individual's hazard of being diagnosed with malaria after CHMI. Hazard ratios less than one suggested that an increase in the TRM–like cell frequency decreased the instantaneous risk of malaria diagnosis over the study period. Hazard ratios greater than one suggested that a decrease in TRM–like cell frequency increased the instantaneous risk of malaria diagnosis over the study period. Log transformation was applied to the TRM–like cell frequency, and regression was performed on these values. The p value was calculated using a Wald test, with a null hypothesis that the parameter did not alter the hazard of malaria diagnosis after CHMI. **(F)** Multivariate Cox regression model using TRM like cells [CD69+ CD11a hi frequency (% CD45RA- CD8+ CD3+ T cells)] measured at two time points: IV and IV+3. Hazard ratios and 95%CI are presented. Log transformation was applied to the TRM–like cell frequency, and regression was performed on these values. The individual variable p values were calculated using a Wald test. The global p value was calculated using a Score (log–rank) test. Events refers to the number of volunteers that were diagnosed with malaria. AIC, Akaike information criterion; C, challenge; CHMI, controlled human malaria infection; D, day; GMFI, geometric mean fluorescence intensity; IV, intravenous viral vector administration; TRM, tissue-resident memory T cell.

0.723, Wald test p value = 0.0077). Both IV and IV+3 were robustly associated with a decreased hazard of malaria diagnosis (61% and 72% reduction per log unit increase, respectively), although individually in the multivariate analysis these variables were not significant (**Supplementary Figures 13B, C**). ELISpot and IFNγ+ (% CD8+, as measured by ICS) responses at several time points were included in forward stepwise model selection. The most parsimonious model $\Delta_?$ analysis was composed of six

parameters (**Supplementary Figure 13D**) but was composed of covariates that were correlated to varying degrees, resulting in multicollinearity. In addition, the parameters were taken from three different assays which, if these correlates were to be further examined in other, larger trials, presents practical difficulties. Lastly, for each model with less than five predictors, the most parsimonious model was composed entirely of TRM–like cell predictors. These results suggest that the benefits of including antigen-specific predictors into multivariate analysis did not outweigh the drawbacks of their inclusion. In this challenge study, we observed that increased frequency of TRM-like cells early post-vaccination correlated with higher levels of sterile protection from liver-stage malaria by infectious mosquito bite challenge. Overall these data would indicate that TRM-like cells are an indicator of bona-fide liver TRM cells, and therefore may be surrogate markers for liver-stage immunity.

DISCUSSION

Given the important role CD8+ T cells and TRM cells have been shown to play in protection from rodent malaria (9–11), an assay to measure TRM-associated cells in human peripheral blood could be a means of measuring liver TRM cells and, potentially, viral vector liver-stage malaria vaccine performance. In our study we identified a population of TRM-like cells in the circulation that correlated quantitatively and qualitatively to TRM cells isolated from the liver by FNA. Mini–bulk RNA-seq showed that although both cell populations displayed unique transcriptional properties, the differences were not a function of organ-specific differences and were substantively distinct to a core TRM cell signature seen by contrasting CD69+ TRM to CD69- TEM cells (14). scRNA-seq profiled these CD69+ TRM cells further, identified heterogeneous subpopulations and shared clonality between tissues. This work points to the potential for using CD69+ TRM-like cells in the periphery to estimate liver CD69+ TRM cells, and vaccine-induced protection from malaria. While our work is consistent with earlier studies indicating comparable frequencies of lymphocytes and that total CD3+ and CD8+ T cells positively correlate between PBMC and FNA samples (12, 30, 39), this study is the first to demonstrate bona fide TRM and TRM–like cells are related both quantitatively and qualitatively.

Previous reports indicate that major transcriptional differences between blood and tissue–residing T cells include apoptosis and cell-matrix interaction genes (23). Our data recapitulate some of these differences, but also shows that TRM and TRM-like cell differences are unique from other T cell comparisons across liver and blood. Pathway analyses indicated TRM-like cells were enriched for genes suggesting they were metabolically active but transcriptionally regulated, and prepared for leucocyte migration, when compared to liver TRM cells. These exploratory analyses, while not followed up with functional assays, could be the basis of further work examining blood CD69+ cells. Indeed, Walsh et al. have shown in mice that CD69 mediates recruitment and uptake of circulating CD8+ T cells in non–lymphoid tissues (47). Therefore, we hypothesise that TRM–like cells in the periphery circulate with a heightened predilection for tissue recruitment, and ability to follow chemotactic gradients, into the liver.

In silico reconstruction of single-cell TCRs confirmed the identity of MAIT cells and showed substantial clonal relationships between PBMC and FNA samples. The finding that clones coexisted and TCR chain sharing occurred between liver and blood is important, as it suggests that TRM-like cells were reflective of the liver TRM cell repertoire. MAIT cells are known to be highly abundant in the liver (48). This has been demonstrated using scRNA–seq gene expression (22) and TCR sequencing (49). MAIT cell oligoclonality among tissues and the circulation, and inter-individual homology have both been shown previously (49, 50). These TCR data were therefore in agreement with established literature regarding MAIT cells. However, this is the first report to comprehensively show the contribution of MAIT cells to the liver CD69+ memory CD8+ T cell compartment, indicating the underappreciated heterogeneity in previous reports defining traditional TRM cells as all hepatic CD69+ T cells (12, 17, 30, 51).

This work has a number of limitations. CD69 is well established as a very early activation marker (52) and it is possible that 'TRM-like' cells seen in the periphery, early after IV viral vector administration could merely be activated memory T cells. CD69 expression is known to decline six hours after activation (52), making it unlikely that the expression on memory T cells at IV+3 and later time points is entirely accounted for by an early inflammatory response. Despite significant evidence from animal models (9, 10, 53), the question as to whether TRMs are specifically induced by IV vaccination in humans remains an ongoing avenue of inquiry. We have seen that IV boosting induces substantially higher numbers of TRM-like cells, compared to IM boosting (data not shown). It is likely that only a proportion of the TRM-like cells identified in human peripheral blood i) were specific to the vaccine antigen and ii) established and maintained themselves in the liver long term. While bystander T cells lack specificity for the heterologous pathogen, they can however influence the immune response to infection, highlighting the importance of non-antigen-specific T cells (54). The pathway analyses presented were designed to be exploratory and could not provide conclusive evidence of functional and biological differences between TRM and TRM-like cells. These analyses could be the basis of future work examining TRM and TRM-like cells.

In this study we used FNAs to compare liver CD8+ TRM cells to circulating TRM-like counterparts, and highlight TRM-like cells as a potential surrogate marker of vaccine-induced protection against malaria. We found that while these peripheral 'TRM-like' cells differed to TRM cells in terms of significant pathways, such as leukocyte adhesion and T cell differentiation, they are phenotypically similar and

indistinguishable in terms of T cell residency transcriptional signatures. Increases in the frequency of these TRM-like cells in the blood early after IV vaccination was associated with a reduced risk of developing malaria. This work provides proof-of-concept of multiple novel methods to investigate liver-stage malaria vaccines, immunological evaluation of a malaria vaccine strategy by CHMI, and insights into correlates of protection after vaccination. A simple, accessible and reproducible correlate of protection would be particularly helpful in trials of liver-stage malaria vaccines as they progress to phase III, large-scale testing in African infants. We provide a blueprint for understanding and monitoring liver TRM cells induced by a prime-target malaria vaccine approach.

DATA AVAILABILITY STATEMENT

The datasets presented in this article are not readily available in order to protect the privacy of the limited clinical trial participants and given the potentially re-identifiable nature of the data. Requests to access the datasets should be directed to author AVSH, adrian.hill@ndm.ox.ac.uk.

ETHICS STATEMENT

The studies involving human participants were reviewed and approved by UK National Research Ethics Service, Committee South Central–Oxford REC A (18/SC/0384). The patients/participants provided their written informed consent to participate in this study.

AUTHOR CONTRIBUTIONS

Conception or design of the work: AN, AS, KE, AH. Acquisition, analysis and/or interpretation of data for the work: AN, MD, AF, DJ, DB, RAM, RM, FL, JS, AH, KE, AS, MH, DV, NP. Drafting the work or revising it critically for important intellectual content: AN, DV, NP, RM, AS, KE, AH. Provide approval for publication of the content: AN, AS, KE, AH. Agree to be accountable for all aspects of the work in ensuring that questions related to the accuracy or integrity of any part of the work are appropriately investigated and resolved: AN, MD, AF, DJ, DB, RAM, RM, FL, JS, AH, KE, AS, MH, DV, NP. All authors contributed to the article and approved the submitted version.

FUNDING

This project has received funding from the European Union's Horizon 2020 research and innovation programme under grant agreement No 733273. This research was funded by the National Institute for Health Research (NIHR) Oxford Biomedical Research Centre (BRC). This work was supported by the Medical Research Council [grant number MR/R015236/1]. AN was supported by The Rhodes Trust. This paper reflects the author's view(s) and the European Commission are not responsible for any use that may be made of the information it contains. The views expressed are those of the author(s) and not necessarily those of the NHS, the NIHR or the Department of Health.

ACKNOWLEDGEMENTS

The authors would like to thank the trial volunteers that took part in this study. The authors would like to thank Julie Furze, Andrew Worth and Nick Edwards for their expert technical assistance throughout the conduct of the study. The authors would like to acknowledge the assistance of Dr Helen Ferry and Dr Neil Ashley in sample collection, preparation and sequencing.

SUPPLEMENTARY MATERIAL

The Supplementary Material for this article can be found online at: https://www.frontiersin.org/articles/10.3389/fimmu.2022.795463/full#supplementary-material

Supplementary Figure 1 | Trial overview and timeline. Detailed schematic of trial. The final study cohort included 35 volunteers, across five groups, with group sizes for the first four (intervention) groups as indicated. Not shown in this figure is the infectivity control group (N=5) that did not receive any vaccinations and underwent CHMI with the vaccinated groups. All intervention group volunteers received either two or three vaccines of viral vectors encoding ME-TRAP. Doses were as indicated. Fine needle aspirates occurred between 16 and 24 days after IV vaccination/boost. Controlled Human Malaria Infection (CHMI, challenge) of volunteers by infected mosquitoes was carried out in a CL3 suite. Volunteers underwent CHMI on two separate days (4/2/2019 and 5/2/2019) and participants were equally and randomly divided across these days. Infectious mosquitos were provided by the Walter Reed Army Institute of Research. Volunteers were exposed to the bites of five infectious mosquitoes per participant for 5-10 minutes. Fed mosquitoes were individually dissected and assessed for sporozoite load, to ensure all fed mosquitoes were infected with P. falciparum. Volunteers were followed up twice per day from five days after challenge. Volunteers were treated with 20mg artemether/120mg lumefantrine (Riamet) upon malaria diagnosis or 21 days after challenge. A diagnosis of malaria infection was made given the following criteria: 1) The presence of symptoms suggestive of malaria in addition to a qPCR result indicating ≥ 1,000 parasites/mL OR 2) Lack of symptoms with a qPCR result indicating ≥ 10,000 parasites/mL. None of the volunteers in the infectivity control group achieved sterile protection.

Supplementary Figure 2 | Gating strategy for paired liver FNA and PBMC samples. Boxes on flow cytometry plots define the representative sequential gating strategy identifying TRM in human liver FNA and TRM-like cells in human PBMC. Singlets, CD45+, live CD20-, lymphocytes, CD3+, CD8+/CD4+, CD56-, CD69+ CD45RA ± CD11a hi ± CD103. FNA, fine needle aspirate; FSC-A/H, forward scatter; LIVE/DEAD Aqua, fixable dead cell stain; PBMC, peripheral blood mononuclear cells; SSC-A, side scatter.

Supplementary Figure 3 | Representative flow cytometry plots from FNA and PBMC of the same donors. Boxes on flow cytometry plots define the representative gating strategy identifying several T cells subsets in human liver FNA and PBMC. Percentages are expressed relative to total singlet, CD45+, live, CD20-, CD3+, CD8+/CD4+, CD56- T cells. Previous gating prior to this included: singlets, CD45+, live CD20-, lymphocytes, CD3+, CD8+/CD4+, CD56-. FNA, fine needle aspirate; PBMC, peripheral blood mononuclear cells.

Supplementary Figure 4 | Expression of TRM markers on FNA TRM and PBMC TRM-like cells. TRM/TRM-like cell expression of the selected markers was compared to paired (within volunteer and within sample) TEM (CD69-) expression of the selected marker. Both the positive fraction of cells and the GMFI of the selected markers is presented. Two-way ANOVA results are presented below each plot. Pairing by tissue and CD69 status was performed. Equal variability of differences was assumed when performing repeated measures two-way ANOVA (based on GLM). ANOVA, Analysis of variance. FNA, fine needle aspirate. GLM, general linear model. PBMC, peripheral blood mononuclear cells.

Supplementary Figure 5 | FNA and PBMC t-distributed stochastic neighbour embedding (tSNE). The tSNE algorithm was run using single cell expression values of 13 markers on 1,068,990 cells pre-gated on CD45+ single live lymphocyte size. These lymphocytes were derived from all 13 volunteers. Each FNA sample contributed on average 32,760 cells (range 6480-50,000), while each PBMC sample contributed 50,000 cells. **(A)** Contour tSNE plot of FNA and PBMC CD8+ and CD8+ TRM cells. Five distinct clusters of TRM can be seen. (B) Contour tSNE plot of TRM/TRM-like cells compared to TEM (non-TRM) from both tissues. The left plot shows only those cells derived from the liver (FNA), while the right shows those from the blood (PBMC). **(C)** Contour tSNE plot of TRM/TRM-like cells from both tissues. The gates of the three tSNE subsets are shown with the corresponding percentage of total cells. **(D)** Phenotype and metaparameter characterisation of the three tSNE subsets. The three subsets can be differentiated by PD-1, CXCR6 and CD103 expression. The tSNE plot shows the positions of the three subsets and the left histograms show the GMFI of the listed markers for the three subsets. The three subsets have been selected due to their over-representation in CD69+ memory T cells compared to CD69- memory T cells. The right histograms show the relative distribution of cells into discrete experimental and technical categories. tSNE subsets are relatively equally spread across each of the metaparameters. Metaparameters were not included when running the tSNE algorithm. FNA, fine needle aspirate. GMFI, geometric mean fluorescence intensity. PBMC, peripheral blood mononuclear cells. tSNE, t-distributed stochastic neighbour embedding.

Supplementary Figure 6 | Pathway analyses. **(A)** Over-representation analysis plots for gene ontology categories of the FNA CD69+ vs PBMC CD69+ comparison. A: Over-representation analysis gene-concept network plots for enriched Gene Ontology biological process and molecular function categories. A hyper geometric test was used to test for significance of gene category over-representation. Gene categories presented have an FDR < 0.05. Size refers to the number of genes involved in category. **(B)** Enrichment plots for gene ontology categories of the FNA CD69+ vs PBMC CD69+ comparison. Gene set enrichment analyses visualised by category running enrichment score among pre-ranked list of all 11,933 differentially expressed genes. A category's enrichment score is the maximum deviation from zero encountered in the running score. If the normalised enrichment score is positive, this suggests enrichment of the category in FNA CD69 + samples. A negative normalised enrichment score suggests enrichment of the category in PBMC CD69+. The ranked list metric is the binary logarithm of the fold change of gene expression between FNA CD69+ and PBMC CD69+ cells. **(C)** Venn diagram of the FNA CD69- vs PBMC CD69- comparison. Venn diagram demonstrating the overlap of genes that are in both FNA vs PBMC comparisons (where CD69+ cells are compared, left blue circle, and CD69- cells, right orange circle). All genes were differentially expressed with an FDR < 0.01. Ten genes co −occurred in the differential expression lists generated by comparing FNA and PBMC CD69+, and FNA and PBMC CD69- (not significant, hypergeometric test p≃1). **(D)** GSEA plots of the FNA CD69- vs PBMC CD69- comparison. Gene set enrichment analyses of gene ontologies visualised by category running enrichment score among pre-ranked list of all 12,062 differentially expressed genes. A category's enrichment score is approximated by the maximum deviation, from zero, encountered in the running score. If the normalised enrichment score is positive, this suggests enrichment of the category in FNA CD69- samples. A negative normalised enrichment score suggests enrichment of the category in PBMC CD69-. All categories presented had an FDR < 0.05. Considering gene expression differences between PBMC CD69+ and CD69- samples, no terms were enriched with FDR<0.05 on GSEA when using Hallmark MSigDB gene sets or gene ontology sets (data not shown). **(E)** Clustering of the samples in the PBMC CD69+ vs CD69- comparison. Hierarchical clustering tree based on Spearman's correlation of sample rlog normalised count values considering all genes in CD8+ Kumar et al. core TRM transcriptional signature. FDR, false discovery rate. FNA, fine needle aspirate. GSEA, gene set enrichment analysis. PBMC, peripheral blood mononuclear cells. rlog, regularised logarithm. TRM, tissue-resident memory T cell.

Supplementary Figure 7 | PCA plots based on the 500 most variable genes in the single cell RNA sequencing experiment. Each point represents one cell, either a PBMC or FNA live single CD20- CD3+ CD45+ CD8+ CD4- CD45RA- CD69+ lymphocyte FACS sorted and sequenced in plates by the SmartSeq2 protocol. Six hundred and twenty-nine cells are presented in these PC plots. Cell cycle phase was assigned using the cyclone function from the scran package version 1.14.6. **(A)** Plots of the first two PC, according to various technical and biological parameters. PC1 is associated with the number of features per cell (SCT normalisation in Seurat was performed). PC2 does not appear to be substantially separated by the presented parameters. **(B)** Plots of PC2 and PC3, according to various technical and biological parameters. PC3 appears to separate PBMC and FNA cells. FACS, fluorescence-assisted cell sorting. FC, flow cell. G1, gap 1 cell cycle phase. G2, gap 2 cell cycle phase. mtDNA, mitochondrial DNA PC, principal component. PCA, principal component analysis. S, synthesis cell cycle phase. V, volunteer.

Supplementary Figure 8 | T cell clonality and clone size. **(A)** Out of the 690 cells analysed, productive TCR α and β loci were reconstructed in 634 (91.9%) and 639 (92.6%) cells, respectively. There was productive reconstruction of both α and β loci from 603 (87.4%) cells. Most cells had one productive α or β locus identified (Table 4.4). Relatively few cells had two productive α or β loci (Table 4.4), **(B)** TCR alpha (left) and beta (right) loci clone frequency. Bars represent individual clones and bar height represents clone frequency. A clone was defined as any number of cells that had the exact same (alpha or beta) TCR loci and CDR3 nucleotide sequence. Clones with more than two cells are displayed here. Non-productive recombinants and recombinants derived from MAIT cells were excluded from these analyses. Clone sizes are reported as a frequency, in relation to the total number of reconstructed TCR recombinants. **(C)** Clonality by volunteer and sample type. Alpha and beta TCR loci recombinants categorised according to whether they were expanded (shared by more than two cells), clonal (present in two cells) or unique (present in one cell). **(D)** TCR alpha and beta chain usage of expanded clonal T cells by sample type. Chain pairing of TRAV & TRAJ and TRBV & TRBJ are displayed as chord diagrams where ribbons connecting arcs indicate frequency of chain pairing. Only clones of greater than two cells and productive recombinants were included in these analyses. MAIT cells were excluded from these analyses. Ticks on the inside of the arcs are present for every 5 cells that shared the recombinant. Recombinant totals: alpha chain usage FNA n=75, PBMC n=30; beta chain usage FNA n=51, PBMC n=17. The degree of TCR chain usage sharing between samples is representative of all volunteers. **(E)** Clonal relationships between MAIT and non-MAIT cells. The number of recombinants shared between MAIT (left) and non-MAIT (right) cells. Nodes (vertices) represent individual cells and links (edges) represent a unique recombinant shared between the connected cells. Cells could share up to a maximum of four recombinants (two TCR α and two TCR β). Cells are distributed using a force-directed layout algorithm whereby cells have a simulated 'charge', repelling them from other cells, and links have attractive forces for connected cells. For a given number of cells, more links resulted in tighter clusters. A clone was defined as any number of cells that had the exact same (α or β) TCR loci and CDR3 nucleotide sequence. Clones with more than two cells are displayed here. MAIT cells were defined based on TCR α locus: any cell that expressed TRAV1-2 paired with TRAJ33, TRAJ12 or TRAJ20 was defined as a MAIT cell, regardless of the TCR β locus recombinant. **(F)** Flow cytometry index sort information obtained at the time of single-cell isolation for CD69, CD56, CD11a and CD16 molecules. Values represent fluorochrome geometric mean fluorescence intensity that has been compensated, but not transformed. FNA, fine needle aspirate. MAIT, mucosal associated invariant T cell. PBMC, peripheral blood mononuclear cell. recomb(s), TCR recombinant. TCR, T cell receptor. TCRA, T cell receptor alpha locus. TCRB, T cell receptor beta locus. Vol, volunteer.

Supplementary Figure 9 | TRM-like cells gating strategy. Boxes on flow cytometry plots define the representative sequential gating strategy identifying TRM-like cells in human PBMC. Singlets, lymphocytes, live, (CD4 & CD20)-, CD3+, CD8+, CD45RA- and CD69+ CD11a hi using 16-color flow cytometry. FSC-A/H, forward scatter; LIVE/DEAD Aqua, fixable dead cell stain; PBMC, peripheral blood mononuclear cells; SSC-A, side scatter.

Supplementary Figure 10 | Representative flow cytometry plots from representative two volunteers samples at different time points. Boxes on flow cytometry plots define the representative gating strategy identifying TRM like cells in PBMC. Percentages are expressed relative to total singlet, live, (CD4 & CD20)-, CD3+, CD8+, CD45RA-T cells. Previous gating prior to this included: singlets, lymphocytes, live, (CD4 & CD20)-, CD3+, CD8+, CD45RA- and CD69+ CD11a hi using 16-colour flow cytometry. PBMC, peripheral blood mononuclear cells.

Supplementary Figure 11 | TRM like cells after IV vaccination. **(A)** CD69+ CD11a hi cells as proportions of CD8+ CD3+ T cells at six time points after IV vaccination. **(B)** CD69+ CD11a hi cells as proportions of CD45RA- CD8+ CD3+ T cells by time after IV vaccination. For each time point, there was a window in which volunteers could attend for blood sampling. **(C)** CD69+ CD11a hi CD45RA- CD8+ CD3+ T cell concentration calculated using volunteers' clinical haematology value for total lymphocytes. Mean values are presented, and error bars represent the standard deviation. Significance testing of differences between time points was performed using ratio paired t tests and the resultant p values of all tested comparisons are shown (unless specifically mentioned). An α of less than 0.05 was considered statistically significant. These analyses were performed by assuming that 30% of lymphocytes were CD8+ CD3+, as has been previously demonstrated in Caucasian UK and US populations (!ref,!ref). **(D)** Ki67+ frequencies of CD69+ and CD69- CD11a hi CD45RA- CD8+ CD3+ T cells (left), and Ki67 geometric mean fluorescence intensities of CD69+ and CD69- CD11a hi CD45RA- CD8+ CD3+ T cells (right). CD69- (effector memory T cell) frequency and expression of the markers are presented as an internal comparator. All comparisons between CD69+ and CD69- cells were significant ($p<0.001$). Significance testing of differences between individual groups was performed using ratio paired t-tests, and the resultant p values of all tested comparisons are shown. Statistics were performed on non-transformed data.

Supplementary Figure 12 | IV+3 TRM–like cells vs indicators of vaccine-induced immunity and protection.**(A–C)** X-axes and values are shared between all plots. Empty grey triangles represent volunteers that achieved sterile protection and were removed from the "without protection" analyses. **(A)** TRM–like cell frequencies; CD69+ CD11a hi CD45RA- (% CD8+ CD3+ T cells) cell frequencies, at IV+3, compared to IFNγ ELISpot AgSp T cell response at C-1 (left), C+35 (middle) and C +90 (right). **(B)** TRM–like cell frequencies at IV+3, compared to IFNγ+ cell (% CD8+ CD3+ T cells) response at C-1 (left) and C+7 (right). **(C)** TRM–like cell frequencies at IV+3, compared to the maximum IFN–γ ELISpot AgSp T cell response (left) and the maximum IFNγ+ cell (% CD8+ CD3+ T cells) response as measured by ICS (right). IFN–γ ELISpot was performed at between 10 and 13 time points, and ICS was performed at three time points. Spearman's rank correlation coefficient, the correlation coefficient 95% confidence interval and an approximate, unadjusted p value are reported. **(D)** TRM–like cell frequencies (CD69+ CD11a hi CD45RA- (% CD8+ CD3+ T cells)) measured at IV+3 compared across volunteers who experienced any (sterile or partial) vaccine-induced protection and those with no protection. Partial protection was defined as volunteers with a diagnosis of malaria 14 days or later, after infectious mosquito bite [!ref] **(E)** Associations of TRM–like cell frequencies at IV+3, and time to malaria diagnosis (left) and the mean number of parasites in the first three replication cycles (right). Empty grey triangles represent volunteers that were right-censored from the study and deemed to have achieved sterile protection from malaria. These volunteers did not reach 1000 blood-stage parasites, therefore were not included in this analysis. Spearman's rank correlation coefficient, the correlation coefficient 95% confidence interval and an approximate, unadjusted p value are reported. Statistics were performed on non-transformed data. For log-transformed PCR data, a pseudocount value of one was added to each qPCR value to allow log transformation of zero values (y=log(1+qPCR)). **(F)** Kaplan–Meier curve comparisons using TRM–like cells one day after IV vaccination. Volunteers were stratified according to whether their CD69+ CD11a hi CD45RA- frequency (% CD8+ CD3+ T cells) above or below the median of all values. A log–rank test was performed to test for difference in survival (delay/lack of malaria diagnosis), and the p value is reported in the plot. The risk table shows the percentage of volunteers, in each stratum, at risk of malaria diagnosis at five representative time points. Right censoring occurred at 21 days as all undiagnosed volunteers received antimalarial therapy. Time, on the x-axes, refers to the time after CHMI. Kaplan Meier curve comparisons using AgSp responses at C-1 to stratify volunteers: IFNγ ELISpot ME-TRAP SFC per million PBMC (left) and IFNγ+ frequency (% CD8+) as measured by intracellular cytokine staining (right).

Supplementary Figure 13 | (A) Univariate Cox regression models using antigen-specific responses: IFNγ ELISpot ME-TRAP SFC per million PBMC (left) and IFNγ+ frequency (% CD8+) as measured by intracellular cytokine staining (right). **(B)** Univariate Cox regression models using non-antigen-specific T cell subsets: CD69- CD11a hi CD45RA- CD8+ CD3+ T cells (left) and CD45RA- CD8+ CD3+ T cells (right). **(C)** Schoenfeld residuals plotted to test the proportional hazards assumption (top). Systematic departures from a horizontal line when plotting Schoenfeld residuals would indicate non-proportional hazards. The assumption of proportional hazards was supported for both covariates and overall, for the model ($p=0.304$). The blue dashed lines are fit by local linear regression (lowess), to aid in interpretation; the shading represents ± 2-standard-error envelopes around the fit. The red dashed line is at y=0. C: Dfbetas plotted to assess influential observations. Plotting dfbetas estimated the changes in regression coefficients upon deleting each observation in turn (bottom). Comparing the magnitudes of the largest dfbeta values to the regression coefficients suggests that none of the observations were largely influential. The model satisfied the proportional hazards assumption ($p=0.304$ overall) and there were no vastly influential observations. IV and IV+3 TRM –like cell parameters were previously shown to be moderately positively correlated (p=3.433x10-4,,). The variance inflation factor, which measures the inflation in variance due to parameter correlation, of both variables was 1.38. **(D)** Akaike information criterion values of models composed of all permutations of ten log-transformed TRM–like cell, IFNγ+ (%CD8+ as measured by ICS) and IFNγ ELISpot parameters.

Supplementary Data Sheet 1 | Differentially expressed gene list, adjusted p values and shrunken log2 fold change values for FNA CD69+ vs FNA CD69- comparison.

Supplementary Data Sheet 2 | Results of gene set enrichment analysis using custom gene sets obtained from Kumar et al., Zhao et al. and Szabo et al.

Supplementary Data Sheet 3 | Differentially expressed gene list, adjusted p values and shrunken log2 fold change values for FNA CD69+ vs PBMC CD69+ comparison.

Supplementary Data Sheet 4 | Differentially expressed gene list, adjusted p values and average natural log fold change values for cluster 0 FNA CD69+ vs cluster 1 FNA CD69+ single cell comparison.

Supplementary Data Sheet 5 | Differentially expressed gene list, adjusted p values and average natural log fold change values for cluster 0 FNA CD69+ vs cluster 0 PBMC CD69+ single cell comparison.

Supplementary Data Sheet 6 | Differentially expressed gene list, adjusted p values and average natural log fold change values for cluster 1 FNA CD69+ vs cluster 1 PBMC CD69+ single cell comparison.

REFERENCES

1. Romero P, Maryanski JL, Corradin G, Nussenzweig RS, Nussenzweig V, Zavala F. Cloned Cytotoxic T Cells Recognize an Epitope in the Circumsporozoite Protein and Protect Against Malaria. *Nature* (1989) 341(6240):323–6. doi: 10.1038/341323a0
2. Bliss CM, Bowyer G, Anagnostou NA, Havelock T, Snudden CM, Davies H, et al. Assessment of Novel Vaccination Regimens Using Viral Vectored Liver Stage Malaria Vaccines Encoding ME-TRAP. *Sci Rep* (2018) 8(1):3390. doi: 10.1038/s41598-018-21630-4
3. Ewer KJ, Lambe T, Rollier CS, Spencer AJ, Hill AV, Dorrell L. Viral Vectors as Vaccine Platforms: From Immunogenicity to Impact. *Curr Opin Immunol* (2016) 41:47–54. doi: 10.1016/j.coi.2016.05.014
4. Ewer KJ, O'Hara GA, Duncan CJ, Collins KA, Sheehy SH, Reyes-Sandoval A, et al. Protective CD8+ T-Cell Immunity to Human Malaria Induced by

Chimpanzee Adenovirus-MVA Immunisation. *Nat Commun* (2013) 4:2836. doi: 10.1038/ncomms3836
5. Hodgson SH, Ewer KJ, Bliss CM, Edwards NJ, Rampling T, Anagnostou NA, et al. Evaluation of the Efficacy of ChAd63-MVA Vectored Vaccines Expressing Circumsporozoite Protein and ME-TRAP Against Controlled Human Malaria Infection in Malaria-Naive Individuals. *J Infect Dis* (2015) 211(7):1076–86. doi: 10.1093/infdis/jiu579
6. Rodrigues EG, Zavala F, Eichinger D, Wilson JM, Tsuji M. Single Immunizing Dose of Recombinant Adenovirus Efficiently Induces CD8+ T Cell-Mediated Protective Immunity Against Malaria. *J Immunol* (1997) 158(3):1268–74.
7. Bruna-Romero O, Gonzalez-Aseguinolaza G, Hafalla JC, Tsuji M, Nussenzweig RS. Complete, Long-Lasting Protection Against Malaria of Mice Primed and Boosted With Two Distinct Viral Vectors Expressing the Same Plasmodial Antigen. *Proc Natl Acad Sci USA* (2001) 98(20):11491–6. doi: 10.1073/pnas.191380898
8. Ogwang C, Kimani D, Edwards NJ, Roberts R, Mwacharo J, Bowyer G, et al. Prime-Boost Vaccination With Chimpanzee Adenovirus and Modified Vaccinia Ankara Encoding TRAP Provides Partial Protection Against Plasmodium Falciparum Infection in Kenyan Adults. *Sci Transl Med* (2015) 7(286):286re5. doi: 10.1126/scitranslmed.aaa2373
9. Gola A, Silman D, Walters AA, Sridhar S, Uderhardt S, Salman AM, et al. Prime and Target Immunization Protects Against Liver-Stage Malaria in Mice. *Sci Transl Med* (2018) 10(460). doi: 10.1126/scitranslmed.aap9128
10. Fernandez-Ruiz D, Ng WY, Holz LE, Ma JZ, Zaid A, Wong YC, et al. Liver-Resident Memory CD8(+) T Cells Form a Front-Line Defense Against Malaria Liver-Stage Infection. *Immunity* (2016) 45(4):889–902. doi: 10.1016/j.immuni.2016.08.011
11. Olsen TM, Stone BC, Chuenchob V, Murphy SC. Prime-And-Trap Malaria Vaccination To Generate Protective CD8(+) Liver-Resident Memory T Cells. *J Immunol* (2018) 201(7):1984–93. doi: 10.4049/jimmunol.1800740
12. Pallett LJ, Davies J, Colbeck EJ, Robertson F, Hansi N, Easom NJW, et al. IL-2 (High) Tissue-Resident T Cells in the Human Liver: Sentinels for Hepatotropic Infection. *J Exp Med* (2017) 214(6):1567–80. doi: 10.1084/jem.20162115
13. Kumar BV, Kratchmarov R, Miron M, Carpenter DJ, Senda T, Lerner H, et al. Functional Heterogeneity of Human Tissue-Resident Memory T Cells Based on Dye Efflux Capacities. *JCI Insight* (2018) 3(22). doi: 10.1172/jci.insight.123568
14. Kumar BV, Ma W, Miron M, Granot T, Guyer RS, Carpenter DJ, et al. Human Tissue-Resident Memory T Cells Are Defined by Core Transcriptional and Functional Signatures in Lymphoid and Mucosal Sites. *Cell Rep* (2017) 20 (12):2921–34. doi: 10.1016/j.celrep.2017.08.078
15. Szabo PA, Miron M, Farber DL. Location, Location, Location: Tissue Resident Memory T Cells in Mice and Humans. *Sci Immunol* (2019) 4(34). doi: 10.1126/sciimmunol.aas9673
16. Kim JH, Han JW, Choi YJ, Rha MS, Koh JY, Kim KH, et al. Functions of Human Liver CD69(+)CD103(-)CD8(+) T Cells Depend on HIF-2alpha Activity in Healthy and Pathologic Livers. *J Hepatol* (2020) 72(6):1170–81. doi: 10.1016/j.jhep.2020.01.010
17. Stelma F, de Niet A, Sinnige MJ, van Dort KA, van Gisbergen K, Verheij J, et al. Human Intrahepatic CD69 + CD8+ T Cells Have a Tissue Resident Memory T Cell Phenotype With Reduced Cytolytic Capacity. *Sci Rep* (2017) 7 (1):6172. doi: 10.1038/s41598-017-06352-3
18. Thome JJ, Yudanin N, Ohmura Y, Kubota M, Grinshpun B, Sathaliyawala T, et al. Spatial Map of Human T Cell Compartmentalization and Maintenance Over Decades of Life. *Cell* (2014) 159(4):814–28. doi: 10.1016/j.cell.2014.10.026
19. Wherry EJ. T Cell Exhaustion. *Nat Immunol* (2011) 12(6):492–9. doi: 10.1038/ni.2035
20. Heydtmann M, Lalor PF, Eksteen JA, Hubscher SG, Briskin M, Adams DH. CXC Chemokine Ligand 16 Promotes Integrin-Mediated Adhesion of Liver-Infiltrating Lymphocytes to Cholangiocytes and Hepatocytes Within the Inflamed Human Liver. *J Immunol* (2005) 174(2):1055–62. doi: 10.4049/jimmunol.174.2.1055
21. Tse SW, Radtke AJ, Espinosa DA, Cockburn IA, Zavala F. The Chemokine Receptor CXCR6 Is Required for the Maintenance of Liver Memory CD8(+) T Cells Specific for Infectious Pathogens. *J Infect Dis* (2014) 210(9):1508–16. doi: 10.1093/infdis/jiu281
22. Zhao J, Zhang S, Liu Y, He X, Qu M, Xu G, et al. Single-Cell RNA Sequencing Reveals the Heterogeneity of Liver-Resident Immune Cells in Human. *Cell Discov* (2020) 6:22. doi: 10.1038/s41421-020-0157-z
23. Szabo PA, Levitin HM, Miron M, Snyder ME, Senda T, Yuan J, et al. Single-Cell Transcriptomics of Human T Cells Reveals Tissue and Activation Signatures in Health and Disease. *Nat Commun* (2019) 10(1):4706. doi: 10.1038/s41467-019-12464-3
24. He S, Wang L-H, Liu Y, Li Y-Q, Chen H, Xu J, et al. Single-Cell Transcriptome Profiling an Adult Human Cell Atlas of 15 Major Organs. *Genome Biol* (2020) 21(1):294. doi: 10.1186/s13059-020-02210-0
25. Fonseca R, Beura LK, Quarnstrom CF, Ghoneim HE, Fan Y, Zebley CC, et al. Developmental Plasticity Allows Outside-in Immune Responses by Resident Memory T Cells. *Nat Immunol* (2020) 21(4):412–21. doi: 10.1038/s41590-020-0607-7
26. Klicznik MM, Morawski PA, Hollbacher B, Varkhande SR, Motley SJ, Kuri-Cervantes L, et al. Human CD4(+)CD103(+) Cutaneous Resident Memory T Cells are Found in the Circulation of Healthy Individuals. *Sci Immunol* (2019) 4(37). doi: 10.1126/sciimmunol.aav8995
27. Li N, van Unen V, Abdelaal T, Guo N, Kasatskaya SA, Ladell K, et al. Memory CD4(+) T Cells are Generated in the Human Fetal Intestine. *Nat Immunol* (2019) 20(3):301–12. doi: 10.1038/s41590-018-0294-9
28. Beura LK, Mitchell JS, Thompson EA, Schenkel JM, Mohammed J, Wijeyesinghe S, et al. Intravital Mucosal Imaging of CD8(+) Resident Memory T Cells Shows Tissue-Autonomous Recall Responses That Amplify Secondary Memory. *Nat Immunol* (2018) 19(2):173–82. doi: 10.1038/s41590-017-0029-3
29. Pembroke T, Gallimore A, Godkin A. Tracking the Kinetics of Intrahepatic Immune Responses by Repeated Fine Needle Aspiration of the Liver. *J Immunol Methods* (2015) 424:131–5. doi: 10.1016/j.jim.2015.04.011
30. Gill US, Pallett LJ, Thomas N, Burton AR, Patel AA, Yona S, et al. Fine Needle Aspirates Comprehensively Sample Intrahepatic Immunity. *Gut* (2019) 68 (8):1493–503. doi: 10.1136/gutjnl-2018-317071
31. Lee JM, Lee HS, Hyun JJ, Lee JM, Yoo IK, Kim SH, et al. Slow-Pull Using a Fanning Technique Is More Useful Than the Standard Suction Technique in EUS-Guided Fine Needle Aspiration in Pancreatic Masses. *Gut Liver* (2018) 12(3):360–6. doi: 10.5009/gnl17140
32. McConkey SJ, Reece WH, Moorthy VS, Webster D, Dunachie S, Butcher G, et al. Enhanced T-Cell Immunogenicity of Plasmid DNA Vaccines Boosted by Recombinant Modified Vaccinia Virus Ankara in Humans. *Nat Med* (2003) 9 (6):729–35. doi: 10.1038/nm881
33. Picelli S, Faridani OR, Bjorklund AK, Winberg G, Sagasser S, Sandberg R. Full-Length RNA-Seq From Single Cells Using Smart-Seq2. *Nat Protoc* (2014) 9(1):171–81. doi: 10.1038/nprot.2014.006
34. Dobin A, Davis CA, Schlesinger F, Drenkow J, Zaleski C, Jha S, et al. STAR: Ultrafast Universal RNA-Seq Aligner. *Bioinformatics* (2013) 29(1):15–21. doi: 10.1093/bioinformatics/bts635
35. Liao Y, Smyth GK, Shi W. Featurecounts: An Efficient General Purpose Program for Assigning Sequence Reads to Genomic Features. *Bioinformatics* (2014) 30(7):923–30. doi: 10.1093/bioinformatics/btt656
36. Love MI, Huber W, Anders S. Moderated Estimation of Fold Change and Dispersion for RNA-Seq Data With Deseq2. *Genome Biol* (2014) 15(12):550. doi: 10.1186/s13059-014-0550-8
37. Butler A, Hoffman P, Smibert P, Papalexi E, Satija R. Integrating Single-Cell Transcriptomic Data Across Different Conditions, Technologies, and Species. *Nat Biotechnol* (2018) 36(5):411–20. doi: 10.1038/nbt.4096
38. Stuart T, Butler A, Hoffman P, Hafemeister C, Papalexi E, Mauck WM3rd, et al. Comprehensive Integration of Single-Cell Data. *Cell* (2019) 177(7):1888–902.e21. doi: 10.1016/j.cell.2019.05.031
39. Gill US, Pallett LJ, Kennedy PTF, Maini MK. Liver Sampling: A Vital Window Into HBV Pathogenesis on the Path to Functional Cure. *Gut* (2018) 67 (4):767–75. doi: 10.1136/gutjnl-2017-314873
40. Stamataki Z, Swadling L. The Liver as an Immunological Barrier Redefined by Single-Cell Analysis. *Immunology* (2020) 160(2):157–70. doi: 10.1111/imm.13193
41. Mackay LK, Rahimpour A, Ma JZ, Collins N, Stock AT, Hafon ML, et al. The Developmental Pathway for CD103(+)CD8+ Tissue-Resident Memory T Cells of Skin. *Nat Immunol* (2013) 14(12):1294–301. doi: 10.1038/ni.2744
42. Hombrink P, Helbig C, Backer RA, Piet B, Oja AE, Stark R, et al. Programs for the Persistence, Vigilance and Control of Human CD8(+) Lung-Resident Memory T Cells. *Nat Immunol* (2016) 17(12):1467–78. doi: 10.1038/ni.3589

43. Mackay LK, Minnich M, Kragten NA, Liao Y, Nota B, Seillet C, et al. Hobit and Blimp1 Instruct a Universal Transcriptional Program of Tissue Residency in Lymphocytes. *Science* (2016) 352(6284):459–63. doi: 10.1126/science.aad2035
44. Pont F, Tosolini M, Fournie JJ. Single-Cell Signature Explorer for Comprehensive Visualization of Single Cell Signatures Across scRNA-Seq Datasets. *Nucleic Acids Res* (2019) 47(21):e133. doi: 10.1093/nar/gkz601
45. Stubbington MJT, Lonnberg T, Proserpio V, Clare S, Speak AO, Dougan G, et al. T Cell Fate and Clonality Inference From Single-Cell Transcriptomes. *Nat Methods* (2016) 13(4):329–32. doi: 10.1038/nmeth.3800
46. Burnham KP, Anderson DR. Multimodel Inference:Understanding AIC and BIC in Model Selection. *Sociol Methods Res* (2004) 33(2):261–304. doi: 10.1177/0049124104268644
47. Walsh DA, Borges da Silva H, Beura LK, Peng C, Hamilton SE, Masopust D, et al. The Functional Requirement for CD69 in Establishment of Resident Memory CD8(+) T Cells Varies With Tissue Location. *J Immunol* (2019) 203 (4):946–55. doi: 10.4049/jimmunol.1900052
48. Rha MS, Han JW, Kim JH, Koh JY, Park HJ, Kim SI, et al. Human Liver CD8(+) MAIT Cells Exert TCR/MR1-Independent Innate-Like Cytotoxicity in Response to IL-15. *J Hepatol* (2020) 73(3):640–50. doi: 10.1016/j.jhep.2020.03.033
49. Lepore M, Kalinichenko A, Colone A, Paleja B, Singhal A, Tschumi A, et al. Parallel T-Cell Cloning and Deep Sequencing of Human MAIT Cells Reveal Stable Oligoclonal TCRbeta Repertoire. *Nat Commun* (2014) 5:3866. doi: 10.1038/ncomms4866
50. Carnero Contentti E, Farez MF, Correale J. Mucosal-Associated Invariant T Cell Features and TCR Repertoire Characteristics During the Course of Multiple Sclerosis. *Front Immunol* (2019) 10:2690. doi: 10.3389/fimmu.2019.02690
51. Pallett LJ, Burton AR, Amin OE, Rodriguez-Tajes S, Patel AA, Zakeri N, et al. Longevity and Replenishment of Human Liver-Resident Memory T Cells and Mononuclear Phagocytes. *J Exp Med* (2020) 217(9). doi: 10.1084/jem.20200050
52. Cibrian D, Sanchez-Madrid F. CD69: From Activation Marker to Metabolic Gatekeeper. *Eur J Immunol* (2017) 47(6):946–53. doi: 10.1002/eji.201646837
53. Darrah PA, Zeppa JJ, Maiello P, Hackney JA, Wadsworth MH2nd, Hughes TK, et al. Prevention of Tuberculosis in Macaques After Intravenous BCG Immunization. *Nature* (2020) 577(7788):95–102. doi: 10.1038/s41586-019-1817-8
54. Kim TS, Shin EC. The Activation of Bystander CD8(+) T Cells and Their Roles in Viral Infection. *Exp Mol Med* (2019) 51(12):1–9. doi: 10.1038/s12276-019-0316-1

Conflict of Interest: The authors declare that the research was conducted in the absence of any commercial or financial relationships that could be construed as a potential conflict of interest.

Publisher's Note: All claims expressed in this article are solely those of the authors and do not necessarily represent those of their affiliated organizations, or those of the publisher, the editors and the reviewers. Any product that may be evaluated in this article, or claim that may be made by its manufacturer, is not guaranteed or endorsed by the publisher.

Citation: *Noé A, Datoo MS, Flaxman A, Husainy MA, Jenkin D, Bellamy D, Makinson RA, Morter R, Ramos Lopez F, Sheridan J, Voukantsis D, Prasad N, Hill AVS, Ewer KJ and Spencer AJ (2022) Deep Immune Phenotyping and Single-Cell Transcriptomics Allow Identification of Circulating TRM-Like Cells Which Correlate With Liver-Stage Immunity and Vaccine-Induced Protection From Malaria. Front. Immunol. 13:795463. doi: 10.3389/fimmu.2022.795463*

frontiers | Frontiers in Immunology

ORIGINAL RESEARCH
published: 12 April 2022
doi: 10.3389/fimmu.2022.836492

SARS-CoV-2 Spike Protein Expression *In Vitro* and Hematologic Effects in Mice Vaccinated With AZD1222 (ChAdOx1 nCoV-19)

Richard Stebbings[1], Christopher Jones[2], Peter Cotton[3†], Gillian Armour[4], Shaun Maguire[4], Vicky Skellett[2], Chi-Man Tang[2], Joanne Goodman[2], Tyler Brady[5], Virginia Takahashi[6], Andrew Daunt[7], Jean-Martin Lapointe[8] and Taylor S. Cohen[6]*

[1] Oncology Safety, Clinical Pharmacology and Safety Sciences, BioPharmaceuticals R&D, AstraZeneca, Melbourn, United Kingdom, [2] Integrated Bioanalysis, Clinical Pharmacology and Safety Sciences, BioPharmaceuticals R&D, AstraZeneca, Cambridge, United Kingdom, [3] Research and Development, BioPharmaceuticals R&D, AstraZeneca, Macclesfield, United Kingdom, [4] Regulatory Toxicology and Safety Pharmacology, Clinical Pharmacology and Safety Sciences, BioPharmaceuticals R&D, AstraZeneca, Melbourn, United Kingdom, [5] Translational Medicine, Vaccines & Immune Therapies, BioPharmaceuticals Medical, AstraZeneca, Gaithersburg, MD, United States, [6] Microbiome Discovery, Vaccines & Immune Therapies, BioPharmaceuticals Medical, AstraZeneca, Gaithersburg, MD, United States, [7] Labcorp Early Development Laboratories Limited, Harrogate, United Kingdom, [8] Oncology Safety Pathology, Clinical Pharmacology and Safety Sciences, BioPharmaceuticals R&D, AstraZeneca, Cambridge, United Kingdom

OPEN ACCESS

Edited by:
Simon Daniel Van Haren, Boston Children's Hospital and Harvard Medical School, United States

Reviewed by:
Aarón Silva-Sánchez, University of Alabama at Birmingham, United States
Javier Castillo-Olivares, University of Cambridge, United Kingdom

***Correspondence:**
Richard Stebbings
richard.stebbings@astrazeneca.com

[†]This author contributed to this research prior to their retirement from AstraZeneca

Specialty section:
This article was submitted to Vaccines and Molecular Therapeutics, a section of the journal Frontiers in Immunology

Received: *15 December 2021*
Accepted: *14 March 2022*
Published: *12 April 2022*

Citation:
Stebbings R, Jones C, Cotton P, Armour G, Maguire S, Skellett V, Tang C-M, Goodman J, Brady T, Takahashi V, Daunt A, Lapointe J-M and Cohen TS (2022) SARS-CoV-2 Spike Protein Expression In Vitro and Hematologic Effects in Mice Vaccinated With AZD1222 (ChAdOx1 nCoV-19). Front. Immunol. 13:836492. doi: 10.3389/fimmu.2022.836492

Severe COVID-19 can be associated with a prothrombotic state, increasing risk of morbidity and mortality. The SARS-CoV-2 spike glycoprotein is purported to directly promote platelet activation *via* the S1 subunit and is cleaved from host cells during infection. High plasma concentrations of S1 subunit are associated with disease progression and respiratory failure during severe COVID-19. There is limited evidence on whether COVID-19 vaccine-induced spike protein is similarly cleaved and on the immediate effects of vaccination on host immune responses or hematology parameters. We investigated vaccine-induced S1 subunit cleavage and effects on hematology parameters using AZD1222 (ChAdOx1 nCoV-19), a simian, replication-deficient adenovirus-vectored COVID-19 vaccine. We observed S1 subunit cleavage *in vitro* following AZD1222 transduction of HEK293x cells. S1 subunit cleavage also occurred *in vivo* and was detectable in sera 12 hours post intramuscular immunization ($1x10^{10}$ viral particles) in CD-1 mice. Soluble S1 protein levels decreased within 3 days and were no longer detectable 7–14 days post immunization. Intravenous immunization ($1x10^{9}$ viral particles) produced higher soluble S1 protein levels with similar expression kinetics. Spike protein was undetectable by immunohistochemistry 14 days post intramuscular immunization. Intramuscular immunization resulted in transiently lower platelet (12 hours) and white blood cell (12–24 hours) counts relative to vehicle. Similarly, intravenous immunization resulted in lower platelet (24–72 hours) and white blood cell (12–24 hours) counts, and increased neutrophil (2 hours) counts. The responses observed with either route of immunization represent transient hematologic changes and correspond to expected innate immune responses to adenoviral infection.

Keywords: AZD1222 (ChAdOx1 nCoV-19), adenovirus-vectored vaccine, SARS-CoV-2 spike protein, COVID-19 vaccination, platelet and white blood cell parameters

INTRODUCTION

The COVID-19 pandemic has produced substantial global morbidity and mortality, with more than 5 million deaths reported as of November 15, 2021 (1). Individuals with severe and critically severe COVID-19 commonly present with abnormal platelet parameters, including decreased platelet counts, compared with healthy individuals and those with mild/moderate COVID-19 (2). Poor coagulation outcomes including venous thromboembolism and arterial thromboembolism are associated with hospitalization and mortality from COVID-19 (3).

The SARS-CoV-2 structural surface glycoprotein antigen ('spike protein') has been observed to directly bind platelet Angiotensin-Converting Enzyme 2 (ACE2) receptors, enhancing platelet activation *in vitro* and potentiating thrombus formation *in vivo* (2). Cleavage of the spike protein S1 subunit ('S1 subunit') from host cells occurs during SARS-CoV-2 infection, and high plasma S1 subunit concentrations correlate with disease progression and respiratory failure in patients with severe COVID-19 (4). Due to its indispensable functions in mediating virus host-cell entry (5), the first wave of COVID-19 vaccine candidates were predominantly developed to target the spike protein, with several genetic vaccine platforms inducing its expression in vaccinees (6). Although gene-based spike protein vaccines have substantially reduced the risk of hospitalization and death from COVID-19 (7–10), it is unknown if vaccine-induced S1 subunit is similarly cleaved and present in the blood at high concentrations, and whether this has implications for the host immune response (11). There is also limited evidence on host immune responses or effects on blood parameters immediately following COVID-19 vaccination.

AZD1222 (ChAdOx1 nCoV-19), is a simian, replication-deficient adenovirus-vectored COVID-19 vaccine that is being used globally (1, 7), with >2 billion doses administered at the time of manuscript preparation. We conducted these experiments to test the hypothesis that S1 subunit is cleaved *in vivo* following AZD1222 immunization and to assess the potential effects of AZD1222 vaccination on host hematologic parameters.

MATERIALS AND METHODS

In Vitro Assessment of Spike Protein Expression and Cleavage

Cell Culture, AZD1222 Transduction, and Cytotoxicity Assessment

Human embryonic kidney (HEK) 293x cells (American Type Culture Collection) were grown at 37°C, 8% CO_2, in FreeStyle™ 293 Expression Medium at a starting density of $1x10^6$ cells/mL. Cell cultures were transduced with AZD1222 at increasing multiplicities of infection (MOI); ChAdOx1-GFP at MOI=10 and mock transduction (FreeStyle™ 293 Expression Medium) were used as controls (**Figure 1A**). Cell pellets and culture supernatants were collected 48 and 72 hours post transduction for further analysis.

Cytotoxicity was assessed using the LDH-Glo™ assay (Promega, J2380/J2381) per the manufacturer's instructions (12). An aliquot of culture media from mock transduction control received 40 µL of 10% Triton X-100 and was incubated at room temperature for a minimum of 15 minutes. Cellular supernatants for the assessment of lactate dehydrogenase (LDH) were diluted 1:20 in LDH storage buffer [200 mM Tris-HCl (pH = 7.3); glycerol 10%; bovine serum albumin 1%]. Supernatant from Triton-X-100-treated cells was serially diluted to within the linear range of the assay. Diluted samples were combined 1:1 with detection reagent (LDH Detection Enzyme Mix with Reductase Substrate) and added to a 384-well plate in duplicate. A standard curve was prepared from the positive control and added to the plate in triplicate. Samples were analyzed using an EnVision® plate reader (PerkinElmer) following a 50-minute incubation at room temperature.

SARS-CoV-2 S1 and S2 Subunit Western Blot and ELISA

Cell pellets were examined for expression of spike protein by Western blot. Cell pellet (10 µg protein per lane) samples were run on sodium dodecyl sulphate–polyacrylamide gel electrophoresis (SDS-PAGE) gels and then transferred onto polyvinylidene fluoride (PVDF) membranes using the iBlot® 2 dry blotting system (Thermo Fisher Scientific). PVDF membranes were blocked, washed and incubated with primary and secondary antibodies using an iBind™ (Thermo Fisher Scientific) system. Anti-SARS-CoV-2/2019-n-CoV Spike receptor binding domain (RBD) and Spike S2 (Sino Biological, 40592-T62 and 40590-T62) were used as primary antibodies. Anti-β-Actin (Sigma, A1978) was used as a loading control. IRDye 680CW (Licor, 926-68073) and IRDye 800CW (Licor, 926-32212) were used as secondary antibodies. Fluorescence was visualized using an Odyssey CLx imager (Li-Cor Biosciences).

Spike protein S1 and S2 subunit expression levels in culture supernatant were measured by ELISA using 2130-wt or 2196-wt, two monoclonal SARS-CoV-2 spike protein RBD neutralizing antibodies (13), at 100 µg/mL as capture antibodies. 96-well high-binding plates were coated with 100 µg/mL 2130-wt or 2196-wt in 1X PBS at 100 µL per well and incubated at 40°C overnight. Wells were washed 4 times with Blocker™ Casein phosphate buffered saline (PBS) buffer (Thermo 37528) and blocked with 200 µL per well of casein for 1 hour at room temperature. For spike protein standard curve, purified SARS-CoV-2 S trimer was serially diluted 1:3 beginning with high concentration of 3 µg/mL down to 0.001 ng/mL in casein. Samples were tested undiluted and at 1:5 dilutions in casein. Standards and samples were added to wells at 100 µL per well and incubated for 1 hour at room temperature. Wells were washed 4 times with 300 µL per well of casein. Next, secondary antibodies (anti-mouse HRP [Dako P0447] or anti-rabbit HRP (Cell Signaling, 7074S) were diluted 1:10,000 in casein and added to wells at 100 µL per well and incubated for 1 hour at room temperature. Wells were again washed four times with 300 µL per well of casein. 3,3,5,5-Tetramethylbenzidine (TMB) KPL SureBlue (SeraCare, 5120-0074) (equilibrated to room temperature) was added to wells at 100 µL per well and incubated in the dark at room temperature for 5–10 minutes. Reactions were stopped by adding 2N H_2SO_4 at 100 µL per well.

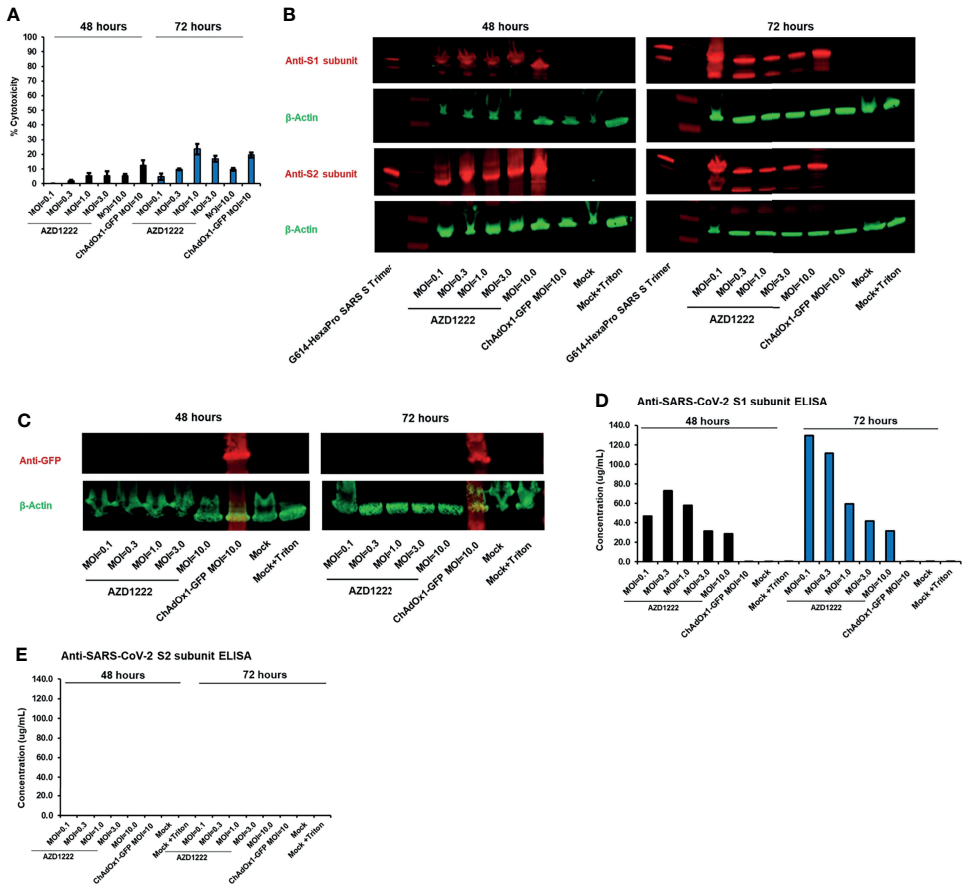

FIGURE 1 | The S1 subunit of the SARS-CoV-2 spike glycoprotein is cleaved *in vitro* following AZD1222 transduction. **(A)** Viability of HEK293x cell lines 48 and 72 hours following transduction with AZD1222 at increasing input MOIs or ChAdOx1-GFP control. Error bars show the associated standard deviation for each sample. **(B)** Expression of SARS-CoV-2 S1 and S2 spike protein subunits 48 or 72 hours post transduction with AZD1222. **(C)** Expression of GFP control 48 or 72 hours post transduction with ChAdOx1-GFP. **(D)** Levels of SARS-CoV-2 S1 subunit and **(E)** full-length spike protein in cell culture supernatants at 48- and 72-hours post-transduction.

Plates were analyzed with an EnVision® plate reader (PerkinElmer) to read absorbance at 450 nm.

In Vivo Animal Procedures and Study Design

Animals

All *in vivo* experimental procedures were approved by the Home Office, United Kingdom, with adherence to the Animals (Scientific Procedures) Act 1986. The regulations conform to EU Directive 2010/63/EU and achieve the standard of care required by the US Department of Health and Human Services' Guide for the Care and Use of Laboratory Animals. Animal studies were conducted according to Good Laboratory Practice regulations for nonclinical laboratory studies and complied with ARRIVE guidelines.

Animal procedures used equal numbers of male and female CD-1 mice aged 8–12 weeks and weighing 20–50 g at the time of dosing. Animals were obtained from Charles River Laboratories (Charles River UK Limited). Mice were examined prior to allocation to study stock. Mice were excluded if they presented with lesions, masses, and/or swellings upon initial examination. Males and females were randomized separately.

Males were housed individually, while females were housed at 2–3 mice per cage. The targeted conditions for animal room environment were 19–23°C, 40–70% humidity, ventilated with >10 air changes per hour, and with a 12-hour light/dark cycle unless interrupted by study procedures/activities. SDS Rat and Mouse No. 1 Diet SQC Expanded, and water, were provided *ad libitum* throughout the study, except during designated procedures.

Test Agent

AZD1222 (MS00684-92) with a virus particle concentration of 2.13 $x10^{12}$/mL was used as the test agent. For control experiments, a buffer (vehicle) of 10 mM histidine, 7.5% (v/w) sucrose, 35 mM sodium chloride, 1 mM magnesium chloride, 0.1% (v/w) Polysorbate-80, 0.1 mM ethylenediaminetetraacetic acid (EDTA), and 0.5% (v/w) ethanol, pH 6.6, was used.

Study Design

This study was performed unblinded. Mice were randomly assigned to receive control (n = 12) or AZD1222 *via* intravenous (IV) (n=48) or intramuscular (IM) (n = 48) injection. Mice assigned to the IV

route-of-administration group received AZD1222 at a concentration of 1 x10^9 viral particles (VP) by single injection at a fixed volume of 30 µL on Day 1. As this was the first time AZD1222 was administrated by IV dosing, mice were split into three batches of increasing size, and 1-day pauses were added between dosing batches 1, 2, and 3 to ensure the tolerability of test agent before dosing larger cohorts of animals. Mice assigned to the IM route-of-administration group received AZD1222 at a concentration of 1x10^{10} VP by single injection of a fixed volume of 30 µL to the right hind limb (thigh) on Day 1.

In Life Procedures and Assessments

Mortality/moribundity were checked throughout the study at the beginning and end of the working day. All mice received at least one physical examination during the pre-treatment portion of the study. Mice were examined regularly throughout the day post dosing for potential reactions to AZD1222 or control, with particular attention paid to the mice during and for the first hour after dosing.

Body weights were collected as deemed necessary by the technical staff for welfare purposes only. Therefore, due to the lack of concurrent data, body weights were compared to pretreatment values and no conclusions are drawn from this dataset. In animals dosed with AZD1222 IV at 1x10^9 VP a decrease in body weight was observed at various timepoints throughout the first week of this study. There were no changes in body weight in animals dosed with AZD1222 IM at 1x10^{10} VP.

Blood Sample Collection and Storage

Blood samples were collected from the orbital sinus following non-recoverable isoflurane anesthesia for serum biomarker bioanalysis and assessment of hematology parameters (**Supplemental Table 1**). Blood samples for hematology assessments were combined with K_2EDTA anticoagulant. Serum samples for S1 sequential sandwich electrochemiluminescence immunoassay were allowed to clot at ambient temperature for ≥60 mins before centrifugation at 1500 x g for 10 mins at 4°C. Resultant serum was separated and stored at −80°C prior to analysis.

Serum S1 Sequential Sandwich Electrochemiluminescence (ECL) Immunoassay

S1 subunit levels in serum were assessed using a validated immunoassay. MSD 96-well small spot streptavidin plates were coated with biotinylated SARS-CoV-2 spike capture antibody (MSD, C20ADB-3) and incubated overnight at 2–8°C. Wells were washed three times with 1x Tris buffer. MSD diluent 11 was added to the wells and allowed to incubate for 30 mins at 25°C. Standard curve and samples were added to wells and allowed to incubate for 120 mins at 25°C. Wells were washed three times with 1x Tris buffer. Detection reagent was added to the wells and allowed to incubate for 60 mins at 25°C. Wells were washed for a final three times with 1x Tris buffer prior to the addition of MSD Gold Read buffer. Spike protein was detected using SULFO-TAG SARS-CoV-2 Spike detection antibody (MSD, D20ADB-3). Plates were analyzed using a MSD S600 Meso Sector Imager Microplate Reader within 10 mins of the addition of read buffer. The lower limit of quantification for the assay was 6.30 pg/mL relative to the SARS-CoV-2 calibrator (MSD, C00ADB-2).

Assessment of Effects on Hematology Parameters

Changes in hematology parameters were assessed based on reference ranges observed in mice under similar study conditions at concurrent and non-concurrent timepoints from historical control data for the testing facility. Group mean values were determined for each timepoint post-vaccination and compared to the reference range to assess for any potential AZD1222-related changes.

Histology, Histopathology, and Immunohistochemistry

Samples of injection site, spleen and bone marrow (sternum and femora-tibial joint) from animals sacrificed at Day 14 post IM injection were fixed in 10% neutral-buffered formalin and processed to paraffin blocks using routine methods. Tissues were sectioned at 4 µm thickness and stained with an immunohistochemical method using a rabbit monoclonal antibody specific to the SARS-Cov2 spike protein (E5S3V, Cell Signaling Technology) at 0.1 µg/ml dilution, on an automated Bond-RX immunostainer (Leica Biosystems), using DAB as a chromogen. Whole slide images were obtained using an Aperio scanner (Leica Biosystems), and were examined by a board-certified veterinary pathologist.

Statistical Analyses

A formal power analysis was considered inappropriate due to the exploratory nature of this study. Three male and three female mice were used per timepoint per vaccination group to ensure reliability of the toxicokinetic and tolerability estimates. Means and standard deviations were calculated where appropriate.

RESULTS

S1 Subunit Is Cleaved *In Vitro* Following AZD1222 Transduction of HEK293x Cells

We assessed the impact of SARS-CoV-2 transgene expression on HEK293x cytotoxicity. Minor levels of cytotoxicity were expected as HEK293x cells are permissive to adenovector propagation by virtue of expressing the adenovirus E1A and E1B genes in *trans* (14), thus incurring the lytic portion of the late-stage adenovirus replication cycle (15). AZD1222-induced cytotoxicity was greatest with MOI=1 and MOI=3 (both 5.5%) at 48 hours post-transduction and with MOI=1 (23.6%) at 72 hours post-transduction (**Figure 1A**, **Supplemental Table 2**). Cell death was not a result of the spike transgene expression as cytotoxicity was also observed 48 hours (12.6%) and 72 hours (19.5%) post transduction with ChAdOx-1-GFP at MOI=10.

Presence of full-length spike protein in cell pellets was confirmed by detection of S1 and S2 subunits by Western blot (**Figure 1B**). S1 and S2 subunit expression was absent in cells transduced with ChAdOx1-GFP or non-transduced controls (**Figures 1B, C**). We observed the presence of cleaved S1 subunit in culture supernatant at 48 and 72 hours following AZD1222 transduction (**Figure 1D**). Higher S1 subunit levels

were observed in cells transduced with lower MOIs at 72 hours, perhaps due to more efficient production of spike protein, or due to lesser cytotoxicity, with lower virus-to-cell ratios. Full-length spike protein was not observed in the supernatant at either 48- or 72-hours post-transduction (**Figure 1E**). Similar results were observed with Western blots of culture supernatants (data not shown).

S1 Subunit Is Cleaved and Rapidly Cleared *In Vivo* Following IM or IV AZD1222 Immunization With Similar Kinetics

We next assessed whether S1 subunit cleavage occurs *in vivo* using CD-1 mice. Mice received higher doses of AZD1222 (per dose/weight ratio) than those in clinical use (7) to maximize the potential for detecting cleaved S1 subunit and to evaluate the effects of exaggerated AZD1222 pharmacology. S1 subunit was detectable in murine sera 12 hours post IM immunization (**Figure 2A**). Mean soluble S1 subunit protein levels decreased within 3 days (**Table 1**) and were below the limit of quantification in 4/6 samples at 7 days and in 6/6 samples at 14 days post-IM immunization (**Supplemental Table 3**). IV immunization produced higher mean levels of soluble S1 subunit protein with similar expression kinetics to IM immunization (**Figure 2B**; **Table 1**; **Supplemental Table 3**).

It is possible that absence of S1 subunit detection after 14 days is due to formation of host anti-S1-subunit antibodies, which would inhibit detection by serum immunoassay. However, immunohistochemistry analyses on IM injection sites revealed no significant expression of spike protein 14 days post AZD1222 immunization (**Supplemental Figure 1**). Bone marrow samples from all animals contained abundant amounts of hematopoietic cells of various lineages, including megakaryocytes. Spleen samples contained variable numbers of hematopoietic cells, as is common in mice. Although another study observed persistence of AZD1222 at IM injection sites by quantitative polymerase chain reaction 29 days post-immunization (16), none of the tissue samples showed evidence of spike protein. Sections of blood vessels did not show evidence of intravascular positive staining in circulating cells including platelets.

AZD1222 Induced Modest/Transient Changes to Host Hematology Parameters Immediately Following Immunization

The effects of AZD1222 vaccination on host hematology parameters and initial immune responses were assessed through evaluating platelet and total white blood cell (consisting of lower lymphocytes, monocytes, and/or eosinophils) counts immediately following immunization (**Table 2**). IM administration of AZD1222 resulted in transiently lower platelets (~73% of vehicle mean; 12 hours), and lower total white blood cells (12–24 hours) counts post immunization. IV administration resulted in lower platelets (69–

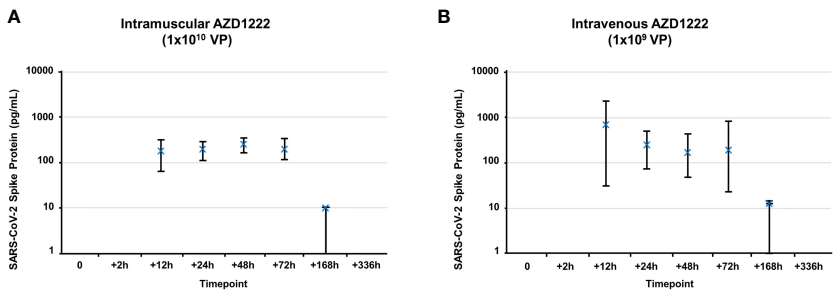

FIGURE 2 | Kinetics of S1 subunit detection following AZD1222 immunization. Levels of SARS-CoV-2 spike protein S1 subunit detected in serum following IM **(A)** or IV **(B)** AZD1222 immunization. Data points represent mean SARS-CoV-2 Spike protein concentrations observed in male and female mice. Error bars indicate minimum and maximum concentrations per timepoint.

TABLE 1 | Mean SARS-CoV-2 soluble S1 subunit levels post-AZD1222 immunization (pg/mL).

Total Viral Particle (VP)/Dose Hours post-AZD1222 immunization	Males		Females	
	$1x10^9$ IV	$1x10^{10}$ IM	$1x10^9$ IV	$1x10^{10}$ IM
0	BLQ	BLQ	BLQ	BLQ
2 hours	BLQ	BLQ	BLQ	BLQ
12 hours	356.0	233.0	1043.0	126.1
24 hours	244.0	206.3	249.0	187.0
48 hours	165.6	276.3	208.7	233.0
72 hours	325.3	166.7	55.2	227.3
168 hours	13.0	10.2	BLQ	10.6
336 hours	BLQ	BLQ	BLQ	BLQ

BLQ, below the limit of quantification (6.3 pg/mL); IM, intramuscular; IV, intravenous; VP, viral particles.

TABLE 2 | Effects on host immune response and hematology parameters immediately following AZD1222 immunization.

Hours post-AZD1222 immunization	Platelets (10^9/L)			Total White Blood Cells (10^9/L)			Neutrophils (10^9/L)		
	Vehicle	IV 1x10^9 VP	IM 1x10^{10} VP	Vehicle	IV 1x10^9 VP	IM 1x10^{10} VP	Vehicle	IV 1x10^9 VP	IM 1x10^{10} VP
0	1033.0	–	–	6.933	–	–	0.840	–	–
2	NA	–	–	NA	–	–	NA	2.940↑	–
12	NA	–	753.5↓	NA	1.593↓	1.040↓	NA	–	–
24	NA	868.0↓	–	NA	1.913↓	3.267↓	NA	–	–
48	NA	721.3↓	–	NA	–	–	NA	–	–
72	NA	815.3↓	–	NA	–	–	NA	–	–
166	NA	–	–	NA	–	–	NA	–	–
336	1295.0	–	–	6.977	–	–	0.890	–	–

Values presented are group mean absolute values that were outside of the reference ranges observed in mice under similar study conditions at concurrent and non-concurrent timepoints from historical control data for the testing facility.

IM, intramuscular; IV, intravenous; NA, Not applicable; VP, viral particles; – = Group mean value was within the reference range, indicating no AZD1222-related change; ↓ = decreased versus reference range; ↑ = increased versus reference range.

84% of vehicle mean; 24–72 hours) and lower white blood cells (12–24 hours) post immunization. Neutrophils were transiently higher 2 hours post IV immunization. Hematology parameters at other timepoints were considered unrelated to AZD1222 and were attributed to biological variation, as similar variations were seen in vehicle control and/or were of a magnitude of change commonly observed in mice under similar study conditions at concurrent and non-concurrent timepoints, or within historical control data for the testing facility.

DISCUSSION

The COVID-19 pandemic continues to cause substantial global morbidity and mortality, with an estimated 28 million life-years lost in 2020 (17). Gene-based vaccines that elicit production of the spike protein in vaccinees have substantially reduced the risk of severe disease and death from COVID-19 (7–10), and are an invaluable tool for mitigating future SARS-CoV-2 outbreaks (18, 19). *In vitro* studies of SARS-CoV-2 have suggested that the spike protein is directly responsible for mediating the thromboembolic complications observed during severe COVID-19 (2, 20, 21). Therefore, it was important to evaluate the effects of COVID-19 vaccine-induced spike protein on host immune and hematologic parameters immediately following immunization.

Within this manuscript we demonstrate that AZD1222-induced S1 subunit is cleaved *in vitro* and *in vivo*. S1 subunit cleavage is likely the result of host proteolytic cleavage [e.g., *via* transmembrane serine protease 2, cathepsin or furin (22, 23)] rather than due to adenovirus-induced cell death (15), as suggested by the low cytotoxicity and lack of S2 subunit detection following AZD1222 transduction. We also demonstrated that, following cleavage, the S1 subunit is rapidly cleared and is no longer detectable from 7–14 days following either IM or IV immunization. Similar quantities of S1 subunit have also been observed in individuals with severe COVID-19 (4). We also observe similar expression kinetics to those observed following IM immunization with mRNA-1273 COVID-19 vaccine (24). Cleavage of vaccine-induced spike protein from host cells may complement other modes of host cell secretion (e.g., endosomal secretion) and facilitate subsequent processing by antigen-presenting cells and the initiation of adaptive immune responses (25).

We observed that IM vaccination induced modest/transient changes to host platelet counts 12 hours following immunization, with similar scale decreases observed 24–72 hours following IV immunization. Murine models of thrombocytopenia (26), with demonstrated physiological relevance to human platelet count/function, suggest that the transient platelet reductions observed following AZD1222 vaccination should not affect host thrombosis or hemostasis. Total white blood cell counts were decreased within the reference range for leukopenia (i.e., <2.0x10^9 total white blood cells per liter) (27) 12 hours following IM and IV immunization but increased to within normal reference ranges (i.e., 2.0–10.0x10^9 total white blood cells per liter) by 24 hours following IM immunization. Transient leukopenia is a characteristic sign of early responses to viral infections and is routinely documented following vaccination (28–33). Following immunization, AZD1222 enters host cells *via* the widely expressed coxsackie and adenovirus receptor (34), wherein detection of AZD1222-derived viral nucleic acids by host cell pathogen recognition receptors initiates production of pro-inflammatory cytokines, chemokines, and type I interferons (35). Neutrophil cell counts were increased 2 hours following IV vaccination, corresponding to expected initial cytokine and chemokine responses to adenoviral infection (36). The initial innate immune response also attracts antigen-presenting cells to the site of immunization, facilitating an induction of S glycoprotein-specific CD8+ and CD4+ T helper 1 T cells, and antibodies that have been observed from 14 days post-immunization in other murine studies of AZD1222 (37–41). Platelet, total white blood cell, and neutrophil counts were unchanged at subsequent timepoints, suggesting that the changes elicited by AZD1222 vaccination are transient and quickly resolved following immunization.

It is important to note that we observed S1 subunit cleavage *in vivo* using AZD1222 concentrations ~30 (IV dose; 1x10^9 VP) to ~300 (IM dose; 1x10^{10} VP) times greater than in current clinical use (based on dose/weight ratio (7)) and therefore are assessing the effects of exaggerated AZD1222 pharmacology within these experiments. Additionally, a limitation of our study is the distinct differences in

COVID-19 pathophysiology between humans and murine models, which may limit the wider interpretation of our findings (42). Although, the SARS-CoV-2 virus can be adapted to improve spike protein binding to the murine ACE2 receptor by serial passage or by using reverse genetics to improve RBD-murine ACE2 receptor binding (43, 44), these adapted viruses still only confer mild forms of COVID-19 disease. Thus, it would be interesting to explore the kinetics and implications of S1 cleavage, and potential effects of AZD1222 and other COVID-19 vaccines on host hematology parameters immediately following vaccination in other animal models (e.g., non-human primates, Syrian hamsters) that may better reflect COVID-19 disease. K18-hACE2 is a transgenic mouse strain that expresses a human ACE2 receptor driven by the cytokeratin-18 (K18) gene promotor, and that has been observed to succumb to SARS-CoV-2 infection due to lung and brain pathology from severe lethal cytokine storm 4–6 days post-SARS-CoV-2 challenge (45, 46). Recombinant SARS-CoV-2 spike protein has been observed to directly bind K18-hACE2 platelets and potentiate thrombosis formation in wild-type mice following K18-hACE2 platelets transfusion (2), albeit using concentrations of spike protein that greatly exceed the concentration of S1 subunit observed in sera of individuals with COVID-19 (4) or following mRNA-1273 vaccination (24). It not yet known whether this finding can be replicated with 'live' SARS-CoV-2 virus or whether spike protein can be induced in sufficient quantities by COVID-19 vaccines to produce a similar result. However, insights from this model may prove invaluable for exploring the etiology of the rare hematologic and vascular complications following COVID-19 vaccination (3).

In conclusion, our results provide further insight to the host response to AZD1222 vaccination. We demonstrate the cleavage of vaccine-induced SARS-CoV-2 spike protein S1 subunit *in vitro* and *in vivo* following IM and IV immunization using concentrations several magnitudes higher than currently used in humans, without deleterious effects on the host. It is unlikely that any potential adverse effects following AZD1222 vaccination can be attributed to persistent S1 subunit expression as this protein is no longer detectable in host sera by 14 days post-vaccination. We also describe transient and quickly resolved effects on host blood parameters immediately following AZD1222 immunization. Collectively these findings, alongside data from pivotal Phase 3 studies (7, 47) and ongoing pharmacosurveillance, support the continued use of AZD1222 to mitigate the COVID-19 pandemic.

DATA AVAILABILITY STATEMENT

Data associated with this study are available in the main text or the **Supplementary Materials**.

ETHICS STATEMENT

The animal study was reviewed and approved by the Home Office, United Kingdom, with adherence to the Animals (Scientific Procedures) Act 1986. The regulations conform to EU Directive 2010/63/EU and achieve the standard of care required by the US Department of Health and Human Services' Guide for the Care and Use of Laboratory Animals. Animal studies were conducted according to Good Laboratory Practice regulations for nonclinical laboratory studies and complied with ARRIVE guidelines.

AUTHOR CONTRIBUTIONS

Study design: RS and TC. HEK 293x transduction: TB. LDH assay: TB. Western blots: VT. ELISA: VT. *In vivo* study monitor: GA and SM. Assessment of hematology parameters: PC. Serum biomarker analysis: JG, CJ, CMT, and VS. Immunohistochemistry experiments and analysis: AD and JML. Critical revision of the manuscript and approval of the final draft: COH under direction of all authors. Confirmation of data accuracy and approval of the final draft: All authors.

FUNDING

This research was funded by AstraZeneca.

ACKNOWLEDGMENTS

The authors thank the staff at Charles River Laboratories for the provision of mice and support with the animal studies described in this report. The authors thank Professor Dame Sarah Gilbert, FMedSci, at the University of Oxford for advice and for help with the supply of test material for this investigation. Medical writing support was provided by Craig O'Hare, PhD, of Ashfield MedComms, an Ashfield company, which was in accordance with Good Publication Practice (GPP3) guidelines and funded by AstraZeneca.

SUPPLEMENTARY MATERIAL

The Supplementary Material for this article can be found online at: https://www.frontiersin.org/articles/10.3389/fimmu.2022.836492/full#supplementary-material

REFERENCES

1. World Health Organization (WHO). *WHO Coronavirus (COVID-19) Dashboard* (2021). Available at: https://covid19.who.int/.
2. Zhang S, Liu Y, Wang X, Yang L, Li H, Wang Y, et al. SARS-CoV-2 Binds Platelet ACE2 to Enhance Thrombosis in COVID-19. *J Hematol Oncol* (2020) 13(1):120. doi: 10.1186/s13045-020-00954-7
3. Hippisley-Cox J, Patone M, Mei XW, Saatci D, Dixon S, Khunti K, et al. Risk of Thrombocytopenia and Thromboembolism After Covid-19 Vaccination and SARS-CoV-2 Positive Testing: Self-Controlled Case Series Study. *BMJ* (2021) 374:n1931. doi: 10.1136/bmj.n1931
4. Ogata AF, Maley AM, Wu C, Gilboa T, Norman M, Lazarovits R, et al. Ultra-Sensitive Serial Profiling of SARS-CoV-2 Antigens and Antibodies in Plasma to Understand Disease Progression in COVID-19 Patients With

Severe Disease. *Clin Chem* (2020) 66(12):1562–72. doi: 10.1093/clinchem/hvaa213
5. Huang Y, Yang C, Xu XF, Xu W, Liu SW. Structural and Functional Properties of SARS-CoV-2 Spike Protein: Potential Antivirus Drug Development for COVID-19. *Acta Pharmacol Sin* (2020) 41(9):1141–9. doi: 10.1038/s41401-020-0485-4
6. Kyriakidis NC, Lopez-Cortes A, Gonzalez EV, Grimaldos AB, Prado EO. SARS-CoV-2 Vaccines Strategies: A Comprehensive Review of Phase 3 Candidates. *NPJ Vaccines* (2021) 6(1):28. doi: 10.1038/s41541-021-00292-w
7. Voysey M, Costa Clemens SA, Madhi SA, Weckx LY, Folegatti PM, Aley PK, et al. Safety and Efficacy of the ChAdOx1 nCoV-19 Vaccine (AZD1222) Against SARS-CoV-2: An Interim Analysis of Four Randomised Controlled Trials in Brazil, South Africa, and the UK. *Lancet* (2021) 397(10269):99–111. doi: 10.1016/S0140-6736(20)32661-1
8. Sadoff J, Gray G, Vandebosch A, Cardenas V, Shukarev G, Grinsztejn B, et al. Safety and Efficacy of Single-Dose Ad26.Cov2.S Vaccine Against Covid-19. *N Engl J Med* (2021) 384(23):2187–201. doi: 10.1056/NEJMoa2101544
9. Baden LR, El Sahly HM, Essink B, Kotloff K, Frey S, Novak R, et al. Efficacy and Safety of the mRNA-1273 SARS-CoV-2 Vaccine. *N Engl J Med* (2021) 384 (5):403–16. doi: 10.1056/NEJMoa2035389
10. Polack FP, Thomas SJ, Kitchin N, Absalon J, Gurtman A, Lockhart S, et al. Safety and Efficacy of the BNT162b2 mRNA Covid-19 Vaccine. *N Engl J Med* (2020) 383(27):2603–15. doi: 10.1056/NEJMoa2034577
11. Watanabe Y, Mendonça L, Allen ER, Howe A, Lee M, Allen JD, et al. Native-Like SARS-CoV-2 Spike Glycoprotein Expressed by ChAdOx1 nCoV-19/AZD1222 Vaccine. *ACS Cent Sci* (2021) 7(4):594–602. doi: 10.1021/acscentsci.1c00080
12. Promega. *LDH-Glo™ Cytotoxicity Assay. Technical Manual* (2021). Available at: https://www.promega.co.uk/-media/files/resources/protocols/technical-manuals/500/ldh-glo-cytotoxicity-assay-technical-manual.pdf?rev=9177f5e2ec194ecfacc9d537dacc0416&sc_lang=en.
13. Zost SJ, Gilchuk P, Case JB, Binshtein E, Chen RE, Nkolola JP, et al. Potently Neutralizing and Protective Human Antibodies Against SARS-CoV-2. *Nature* (2020) 584(7821):443–9. doi: 10.1038/s41586-020-2548-6
14. Braithwaite AW, Russell IA. Induction of Cell Death by Adenoviruses. *Apoptosis* (2001) 6(5):359–70. doi: 10.1023/a:1011338119712
15. Almuqrin A, Davidson AD, Williamson MK, Lewis PA, Heesom KJ, Morris S, et al. SARS-CoV-2 Vaccine ChAdOx1 nCoV-19 Infection of Human Cell Lines Reveals Low Levels of Viral Backbone Gene Transcription Alongside Very High Levels of SARS-CoV-2 S Glycoprotein Gene Transcription. *Genome Med* (2021) 13(1):43. doi: 10.1186/s13073-021-00859-1
16. Stebbings R, Armour G, Pettis V, Goodman J. AZD1222 (ChAdOx1 nCoV-19): A Single-Dose Biodistribution Study in Mice. *Vaccine* (2021) 40(2):192–5. doi: 10.1016/j.vaccine.2021.11.028
17. Islam N, Jdanov DA, Shkolnikov VM, Khunti K, Kawachi I, White M, et al. Effects of Covid-19 Pandemic on Life Expectancy and Premature Mortality in 2020: Time Series Analysis in 37 Countries. *BMJ* (2021) 375:e066768. doi: 10.1136/bmj-2021-066768
18. Pritchard E, Matthews PC, Stoesser N, Eyre DW, Gethings O, Vihta KD, et al. Impact of Vaccination on New SARS-CoV-2 Infections in the United Kingdom. *Nat Med* (2021) 27(8):1370–8. doi: 10.1038/s41591-021-01410-w
19. Moghadas SM, Vilches TN, Zhang K, Wells CR, Shoukat A, Singer BH, et al. The Impact of Vaccination on COVID-19 Outbreaks in the United States. *Clin Infect Dis* (2021) 73(12):2257–64. doi: 10.1093/cid/ciab079
20. Wang J, Pendurthi UR, Yi G, Rao LVM. SARS-CoV-2 Infection Induces the Activation of Tissue Factor-Mediated Coagulation *Via* Activation of Acid Sphingomyelinase. *Blood* (2021) 138(4):344–9. doi: 10.1182/blood.2021010685
21. Connors JM, Levy JH. COVID-19 and its Implications for Thrombosis and Anticoagulation. *Blood* (2020) 135(23):2033–40. doi: 10.1182/blood.2020006000
22. Shang J, Wan Y, Luo C, Ye G, Geng Q, Auerbach A, et al. Cell Entry Mechanisms of SARS-CoV-2. *Proc Natl Acad Sci USA* (2020) 117(21):11727–34. doi: 10.1073/pnas.2003138117
23. Jackson CB, Farzan M, Chen B, Choe H. Mechanisms of SARS-CoV-2 Entry Into Cells. *Nat Rev Mol Cell Biol* (2022) 23(1):3–20. doi: 10.1038/s41580-021-00418-x
24. Ogata AF, Cheng CA, Desjardins M, Senussi Y, Sherman AC, Powell M, et al. Circulating SARS-CoV-2 Vaccine Antigen Detected in the Plasma of mRNA-1273 Vaccine Recipients. *Clin Infect Dis* (2022) 74(4):715–8. doi: 10.1093/cid/ciab465
25. Teijaro JR, Farber DL. COVID-19 Vaccines: Modes of Immune Activation and Future Challenges. *Nat Rev Immunol* (2021) 21(4):195–7. doi: 10.1038/s41577-021-00526-x
26. Morowski M, Vogtle T, Kraft P, Kleinschnitz C, Stoll G, Nieswandt B. Only Severe Thrombocytopenia Results in Bleeding and Defective Thrombus Formation in Mice. *Blood* (2013) 121(24):4938–47. doi: 10.1182/blood-2012-10-461459
27. O'Connell KE, Mikkola AM, Stepanek AM, Vernet A, Hall CD, Sun CC, et al. Practical Murine Hematopathology: A Comparative Review and Implications for Research. *Comp Med* (2015) 65(2):96–113.
28. Black FL, Sheridan SR. Blood Leukocyte Response to Live Measles Vaccine. *Am J Dis Child* (1967) 113(3):301–4. doi: 10.1001/archpedi.1967.02090180061002
29. Goshen-Lago T, Waldhorn I, Holland R, Szwarcwort-Cohen M, Reiner-Benaim A, Shachor-Meyouhas Y, et al. Serologic Status and Toxic Effects of the SARS-CoV-2 BNT162b2 Vaccine in Patients Undergoing Treatment for Cancer. *JAMA Oncol* (2021) 7(10):1507–13. doi: 10.1001/jamaoncol.2021.2675
30. Bancroft WH, Top FHJr., Eckels KH, Anderson JH Jr., McCown JM, Russell PK. Dengue-2 Vaccine: Virological, Immunological, and Clinical Responses of Six Yellow Fever-Immune Recipients. *Infect Immun* (1981) 31(2):698–703. doi: 10.1128/iai.31.2.698-703.1981
31. Muturi-Kioi V, Lewis D, Launay O, Leroux-Roels G, Anemona A, Loulergue P, et al. Neutropenia as an Adverse Event Following Vaccination: Results From Randomized Clinical Trials in Healthy Adults and Systematic Review. *PloS One* (2016) 11(8):e0157385. doi: 10.1371/journal.pone.0157385
32. Laoprasopwattana K, Limpitikul W, Geater A. Using Clinical Profiles and Complete Blood Counts to Differentiate Causes of Acute Febrile Illness During the 2009-11 Outbreak of Typhoid and Chikungunya in a Dengue Endemic Area. *J Trop Pediatr* (2020) 1(5):504–10. doi: 10.1093/tropej/fmaa006
33. Cummins D, Wilson ME, Foulger KJ, Dawson D, Hogarth AM. Haematological Changes Associated With Influenza Vaccination in People Aged Over 65: Case Report and Prospective Study. *Clin Lab Haematol* (1998) 20(5):285–7. doi: 10.1046/j.1365-2257.1998.00149.x
34. Hasanpourghadi M, Novikov M, Ertl HCJ. COVID-19 Vaccines Based on Adenovirus Vectors. *Trends Biochem Sci* (2021) 46(5):429–30. doi: 10.1016/j.tibs.2021.03.002
35. Tan X, Sun L, Chen J, Chen ZJ. Detection of Microbial Infections Through Innate Immune Sensing of Nucleic Acids. *Annu Rev Microbiol* (2018) 72:447–78. doi: 10.1146/annurev-micro-102215-095605
36. Johansson C, Kirsebom FCM. Neutrophils in Respiratory Viral Infections. *Mucosal Immunol* (2021) 14(4):815–27. doi: 10.1038/s41385-021-00397-4
37. Stebbings R, Maguire S, Armour G, Jones C, Goodman J, Maguire AK, et al. Developmental and Reproductive Safety of AZD1222 (ChAdOx1 nCov-19) in Mice. *Reprod Toxicol* (2021) 104:134–42. doi: 10.1016/j.reprotox.2021.07.010
38. AstraZeneca. *Vaxzevria (Previously COVID-19 Vaccine AstraZeneca, Suspension for Injection) COVID-19 Vaccine (ChAdOx1-S [Recombinant]) Public Assessment Report*. Available at: https://assets.publishing.service.gov.uk/government/uploads/system/uploads/attachment_data/file/1003840/CMA_UKPAR_COVID_19_Vaccine_AstraZeneca_PAR_16.07.2021.pdf.
39. Graham SP, McLean RK, Spencer AJ, Belij-Rammerstorfer S, Wright D, Ulaszewska M, et al. Evaluation of the Immunogenicity of Prime-Boost Vaccination With the Replication-Deficient Viral Vectored COVID-19 Vaccine Candidate ChAdOx1 nCov-19. *NPJ Vaccines* (2020) 5(1):69. doi: 10.1038/s41541-020-00221-3
40. Silva-Cayetano A, Foster WS, Innocentin S, Belij-Rammerstorfer S, Spencer AJ, Burton OT, et al. A Booster Dose Enhances Immunogenicity of the COVID-19 Vaccine Candidate ChAdOx1 nCov-19 in Aged Mice. *Med (N Y)* (2021) 2(3):243–62.e8. doi: 10.1016/j.medj.2020.12.006
41. van Doremalen N, Lambe T, Spencer A, Belij-Rammerstorfer S, Purushotham JN, Port JR, et al. ChAdOx1 nCov-19 Vaccine Prevents SARS-CoV-2 Pneumonia in Rhesus Macaques. *Nature* (2020) 586(7830):578–82. doi: 10.1038/s41586-020-2608-y
42. Muñoz-Fontela C, Dowling WE, Funnell SGP, Gsell PS, Riveros-Balta AX, Albrecht RA, et al. Animal Models for COVID-19. *Nature* (2020) 586 (7830):509–15. doi: 10.1038/s41586-020-2787-6
43. Gu H, Chen Q, Yang G, He L, Fan H, Deng YQ, et al. Adaptation of SARS-CoV-2 in BALB/c Mice for Testing Vaccine Efficacy. *Science* (2020) 369 (6511):1603–7. doi: 10.1126/science.abc4730

44. Dinnon KH 3rd, Leist SR, Schafer A, Edwards CE, Martinez DR, Montgomery SA, et al. A Mouse-Adapted Model of SARS-CoV-2 to Test COVID-19 Countermeasures. *Nature* (2020) 586(7830):560–6. doi: 10.1038/s41586-020-2708-8
45. Oladunni FS, Park JG, Pino PA, Gonzalez O, Akhter A, Allué-Guardia A, et al. Lethality of SARS-CoV-2 Infection in K18 Human Angiotensin-Converting Enzyme 2 Transgenic Mice. *Nat Commun* (2020) 11(1):6122. doi: 10.1038/s41467-020-19891-7
46. Winkler ES, Bailey AL, Kafai NM, Nair S, McCune BT, Yu J, et al. SARS-CoV-2 Infection of Human ACE2-Transgenic Mice Causes Severe Lung Inflammation and Impaired Function. *Nat Immunol* (2020) 21(11):1327–35. doi: 10.1038/s41590-020-0778-2
47. Falsey AR, Sobieszczyk ME, Hirsch I, Sproule S, Robb ML, Corey L, et al. Phase 3 Safety and Efficacy of AZD1222 (ChAdOx1 nCov-19) Covid-19 Vaccine. *N Engl J Med* (2021) 385(25):2348–60. doi: 10.1056/NEJMoa2105290

Conflict of Interest: AD is an employee of LabCorp Early Development Laboratories Limited, a contract research organization that supported AstraZeneca with immunohistochemistry analyses during this investigation. All other authors report a relationship with AstraZeneca that includes employment and stock options.

This study received funding from AstraZeneca. The funder had the following involvement with the study: study design; collection, analysis and interpretation of data; the writing of this article and the decision to submit it for publication.

Publisher's Note: All claims expressed in this article are solely those of the authors and do not necessarily represent those of their affiliated organizations, or those of the publisher, the editors and the reviewers. Any product that may be evaluated in this article, or claim that may be made by its manufacturer, is not guaranteed or endorsed by the publisher.

frontiers | Frontiers in Immunology

ORIGINAL RESEARCH
published: 13 April 2022
doi: 10.3389/fimmu.2022.878832

Intranasal Immunization With a c-di-GMP-Adjuvanted Acellular Pertussis Vaccine Provides Superior Immunity Against *Bordetella pertussis* in a Mouse Model

Wenwen Jiang[1†], Xiaoyu Wang[1†], Yuhao Su[2], Lukui Cai[3], Jingyan Li[3], Jiangli Liang[1], Qin Gu[1], Mingbo Sun[1,3] and Li Shi[2*]*

[1] Yunnan Key Laboratory of Vaccine Research and Development on Severe Infectious Diseases, Institute of Medical Biology, Chinese Academy of Medical Science & Peking Union Medical College, Kunming, China, [2] Laboratory of Immunogenetics, Institute of Medical Biology, Chinese Academy of Medical Science & Peking Union Medical College, Kunming, China, [3] Laboratory of Vaccine Development, Institute of Medical Biology, Chinese Academy of Medical Science & Peking Union Medical College, Kunming, China

OPEN ACCESS

Edited by:
Simon Daniel Van Haren, Boston Children's Hospital and Harvard Medical School, United States

Reviewed by:
Dominique Raze, U1019 Centre d'Infection et Immunité de Lille (CIIL) (INSERM), France
Bodo Linz, Friedrich Alexander University Erlangen-Nuremberg, Germany

***Correspondence:**
Mingbo Sun
smb@imbcams.com.cn
Li Shi
shili.imb@gmail.com

[†]These authors have contributed equally to this work

Specialty section:
This article was submitted to Vaccines and Molecular Therapeutics, a section of the journal Frontiers in Immunology

Received: 18 February 2022
Accepted: 22 March 2022
Published: 13 April 2022

Citation:
Jiang W, Wang X, Su Y, Cai L, Li J, Liang J, Gu Q, Sun M and Shi L (2022) Intranasal Immunization With a c-di-GMP-Adjuvanted Acellular Pertussis Vaccine Provides Superior Immunity Against Bordetella pertussis in a Mouse Model. Front. Immunol. 13:878832. doi: 10.3389/fimmu.2022.878832

Pertussis, caused by the gram-negative bacterium *Bordetella pertussis*, is a highly contagious respiratory disease. Intranasal vaccination is an ideal strategy to prevent pertussis, as the nasal mucosa represents the first-line barrier to *B. pertussis* infection. The current intramuscular acellular pertussis (aP) vaccines elicit strong antibody and Th2-biased responses but not necessary cellular and mucosal immunity. Here, we formulated two cyclic dinucleotide (CDN)-adjuvanted aP subunit vaccines, a mammalian 2',3'-cGAMP-adjuvanted aP vaccine and a bacterial-derived c-di-GMP-adjuvanted aP vaccine, and evaluated their immunogenicity in a mouse model. We found that the aP vaccine alone delivered intranasally (IN) induced moderate systemic and mucosal humoral immunity but weak cellular immunity, whereas the alum-adjuvanted aP vaccine administered intraperitoneally elicited higher Th2 and systemic humoral immune responses but weaker Th1 and Th17 and mucosal immune responses. In contrast, both CDN-adjuvanted aP vaccines administered *via* the IN route induced robust humoral and cellular immunity systemically and mucosally. Furthermore, the c-di-GMP-adjuvanted aP vaccine generated better antibody production and stronger Th1 and Th17 responses than the 2′,3′-cGAMP-adjuvanted aP vaccine. In addition, following *B. pertussis* challenge, the group of mice that received IN immunization with the c-di-GMP-adjuvanted aP vaccine showed better protection than all other groups of vaccinated mice, with decreased inflammatory cell infiltration in the lung and reduced bacterial burden in both the upper and lower respiratory tracts. In summary, the c-di-GMP-adjuvanted aP vaccine can elicit a multifaceted potent immune response resulting in robust bacterial clearance in the respiratory tract, which indicates that c-di-GMP can serve as a potential mucosal adjuvant for the pertussis vaccine.

Keywords: *Bordetella pertussis*, acellular pertussis vaccine (aP), c-di-GMP, 2',3'-cGAMP, cyclic dinucleotides (CDNs), mucosal immunity

INTRODUCTION

Pertussis is a highly infectious respiratory disease caused by *Bordetella pertussis (B. pertussis)* and remains a lethal threat in unvaccinated infants. Vaccination is the most effective way to prevent pertussis. To date, acellular pertussis (aP) vaccines have gradually replaced whole pertussis (wP) vaccines due to their fewer adverse side effects (1, 2). However, recent epidemiological data show that pertussis has experienced a resurgence in several countries, even in countries with nearly universal vaccine coverage, in the last 20 years (3, 4). Many hypotheses have been proposed to explain the pertussis resurgence, including increased detection sensitivity, vaccine-driven evolution of *B. pertussis* strains, waning of protective efficacy of aP vaccines, and asymptomatic transmission (5–7). Among all these reasons, the inefficient protection afforded by current aP vaccines may be the major issue for the insufficient prevention and control of whooping cough. Several studies have suggested that current aP vaccines cannot prevent *B. pertussis* infection and transmission because they induce only humoral immune responses but not efficient cellular and mucosal immune responses (8–10). The current intramuscular acellular pertussis (aP) vaccines elicit strong antibody and Th2-biased responses but not necessary cellular and mucosal immunity. Th1 cells-mediated immune responses is generally considered to be cellular or cell-mediated immunity (CMI), while Th2 cells can provide optimal help for humoral immune responses (11). Since routine aP vaccines are formulated with several pertussis components with an aluminum adjuvant, administered *via* intramuscular injection and mainly induce antibody protection, novel aP vaccines with appropriate adjuvants administered *via* intranasal (IN) inoculation have been a research hotspot.

The upper respiratory tract (URT) is the site of infection for *B. pertussis*, and the pre-existing immunity on mucosal surfaces of the respiratory tract plays a crucial role in defense against *B. pertussis* infection (12). Studies on nonhuman primates have shown that potent local humoral and cellular immune responses, especially Th17 responses, induced by natural *B. pertussis* infection can provide complete protection against reinfection (8, 13). In addition, many studies have shown that the IN administration of aP vaccines combined with an appropriate adjuvant induced optimal protection against infection, especially in the URT (14–16). Therefore, mucosal immunity might offer a crucial mechanism to prevent nasal colonization and infection.

Cyclic dinucleotides (CDNs), which can trigger the innate immune response in mammalian cells *via* the stimulator of interferon genes (STING) signaling pathway, leading to type I interferon (IFN) generation, have been studied as novel vaccine adjuvants (17). Many studies have shown that CDNs have strong mucosal adjuvant properties (18–21). CDNs, consisting of two nucleotide residues linked by two phosphodiester bonds, have been recognized as a class of crucial secondary signaling molecules in bacteria and in mammalian cells, with robust immunomodulatory and immunostimulatory functions. Depending on the pair of phosphodiester linkages, CDNs have several isomers. There are four common CDNs, three in bacteria (c-di-GMP, c-di-AMP, and 3',3'-cGAMP) and one in eukaryotic cells (2',3'-cGAMP), and the bacterial Sting pathway, which plays an important role in the defense against bacteriophages, prefers canonical 3'–5'-linked CDNs (22). c-di-GMP is a universal bacterial secondary messenger in gram-negative bacteria and is defined as two GMP molecules linked *via* two 3′-5′ phosphodiester bonds (22, 23). c-di-GMP participates in many bacterial processes, including virulence, stress survival, motility, metabolism, antibiotic production, differentiation, biofilm formation, and other processes (24). Recent research has shown that c-di-GMP, acting as a danger signal in eukaryotic cells, is recognized by mammalian immune systems and therefore is considered a potential vaccine adjuvant (25). Another CDN, 2',3'-cGAMP, containing mixed phosphodiester linkages connecting the two nucleosides from the 2 and 5 positions of guanosine and the 3 and 5 positions of adenosine, is synthesized by cGAS from ATP and GTP upon cytosolic DNA stimulation and was first discovered in 2012 (26, 27). This mammalian CDN isomer is different from all characterized bacterial CDNs. Eukaryotic cells employ a phosphodiester linkage (2′-5′) to promote greater CDN stability, thus allowing stronger and more prolonged signal amplification. In addition, the unique 2′-5′- phosphodiester linkage might be a defense mechanism of eukaryotic cells that allows them to avoid subversion of the innate immune response by bacteria because bacterial cells might not be able to degrade 2′-5′ phosphodiester linkages (22). As seen with other CDNs, 2′,3′-cGAMP also has potential applications as an adjuvant (28). All CDNs can bind and stimulate the STING signaling pathway in eukaryotic cells, but 2′,3′-cGAMP binds to mammalian sting with a much greater affinity than bacterial CDNs because of their different phosphodiester linkage positions (27, 29). Moreover, 2′,3′-cGAMP induces stronger type I IFN production than other CDNs derived from bacteria (27). Thus, we selected 2′,3′-cGAMP and c-di-GMP as adjuvants to determine which could provide a superior mucosal immune response against *B. pertussis*.

In this study, we compared and evaluated the efficacy of two common CDNs *in vitro* by using bone marrow-derived dendritic cells (BMDCs). Subsequently, we formulated the test aP vaccine containing pertussis toxoid (PT), filamentous hemagglutinin (FHA), and pertactin (PRN) using the two types of CDNs as adjuvants. We examined the two test aP vaccine-induced immune responses and protective efficacy against *B. pertussis* in a mouse model to evaluate whether the 2′,3′-cGAMP- or c-di-GMP-adjuvanted aP vaccine could be a candidate vaccine against *B. pertussis*.

MATERIALS AND METHODS

Mice and Ethics Statements

Specific pathogen-free (SPF) 4- to 5-week-old male and female BALB/c mice were purchased from Beijing Charles River Laboratory (Beijing, China). All mice used in this study were treated in accordance with the Guide for the Care and Use of Laboratory Animals of the People's Republic of China.

All protocols were reviewed and approved by the Committee on Ethics of the Institute of Medical Biology, Chinese Academy of Medical Sciences (IMBCAMS; assurance number: DWSP2021 06004). Animals were bred and maintained under SPF conditions at IMBCAMS at a constant temperature (20–24 °C) and humidity (45–65%), with lighting on a fixed light/dark cycle (12 h/12 h).

Bacterial Strains, Media, and Growth Conditions

The *B. pertussis* strain *B.p-L1* used in this study was recently isolated from a patient in Yunnan Province, China. Total DNA was extracted from the recovered *B. pertussis*, which was characterized as carrying the ptxP3 genotype by DNA sequencing of the pertussis toxin promoter (ptxP) (30). For *B. pertussis* infection experiments, bacteria were grown on Bordet-Gengou agar (B-G) plates (Hopebio) containing 20% defibrinated sheep blood (Nanjinglezhen) for 24 to 48 h at 37°C. Colonies from fresh B-G plates were resuspended in phosphate-buffered solution (PBS), diluted to a concentration of 10^{11} CFU/mL by using a turbidimetric method, and used within 2 h of preparation. For culture of bacteria from tissues, Regan-Lowe plates prepared from Regan-Lowe charcoal agar base (Oxoid) supplemented with 10% defibrinated sheep blood and 40 μg/mL cephalexin (Oxoid) were used.

Isolation and Stimulation of Dendritic Cells

BMDCs were isolated from mouse bone marrow cells as previously described (31). Briefly, bone marrow cells were isolated and cultured in RPMI 1640 medium containing 20 ng/mL recombinant GM-CSF (Peprotech), 100 U/mL penicillin, 100 μg/mL streptomycin, and 10% FBS. Petri dishes containing 2×10^6 cells in 10 mL were incubated at 37°C in 5% CO_2. At day 3 of incubation, an additional 10 mL of fresh complete medium containing GM-CSF was added, and 10 mL of medium was replaced with fresh medium supplemented with GM-CSF on day 6. Immature BMDCs were collected on day 7 for experiments. The BMDCs were treated with 2′,3′-cGAMP (5 μg/mL, *In vivo*Gen, California, USA) or c-di-GMP (5 μg/mL, *In vivo*Gen, California, USA) *in vitro* for 24 h. Cells were treated with lipopolysaccharide (LPS, 1 μg/mL, Sigma–Aldrich) as a positive control or sterile PBS as a negative control. Cytokine (IFN-β and TNF-α) levels in the supernatant were quantified by ELISA. The stimulated BMDCs were stained with the specific antibodies described below and analyzed by using FlowJo software.

Mouse Immunization and Sample Collection

BALB/c mice (half of which were male and half of which were female, 4–5 weeks old) were immunized *via* the IN (20 μL volume) or intraperitoneal (IP, 200 μl volume) route three times at three-week intervals with the different tested vaccines (**Table 1**). Antigens of the aP vaccine were produced by the IMBCAMS under good manufacturing practice conditions (32). All vaccinations were performed under anesthesia (isoflurane). Blood, nasal washes (NWs), and bronchoalveolar lavage fluid (BALF) were collected two weeks after the last immunization. Blood was collected and centrifuged at 860 g for 10 min to obtain plasma. NW and BALF samples were obtained by washing the nasal cavity and lung with 0.2 mL and 1 ml of cold PBS containing protease inhibitor, respectively. Nasal cavity and lung wash fluids were centrifuged at 2400 g for 10 min, and the supernatants were collected. Plasma, NW, and BALF samples were stored frozen at -20°C until the detection of antibodies (**Figure 1**).

Preparation of Monocellular Suspensions From Organs

Spleen tissues were minced, filtered through a 70-μm nylon mesh (BD Biosciences), and diluted 1:1 in RPMI 1640. The mixture was loaded onto a Ficoll-Paque (GE, USA) layer and centrifuged at 1500 rpm for 30 minutes at room temperature. For monocellular isolation from lungs, tissues were minced and digested with collagenase D (1 mg/mL; Roche) and DNase I (20 U/mL; Roche) for 45 min at 37°C on a shaker. Next, tissues were passed through a 70-μm cell strainer, washed twice in complete RPMI 1640 medium, mixed with 40% Percoll, loaded onto a 70% Percoll layer and centrifuged at 1800 rpm for 30 minutes at room temperature. The cells obtained from organs were washed twice with RPMI 1640 and/or resuspended in complete cell culture medium (RPMI 1640 supplemented with 10% (V/V) fetal calf serum (FCS) and a 1% (v/v) premixed penicillin–streptomycin solution). The cells were used for cytokine detection, ELISpot, and/or flow cytometry.

Enzyme-Linked Immune Sorbent Assay (ELISA)

Microplates (96-well) were coated with PT, FHA, or PRN at 3 μg/mL and incubated at 4°C overnight. Then, the plates were blocked with 3% (w/v) bovine serum albumin (BSA, Abcam) in PBS at 37°C for 2 h. Diluted serum, NW, or BALF sample was

TABLE 1 | The detail of immunization regimens.

Vaccine components (μg/dose)	PBS/IN	aP/IN	aP + $Al(OH)_3$/IP	aP + 2',3'-cGAMP/IN	aP + c-di-GMP/IN
PT	–	1.25	1.25	1.25	1.25
FHA	–	1.25	1.25	1.25	1.25
PRN	–	0.4	0.4	0.4	0.4
$Al(OH)_3$	–	–	37.5	–	–
2',3'-cGAMP	–	–	–	5	–
c-di-GMP	–	–	–	–	5

"IN" and "IP" indicate intranasally and intraperitoneally immunized, respectively.
"PT", "FHA", and "PRN" indicate pertussis toxoid, filamentous hemagglutinin, and pertactin.

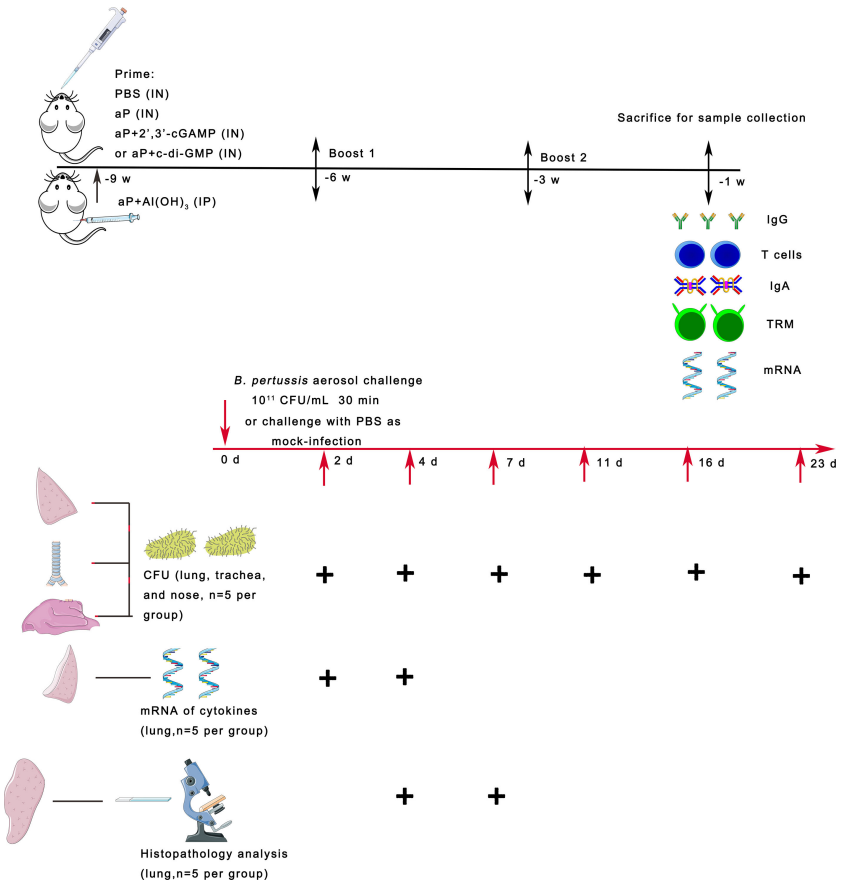

FIGURE 1 | Scheme of mouse immunization and *B. pertussis* challenge. BALB/c mice were immunized with three doses of the different vaccines *via* the intranasal (IN) or intraperitoneal (IP) route at 3-week intervals. Control mice received PBS *via* the IN route. To evaluate specific immune responses, including systemic and mucosal immune responses, mice were bled and sacrificed two weeks after the last immunization for sample collection. Three weeks after the last immunization, the mice were infected with *B. pertussis* by aerosol challenge. In parallel, naïve mice were challenged with PBS as a mock-infection group. On days 2, 4, 7, 11, 16, and 23 after *B. pertussis* infection (dpi), lungs, trachea, and nasal mucosa were collected from each group of mice, and the numbers of *B. pertussis* CFU in the upper and lower respiratory tracts were determined by dilution plating. On days 2 and 4 after infection, the mRNA expression levels of the indicated cytokines were determined by real-time quantitative PCR (RT–qPCR) in the lung tissues. On days 4 and 7 after infection, lung tissues were collected, processed into paraffin sections and stained with H&E.

added to each microplate and incubated at 37°C for 1 h. After washing, a horseradish peroxidase (HRP)-labeled sheep anti-mouse IgG (Jackson ImmunoResearch, USA), anti-mouse IgG1 (Southern Biotech, USA), anti-IgG2a (Southern Biotech, USA), or anti-mouse IgA (Southern Biotech, USA) antibody was added to the microplate, and the plate was incubated at 37°C for 1 h. All the ELISA plates were developed using tetramethylbenzidine (TMB; Solarbio, CHN) to generate a colorimetric reaction, and the reaction was terminated with 2 mmol/L H_2SO_4. The absorbance of the plates at 450 nm was read. Endpoint titers were determined as the dilution that exhibited an optical density exceeding ≥2.1 times the background level (secondary antibody alone).

Enzyme-Linked Immunospot (ELISpot)

T cell detection by IFN-γ, IL-4 and IL-17 ELISpot assays was performed according to the manufacturer's instructions (Cellular Technology Limited, USA). Briefly, precoated 96-well plates were seeded with 5 μg/mL specific stimulants and 4×10^5 mouse splenocytes or pneumonocytes in a total volume of 100 μL and incubated. Following a 24-h incubation at 37°C with 5% CO_2, the cells were removed, and an anti-IFN-γ, anti-IL-4 or anti-IL-17 detection antibody was added, followed by the addition of streptavidin-ALP. For antigen-specific IgA or IgG plasma cell detection, MultiScreen filter 96-well plates (Millipore, USA) were precoated with PT, FHA, or PRN (each 5 μg) for each well overnight at 4°C. After rinsing with PBS, the plates were blocked with culture medium for 30 min at room temperature. Single-cell suspensions of splenocytes or pneumonocytes in culture medium were added to the coated plates and incubated at 37°C with 5% CO_2 for 24 h. After washing with PBS, the plates were incubated with biotinylated anti-IgA or anti-IgG antibodies (Southern Biotech, USA) followed by incubation with streptavidin-conjugated horseradish peroxidase (Jackson

ImmunoResearch, USA), each for 1 h at room temperature. After additional washes with PBS, AEC substrate solution (BD Bioscience, USA) was added for spot development. The reaction was stopped by rinsing with water. Spots were developed using BCIP/NBT and analyzed by a Cellular Technology Limited (CTL) ELISpot reader.

ELISA for Cytokines

Cytokine levels in the supernatant of cultured cells were measured by an ELISA kit according to the manufacturer's recommendation. Values were calculated based on a standard curve of recombinant cytokines. The results are expressed as picograms per milliliter (pg/mL). IFN-β (Cat# VAL612, Novus Biologicals) and TNF-α (Cat# VAL609, Novus Biologicals) levels in the supernatant of BMDCs were quantified. For detecting the cytokines level in the supernatant of cultured splenic or pulmonary lymphocytes, cells were cultured at a concentration of 2×10^6/ml and stimulated with the antigens PT (2 μg/ml), FHA (2 μg/ml), and PRN (2 μg/ml). Supernatants were removed after 3 days and stored at -20°C before testing. IFN-γ (Cat# VAL607, Novus Biologicals), TNF-a (Cat# VAL609, Novus Biologicals), and IL-2 (Cat# VAL602, Novus Biologicals) levels were measured for Th1 responses; IL-5 (Cat# KA0253, Novus Biologicals) and IL-6 (Cat# VAL604, Novus Biologicals) levels were detected for Th2 responses; and IL-17A (Cat# VAL610, Novus Biologicals) and IL-22 (Cat# M2200, R&D Systems) levels were tested for Th17 responses (33, 34).

Flow Cytometry

Single-cell suspensions were obtained from BMDCs or lung tissues. To detect BMDC maturation, cells were blocked with anti-mouse CD16/32 antibodies and stained for surface markers with anti-CD11c (Biolegend, clone: N418, Cat# 117338), anti-CD80 (Biolegend, clone: 16-10A1, Cat# 104729), anti-CD86 (eBioscience, clone: GL1, Cat# 25-0862-82), anti-CD40 (BD Bioscience, clone: 3/23, Cat# 562846), and anti- major histocompatibility complex molecule class II (MHC II) antibodies (I-A/I-E, eBioscience, clone: M5/114.15.2, Cat# 12-5321-8282). To discriminate circulating cells from lung-resident cells, intravascular staining was performed as previously described (31). In brief, mice were intravenously (i.v.) delivered with 3 μg of PE-labeled anti-CD45 antibody (eBioscience, clone: 30-F11, Cat# 12-0451-82) and sacrificed 10 min after i.v. injection, and lungs were isolated immediately to obtain a single-cell suspension as described. For the detection of lung tissue-resident memory T (TRM) cells, lung cells were stained for cell surface markers with anti-CD3 (Biolegend, clone: 17A2, Cat# 100216), anti-CD4 (Biolegend, clone: GK1.5, Cat# 100406), anti-CD8 (Biolegend, clone: 53-6.7, Cat# 100752), anti-CD44 (Biolegend, IM7, Cat# 103040), anti-CD69 (eBioscience, clone: H1.2F3, Cat# 25-0691-82), and anti-CD62L antibodies (Biolegend, clone: MEL-14, Cat# 104412). Dead cells were excluded by 7-AAD staining (BD Bioscience). All samples were assessed on a flow cytometer (Beckman, USA), and data were analyzed with FlowJo software (TreeStar).

RNA-Seq

The nasal mucosa was collected on day 14 after the third immunization and homogenized with TRIzol reagent (Invitrogen, CA), and total RNA was isolated with chloroform/isopropanol, followed by purification with a RNeasy Mini Kit (Qiagen). For library and sequencing, the mRNA was isolated and purified from total RNA *via* Oligo(dT)-attached magnetic beads. Subsequently, purified mRNA was fragmented into small pieces with fragment buffer. Then first-strand cDNA was generated using random hexamer-primed reverse transcription, followed by a second-strand cDNA synthesis. Afterwards, A-Tailing Mix and RNA Index Adapters were added by incubating to end repair. The obtained cDNA fragments were amplified by PCR, and the products were purified by Ampure XP Beads and validated on the Agilent Technologies 2100 bioanalyzer for quality control. The double stranded PCR products were heated, denatured, and circularized by the splint oligo sequence to obtain the final library. The single strand circle DNA was formatted as the final library. The final library was amplified with phi29 to make DNA nanoballs (DNBs) which had more than 300 copies of one molecular, DNBs were loaded into the patterned nanoarray and pair end 100 bases reads were generated on BGIseq500 platform. The raw data were filtered by SOAPnuke software (35). The clean data were mapped on the reference Mus-musculus_GRCm38.p6 with hierarchical indexing for spliced alignment of transcripts (HISAT) software (36). Differentially expressed genes (DEGs) were identified and log2 transformed with DEseq2 (37). The resulting *p* values were adjusted to the Q value (adjusted p value) using the method of multiple testing adjustment with the R package (https://bioconductor.org/packages/release/bioc/html/qvalue.html). The DEGs identified according to the absolute value of log2(fold change) ≥1 and Q value (adjusted *P* value) ≤ 0.05. The enriched Gene Ontology (GO) and Kyoto Encyclopedia of Genes and Genomes (KEGG) pathways of the DEGs were analyzed by ClusterProfiler in RStudio. Heatmaps were drawn with the pheatmap R package.

B. pertussis Challenge

Three weeks after the third immunization, all immunized mice were challenged with strain *B.p-L1 via* aerosol exposure using an aerosolization apparatus (38). Animals were infected *via* the challenge chamber for 30 min. Within the 30 min period, the air sample was removed from the sampling port at 5, 10, 20, and 30 min for assessment of the concentration of *B. pertussis* inside the chamber. The mock-infected animals received PBS aerosol exposure. At the indicated timepoints (2, 4, 7, 11, 16, and 23 days post infection), the lung, trachea, and nasal turbinate were harvested from mice to measure the bacterial burden (**Figure 1**).

Quantitative Real-Time PCR (RT–qPCR)

Total RNA from lung tissues was extracted using TRIzol reagent (Invitrogen, USA) according to the manufacturer's recommendations. Total RNA concentration and quality were measured by using a Thermo Scientific Varioskan Flash (Thermo Fisher Scientific, USA). cDNA was synthesized from 1 μg of RNA

with oligo-dT primers and a PrimeScriptTM RT kit (Accurate Biotechnology, CHN). Cytokine mRNA levels were determined by RT–PCR performed on a LightCycler 96 system (Applied Biosystems, USA) using gene-specific primers (**Supplementary Table 1**) and a SYBR Green Premix Pro Taq HS qPCR Kit (Accurate Biotechnology, CHN). The expression of the housekeeping gene GAPDH was quantified in parallel for RNA normalization. The relative expression of the target genes was calculated by the ΔΔCt method.

Histopathology

For histopathologic analysis, lung tissues from necropsied mice were fixed in 10% neutral buffered formalin, embedded in paraffin, and sectioned at 3-5 μm. Then, the sections were stained with hematoxylin and eosin (H&E) after dehydration. The pathological sections were observed and photographed under a microscope (Leica, Germany).

Statistical Analysis

The results are presented as the means ± SEMs or GMTs and their 95% confidence intervals (CIs). For the data in accordance with normal distribution, one-way ANOVA followed by Tukey's multiple comparisons test was used to compare the difference, while for the data not in accordance with normal distribution, Kruskal-Wallis followed by Dunn's multiple comparisons test was used to compare the difference. A value of $P < 0.05$ was considered significant. Statistical analysis and plots were performed with the Prism version 8.0 (GraphPad Software, Inc.).

RESULTS

c-di-GMP Can Better Promote BMDC Maturation Than Mammalian 2',3'-cGAMP

We studied the maturation efficacy of BMDCs by evaluating the BMDC maturation markers MHC II and the costimulatory molecules CD86, CD80, and CD40. In comparison, c-di-GMP treatment resulted in significantly higher expression of both MHC II and costimulatory molecules (CD86, CD80, and CD40) than 2',3'-cGAMP, as revealed by the enhanced mean fluorescence intensity (MFI) (**Figures 2A, B**). Additionally, we measured the cytokine (IFN-β and TNF-α) levels secreted from BMDCs treated with LPS, PBS, 2',3'-cGAMP, or c-di-GMP. The PBS-treated BMDCs showed undetectable amounts of IFN-β in the culture supernatant. Interestingly, compared with 2',3'-cGAMP treatment, c-di-GMP treatment enhanced IFN-β secretion (**Figure 2C**). Moreover, compared with 2',3'-cGAMP treatment, c-di-GMP treatment caused a slight increase in TNF-α production; however, the difference did not reach statistical significance (**Figure 2D**). Overall, these results indicated that c-di-GMP

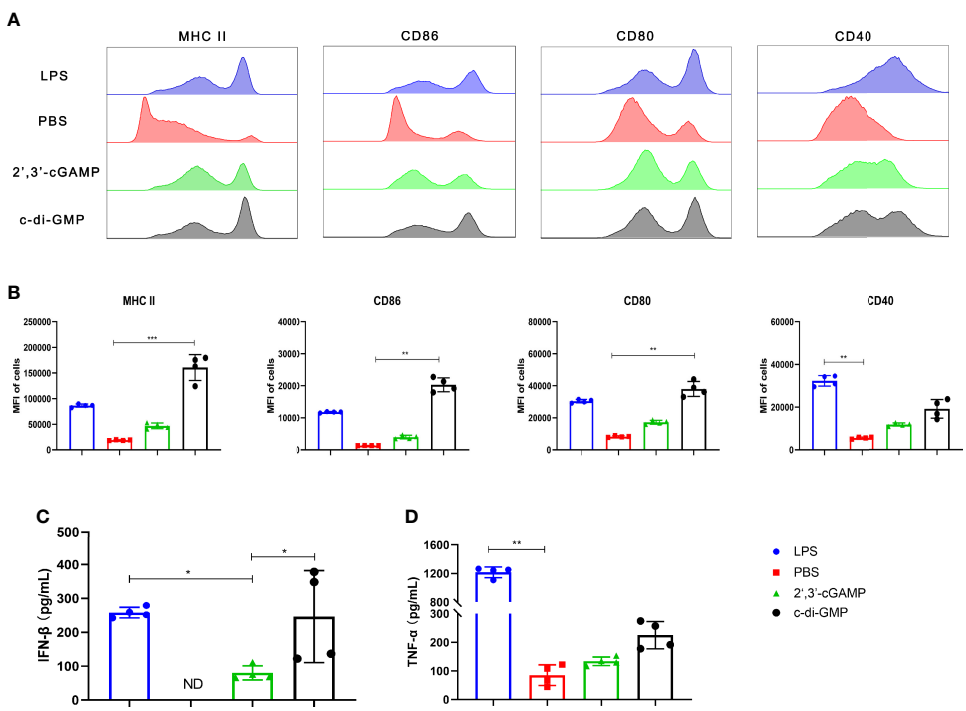

FIGURE 2 | c-di-GMP can better promote BMDC maturation than mammalian 2',3'-cGAMP. BMDCs were incubated with 2',3'-cGAMP (5 μg/mL) or c-di-GMP (5 μg/mL) *in vitro* for 24 h. The cells were treated with lipopolysaccharide (LPS, 1 μg/mL) or sterile PBS as positive and negative controls, respectively. **(A, B)** BMDCs were collected and analyzed *via* flow cytometry to determine the surface expression of MHC II, CD86, CD80, and CD40. **(C, D)** Supernatants were collected, and the levels of IFN-β **(C)** and TNF-α **(D)** were analyzed. The data are expressed as the mean ± SEM of four independent experiments. "ND" indicates that no individuals in this group had detectable levels. The *P* value is indicated as follows: $^{*}P < 0.05$, $^{**}P < 0.01$, $^{***}P < 0.001$.

could better promote the production of the cytokines IFN-β and TNF-α and stimulate DC maturation than 2',3'-cGAMP.

The c-di-GMP-Adjuvanted aP Vaccine Elicits Robust Humoral and Mucosal Humoral Responses

To evaluate the systemic and mucosal humoral immune responses induced by different vaccines (**Table 1**), PT-, FHA-, and PRN-specific antibodies in serum, nasal washes (NW), and bronchoalveolar lavage fluid (BALF) were detected using ELISA method, and splenocytes and pneumonocytes producing antigen-specific IgA or IgG were detected using the ELISpot method at 14 days after the third immunization.

In serum, the aP+c-di-GMP group vaccinated *via* IN administration (aP+c-di-GMP/IN) showed comparable levels of PT-, FHA-, and PRN-specific IgG as the aP+Al(OH)$_3$ group vaccinated *via* IP administration (aP+Al(OH)$_3$/IP), but both groups showed higher PT-specific IgG than the group vaccinated with aP vaccine without any adjuvant (aP/IN) or aP+2',3'-cGAMP *via* IN immunization (aP+2',3'-cGAMP/IN) (**Figure 3A**).

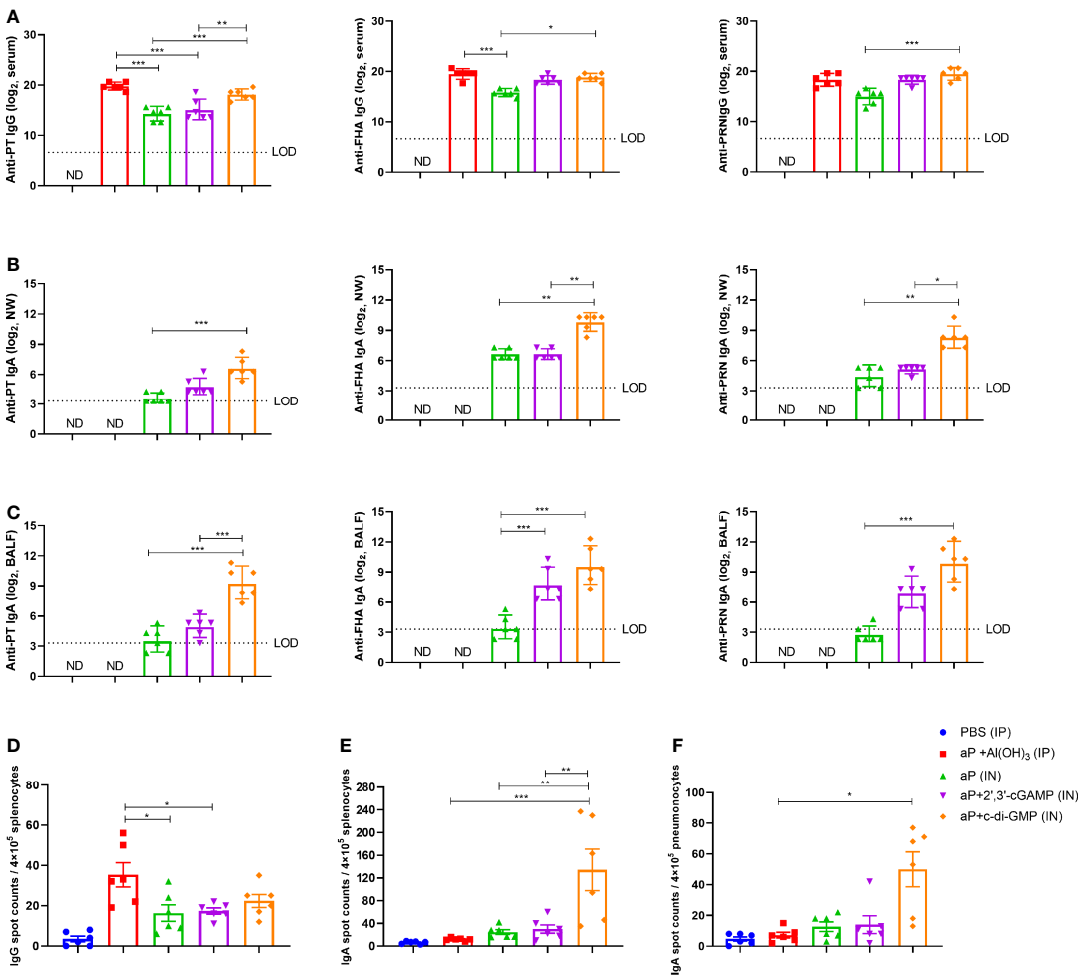

FIGURE 3 | c-di-GMP elicits robust systemic and mucosal humoral responses to the acellular pertussis (aP) vaccine. Mice were intranasally administered the aP vaccine alone or adjuvanted with 2',3'-cGAMP or c-di-GMP three times at three-week intervals and euthanized on day 14 after the last immunization. These groups were compared to a group that received a reference alum-adjuvanted aP vaccine *via* the intraperitoneal (IP) route three times at three-week intervals. Mice intranasally immunized with PBS served as the control group. ELISAs were used to compare antibody responses from mice immunized with different vaccines. ELISpot was conducted to assay the antibody-secreting splenocytes and pneumonocytes producing IgA or IgG against pertussis-specific antigens. **(A)** Total serum IgG titers against pertussis toxoid (PT), filamentous hemagglutinin (FHA), and pertactin (PRN) at day 14 after the last immunization. **(B)** Nasal wash (NW) IgA titers against PT, FHA, and PRN at day 14 after the last immunization. **(C)** Bronchoalveolar lavage fluid (BALF) IgA titers against PT, FHA, and PRN at day 14 after the last immunization. **(D)** Spleen tissues were harvested for the detection of PT-, FHA-, and PRN-specific IgG-secreting cells by ELISpot assay. **(E, F)** Spleen **(E)** and lung **(F)** tissues were assayed by ELISpot to assess PT-, FHA-, and PRN-specific IgA-secreting cells. Data are expressed as the mean ± SEM. The antibody results are expressed as the GMTs and their 95% confidence intervals (CIs). The dotted line indicates the limit of detection (LOD), and values that fell below the detection limit are represented by the limit of detection value for statistical analysis. "ND" indicates that no individuals in this group had detectable levels. Statistical differences between the results of vaccine-immunized groups and those of the PBS group are not marked. The *P* value is indicated as follows: **P* < 0.05, ***P* < 0.01, ****P* < 0.001.

In addition, the FHA- and PRN-specific IgG of the aP+c-di-GMP/IN group was not significantly different from that of the aP-2',3'-cGAMP group but was significantly higher than that of the aP/IN group (**Figure 3A**). The aP+c-di-GMP/IN treatment also elicited higher serum PT-, FHA-, and PRN-specific IgA antibody levels than the aP+$Al(OH)_3$/IP treatment and higher PRN-specific IgA antibody levels than the aP/IN treatment (**Supplementary Figure 1A**). Regarding antibody subclasses (IgG1 and IgG2a), aP+c-di-GMP/IN-immunized mice showed higher serum PT-specific IgG1 than aP/IN-immunized mice but comparable FHA- and PRN- specific IgG1 than aP+$Al(OH)_3$/IP-immunized mice (**Supplementary Figures 1B–D**). In contrast, compared to aP+$Al(OH)_3$/IP and aP/IN treatment, aP+c-di-GMP/IN treatment induced a significant increase in the levels of IgG2a against PT and PRN, and there was no significant difference in the levels of IgG2a against PT, FHA, and PRN between the two CDN-adjuvanted aP vaccine groups (**Supplementary Figures 1B–D**). These data suggested that the c-di-GMP-adjuvanted aP vaccine delivered *via* IN administration induced a balanced Th1 and Th2 immune response.

Regarding nasal washes (NW), aP+c-di-GMP/IN-vaccinated mice showed higher PT, FHA, and PRN-specific IgA levels than aP/IN-vaccinated mice and higher FHA and PRN-specific IgA levels than aP+2',3'-cGAMP/IN-vaccinated mice, while there were no differences between the aP/IN and aP+2',3'-cGAMP/IN groups (**Figure 3B**). Regarding BALF, aP+c-di-GMP/IN-vaccinated mice also showed the higher levels of IgA against PT, FHA, and PRN than aP/IN-vaccinated mice, but there was no significant difference in anti-PT, FHA, and PRN IgA levels in BALF between the two CDN-adjuvanted groups (**Figure 3C**).

For the antibody-secreting splenocytes and pneumonocytes producing IgA or IgG, the number of B cells secreting PT-, FHA-, and PRN-specific IgG in splenocytes from the alum-adjuvanted aP group was higher than that from the aP/IN and aP+2',3'-cGAMP/IN groups, but it showed no difference from the aP+c-di-GMP/IN group (**Figure 3D**). However, in the pneumonocytes, both CDNs adjuvanted with aP vaccines produced a slight increase in the number of IgG-producing B cells (**Supplementary Figure 1E**). Of note, a higher frequency of B cells secreting anti-PT, anti-FHA, or anti-PRN IgA was observed in splenocytes from the aP+c-di-GMP/IN group than in those from all other groups, with a 4.5-fold higher frequency than in the aP+2',3'-cGAMP/IN group (**Figure 3E**). And a higher frequency of B cells secreting anti-PT, anti-FHA, or anti-PRN IgA was also observed in pneumonocytes from the aP+c-di-GMP/IN group than in those from aP/IN group (**Figure 3F**). Although the frequency of B cells secreting anti-PT, anti-FHA, or anti-PRN IgA in pneumonocytes did not show statistical difference between the two CDN-adjuvanted groups, aP+c-di-GMP/IN-immunized mice caused a slight increase with 3.7-fold higher frequency than in the aP+2',3'-cGAMP/IN group (**Figure 3F**). Taken together, these results suggest that aP+c-di-GMP treatment can elicit stronger systemic and mucosal humoral responses than 2',3'-cGAMP.

Intranasal Immunization With the c-di-GMP-Adjuvanted aP Vaccine Induces Strong Systemic and Mucosal Cellular Immune Responses and Potent Tissue-Resident Memory (TRM) Cells

The *B. pertussis*-specific cellular immune responses were assessed *in vitro* by exposing splenic and pulmonary lymphocytes from immunized mice to the specific antigens PT, FHA, and PRN. Regarding frequencies of IFN-γ secreting T cells, aP+c-di-GMP/IN-treated mice showed increased frequency, but there was no significant difference compared to mice in other groups in splenic lymphocytes (**Figure 4A**), while the frequency was significantly higher than aP/IN-immunized mice, reaching a mean response of 542 spot-forming cells (SFC) per 4×10^5 input splenocytes (**Figure 4D**). For frequencies of IL-17-secreting T cells, aP+c-di-GMP/IN-treated mice showed higher frequencies than mice in aP/IN and aP+$Al(OH)_3$/IP groups and comparable frequencies to aP+2',3'-cGAMP/IN-treated mice in splenic lymphocytes and comparable frequencies to aP+2',3'-cGAMP/IN- and aP/IN-treated mice but higher than aP+$Al(OH)_3$/IP- treated mice in pulmonary lymphocytes (**Figures 4B, E**). For IL-4-secreting T cells, the aP+c-di-GMP/IN group showed levels comparable to those in the aP+$Al(OH)_3$/IP group but higher levels than the aP/IN and aP+2',3'-cGAMP/IN groups in the spleen (**Figure 4C**), while the level increased but did not show significant differences from that in all other vaccine groups in pulmonary lymphocytes (**Figure 4F**).

To further examine whether TRM cells were induced by CDN-adjuvanted aP vaccines, flow cytometry was performed on lung tissues from mice (the TRM cell gating strategy is shown in **Supplementary Figure 2**). Not surprisingly, IP administration of the aP+$Al(OH)_3$/IP vaccine did not generate an increased population of lung TRM cells (**Figures 4G, H**). IN immunization with aP vaccine alone also failed to promote the population of lung TRM cells (**Figures 4G, H**), indicating that mucosal immunization alone is not sufficient to induce lung TRM cells. In contrast, mice immunized with aP+2',3'-cGAMP/IN or aP+c-di-GMP/IN showed significantly promotion of the population of lung TRMs (**Figures 4G, H**). Together, these data suggested that IN immunization with both CDN-adjuvanted aP vaccines promoted the generation of CD4+ TRM populations.

The c-di-GMP-Adjuvanted aP Vaccine Generates Mixed Th1, Th2, and Th17 Responses

After incubation with PT, FHA, and PRN for 3 days, cultures of splenic and pulmonary lymphocytes isolated after the third immunization were tested for cytokines in the supernatant. In culture supernatants of splenic lymphocytes, the levels of cytokines associated with Th1 responses (IFN-γ, TNF-α, and IL-2) and Th17 responses (IL-22) were significantly increased in the aP+c-di-GMP/IN group compared with those in the aP+$Al(OH)_3$/IP or aP/IN group (**Figures 5A, B**). The aP+c-di-GMP/IN treatment also induced a slight increase in Th1 (IFN-γ, TNF-α, and IL-2) and Th17 (IL-17A and IL-22) related cytokine levels

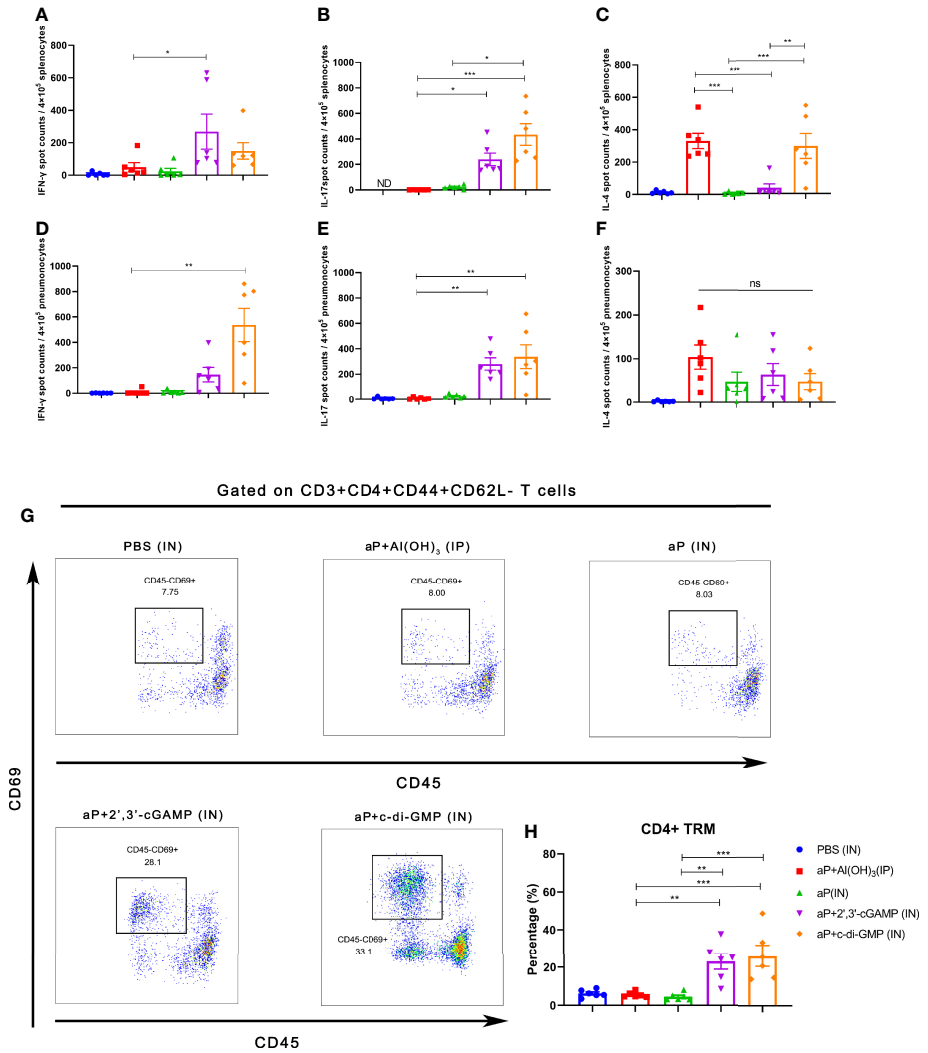

FIGURE 4 | Intranasal immunization with a CDN-adjuvanted aP vaccine induces strong systemic and mucosal cellular immune responses and potent TRM cells. **(A–C)** Splenocytes were assayed by ELISpot assay for IFN-γ **(A)**, IL-17 **(B)**, and IL-4 **(C)** cell production after restimulation with the antigens PT (2 μg/mL), FHA (2 μg/mL), and PRN (2 μg/mL) (n=6 mice per group). **(D-F)** Lung tissues were assayed by ELISpot assay for cell production of IFN-γ **(D)**, IL-17 **(E)**, and IL-4 **(F)** after restimulation with the antigens PT (2 μg/ml), FHA (2 μg/ml), and PRN (2 μg/ml) (n=6 mice per group). **(G, H)** Mice were i.v. injected with an anti-CD45 antibody 10 min prior to euthanasia. The lungs were harvested, and lung mononuclear cells were stained with mAbs specific for CD3, CD4, CD44, CD62L, and CD69 for flow cytometric analysis. The results are expressed as CD4+ tissue resident cells (TRM): CD3+CD4+CD44+CD62L-CD45-CD69+; representative flow cytometry gating strategies for CD4+ TRM cells in the lungs are shown in **Supplementary Figure 2** (n=6 mice per group). Representative dot plots from flow cytometry analysis in **(G)** show the identification of CD4+ TRM cells. The relative proportion of CD4+ TRM cells in the lung tissues induced by different vaccines is shown in **(H)**. Data are expressed as the mean ± SEM. "ND" indicates that no individuals in this group had detectable levels. The *P* value is indicated as follows: $^{*}P < 0.05$, $^{**}P < 0.01$, $^{***}P < 0.001$, ns, no significance.

than aP+2′, 3′-cGAMP/IN treatment, but there was no significant difference (**Figures 5A, B**). Compared with aP/IN and aP+c-di-GMP/IN groups, the aP+Al(OH)$_3$/IP group produced the higher IL-5, which is a Th2-related cytokine, in the supernatant of splenic lymphocyte cultures, while there was no significant difference in IL-6 levels between the aP+Al(OH)$_3$/IP and aP+c-di-GMP/IN groups (**Figure 5C**).

In culture supernatants of pulmonary lymphocytes, similar to the results for splenic lymphocytes, compared with aP+Al(OH)$_3$/IP or aP/IN treatment, aP+c-di-GMP/IN treatment greatly promoted the secretion of Th1 and Th17 response-related cytokines by pulmonary lymphocytes (**Figures 5D, E**). And aP+c-di-GMP/IN treatment also induced a slight increase in Th1 (IFN-γ, TNF-α, and IL-2) and Th17 (IL-17A and IL-22) related cytokine levels than aP+2′, 3′-cGAMP treatment, but there was no significant difference (**Figures 5D, E**). Similarly, the alum-adjuvanted aP vaccine induced higher IL-5 but not IL-6 levels than all other treatments, and the difference between the 2′, 3′-cGAMP/IN and aP+c-di-GMP/IN treatments was not significant (**Figure 5F**). Overall, these results indicated that IN

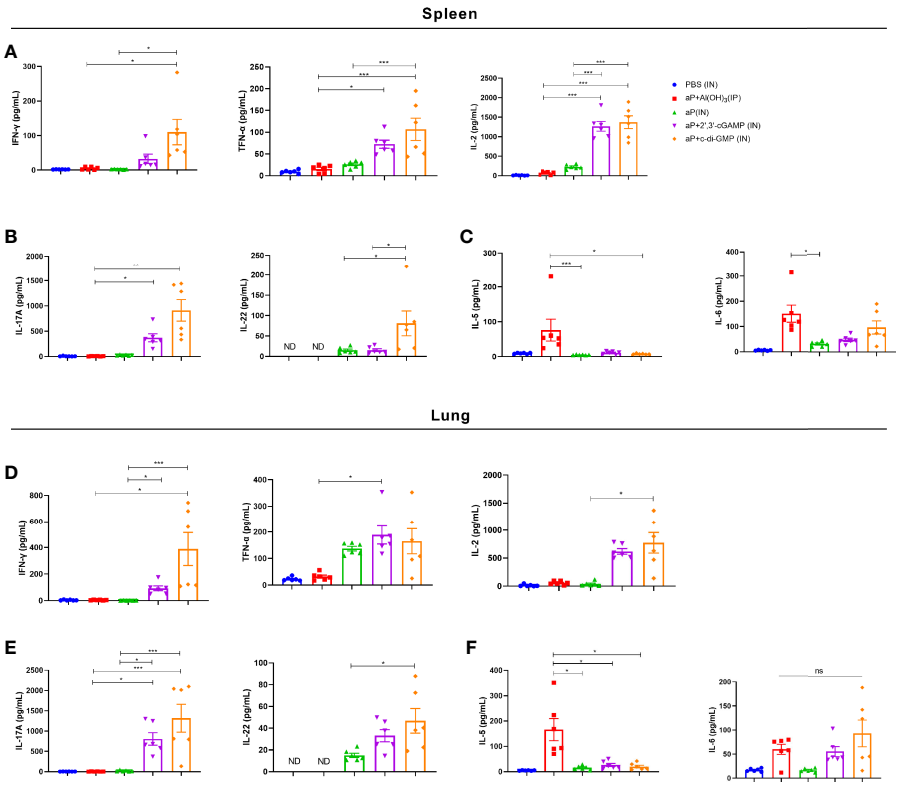

FIGURE 5 | c-di-GMP-adjuvanted aP enhances the expression of Th1/Th17-related cytokines in both splenic and pulmonary lymphocytes. Two weeks after the third immunization, splenic and pulmonary lymphocytes were isolated. Cells were cultured at a concentration of 2 × 10^6/ml at 37°C with 5% CO_2 and stimulated with the *B. pertussis*-specific antigens PT (2 μg/mL), FHA (2 μg/mL), and PRN (2 μg/mL). After incubation for 3 days, the culture supernatant was collected, and multiple cytokines were assayed by ELISA. **(A)** Th1 response-associated cytokines (IFN-γ, TNF-α, and IL-2), **(B)** Th17 response-associated cytokines (IL-17A and IL-22), and **(C)** Th2 response-associated cytokines (IL-5 and IL-6) in the culture supernatant of splenic lymphocytes. **(D)** Th1 response-associated cytokines (IFN-γ, TNF-α, and IL-2), **(E)** Th17 response-associated cytokines (IL-17A and IL-22), and **(F)** Th2 response-associated cytokines (IL-5 and IL-6) in the culture supernatant of pulmonary lymphocytes. Data are expressed as the mean ± SEM. "ND" indicates that no individuals in this group had detectable levels. Statistical differences between the results of vaccine-immunized groups and those of the PBS group are not marked. The *P* value is indicated as follows: $^*P < 0.05$, $^{**}P < 0.01$, $^{***}P < 0.001$, ns, no significance (n=6).

delivering c-di-GMP-adjuvanted aP vaccine generates balanced Th1, Th2, and Th17 responses in both the spleen and lungs and that this effect is better than that with the 2′, 3′-cGAMP-adjuvanted aP vaccine.

The c-di-GMP-Adjuvanted aP Vaccine-Immunized Mice Upregulated Th1, Th2, and Th17 Cell Differentiation and IgA Production Signaling in the Nasal Mucosa

RNA-seq analysis of the nasal mucosa in all immunized mice revealed 44 (7 upregulated, 37 downregulated), 42 (37 upregulated, 5 downregulated), 561 (407 upregulated, 154 downregulated), and 2076 (860 upregulated, 1216 downregulated) DEGs (|fold change| ≥2) in aP+$Al(OH)_3$/IP-, aP/IN-, aP+2',3'-cGAMP/IN-, and aP+c-di-GMP/IN-immunized mice, respectively, compared with PBS (IN)-immunized mice (**Figure 6A**).

The KEGG pathway functional enrichment results showed 20 top significant pathways (**Figure 6B**), among which Th1 and Th2 cell differentiation, Th17 cell differentiation, and IgA production signaling pathways were observed. Using a heatmap, 59 genes involved in these three signaling pathways were identified. Th1 and Th2 cell differentiation-, Th17 cell differentiation-, and IgA production signaling pathway-related genes were noticeably upregulated in aP+c-di-GMP-immunized mice (**Figure 6C**).

The c-di-GMP-Adjuvanted aP Vaccine Reduces *B. pertussis* Burden in the Respiratory Tract

To assess protective efficacy against pertussis, immunized mice were challenged with aerosolized *B. pertussis*, and the bacterial colony-forming units (CFU) in nasal, tracheal, and lung homogenates were counted at the indicated times. aP+c-di-GMP/IN immunization provided a high level of protection against lung infection with *B. pertussis*, resulting undetectable bacterial colonization at 4 days post infection (dpi) with the lowest level of the areas under the bacterial clearance curve (AUC, 0.7195) among all groups (**Figures 7A, B**). When

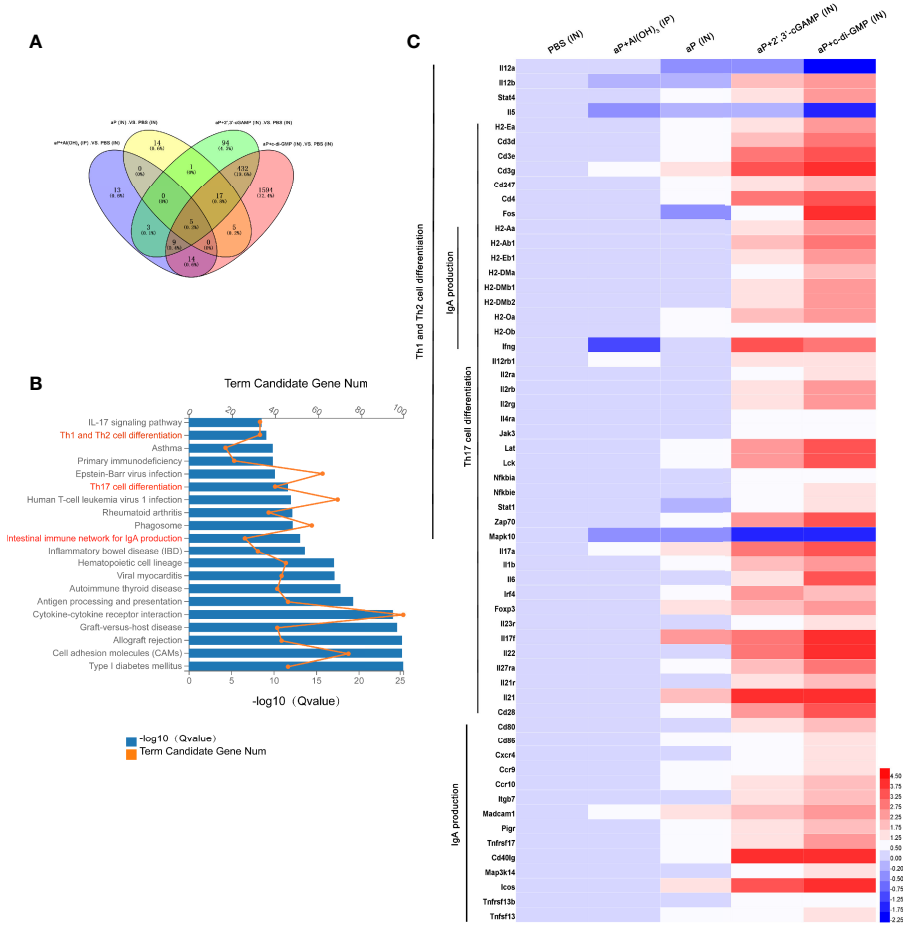

FIGURE 6 | Differentially expressed genes (DEGs) in the nasal mucosa from c-di-GMP-adjuvanted aP immunized mice. **(A)** The DEGs for different vaccine-immunized mice. PBS-immunized mice at 14 days after the last immunization were used for comparison, and the overlap is shown as a Venn diagram. **(B)** The top 20 and KEGG pathways of the DEGs detected in the nasal mucosa of aP+c-di-GMP/IN- and PBS/IN-immunized mice are shown. **(C)** RNA-seq heatmap for the nasal mucosa from mice immunized with PBS/IN, aP+Al(OH)3/IP, aP/IN, aP+2',3'-cGAMP/IN, or aP+c-di-GMP/IN (n = 5). The heatmap shows 59 significantly upregulated genes in aP+c-di-GMP/IN-immunized mice compared to those in other vaccine-immunized mice. Red (4.50) to blue (-2.25) were ranked by values of log2(value of gene expression).

compared with those in PBS-immunized mice, the CFU counts in the lungs after *B. pertussis* aerosol challenge were significantly reduced in mice IP immunized with aP+Al$(OH)_3$, resulting in undetectable CFU counts at 7 dpi and an AUC of 1.385, but the reduction was not as rapid as that seen in mice IN immunized with the aP+c-di-GMP vaccine (**Figures 7A, B**). Additionally, there was a significant reduction in the number of CFU in the lungs from aP (IN)- and aP+2',3'-cGAMP (IN)-immunized mice at 4 dpi; however, these changes were not observed at 2 dpi, and the AUC of each was very similar (aP/IN: 6.209; aP+2',3'-cGAMP/IN: 5.739) (**Figures 7A, B**).

In the trachea, *B. pertussis* colonization was not detected at any indicated time in the aP+di-GMP/IN group (**Figures 7C, D**). aP/IN- and aP+2',3'-cGAMP/IN-immunized mice showed very low bacterial burdens at 2 dpi and 4 dpi, with AUCs of 0.30 and 0.24, respectively (**Figures 7C, D**). Surprisingly, aP+Al$(OH)_3$/IP group mice did not exhibit detectable CFU counts in the trachea at 2 dpi; however, rebound was observed at 4 dpi, the numbers peaked at 7 dpi, and the bacteria were completely cleared at 23 dpi (**Figures 7C, D**).

Regarding nasal homogenate, PBS-immunized mice were heavily colonized at 2 days post *B. pertussis* challenge and reached the highest level, 1.0×10^6 CFU/mL, at 7 dpi; the number of colonies gradually decreased until 23 dpi, with an AUC of 16.36 (**Figures 7E, F**). In contrast, mice immunized with aP+c-di-GMP/IN had very low CFU counts at 2 dpi and 4 dpi, and bacteria were completely cleared by day 7, with an AUC of 1.20 (**Figures 7E, F**). aP+2',3'-cGAMP/IN treatment also resulted in protection in the nose, although not as effectively as that seen with aP+c-di-GMP/IN treatment, with an AUC of 4.191 (**Figures 7E, F**). Intriguingly, aP+Al$(OH)_3$/IP treatment did not confer any protection against *B. pertussis* colonization of the mouse nose, resulting in a steady level of nasal colonization at 10^3 CFU/mL through at least 23 dpi (**Figures 7E, F**). In contrast,

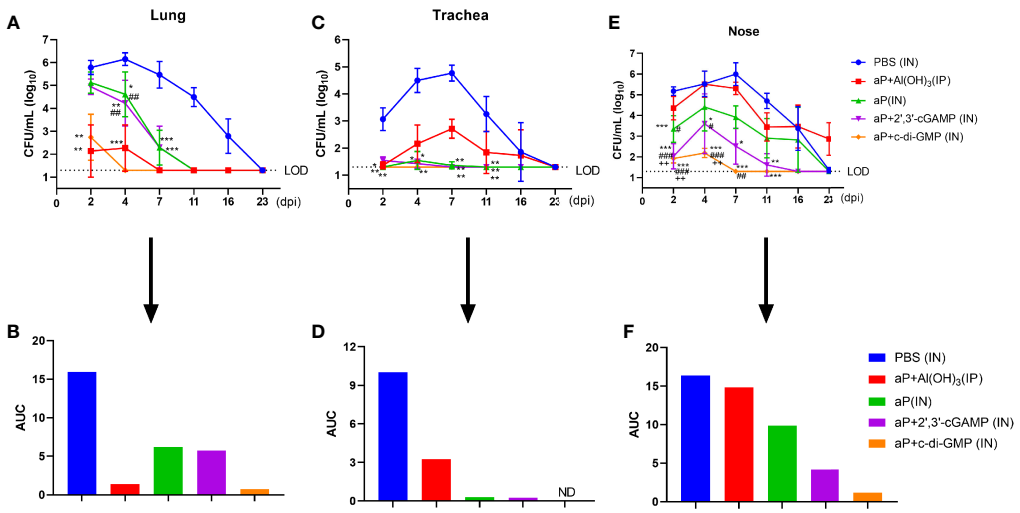

FIGURE 7 | Intranasal administration of the c-di-GMP-adjuvanted aP vaccine reduces the respiratory *B. pertussis* burden. Mice were intranasally administered aP vaccine alone or adjuvanted with 2',3'-cGAMP or c-di-GMP three times at three-week intervals and euthanized on day 14 after the last immunization. These groups were compared to a group that received a reference alum-adjuvanted aP vaccine *via* the intraperitoneal (IP) route three times at three-week intervals. Mice intranasally immunized with PBS served as the control group. Immunized mice were challenged by exposure to live *B. pertussis* three weeks after the third immunization. Analysis of bacterial burden was determined at 2, 4, 7, 11, 16, and 23 dpi. Bacteria were quantified by counting CFU from serial dilutions following challenge. **(A)** CFU counts were determined from lung homogenate. **(B)** The areas under the bacterial clearance curves corresponding to the curves of CFU counts from lung homogenate. **(C)** CFU counts were determined from tracheal homogenate. **(D)** The areas under the bacterial clearance curves corresponding to the curves of CFU counts from tracheal homogenate. **(E)** CFU counts were determined from nasal homogenate. **(F)** The areas under the bacterial clearance curves corresponding to the CFU counts from nasal homogenate. The results are the mean ± SEM (n = 5). The dashed line represents the lower limit of detection (LOD). ND" indicates that no individuals in this group had detectable levels. The *P* value is indicated as follows: $^{*}P < 0.05$, $^{**}P < 0.01$, $^{***}P < 0.001$ vs. PBS-immunized mice; $^{\#}P < 0.05$, $^{\#\#}P < 0.01$, $^{\#\#\#}P < 0.001$ vs. alum-adjuvanted aP vaccine-immunized mice; and $^{++}P < 0.01$ vs. aP vaccine-immunized mice.

the PBS-immunized mice completely cleared the nasal infection by that time. Together, these results indicated that IN immunization with the aP+c-di-GMP/IN vaccine enabled accelerated bacterial clearance in the respiratory tract following *B. pertussis* infection compared to that in aP+Al(OH)$_3$/IP- or aP-2',3'-cGAMP/IN-immunized animals.

IN Immunization With the c-di-GMP-Adjuvanted aP Vaccine Protects Mice Against Lung Disease Caused by *B. pertussis* Infection

We evaluated the pathological changes in the different vaccination groups after *B. pertussis* challenge. We observed lung histopathological changes by hematoxylin & eosin (H&E) staining at 4 and 7 dpi. Large amounts of inflammatory cell infiltration, especially neutrophils (blue arrows), lung interstitial thickening, and severe bronchial obstruction, were observed in the lungs of PBS-immunized mice after challenge (**Figure 8A**). A small quantity of inflammatory cells and relatively slight bronchial obstruction were also observed in lungs from aP/IN- or AP+2',3'-cGAMP/IN-immunized mice (**Figure 8A**). Both aP+Al(OH)$_3$/IP- and aP+c-di-GMP/IN-immunized mice showed less evidence of histopathological lesions in the lungs, especially no bronchial obstruction (**Figure 8A**). Interestingly, eosinophil infiltration was observed in mice IP immunized with the alum-adjuvanted aP vaccine, which was not found in other groups. And bronchial-associated lymphoid tissue (BALT) hyperplasia was observed in three groups of mice IN immunized vaccines, and with the c-di-GMP-adjuvanted aP vaccine most obviously, which was not found in control mice or mice IP immunized with the alum-adjuvanted aP vaccine (**Figure 8A** and **Supplementary Figure 3**).

Moreover, mRNA levels of cytokines in the lung tissues on 2 and 4 dpi were detected by RT-qPCR. The production of proinflammatory cytokines (IL-1β, TNF-α, and IL-6) in the lung tissues of *B. pertussis*-infected mice was expressed as a fold change compared to that in lung tissues from mock-infected mice (**Figure 8B**). At 2 dpi, PBS-immunized mice showed induction of only IL-1β levels in the lung tissues. However, the mRNA levels of IL-1β, TNF-α, and IL-6 were significantly increased at 4 dpi and were 14-, 5- and 28-fold higher than the levels in mock-infected lung tissues, respectively (**Figure 8C**). As expected, the levels of IL-1β, TNF-α, and IL-6 from mice immunized with aP+Al(OH)$_3$/IP did not show obvious changes at 2 dpi and 4 dpi compared with those from mock-infected mice (**Figures 8B, C**). Interestingly, both CDN-adjuvanted groups showed higher TNF-α production than the mock-infected group at the two detected time points (**Figures 8B, C**). The difference was that the aP/IN and aP + 2',3'-cGAMP/IN groups showed a slight increase and indistinguishable IL-6 production at 2 dpi compared with the mock-infected group, while no increase was observed in the aP+c-di-GMP/IN group (**Figures 8B, C**). We also analyzed the Th cell bias in the lungs of immunized mice at 2 dpi and 4 dpi by detecting the mRNA levels of IFN-γ, IL-17A, and IL-5, which are indicators of Th1, Th17, and Th2 activation, respectively. Mice immunized with aP+c-di-GMP/

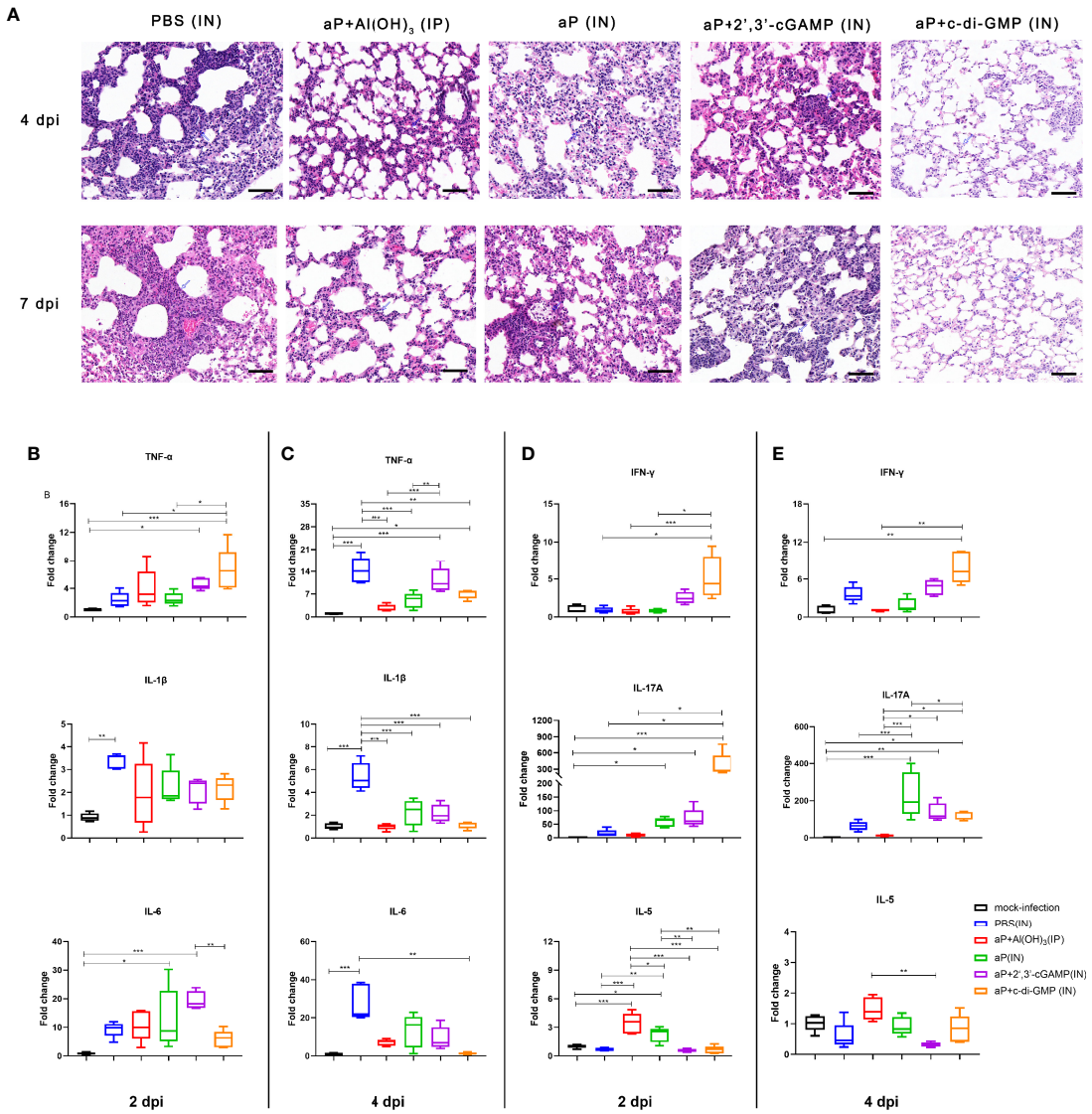

FIGURE 8 | IN immunization with the c-di-GMP-adjuvanted aP vaccine protects mice against lung disease caused by *B. pertussis* infection. **(A)** Images showing H&E staining following infection with *B. pertussis*. The images shown are from 4 dpi and 7 dpi for all groups. Scale bar, 50 μm. Each image is representative of a group of 5 mice at 4 dpi and 7 dpi. **(B–E)** Total RNA was extracted from the lungs of mice euthanized at day 2 and day 4 after *B. pertussis* challenge. Mouse TNF-α, IL-1β, and IL-6 mRNA levels at 2 dpi **(B)** and 4 dpi **(C)** were quantified by RT–PCR. Mouse IFN-γ, IL-17A, and IL-5 mRNA levels at 2 dpi **(D)** and 4 dpi **(E)** were quantified by RT–PCR. GAPDH mRNA was used as an internal control. Data are shown as the fold change in gene expression compared to that in mock-infected animals (unimmunized and challenged with PBS) after normalization. n = 5 animals for each time point. Data are expressed as the mean ± SEM. The *P* value is indicated as follows: $^{*}P < 0.05$, $^{**}P < 0.01$, $^{***}P < 0.001$. See also **Supplementary Figure 3**.

IN showed the higher levels of IL-17A and IFN-γ gene expression at 2 dpi than PBS- and aP+$Al(OH)_3$/IP- immunized mice (**Figure 8D**). The aP/IN and aP+2',3'-cGAMP/IN groups showed moderate upregulation of IL-17A gene expression at 2 dpi compared with that of the mock-infected group (**Figure 8D**). However, mice immunized with aP+$Al(OH)_3$/IP did not show obvious changes in IL-17A and IFN-γ gene expression at 2 dpi and 4 dpi compared with that of mock-infected mice (**Figures 8D, E**), while they showed a significant increase in IL-5 expression at 2 dpi (**Figure 8D**).

DISCUSSION

Vaccination is important to control *B. pertussis* infection. However, pertussis has reemerged in recent years even with high vaccine coverage, which makes it remaining as a major global public health problem. Indeed, the high incidence of asymptomatic infection and the fact that current aP vaccines cannot prevent *B. pertussis* transmission highlight the necessity to develop a more effective vaccine that can protect against disease and prevent *B. pertussis* infection and transmission

(8–10). Considering that *B. pertussis* is a respiratory pathogen and highly contagious, efficacious prophylaxis would benefit from a mucosal immunization strategy to block bacterial replication at a very early stage and prevent *B. pertussis* infection and transmission. Here, we explored the potential of bacterial-derived c-di-GMP and mammalian 2′,3′-cGAMP as mucosal adjuvants for an aP vaccine against *B. pertussis*. Our results indicated that although both CDN adjuvants could produce in a certain reduction in *B. pertussis* burden in the URT compared with the aP vaccine alone administered *via* the IN route (aP/IN) or a conditional alum-adjuvanted aP vaccine administered *via* the IP route (aP +$Al(OH)_3$/IP), the bacterial-derived c-di-GMP-adjuvanted aP vaccine (aP +c-di-GMP/IN) resulted in stronger systemic and local mucosal immune responses and better inhibited *B. pertussis* replication in both the upper and lower respiratory tract than the mammalian 2′, 3′-cGAMP-adjuvanted aP vaccine (aP+ 2′, 3′-cGAMP/IN).

Although CDN molecules have been explored as mucosal adjuvants, the immunostimulatory and immunoregulatory properties of different CDNs vary significantly (39, 40). Zhang et al. (27) demonstrated that 2′,3′-cGAMP induces stronger type I IFN production than other CDNs derived from bacteria. However, in the present study, we found that c-di-GMP elicited more IFN-β production in BMDCs than 2′,3′-cGAMP, resulting in stronger capacities to promote the activation and maturation of BMDCs. One of the reasons for this phenomenon may be related to different cell treatments. In a study by Zhang et al. (27), cells were permeabilized with digitonin, which allowed CDNs to more easily enter the intracellular space, where 2′,3′-cGAMP and STING possessed higher affinity than sting and other CDNs, resulting in more IFN-β production. In addition, in the current study, we found that c-di-GMP showed a better immunologic adjuvant effect for the aP vaccine than 2′, 3′-cGAMP *in vivo*. Blaauboer et al. (41) also found that c-di-GMP elicited higher antigen-specific antibody production, stronger T cell responses, and better protection against pneumococcal infection *in vivo* than mammalian 2′,3′-cGAMP. Indeed, CDNs, which were unable to penetrate the cell membrane and bind STING protein, enhanced antigen uptake *via* both pinocytosis and receptor-mediated endocytosis. However, the phosphodiester endogenic mammalian 2′,3′-cGAMP is unstable and more likely to be hydrolyzed by phosphodiesterases, especially ectonucleotide phosphodiesterase (ENPP1) of mammalian cells (42, 43). Thus, we considered that endogenous mammalian 2′,3′-cGAMP is more easily hydrolyzed by phosphodiesterases *in vivo*, which may result in its inferior adjuvant properties compared to bacterial-derived c-di-GMP. However, the specific mechanisms need to be further studied.

In the present study, aP+c-di-GMP/IN treatment significantly enhanced both systemic and mucosal immune responses and resulted in the fastest clearance of *B. pertussis* and an almost undetectable bacterial load in the respiratory tract among all vaccination regimens. In addition to strong IgG antibody responses in serum, strong mucosal humoral and Th17 responses should be considered important factors in bacterial clearance from the respiratory tract. In the current study, we found the highest level of IL-17-producing cells in the lung tissues in the aP+c-di-GMP/IN group after the last immunization, among all four vaccination groups. Moreover, we clearly identified significantly upregulated IL-17 expression in the lungs of aP+c-di-GMP/IN-immunized mice at 2 dpi. Substantial evidence has shown that Th17 and IL-17 play a pivotal role in protection against *B. pertussis* infection (13, 44, 45). Other intranasally delivered adjuvants, such as TLR agonists and combinations of TLR2 agonists and STING agonists, when delivered with *B. pertussis* antigens in mice, have all been shown to induce robust Th17 responses and confer *B. pertussis* control (14, 46). Thus, aP+c-di-GMP/IN inducing efficient Th17-related immune responses may contribute to resulting in rapid clearance of *B. pertussis* from the respiratory tract, with a lower bacterial load in the present study. More importantly, the aP+c-di-GMP/IN-immunized mice showed significantly higher IgA levels in NWs than the aP/IN- and aP+2',3'-cGAMP/IN-immunized mice after the third immunization, which was also demonstrated by the upregulation of IgA production-associated genes in the nasal mucosa. Mucosal IgA is important to protect the nasal mucosa against *B. pertussis*. Solans et al. (47) found that BPZE1, the only mucosal aP vaccine candidate tested in clinical trials, induced protection in the nasal mucosa that was significantly diminished in IgA-deficient animals. Neither NW secretory IgA (sIgA) nor serum IgA from *B. pertussis* convalescent patients could inhibit adherence of *B. pertussis* to respiratory epithelial cells (48). In addition, sIgA production could be mediated by IL-17 (47), and IL-17 was central to protection against nasal infection with *B. pertussis* by recruiting neutrophils, especially siglec-F+ neutrophils (49). The RNA-seq results in this study suggested that the levels of many genes associated with Th17 proliferation were increased in the nasal mucosa of aP+c-di-GMP/IN mice, which may contribute to the clearance of bacteria from the nasal mucosa. Thus, we considered that the robust Th17 response and high level of IgA induced by aP+c-di-GMP/IN may contribute to the strong protection against *B. pertussis* in the entire respiratory tract, especially the URT. Third, Th1-related immune response elements, such as CD4+ T cells, may also contribute to immune protection during *B. pertussis* infection through IFN-γ-dependent mechanisms (45). We found a higher level of IFN-γ-producing cells in the lung tissues in the aP+c-di-GMP/IN-treated mice than in the aP+2',3' cGAMP-/IN-treated mice after the last immunization. Furthermore, we identified significantly upregulated IFN-γ expression in the lung in aP+c-di-GMP/IN mice 2 dpi. Evidence from both mouse models and clinical experiments has shown that cellular responses mediated by Th1 cells play an important role in protective immunity against *B. pertussis* and wP vaccine-mediated immune protection (44, 50–53). In addition, IFN-γ receptor knockout mice developed a disseminated lethal infection after challenge with *B. pertussis* (54). Moreover, many studies have shown that satisfactory protective results have been obtained *via* the addition of Th1-polarizing adjuvants to the existing aP vaccine (46, 55, 56). Thus,

we considered that strong Th1 responses induced by aP+c-di-GMP/IN may also contribute to the clearance of bacteria from the airway.

One of the interesting results in this study was that although aP+c-di-GMP/IN provided the best protection for the lungs of the mice, with the fastest clearance of *B. pertussis*, followed by aP+Al$(OH)_3$/IP, there was no significant difference between aP+2',3'-cGAMP/IN and the nonadjuvanted aP vaccine administered *via* IN (aP/IN). In agreement with previous studies, mice immunized with aP+Al$(OH)_3$/IP showed a small, limited amount of *B. pertussis* colonization and rapid clearance in the lungs after *B. pertussis* infection, causing only minor pathological damage to the lungs (8, 57). Compared with those from control mice or the three groups of IN immunized mice, lung tissue sections stained by HE from aP+Al$(OH)_3$/IP mice showed that pulmonary neutrophilia was reduced, whereas eosinophilia was strongly increased, which we have rarely noticed previously. Moreover, IL-5 expression was significantly increased in the lung tissues of aP+Al$(OH)_3$/IP-immunized mice after *B. pertussis* challenge. Verhoef et al. (58) found that IL-5 from type 2 innate lymphoid cells (ILC2s) in the lung could recruit eosinophils. In addition, clinical studies have demonstrated that eosinophil counts correlated with survival among patients with acute pulmonary infections (59, 60). Furthermore, a study from Linch et al. (61) highlighted that eosinophils possess strong antibacterial properties. Krishack et al. (62) revealed that eosinophilia was critical for the protection against *Staphylococcus aureus*, which further suggested a potential protective effect of eosinophilia against bacterial infection. Thus, we inferred that moderate infiltration of eosinophils in the lung tissues after *B. pertussis* challenge may contribute to the aP+Al$(OH)_3$/IP protection mechanism, except for the high level of antibodies. Another interesting result in this study was that we observed a phenomenon similar to that in a study by Holubová et al. (57) in which an IP administered commercial alum-adjuvanted aP vaccine inhibited *B. pertussis* clearance from the nasal mucosa in a mouse model. In this study, mice given the aP+Al$(OH)_3$/IP vaccine stabilized at a high level of *B. pertussis* colonization in NWs even at 23 dpi, with an average of 10^3 CFU/mL. However, the control mice receiving only PBS had cleared the nasal bacteria by that time. Expectedly, mice IN immunized with the aP vaccine showed a lower bacterial load in the nasal mucosa than control mice, although both cleared nasal *B. pertussis* by 23 dpi. Indeed, Dubois et al. (63) also found that aP+Al$(OH)_3$/IP immunization prolonged nasal carriage of *B. pertussis*. They further revealed the mechanism of this phenomenon in which the predominant Th2 immune response induced by aP+Al$(OH)_3$/IP immunization may suppress the mucosal Th17 memory response, resulting in prolonged nasal carriage of *B. pertussis*. However, in contrast to the study of Boehm et al. (15), we found that IN delivery of an aP vaccine without mucosal adjuvant (aP/IN) did not elicit the same anti-PT IgG level, increased IL-17 level, or CD4+ TRM cell counts as aP +Al$(OH)_3$/IP. Although aP/IN-immunized mice showed lower levels of specific IgA in NW and BALF samples and a reduction in bacterial load in the respiratory tract compared with those of control mice, they showed a lower bacterial load in the trachea and nasal mucosa but not in the lung tissue than aP+Al$(OH)_3$/IP-immunized mice. This finding suggested that just simply modifying the aP vaccine immunization route, at least at the doses used in this study, did not accelerate the clearance of lung infection. In contrast, Boehm et al. (15) observed that an aP vaccine administered *via* the IN route induced protection of mouse lungs against *B. pertussis* comparable to that with the IP administered alum-adjuvanted aP vaccine. This discrepancy could be due to different doses of the aP vaccine used and different *B. pertussis* infection methods.

In summary, the obtained results showed that c-di-GMP, as a mucosal adjuvant, generated better antigen-specific antibody production and stronger Th1 and Th17 responses than the mammalian cyclic dinucleotide 2′3′-cGAMP. This difference translated into better protection against *B. pertussis* infection in a mouse model, with more efficient bacterial clearance in the respiratory tract. These results also indicated that c-di-GMP may be a better candidate mucosal adjuvant for regulating immune responses.

DATA AVAILABILITY STATEMENT

The datasets presented in this study can be found in online repositories. The names of the repository/repositories and accession number(s) can be found below: https://www.ncbi.nlm.nih.gov/bioproject/?term=PRJNA806201.

ETHICS STATEMENT

The animal study was reviewed and approved by Committee on Ethics of the Institute of Medical Biology, Chinese Academy of Medical Sciences.

AUTHOR CONTRIBUTIONS

LS and MS conceived and designed the research. WJ, XW, and YS performed experiments. and data analysis. LC and JYL analyzed the data. JLL and QG contributed reagents and materials. WJ wrote the manuscript. LS and MS reviewed the manuscript. All authors contributed to the article and approved the submitted version.

FUNDING

This work was supported by the by the Yunnan Provincial Science and Technology Department [Grant number 202002AA100009]; and the Kunming Science and Technology Bureau [Grant number 2019-1-N-25318000003332]; and the Special Funds for High-Level Health Talents of Yunnan Province [Grant number L-201615]. The funders had no role in the design of the study, data collection and analysis, decision to publish, or preparation of the manuscript.

ACKNOWLEDGMENTS

We thank Donghong Tang and Meihua Fan for their excellent technical assistance with animal husbandry. We also thank for Xi Wang and Dong Shen for their technical assistance with histopathological analysis.

SUPPLEMENTARY MATERIAL

The Supplementary Material for this article can be found online at: https://www.frontiersin.org/articles/10.3389/fimmu.2022.878832/full#supplementary-material

REFERENCES

1. Herzog C. Changing From Whole-Cell to Acellular Pertussis Vaccines Would Trade Superior Tolerability for Inferior Protection. *Expert Rev Vaccines* (2015) 14:1065–72. doi: 10.1586/14760584.2015.1059759
2. Patterson J, Kagina BM, Gold M, Hussey GD, Muloiwa R. Comparison of Adverse Events Following Immunisation With Acellular and Whole-Cell Pertussis Vaccines: A Systematic Review. *Vaccine* (2018) 36:6007–16. doi: 10.1016/j.vaccine.2018.08.022
3. Barkoff AM, Mertsola J, Pierard D, Dalby T, Hoegh SV, Guillot S, et al. Pertactin-Deficient Bordetella Pertussis Isolates: Evidence of Increased Circulation in Europe, 1998 to 2015. *Euro Surveill* (2019) 24:1700832. doi: 10.2807/1560-7917.Es.2019.24.7.1700832
4. Bouchez V, Guillot S, Landier A, Armatys N, Matczak S, Toubiana J, et al. Evolution of Bordetella Pertussis Over a 23-Year Period in France, 1996 to 2018. *Euro Surveill* (2021) 26:2001213. doi: 10.2807/1560-7917.Es.2021.26.37.2001213
5. Klein NP, Bartlett J, Rowhani-Rahbar A, Fireman B, Baxter R. Waning Protection After Fifth Dose of Acellular Pertussis Vaccine in Children. *N Engl J Med* (2012) 367:1012–9. doi: 10.1056/NEJMoa1200850
6. Klein NP, Bartlett J, Fireman B, Rowhani-Rahbar A, Baxter R. Comparative Effectiveness of Acellular Versus Whole-Cell Pertussis Vaccines in Teenagers. *Pediatrics* (2013) 131:e1716–22. doi: 10.1542/peds.2012-3836
7. Althouse BM, Scarpino SV. Asymptomatic Transmission and the Resurgence of Bordetella Pertussis. *BMC Med* (2015) 13:146. doi: 10.1186/s12916-015-0382-8
8. Warfel JM, Zimmerman LI, Merkel TJ. Acellular Pertussis Vaccines Protect Against Disease But Fail to Prevent Infection and Transmission in a Nonhuman Primate Model. *Proc Natl Acad Sci USA* (2014) 111:787–92. doi: 10.1073/pnas.1314688110
9. Craig R, Kunkel E, Crowcroft NS, Fitzpatrick MC, de Melker H, Althouse BM, et al. Asymptomatic Infection and Transmission of Pertussis in Households: A Systematic Review. *Clin Infect Dis* (2020) 70:152–61. doi: 10.1093/cid/ciz531
10. Gill CJ, Gunning CE, MacLeod WB, Mwananyanda L, Thea DM, Pieciak RC, et al. Asymptomatic Bordetella Pertussis Infections in a Longitudinal Cohort of Young African Infants and Their Mothers. *Elife* (2021) 10:e65663. doi: 10.7554/eLife.65663
11. Romagnani S. Th1/Th2 Cells. *Inflamm Bowel Dis* (1999) 5:285–94. doi: 10.1097/00054725-199911000-00009
12. Solans L, Locht C. The Role of Mucosal Immunity in Pertussis. *Front Immunol* (2019) 9:3068. doi: 10.3389/fimmu.2018.03068
13. Warfel JM, Merkel TJ. Bordetella Pertussis Infection Induces a Mucosal IL-17 Response and Long-Lived Th17 and Th1 Immune Memory Cells in Nonhuman Primates. *Mucosal Immunol* (2013) 6:787–96. doi: 10.1038/mi.2012.117
14. Allen AC, Wilk MM, Misiak A, Borkner L, Murphy D, Mills KHG. Sustained Protective Immunity Against Bordetella Pertussis Nasal Colonization by Intranasal Immunization With a Vaccine-Adjuvant Combination That Induces IL-17-Secreting T(RM) Cells. *Mucosal Immunol* (2018) 11:1763–76. doi: 10.1038/s41385-018-0080-x
15. Boehm DT, Wolf MA, Hall JM, Wong TY, Sen-Kilic E, Basinger HD, et al. Intranasal Acellular Pertussis Vaccine Provides Mucosal Immunity and Protects Mice From Bordetella Pertussis. *NPJ Vaccines* (2019) 4:40. doi: 10.1038/s41541-019-0136-2
16. Hall JM, Bitzer GJ, DeJong MA, Kang J, Wong TY, Wolf MA, et al. Mucosal Immunization With DTaP Confers Protection Against Bordetella Pertussis Infection and Cough in Sprague-Dawley Rats. *Infect Immun* (2021) 89(12):e0034621. doi: 10.1128/iai.00346-21
17. Yan H, Chen W. The Promise and Challenges of Cyclic Dinucleotides as Molecular Adjuvants for Vaccine Development. *Vaccines (Basel)* (2021) 9:917. doi: 10.3390/vaccines9080917
18. Chen W, Kuolee R, Yan H. The Potential of 3',5'-Cyclic Diguanylic Acid (C-Di-GMP) as an Effective Vaccine Adjuvant. *Vaccine* (2010) 28:3080–5. doi: 10.1016/j.vaccine.2010.02.081
19. Ebensen T, Debarry J, Pedersen GK, Blazejewska P, Weissmann S, Schulze K, et al. Mucosal Administration of Cycle-Di-Nucleotide-Adjuvanted Virosomes Efficiently Induces Protection Against Influenza H5N1 in Mice. *Front Immunol* (2017) 8:1223. doi: 10.3389/fimmu.2017.01223
20. Martin TL, Jee J, Kim E, Steiner HE, Cormet-Boyaka E, Boyaka PN. Sublingual Targeting of STING With 3'3'-cGAMP Promotes Systemic and Mucosal Immunity Against Anthrax Toxins. *Vaccine* (2017) 35:2511–9. doi: 10.1016/j.vaccine.2017.02.064
21. Luo J, Liu X-P, Xiong F-F, Gao F-X, Yi Y-L, Zhang M, et al. Enhancing Immune Response and Heterosubtypic Protection Ability of Inactivated H7N9 Vaccine by Using STING Agonist as a Mucosal Adjuvant. *Front Immunol* (2019) 10:2274. doi: 10.3389/fimmu.2019.02274
22. Danilchanka O, Mekalanos JJ. Cyclic Dinucleotides and the Innate Immune Response. *Cell* (2013) 154:962–70. doi: 10.1016/j.cell.2013.08.014
23. Ross P, Weinhouse H, Aloni Y, Michaeli D, Weinberger-Ohana P, Mayer R, et al. Regulation of Cellulose Synthesis in Acetobacter Xylinum by Cyclic Diguanylic Acid. *Nature* (1987) 325:279–81. doi: 10.1038/325279a0
24. Römling U, Galperin MY, Gomelsky M. Cyclic Di-GMP: The First 25 Years of a Universal Bacterial Second Messenger. *Microbiol Mol Biol Rev* (2013) 77:1–52. doi: 10.1128/mmbr.00043-12
25. Karaolis DK, Cheng K, Lipsky M, Elnabawi A, Catalano J, Hyodo M, et al. 3',5'-Cyclic Diguanylic Acid (C-Di-GMP) Inhibits Basal and Growth Factor-Stimulated Human Colon Cancer Cell Proliferation. *Biochem Biophys Res Commun* (2005) 329:40–5. doi: 10.1016/j.bbrc.2005.01.093
26. Sun L, Wu J, Du F, Chen X, Chen ZJ. Cyclic GMP-AMP Synthase is a Cytosolic DNA Sensor That Activates the Type I Interferon Pathway. *Science* (2013) 339:786–91. doi: 10.1126/science.1232458
27. Zhang X, Shi H, Wu J, Zhang X, Sun L, Chen C, et al. Cyclic GMP-AMP Containing Mixed Phosphodiester Linkages is an Endogenous High-Affinity Ligand for STING. *Mol Cell* (2013) 51:226–35. doi: 10.1016/j.molcel.2013.05.022
28. Su M, Zheng J, Gan L, Zhao Y, Fu Y, Chen Q. Second Messenger 2'3'-Cyclic GMP-AMP (2'3'-cGAMP):Synthesis, Transmission, and Degradation. *Biochem Pharmacol* (2022) 198:114934. doi: 10.1016/j.bcp.2022.114934
29. Morehouse BR, Govande AA, Millman A, Keszei AFA, Lowey B, Ofir G, et al. STING Cyclic Dinucleotide Sensing Originated in Bacteria. *Nature* (2020) 586:429–33. doi: 10.1038/s41586-020-2719-5
30. Kamachi K, Toyoizumi-Ajisaka H, Toda K, Soeung SC, Sarath S, Nareth Y, et al. Development and Evaluation of a Loop-Mediated Isothermal Amplification Method for Rapid Diagnosis of Bordetella Pertussis Infection. *J Clin Microbiol* (2006) 44:1899–902. doi: 10.1128/jcm.44.5.1899-1902.2006
31. Jiang W, Shi L, Cai L, Wang X, Li J, Li H, et al. A Two-Adjuvant Multiantigen Candidate Vaccine Induces Superior Protective Immune Responses Against SARS-CoV-2 Challenge. *Cell Rep* (2021) 37:110112. doi: 10.1016/j.celrep.2021.110112
32. Sun M, Ma Y, Xu Y, Yang H, Shi L, Che Y, et al. Dynamic Profiles of Neutralizing Antibody Responses Elicited in Rhesus Monkeys Immunized With a Combined Tetravalent DTaP-Sabin IPV Candidate Vaccine. *Vaccine* (2014) 32:1100–6. doi: 10.1016/j.vaccine.2013.12.025
33. Raeven RHM, Rockx-Brouwer D, Kanojia G, van der Maas L, Bindels THE, Ten Have R, et al. Intranasal Immunization With Outer Membrane Vesicle Pertussis Vaccine Confers Broad Protection Through Mucosal IgA and Th17 Responses. *Sci Rep* (2020) 10:7396–. doi: 10.1038/s41598-020-63998-2
34. Romagnani S. T-Cell Subsets (Th1 Versus Th2). *Ann Allergy Asthma Immunol* (2000) 85:9–21. doi: 10.1016/S1081-1206(10)62426-X
35. Cock PJ, Fields CJ, Goto N, Heuer ML, Rice PM. The Sanger FASTQ File Format for Sequences With Quality Scores, and the Solexa/Illumina FASTQ Variants. *Nucleic Acids Res* (2010) 38:1767–71. doi: 10.1093/nar/gkp1137

36. Kim D, Langmead B, Salzberg SL. HISAT: A Fast Spliced Aligner With Low Memory Requirements. *Nat Methods* (2015) 12:357–60. doi: 10.1038/nmeth.3317
37. Love MI, Huber W, Anders S. Moderated Estimation of Fold Change and Dispersion for RNA-Seq Data With Deseq2. *Genome Biol* (2014) 15:550. doi: 10.1186/s13059-014-0550-8
38. Jiang W, Wei C, Mou D, Zuo W, Liang J, Ma X, et al. Infant Rhesus Macaques as a non-Human Primate Model of Bordetella Pertussis Infection. *BMC Infect Dis* (2021) 21:407. doi: 10.1186/s12879-021-06090-y
39. Libanova R, Ebensen T, Schulze K, Bruhn D, Nörder M, Yevsa T, et al. The Member of the Cyclic Di-Nucleotide Family Bis-(3', 5')-Cyclic Dimeric Inosine Monophosphate Exerts Potent Activity as Mucosal Adjuvant. *Vaccine* (2010) 28:2249–58. doi: 10.1016/j.vaccine.2009.12.045
40. Zhao T, Mo Z, Ying Z, Huang T, Che Y, Li G, et al. *Post Hoc* Analysis of Two Clinical Trials to Compare the Immunogenicity and Safety of Different Polio Immunization Schedules in Chinese Infants. *Ann Transl Med* (2021) 9:253. doi: 10.21037/atm-20-2537
41. Blaauboer SM, Mansouri S, Tucker HR, Wang HL, Gabrielle VD, Jin L. The Mucosal Adjuvant Cyclic Di-GMP Enhances Antigen Uptake and Selectively Activates Pinocytosis-Efficient Cells In Vivo. *Elife* (2015) 4:e06670. doi: 10.7554/eLife.06670
42. Li L, Yin Q, Kuss P, Maliga Z, Millán JL, Wu H, et al. Hydrolysis of 2'3'-cGAMP by ENPP1 and Design of Nonhydrolyzable Analogs. *Nat Chem Biol* (2014) 10:1043–8. doi: 10.1038/nchembio.1661
43. Ding C, Song Z, Shen A, Chen T, Zhang A. Small Molecules Targeting the Innate Immune cGAS–STING–TBK1 Signaling Pathway. *Acta Pharm Sin B* (2020) 10:2272–98. doi: 10.1016/j.apsb.2020.03.001
44. Ross PJ, Sutton CE, Higgins S, Allen AC, Walsh K, Misiak A, et al. Relative Contribution of Th1 and Th17 Cells in Adaptive Immunity to Bordetella Pertussis: Towards the Rational Design of an Improved Acellular Pertussis Vaccine. *PloS Pathog* (2013) 9:e1003264. doi: 10.1371/journal.ppat.1003264
45. Kapil P, Merkel TJ. Pertussis Vaccines and Protective Immunity. *Curr Opin Immunol* (2019) 59:72–8. doi: 10.1016/j.coi.2019.03.006
46. Misiak A, Leuzzi R, Allen AC, Galletti B, Baudner BC, D'Oro U, et al. Addition of a TLR7 Agonist to an Acellular Pertussis Vaccine Enhances Th1 and Th17 Responses and Protective Immunity in a Mouse Model. *Vaccine* (2017) 35:5256–63. doi: 10.1016/j.vaccine.2017.08.009
47. Solans L, Debrie AS, Borkner L, Aguiló N, Thiriard A, Coutte L, et al. IL-17-Dependent SIgA-Mediated Protection Against Nasal Bordetella Pertussis Infection by Live Attenuated BPZE1 Vaccine. *Mucosal Immunol* (2018) 11:1753–62. doi: 10.1038/s41385-018-0073-9
48. Tuomanen EI, Zapiain LA, Galvan P, Hewlett EL. Characterization of Antibody Inhibiting Adherence of Bordetella Pertussis to Human Respiratory Epithelial Cells. *J Clin Microbiol* (1984) 20:167–70. doi: 10.1128/jcm.20.2.167-170.1984
49. Borkner L, Curham LM, Wilk MM, Moran B, Mills KHG. IL-17 Mediates Protective Immunity Against Nasal Infection With Bordetella Pertussis by Mobilizing Neutrophils, Especially Siglec-F(+) Neutrophils. *Mucosal Immunol* (2021) 14:1183–202. doi: 10.1038/s41385-021-00407-5
50. Mills KH, Barnard A, Watkins J, Redhead K. Cell-Mediated Immunity to Bordetella Pertussis: Role of Th1 Cells in Bacterial Clearance in a Murine Respiratory Infection Model. *Infect Immun* (1993) 61:399–410. doi: 10.1128/iai.61.2.399-410.1993
51. Redhead K, Watkins J, Barnard A, Mills KH. Effective Immunization Against Bordetella Pertussis Respiratory Infection in Mice is Dependent on Induction of Cell-Mediated Immunity. *Infect Immun* (1993) 61:3190–8. doi: 10.1128/iai.61.8.3190-3198.1993
52. Ryan M, Murphy G, Gothefors L, Nilsson L, Storsaeter J, Mills KH. Bordetella Pertussis Respiratory Infection in Children is Associated With Preferential Activation of Type 1 T Helper Cells. *J Infect Dis* (1997) 175:1246–50. doi: 10.1086/593682
53. Mascart F, Verscheure V, Malfroot A, Hainaut M, Piérard D, Temerman S, et al. Bordetella Pertussis Infection in 2-Month-Old Infants Promotes Type 1 T Cell Responses. *J Immunol* (2003) 170:1504–9. doi: 10.4049/jimmunol.170.3.1504
54. Mahon BP, Sheahan BJ, Griffin F, Murphy G, Mills KH. Atypical Disease After Bordetella Pertussis Respiratory Infection of Mice With Targeted Disruptions of Interferon-Gamma Receptor or Immunoglobulin Mu Chain Genes. *J Exp Med* (1997) 186:1843–51. doi: 10.1084/jem.186.11.1843
55. Geurtsen J, Fransen F, Vandebriel RJ, Gremmer ER, de la Fonteyne-Blankestijn LJ, Kuipers B, et al. Supplementation of Whole-Cell Pertussis Vaccines With Lipopolysaccharide Analogs: Modification of Vaccine-Induced Immune Responses. *Vaccine* (2008) 26:899–906. doi: 10.1016/j.vaccine.2007.12.012
56. Li P, Asokanathan C, Liu F, Khaing KK, Kmiec D, Wei X, et al. PLGA Nano/Micro Particles Encapsulated With Pertussis Toxoid (PTd) Enhances Th1/Th17 Immune Response in a Murine Model. *Int J Pharm* (2016) 513:183–90. doi: 10.1016/j.ijpharm.2016.08.059
57. Holubová J, Staněk O, Brázdilová L, Mašín J, Bumba L, Gorringe AR, et al. Acellular Pertussis Vaccine Inhibits Bordetella Pertussis Clearance From the Nasal Mucosa of Mice. *Vaccines (Basel)* (2020) 8:695. doi: 10.3390/vaccines8040695
58. Verhoef PA, Constantinides MG, McDonald BD, Urban JFJr., Sperling AI, Bendelac A. Intrinsic Functional Defects of Type 2 Innate Lymphoid Cells Impair Innate Allergic Inflammation in Promyelocytic Leukemia Zinc Finger (PLZF)-Deficient Mice. *J Allergy Clin Immunol* (2016) 137:591–600.e1. doi: 10.1016/j.jaci.2015.07.050
59. Du Y, Tu L, Zhu P, Mu M, Wang R, Yang P, et al. Clinical Features of 85 Fatal Cases of COVID-19 From Wuhan. A Retrospective Observational Study. *Am J Respir Crit Care Med* (2020) 201:1372–9. doi: 10.1164/rccm.202003-0543OC
60. Zhou F, Yu T, Du R, Fan G, Liu Y, Liu Z, et al. Clinical Course and Risk Factors for Mortality of Adult Inpatients With COVID-19 in Wuhan, China: A Retrospective Cohort Study. *Lancet* (2020) 395:1054–62. doi: 10.1016/s0140-6736(20)30566-3
61. Linch SN, Kelly AM, Danielson ET, Pero R, Lee JJ, Gold JA. Mouse Eosinophils Possess Potent Antibacterial Properties In Vivo. *Infect Immun* (2009) 77:4976–82. doi: 10.1128/iai.00306-09
62. Krishack PA, Hollinger MK, Kuzel TG, Decker TS, Louviere TJ, Hrusch CL, et al. IL-33-Mediated Eosinophilia Protects Against Acute Lung Injury. *Am J Respir Cell Mol Biol* (2021) 64:569–78. doi: 10.1165/rcmb.2020-0166OC
63. Dubois V, Chatagnon J, Thiriard A, Bauderlique-Le RH, Debrie AS, Coutte L, et al. Suppression of Mucosal Th17 Memory Responses by Acellular Pertussis Vaccines Enhances Nasal Bordetella Pertussis Carriage. *NPJ Vaccines* (2021) 6:6. doi: 10.1038/s41541-020-00270-8

Conflict of Interest: The authors declare that the research was conducted in the absence of any commercial or financial relationships that could be construed as a potential conflict of interest.

Publisher's Note: All claims expressed in this article are solely those of the authors and do not necessarily represent those of their affiliated organizations, or those of the publisher, the editors and the reviewers. Any product that may be evaluated in this article, or claim that may be made by its manufacturer, is not guaranteed or endorsed by the publisher.

frontiers | Frontiers in Immunology

MINI REVIEW
published: 03 May 2022
doi: 10.3389/fimmu.2022.884862

Oral mRNA Vaccines Against Infectious Diseases- A Bacterial Perspective [Invited]

Vijayakumar Jawalagatti[†‡], *Perumalraja Kirthika*[†‡] *and John Hwa Lee*[*]

Department of Veterinary Public Health, College of Veterinary Medicine, Jeonbuk National University, Iksan, South Korea

OPEN ACCESS

Edited by:
Gabriel Pedersen,
Statens Serum Institut (SSI), Denmark

Reviewed by:
Irina V. Kiseleva,
Institute of Experimental Medicine (RAS), Russia
Bert Devriendt,
Ghent University, Belgium
Shankargouda Patil,
Jazan University, Saudi Arabia

***Correspondence:**
John Hwa Lee
johnhlee@jbnu.ac.kr

[†]Present addresses:
Vijayakumar Jawalagatti, Urology Department, Mayo Clinic, Rochester, MN, United States
Perumalraja Kirthika, Biochemistry and Molecular Biology Department, Mayo Clinic, Rochester, MN, United States

[‡]*These authors have contributed equally to this work*

Specialty section:
This article was submitted to Vaccines and Molecular Therapeutics, a section of the journal Frontiers in Immunology

Received: *27 February 2022*
Accepted: *11 April 2022*
Published: *03 May 2022*

Citation:
Jawalagatti V, Kirthika P and Lee JH (2022) Oral mRNA Vaccines Against Infectious Diseases- A Bacterial Perspective [Invited]. Front. Immunol. 13:884862. doi: 10.3389/fimmu.2022.884862

The mRNA vaccines from Pfizer/BioNTech and Moderna were granted emergency approval in record time in the history of vaccinology and played an instrumental role in limiting the pandemic caused by SARS-CoV-2. The success of these vaccines resulted from over 3 decades of research from many scientists. However, the development of orally administrable mRNA vaccine development is surprisingly underexplored. Our group specializing in *Salmonella*-based vaccines explored the possibility of oral mRNA vaccine development. Oral delivery was made possible by the exploitation of the Semliki Forest viral replicon and *Salmonella* vehicle for transgene amplification and gene delivery, respectively. Herein we highlight the prospect of developing oral replicon-based mRNA vaccines against infectious diseases based on our recent primary studies on SARS-CoV-2. Further, we discuss the potential advantages and limitations of bacterial gene delivery.

Keywords: bacterial delivery, alphaviral replicon, mRNA vaccine, oral, mucosal vaccine, SARS-CoV-2, infectious diseases

INTRODUCTION

Edward Jenner's innovative contribution played a pivotal role in the ultimate eradication of smallpox and served as the harbinger of vaccination. This was followed by the works of Louis Pasteur, who spearheaded the development of live-attenuated cholera vaccine and inactivated anthrax vaccine in humans in 1897 and 1904, respectively. The field of vaccine research soon became popular, and vaccines were developed against a plethora of infectious diseases of medical and veterinary importance. First-generation traditional vaccines based on the use of live, live-attenuated, and inactivated organisms were instrumental in the control of measles, polio, rubella, mumps, classical swine fever, and many other diseases, and responsible for the eradication of smallpox in humans and rinderpest in cattle. Although live and live-attenuated vaccines are effective, they may pose significant health risks to vaccinated individuals, including the development of disease, transmission to healthy individuals, and reversion to a virulent form and particularly in individuals with compromised immune system (1–5). All this changed with the advent of molecular biology and recombinant DNA technology, which paved the way for the development of safer vaccines. However, DNA vaccines did not achieve their expected clinical success owing to limited or poor immunogenicity (6, 7). Technological refinements were made to improve DNA vaccine efficacy (8–15), but the risk of mutagenesis induced by exogenous DNA integration has limited their use in humans (16–19). This has led to a renewed interest in the use of RNA in vaccines and therapeutics.

Synthetic RNA vaccines fall into two main categories: non-replicating and self-amplifying mRNA vaccines. The non-replicating mRNA vaccine is a straightforward approach wherein administered mRNA is directly translated in the cytoplasm of transfected cells to produce immunogenic proteins. The extent of non-replicating mRNA vaccine-induced antigen expression is proportional to the number of transfected cells and thus, requires the injection of a large dose of mRNA. This can be overcome by the use of self-amplifying RNA replicons from alphaviruses, such as Sindbis virus (20), Semliki Forest virus (SFV) (21), and Venezuelan equine encephalitis virus (VEE) (22). Different vector systems, namely replication-competent viral particles, replication-deficient viral particles, and DNA-launched-mRNA vector approaches, have been exploited for transgene expression (reviewed in 23, 24). DNA-launched-mRNA vectors were engineered by deleting the structural genes from the genome and replacing them with the target genes (21, 25). The resulting vector backbone with non-structural proteins (nsp1–4) forms a replicase complex that drives efficient transgene expression by a self-amplifying mechanism (21, 24). The mRNA vaccines developed to combat SARS-CoV-2 constitute the first success story in the long history of mRNA vaccine development. Nonetheless, oral delivery of an mRNA vaccine has surprisingly not been exploited. In this article, we highlight a strategy for the development of oral replicon-based mRNA vaccines by taking cues from our recent publications and discussing the advantages of *Salmonella*-mediated oral gene delivery.

mRNA VACCINES: A BRIEF HISTORICAL BACKGROUND

The vaccines developed against SARS-CoV-2 by Pfizer/BioNTech and Moderna constitute the first success stories in mRNA vaccine history. Although the delivery of mRNA wrapped in cationic liposomes was shown to produce proteins in human cells in 1989 (26), the potential of mRNA as a vaccine has yet to be exploited. During these past 3 decades, many scientists studied mRNA, and collective scientific advances enabled the production of the first successful mRNA vaccine in record time (**Figure 1A**). Some of the most important inventions to the adaptation of mRNA vaccination were the chemical modification of mRNA and lipid nanoparticles for delivery. Without lipid nanoparticle encapsulation, administered mRNA would be detected by the immune system and probably degraded by RNases. Of note, mRNA was shown to elicit TLR3-mediated immune activation of dendritic cells (DCs) (30), and bacterial RNA can prime DCs for higher IL-12 secretion (31). Replacing

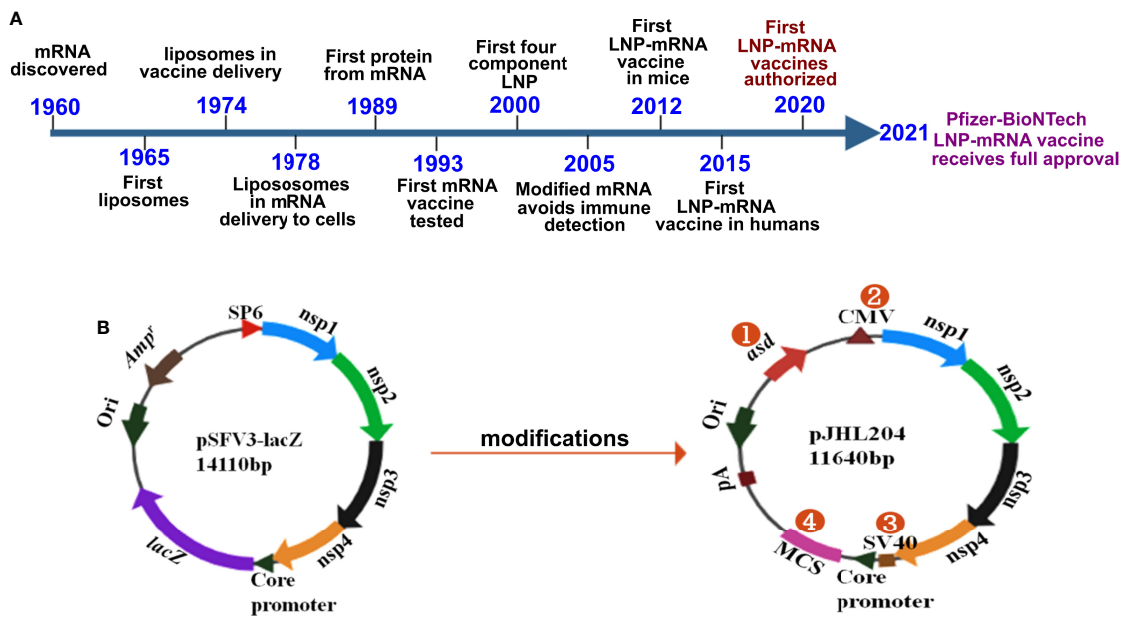

FIGURE 1 | History and design of mRNA vaccines. **(A)** Timeline depicting some of the key milestones that contributed to the first successful mRNA vaccines developed against COVID-19. The timeline was adapted from Sahin et al., 2014 (ref. 27) Hou et al., 2021 (28); and Dolgin, 2021 (29). **(B)** The DNA-launched-mRNA vaccine design for bacterial delivery. pSFV3-lacZ, an SFV replicon-based vector, was used after making several modifications. 1- The ampicillin resistance marker was replaced with asd, an auxotrophic marker to enable antibiotic-free maintenance and delivery of the vector. 2- The SP6 promoter was replaced with the cytomegalovirus (CMV) promoter. 3- The SV40 promoter was placed just before the SFV sub-genomic core promoter to enable direct nuclear transcription of the vaccine constructs. 4- *lacZ* was replaced with multiple cloning site (MCS) sequences. nsp 1-4 from SFV constitute the replicon, which drives efficient transgene expression through RdRp. pA, polyadenylation signal; Ori, pBR origin of replication; RdRp, RNA dependent RNA polymerase; nsp, non-structural protein; SFV, Semliki Forest virus.

uridine with pseudouridine, the chemical modification that diminished immune recognition of administered mRNA, paved the way for mRNA treatments (32). The encapsulation of mRNA by lipid nanoparticles (LNPs) provided an effective and safe delivery platform (reviewed in 33). The discovery of increased protein expression and potent antibody responses to the SARS-CoV-2 spike protein in its stabilized prefusion conformation (34) is vital to the efficacy of mRNA vaccines. The developments and progress in mRNA vaccines against infectious diseases have been reviewed elsewhere (35, 36).

mRNA DELIVERY TECHNOLOGIES: PROGRESS AND LIMITATIONS

The poor uptake of mRNA by cells is associated with the rapid degradation of naked mRNA by extracellular RNAses (37–41). Developments of efficient mRNA delivery platforms have been fruitful in the last decade. From advancements in transfection reagents and liposomes to nanoparticles and nanoemulsions, *in vivo* antigen presentation and the immune response to mRNA-based vaccines have recently improved (42–51). The aforementioned mRNA complexing strategies have been shown to affect mRNA stability during storage (52). Thus, a continuous supply of raw materials is crucial for the uninterrupted production of mRNA vaccines. Such requirements can prove challenging at times when the demand is high (52–57). Additionally, substituting rare codons with frequently used synonymous codons and introducing modified nucleosides have been shown to enhance mRNA translation and stability in the context of vaccination (reviewed in 38). A major disadvantage associated with base modifications is that they may result in altered mRNA secondary structure, which may influence translation and protein folding. These alterations may, in turn, prove detrimental to efficacy (58–60). One of the major drawbacks with *in vitro* transcribed RNA is the presence of dsRNAs that trigger the innate immune response and reduces the vaccine efficacy. Advancement such as cellulose-based purification was shown to remove the dsRNA byproducts leading to the lower type I interferon response and improving the efficacy of a self-amplifying mRNA vaccine against Zika virus (61). Continuous efforts have been made to minimize the drawbacks associated with mRNA vaccines, enabling an array of these vaccines to enter phase IIb clinical trials (38, 62–67). Most of the current mRNA vaccines against infectious disease are administered using the conventional delivery routes, namely intramuscular, subcutaneous, intradermal, or intranodal routes. Most of these routes of administration require injection and specific conditions for storage and transport. Furthermore, the concerns associated with the stability of these vaccines and the addition of adjuvants to enhance immunogenicity increase the cost of production and pose toxicity threats (68, 69). Despite the success of mRNA vaccines in controlling infectious diseases, the limitations associated with their production and administration demonstrate the need to develop better and safer routes of administration for mRNA vaccines (70, 71).

IS IT POSSIBLE TO ORALLY DELIVER mRNA VACCINES?

Despite three decades of history supporting mRNA vaccine development and the successful rollout of mRNA vaccines during the COVID-19 pandemic, the possibility of oral delivery has surprisingly been underexplored (71). This could be attributed to the highly unstable nature of mRNA and the gut posing a significant barrier for mRNA delivery. However, some of the oral antigen delivery strategies such as yeast ghosts, microencapsulated antigens and microbial adhesions have been developed to overcome the harsh conditions in the gut (reviewed in 72). But they suffer from major limitation of poor intestinal epithelial barrier crossing and have not been explored to deliver mRNA (72). Further, lipid-based approaches such as liposomes, bilosomes and immunestimulating complexes (ISCOMs) also provide with a potential delivery vehicle for oral biologic delivery (reviewed in 71). The oral delivery of mRNA vaccines is possible due to the exploitation of an alphaviral replicon and *Salmonella* bactofection for mRNA amplification and gene delivery, respectively. Our group specialized in the development of *Salmonella*-based vaccines against diseases of veterinary and medical importance (73–79), exploited this platform for the development of an oral mRNA vaccine. Further, we exploited the Semliki Forest virus replicon for mRNA amplification (23, 24). We made several modifications to the original vector backbone (pSFV3) to enable transcription in host cells and plasmid maintenance in bacteria (**Figure 1B**) (25). The SP6 promoter was replaced with the Cytomegalovirus (CMV) promoter to enable transcription by mammalian RNA polymerase. The replacement of the ampicillin selection marker with the aspartate-semialdehyde dehydrogenase (asd) auxotrophic marker allows for antibiotic-free plasmid maintenance and delivery (80). The *Salmonella* strains used for gene delivery carry a deletion in the *asd* gene, creating balanced-lethal host-vector systems. Diaminopimelic acid (DAP), the product of asd, is a vital component of the bacterial cell wall, and asd mutants will not survive unless DAP is supplemented in growth media or the *asd* gene is complemented from a plasmid vector. Thus, asd serves as a powerful antibiotic-independent selection maker for bacterial delivery. This DNA-launched-mRNA vector design was exploited for the *Salmonella*-enabled oral delivery of a replicon-based mRNA vaccine against SARS-CoV-2 (25, 81, 82). The detailed mechanism of vector delivery, transgene amplification, and the generation of an immune response upon oral administration of *Salmonella* carrying the SFV replicon vector encoding vaccine immunogens is furnished in **Figure 2**. The findings demonstrate the possibility and potential of bacteria-mediated gene delivery for the development of oral replicon-based mRNA vaccines against infectious diseases.

ADVANTAGES AND LIMITATIONS OF *Salmonella*-MEDIATED ORAL GENE DELIVERY

The delivery of vaccines through the oral route can elicit a potent mucosal response considering the extensive presence of

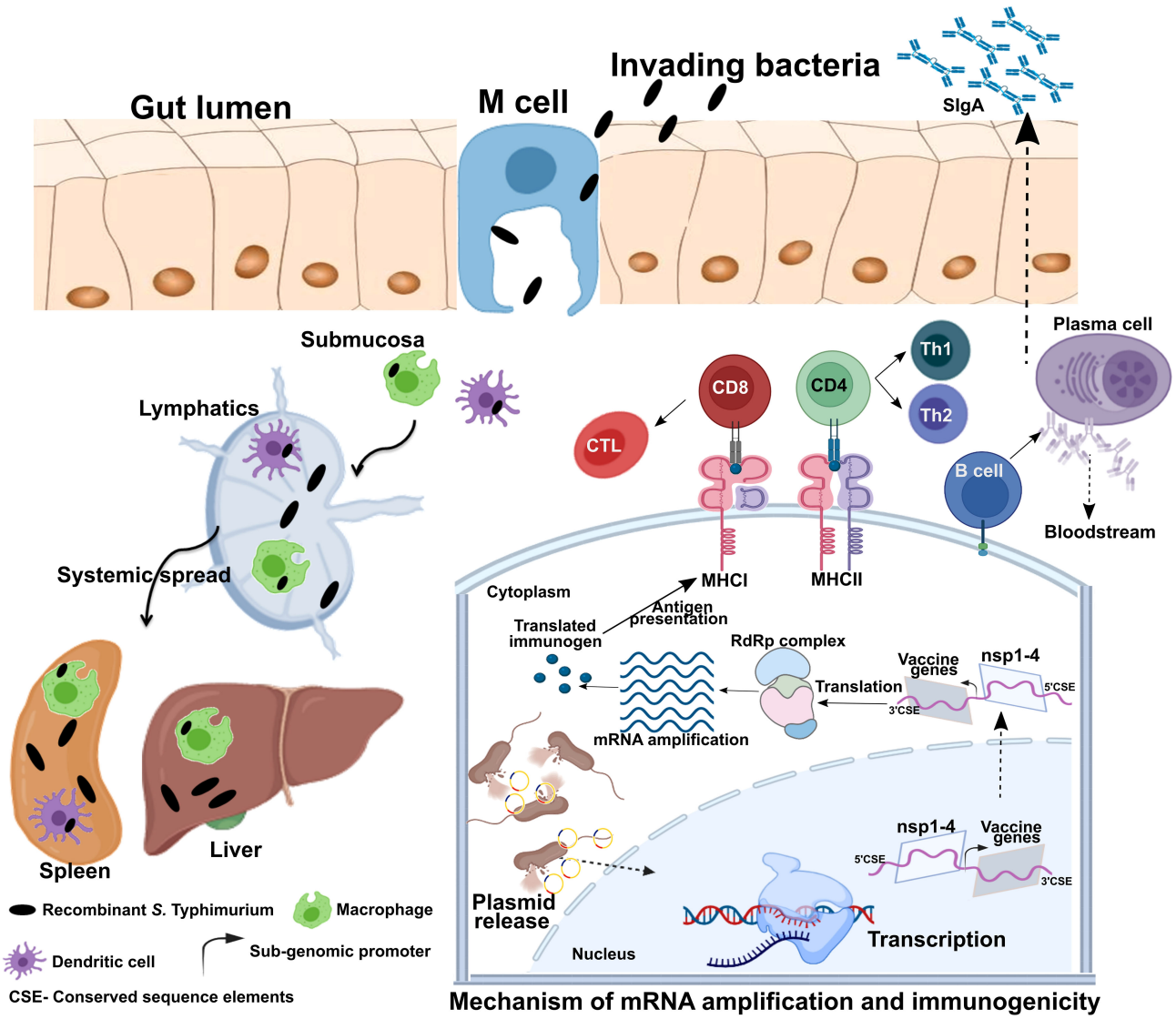

FIGURE 2 | Mechanism of gene delivery, transgene expression, and induction of immune response. Upon oral administration, *Salmonella* Typhimurium is translocated from the luminal surface to submucosa by specialized M cells in the gut epithelium. Bacteria then invade antigen-presenting cells (APCs), such as macrophages and dendritic cells (DCs), and spread to different organs like the liver and spleen through lymphatics and the bloodstream. The vector encoding the Semliki Forest virus (SFV) replicon (nsp1-4) and SARS-CoV-2 immunogens is released within the host cell cytoplasm through bacterial lysis. Transcription of the delivered plasmid takes place in the cell nucleus, and, following *in situ* translation, the nsp1-4 proteins form an RNA-dependent RNA polymerase (RdRp) complex. The RdRp complex then recognizes the sub-genomic promoter and flanking conserved sequence elements (CSE), leading to enhanced mRNA amplification of vaccine genes. The resulting mRNAs translated to produce immunogenic proteins. The APCs process and present antigens to CD8+ and CD4+ T cells *via* MHC I and MHC II, respectively, leading to the elicitation of the T cell response. DCs can present antigens directly to B cells or follicular DCs (FDCs). FDC stores antigens for a longer time, periodically displaying them to cognate B cells. B cells then differentiate to specific antibody-secreting plasma cells and memory B cells. MHC, major histocompatibility complex; nsp, non-structural protein; CD, cluster of differentiation; CTL, cytotoxic T cell; Th, T helper cell; CSE- Conserved sequence elements. This figure was created with the help of the Biorender online tool (https://app.biorender.com/). The figure and description are reproduced with permission from Jawalagatti et al., 2022 (reference 82). ©The American Society of Gene and Cell Therapy.

gut-associated lymphoid tissues (GALT). The bacterial species, *Salmonella* has the ability to interact with immune cells in Payer's patch, leading to efficient induction of the mucosal response (83, 84). Mucosal vaccines play a pivotal role in limiting infections caused by digestive and respiratory pathogens. Moreover, gut bacteria can influence SIgA production in the lungs through $CD103^+$ DCs (85). In agreement, we and others have documented the elicitation of mucosal response in respiratory sites by oral *Salmonella*-based vaccine administration (82, 86). Further, *Salmonella* can translocate through M cells in the intestine and reach organs such as the liver and spleen, eliciting a systemic response as well

(87–89). One of the most important advantages of *Salmonella* is its innate ability to invade and proliferate in professional antigen-presenting cells (APCs), such as dendritic cells (DCs) (90) and macrophages (91), during which it directly delivers the DNA cargo to these cells. As antigens must be formed within the APC or cross-presented to an APC to elicit a cellular response (92), gene delivery and antigen expression within APCs result in robust cellular immunity along with the induction of a potent humoral response. Moreover, vaccine production can be easily scaled up, and a high number of doses can be prepared rapidly at an inexpensive rate. Importantly, bacteria-mediated vaccine delivery does not require additional adjuvants or delivery systems, which further cuts down the cost of manufacturing and limits the frequency of vaccine-associated adverse events (68, 69). Most important of all, the availability of licensed oral *Salmonella* Typhi vaccines provides the possibility of direct translation to humans. Further, the availability of a licensed live-attenuated *Vibrio cholerae* vaccine (Vaxchora; https://www.fda.gov/media/98688/download) provides with additional bacterial vector to develop vaccines against diseases of medical importance. The fact that *Salmonella* can be lyophilized permits a thermostable way to dispatch the vaccines and represents progress towards needle-free mass oral immunizations. Collectively, the data suggest the highly prospective nature of exploiting bacteria to develop oral mRNA vaccines with the ability to elicit potent systemic and mucosal immune responses. The intranasal delivery could also be exploited to develop potent mucosal mRNA vaccines. However, as the vaccine uses live-attenuated bacterium poses a significant safety and regulatory hurdle. The intranasal route is more suitable and safer for delivery of mRNA through polymeric delivery systems. The advantage of oral vaccine over an intranasal vaccine would be superior patient compliance and easy mass administration. Therefore, bacteria-mediated delivery of mRNA vaccines for mucosal vaccine development would be feasible when administered orally rather than intranasally.

One of the major limitations of live-attenuated bacteria is safety. However, the availability of tested and proven licensed vaccines provides safer delivery options. Furthermore, well-established tools to modify the bacterial genome provide an opportunity to create safer mutants (93). Another major limitation of using live-attenuated organisms for gene delivery is a hindrance from pre-existing immunity that can seriously affect vaccine efficacy (94, 95). Both SIgA and IgG could contribute to the pre-existing immunity against *Salmonella.* Nevertheless, this limitation could be overcome by deleting the O-antigen ligase (*rfaL*) or any other gene(s) from the bacterial genome that mask the bacteria from detection by the immune system (77). However, several studies have shown the positive influence of pre-existing immunity and recorded stronger immune responses against the delivered antigen by *Salmonella* vectors (reviewed in 96). Thus, the effect of pre-existing immunity on heterologous antigen delivery is likely negligible or less variable. Of note, the effect of pre-existing immunity on viral vectors is more pronounced than on bacterial vectors (96).

ORAL REPLICON-BASED mRNA VACCINE AGAINST SARS-COV-2

Our proof-of-principle studies using SARS-CoV-2 (25, 81, 82) provide evidence for the development of oral replicon-based mRNA vaccines against infectious diseases. *Salmonella* is an ideal bacterial vector owing to its unique ability to target GALT upon oral administration, resulting in both systemic and mucosal immune responses in vaccinated individuals. The possibility of oral delivery was partly enabled by creating a DNA-launched-mRNA design of the SFV replicon that essentially drives gene expression by a self-amplifying mRNA mechanism (25). Although the research on RNA vaccines and therapeutics spans over 3 decades, the possibility of oral mRNA vaccine delivery was yet to be explored. To the best of our knowledge, our studies are the first to demonstrate oral replicon-based mRNA vaccine delivery. To this end, we designed a multivalent SFV replicon-based vaccine targeting receptor-binding domain (RBD), heptad repeat domain (HR), membrane glycoprotein (M), and epitopes of nsp13 and employed *Salmonella* Typhimurium for gene delivery (25). The administration of the vaccine was highly safe in mice and hamsters inoculated both orally and intramuscularly (25, 82). The vaccine elicited potent Th1-dominated humoral and cellular immune responses in mice against all the target antigens, suggesting efficient antigen production and presentation (25, 82). Furthermore, RBD expressed after *Salmonella* delivery was confirmed to be antigenically intact in macrophage-like cells (82). We recorded the difference in mucosal immune response induction between oral and intramuscular routes of vaccine administration, highlighting the feasibility of exploiting oral administration for mucosal vaccine development (82). Most importantly, the vaccine protected hamsters against live SARS-CoV-2, and complete protection was elicited by oral immunization against viral replication and lung disease (82). Moreover, a robust cross-protection against the B.1.617.2 delta variant was evidenced following oral immunization in hamsters (82) and mice (81). The fact that an intranasal vaccine durably protected against SARS-CoV-2 variants (97, 98) and dimeric IgA had superior neutralizing activity (99) underscore the efficacy of the mucosal response exerted by oral vaccines in protection against rapidly replicating variants.

CONCLUSIONS AND FUTURE DIRECTIONS

Our proof-of-principle studies have unraveled a novel method for the development of oral mRNA vaccines. The availability of some licensed live-attenuated bacterial vaccines increases the prospects of adopting such vaccines in the clinic. However, more studies using relevant bacterial species in suitable preclinical models are necessary to prove the hypothesis. Moreover, the possibility of other bacterial species, such as *Shigella*, could also be tested to optimize the choice of a bacterial vector.

AUTHOR CONTRIBUTIONS

VJ and PK: prepared the figures and wrote the article. JL: acquired funding and commented on the manuscript. All authors contributed to the article and approved the submitted version.

FUNDING

This research was supported by Basic Science Research Program through the National Research Foundation of Korea (NRF) funded by the Ministry of Education (2019R1A6A1A03033084).

REFERENCES

1. Minor PD. Live Attenuated Vaccines: Historical Successes and Current Challenges. *Virol* (2015) 479–480:379–92. doi: 10.1016/j.virol.2015.03.032
2. Minor PD. The Polio-Eradication Programme and Issues of the End Game. *J Gen Virol* (2012) 93:457–74. doi: 10.1099/vir.0.036988-0
3. Marsden SA, Boulger LR, Magrath DI, Reeve P, Schild GC, Taffs LF. Monkey Neurovirulence of Live, Attenuated (Sabin) Type I and Type II Poliovirus Vaccines. *J Biol Stand* (1980) 8:303–9. doi: 10.1016/S0092-1157(80)80008-4
4. Shaghaghi M, Parvaneh N, Ostad-Rahimi P, Fathi SM, Shahmahmoodi S, Abolhassani H, et al. Combined Immunodeficiency Presenting With Vaccine-Associated Paralytic Poliomyelitis: A Case Report and Narrative Review of Literature. *Immunol Invest* (2014) 43:292–8. doi: 10.3109/08820139.2013.859156
5. Rubin LG, Levin MJ, Ljungman P, Davies EG, Avery R, Tomblyn M, et al. IDSA Clinical Practice Guideline for Vaccination of the Immunocompromised Host. *Clin Infect Dis* (2014) 58:e44–e100. doi: 10.1093/cid/cit684
6. Kutzler MA, Weiner DB. DNA Vaccines: Ready for Prime Time? *Nat Rev Genet* (2008) 9:776–88. doi: 10.1038/nrg2432
7. MacGregor RR, Boyer JD, Ugen KE, Lacy KE, Gluckman SJ, Bagarazzi ML, et al. First Human Trial of a DNA-Based Vaccine for Treatment of Human Immunodeficiency Virus Type 1 Infection: Safety and Host Response. *J Infect Dis* (1998) 178:92–100. doi: 10.1086/515613
8. Cheung Y-K, Cheng SC-S, Sin FW-Y, Xie Y. Plasmid Encoding Papillomavirus Type 16 (HPV16) DNA Constructed With Codon Optimization Improved the Immunogenicity Against HPV Infection. *Vaccine* (2004) 23:629–38. doi: 10.1016/j.vaccine.2004.07.010
9. Narum DL, Kumar S, Rogers WO, Fuhrmann SR, Liang H, Oakley M, et al. Codon Optimization of Gene Fragments Encoding Plasmodium Falciparum Merzoite Proteins Enhances DNA Vaccine Protein Expression and Immunogenicity in Mice. *Infect Immun* (2001) 69:7250–3. doi: 10.1128/IAI.69.12.7250-7253.2001
10. Yan J, Yoon H, Kumar S, Ramanathan MP, Corbitt N, Kutzler M, et al. Enhanced Cellular Immune Responses Elicited by an Engineered HIV-1 Subtype B Consensus-Based Envelope DNA Vaccine. *Mol Ther* (2007) 15:411–21. doi: 10.1038/sj.mt.6300036
11. Xu Z-L, Mizuguchi H, Ishii-Watabe A, Uchida E, Mayumi T, Hayakawa T. Optimization of Transcriptional Regulatory Elements for Constructing Plasmid Vectors. *Gene* (2001) 272:149–56. doi: 10.1016/S0378-1119(01)00550-9
12. Kaur R, Rauthan M, Vrati S. Immunogenicity in Mice of a Cationic Microparticle-Adsorbed Plasmid DNA Encoding Japanese Encephalitis Virus Envelope Protein. *Vaccine* (2004) 22:2776–82. doi: 10.1016/j.vaccine.2004.01.040
13. Pai Kasturi S, Qin H, Thomson KS, El-Bereir S, Cha S, Neelapu S, et al. Prophylactic Anti-Tumor Effects in a B Cell Lymphoma Model With DNA Vaccines Delivered on Polyethylenimine (PEI) Functionalized PLGA Microparticles. *J Control Release* (2006) 113:261–70. doi: 10.1016/j.jconrel.2006.04.006
14. Jilek S, Merkle H, Walter E. DNA-Loaded Biodegradable Microparticles as Vaccine Delivery Systems and Their Interaction With Dendritic Cells. *Adv Drug Delivery Rev* (2005) 57:377–90. doi: 10.1016/j.addr.2004.09.010
15. Vandervoort J. Microneedles for Transdermal Drug Delivery: A Minireview. *Front Biosci* (2008) 13:1711. doi: 10.2741/2794
16. Nichols WW, Ledwith BJ, Manam SV, Troilo PJ. Potential DNA Vaccine Integration Into Host Cell Genome. *Ann N Y Acad Sci* (1995) 772:30–9. doi: 10.1111/j.1749-6632.1995.tb44729.x
17. Martin T, Parker SE, Hedstrom R, Le T, Hoffman SL, Norman J, et al. Plasmid DNA Malaria Vaccine: The Potential for Genomic Integration After Intramuscular Injection. *Hum Gene Ther* (1999) 10:759–68. doi: 10.1089/10430349950018517
18. Wang Z, Troilo PJ, Wang X, Griffiths TG, Pacchione SJ, Barnum AB, et al. Detection of Integration of Plasmid DNA Into Host Genomic DNA Following Intramuscular Injection and Electroporation. *Gene Ther* (2004) 11:711–21. doi: 10.1038/sj.gt.3302213
19. Liu MA. DNA Vaccines: An Historical Perspective and View to the Future. *Immunol Rev* (2011) 239:62–84. doi: 10.1111/j.1600-065X.2010.00980.x
20. Xiong C, Levis R, Shen P, Schlesinger S, Rice CM, Huang HV. Sindbis Virus: An Efficient, Broad Host Range Vector for Gene Expression in Animal Cells. *Science (80-)* (1989) 243:1188–91. doi: 10.1126/science.2922607
21. Liljeström P, Garoff H. A New Generation of Animal Cell Expression Vectors Based on the Semliki Forest Virus Replicon. *Bio/Technology* (1991) 9:1356–61. doi: 10.1038/nbt1291-1356
22. Davis NL, Willis LV, Smitht JF, Johnston RE. *In Vitro* Synthesis of Infectious Venezuelan Equine Encephalitis Virus RNA From a cDNA Clone: Analysis of a Viable Deletion Mutant. *Virology* (1989) 171:189–204. doi: 10.1016/0042-6822(89)90526-6
23. Lundstrom K. Biology and Application of Alphaviruses in Gene Therapy. *Gene Ther* (2005) 12:S92–7. doi: 10.1038/sj.gt.3302620
24. Lundstrom K. Alphaviruses in Gene Therapy. *Viruses* (2015) 7:2321–33. doi: 10.3390/v7052321
25. Jawalagatti V, Kirthika P, Park J-Y, Hewawaduge C, Lee JH. Highly Feasible Immunoprotective Multicistronic SARS-CoV-2 Vaccine Candidate Blending Novel Eukaryotic Expression and Salmonella Bactofection. *J Adv Res* (2022) 36:211–22. doi: 10.1016/j.jare.2021.07.007
26. Malone RW, Felgner PL, Verma IM. Cationic Liposome-Mediated RNA Transfection. *Proc Natl Acad Sci* (1989) 86:6077–81. doi: 10.1073/pnas.86.16.6077
27. Sahin U, Karikó K, Türeci Ö. mRNA-Based Therapeutics — Developing a New Class of Drugs. *Nat Rev Drug Discov* (2014) 13:759–80. doi: 10.1038/nrd4278
28. Hou X, Zaks T, Langer R, Dong Y. Lipid Nanoparticles for mRNA Delivery. *Nat Rev Mater* (2021) 6:1078–94. doi: 10.1038/s41578-021-00358-0
29. Dolgin E. The Tangled History of mRNA Vaccines. *Nature* (2021) 597:318–24. doi: 10.1038/d41586-021-02483-w
30. Karikó K, Ni H, Capodici J, Lamphier M, Weissman D. mRNA Is an Endogenous Ligand for Toll-Like Receptor 3. *J Biol Chem* (2004) 279:12542–50. doi: 10.1074/jbc.M310175200
31. Koski GK, Karikó K, Xu S, Weissman D, Cohen PA, Czerniecki BJ. Cutting Edge: Innate Immune System Discriminates Between RNA Containing Bacterial Versus Eukaryotic Structural Features That Prime for High-Level IL-12 Secretion by Dendritic Cells. *J Immunol* (2004) 172:3989–93. doi: 10.4049/jimmunol.172.7.3989
32. Karikó K, Buckstein M, Ni H, Weissman D. Suppression of RNA Recognition by Toll-Like Receptors: The Impact of Nucleoside Modification and the Evolutionary Origin of RNA. *Immunity* (2005) 23:165–75. doi: 10.1016/j.immuni.2005.06.008
33. Buschmann MD, Carrasco MJ, Alishetty S, Paige M, Alameh MG, Weissman D. Nanomaterial Delivery Systems for mRNA Vaccines. *Vaccines* (2021) 9:65. doi: 10.3390/vaccines9010065
34. Pallesen J, Wang N, Corbett KS, Wrapp D, Kirchdoerfer RN, Turner HL, et al. Immunogenicity and Structures of a Rationally Designed Prefusion MERS-CoV Spike Antigen. *Proc Natl Acad Sci* (2017) 114:E7348–57. doi: 10.1073/pnas.1707304114
35. Bloom K, van den Berg F, Arbuthnot P. Self-Amplifying RNA Vaccines for Infectious Diseases. *Gene Ther* (2021) 28:117–29. doi: 10.1038/s41434-020-00204-y

36. Zhang C, Maruggi G, Shan H, Li J. Advances in mRNA Vaccines for Infectious Diseases. *Front Immunol* (2019) 10:594. doi: 10.3389/fimmu.2019.00594
37. Kowalski PS, Rudra A, Miao L, Anderson DG. Delivering the Messenger: Advances in Technologies for Therapeutic mRNA Delivery. *Mol Ther* (2019) 27:710–28. doi: 10.1016/j.ymthe.2019.02.012
38. Pardi N, Hogan MJ, Porter FW, Weissman D. mRNA Vaccines — A New Era in Vaccinology. *Nat Rev Drug Discov* (2018) 17:261–79. doi: 10.1038/nrd.2017.243
39. Tsui NBY, Ng EKO, Lo YMD. Stability of Endogenous and Added RNA in Blood Specimens, Serum, and Plasma. *Clin Chem* (2002) 48:1647–53. doi: 10.1093/clinchem/48.10.1647
40. Kauffman KJ, Webber MJ, Anderson DG. Materials for Non-Viral Intracellular Delivery of Messenger RNA Therapeutics. *J Control Release* (2016) 240:227–34. doi: 10.1016/j.jconrel.2015.12.032
41. Guan S, Rosenecker J. Nanotechnologies in Delivery of mRNA Therapeutics Using Nonviral Vector-Based Delivery Systems. *Gene Ther* (2017) 24:133–43. doi: 10.1038/gt.2017.5
42. Bahl K, Senn JJ, Yuzhakov O, Bulychev A, Brito LA, Hassett KJ, et al. Preclinical and Clinical Demonstration of Immunogenicity by mRNA Vaccines Against H10N8 and H7N9 Influenza Viruses. *Mol Ther* (2017) 25:1316–27. doi: 10.1016/j.ymthe.2017.03.035
43. Pollard C, Rejman J, De Haes W, Verrier B, Van Gulck E, Naessens T, et al. Type I IFN Counteracts the Induction of Antigen-Specific Immune Responses by Lipid-Based Delivery of mRNA Vaccines. *Mol Ther* (2013) 21:251–9. doi: 10.1038/mt.2012.202
44. Uchida S, Kinoh H, Ishii T, Matsui A, Tockary TA, Takeda KM, et al. Systemic Delivery of Messenger RNA for the Treatment of Pancreatic Cancer Using Polyplex Nanomicelles With a Cholesterol Moiety. *Biomaterials* (2016) 82:221–8. doi: 10.1016/j.biomaterials.2015.12.031
45. Mockey M, Bourseau E, Chandrashekhar V, Chaudhuri A, Lafosse S, Le Cam E, et al. mRNA-Based Cancer Vaccine: Prevention of B16 Melanoma Progression and Metastasis by Systemic Injection of MART1 mRNA Histidylated Lipopolyplexes. *Cancer Gene Ther* (2007) 14:802–14. doi: 10.1038/sj.cgt.7701072
46. Perche F, Benvegnu T, Berchel M, Lebegue L, Pichon C, Jaffrès P-A, et al. Enhancement of Dendritic Cells Transfection *In Vivo* and of Vaccination Against B16F10 Melanoma With Mannosylated Histidylated Lipopolyplexes Loaded With Tumor Antigen Messenger RNA. *Nanomed Nanotechnol Biol Med* (2011) 7:445–53. doi: 10.1016/j.nano.2010.12.010
47. Démoulins T, Milona P, Englezou PC, Ebensen T, Schulze K, Suter R, et al. Polyethylenimine-Based Polyplex Delivery of Self-Replicating RNA Vaccines. *Nanomed Nanotechnol Biol Med* (2016) 12:711–22. doi: 10.1016/j.nano.2015.11.001
48. Maruggi G, Chiarot E, Giovani C, Buccato S, Bonacci S, Frigimelica E, et al. Immunogenicity and Protective Efficacy Induced by Self-Amplifying mRNA Vaccines Encoding Bacterial Antigens. *Vaccine* (2017) 35:361–8. doi: 10.1016/j.vaccine.2016.11.040
49. Brazzoli M, Magini D, Bonci A, Buccato S, Giovani C, Kratzer R, et al. Induction of Broad-Based Immunity and Protective Efficacy by Self-Amplifying mRNA Vaccines Encoding Influenza Virus Hemagglutinin. *J Virol* (2016) 90:332–44. doi: 10.1128/JVI.01786-15
50. Brito LA, Chan M, Shaw CA, Hekele A, Carsillo T, Schaefer M, et al. A Cationic Nanoemulsion for the Delivery of Next-Generation RNA Vaccines. *Mol Ther* (2014) 22:2118–29. doi: 10.1038/mt.2014.133
51. McCullough KC, Bassi I, Milona P, Suter R, Thomann-Harwood L, Englezou P, et al. Self-Replicating Replicon-RNA Delivery to Dendritic Cells by Chitosan-Nanoparticles for Translation *In Vitro* and *In Vivo*. *Mol Ther - Nucleic Acids* (2014) 3:e173. doi: 10.1038/mtna.2014.24
52. Crommelin DJA, Anchordoquy TJ, Volkin DB, Jiskoot W, Mastrobattista E. Addressing the Cold Reality of mRNA Vaccine Stability. *J Pharm Sci* (2021) 110:997–1001. doi: 10.1016/j.xphs.2020.12.006
53. Reichmuth AM, Oberli MA, Jaklenec A, Langer R, Blankschtein D. mRNA Vaccine Delivery Using Lipid Nanoparticles. *Ther Deliv* (2016) 7:319–34. doi: 10.4155/tde-2016-0006
54. Hassett KJ, Benenato KE, Jacquinet E, Lee A, Woods A, Yuzhakov O, et al. Optimization of Lipid Nanoparticles for Intramuscular Administration of mRNA Vaccines. *Mol Ther - Nucleic Acids* (2019) 15:1–11. doi: 10.1016/j.omtn.2019.01.013
55. Lutz J, Lazzaro S, Habbeddine M, Schmidt KE, Baumhof P, Mui BL, et al. Unmodified mRNA in LNPs Constitutes a Competitive Technology for Prophylactic Vaccines. *NPJ Vaccines* (2017) 2:29. doi: 10.1038/s41541-017-0032-6
56. Sedic M, Senn JJ, Lynn A, Laska M, Smith M, Platz SJ, et al. Safety Evaluation of Lipid Nanoparticle–Formulated Modified mRNA in the Sprague-Dawley Rat and Cynomolgus Monkey. *Vet Pathol* (2018) 55:341–54. doi: 10.1177/0300985817738095
57. Golan MS, Mahoney E, Trump B, Linkov I. Resilience and Efficiency for the Nanotechnology Supply Chains Underpinning COVID-19 Vaccine Development. *Curr Opin Chem Eng* (2021) 34:100759. doi: 10.1016/j.coche.2021.100759
58. Mauro VP, Chappell SA. A Critical Analysis of Codon Optimization in Human Therapeutics. *Trends Mol Med* (2014) 20:604–13. doi: 10.1016/j.molmed.2014.09.003
59. Buhr F, Jha S, Thommen M, Mittelstaet J, Kutz F, Schwalbe H, et al. Synonymous Codons Direct Cotranslational Folding Toward Different Protein Conformations. *Mol Cell* (2016) 61:341–51. doi: 10.1016/j.molcel.2016.01.008
60. Yu C-H, Dang Y, Zhou Z, Wu C, Zhao F, Sachs MS, et al. Codon Usage Influences the Local Rate of Translation Elongation to Regulate Co-Translational Protein Folding. *Mol Cell* (2015) 59:744–54. doi: 10.1016/j.molcel.2015.07.018
61. Zhong Z, McCafferty S, Opsomer L, Wang H, Huysmans H, De Temmerman J, et al. Corticosteroids and Cellulose Purification Improve, Respectively, the *In Vivo* Translation and Vaccination Efficacy of sa-mRNAs. *Mol Ther* (2021) 29:1370–81. doi: 10.1016/j.ymthe.2021.01.023
62. Jacobson JM, Routy J-P, Welles S, DeBenedette M, Tcherepanova I, Angel JB, et al. Dendritic Cell Immunotherapy for HIV-1 Infection Using Autologous HIV-1 RNA. *JAIDS J Acquir Immune Defic Syndr* (2016) 72:31–8. doi: 10.1097/QAI.0000000000000926
63. Schnee M, Vogel AB, Voss D, Petsch B, Baumhof P, Kramps T, et al. An mRNA Vaccine Encoding Rabies Virus Glycoprotein Induces Protection Against Lethal Infection in Mice and Correlates of Protection in Adult and Newborn Pigs. *PloS Negl Trop Dis* (2016) 10:e0004746. doi: 10.1371/journal.pntd.0004746
64. Alberer M, Gnad-Vogt U, Hong HS, Mehr KT, Backert L, Finak G, et al. Safety and Immunogenicity of a mRNA Rabies Vaccine in Healthy Adults: An Open-Label, Non-Randomised, Prospective, First-in-Human Phase 1 Clinical Trial. *Lancet* (2017) 390:1511–20. doi: 10.1016/S0140-6736(17)31665-3
65. Gandhi RT, Kwon DS, Macklin EA, Shopis JR, McLean AP, McBrine N, et al. Immunization of HIV-1-Infected Persons With Autologous Dendritic Cells Transfected With mRNA Encoding HIV-1 Gag and Nef. *JAIDS J Acquir Immune Defic Syndr* (2016) 71:246–53. doi: 10.1097/QAI.0000000000000852
66. Routy J-P, Boulassel M-R, Yassine-Diab B, Nicolette C, Healey D, Jain R, et al. Immunologic Activity and Safety of Autologous HIV RNA-Electroporated Dendritic Cells in HIV-1 Infected Patients Receiving Antiretroviral Therapy. *Clin Immunol* (2010) 134:140–7. doi: 10.1016/j.clim.2009.09.009
67. Richner JM, Himansu S, Dowd KA, Butler SL, Salazar V, Fox JM, et al. Modified mRNA Vaccines Protect Against Zika Virus Infection. *Cell* (2017) 168:1114–1125.e10. doi: 10.1016/j.cell.2017.02.017
68. Ruiz JT, Luján L, Blank M, Shoenfeld Y. Adjuvants- and Vaccines-Induced Autoimmunity: Animal Models. *Immunol Res* (2017) 65:55–65. doi: 10.1007/s12026-016-8819-5
69. Nicholls EF, Madera L, Hancock REW. Immunomodulators as Adjuvants for Vaccines and Antimicrobial Therapy. *Ann N Y Acad Sci* (2010) 1213:46–61. doi: 10.1111/j.1749-6632.2010.05787.x
70. D'Amico C, Fontana F, Cheng R, Santos HA. Development of Vaccine Formulations: Past, Present, and Future. *Drug Deliv Transl Res* (2021) 11:353–72. doi: 10.1007/s13346-021-00924-7
71. Coffey JW, Das Gaiha G, Traverso G. Oral Biologic Delivery: Advances Toward Oral Subunit, DNA, and mRNA Vaccines and the Potential for Mass Vaccination During Pandemics. *Annu Rev Pharmacol Toxicol* (2021) 61:517–40. doi: 10.1146/annurev-pharmtox-030320-092348
72. Devriendt B, De Geest BG, Goddeeris BM, Cox E. Crossing the Barrier: Targeting Epithelial Receptors for Enhanced Oral Vaccine Delivery. *J Control Release* (2012) 160:431–9. doi: 10.1016/j.jconrel.2012.02.006

73. Jawale CV, Lee JH. Salmonella Enterica Serovar Enteritidis Ghosts Carrying the Escherichia Coli Heat-Labile Enterotoxin B Subunit Are Capable of Inducing Enhanced Protective Immune Responses. *Clin Vaccine Immunol* (2014) 21:799–807. doi: 10.1128/CVI.00016-14
74. Jawale CV, Chaudhari AA, Jeon BW, Nandre RM, Lee JH. Characterization of a Novel Inactivated Salmonella Enterica Serovar Enteritidis Vaccine Candidate Generated Using a Modified Ci857/λ P R/Gene E Expression System. *Infect Immun* (2012) 80:1502–9. doi: 10.1128/IAI.06264-11
75. Hyoung KJ, Hajam IA, Lee JH. A Consensus-Hemagglutinin-Based Vaccine Delivered by an Attenuated Salmonella Mutant Protects Chickens Against Heterologous H7N1 Influenza Virus. *Oncotarget* (2017) 8:38780–92. doi: 10.18632/oncotarget.16353
76. Kim JH, Hajam IA, Lee JH. Oral Immunization With a Novel Attenuated Salmonella Typhimurium Encoding Influenza HA, M2e and NA Antigens Protects Chickens Against H7N9 Infection. *Vet Res* (2018) 49:12. doi: 10.1186/s13567-018-0509-y
77. Lalsiamthara J, Kim JH, Lee JH. Engineering of a Rough Auxotrophic Mutant Salmonella Typhimurium for Effective Delivery. *Oncotarget* (2018) 9:25441–57. doi: 10.18632/oncotarget.25192
78. Kim B, Won G, Lee JH. Construction of an Inactivated Typhoid Vaccine Candidate Expressing Escherichia Coli Heat-Labile Enterotoxin B Subunit and Evaluation of Its Immunogenicity in a Murine Model. *J Med Microbiol* (2017) 66:1235–43. doi: 10.1099/jmm.0.000543
79. Lalsiamthara J, Lee JH. Brucella Lipopolysaccharide Reinforced Salmonella Delivering Brucella Immunogens Protects Mice Against Virulent Challenge. *Vet Microbiol* (2017) 205:84–91. doi: 10.1016/j.vetmic.2017.05.012
80. Nakayama K, Kelly SM, Curtiss R. Construction of an ASD+ Expression-Cloning Vector: Stable Maintenance and High Level Expression of Cloned Genes in a Salmonella Vaccine Strain. *Nat Biotechnol* (1988) 6:693–7. doi: 10.1038/nbt0688-693
81. Jawalagatti V, Kirthika P, Hewawaduge C, Park J-Y, Yang M, Oh B, et al. A Simplified SARS-CoV-2 Mouse Model Demonstrates Protection by an Oral Replicon-Based mRNA Vaccine. *Front Immunol* (2022) 13:811802. doi: 10.3389/fimmu.2022.811802
82. Jawalagatti V, Kirthika P, Hewawaduge C, Yang M, Park J-Y, Oh B, et al. Bacteria-Enabled Oral Delivery of a Replicon-Based mRNA Vaccine Candidate Protects Against Ancestral and Delta Variant SARS-CoV-2. *Mol Ther* (2022) 30. doi: 10.1016/j.ymthe.2022.01.042
83. Martinoli C, Chiavelli A, Rescigno M. Entry Route of Salmonella Typhimurium Directs the Type of Induced Immune Response. *Immunity* (2007) 27:975–84. doi: 10.1016/j.immuni.2007.10.011
84. Sato A, Hashiguchi M, Toda E, Iwasaki A, Hachimura S, Kaminogawa S. CD11b + Peyer's Patch Dendritic Cells Secrete IL-6 and Induce IgA Secretion From Naive B Cells. *J Immunol* (2003) 171:3684–90. doi: 10.4049/jimmunol.171.7.3684
85. Lycke NY, Bemark M. The Regulation of Gut Mucosal IgA B-Cell Responses: Recent Developments. *Mucosal Immunol* (2017) 10:1361–74. doi: 10.1038/mi.2017.62
86. Hopkins S, Kraehenbuhl JP, Schödel F, Potts A, Peterson D, de Grandi P, et al. A Recombinant Salmonella Typhimurium Vaccine Induces Local Immunity by Four Different Routes of Immunization. *Infect Immun* (1995) 63:3279–86. doi: 10.1128/iai.63.9.3279-3286.1995
87. Jang MH, Kweon M-N, Iwatani K, Yamamoto M, Terahara K, Sasakawa C, et al. Intestinal Villous M Cells: An Antigen Entry Site in the Mucosal Epithelium. *Proc Natl Acad Sci* (2004) 101:6110–5. doi: 10.1073/pnas.0400969101
88. Jones BD, Ghori N, Falkow S. Salmonella Typhimurium Initiates Murine Infection by Penetrating and Destroying the Specialized Epithelial M Cells of the Peyer's Patches. *J Exp Med* (1994) 180:15–23. doi: 10.1084/jem.180.1.15
89. Penheiter KL, Mathur N, Giles D, Fahlen T, Jones BD. Non-Invasive Salmonella Typhimurium Mutants Are Avirulent Because of an Inability to Enter and Destroy M Cells of Ileal Peyer's Patches. *Mol Microbiol* (1997) 24:697–709. doi: 10.1046/j.1365-2958.1997.3741745.x
90. Wick MJ. The Role of Dendritic Cells During Salmonella Infection. *Curr Opin Immunol* (2002) 14:437–43. doi: 10.1016/S0952-7915(02)00364-3
91. Gog JR, Murcia A, Osterman N, Restif O, McKinley TJ, Sheppard M, et al. Dynamics of Salmonella Infection of Macrophages at the Single Cell Level. *J R Soc Interface* (2012) 9:2696–707. doi: 10.1098/rsif.2012.0163
92. Liu MA. A Comparison of Plasmid DNA and mRNA as Vaccine Technologies. *Vaccines* (2019) 7:37. doi: 10.3390/vaccines7020037
93. Datsenko KA, Wanner BL. One-Step Inactivation of Chromosomal Genes in Escherichia Coli K-12 Using PCR Products. *Proc Natl Acad Sci* (2000) 97 (12):6640–5. doi: 10.1073/pnas.120163297
94. Roberts M, Bacon A, Li J, Chatfield S. Prior Immunity to Homologous and Heterologous Salmonella Serotypes Suppresses Local and Systemic Anti-Fragment C Antibody Responses and Protection From Tetanus Toxin in Mice Immunized With Salmonella Strains Expressing Fragment C. *Infect Immun* (1999) 67:3810–5. doi: 10.1128/IAI.67.8.3810-3815.1999
95. Mok DZL, Chan KR. The Effects of Pre-Existing Antibodies on Live-Attenuated Viral Vaccines. *Viruses* (2020) 12:520. doi: 10.3390/v12050520
96. Saxena M, Van TTH, Baird FJ, Coloe PJ, Smooker PM. Pre-Existing Immunity Against Vaccine Vectors – Friend or Foe? *Microbiology* (2013) 159:1–11. doi: 10.1099/mic.0.049601-0
97. Hassan AO, Shrihari S, Gorman MJ, Ying B, Yaun D, Raju S, et al. An Intranasal Vaccine Durably Protects Against SARS-CoV-2 Variants in Mice. *Cell Rep* (2021) 36:109452. doi: 10.1016/j.celrep.2021.109452
98. Hassan AO, Kafai NM, Dmitriev IP, Fox JM, Smith BK, Harvey IB, et al. A Single-Dose Intranasal ChAd Vaccine Protects Upper and Lower Respiratory Tracts Against SARS-CoV-2. *Cell* (2020) 183:169–184.e13. doi: 10.1016/j.cell.2020.08.026
99. Wang Z, Lorenzi JCC, Muecksch F, Finkin S, Viant C, Gaebler C, et al. Enhanced SARS-CoV-2 Neutralization by Dimeric IgA. *Sci Transl Med* (2021) 13:eabf1555. doi: 10.1126/scitranslmed.abf1555

Conflict of Interest: The authors declare that the research was conducted in the absence of any commercial or financial relationships that could be construed as a potential conflict of interest.

frontiers | Frontiers in Immunology

ORIGINAL RESEARCH
published: 09 May 2022
doi: 10.3389/fimmu.2022.873351

Orf Virus-Based Vectors Preferentially Target Professional Antigen-Presenting Cells, Activate the STING Pathway and Induce Strong Antigen-Specific T Cell Responses

Melanie Müller[1], *Alena Reguzova*[1], *Markus W. Löffler*[1,2,3,4*] *and Ralf Amann*[1*]

[1] Department of Immunology, Interfaculty Institute for Cell Biology, University of Tübingen, Tübingen, Germany, [2] Department of General, Visceral and Transplant Surgery, University Hospital Tübingen, Tübingen, Germany, [3] Department of Clinical Pharmacology, University Hospital Tübingen, Tübingen, Germany, [4] Cluster of Excellence iFIT (EXC2180) 'Image-Guided and Functionally Instructed Tumor Therapies', University of Tübingen, Tübingen, Germany

OPEN ACCESS

Edited by:
Gabriel Pedersen,
Statens Serum Institut (SSI), Denmark

Reviewed by:
Felix Ngosa Toka,
Ross University School of Veterinary Medicine, Saint Kitts and Nevis
Carlos Maluquer De Motes,
University of Surrey, United Kingdom
Christine Luttermann,
Friedrich-Loeffler-Institute, Germany

***Correspondence:**
Ralf Amann
ralf.amann@ifiz.uni-tuebingen.de
Markus W. Löffler
markus.loeffler@uni-tuebingen.de

Specialty section:
This article was submitted to Vaccines and Molecular Therapeutics, a section of the journal Frontiers in Immunology

Received: 10 February 2022
Accepted: 28 March 2022
Published: 09 May 2022

Citation:
Müller M, Reguzova A, Löffler MW and Amann R (2022) Orf Virus-Based Vectors Preferentially Target Professional Antigen-Presenting Cells, Activate the STING Pathway and Induce Strong Antigen-Specific T Cell Responses. Front. Immunol. 13:873351. doi: 10.3389/fimmu.2022.873351

Background: Orf virus (ORFV)-based vectors are attractive for vaccine development as they enable the induction of potent immune responses against specific transgenes. Nevertheless, the precise mechanisms of immune activation remain unknown. This study therefore aimed to characterize underlying mechanisms in human immune cells.

Methods: Peripheral blood mononuclear cells were infected with attenuated ORFV strain D1701-VrV and analyzed for ORFV infection and activation markers. ORFV entry in susceptible cells was examined using established pharmacological inhibitors. Using the THP1-Dual™ reporter cell line, activation of nuclear factor-κB and interferon regulatory factor pathways were simultaneously evaluated. Infection with an ORFV recombinant encoding immunogenic peptides (PepTrio-ORFV) was used to assess the induction of antigen-specific CD8+ T cells.

Results: ORFV was found to preferentially target professional antigen-presenting cells (APCs) *in vitro*, with ORFV uptake mediated primarily by macropinocytosis. ORFV-infected APCs exhibited an activated phenotype, required for subsequent lymphocyte activation. Reporter cells revealed that the stimulator of interferon genes pathway is a prerequisite for ORFV-mediated cellular activation. PepTrio-ORFV efficiently induced antigen-specific CD8+ T cell recall responses in a dose-dependent manner. Further, activation and expansion of naïve antigen-specific CD8+ T cells was observed in response.

Discussion: Our findings confirm that ORFV induces a strong antigen-specific immune response dependent on APC uptake and activation. These data support the notion that

ORFV D1701-VrV is a promising vector for vaccine development and the design of innovative immunotherapeutic applications.

Keywords: parapoxvirus, ORFV, viral vector, vaccine, antigen-presenting cell, STING pathway, T cell response

INTRODUCTION

Orf virus (ORFV) is a large (~ 140 kb) double-stranded DNA (dsDNA) *Parapoxvirus* (1). The wildtype ORFV genome contains highly conserved regions comprising genes implicated in virulence and host immunomodulation (2). As a zoonotic pathogen ORFV primarily infects goats and sheep as its natural host. Humans are rarely affected and infections are typically associated with minor self-limiting symptoms (3, 4). The ORFV strain D1701, which was attenuated by successive *in vitro* passages in primary bovine and ovine cells, was used as a vaccine against Orf disease in its natural host animals, but it was discontinued due to lacking long-term protective effects (5, 6). Further *in vitro* passaging in Vero cells generated the Vero-adapted attenuated ORFV strain D1701-V, which lacks any pathogenic features, even in immunosuppressed sheep (7–10).

Further, substitution of the viral *vegf-e* gene by foreign transgenes generated the ORFV strain D1701-VrV. The poxviral early vegf promotor enables transgene expression without the requirement of viral replication, thus allowing ORFV to be used in non-permissive cells (10). ORFV D1701-VrV therefore represents an optimal viral vector candidate for animal and human use and possesses several desirable characteristics, including: 1.) a beneficial safety profile; 2.) a large genome, allowing for the integration of multiple/large genes; 3.) negligible induction of ORFV-specific immunity, allowing for repeated administration; 4.) potent induction of innate and adaptive immune responses against inserted transgenes; and 5.) large virus production capacity in cell cultures, facilitating the rapid generation of vaccine prototypes (11, 12). Meanwhile, recombinant ORFV D1701-VrV-based vaccines have been generated against several zoonotic pathogens, including avian influenza (13), rabies (11), pseudorabies (14), and Borna disease virus (15). Various animal models provided promising results, demonstrating protective immunity through respective vaccines with limited adverse effects (1, 16). Of note, recent studies with ORFV D1701-VrV by Reguzova et al. showed successful T cell induction against transgenes, while ORFV-specific epitopes remained unaffected (12, 17).

In spite of the emerging role as a vaccine vector and potential immunotherapeutic applications, the mechanisms by which ORFV D1701-VrV induces immunity, and effects observed in human cells, remain to be characterized. Respective knowledge is essential for the development of ORFV-based vaccine platforms and potential clinical applications for human use. Therefore, this study focused on the mechanisms involved in ORFV-induced immune responses in human cells. To this end, we sought to investigate: 1) the susceptibility of human primary lymphocytes to ORFV infection and the respective cell tropism; 2) the activation of peripheral blood mononuclear cells (PBMCs) subsets and antigen-presenting cells (APCs) after ORFV infection; 3) ORFV entry into susceptible cells; 4) the signaling pathway(s) involved after ORFV-infection of cells; and 5) induction of antigen-specific T cell responses through ORFV D1701-VrV *in vitro*.

MATERIALS AND METHODS

Generation of ORFV D1701-V-D12-mCherry and ORFV D1701-V12-PepTrio-D12-Cherry

ORFV strain D1701-V-D12-mCherry (V-D12-Cherry) was generated as described previously (6, 10) to enable visualization of viral infection through the detection of mCherry florescence by flow cytometry. The novel artificial antigen "PepTrio", designed specifically for use in this work, consists of three immunodominant epitopes from human cytomegalovirus (HCMV) proteins IE-1 (316-324; VLEETSVML) and pUL83/pp65 (495-503; NLVPMVATV and 120-128; MLNIPSINV), which all bind to the major histocompatibility complex (MHC) class I molecule HLA-A*02:01. The PepTrio-encoding gene (synthesized by Gene Art, Thermo Fisher Scientific, Waltham, MA, USA) was isolated as a *Bgl*II–*Eco*RI DNA fragment (164 bp) by agarose gel electrophoresis and Qiaex II gel extraction (Qiagen, Hilden, Germany) followed by ligation (Quick Ligation Kit, New England BioLabs, Frankfurt am Main, Germany) into *Bgl*II–*Eco*RI-digested pV12-Cherry (10). The resulting transfer plasmid, pV12-PepTrio, was used to transfect D1710-V-GFP-D12-mCherry-infected Vero cells using nucleofection (Cell Line V Nucleofector® Kit, Lonza, Köln, Germany) to replace the GFP-encoding gene with PepTrio, as described previously (10). The new ORFV recombinant D1701-V12-PepTrio-D12-mCherry (V12-PepTrio-D12-Cherry, PepTrio-ORFV) was selected and purified by fluorescence-based negative selection, as described previously (10). PCR primers spanning the *vegf* locus [5'-GGTGCTCAGCGTGGTGGCGGTTTC-3' (forward) and 5'-ACCACAAGGCCGCCCAGAAGACGCCGCTAG-3' (reverse)] were commercially obtained (Metabion, Planegg, Germany) and were used to confirm the presence of a 738-bp amplicon for the PepTrio gene and the loss of an 1129-bp amplicon for the GFP-encoding gene. Sequencing confirmed the correct integration of the PepTrio gene into the *vegf* locus. The ORFV recombinants were purified, propagated, and titrated in Vero cells, as described previously (10).

Donor Cells and Cell Lines

PBMCs were isolated from buffy coats obtained at the University Hospital Tübingen, Center for Clinical Transfusion Medicine, from HCMV-seronegative and HCMV-seropositive donors. The use of biomaterials was approved by the Ethics Committee of the Medical Faculty of Eberhard Karls University and the University Hospital of Tübingen (project number: 507/2017B01).

African green monkey kidney (Vero) cells (ATCC®) were cultured in Dulbecco's Modified Eagle's Medium (DMEM; Life

Technologies) containing 5% fetal calf serum (FCS; Capricorn Scientific, Ebsdorfergrund, Germany) with 0.5% penicillin–streptomycin. All cells were cultured at 37°C with 5% CO_2 in a humidified incubator.

Cell Isolation and Macrophage and Dendritic Cell (DC) Differentiation

PBMCs were isolated from buffy coats by Ficoll density gradient centrifugation (Biocoll Separation Solution, Merck KGaA, Darmstadt, Germany). CD14+ monocytes were isolated from total PBMCs by magnetic cell sorting using CD14 microbeads (MACS, Miltenyi Biotec, Bergisch Gladbach, Germany). PBMCs or CD14+ monocytes were seeded at a density of 1×10^6 or 1×10^5 per well in a 96-well plate, respectively, and cultured with 200 µL Iscove's Modified Dulbecco's Medium (IMDM; Lonza, Köln, Germany) supplemented with 10% heat-inactivated FCS (Sigma-Aldrich, St. Louis, MO, USA). Monocyte-derived macrophages were differentiated from CD14+ cells with 50 ng/mL granulocyte-macrophage colony-stimulating factor (GM-CSF; Leukine® (Sargramostim), Sanofi, Paris, France), immature dendritic cells (iDCs) were differentiated from CD14+ cells with 50 ng/mL GM-CSF and 50 ng/mL interleukin (IL)-4 (Peprotech, Rocky Hill, NJ, USA). Mature DCs (mDCs) were generated by stimulating iDCs with 100 ng/mL lipopolysaccharide (LPS; Sigma-Aldrich) for 24 h.

Infection of Vero Cells With Virus Lysates From Infected APCs

DCs and macrophages were infected with V-D12-Cherry at MOI 1.0 and MOI 5.0 for 6 h, 24 h, and 96 h, respectively and lysed by repeated freezing and thawing. Vero cells were infected using DC- and macrophage-lysates (infection at MOI 5.0) with different dilutions for 24 h. The percentage of infected Vero cells was assessed by flow cytometry and viral infection was determined in respective samples, confirming a linear range of infection from 0.5-30%.

Monocyte Depletion

Monocytes were depleted from total PBMCs using CD14 microbeads and depletion columns (MACS) in accordance with the manufacturer's instructions. Successful depletion (98-100%) was verified by flow cytometry.

Viral Infection

PBMCs, monocytes, macrophages and DCs were inoculated with V-D12-Cherry for *in vitro* infection at a multiplicity of infection (MOI) of 5.0 for the indicated times, if not specifically indicated otherwise.

Inhibition of Phagocytosis and Macropinocytosis

Phagocytosis was inhibited by incubating cells with 20 µM cytochalasin D (Sigma-Aldrich) for 30 min before infection. Macropinocytosis was inhibited by incubating cells with 3 µM rottlerin (Sigma-Aldrich) for 30 min before infection.

Cytometric Bead Array

For analysis of CXCL10 production, DCs were infected with V-D12-Cherry for 24 h (MOI 5.0). Quantification of CXCL10 in the supernatants of ORFV-infected DCs was performed using BD™ Cytometric Bead Array (CBA) (BD Biosciences, Franklin Lakes, NJ, USA) according to the manufacturer's instructions.

Activation of THP1-Dual™ Cells

THP1-Dual™ cells, THP1-Dual™ KO-IFNAR2 cells, THP1-Dual™ KO-MyD88 cells, and THP1-Dual™ KO-STING cells were purchased (InvivoGen, San Diego, CA, USA). Secreted embryonic alkaline phosphatase (SEAP) and luciferase activity were assessed after infection with V-D12-Cherry (MOI 10.0) in accordance with the manufacturer's protocol for THP1-Dual™ cells. Infection rates were determined by flow cytometry and established at 25% ± 5%.

Memory T Cell Expansion

A total of 5×10^6 PBMCs per well, obtained from HCMV-seropositive blood donors, were seeded into a 24-well plate in 2 mL medium (RPMI-1640 with 10% heat-inactivated FCS) and incubated for 6 h. PBMCs were infected with PepTrio-ORFV or V-D12-Cherry (mock virus control) at the indicated MOI, or stimulated with 1 µg/mL HCMV pp65 $_{495–503}$ NLVPMVATV peptide (positive control) for CD8+ T cell activation. Every 2–3 days, 500 µL of medium was replaced with 500 µL fresh medium containing 20 U/mL IL-2 (R&D Systems, Minneapolis, MN, USA). After 12 days of stimulation, analysis of T cell expansion and antigen-specific T cell functionality was performed by HLA-tetramer and intracellular cytokine staining, respectively.

Priming of Naïve T Cells

A total of 1×10^8 PBMCs from HCMV-seronegative blood donors were used to isolate CD14+ monocytes and to subsequently induce differentiation into DCs as described above. DCs (2×10^5) were seeded into a 96-well pate in 200 µL medium per well. After one week, DCs were infected with PepTrio-ORFV (MOI 5.0) for 6 h or stimulated with 10 ng/mL IL-4 (Peprotech), 800 U/mL GM-CSF, 10 ng/mL LPS, and 100 U/mL IFN-γ (Peprotech) for 24 h and loaded with 25 µg/mL HCMV pp65 $_{495–503}$ NLVPMVATV peptide for 2 h. Isolation of CD8+ T cells from cryopreserved PBMCs was performed by magnetic cell sorting using CD8 microbeads (MACS). Subsequently, 1×10^6 CD8+ T cells were added to the infected or peptide-loaded DCs in the presence of 5 ng/mL IL-12 (PromoCell, Heidelberg, Germany). Every 2–3 days, 100 µL medium was replaced with 100 µL fresh medium containing 40 U/mL IL-2. After one week of co-culture of DCs and CD8+ T cells, the latter were restimulated with autologous peptide-loaded PBMCs. For this purpose, autologous PBMCs were thawed and loaded with 25 µg/mL HCMV pp65 $_{495–503}$ NLVPMVATV peptide and incubated for 2 h. A total of 1×10^6 peptide-loaded PBMCs were added to each well following irradiation (30 Gy). T cells were stimulated three or four times in total with 7-day intervals. One week after the last re-stimulation,

analysis of antigen-specific CD8+ T cell responses was performed by HLA-tetramer staining.

Antibody Staining and Flow Cytometry

To prevent non-specific antibody binding, cells were treated with Fc block (BioLegend, San Diego, CA, USA) before antibody staining according to the manufacturer's instructions. To stain for viability, cells were washed with PBS and stained using the Zombie Aqua™ Fixable Viability Kit (BioLegend). Before extracellular staining, cells were washed twice with staining buffer (2 mM ethylenediaminetetraacetic acid [EDTA], 2% FCS, and 0.02% NaN_3 in PBS).

To analyze PBMC activation, cells were stained with antibodies specific for $CD4^{PacificBlue}$, $CD8^{APC/Cy7}$, $CD14^{AlexaFluor700}$, $CD19^{PerCP}$, $CD56^{BV605}$, and $CD69^{PE}$ (all BioLegend). Infected monocytes were stained for $CD14^{AlexaFluor700}$ and the activation marker human leukocyte antigen (HLA)-DR^{BV711}. Monocyte-derived macrophages were stained for $CD14^{AlexaFluor700}$, the activation markers HLA-DR^{BV711}, $CD80^{FITC}$, $CD86^{BV605}$, and $CD40^{PE/Cy7}$ (all BioLegend). Monocyte-derived DCs were stained for $CD11c^{BV421}$, the activation markers HLA-DR^{BV711}, $CD80^{FITC}$, $CD86^{BV605}$, and $CD40^{PE/Cy7}$, and the maturation marker $CD83^{APC}$ (all BioLegend). All staining steps were performed by incubating the cells and antibodies at 4°C for 30 min followed by two washing steps with staining buffer.

For HLA-tetramer staining, cells were washed twice with 200 µL PBS and then resuspended in 50 µL tetramer buffer (50% FCS, 2 mM EDTA in PBS) with 1 µL phycoerythrin (PE)-conjugated HLA-tetramer. Incubation was performed at room temperature for 30 min in the dark. After incubation, cells were stained for viability (Zombie Aqua™ Fixable Viability Kit) and for extracellular markers using antibodies specific for $CD4^{PacificBlue}$ and $CD8^{APC/Cy7}$ (BioLegend).

For intracellular cytokine staining, expanded CD8+ memory T cells were stimulated with HCMV $pp65_{495–503}$ peptide NLVPMVATV (1 µg/mL) in the presence of 10 µg/mL brefeldin A (Sigma-Aldrich) for 16 h. After incubation, cell viability staining was performed (Zombie Aqua™ Fixable Viability Kit), followed by cell surface staining with antibodies specific for $CD4^{PacificBlue}$ and $CD8^{APC/Cy7}$ (BioLegend). The cells were subsequently fixed and permeabilized using BD Cytofix/Cytoperm (BD Biosciences, Franklin Lakes, NJ, USA) at 4°C for 30 min and incubated with antibodies specific for IFN-γ^{APC} and tumor necrosis factor (TNF)$^{PE/Cy7}$ (BioLegend).

Samples were analyzed using a LSR Fortessa™ flow cytometer (BD Biosciences) and data processing was performed with FlowJo® software (TreeStar Inc., Ashland, OR, USA).

Statistical Analysis

All statistical analyses were performed using GraphPad Prism 9 software. Data are presented as means ± standard deviation. Normality of data was tested using the Shapiro-Wilk test. Comparisons between groups were performed using a two-tailed Student´s *t*-test. A $p < 0.05$ was considered to indicate statistical significance.

RESULTS

ORFV Preferentially Targets Antigen-Presenting Cells *In Vitro*

To examine whether ORFV infects and drives the expression of transgenes in leukocytes, PBMCs were infected with ORFV encoding mCherry (V-D12-Cherry) for 24 h *in vitro*, stained and assessed by flow cytometry to identify cell subsets (T cells, B cells, NK cells and monocytes) susceptible for infection. Expression of mCherry is driven by an early poxviral promoter that enables strong early transgene expression without the need for ORFV genome replication or infectious virus production. After infection, mCherry expression, indicating viral infection, remained restricted to CD14+ monocytes and resulted in a mean infection rate of ~15% (**Figure 1A**). All other assessed cell populations were unaffected.

Since ORFV incubation with PBMCs only infected monocytes, we next analyzed whether other APCs (*i.e.*, macrophages and DCs) were also susceptible for infection. When infecting monocyte-derived macrophages and DCs with ORFV for different periods, the percentage of mCherry-positive macrophages and DCs increased and peaked at 24 h, subsequently decreasing until 96 h (**Figure 1B**).

Next, we determined whether ORFV replicates in human APCs. This was investigated by assessing the percentage of Vero cells that were infected through incubation with cell lysates from macrophages and DCs previously infected with ORFV and then cultured for different periods of time.

The infection rates of Vero cells lay in the linear range from 0.5 – 30% of infected cells at 24 hours post infection. Significantly fewer Vero cells became infected when incubated with cell lysates from both macrophages and DCs harvested 96 h after ORFV incubation as compared to incubation with respective cell lysates harvested earlier at 6 h (**Figure 1C**), suggesting that after 96 h less ORFV virus is present in the APC lysate than after 6 h. Thus, the decreasing amount of virus over time indicates a lack of productive generation of infectious virus particles in APCs.

Overall, these results demonstrate that professional APCs are susceptible to ORFV infection and enable expression of the transgene without the need for viral replication.

ORFV Is Taken Up by Professional APCs *via* Macropinocytosis

After establishing the susceptibility of APCs for ORFV infection, we aimed to investigate the mechanisms of ORFV entry into these cells. APCs take up pathogens either *via* receptor-mediated endocytosis (*e.g.*, phagocytosis) or *via* receptor-independent macropinocytosis, but both processes require actin polymerization (18, 19). Therefore, we inhibited actin polymerization in monocyte-derived macrophages and DCs by cytochalasin D before ORFV infection. Treated APCs remained negative for ORFV infection, while untreated APCs became infected ($p < 0.01$; **Figure 2A**), indicating that actin cytoskeleton rearrangement is required for ORFV uptake.

To differentiate an uptake *via* phagocytosis from macropinocytosis, the cells were treated with the protein kinase C delta inhibitor rottlerin that specifically inhibits macropinocytosis at

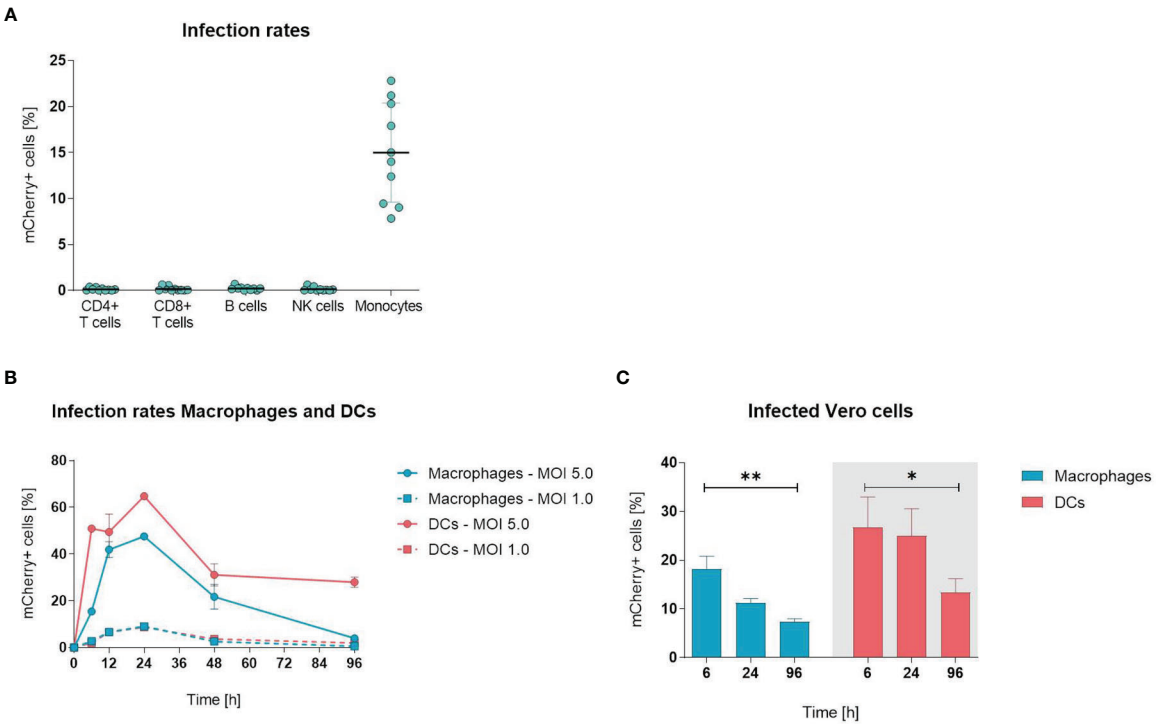

FIGURE 1 | Orf virus (ORFV) preferentially targets antigen-presenting cells *in vitro*. **(A)** Human peripheral blood mononuclear cells (PBMCs) were inoculated with V-D12-Cherry [multiplicity of infection (MOI) 5.0, 24 h]. Different cell subsets were identified by extracellular staining [CD4: CD4+ T cells, CD8: CD8+ T cells, CD19: B cells; CD56: natural killer (NK) cells; CD14: monocytes] and the percentage of viable mCherry+ cells was determined by flow cytometry analysis. Data represent mean ± SD of biological replicates. **(B)** Macrophages and DCs were infected with V-D12-Cherry (MOI 1.0 and MOI 5.0). The percentage of viable mCherry+ cells was determined at 6, 12, 24, 48 and 96 h post-infection by flow cytometry. X-axis: time post-infection (h); Y-axis: percentage of mCherry+ cells. Data represent mean ± SD of technical replicates (n=3). **(C)** Cell lysate of V-D12-Cherry-infected (MOI 5.0) macrophages and DCs at 6 h post-infection (hpi), 24 hpi, and 96 hpi was used to infect Vero cells. The percentage of mCherry+ Vero cells was determined 24 hpi. X-axis: time point after macrophage or DC infection; Y-axis: percentage of mCherry+ Vero cells. Data represent mean ± SD of technical replicates (n=3) and are representative for 3 independent experiments. Statistical differences are shown (unpaired *t*-test). *P < 0.05; **P < 0.01.

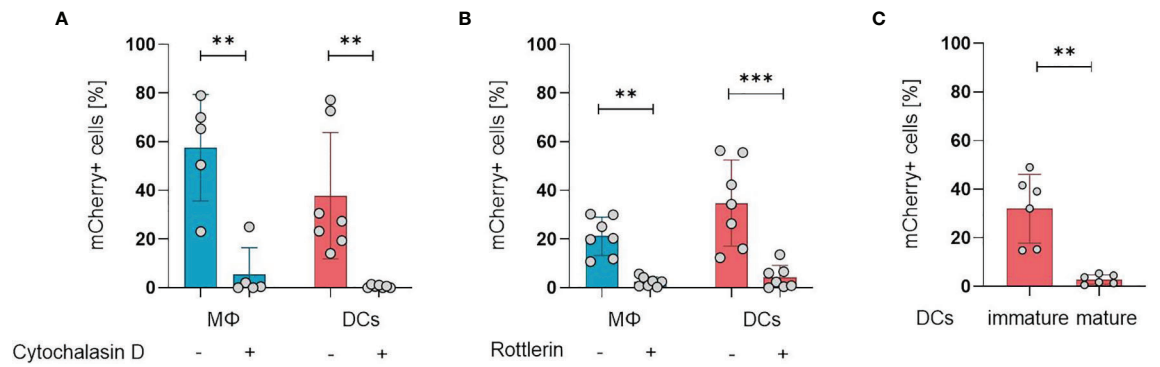

FIGURE 2 | ORFV is taken up by professional APCs *via* macropinocytosis. **(A)** Macrophages (MΦ) and DCs were treated with 20 µM cytochalasin D or left untreated. After infection with V-D12-Cherry (MOI 5.0, 24 h) the level of mCherry expression was measured using flow cytometry. The percentage of positive cells is indicated. **(B)** Macrophages and DCs were treated with 3 µM rottlerin or left untreated. After infection with V-D12-Cherry (MOI 5.0, 24 h) mCherry expression was measured using flow cytometry. The percentage of positive cells is indicated. **(C)** Immature DCs and LPS-matured DCs were infected with V-D12-Cherry (MOI 5.0, 24 h). The percentage of mCherry+ cells was determined using flow cytometry. Of note: cells of different donors were used for experiments shown in **(A–C)**. Data represent mean ± SD of biological replicates. Statistical differences are shown (paired *t*-test). **P < 0.01; ***P < 0.001.

low concentrations (20, 21). The infection rate in DCs after treatment was significantly reduced compared to controls ($p < 0.001$), however, a baseline infection was discernible in the latter (**Figure 2B**), confirming that ORFV mainly enters DCs *via* macropinocytosis. Respective findings could also be shown in macrophages (**Figure 2B**).

While phagocytosis and macropinocytosis are well-known uptake mechanisms of immature DCs, this ability is lost during DC maturation and activation (22). Therefore, we tested whether DC maturation influences the uptake of ORFV. Both immature DCs (iDCs) and matured DCs (mDCs) were incubated with ORFV. Results confirmed that iDCs were significantly more frequently infected than mDCs ($p < 0.001$; **Figure 2C**).

PBMCs and Professional APCs Are Activated After ORFV Infection *In Vitro*

Next, we examined whether incubation with ORFV induces activation of leukocytes *in vitro*. First, we analyzed the activation state of APCs upon ORFV uptake. To characterize monocyte activation, CD14+ cells among PBMCs were purified and stained for HLA-DR 24 h after ORFV infection. Results revealed that HLA-DR expression was significantly increased in the ORFV-infected monocytes when compared to untreated controls ($p < 0.01$; **Figure 3A**).

To investigate activation of professional APCs after ORFV-infection, macrophages and DCs were incubated with ORFV for 24 h and subsequently expression of CD80, CD86, HLA-DR, and CD40 were assessed on CD14+ macrophages and CD11c+ DCs. DCs were further examined for the maturation marker CD83 (23). The expression of activation markers CD80, CD86 and HLA-DR was strongly increased on macrophages following infection compared to the non-infected control. The expression of all assessed activation markers observed on DCs from different donors varied substantially. However, the proportion of HLA-DR- and CD83-positive DCs were found markedly increased following infection (**Figure 3B**). In addition, analysis of cell culture supernatant 24 h after ORFV infection showed that DCs produced a significantly increased amount of CXCL10 after incubation with ORFV compared to uninfected DCs (**Figure 3C**). To investigate the effect of APC activation on activation of lymphocytes, we next analyzed the activation state of cell subsets in human PBMCs after incubation with ORFV *in vitro*. Following incubation with ORFV a significantly increased percentage of CD4+ and CD8+ T cells, B cells as well as NK cells expressed CD69, as compared to untreated controls (all $p < 0.001$; **Figure 3D**). This activation state was found particularly pronounced in NK cells.

These results indicate that infection with ORFV induces activation of APCs upon virus uptake and subsequently leads to the activation of T cells, B cells, and NK cells.

Lymphocyte Activation Depends on ORFV-Infected Monocytes

Since infection of PBMCs with ORFV led to an increase of CD69+ cells among lymphocytes, we sought to investigate the role of monocytes in the activation of other cell subsets. Thus, both total PBMCs and monocyte-depleted PBMCs were infected with ORFV and assessed for CD69 expression. While the infection of total PBMCs led to the activation of the different cell subsets, as evidenced before, the proportion of CD69-expressing CD4+ and CD8+ T cells, B cells, or NK cells among lymphocytes was not increased when monocytes were depleted (**Figures 4A–D**).

These data suggest that uptake of ORFV by APCs is a prerequisite for subsequent lymphocyte activation.

Activation of the Stimulator of Interferon Genes (STING) Pathway in APCs Through ORFV Infection

To investigate ORFV-mediated APC activation in more detail, a monocytic reporter cell line (THP1-Dual cells) was used to investigate pathways involved in monocyte activation. These cells allow for simultaneous studies of the NF-κB and interferon regulatory factor pathways through SEAP and luciferase activity, respectively. To assess pathways required for APC activation, THP1-Dual reporter cells were infected with ORFV. Infected THP1-Dual KO MyD88 cells exhibited comparable SEAP production as infected THP1-Dual control cells (**Figure 5A**), indicating that ORFV-mediated APC activation occurs independent of MyD88. Luciferase activity in infected THP1-Dual KO IFNAR cells was less compared to Luciferase activity in THP1-Dual cells (**Figure 5B**), suggesting that ORFV-mediated APC activation occurs partially dependent of IFNAR2. However, infection of THP1-Dual KO STING cells failed to induce luciferase activity, indicating that the activation of APCs by ORFV is mediated by the STING pathway (**Figure 5C**).

Induction of Cellular Immune Responses *In Vitro*

We assessed whether ORFV-infected APCs present encoded HLA class I-restricted epitopes leading to the activation of antigen-specific T cells. To this end, a recombinant ORFV encoding the artificial antigen PepTrio (V12-PepTrio-D12-Cherry; abbreviated as PepTrio-ORFV) was used, encoding three HLA-A*0201 restricted epitopes from cytomegalovirus (HCMV), i.e. $pp65_{495-503}$ NLVPMVATV, $pp65_{120-128}$ MLNIPSINV, and IE-$1_{316-324}$ VLEETSVML (**Figure 6A**). First the activation and expansion of antigen-specific memory CD8+ T cells with different antigen specificities was assessed. Therefore, PBMCs from a HCMV-seropositive donor were infected with PepTrio-ORFV (MOI 5.0) and the frequency of transgene-specific CD8+ T cells was determined by flow cytometry after 12 days. PBMC stimulation with PepTrio-ORFV activated a robust peptide-specific CD8+ T cell recall response against all encoded epitopes (**Figure 6B**).

Further, the relation between ORFV infection dose and the proliferation and activation of memory CD8+ T cells was investigated. Again, PBMCs from a HCMV-seropositive donor were infected with PepTrio-ORFV at different MOIs (0.1, 1.0 or 5.0). The frequency of HCMV $pp65_{495-503}$-specific CD8+ T cells was assessed 12 days after ORFV infection by flow cytometry using HLA-tetramer staining as well as intracellular cytokine staining for TNF and IFN-γ. Thereby, antigen-specific CD8+ T cell recall

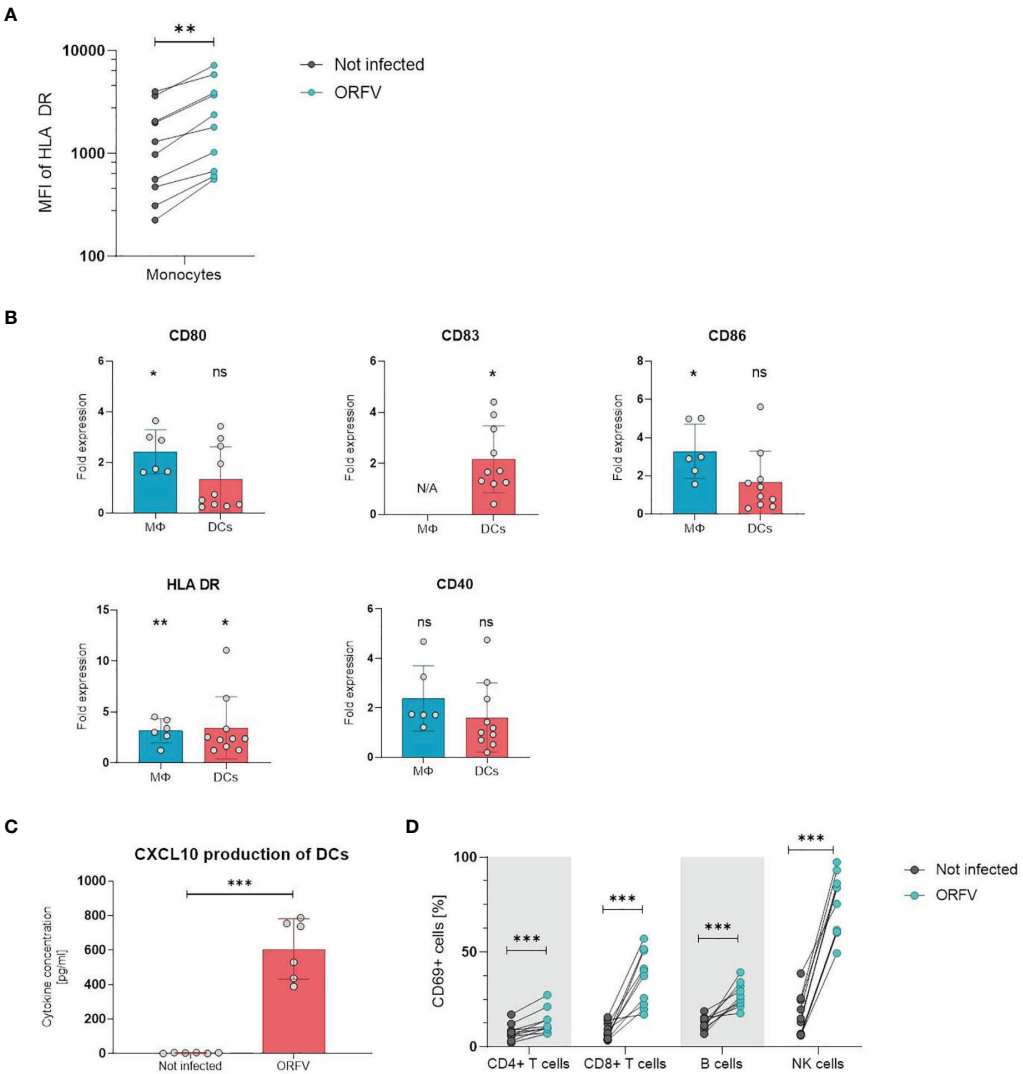

FIGURE 3 | PBMCs and professional APCs are activated after ORFV infection *in vitro*. **(A)** Monocytes were inoculated with V-D12-Cherry (MOI 5.0, 24 h). Expression of human leukocyte antigen (HLA)-DR after infection was determined by flow cytometry. Expression of the activation marker HLA-DR on monocytes is depicted as the specific mean fluorescent intensity (sMFI) calculated as: MFI of the sample *minus* MFI of the isotype control. The change in HLA-DR expression was compared between non-infected and V-D12-Cherry-infected monocytes. Statistical differences are shown (paired *t*-test). **P < 0.01. **(B)** Macrophages (MΦ) and DCs were infected with V-D12-Cherry (MOI 5.0, 24 h). The expression of surface markers CD80, CD83, CD86, HLA-DR, and CD40 was analyzed between non-infected and V-D12-Cherry-infected cells and is indicated as the fold expression compared to expression on non-infected cells. Data represent mean ± SD of biological replicates. Statistical differences are shown for each marker (one sample *t*-test). ns, not statistically significant; *P < 0.05; **P < 0.01. **(C)** DCs were infected with V-D12-Cherry (MOI 5.0, 24 h). The concentration of CXCL10 in cell culture supernatant was determined *via* Cytometric Bead Array (CBA). Statistical differences are shown (paired *t*-test). ***P < 0.001. **(D)** Human peripheral blood mononuclear cells (PBMCs) were inoculated with V-D12-Cherry (MOI 5.0, 24 h). Expression of the activation marker CD69 after infection was determined by flow cytometry. The percentage of T cells, B cells, and NK cells expressing the early activation marker CD69 is indicated. Statistical differences are shown for all analyzed cell subsets (paired *t*-test). ***P < 0.001.

responses could be shown as depending on the ORFV infection dose (**Figure 6C**). In summary, proliferation and activation of memory CD8+ T cells was demonstrated in PBMCs of 7 individual HCMV-seropositive donors. Overall, infection with PepTrio-ORFV (MOI 5.0) resulted in the highest frequency of HCMV $pp65_{495–503}$-specific CD8+ T cells (**Figure 6D**).

Finally, priming of naive CD8+ T cells with PepTrio-ORFV-encoded peptides was also assessed *in vitro*. HLA-tetramer staining showed that HCMV $pp65_{495–503}$-specific CD8+ T cells could be successfully induced by ORFV-infected DCs (**Figure 6E**). Thereby, successful priming with ORFV-infected DCs was shown more frequently than when using peptide-loaded DCs.

Altogether, these data demonstrate that APCs infected with PepTrio-ORFV enable priming of naïve CD8+ T cells and induce the activation of functional memory CD8+ T cells against encoded HLA class I-restricted epitopes.

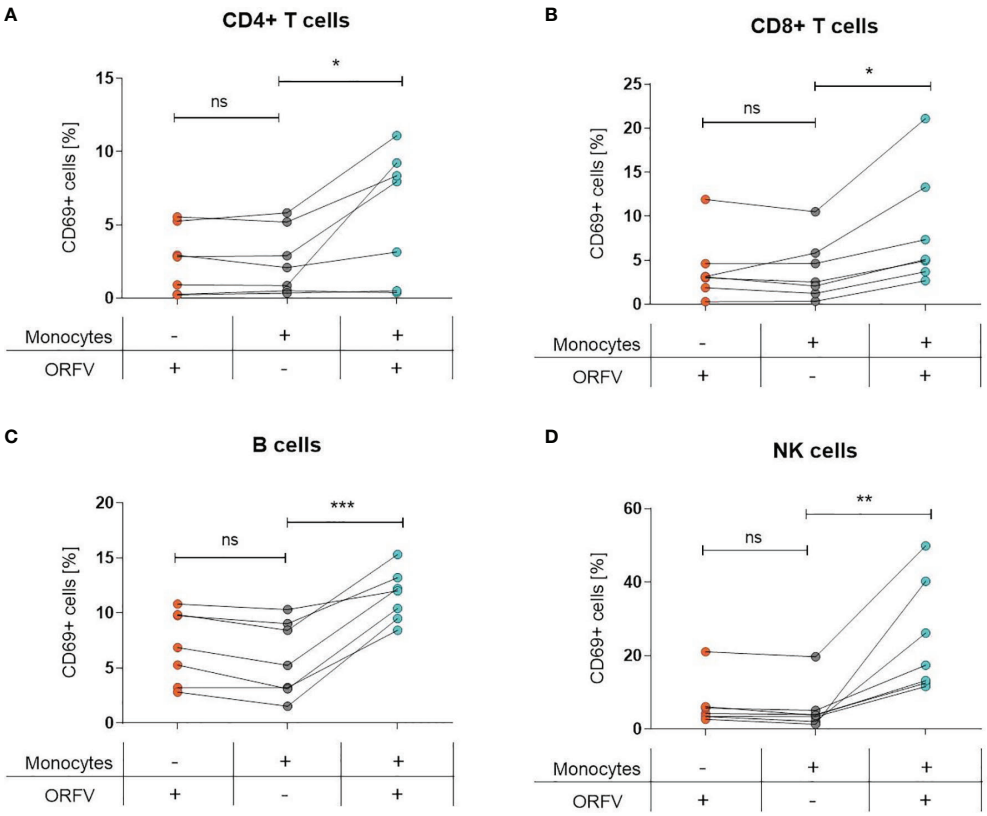

FIGURE 4 | Lymphocyte activation is dependent on ORFV-infected monocytes. PBMCs and monocyte-depleted PBMCs were infected with V-D12-Cherry (MOI 5.0, 24 h) and stained with a specific antibody against the early activation marker CD69. The percentage of CD69+ cells is indicated. The change in CD69 expression was compared between non-infected and V-D12-Cherry-infected PBMCs, as well as V-D12-Cherry-infected monocyte-depleted PBMCs. Statistical differences (paired *t*-test) are shown for **(A)** CD4+ T cells, **(B)** CD8+ T cells, **(C)** B cells, and **(D)** NK cells. ns, not statistically significant; *P < 0.05; **P < 0.01; ***P < 0.001.

DISCUSSION

ORFV D1701-VrV is a promising viral vector both for the development of novel vaccines and innovative immunotherapeutic approaches, enabling potent antigen-specific immune responses. Details on the precise mechanisms by which ORFV activates immune responses remain to be elucidated. The presented findings now demonstrate that ORFV-mediated T cell activation depends on the uptake of ORFV by APCs and on their activation *via* the STING pathway.

Analysis of cell tropism of ORFV revealed that only professional APCs such as monocytes, macrophages and DCs were shown to be susceptible to ORFV infection. In contrast, infection of T cells, B cells, and NK cells was neither detected in PBMCs nor in monocyte-depleted PBMCs. Experiments with rabbit PBMCs recently indicated this ORFV tropism. After infection of isolated rabbit PBMCs with D1701-V-Cherry, expression of mCherry was observed only in monocytes (24). The preferential targeting of professional APCs has also been observed in the context of other members of the *Poxviridae* family. In 2011, Flechsig et al. showed the preferential infection of monocytes when elucidating the cell tropism of modified vaccinia Ankara virus (MVA) in human PBMCs (25) and later confirmed by Altenburg et al. (26). In a large-scale study, cell tropism of MVA was investigated *in vitro* in human PBMCs, *ex vivo* in murine lung explants, and *in vivo* in mice, ferrets, and macaques after intranasal droplet infusion and following intramuscular injection. Regardless of the experimental set-up, animal model, or route of administration, the preferential infection of professional APCs was demonstrated.

By infecting professional APCs for different periods, we observed an increasing percentage of mCherry-positive cells until 24 h after infection, which subsequently decreased. Since infection of APCs was not synchronized, the observed increase of infected cells over the first 24 h was expected. Considering that infectious ORFV particles are produced considerably later than it is known for other poxviruses (27, 28), these results indicate the lack of viral spread in APCs. The absence of productive infectious virus particle generation in APCs was further demonstrated by incubating Vero cells with cell lysates from macrophages and DCs harvested 6 h and 96 h post infection. Moreover, since mCherry expression is driven by an early poxviral promoter, these results prove that expression of a transgene by ORFV is possible despite abortive infection.

Using established pharmacological inhibitors that prevent the entry of ORFV into APCs, we could determine entry *via* macropinocytosis as a main route. This is in line with other

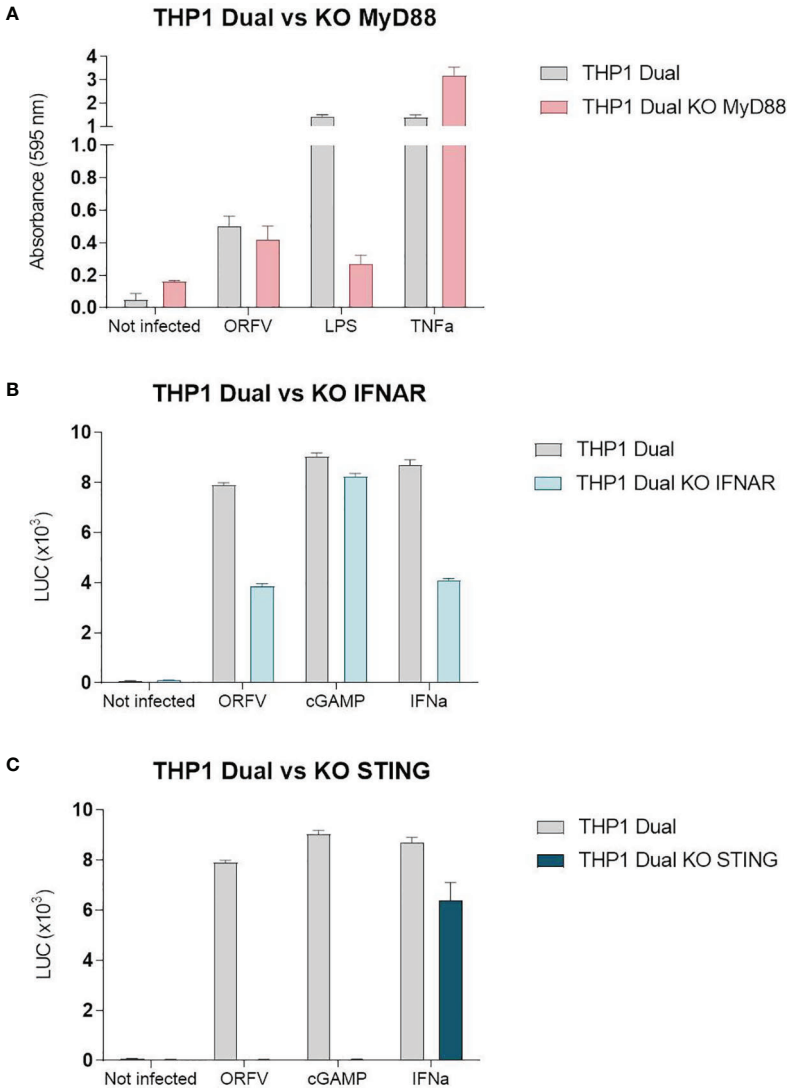

FIGURE 5 | The stimulator of interferon genes (STING) pathway is required for the activation of THP1-Dual cells. **(A)** THP1-Dual cells and THP1-Dual KO myeloid differentiation primary response 88 (MyD88) cells were infected with V-D12-Cherry (MOI 10.0, 24 h). Secreted embryonic alkaline phosphatase (SEAP) was analyzed in the cell culture supernatant. LPS stimulation (100 ng/ml) and tumor necrosis factor (TNF) stimulation (100 ng/ml) served as positive controls. Non-infected cells served as a negative control. **(B)** THP1-Dual cells and THP1-Dual KO interferon alpha receptor cells (IFNAR) were infected with V-D12-Cherry (MOI 10.0, 24 h). Luciferase secretion was analyzed in the cell culture supernatant. cGAMP (10 µ/ml) and interferon (IFN)-α stimulation (10^6 U/ml) served as a positive control. Non-infected cells served as a negative control. **(C)** THP1-Dual cells and THP1-Dual KO STING cells, were infected with V-D12-Cherry (MOI 10.0, 24 h). Luciferase secretion was analyzed in the cell culture supernatant. cGAMP (10 µ/ml) and interferon (IFN)-α stimulation (10^6 U/ml) served as a positive control. Non-infected cells served as a negative control. SEAP and luciferase activity was assessed in cells with infection rates of 25% ± 5%. Data represent mean ± SD of technical replicates (n=3) and are representative for 3 independent experiments.

members of the *Poxviridae* family. For example, Sangren et al. demonstrated that vaccinia virus enters monocyte-derived DCs *via* macropinocytosis (29). Nevertheless, phagocytosis and other forms of endocytosis may still represent ancillary forms of entry (30). Our observations that following maturation, APCs lose the ability to take up ORFV conforms with results from Sallusto et al., who found that DC maturation led to an irreversible loss of macropinocytosis (20). It has been suggested that this loss in antigen capture and processing capacity may be required for optimal antigen presentation to T cells (20).

Previous studies have investigated the activation of APCs by ORFV strain D1701-B, the original strain from which ORFV strain D1701-VrV was derived. After infection of murine bone marrow-derived DCs, increased expression of MHC class I and class II as well as CD86 was shown (31, 32). In this study, enhanced expression of the co-stimulatory molecules CD80, CD86, and CD40 as well as the MHC class II molecule HLA-DR and the production of CXCL10 successfully demonstrated the activation of human APCs by ORFV strain D1701-VrV for the first time. It was further shown that infection and activation

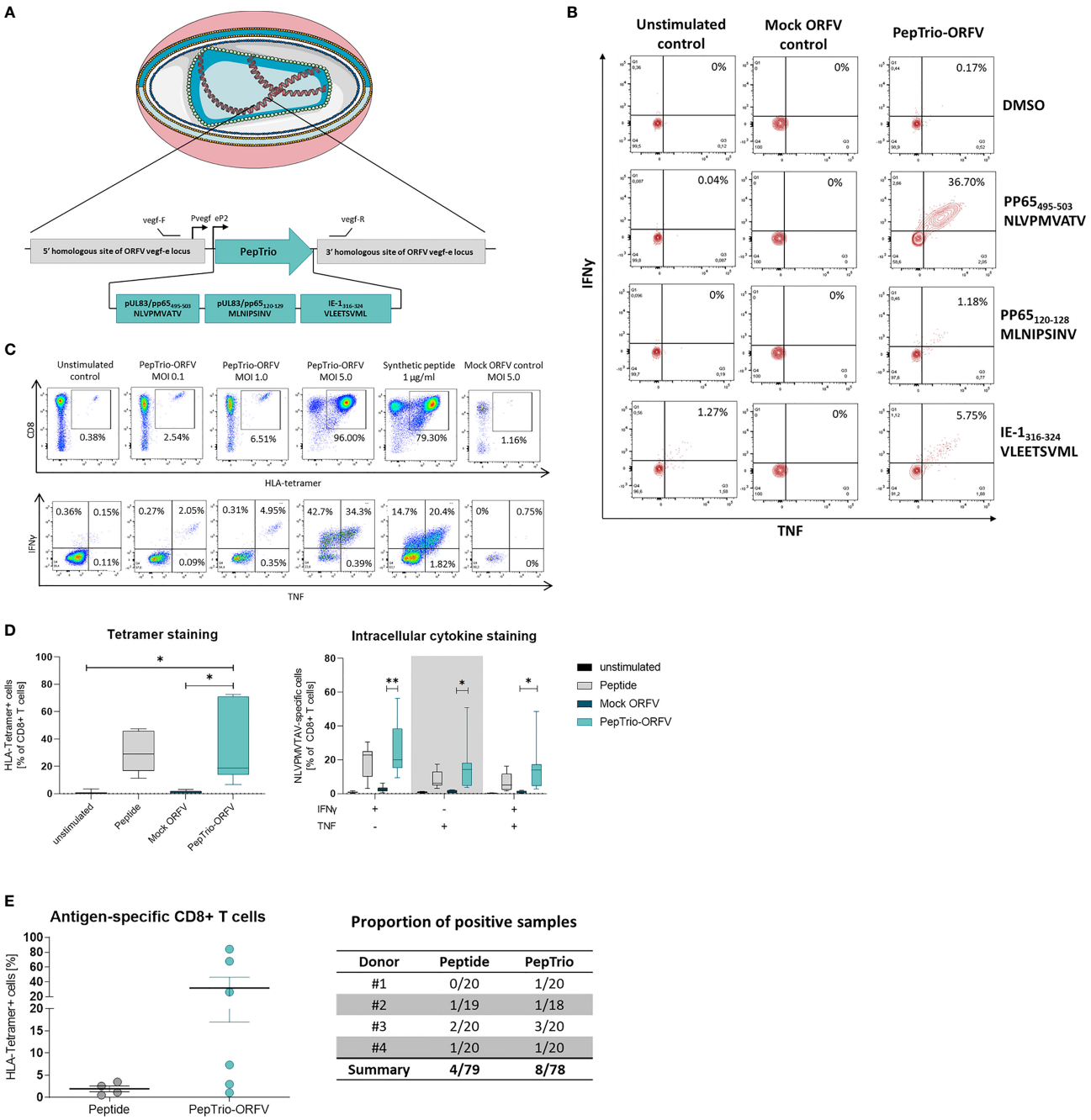

Donor	Peptide	PepTrio
#1	0/20	1/20
#2	1/19	1/18
#3	2/20	3/20
#4	1/20	1/20
Summary	**4/79**	**8/78**

FIGURE 6 | PepTrio-ORFV induces robust antigen-specific CD8+ T cell responses *in vitro*. **(A)** Schematic illustration of PepTrio integrated into the ORFV genome. PepTrio consists of minigenes that encode the HLA-A*0201 restricted epitopes HCMV pp65 $_{495–503}$ NLVPMVATV, pp65 $_{120–128}$ MLNIPSINV, and IE-1 $_{316–324}$ VLEETSVML. Each epitope is encoded with its own start and stop codon. Pvegf and eP2 denote the early promoters, and vegf forward and vegf reverse indicate the primer-binding locations. **(B)** PBMCs from human cytomegalovirus (HCMV)-seropositive blood donors were presensitized for 12 days with Mock-ORFV or PepTrio-ORFV (MOI 5.0) or kept unstimulated. Activation of HCMV pp65 NLVPMVATV-, pp65 MLNIPSINV- and IE-1 VLEETSVML-specific CD8+ cells upon stimulation was determined by intracellular cytokine staining. **(C, D)** PBMCs from human cytomegalovirus (HCMV)-seropositive blood donor were presensitized for 12 days with PepTrio-ORFV or Mock-ORFV at the indicated MOIs, or kept unstimulated. Synthetic HCMV pp65 $_{495–503}$ NLVPMVATV peptide was used as a control. Activation of HCMV pp65 NLVPMVATV-specific CD8+ cells upon stimulation was determined by HLA-tetramer staining and subsequent intracellular cytokine staining. **(D)** Data represent mean ± SD of biological replicates (n=7). Statistical differences (paired *t*-test) are shown. *P < 0.05; **P < 0.01. **(E)** Human monocyte-derived DCs of 4 donors were exposed to PepTrio-ORFV (MOI 5.0) for 6 h, followed by co-cultivation with autologous CD8+ T cells. After 4 weeks, the activation of naïve CD8+ T cells was assessed by HLA-tetramer staining. Peptide-loaded DCs used to stimulate CD8+ T cells served as a control.

of APCs is required for subsequent activation of T cells, B cells, and NK cells. A similar dependence was also demonstrated in studies conducted with MVA. Using an *in vivo* mouse model, Liu et al. demonstrated that MVA-infection of DCs was required to induce MVA-specific CD8+ T cell responses *via* both direct- and cross-presentation of viral antigens (33).

A main finding of our study was that APC activation involves the STING pathway. This was evidenced both through CXCL10 production by ORFV-infected DCs and the lack of activation of THP1-Dual KO STING cells. STING is a well-characterized adaptor molecule relevant for the cellular response to self and foreign cytosolic dsDNA (34). After detection of cytosolic dsDNA by cGAMP it binds to STING and induces IFN gene transcription (35). This is why STING-dependent signaling has been shown central for the induction of both innate and adaptive immunity in response to dsDNA viruses (36, 37) and was found to be critically involved in the induction of type I IFN induction in cDCs by MVA as well as a robust cytotoxic lymphocyte response connected with an MVA-based vaccination (36). However, we cannot exclude that activation of APCs by ORFV also occurs *via* additional pathways. Whereas MyD88 does not play a role in the activation of THP1-Dual cells in our experiment, Siegemund et al. showed that the activation of plasmacytoid bone-marrow derived dendritic cells (BM-pDCs) is dependent on this adaptor protein (31). Von Buttlar et al. further identified the endosomal receptor TLR9 as an ORFV-sensing receptor in BM-pDCs (32). To what extent ORFV is also recognized by TLR9 in human APCs remains to be determined by future experiments.

Initially, MVA infections were known to be recognized not only by DNA sensing pathways but also by TLR-dependent and -independent signaling pathways, including the RNA sensor melanoma differentiation-associated protein (MDA)-5, TLR2/TLR6 and NALP3 (38–42). In addition to cGAS, the STING-independent DNA sensors DNA-dependent protein kinase (DNA-PK) and Gamma-interferon-inducible protein (IFI16) are involved in immune activation by MVA (42) and therefore represent potential DNA sensors recognizing ORFV.

ORFV-based recombinant vectors have been successfully used in the past to develop prophylactic vaccines. A strong, long-lasting humoral immune response was elicited and protection against various infectious diseases was achieved in a wide range of animal species (11, 13–15, 43). However, whether and to what extent cellular immune responses are induced was not subject of these studies. Anyhow, depletion of CD8+ T cells after immunization with ORFV had no negative effect on protection against rabies or influenza virus infections (11, 13). In contrast, Rohde et al. suggested a T-cell-based protection of rabbits against infection with rabbit hemorrhagic disease virus, but without direct evidence for antigen-specific T cells (43). Schneider et al. recently demonstrated that an ORFV-based antitumor vaccine significantly inhibited tumor growth through inducing robust cellular immune responses, connected with complete tumor regression in rabbits after repeated administrations (24). Importantly, repeated vaccination with ORFV D1701-VrV did not induce ORFV-specific CD8+ T cell responses but induced respective immune responses towards an encoded transgene (12). In this study, the activation of both memory T cells and naïve T cells against ORFV-encoded transgenes was successfully demonstrated. This is in line with results from a very recently published proof-of-concept study of a D1701-VrV-based dengue virus (DENV) vaccine candidate (17).

However, our study has also some limitations. *In vitro* experiments with human PBMCs are subject to inherent variability, as these were obtained from a limited number of donors and such sample materials usually show considerable variance. Hence, the precise mechanisms of ORFV uptake and activation in tissue-resident APCs may differ and cannot be extrapolated from our data with absolute security. Although ORFV uptake by phagocytosis and macropinocytosis was established, a more detailed understanding of the molecular mechanisms would be desirable. In addition, although it has been shown that ORFV-mediated DC activation involves the STING pathway, the specific signaling cascade remains to be elucidated also in primary cells, as well as the potential role of other signaling pathways.

In conclusion, we successfully demonstrated that ORFV-mediated cellular immune responses involve virus uptake by APCs and their subsequent activation *via* the STING pathway. Activated APCs subsequently activate surrounding T cells, B cells, and NK cells. Furthermore, ORFV-infected DCs prime naïve T cells against encoded antigens and induce a potent recall response. These results support that ORFV is a promising viral vector for the induction of strong adaptive immune responses towards encoded antigens.

DATA AVAILABILITY STATEMENT

The original contributions presented in the study are included in the article/supplementary material. Further inquiries can be directed to the corresponding authors.

ETHICS STATEMENT

The use of human biomaterials was reviewed and approved by the Ethics Committee of the Medical Faculty of Eberhard Karls University and the University Hospital of Tübingen (project number: 507/2017B01). All blood donors provided their written informed consent before study participation and use of their biomaterials.

AUTHOR CONTRIBUTIONS

Conceptualization, MM, AR, and RA. Methodology, MM and AR. Validation, MM, AR, and RA. Formal analysis, MM and AR. Investigation, MM and AR. Resources, RA. Data curation, MM, AR, and RA. Writing—original draft preparation, MM and AR. Writing—review and editing, MWL and RA. Visualization, MM, AR, and MWL. Supervision, MWL and RA. Project administration, RA and MWL. Funding acquisition, RA. All authors have read and agreed to the final version of the manuscript.

FUNDING

This research was supported in part by the Institutional Strategy of the University of Tübingen (Deutsche Forschungsgemeinschaft ZUK63), the EXIST Forschungstransfer of the German Ministry for Economic Affairs and Energy, which is co-financed by the European Social Fund. We acknowledge support by Open Access Publishing Fund of the University of Tübingen.

ACKNOWLEDGMENTS

The authors thank Prof. Dr. Stefan Stevanović (University of Tübingen, Germany) and members of his laboratory for the peptide synthesis and HLA class I monomer complexes as well as the Center for Clinical Transfusion Medicine at the University Hospital Tübingen for the provision of buffy coats from blood donors and their support of this research.

REFERENCES

1. Wang R, Wang Y, Liu F, Luo S. Orf Virus: A Promising New Therapeutic Agent. *Rev Med Virol* (2019) 29(1):e2013. doi: 10.1002/jmv.25282
2. Mercer AA, Fraser K, Barns G, Robinson AJ. The Structure and Cloning of Orf Virus DNA. *Virology* (1987) 157(1):1–12. doi: 10.1016/0042-6822(87)90307-2
3. Al-Salam S, Nowotny N, Sohail MR, Kolodziejek J, Berger TG. Ecthyma Contagiosum (Orf)–Report of a Human Case From the United Arab Emirates and Review of the Literature. *J Cutan Pathol* (2008) 35(6):603–7. doi: 10.1111/j.1600-0560.2007.00857.x
4. Estela Cubells JR, Braverman I, Kashgarian M, Lazova R. A 65-Year-Old Female From Connecticut With Orf Infection. *Dermatopathology* (2016) 3(2):55–60. doi: 10.1159/000447125
5. Mayr A, Herlyn M, Mahnel H, Danco A, Zach A, Bostedt H. Control of Ecthyma Contagiosum (Pustular Dermatitis) of Sheep With a New Parenteral Cell Culture Live Vaccine. *Zentralbl Veterinarmed B* (1981) 28(7):535–52. doi: 10.1111/j.1439-0450.1981.tb01772.x
6. Rziha HJ, Büttner M, Müller M, Salomon F, Reguzova A, Laible D. Genomic Characterization of Orf Virus Strain D1701-V (Parapoxvirus) and Development of Novel Sites for Multiple Transgene Expression. *Viruses* (2019) 11(2):E127. doi: 10.3390/v11020127
7. Büttner M, Rziha HJ. Parapoxviruses: From the Lesion to the Viral Genome. *J Vet Med B Infect Dis Vet Public Health* (2002) 49(1):7–16. doi: 10.1046/j.1439-0450.2002.00539.x
8. Rziha H, Henkel M, Cottone R, Bauer B, Auge U, Götz F. Generation of Recombinant Parapoxviruses: Non-Essential Genes Suitable for Insertion and Expression of Foreign Genes. *J Biotechnol* (2000) 83(1–2):137–45. doi: 10.1016/S0168-1656(00)00307-2
9. Rziha HJ, Henkel M, Cottone R, Meyer M, Dehio C, Büttner M. Parapoxviruses: Potential Alternative Vectors for Directing the Immune Response in Permissive and Non-Permissive Hosts. *J Biotechnol* (1999) 73(2–3):235–42. doi: 10.1016/S0168-1656(99)00141-8
10. Rziha HJ, Rohde J, Amann R. Generation and Selection of Orf Virus (ORFV) Recombinants. *Methods Mol Biol* (2016) 1349:177–200. doi: 10.1007/978-1-4939-3008-1_12
11. Amann R, Rohde J, Wulle U, Conlee D, Raue R, Martinon O. A New Rabies Vaccine Based on a Recombinant ORF Virus (Parapoxvirus) Expressing the Rabies Virus Glycoprotein. *J Virol* (2013) 87(3):1618–30. doi: 10.1128/JVI.02470-12
12. Reguzova A, Ghosh M, Müller M, Rziha HJ, Amann R. Orf Virus-Based Vaccine Vector D1701-V Induces Strong CD8+ T Cell Response Against the Transgene But Not Against ORFV-Derived Epitopes. *Vaccines* (2020) 8(2):E295. doi: 10.3390/vaccines8020295
13. Rohde J, Amann R, Rziha HJ. New Orf Virus (Parapoxvirus) Recombinant Expressing H5 Hemagglutinin Protects Mice Against H5N1 and H1N1 Influenza A Virus. *PloS One* (2013) 8(12):e83802. doi: 10.1371/journal.pone.0083802
14. van Rooij EMA, Rijsewijk FAM, Moonen-Leusen HW, Bianchi ATJ, Rziha HJ. Comparison of Different Prime-Boost Regimes With DNA and Recombinant Orf Virus Based Vaccines Expressing Glycoprotein D of Pseudorabies Virus in Pigs. *Vaccine* (2010) 28(7):1808–13. doi: 10.1016/j.vaccine.2009.12.004
15. Henkel M, Planz O, Fischer T, Stitz L, Rziha HJ. Prevention of Virus Persistence and Protection Against Immunopathology After Borna Disease Virus Infection of the Brain by a Novel Orf Virus Recombinant. *J Virol* (2005) 79(1):314–25. doi: 10.1128/JVI.79.1.314-325.2005
16. Voigt H, Merant C, Wienhold D, Braun A, Hutet E, Le Potier MF. Efficient Priming Against Classical Swine Fever With a Safe Glycoprotein E2 Expressing Orf Virus Recombinant (ORFV VrV-E2). *Vaccine* (2007) 25(31):5915–26. doi: 10.1016/j.vaccine.2007.05.035
17. Reguzova A, Fischer N, Müller M, Salomon F, Jaenisch T, Amann R. A Novel Orf Virus D1701-VrV-Based Dengue Virus (DENV) Vaccine Candidate Expressing HLA-Specific T Cell Epitopes: A Proof-Of-Concept Study. *Biomedicines* (2021) 9(12):1862. doi: 10.3390/biomedicines9121862
18. Mercer J, Helenius A. Virus Entry by Macropinocytosis. *Nat Cell Biol* (2009) 11(5):510–20. doi: 10.1038/ncb0509-510
19. Quemin ER, Corroyer-Dulmont S, Krijnse-Locker J. Entry and Disassembly of Large DNA Viruses: Electron Microscopy Leads the Way. *J Mol Biol* (2018) 430(12):1714–24. doi: 10.1016/j.jmb.2018.04.019
20. Sallusto F, Cella M, Danieli C, Lanzavecchia A. Dendritic Cells Use Macropinocytosis and the Mannose Receptor to Concentrate Macromolecules in the Major Histocompatibility Complex Class II Compartment: Downregulation by Cytokines and Bacterial Products. *J Exp Med* (1995) 182(2):389–400. doi: 10.1084/jem.182.2.389
21. Sarkar K, Kruhlak MJ, Erlandsen SL, Shaw S. Selective Inhibition by Rottlerin of Macropinocytosis in Monocyte-Derived Dendritic Cells. *Immunology* (2005) 116(4):513–24. doi: 10.1111/j.1365-2567.2005.02253.x
22. Norbury CC, Chambers BJ, Prescott AR, Ljunggren HG, Watts C. Constitutive Macropinocytosis Allows TAP-Dependent Major Histocompatibility Complex Class I Presentation of Exogenous Soluble Antigen by Bone Marrow-Derived Dendritic Cells. *Eur J Immunol* (1997) 27(1):280–8. doi: 10.1002/eji.1830270141
23. Randolph GJ, Beaulieu S, Lebecque S, Steinman RM, Muller WA. Differentiation of Monocytes Into Dendritic Cells in a Model of Transendothelial Trafficking. *Science* (1998) 282(5388):480–3. doi: 10.1126/science.282.5388.480
24. Schneider M, Müller M, Yigitliler A, Xi J, Simon C, Feger T. Orf Virus-Based Therapeutic Vaccine for Treatment of Papillomavirus-Induced Tumors. *J Virol* (2020) 94(15):e00398-20. doi: 10.1128/JVI.00398-20
25. Flechsig C, Suezer Y, Kapp M, Tan SM, Löffler J, Sutter G. Uptake of Antigens From Modified Vaccinia Ankara Virus-Infected Leukocytes Enhances the Immunostimulatory Capacity of Dendritic Cells. *Cytotherapy* (2011) 13(6):739–52. doi: 10.3109/14653249.2010.549123
26. Altenburg AF, van de Sandt CE, Li BWS, MacLoughlin RJ, Fouchier RAM, van Amerongen G. Modified Vaccinia Virus Ankara Preferentially Targets Antigen Presenting Cells *In Vitro*, Ex Vivo and *In Vivo*. *Sci Rep* (2017) 7(1):8580. doi: 10.1038/s41598-017-08719-y
27. Rziha HJ, Büttner M. Parapoxviruses (Poxviridae). In: Bamford D. H., Zuckerman M, editors. *Encyclopedia of Virology*. Amsterdam, Oxford, Cambridge MA: Elsevier (2021). p. 666–74. Available at: https://linkinghub.elsevier.com/retrieve/pii/B9780128145159000588.
28. Kieser Q, Noyce RS, Shenouda M, James Lin YC, Evans DH. Cytoplasmic Factories, Virus Assembly, and DNA Replication Kinetics Collectively Constrain the Formation of Poxvirus Recombinants. *PloS One* (2020) 15(1):e0228028. doi: 10.1371/journal.pone.0228028
29. Sandgren KJ, Wilkinson J, Miranda-Saksena M, McInerney GM, Byth-Wilson K, Robinson PJ. A Differential Role for Macropinocytosis in Mediating Entry of the Two Forms of Vaccinia Virus Into Dendritic Cells. *PloS Pathog* (2010) 6(4):e1000866. doi: 10.1371/journal.ppat.1000866
30. Dutta D, Donaldson JG. Search for Inhibitors of Endocytosis: Intended Specificity and Unintended Consequences. *Cell Logist* (2012) 2(4):203–8. doi: 10.4161/cl.23967

31. Siegemund S, Hartl A, von Buttlar H, Dautel F, Raue R, Freudenberg MA. Conventional Bone Marrow-Derived Dendritic Cells Contribute to Toll-Like Receptor-Independent Production of Alpha/Beta Interferon in Response to Inactivated Parapoxvirus Ovis. *J Virol* (2009) 83(18):9411–22. doi: 10.1128/JVI.02362-08
32. von Buttlar H, Siegemund S, Büttner M, Alber G. Identification of Toll-Like Receptor 9 as Parapoxvirus Ovis-Sensing Receptor in Plasmacytoid Dendritic Cells. *PloS One* (2014) 9(8):e106188. doi: 10.1371/journal.pone.0106188
33. Liu L, Chavan R, Feinberg MB. Dendritic Cells are Preferentially Targeted Among Hematolymphocytes by Modified Vaccinia Virus Ankara and Play a Key Role in the Induction of Virus-Specific T Cell Responses *In Vivo*. *BMC Immunol* (2008) 9:15. doi: 10.1186/1471-2172-9-15
34. Xiao TS, Fitzgerald KA. The cGAS-STING Pathway for DNA Sensing. *Mol Cell* (2013) 51(2):135–9. doi: 10.1016/j.molcel.2013.07.004
35. Wu J, Sun L, Chen X, Du F, Shi H, Chen C. Cyclic GMP-AMP Is an Endogenous Second Messenger in Innate Immune Signaling by Cytosolic DNA. *Science* (2013) 339(6121):826–30. doi: 10.1126/science.1229963
36. Georgana I, Sumner RP, Towers GJ, Maluquer de Motes C. Virulent Poxviruses Inhibit DNA Sensing by Preventing STING Activation. *J Virol* (2018) 92(10):e02145-17. doi: 10.1128/JVI.02145-17
37. Lam E, Stein S, Falck-Pedersen E. Adenovirus Detection by the cGAS/STING/TBK1 DNA Sensing Cascade. *J Virol* (2014) 88(2):974–81. doi: 10.1128/JVI.02702-13
38. Guerra S, Nájera JL, González JM, López-Fernández LA, Climent N, Gatell JM. Distinct Gene Expression Profiling After Infection of Immature Human Monocyte-Derived Dendritic Cells by the Attenuated Poxvirus Vectors MVA and NYVAC. *J Virol* (2007) 81(16):8707–21. doi: 10.1128/JVI.00444-07
39. Barbalat R, Lau L, Locksley RM, Barton GM. Toll-Like Receptor 2 on Inflammatory Monocytes Induces Type I Interferon in Response to Viral But Not Bacterial Ligands. *Nat Immunol* (2009) 10(11):1200–7. doi: 10.1038/ni.1792
40. Zhu J, Martinez J, Huang X, Yang Y. Innate Immunity Against Vaccinia Virus Is Mediated by TLR2 and Requires TLR-Independent Production of IFN-Beta. *Blood* (2007) 109(2):619–25. doi: 10.1182/blood-2006-06-027136
41. Andrejeva J, Childs KS, Young DF, Carlos TS, Stock N, Goodbourn S. The V Proteins of Paramyxoviruses Bind the IFN-Inducible RNA Helicase, Mda-5, and Inhibit its Activation of the IFN-Beta Promoter. *Proc Natl Acad Sci USA* (2004) 101(49):17264–9. doi: 10.1073/pnas.0407639101
42. El-Jesr M, Teir M, Maluquer de Motes C. Vaccinia Virus Activation and Antagonism of Cytosolic DNA Sensing. *Front Immunol* (2020) 11:568412. doi: 10.3389/fimmu.2020.568412
43. Rohde J, Schirrmeier H, Granzow H, Rziha HJ. A New Recombinant Orf Virus (ORFV, Parapoxvirus) Protects Rabbits Against Lethal Infection With Rabbit Hemorrhagic Disease Virus (RHDV). *Vaccine* (2011) 29(49):9256–64. doi: 10.1016/j.vaccine.2011.09.121

Conflict of Interest: RA is the inventor of patents on ORFV. RA and MM have ownership interest in Prime Vector Technologies GmbH. MWL is an inventor of patents owned by Immatics Biotechnologies and has acted as a paid consultant in cancer immunology for Boehringer Ingelheim Pharma & Co. KG.

The remaining authors declare that the research was conducted in the absence of any commercial or financial relationships that could be construed as a potential conflict of interest.

Publisher's Note: All claims expressed in this article are solely those of the authors and do not necessarily represent those of their affiliated organizations, or those of the publisher, the editors and the reviewers. Any product that may be evaluated in this article, or claim that may be made by its manufacturer, is not guaranteed or endorsed by the publisher.

frontiers | Frontiers in Immunology

BRIEF RESEARCH REPORT
published: 19 May 2022
doi: 10.3389/fimmu.2022.906457

Comparison of Immune Responses Elicited by SARS-CoV-2 mRNA and Recombinant Protein Vaccine Candidates

Yixin Wu[1], *Huicong Zhang*[2], *Liuxian Meng*[1], *Fusheng Li*[2,3]* *and Changyuan Yu*[1]*

[1] College of Life Science and Technology, Beijing University of Chemical Technology, Beijing, China, [2] Research Department, Sysvax Inc, Beijing, China, [3] Vaccine Division, Sun Yat-sen Biomedical Institute Limited, Hong Kong, China

After the outbreak of COVID-19, billions of vaccines with different types have been administrated, including recombinant protein vaccines and mRNA vaccines. Although both types of SARS-CoV-2 vaccine can protect people from viral infection, their differences in humoral and cellular immune responses are still not clearly understood. In this study, we made a head-to-head comparison between an mRNA vaccine candidate and a recombinant protein vaccine we developed previously. Results demonstrated that both vaccine candidates could elicit high specific binding and neutralizing antibody titers in BALB/c mice, but with bias towards different IgG subtypes. Besides, the mRNA vaccine candidate induces higher cellular immune responses than the recombinant protein vaccine. To date, this is the first reported study to directly compare the immune responses of both arms between SARS-CoV-2 mRNA and recombinant vaccines.

Keywords: SARS-CoV-2, protein vaccine, mRNA vaccine, IgG subclass antibodies, cellular immune response

OPEN ACCESS

Edited by:
Simon Daniel Van Haren, Harvard Medical School, United States

Reviewed by:
Darrell O. Ricke, Massachusetts Institute of Technology, United States
Zhao Zhongpeng, Beijing Institute of Microbiology and Epidemiology, China

***Correspondence:**
Fusheng Li
fushengli@sysvax.com
Changyuan Yu
yucy@mail.buct.edu.cn

Specialty section:
This article was submitted to Vaccines and Molecular Therapeutics, a section of the journal Frontiers in Immunology

Received: *28 March 2022*
Accepted: *19 April 2022*
Published: *19 May 2022*

Citation:
Wu Y, Zhang H, Meng L, Li F and Yu C (2022) Comparison of Immune Responses Elicited by SARS-CoV-2 mRNA and Recombinant Protein Vaccine Candidates. Front. Immunol. 13:906457. doi: 10.3389/fimmu.2022.906457

INTRODUCTION

SARS-CoV-2 becomes one of the most severe health crises in human history. To date, it has caused over 497 million cases including more than 6 million deaths. According to WHO, since it was first reported in December 2019, more than 20 SARS-CoV-2 variants has emerged, and the virus is still mutating. Until now, there have been two variants, Delta and Omicron, listed as Variants of Concern (VOC).

SARS-CoV-2 is an enveloped, single-stranded RNA virus. Its virions are spiral capsids consisting of nucleocapsid (N) proteins bound to the RNA genome, and an envelope composed of membranes (M), envelopes (E), and spike (S) proteins, which can be cleaved into S1 and S2 subunits by proteases. In the infection cycle, the S protein binds to angiotensin-converting enzyme 2 (ACE2), *via* the receptor-binding domain (RBD) at S1 subunit, and then the S2 subunit mediates viral cell membrane fusion by forming a six-helical bundle *via* the two-heptad repeat domain (1, 2). Hence, in the research and development of SARS-CoV-2 vaccines, the full-length S protein, S1, and RBD have been widely researched as potential targets for inducing robust neutralizing antibodies and T cell-mediated immunity (3–5).

After the outbreak, scientists all over the world were devoted to the research of SARS-CoV-2 vaccines. It has been reported that there are 349 vaccine candidates in clinical or pre-clinical

development. Among them, 51 are subunit protein vaccines, which are considered safe and simple to produce. In our previous work, we have also developed an RBD recombinant protein vaccine adjuvanted by innovative delivery of poly I:C for stronger immune responses. In the study, poly I:C was first packed with cationic polymer, poly-L-lysine (PLL), and then poly I:C-PLL, as a polyplex core, was loaded into a lipid shell, consisting of DOTAP, cholesterol, DSPC and DMG-PEG_{2000}. Results demonstrated that this recombinant RBD protein induces strong neutralizing antibody responses and protects mice from SARS-CoV-2 infection.

At the same time, the success of Moderna's mRNA-1273 and BioNTech's BNT162b2 have led to the outbreak in mRNA vaccine research. One of the important benefits of mRNA vaccine is its ability to be scaled up in a fairly short period of time, which is highly beneficial for SARS-CoV-2 with a fast mutation rate. Compared with recombinant protein vaccine, the manufacture of mRNA does not need laboring and expensive cell culture and purification steps. When viral antigen sequences are available, the clinical-scale mRNA vaccines can be rapidly developed and manufactured in a short time period (4). However, current mRNA vaccine has its own shortcomings. It has been reported that BNT162b2 needed to be stored at -80°C for quality control and needed to be shipped in special freezers from corporate centers in Michigan and Wisconsin to distribution centers across the country, and then to designated vaccination centers and individuals. Every step requires diligent care and coordination. The requirements for mRNA-1273 are simpler, but the storage at -20°C also makes shipping and storage a challenge. The two-week interval required for the second dose of the two vaccines also hamper the widespread vaccination (6).

Despite the extensive efforts on developing recombinant protein and mRNA vaccines, their differences in inducing immunity are less explored. In this study, we constructed an mRNA vaccine candidate against SARS-CoV-2 variant B.1.617.2 and made a direct comparison of immune responses with a SARS-CoV-2 RBD recombinant protein vaccine we developed in our previous work. Although both vaccine candidates elicit similar level of humoral responses in BALB/c mice, the superiority of mRNA vaccine in inducing higher cellular immune responses makes it better vaccine candidate for protecting SARS-CoV-2 infection.

RESULTS

mRNA Vaccine Delivers RBD Expression Both *In Vitro* and *In Vivo*

Lipid nanoparticles (LNPs) are of great promise and have been widely used in mRNA delivery (7–9). In this study, we chose the RBD of SARS-CoV-2 B.1.617.2 variant as the target antigen and constructed a vaccine, namely RBD_LNPs, which is based on LNPs encapsulating the modified RBD-encoding mRNA. Dynamic light scattering (DLS) and transmission electron microscopy (TEM) were performed to characterize RBD_LNPs. As shown in **Figure 1A**, the average particle size of RBD_LNPs was 144.76 nm, and TEM analysis demonstrated its formation and structure. HEK 293T cells were incubated with RBD_LNPs at different mRNA concentration for 48 h, and cell supernatant was collected to quantify the expression of recombinant RBD protein by ELISA. Results showed that at the minimum dose of 0.3 μg mRNA, the concentration of RBD in supernatant was 8.01 μg/ml (**Figure 1B**). Immunoblotting was also performed to verify the expression of RBD protein (**Figure 1C**). To further test the *in vivo* expression of this mRNA vaccine, RBD_LNPs were injected into BALB/c mice intramuscularly at 1 mg/kg, and the serum was collected at different time point to quantify the expression of RBD by ELISA. Results demonstrated that at 6 h after injection, the expression of RBD was readily detectable, and it was enhanced with the increase of the treatment time. 24 h after injection, the average concentration of RBD in serum reached 901.8 ng/ml (**Figure 1D**), indicating that RBD_LNPs can express RBD protein in mice successfully. Furthermore, RBD_LNPs were stored at 4°C for three weeks, and the size was monitored by DLS. No significant change in the diameter was found (**Figure 1E**).

mRNA and Recombinant Protein Vaccines Elicited Strong Humoral Responses With Bias Towards Different Subtypes

To further evaluate the immunogenicity of this mRNA vaccine and compare it with RBD recombinant protein vaccine candidate, female BALB/c mice were divided into three groups randomly. All mice were immunized and boosted with the same vaccine candidate on day 14. Serum for antibody assays were collected on day 7,14,21,28 and 35 after the first immunization (**Figure 2A**). As shown in **Figure 2B**, after the first immunization, both mRNA and protein vaccine induced detectable RBD-specific immunoglobulin G (IgG) antibodies. Much higher titers were observed after the second vaccination. We next evaluated the ability of both vaccine candidates to induce specific IgG subtype antibodies with sera collected on Day 28 after the initial immunization. As shown in **Figure 2C**, both mRNA and protein vaccines could induce strong RBD-specific IgG1 antibody, and no significant differences were observed between these two groups. As for RBD-specific IgG2a antibody (**Figure 2D**), mRNA vaccine elicits significantly stronger immune response than protein vaccine. The analysis of Th1/Th2 antibody response demonstrated that mice vaccinated with protein vaccine exhibited specific Th2-biased (IgG1) IgG antibody responses (**Figure 2E**).

mRNA and Recombinant Protein Vaccines Induce Similar Neutralizing Antibodies in BALB/c Mice

For evaluation of a vaccine efficacy, neutralizing antibody titer is an important factor to be considered, for it is critical for the clearance of virus *in vivo*. In this research, we studied the *in vitro* neutralizing antibody titers of two vaccine candidates. Results showed that both vaccine candidates induce high neutralization antibody titers after second vaccination (**Figure 3**). It is noted

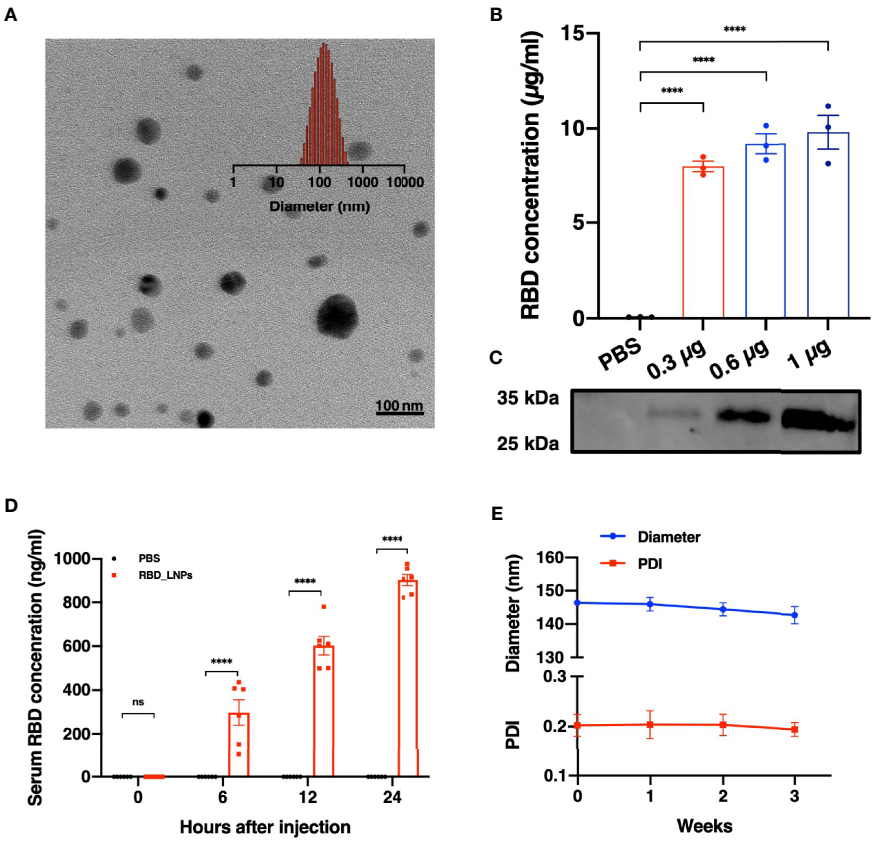

FIGURE 1 | Characterization, expression *in vitro* and *in vivo* delivery of RBD mRNA vaccine. **(A)** TEM and DLS results of RBD_LNPs. **(B)** RBD expression in HEK293T cells. Cells were transfected with RBD_LNPs at different amount of mRNA (0.3μg, 0.6μg, and 1μg/10^6 cells). The concentration was measured by ELISA at 72 h after transfection. **(C)** HEK293T cells were transfected with RBD_LNPs and western blot of cell supernatant was performed at 72 h after transfection. **(D)** Expression of RBD in mice at different time point after injection. **(E)** DLS results of stability test of RBD_LNPs, which were stored at 4°C for three weeks and the diameter and PDI were evaluated by DLS. The data are presented as mean ± SEM. Significance was calculated using unpaired t test (ns, not significant; *$p < 0.05$, **$p < 0.01$, ***$p < 0.001$, ****$p < 0.0001$).

that after the first immunization, the protein vaccine elicited higher neutralizing antibody titer than the mRNA vaccine, while on the day 35 after the initial vaccination, neutralizing antibody titer of mRNA vaccine group reached a significantly higher level than that of protein vaccine group, which was similar to the induction of RBD-specific IgG antibody. Together, both mRNA and protein vaccine tested in this study induce high neutralizing antibody titers in mice but with some differences in response dynamics.

mRNA Vaccine Induces Stronger SARS-CoV-2-Specific Cellular Responses

It has been reported that the antibodies in serum of the recovered patients of SARS vanished in one year (10, 11), while the T cells have existed in the patients for more than six years (12, 13), indicating that cell immunity should be considered in designing SARS-CoV-2 vaccine. On day 35 after the initial vaccination, spleens of mice were harvested and secretion of interferon γ (IFN-γ) in splenocytes was assessed through an ELISpot assay. As shown in **Figure 4A**, the number of IFN-γ-secreting RBD-specific T cells in mRNA vaccine was significantly higher than that in protein vaccine group. In addition to spot counts, IFN-γ spot size should also be considered for illustrating the strength of a single cell to secrete certain cytokines after stimulation. Here, we have found that in the mRNA vaccine group, the average size of IFN-γ spots was significantly larger than the protein vaccine group, as well as the positive control (**Figure 4B**). Taken them together, these results suggested that mRNA vaccines seem better in eliciting cellular immune responses.

DISCUSSION

After the outbreak of COVID-19, billions of vaccines with multiple types have been administrated, including protein vaccine and mRNA vaccine. Although both vaccine types can protect people from infection, their differences in humoral and cellular immune responses are still not clearly understood. In this

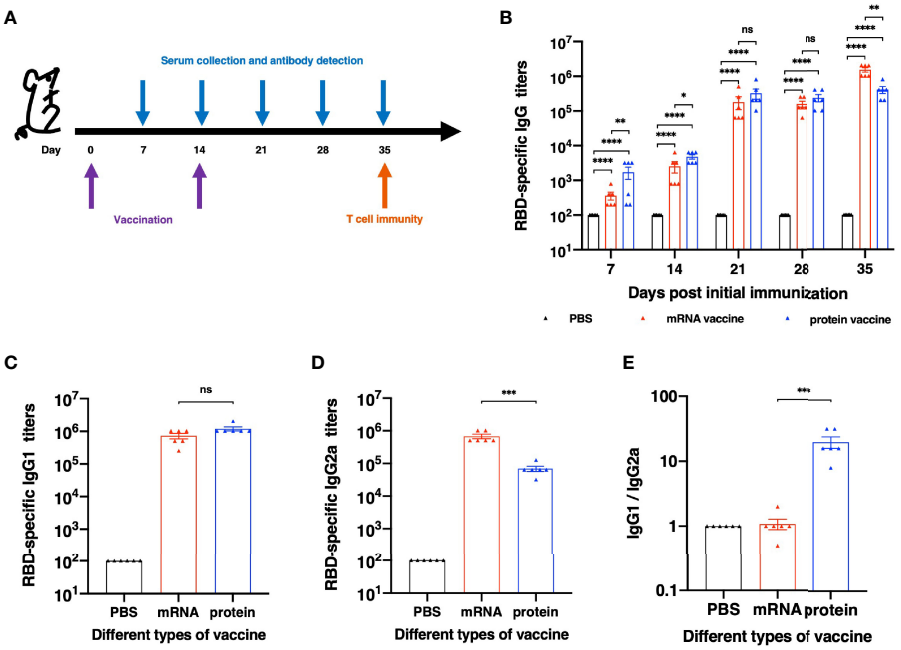

FIGURE 2 | Humoral Immune Response results of different vaccines. **(A)** Schematic diagram of immunization and sample collection schedule. **(B)** SARS-CoV-2-specific IgG antibody titers. **(C)** SARS-CoV-2 RBD-specific IgG1 (Th2) titers and **(D)** IgG2a (Th1) titers of each vaccination group. **(E)** The ratios between specific IgG1 and IgG2a antibody responses. The antibody titers were expressed as the endpoint dilutions that remain positively detectable. The data are presented as mean ± SEM from six mice in each group. PBS was included as the control. Significance was calculated using unpaired t test (ns, not significant; *p < 0.05, **p < 0.01, ***p < 0.001, ****p < 0.0001).

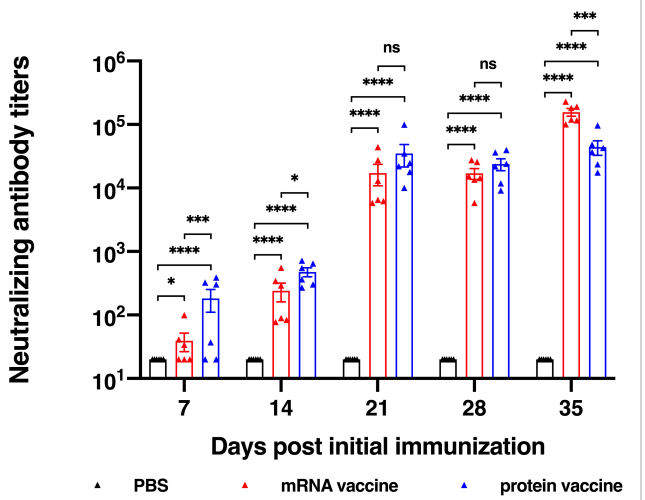

FIGURE 3 | Neutralization ability determined using SARS-CoV-2 pseudovirus. The data are presented as mean± SEM from six mice in each group. PBS was included as the control. Significance was calculated using unpaired t test (ns, not significant; *p < 0.05, **p < 0.01, ***p < 0.001, ****p < 0.0001).

study, we constructed an mRNA vaccine against SARS-CoV-2 Delta variant and compared it with a recombinant protein vaccine we studied in our previous work.

Modified RBD-encoding mRNA was loaded in the LNPs containing DOPE, cholesterol, DMG-PEG_{2000} and an ionizable lipid, DLin-MC3-DMA. Two doses of vaccination with RBD_LNPs induced high specific and neutralizing antibody titer and induce robust T cell immune response as well. These results clearly show the superiority of mRNA vaccine over recombinant protein vaccine for inducing virus-specific immune responses, especially for T-cell responses. However, a major concern for mRNA vaccine is its low stability. To test the stability of our mRNA vaccine candidate, Gluc_LNPs were constructed to verify the stability of this mRNA vaccine platform (**Figure S1**). Results showed that even after the storage at 4°C for three weeks, this mRNA_LNPs could still be effective and express certain protein *in vivo*, indicating that this platform would be a promising strategy for mRNA vaccine development.

To compare the immunogenicity of mRNA and protein vaccines, we first evaluated the level of antibody titers, including RBD-specific IgG titers and *in vitro* neutralizing antibody titers. Both vaccines induced detectable RBD-specific IgG and neutralizing antibodies after the first immunization and elevated much higher after the second vaccination. It is noted that on the day 35 after the initial vaccination, neutralizing antibody titer of mRNA vaccine group reached a significantly higher level than that of protein vaccine group. The antibody titers of protein reached the highest level on day 21 after the first

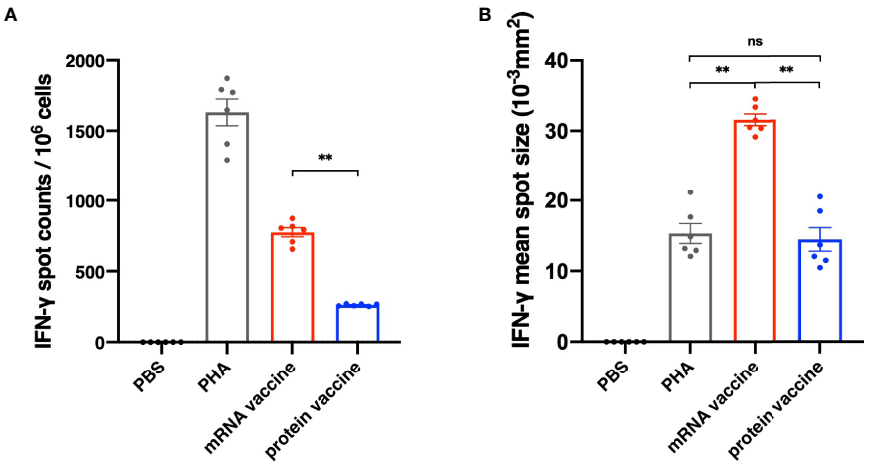

FIGURE 4 | Cellular Immune Response results of different vaccines. **(A)** The number of IFN-γ spot counts per 10^6 splenocytes. **(B)** IFN-γ mean spot size of different vaccine groups. The data are presented as mean± SEM from six mice in each group. PBS was included as the control. Significance was calculated using unpaired t test (ns, not significant; *p < 0.05, **p < 0.01, ***p < 0.001, ****p < 0.0001).

vaccination, while that of mRNA vaccine peaked on the day 35 after the first immunization. To conclude, the protein vaccine could elicit humoral immune response faster than the mRNA vaccine, and it takes longer time for mRNA vaccine to reach its peak responses.

Besides the neutralizing activities, antibodies are capable of mediating host effector functions and facilitating the clearance of pathogens from the host (14). In particular, the Fc portion of IgG2a antibodies mediate a high-affinity interaction with activatory Fc receptors and complement components, which can potently trigger Fc receptor-mediated effector functions, including the stimulation of antibody-dependent cell-mediated cytotoxicity and opsonophagocytosis by macrophages (15, 16). The Fc portion of IgG1 antibodies, however, could not interact with activatory Fc receptors so effectively and does not stimulate Fc receptor-mediated immune responses as well (17, 18). Hence, we evaluated the IgG1 and IgG2a antibody titers of each vaccine in this study. It has found that both vaccines can elicit high IgG1 antibody titers and the mRNA vaccine had induced significantly higher IgG2a titers than the protein vaccine. Analysis of the ratio of IgG1 and IgG2a indicates that BALB/c mice immunized with recombinant protein vaccine with a Th-2 type immune response, as manifested by dominant IgG1 antibodies.

As mentioned above, the T cells could exist a much longer time than the antibodies in the recovered patients of SARS, indicating that cellular immunity responses should be studied carefully in designing SARS-CoV-2 vaccine. As the result shown (**Figure 4**), the mRNA vaccine performed better than the protein vaccine in inducing cellular immune response. Not only were more specific memory T cells observed in the mRNA vaccine group, but also the size of the spots was significantly larger than the protein vaccine and positive control groups as well, indicating that the mRNA vaccine strongly enhanced the ability of IFN-γ secretion in infection. These differences may be caused by the different antigen-presenting mechanisms of the two types of vaccine. For protein vaccines, the antigen proteins are enclosed into endocytic vesicles and presented on the cell surface by MHC-II (major histocompatibility complex class II) molecules to the $CD4^+$ helper T cells (19). However, for the mRNA vaccines, after being transfected into antigen-presenting cells *via* endocytosis, the antigen proteins are translated and processed in cell cytosol, and in this way, not only is the MHC-II pathway activated after the secretion of antigen, but the MHC-I pathway is activated as well, leading to both $CD4^+$ and $CD8^+$ robust T cell responses (20).

In summary, this study compared the humoral and cellular responses of two major SARS-CoV-2 vaccine types, mRNA and recombinant vaccine. As both vaccines demonstrated highly immunogenic, still significant differences in response profiling exist. Specifically, mRNA vaccine can induce higher cellular immune responses than recombinant protein vaccine. To date, this is the first reported study to directly compare the immune responses of both immune arms between SARS-CoV-2 mRNA and recombinant protein vaccines. This work lays a strong foundation for optimizing better vaccines against SARS-CoV-2. To gain further understanding of their differences, viral challenging study in animal model is likely needed. Although safety concerns nowadays prevent us from pursuing such study using live viruses, we believe that challenging study can reveal more important details. In this regard, a clinical trial to compare them in human subjects may be even considered in the future.

MATERIALS AND METHODS

mRNA Synthesis

The linearized DNA template, encoding codon-optimized RBD of SARS-CoV-2 B.1.617.2 variant and incorporating the 5' and 3' untranslated regions and a poly-A tail, was obtained from DNA plasmid A1009 (Tsingke) by using SapI endonuclease. The RBD-

mRNA was produced by *in vitro* transcription using T7 RNA polymerase. The Gluc-encoding mRNA was constructed in the same way from DNA plasmid A1007.

Preparation and Characterization of mRNA Lipid Nanoparticles

mRNA_LNPs were prepared in microfluidic mixing technology with the NanoAssemblr Benchtop (Precision NanoSystems Inc.). Specifically, DLin-MC3-DMA, 1,2-Dioleoyl-sn-glycero-3-PE (DOPE), cholesterol and DMG-PEG_{2000} were dissolved in ethanol in the molar ratio of 50:10:38.5:1.5, and mRNA was dissolved in physiological water. Both of them were injected into the mixer at a 1:3 volume and at a combined final flow rate of 10 mL/min (2.5 mL/min ethanol, 7.5 mL/min aqueous). Residual ethanol in the final mixture was then removed by dialysis. The preparation was performed in a sterile environment at room temperature. DLS and TEM were employed to confirm the formation of the mRNA_LNPs. All of the mRNA_LNPs were kept at 4°C for three weeks, and the size and PDI of them were measured by DLS.

Expression of Recombinant RBD *In Vitro*

HEK 293T cells were seeded in 6-well cell culture plates (2×10^6 cells/well) in KOP 293 medium. Six hours later, RBD_LNPs containing different amount of mRNA (0.3μg, 0.6 μg, and 1 μg) were added into cells. After being cultured at 37°C with 5% CO2 for 48 hours, cells were centrifuged at 1000 rpm for 10 minutes, and the supernatant were collected for further analysis.

Animals

The animal studies were carried out at Beijing University of Chemical Technology, which were in strict accordance with the guidelines evaluated and approved by the ethics committee of University Animal Care and Use Committee and followed the international standards on animal welfare.

Expression of Recombinant RBD *In Vivo*

Twelve mice were divided in groups of six randomly and administrated intramuscularly at 1 mg/kg RBD_LNPs or equivalent volume of PBS. The orbital blood was collected at different time point after administration (0 h, 6 h, 12 h, and 24 h). After being centrifuged at 2000 rpm for 15 minutes, the serum was collected and stored at -20°C for further analysis.

Evaluation of RBD Expression *In Vivo* and *In Vitro*

A standard curve of different concentration of Delta variant RBD protein was established by ELISA. Briefly, a 96-well plate was coated with different concentration of RBD at 4°C overnight, and then the plate was washed three times with PBST and blocked with 2% Difco™ Skim Milk at 37°C for 1 h. After five washes with PBST, the plate was incubated with anti-RBD-hFc antibody at 37°C for 1 h. To develop the reaction, the plates were washed five times and incubated with horseradish peroxidase-conjugated antihuman IgG-Fc secondary antibody at 37°C for 1 h and washed five times. The reaction was visualized by TMB Single-Component Substrate solution and stopped with 2 N HCl. The absorbance at 450 nm (A450) was measured by ELISA plate reader. After constructing the standard curve of different concentration of RBD protein in GraphPad Prism 9, the supernatant or serum was analysis in the same ELISA protocol to quantify the expression of RBD *in vitro* and *in vivo*.

Recombinant RBD Vaccine Candidate

Codon-optimized genes encoding residues 1-13, followed by 331-524, of SARS-CoV-2 spike protein were expressed in HEK 293 cell and purified from culture supernatant. Poly I:C-PLL was prepared in physiological water by adding the poly-L-lysine to poly I:C dropwise in a molar ratio of 0.5:1. The process was under magnetic stirring in a sterile environment. The lipid-based adjuvant was prepared with the NanoAssemblr Benchtop in a sterile environment at room temperature. In brief, the lipid components (DOTAP, DOPE, cholesterol and DMG-PEG were dissolved in ethanol in the molar ratio of 50:10:38.5:1.5) were dissolved in ethanol and the poly I:C-PLL was dissolved in physiological water, both of which were injected into the microfluidic mixer at a 1:3 volume and at a combined final flow rate of 10 mL/min. Residual ethanol in the final mixture was then removed by dialysis.

Animal Vaccination and Sample Collection

Eighteen BALB/c mice were divided into three groups randomly (n=6). One group was vaccinated with 1μg/g mouse weight of recombinant RBD protein (in 100μl physiological water) in the presence of best adjuvant which we selected in our previous work; another group was vaccinated with 100μl RBD_LNPs which contain 5 μg modified RBD-encoding mRNA; the third group was administrated with 100μl PBS as the control. Mice were boosted with the same vaccine formulation or PBS after two weeks. Sera were collected at different time point as schedule (shown in **Figure 2A**) to assess SARS-CoV-2 RBD-specific antibody responses and *in vitro* neutralization assay. All groups of mice were sacrificed on day 35 after the first immunization, and splenocytes were collected to detect SARS-CoV-2 RBD-specific T-cell response.

Evaluation of the Humoral Immune Response

ELISA was used to measure murine antibody responses induced by different vaccines. Briefly, ELISA plates were pre-coated with SARS-CoV-2 recombinant RBD protein overnight at 4°C, After three washes with PBST, serial dilution of mouse sera (from 1:1000 to 1:2048000) were added to plated and incubated at 37°C for 1 h. To develop the reaction, the plates were washed five times and incubated with horseradish peroxidase-conjugated secondary antibody (antimouse IgG, IgG1, or IgG2a) at 37°C for 1 h, and washed five times. The reaction was visualized by TMB Single-Component Substrate solution and stopped with 2 N HCl. The absorbance at 450 nm (A450) was measured by ELISA plate reader.

In Vitro Neutralization Assay

Vero cells were plated in 96-well plates (2×10^5 cells/well) and incubated overnight. Serial dilutions of serum were incubated

with 650 $TCID_{50}$ of the pseudovirus of SARS-CoV-2 B1.617.2 variant for 1 hour at room temperature before transfer to Vero cells. After 72 h of incubation, the supernatant was removed, and luciferase substrate was added. 2 minutes later, luciferase activity was measured and NT_{50} was defined as the serum dilution at which the relative light units (RLUs) were reduced by 50% compared with the virus control wells.

Evaluation of Cytotoxic Immune Response

An ELISpot assay was used to evaluate cytotoxic immune response elicited by different vaccines. Briefly, on day 35 after the initial immunization, spleens from immunized mice were harvested and both grinded and filtered through 40 μm cell strainers. Splenocytes were collected and tested by IFN-γ ELISpot Kit. In brief, the plate was blocked using RPMI Medium 1640 (Solarbio, Beijing, China) containing 10% FBS and incubated for at least 30 minutes. Then, splenocytes collected from immunized mice were plated at 2.5×10^5 cells/well, with overlapped peptide pool derived from SARS-CoV-2 RBD, RPMI Medium 1640 as negative control and Phytohaemagglutinin A (PHA) as positive control. After incubation at 37°C, 5% CO_2 for 48 hours, the plate was washed with PBS for 4 times. Biotinylated anti-mouse IFN-γ antibody was added to each well and was incubated for 2 hours at room temperature. The reaction was visualized by AEC substrate solution, and the plate was read on CTL ELISPOT reader. The number and mean spot size of spot-forming cells (SFC) were recorded.

Statistical Analysis

All statistical analysis were performed using GraphPad Prism 9.0 software (GraphPad Software). Statistical significance among different vaccination groups was analyzed by using two-way multiple ANOVA test, as specified in the figure legends. The values are presented as the means ± SEM unless otherwise noted.

DATA AVAILABILITY STATEMENT

The original contributions presented in the study are included in the article/**Supplementary Material**, further inquiries can be directed to the corresponding authors.

ETHICS STATEMENT

The animal study was reviewed and approved by Beijing University of Chemical Technology.

AUTHOR CONTRIBUTIONS

YW conceived the ideas of research, prepared materials, analyzed the data, and wrote the manuscript. HZ and LM performed the animal surgery. FL and CY provided the lab resource and funding, supervised project, revised and edited the manuscript. All authors contributed to the article and approved the submitted version.

FUNDING

This work was supported by the National Natural Science Foundation of China (Grant No. 82174531).

SUPPLEMENTARY MATERIAL

The Supplementary Material for this article can be found online at: https://www.frontiersin.org/articles/10.3389/fimmu.2022.906457/full#supplementary-material

REFERENCES

1. Hoffmann M, Kleine-Weber H, Schroeder S, Kruger N, Herrler T, Erichsen S, et al. SARS-CoV-2 Cell Entry Depends on ACE2 and TMPRSS2 and Is Blocked by a Clinically Proven Protease Inhibitor. *Cell* (2020) 181(2):271–80.e8. doi: 10.1016/j.cell.2020.02.052
2. Huang Y, Yang C, Xu XF, Xu W, Liu SW. Structural and Functional Properties of SARS-CoV-2 Spike Protein: Potential Antivirus Drug Development for COVID-19. *Acta Pharmacol Sin* (2020) 41(9):1141–9. doi: 10.1038/s41401-020-0485-4
3. Wang Y, Wang L, Cao H, Liu C. SARS-CoV-2 S1 is Superior to the RBD as a COVID-19 Subunit Vaccine Antigen. *J Med Virol* (2021) 93(2):892–8. doi: 10.1002/jmv.26320
4. Verbeke R, Lentacker I, De Smedt SC, Dewitte H. The Dawn of mRNA Vaccines: The COVID-19 Case. *J Control Release* (2021) 333:511–20. doi: 10.1016/j.jconrel.2021.03.043
5. Zhang NN, Li XF, Deng YQ, Zhao H, Huang YJ, Yang G, et al. A Thermostable mRNA Vaccine Against COVID-19. *Cell* (2020) 182 (5):1271–83.e16. doi: 10.1016/j.cell.2020.07.024
6. Cao Y, Gao GF. mRNA Vaccines: A Matter of Delivery. *EClinicalMedicine* (2021) 32:100746. doi: 10.1016/j.eclinm.2021.100746
7. Park KS, Sun X, Aikins ME, Moon JJ. Non-Viral COVID-19 Vaccine Delivery Systems. *Adv Drug Delivery Rev* (2021) 169:137–51. doi: 10.1016/j.addr.2020.12.008
8. Elia U, Rotem S, Bar-Haim E, Ramishetti S, Naidu GS, Gur D, et al. Lipid Nanoparticle RBD-hFc mRNA Vaccine Protects Hace2 Transgenic Mice Against a Lethal SARS-CoV-2 Infection. *Nano Lett* (2021) 21(11):4774–9. doi: 10.1021/acs.nanolett.1c01284
9. Teo SP. Review of COVID-19 mRNA Vaccines: BNT162b2 and mRNA-1273. *J Pharm Pract* (2021) 12:8971900211009650. doi: 10.1177/08971900211009650
10. Bergmann CC, Lane TE, Stohlman SA. Coronavirus Infection of the Central Nervous System: Host-Virus Stand-Off. *Nat Rev Microbiol* (2006) 4(2):121–32. doi: 10.1038/nrmicro1343
11. Shin EC, Sung PS, Park SH. Immune Responses and Immunopathology in Acute and Chronic Viral Hepatitis. *Nat Rev Immunol* (2016) 16(8):509–23. doi: 10.1038/nri.2016.69
12. Tang F, Quan Y, Xin ZT, Wrammert J, Ma MJ, Lv H, et al. Lack of Peripheral Memory B Cell Responses in Recovered Patients With Severe Acute Respiratory Syndrome: A Six-Year Follow-Up Study. *J Immunol* (2011) 186 (12):7264–8. doi: 10.4049/jimmunol.0903490
13. Ng OW, Chia A, Tan AT, Jadi RS, Leong HN, Bertoletti A, et al. Memory T Cell Responses Targeting the SARS Coronavirus Persist Up to 11 Years Post-Infection. *Vaccine* (2016) 34(17):2008–14. doi: 10.1016/j.vaccine.2016.02.063
14. Huber VC, McKeon RM, Brackin MN, Miller LA, Keating R, Brown SA, et al. Distinct Contributions of Vaccine-Induced Immunoglobulin G1 (IgG1) and IgG2a Antibodies to Protective Immunity Against Influenza. *Clin Vaccine Immunol* (2006) 13(9):981–90. doi: 10.1128/CVI.00156-06
15. Kipps TJ, Parham P, Punt J, Herzenberg LA. Importance of Immunoglobulin Isotype in Human Antibody-Dependent, Cell-Mediated Cytotoxicity Directed by Murine Monoclonal Antibodies. *J Exp Med* (1985) 161(1):1–17. doi: 10.1084/jem.161.1.1

16. Takai T, Li M, Sylvestre D, Clynes R, Ravetch JV. FcR Gamma Chain Deletion Results in Pleiotrophic Effector Cell Defects. *Cell* (1994) 76(3):519–29. doi: 10.1016/0092-8674(94)90115-5
17. Nimmerjahn F, Ravetch JV. Divergent Immunoglobulin G Subclass Activity Through Selective Fc Receptor Binding. *Science* (2005) 310(5753):1510–2. doi: 10.1126/science.1118948
18. Nimmerjahn F, Bruhns P, Horiuchi K, Ravetch JV. FcgammaRIV: A Novel FcR With Distinct IgG Subclass Specificity. *Immunity* (2005) 23(1):41–51. doi: 10.1016/j.immuni.2005.05.010
19. Stern LJ, Santambrogio L. The Melting Pot of the MHC II Peptidome. *Curr Opin Immunol* (2016) 40:70–7. doi: 10.1016/j.coi.2016.03.004
20. Wadhwa A, Aljabbari A, Lokras A, Foged C, Thakur A. Opportunities and Challenges in the Delivery of mRNA-Based Vaccines. *Pharmaceutics* (2020) 12(2):102–29. doi: 10.3390/pharmaceutics12020102

Conflict of Interest: Author FL was employed by company Sun Yat-sen Biomedical Institute Limited. Author HZ and FL were employed by the company Sysvax Inc.

The remaining authors declare that the research was conducted in the absence of any commercial or financial relationships that could be construed as a potential conflict of interest.

Publisher's Note: All claims expressed in this article are solely those of the authors and do not necessarily represent those of their affiliated organizations, or those of the publisher, the editors and the reviewers. Any product that may be evaluated in this article, or claim that may be made by its manufacturer, is not guaranteed or endorsed by the publisher.

frontiers | Frontiers in Immunology

ORIGINAL RESEARCH
published: 06 June 2022
doi: 10.3389/fimmu.2022.801111

Innate Immune Responses and *P. falciparum* CS Repeat-Specific Neutralizing Antibodies Following Vaccination by Skin Scarification

Robert A. Mitchell[*†], *Rita Altszuler*, *Sandra Gonzalez*, *Roshawn Johnson*[†], *Ute Frevert* and *Elizabeth Nardin*

Department of Microbiology, New York University School of Medicine, New York, NY, United States

The skin is the site of host invasion by the mosquito-borne *Plasmodium* parasite, which caused an estimated 229 million infections and 409,000 deaths in 2019 according to WHO World Malaria report 2020. In our previous studies, we have shown that skin scarification (SS) with a *P. falciparum* circumsporozoite (CS) peptide in the oil-in-water adjuvant AddaVax containing a combination of TLR 7/8 and TLR 9 agonists can elicit sporozoite neutralizing antibodies. SS with AddaVax + TLR agonists, but not AddaVax alone, elicited CD4+ Th1 cells and IgG2a/c anti-repeat antibody. To explore the innate immune responses that may contribute to development of adaptive immunity following SS, we examined the skin at 4h and 24h post priming with CS peptide in AddaVax with or without TLR agonists. H&E stained and IHC-labeled dorsal skin sections obtained 24h post SS demonstrated a marked difference in the pattern of infiltration with F4/80+, CD11b+ and Ly6G+ cells at the immunization site, with the lowest intensity noted following SS with AddaVax + TLR agonists. Serum collected at 4h post SS, had reproducible increases in IL-6, MIP-3α, IL-22 and IP-10 (CXCL10) following SS with AddaVax + TLR agonists, but not with AddaVax alone. To begin to decipher the complex roles of these pro-inflammatory cytokines/chemokines, we utilized IP-10 deficient (IP-10 -/-) mice to examine the role of this chemokine in the development of anti-repeat antibody response following SS. In the absence of IP-10, the levels of Th1-type IgG2a/c antibody and kinetics of the primary anti-repeat antibody response were reduced following prime and boost. The IP-10 chemokine, present as early as 4h post prime, may provide an early serological marker for rapid screening of adjuvant formulations and delivery platforms to optimize SS-induced humoral immunity to CS repeats as well as other pathogens.

Keywords: *Plasmodium falciparum*, circumsporozoite protein, peptide, skin scarification, Toll-Like Receptor (TLR) agonist adjuvants, innate immunity, IP-10 (CXCL-10), antibody

OPEN ACCESS

Edited by:
Ali M. Harandi,
University of Gothenburg, Sweden

Reviewed by:
Thomas Jacobs,
Bernhard Nocht Institute for Tropical Medicine (BNITM), Germany
Moriya Tsuji,
Columbia University Irving Medical Center, United States
Andrea Berry,
University of Maryland, Baltimore, United States

****Correspondence:***
Robert A. Mitchell
robert.mitchell@isglobal.org

†Present address:
Robert A. Mitchell,
ISGlobal, Hospital Clinic—Universitat de Barcelona, Barcelona, Spain
Roshawn Johnson,
Morehouse School of Medicine, Atlanta, GA, United States

Specialty section:
This article was submitted to Vaccines and Molecular Therapeutics, a section of the journal Frontiers in Immunology

Received: *24 October 2021*
Accepted: *09 May 2022*
Published: *06 June 2022*

Citation:
Mitchell RA, Altszuler R, Gonzalez S, Johnson R, Frevert U and Nardin E (2022) Innate Immune Responses and P. falciparum CS Repeat-Specific Neutralizing Antibodies Following Vaccination by Skin Scarification. Front. Immunol. 13:801111. doi: 10.3389/fimmu.2022.801111

INTRODUCTION

The skin provides the first barrier against pathogens that directly invade the host or that are delivered into the skin by the bite of arthropod vectors, as in the case of the *Plasmodium* parasite. Studies in rodents, non-human primates and human volunteers have shown that sterile immunity can be elicited by sporozoites delivered by the bite of *Plasmodium*-infected mosquitoes (1–6). While immunization by exposure to the bites of infected mosquitoes is not practical for mass vaccination campaigns, the analysis of immune responses in sporozoite-immunized hosts has provided critical information on the immune mechanisms that effectively target the infective sporozoite.

Antibody specific for the major surface antigen of the sporozoite, the circumsporozoite protein (CS), was one of the first protective immune mechanisms identified in sporozoite-immunized experimental hosts (7, 8). Murine monoclonal antibodies (MAB) that target the CS repeats, derived from sporozoite-immunized mice, were shown to neutralize sporozoite infectivity by inhibiting parasite motility in the skin and by blocking liver invasion thus preventing the subsequent development of Plasmodium blood stages responsible for clinical disease (9–11). In more recent studies, human CS-specific MAB derived from volunteers immunized with *P. falciparum* sporozoites were shown to protect human liver-chimeric mice against *P. falciparum* sporozoite challenge (12, 13).

A significant advance in malaria vaccine development has been a CS-based recombinant protein vaccine, termed RTS,S, that was shown in Phase III trials to protect 30-50% of immunized infants and children in Africa (14). RTS,S-induced protection was predominantly antibody-mediated (15, 16). Human MABs targeting CS repeats derived from the RTS,S vaccinees were shown to reduce *P. falciparum* sporozoite infectivity *in vitro* and infection of human liver chimeric mice (17, 18). RTS,S was recently recommended by the WHO for use in children living in moderate to high malaria transmission countries in Africa (19). Encouraged by these advances, efforts continue to improve CS-based vaccine efficacy and delivery methods.

The large scale deployment of vaccines in resource poor areas requires ease of administration by trained community workers, as was successfully used in the WHO Smallpox Eradication Campaign. In previous murine studies, we utilized a two-pronged stylet, as used for administration of smallpox vaccine, to immunize mice by skin scarification (SS) with a *P. falciparum* CS repeat peptide (20). Preclinical testing of highly purified CS-based subunit vaccines have illustrated the critical role of adjuvant in eliciting sporozoite neutralizing antibodies. Potent new adjuvants based on well defined synthetic TLR agonists that specifically target cellular receptors have been developed (21, 22). We therefore utilized adjuvants containing the TLR 7/8 agonist Resiquimod and the TLR 9 agonist CpG (20), as these bind to receptors within the endosome where co-localization with endocytosed antigen may more closely mimic the innate immune patterns elicited by infectious pathogens (23). Our prior SS studies (20) found that induction of anti-repeat antibodies that neutralized infectivity of sporozoites required a combination of TLR 7/8 and TLR 9 agonists in Addvax, a squalene-based oil-in-water nano-emulsion adjuvant.

The current studies were undertaken to explore early innate immune responses that play a role in development of anti-repeat antibody following SS with or without TLR agonists. We examined the SS site using H&E stained and IHC-labeled skin sections as well as measuring systemic cytokines/chemokines in serum collected at 4h and 24h post post prime. A better understanding of innate immune responses associated with the development of anti-repeat IgG antibodies will facilitate optimization of vaccine-induced humoral immunity to target the extracellular sporozoite and prevent development of clinical disease.

Abbreviations: CS, circumsporozoite protein; dLN, draining lymph node; IP-10, interferon gamma induced protein 10 (CXCL-10); MIG, monokine induced by gamma interferon (CXCL9); MIP-3α, MacrophageInflammatory Protein-3 alpha (CCL20); CXCR3, receptor for chemokines containing CXC conserved cysteine motif; MAB, monoclonal antibody; PfPb, transgenic *P. berghei* sporozoites expressing *P. falciparum* CS repeats; SS, skin scarification; TLR, Toll-Like Receptor; TSNA, Transgenic Sporozoite Neutralizing Assay.

MATERIALS AND METHODS

Immunization

C57Bl/6 mice 6-8 weeks of age and breeding pairs of IP-10 -/- mice (B6.129S4-Cxcl10^{tm1Adl}/J) lacking IP-10 (CXCL10) were obtained from Jackson Laboratories (Bar Harbor, Maine). Mice were immunized by SS at 14-28 day intervals with one to four doses of a *P. falciparum* CS peptide delivered into the interscapular dorsal area using a two pronged stylet (Precision Medical Inc., Denver, PA), as previously described (20). The tetrabranched CS peptide used as antigen was comprised of tandem copies of both the major repeats $(NANP)_3$ and the minor repeats (DPNANPNVDPNANPNV) that are contained in the CS repeat region (24, 25). The CS repeat peptide (50 μg) was administered either with or without TLR agonists in AddaVax (InvivoGen, San Diego, CA), a squalene oil-in-water nano-emulsion, comparable to MF59 adjuvant approved for human vaccines, which is known to function as an antigen depot and enhance Th2-type antibody responses (26). A total volume of 100 - 200 μl of vaccine formulation was applied to a 2 cm^2 area of unshaved dorsal skin followed by 10 pricks with the two-pronged stylet. Innate immune responses were measured in serum and skin sections obtained at 4h and 24h after SS priming. For immunogenicity experiments, a prime-boost immunization schedule was performed where two prime doses were administered followed by two additional booster doses. Humoral immunity was measured using serum obtained 14-28 days after each of four SS immunizations delivered at 14 – 28 day intervals. T cell responses were measured using spleen cells obtained after the final immunization. The study was conducted in strict accordance with the recommendations in the Guide for the Care and Use of Laboratory Animals of the National Institutes of Health. The protocol was approved by the Institutional Animal Care and Use Committee, NYU School of Medicine.

TLR Agonists

The TLR agonists used in the adjuvant formulation included the TLR 7/8 agonist Resiquimod (*In vivo*Gen, San Diego, CA), an imidazoquinoline derivative with well-defined adjuvant properties in murine and human hosts (22, 27). The TLR 9 agonist used was CpG, a cytosine:guanine oligodeoxyribonucleotide (ODN) that mimics an unmethylated bacterial DNA motif synthesized on a phosphorothioate backbone (The Certified Midland Reagent Co., Midland, TX) (28). The TLR agonists were tested using the manufacturer's recommended dose per mouse (range 125-150 μg/dose).

Histology and Immunohistochemical (IHC) Staining

Mice from each experimental group (2 – 3 mice/group) were sacrificed at 4h or 24h post first SS immunization and 1cm^2 skin samples were excised from the SS site and fixed in 4% paraformaldehyde. Samples were embedded in paraffin, sectioned and stained with H&E or labeled by immunohistochemistry (IHC) using 2 – 3 sections for each mouse (Histowiz Inc., NY). For IHC, fixed tissue sections were labeled with HRP-conjugated antibodies specific for murine CD11b+ monocytes (Abcam Cambridge, MA), F4/80+ macrophages (Invitrogen Thermo Fisher Scientific, Waltham MA), LY6G+ neutrophils (Abcam, Cambridge, MA), B220+ B cells (Novus Biologicals, Centennial, CO), or CD3+ and CD4+T cells (Abcam, Cambridge, MA). Cellular infiltration at the immunization site was examined in tissue sections from 2-3 mice/group and cellular density in the area under the SS scar was scored manually by two investigators using a range of 1+ to 4+ for intensity of cellular infiltration (**Figures 1S**, **2S**). Two independent experiments were carried out with similar results. Figures show results of a representative experiment.

Cytokine/Chemokine Assays

Cytokines and chemokines were measured in serum collected 4 – 48h post SS priming and stored frozen at -80°C until tested. Samples were screened using a Cytokine/Chemokine Microarray (Cytokine array Q1, RayBiotech Inc, Norcross, GA) to measure IL-1β, IL-2,-3,-5,-6,-10, IL12p70, IL-13,-17,-17F,-21,-22,-23,-28, IFNγ, MIP-3α (CCL20), TGFβ1 and TNFα, according to the manufacturer's protocol. Array slides were read with a 710AL scanner, using Mapix version 8.5.0 scanning software and results were analyzed by RayBiotech using Quantibody Q-Anlyzer software. Quantification of each cytokine/chemokine (pg/ml) was based on standards included in each microarray and the results expressed as fold-increase over limit of detection (LOD) with >3X LOD taken as positive. ELISA assays were used to measure IP-10 (CXCL10) (Abcam, Cambridge, MA) and IL-22 (R&D Systems, Minnesota, MN) in serum obtained at 4h and 24h post SS priming, according to the manufacturer's protocol. All assays were repeated at least twice with results shown for representative experiment.

Humoral immunity

IgG anti-CS repeat antibodies were measured in individual serum samples collected 14d post each SS immunization using a *P. falciparum* CS repeat peptide ELISA, as previously described (20, 29). Results are shown as geometric mean titers (GMT), with the endpoint defined as the final dilution giving an OD greater than three times the OD of BSA-coated control wells. Isotypes of anti-CS repeat IgG antibodies were determined by ELISA using MAB specific for murine Th2-associated IgG1 antibody or Th1-associated IgG2a/c antibody (Southern Biotechnology, Birmingham, AL).

The neutralizing activity of anti-repeat antibody elicited by SS immunization was measured using an *in vitro* Transgenic Sporozoite Neutralization Assay (TSNA), as in previous studies (20, 29, 30). Briefly, 2 X 10^4 transgenic *P. berghei* sporozoites expressing the entire *P. falciparum* CS repeat region (termed PfPb) (31), were incubated with immune or naïve murine serum prior to addition to confluent cultures of human HepG2 hepatoma cells (ATCC HB 8065) in cRPMI (RPMI 1640 supplemented with 10% FBS, 50U Penicillin/50 μg Streptomycin, sodium pyruvate, non-essential amino acids, all from Gibco, ThermoFisher, Waltham, MA). Controls included sporozoites incubated with 25 μg/ml of monoclonal antibody (MAB) 2A10 (ATCC BEI MRA 183), specific for *P. falciparum* CS repeats, or MAB 3D11, specific for *P. berghei* CS repeats (9), as positive and negative controls, respectively. Plates were incubated at 5% CO_2 for 48h, with media change at 24h, followed by extraction of total RNA (PureLink, RNA Mini Kit, ThermoFisher, Waltham, MA). The amounts of parasite 18S rRNA in each culture extract was quantitated by real-time PCR (qRT-PCR) using cDNA primers specific for 18S ribosomal RNA (rRNA) (30, 32). The parasite 18S rRNA copy number was calculated based on a standard curve generated with known amounts of plasmid 18S cDNA. As in previous studies (20), a >90% reduction in parasite copy number was considered biologically relevant as previous studies using injection of known numbers of sporozoites demonstrated that >90% reduction was associated with sterile immunity or delayed prepatent period (1, 33).

Cellular Immunity

Th1- and Th2-type cells were measured in spleen cells obtained following the fourth SS immunization using IFNγ and IL-5 ELISPOT kits, respectively, per the manufacturer's protocol (BD Biosciences, San Jose, CA). Pooled spleens (3-5 mice/group) were stimulated with CS peptide (10 μg/ml) or RPMI medium without peptide. PMA/Ionomycin stimulation served as positive control (Sigma, St. Louis, MO). Results were expressed as number of spot forming cells (SFC)/10^6 spleen cells after subtraction of media control background. The phenotype of the cytokine-producing T cells measured in ELISPOT was determined by treatment with anti-CD4 (MAB GK1.5) or anti-CD8 (MAB 2.43) monoclonal antibodies (Bio X Cell, Lebanon, NH).

Statistics

Statistical analysis was carried out using GraphPad Prism software version 9.2.0 (GraphPad Software, La Jolla, CA). For antibody analysis (**Figure 1A** and **Figure 4SB**), differences between groups were assessed by two-tailed, Mann-Whitney test. Comparison of IP-10 -/- to WT antibody titers (**Figure 6B**) was by one-way ANOVA with Bonferroni's post-test for multiple comparisons. For TSNA, differences between

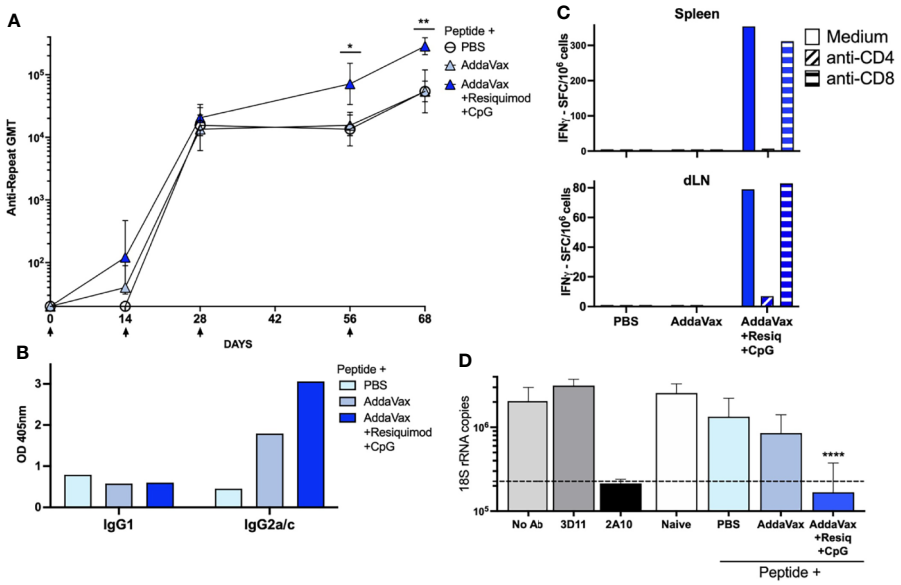

FIGURE 1 | SS with *P. falciparum* CS peptide in AddaVax containing TLR agonists elicits Th1- type neutralizing antibody and cellular responses. **(A)** Kinetics of anti-CS repeat IgG response following SS immunization. Sera was collected 14d post each SS immunization (arrows) with CS peptide in PBS, AddaVax or AddaVax + Resiquimod + CpG. ELISA geometric mean IgG titers (GMT) are shown for sera from individual mice (*n* = 5/group). Mann-Whitney test showed a significant difference in antibody titer post 3rd dose (p = 0.0317) and post 4th dose (p = 0.0079) with SS immunization with CS peptide in AddaVax + Resiquimod + CpG compared to CS peptide in AddaVax only. Error bars show standard deviation. **(B)** Anti-CS repeat IgG isotypes in serum of SS immunized mice. ELISA was carried out using MAB specific for Th2-type IgG1 or Th1-type IgG2a/c. Data are shown as OD of pooled serum (1:320 dilution) obtained post fourth SS immunization from each group of mice (*n* = 5 mice/group). **(C)** T cell cytokine responses in spleen and dLN of SS immunized mice. IFNγ ELISPOT was carried out using pooled spleen or dLN cells (5 mice/group) obtained post fourth SS immunization with CS peptide in PBS, Addavax only or Addavax + Resiquimod + CpG. Data are shown as SFC/10^6 after subtraction of medium only control. **(D)** Sporozoite neutralizing antibody in serum of SS hyperimmunized mice. TSNA was measured using serum (1:5 dilution) of individual mice (n = 5 mice/group) obtained post fourth SS immunization. Mean number of 18S rRNA copies in cultures were quantitated by qRT-PCR. Controls (gray bars) included MAB 2A10 as a inhibitory antibody positive control, or MAB 3D11 as a negative antibody control, and no antibody (No Ab). Dotted line indicates 90% reduction in parasite rRNA copy numbers. Serum from mice immunized SS with CS peptide in AddaVax + Resiquimod + CpG gave >90% inhibition (dotted line), with a significant reduction in parasite copy numbers when compared to naïve serum (One-way ANOVA of log transformed data with Dunnett's multiple comparisons test and adjusted p values, ****p < 0.0001). No significant difference in 18S rRNA copy numbers was found in cultures containing serum of mice immunized SS with PBS or AddaVax compared to naïve. (*p = 0.0317) and (**p = 0.0079).

experimental groups and naïve control were determined by one-way ANOVA with Dunnett's post-test for multiple comparisons. For analysis of parasite 18S rRNA copy number measured in TSNA, the average copy number was calculated across each trial (performed in triplicate) within each group. A P value <0.05 was considered significant and adjusted P values for multiple comparisons are given.

RESULTS

SS With CS Peptide in Adjuvant Containing TLR Agonists Elicits Sporozoite Neutralizing Antibody

SS immunization with CS peptide in AddaVax containing a combination of the TLR 7/8 agonist Resiquimod and the TLR 9 agonist CpG elicited enhanced anti-CS repeat antibody titers when compared to AddaVax without TLR agonists (**Figure 1A**, p = 0.0317 post 3rd dose; p = 0.0079 post 4th dose), consistent with our previous studies (20). The addition to Addavax of Resiquimod and CpG TLR agonists led to production of Th1-type IgG2a/c anti-repeat antibodies (**Figure 1B**). In contrast, SS with CS peptide in AddaVax without TLR agonists, or in PBS, elicited a Th-2 type IgG1 antibody and minimal IgG2a/c antibody.

Spleen cells and draining lymph node (dLN) cells of mice immunized with CS peptide in AddaVax + Resiquimod + CpG had predominantly IFNγ-producing CD4+ T cells (**Figure 1C**), consistent with the shift to IgG2a/c isotype of anti-repeat antibodies. In contrast, cells from mice immunized with CS peptide in AddaVax only, or PBS, did not have detectable IFNγ-producing CD4+ T cells. Minimal IL-5 producing T cells were detected by ELISPOT (data not shown).

When the neutralizing function of the anti-repeat antibodies elicited by SS was assayed by TSNA, only the serum of mice immunized with CS peptide in AddaVax + Resiquimod + CpG neutralized sporozoite infectivity and inhibited >90% of parasite growth *in vitro* (**Figure 1D**). There was a statistically significant reduction in parasite rRNA copy number in cell cultures receiving PfPb sporozoites incubated with immune serum from

mice immunized with CS peptide in AddaVax + Resiquimod + CpG compared to serum of naïve mice ($p = 0.0001$). Reduction in parasite copy number was comparable to that obtained with protective MAB 2A10. No significant difference in rRNA copy number was found using serum of mice immunized with CS peptide in PBS or AddaVax compared to naïve serum.

Presence of TLR Agonists Modulate Cellular Infiltration at Skin Scarification Site

To examine the innate responses associated with induction of Th1-type humoral immunity following SS, dorsal skin obtained from the SS site harvested 4h or 24h post initial SS was stained with H&E (**Figure 2**). At 4h, only minimal histological changes were noted, while at 24h active wound healing and re-epithelization were clear at the SS site (**Figure 1S**). Skin obtained at 24h post SS was therefore examined in more detail in the area under the SS scar (**Figure 2S**).

The intensity of the cellular influx at the SS site, reflected by nuclear (hematoxylin) staining in H&E sections, varied depending on the adjuvant formulation (**Figure 2**). When compared to immunization without adjuvant, SS with CS peptide in Addavax elicited a heavy cellular influx throughout the dermis and subdermis at the SS site (**Figure 2B**). The lowest level of nuclear staining was in skin from mice immunized with CS peptide in AddaVax + Resiquimod + CpG (**Figure 2C**). The intensity of cellular infiltration was AddaVax > PBS > AddaVax + Resiquimod +CpG at the SS site, with a similar pattern observed in two independent experiments.

Efforts to use flow cytometry to analyze the cell populations infiltrating the SS site at 24h was limited by technical difficulties in dissociating murine dorsal skin, as reported by others (34). Immunohistochemistry (IHC) of skin tissue sections was therefore used to examine the cell populations *in situ* at the SS site following labeling for monocytes (CD11b+), macrophages (F4/80+) and neutrophils (Ly6G+), as well as T (CD3+, CD4+) and B (B220+) cells (**Figure 3**).

SS with peptide in AddaVax led to a notable increase in F4/80+ cells at the SS site, when compared to SS without adjuvant (PBS) (**Figures 3A, B**). The lowest F4/80 label intensity was observed following SS with AddaVax + Resiquimod + CpG (**Figure 3C**). CD11b+ monocyte labeling (**Figures 3D, E**) and Ly6G+ neutrophil labeling (**Figures 3G, H**) was also strongest in skin of mice primed with peptide in AddaVax or PBS, with notably lower label intensity at the site following SS with AddaVax + Resiquimod + CpG (**Figures 3F, I**). The pattern of intensity of the IHC label was AddaVax > PBS > AddaVax + Resiquimod + CpG, consistent with the pattern observed in H&E stained sections of skin from the SS site (**Figure 2**).

Immunization with or without adjuvant did not alter levels of T cells (CD3+) and B cells (B220+) detectable in skin sections by IHC at 24h post SS prime (data not shown). Only minimal numbers of B220+ B cells were observed scattered throughout the dermis at 24h post SS with or without adjuvant, similar to levels of B cells in naïve skin. CD3+ T cells were also not visibly increased post SS when compared to naïve mice, with the majority of T cells associated with hair follicles or scattered throughout the epidermis.

Chemokines/Cytokines at 4h and 24h Post SS Prime

Cytokines and chemokines are required for repair of the skin barrier following trauma as well as to initiate adaptive immunity in response to skin infection or invasive pathogens. To examine the cytokines/chemokines that may have contributed to cellular responses noted at 24h, serum collected at 4h and 24h post prime was screened using a multiplex chemokine/cytokine microassay (RayBiotech Inc, Norcross, GA).

As early as 4h post SS, elevated levels of pro-inflammatory cytokine IL-6 (**Figure 4A**) and chemokine MIP-3α (CXCL20) (**Figure 4B**) were detected in serum of mice immunized with peptide in AddaVax + Resiquimod + CpG (**Figure 4**, solid blue bars). Tissue extracts obtained from draining lymph node (dLN) and spleen at 4h post prime with CS peptide in Addavax +

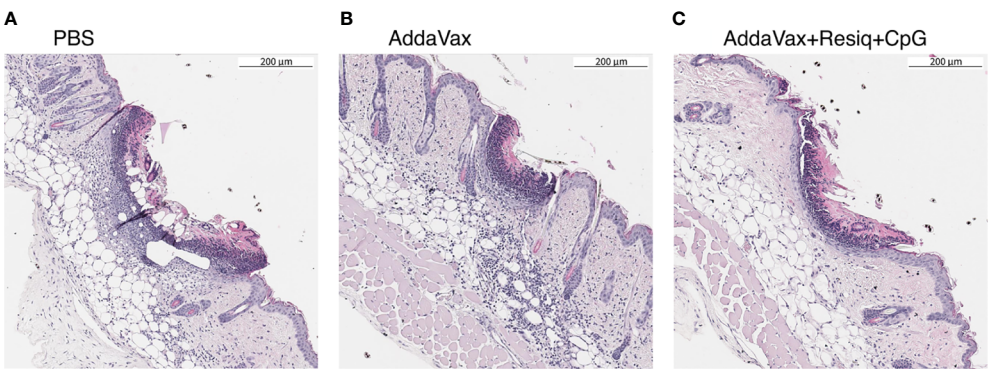

FIGURE 2 | Cellular infiltration into dorsal skin 24h post SS prime. Nuclear staining with hematoxylin (H&E) was used as a measure of cellular infiltration. Dorsal skin sample were obtained at 24h post SS with CS peptide in **(A)** PBS, **(B)** Addavax, or **(C)** Addavax + Resiquimod + CpG. The pattern of intensity of cell infiltration, Addavax > PBS > AddaVax + Resiquimod + CpG was similar in dorsal skin from two independent experiments, with representative results of one experiment shown.

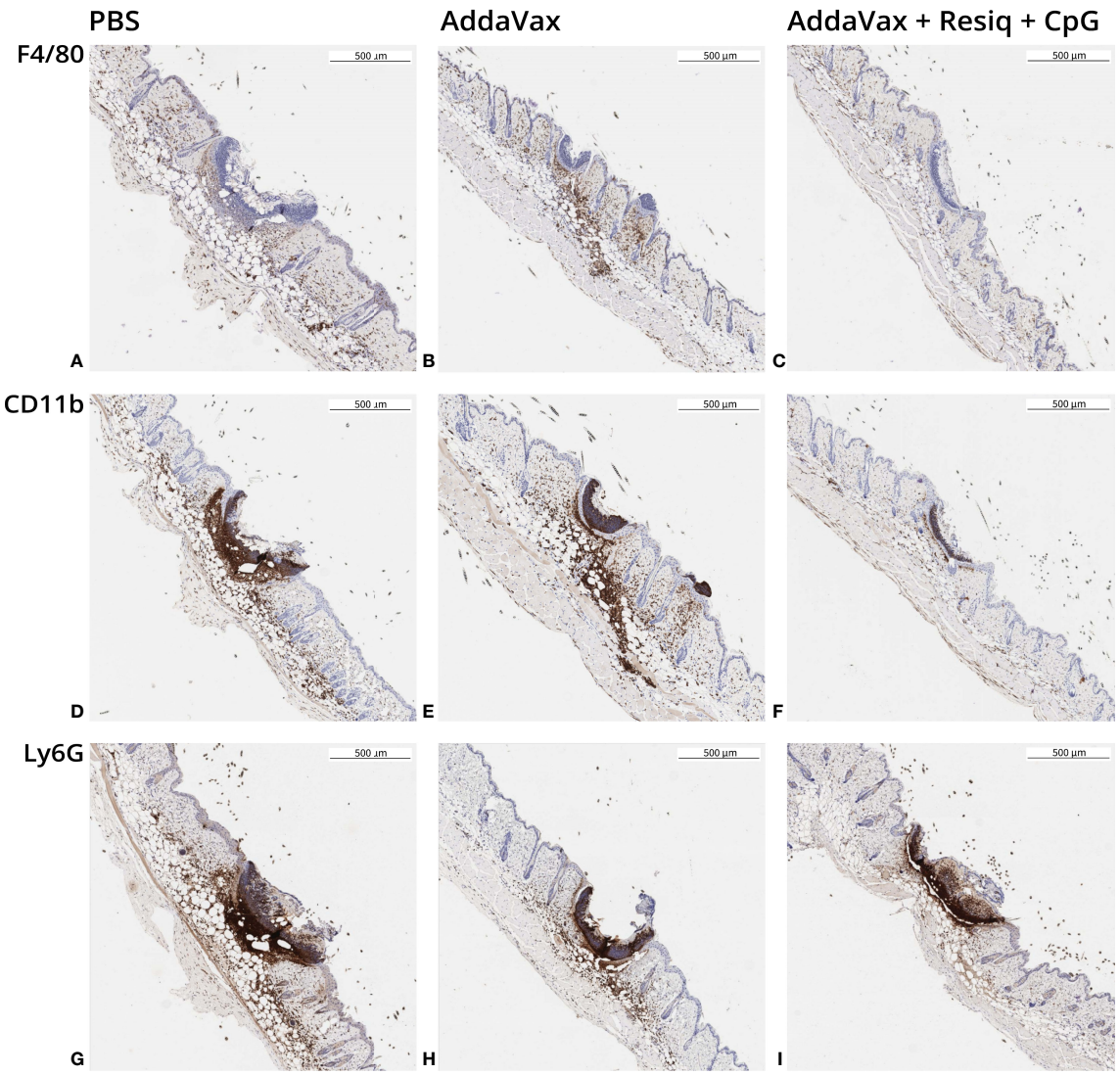

FIGURE 3 | Immunohistochemistry (IHC) of dorsal skin obtained 24h post SS prime. Skin sections were obtained from 2-3 mice/experimental group at 24h post SS with CS peptide in PBS (first column), Addavax (second column) or Addavax + Resiquimod + CpG (third column). Cellular infiltration was assessed in skin sections from SS site labeled by IHC with antibody to F4/80 **(A–C)**, CD11b **(D–F)** or Ly6G **(G–I)**. Similar results were obtained in three experiments with results of a representative experiment shown.

Resiquimod + CpG also had increased levels of IL-6 and MIP-3α (hatched blue bars). The elevated levels of cytokines/chemokines were elicited primarily by the TLR 7/8 agonist Resiquimod, as SS with AddaVax + CpG did not elicit detectable IL-6 or MIP-3α in serum or extracts of dLN and spleen (**Figures 4A, B**, gray bars). The increase in IL-6 and MIP-3α was transient, as sera collected at 24h post prime showed minimal IL-6 or MIP-3α signals (data not shown). Serum collected at 4h or 24h post prime with CS peptide in Addavax without TLR agonists, or peptide without adjuvant (PBS) did not have detectable levels of IL-6 or MIP-3α (<3X LOD). Tissue extracts from naïve mice were also negative at both time points (data not shown). All tissue and serum samples were negative for other cytokines/chemokines included in the microassay: IL-1β, IL-2,-3,-5,-10, IL12p70, IL-13,-17,-17F,-21,-22,-23,-28, IFNγ, TGFβ1 and TNFα.

The composition of the antigen used in SS could potentially contribute to the cytokine/chemokine pattern if the immunogen contained TLR ligands due to microbial contaminants. In the current study, the CS synthetic peptide did not contribute to the chemokine/cytokine responses measured at 4h, as IL-6 and MIP-3α were also detected in serum of mice immunized with AddaVax + Resiquimod + CpG without CS peptide (**Table 1S**). As found following SS with CS peptide with AddaVax + Resiquimod + CpG, the elevated cytokines/chemokine responses post immunization without peptide were transient. IL-6 levels decreased from 36.9X LOD at 4h to 8.9X

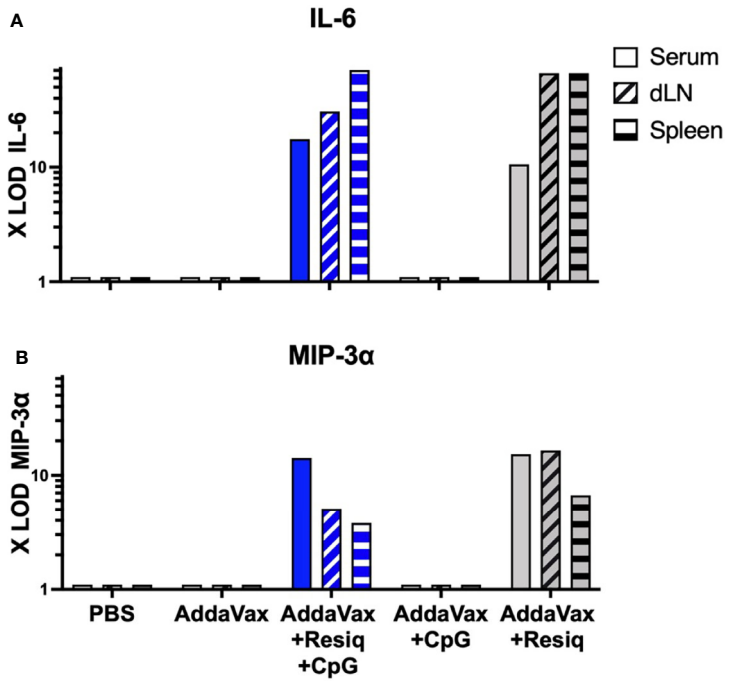

FIGURE 4 | Cytokines/chemokines detectable by microarray at 4h post SS prime. Serum and extracts of spleen or dLN collected at 4h post SS from 3-4 mice/group were tested for levels of cytokines/chemokines by microarray. IL-6 **(A)** and MIP-3α **(B)** were detected in serum (solid blue bar) and extracts of spleen and dLN (hatched blue bars) obtained from mice immunized with AddaVax + Resiquimod + CpG, but not Addavax only or PBS. Induction of IL-6 and MIP-3α was primarily due to inclusion of Resiquimod (gray bars). All samples were negative (<3X LOD) for IL-1β, IL-2,-3,-5,-10, IL-12p70, IL-13,-17,-17F,-21,-23,-28, IFNγ, TGFβ1 and TNFα when tested by microarray.

LOD, while MIP-3α levels decreased from 319.7X LOD at 4h to 16X LOD at 24h post SS. Similar to SS with CS peptide, the elevated cytokines/chemokines were elicited primarily by the TLR 7/8 agonist Resiquimod, with only low levels of IL-6 (3.1 X LOD) and MIP-3α (26.3X LOD) detectable in serum following SS with AddaVax + CpG. The serum from mice immunized with AddaVax + Resiquimod + CpG, or with AddaVax + Resiquimod also had low levels of IL-12 and IL-22 detectable at 4h post prime. SS with AddaVax did not elicit IL-6, IL-12 or IL-22, while minimal levels of MIP-3α were detected at 4h and 24h. TNFα was only detected is serum following immunization without TLR agonists (PBS, AddaVax).

While the microarray provided a significant advantage in screening for multiple cytokines/chemokines in single samples, the assay did not include chemokines such as IP-10 (CXCL10) which is known to play a role in the initiation of Th1-type adaptive immunity (35). An ELISA was therefore used to measure IP-10 in serum collected at 4h and 24h post SS prime. Elevated levels of IP-10 were detected in serum at 4h (18,690 IP-10 pg/mL, with decreased levels at 24h, post SS with peptide in AddaVax + Resiquimod + CpG (**Figure 5A**). A second experiment detected 15,911 IP-10 pg/mL confirming the elevated level of IP-10 at 4 hours post prime (data not shown). IP-10 was not detected in serum following SS with peptide in Addavax only, or with peptide in PBS, at either 4h or 24h post prime. Elevated IP-10 at 4h, with reduced levels at 24h, was also observed following SS with AddaVax + Resiquimod + CpG without peptide (**Figure 5B**), indicating that the CS peptide did not contribute to the induction of the IP-10 chemokine, consistent with cytokines/chemokines detected by microarray. Additionally, SS using single TLR agonists demonstrated that IP-10 was elicited primarily by the formulation containing Resiquimod, with little or no IP-10 detected in the AddaVax + CpG group (data not shown).

Innate and Adaptive Immune Responses in IP-10 -/- Mice

The pro-inflammatory cytokines/chemokines reproducibly detected at 4h post prime, IL-6, MIP-3α, IL-22 and IP-10, have pleomorphic functions in tissue regeneration, inflammation, as well as initiation and modulation of adaptive immune responses. To begin to explore the roles of the complex array of cytokines/chemokines elicited by SS with AddaVax + Resiquimod + CpG in the adaptive immune response, we focused on IP-10 (CXCL10). Previous studies in non-human primates (NHP) had shown that the intradermal injection of adjuvant containing Resiquimod + CpG led to detectable IP-10 in serum at 3h, and increased inflammatory monocytes in dLN at 24h (36). IP-10 was also the most consistently elevated early chemokine detected in NHP plasma at 6h - 24h post priming

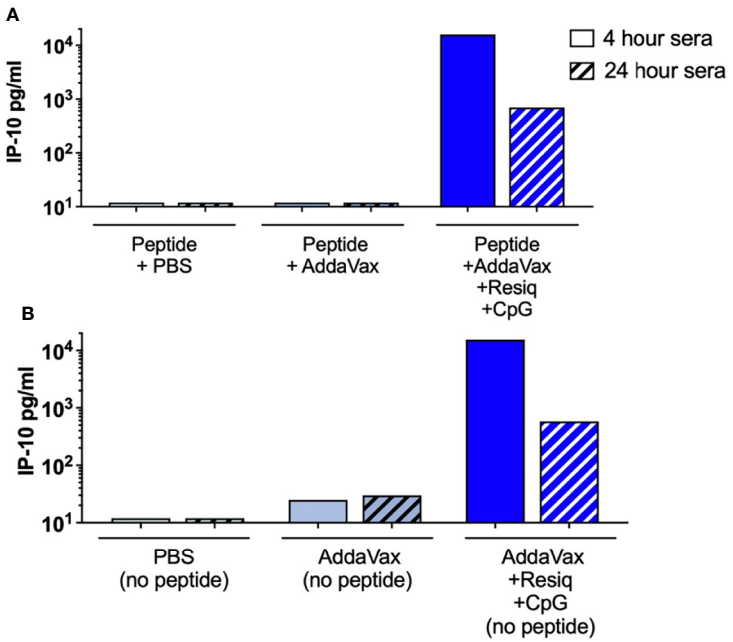

FIGURE 5 | IP-10 (CXCL10) in serum 4h and 24h post SS with AddaVax + Resiquimod + CpG. ELISA quantitation of chemokine IP-10 (CXCL10) in serum of mice immunized by SS either with CS peptide **(A)** or without peptide **(B)**. IP-10 concentrations (pg/ml) were measured in serum collected at 4h (solid bars) or 24h (hatched bars) post SS prime.

with HIV gp140 in an oil adjuvant containing Resiquimod + CpG and was associated with strong antibody responses following multiple IM injections (37).

To examine the role of IP-10 in innate and adaptive immune responses following immunization, mice lacking IP-10 (IP-10 -/-) were immunized with CS peptide in Addavax with or without TLR agonists. When skin samples obtained at 24h post SS were labeled by IHC, the IP-10 -/- mice immunized SS with AddaVax demonstrated strong F4/80+ and Ly6G+ cellular infiltration, similar to WT controls (**Table 1**). Similar to WT, skin from the IP-10 -/- mice immunized with AddaVax + Resiquimod + CpG had reduced F4/80 and Ly6G labeling when compared to skin from IP-10 -/- mice immunized with CS peptide in AddaVax or PBS. However, in contrast to WT, the IP-10 -/- mice had increased CD11b+ cells following SS with AddaVax + Resiquimod + CpG.

TABLE 1 | IHC of skin tissue from SS site of IP-10 -/- vs WT mice.

SS with CS peptide in	CD11b		F4/80		Ly6G	
	WT	IP-10 -/-	WT	IP-10 -/-	WT	IP-10 -/-
PBS	2.5	2.25	1.5	2.0	2.5	2.5
AddaVax	3.3	4.0	3.0	3.0	3.2	3.0
AddaVax + Resiquimod +CpG	1.9	3.25	1.25	1.0	2.0	1.25

IHC-labeled dorsal skin obtained 24h post SS prime was scored manually by microscopy: 1+, scattered positive cells; 2+, staining localized to SS site; 3+, increased cellular infiltration localized to SS; 4+, strong cell infiltration localized to SS. Skin sections from naive WT or IP-10 -/- mice were scored 1+. Results are shown as average scores for slides from 2-3 mice/group. IHC using antibodies for CD3, CD4 and B220 scored 1+ for all experimental conditions (data not shown).

When serum of IP-10 -/- mice was assayed for cytokines/chemokines by microarray, elevated IL-6 and MIP-3α were detected in serum at 4h post prime with AddaVax + Resiquimod + CpG, similar to WT mice (**Table 2**). The concentrations of IL-6 and MIP-3α were 6-7 fold higher in the IP-10 -/- mice compared to WT mice. Low levels of IL-22 and TNFα were also detected in the serum of the IP-10 -/- mice following SS with Addavax + Resiquimod + CpG. A more sensitive IL-22 ELISA confirmed the presence of IL-22 in serum of both IL-10 -/- and WT mice at 4hrs post prime with peptide in AddaVax + Resiquimod + CpG (**Figure 3S**). Despite the enhanced sensitivity of the ELISA compared to microarray, minimal or no IL-22 was detected in serum of either IP-10 -/- or WT mice immunized SS with CS peptide in AddaVax or PBS.

The adaptive immune response in IP-10 -/- mice was assayed by measuring IgG anti-repeat antibody following SS priming and boost. Previous studies in IP-10 -/- mice had demonstrated reduced primary IgG2a/c antibody responses following i.p. immunization with ovalbumin in Freund's adjuvant (38). Following SS with peptide in AddaVax + Resiquimod + CpG, the IP-10 -/- mice had lower Th1-type anti-repeat IgG2a/c antibody when compared to WT mice (**Figure 6A**, right panel). In contrast, following SS with AddaVax + Resiquimod + CpG, the Th-2 type IgG1 response was similar in WT as compared to IP-10 -/- mice (left panel).

TABLE 2 | Chemokines/Cytokines in IP-10 -/- vs WT mice.

Chemokine/ Cytokine	LOD (pg/ml)	Serum obtained +4h post SS with CS peptide in					
		PBS		Addavax		AddaVax + Resiq + CpG	
		WT	IP-10 -/-	WT	IP-10 -/-	WT	IP-10 -/-
IL-6	19.6	<3X	<3X	<3X	<3X	17.6X	98.7X
IL-22	58.6	<3X	<3X	<3X	<3X	<3X	6.7X
MIP-3α	7.5	<3X	<3X	<3X	<3X	14.2X	104.9X
TNFα	31.8	<3X	<3X	<3X	<3X	<3X	6.8X

Chemokines/cytokines in serum obtained 4h post SS were quantitated by microarray. Results are shown as fold-increase over limit of detection (LOD), with <3X LOD considered negative. Serum from naïve WT or naïve IP-10 -/- mice were negative for all chemokines/cytokines (data not shown). Sera of IP-10 -/- and WT mice obtained 4h post SS prime with CS peptide with or without adjuvant were negative for: IL1-β, IL-2,-3,-5,-10, IL-12p70, IL-13,-21,-23,-28, IFNγ, and TGFβ1. IP-10 -/- mice immunized SS with AddaVax + Resiquimod + CpG had low levels of IL-17F (3.4X LOD) (not shown).

The primary anti-repeat antibody titers in the IP-10 -/- mice immunized SS with CS peptide in AddaVax + Resiquimod + CpG were significantly reduced when compared to WT mice (**Figure 6B**, p<0.0001). The reduced IgG2a/c concentrations and lower antirepeat antibody titers in the IP-10 -/- mice suggest that IP-10 plays a critical role in the shift to the Th1-type IgG subtype as well as the kinetics of the primary anti-repeat antibody response following SS immunization.

To investigate the function of antibodies elicited in the absence of IP-10, the IP-10 -/- mice received two additional boosters for a total of four SS immunizations (hyperimmunized), as our previous studies had found that development of neutralizing antibodies requires multiple boosters (20). Following a total of four immunizations with CS peptide in AddaVax + Resiquimod + CpG, hyperimmunized IP-10 -/- mice demonstrated a shift to IgG2a/c (**Figure 4SA**) and kinetics of anti-repeat antibody response (**Figure 4SB**) similar to that observed in WT mice (**Figure 1**). When hyperimmune serum of IP-10 -/- and WT mice were tested in parallel in TSNA, comparable neutralizing antibody levels were obtained in serum from IP-10 -/- mice and WT mice (**Figure 7**). A 1:5 dilution of hyperimmune serum of both IP-10 -/- and WT mice immunized

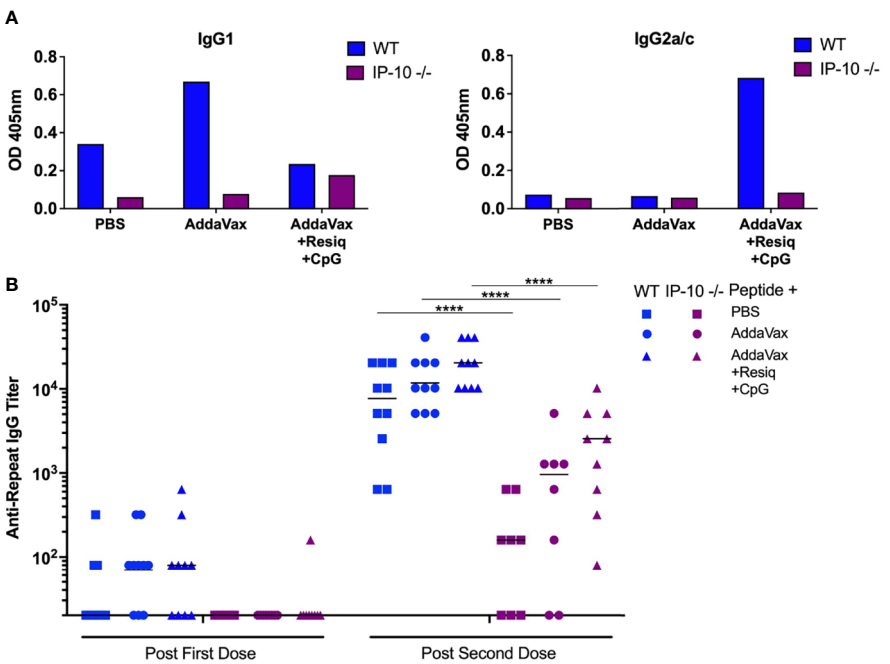

FIGURE 6 | Anti-repeat antibody responses in IP-10 -/- mice post SS prime and boost. **(A)** IgG1 (left panel) and IgG2a/c (right panel) anti-CS repeat antibodies were measured by ELISA in pooled serum (3-4 mice/group) in IP-10 -/- mice (purple bars) or WT controls (blue bars). Serum was collected following SS prime and boost with CS peptide in PBS, Addavax or Addavax + Resiquimod + CpG. Results are shown as OD at 1:80 serum dilution. **(B)** Anti-repeat antibody response in serum of individual IP-10 -/- mice (purple symbols) compared to WT mice (blue symbols) following SS prime and boost with CS peptide without adjuvant (PBS), with AddaVax, or with AddaVax + Resiquimod + CpG. Results of two experiments were pooled with individual mice shown as data points and geometric mean indicated by bar. One-way ANOVA of log-transformed values followed by Bonferroni's multiple comparisons test with adjusted p values, ****p <0.0001.

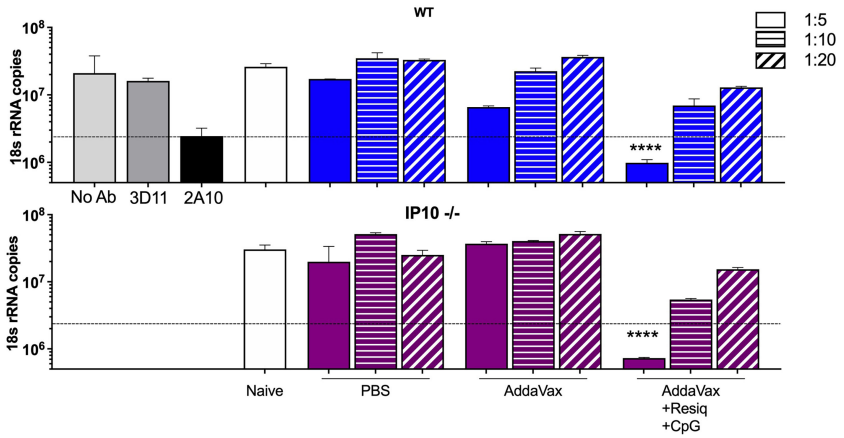

FIGURE 7 | Sporozoite neutralizing antibody in hyperimmune serum of SS immunized IP-10 -/- compared to WT mice. TSNA was carried out with pooled immune sera (5 mice/group) obtained post 4th SS immunization from WT (upper panel, blue bars) or IP-10 -/- mice (purple bars) tested in parallel at 1:5 –1:20 serum dilution. Controls (grey bars) include PfPb sporozoites incubated with inhibitory MAB 2A10 or with negative control MAB 3D11 or without antibody (No Ab). Dotted line represents >90% inhibition of parasite levels in liver cell cultures measured by qRT-PCR. Significant reduction of parasite copy number was obtained with hyperimmune serum from both IP-10 -/- mice and WT mice following four SS immunizations with peptide in AddaVax + Resiquimod + CpG compared to serum from naïve mice (one-way ANOVA of log-transformed data with Dunnett's multiple comparisons test and adjusted p values, ****p <0.0001).

SS with AddaVax + Resiquimod + CpG reduced parasite levels *in vitro* >90%. A statistically significant reduction in rRNA copy number was found in cell cultures containing hyperimmune serum of IP10 -/- or WT mice when compared to serum from naïve mice ($p<0.0001$). No significant difference in parasite levels was found in cultures receiving sporozoities incubated in serum of IP-10 -/- or WT mice immunized with peptide in AddaVax or PBS.

DISCUSSION

Skin scarification (SS) with a *P. falciparum* CS repeat peptide delivered in an adjuvant formulation comprised of AddaVax containing a combination of the TLR 7/8 agonist Resiquimod and TLR 9 agonist CpG elicited anti-repeat antibodies that neutralized sporozoite infectivity (**Figure 1**), confirming our previous study (20). As early as 24h post prime, dorsal skin from the SS site, stained by H&E or labeled by IHC, demonstrated that the innate immune responses differed depending on the presence or absence of TLR agonists (**Figures 2**, **3**). Of note was the reduced cellular infiltration in the skin following treatment with AddaVax + TLR agonists (**Figure 2C**, **Figures 3C, F, I**) when compared to AddaVax only. Previous murine studies using a skin laser adjuvant, also noted a reduced cellular infiltrate following topical treatment with a TLR 7 agonist which the authors demonstrated was due to increased rapid transit of APC from the skin to the dLN (39).

The reduced cellular infiltration observed in the skin at 24h post SS with AddaVax + Resiquimod + CpG correlated with the presence of pro-inflammatory cytokines/chemokines, including IL-6, IL-22, MIP-3α (CCL20) and IP-10 (CXCL10), detectable at 4h post prime in serum as well as in extracts of dLN and spleen (**Figures 4**, **5**). These pro-inflammatory cytokines/chemokines were not detected in serum obtained 4h or 24h post SS with either AddaVax or PBS.

In this initial exploration of the potential role of the pro-inflammatory cytokines/chemokines detected at 4h in the induction of the adaptive immune response, we focused on IP-10 (CXCL10). IP-10 and the CXCR3 receptor in dLN are known to be of importance in the interaction of CD4+ T cells and dendritic cells and localization of Th cells to B cell areas to facilitate antibody isotype switching and affinity maturation (35, 40). Direct administration of IP-10 as adjuvant for peptide or protein antigens has been shown to elicit murine Th1-type antibody and CD8+ T cells (41). In addition to murine studies, intradermal injection of Resiquimod or CpG into Rhesus monkeys elicited IP-10 in serum detected 3-8h post injection and increased expression of IP-10 mRNA in LN (36). When serum of NHP immunized IM with HIV gp140 in an oil emulsion containing Resiquimod + CpG was tested using a panel of 30 cytokines/chemokines, only elevated serum IP-10 at 24h post prime correlated with enhanced anti-HIV antibody responses following additional boosters (37).

In the current studies, IP-10 -/- mice had reduced Th1-type IgG2a/c antibody and significantly lower anti-repeat titers following SS prime and boost with CS peptide in AddaVax + Resiquimod + CpG (**Figure 6**). These results are consistent with previous studies in IP-10 -/- mice that found impaired CD4+ Th1 cell responses and decreased IgG2a/c antibody titers following priming with soluble antigen (38). In the current studies, serum of IP-10 -/- mice had levels of IL-6, IL-22 and MIP-3α equal to or greater than WT mice at 4h post SS with AddaVax + Resiquimod + CpG (**Table 2**, **Figure 3S**), suggesting that these pro-inflammatory cytokines/chemokines were not sufficient to overcome the lack of IP-10 in the initiation of IgG2a/c antibody response.

In the IP-10 -/- mice, IHC labeling of skin sections obtained 24h following SS with AddaVax + Resiquimod + CpG demonstrated that CD11b+ cells were increased in IP-10 -/- mice compared to WT (**Table 1**). In contrast, the pattern of infiltration with F4/80+ and Ly6G+ cells was reduced, similar to the pattern observed in WT mice. CD11b+ antigen presenting cells (APC) are important in the transport of antigen from the injection site to the dLN. Following sporozoite injection ID or by mosquito bite, intravital microscopy of ear pinnae demonstrated increased numbers of CD11b+ cells at 2-4h and sporozoites associated with CD11b+ cells in dLN (42, 43). While the role of CD11b+ cells as APC following SS remains to be explored, the increase of CD11b+ cells at the SS site in IP-10 -/- mice immunized with AddaVax + Resiquimod + CpG could reflect a failure or delay of APC to transit out of skin to the dLN in the absence of an IP-10 signal. The resulting reduced APC:T cell interaction and Th1 differentiation in the dLN could potentially lead to reduced levels of anti-repeat IgG2a/c, as found in the IP-10 -/- mice following prime and boost with AddVax + TLR agonists (**Figure 6**).

Of note was the finding that multiple SS immunizations could overcome the reduced primary anti-repeat antibody found in the IP-10 -/- mice. Following four immunizations with AddaVax + Resiquimod + CpG, the skewing to IgG2a/c isotype and the magnitude of anti-repeat and neutralizing antibodies in serum of hyperimmunized IP-10 -/- mice were comparable to WT mice (**Figure 4S**, **Figure 7**). These finding suggest compensatory pro-inflammatory chemokines may be functioning in anti-repeat antibody response in IP-10 -/- mice following multiple SS immunizations. MIG (CXCL9) is also an agonist for the CXCR3 receptor which can function in differentiation of Th1 cells and antibody responses (35, 44). Whether CXCL9 can compensate for the lack of IP-10 in the hyperimmunized IP-10 -/- mice remains to be explored.

The reduced primary antibody responses in the SS primed IP-10 -/- mice suggest that IP-10 may provide a potential early biomarker for the initiation of Th1-type anti-repeat antibody response. Consistent with the murine studies, in NHP the presence of IP-10 following priming with HIV antigen in an oil adjuvant containing Resiquimod + CpG correlated with subsequent antibody development following five IM immunizations (37). It is encouraging that despite the variation in TLR distribution in mice versus NHP, the murine innate immune responses observed in the current studies were consistent with TLR stimulated antibody responses in NHP (45, 46). Measurement of IP-10 may therefore provide a useful early serologic marker for rapid screening of TLR agonist based adjuvants not only in murine, but also in primate hosts.

The ability to rapidly and easily test multiple iterations of TLR agonist concentrations and combinations is critical for the successful optimization of vaccine formulations for delivery to the skin. Skin delivery of vaccines provide the advantage of simplifying vaccination strategies and reducing costs by eliminating the need for trained medical personnel required for sterile injections. Co-delivery of antigen in TLR agonist adjuvants to skin APC by SS may more accurately mimic delivery of sporozoite and pathogen associated molecular patterns (PAMP) into the skin. The current studies demonstrate that a simple bifurcated needle can provide an inexpensive tool to deliver subunit vaccines to the skin. Further modifications of vaccine formulations by conjugation of TLR agonist and antigen may enhance vaccine potency (23, 42). Moreover, the use of more technologically advanced skin delivery systems, such as patches comprised of microneedles (47), would be expected to further improve vaccine immunogenicity by increasing the dose of antigen and/or TLR agonists delivered to the skin. Phase I trials of flu vaccine delivered to skin *via* a microneedle patch demonstrated that self-administered vaccines can elicit virus neutralizing antibody titers similar to IM immunization by trained healthcare personnel (48). Measurement of IP-10 in serum may facilitate rapid testing of various TLR agonist combinations and delivery systems, to determine whether these modifications lead to increased levels of IP-10 that correlate with increases in vaccine efficacy.

DATA AVAILABILITY STATEMENT

The raw data supporting the conclusions of this article will be made available by the authors, without undue reservation.

ETHICS STATEMENT

The animal study was reviewed and approved by Institutional Animal Care and Use Committee, NYU School of Medicine.

AUTHOR CONTRIBUTIONS

EN, RM, and UF contributed to the design of the study. RM, RJ, SG, and RA performed the experiments. EN and RM wrote the manuscript. All authors reviewed the manuscript.

FUNDING

We are grateful for the research support provided by NIH grant AI098302.

ACKNOWLEDGMENTS

We gratefully acknowledge Ico Romero Reyes for assistance with images.

SUPPLEMENTARY MATERIAL

The Supplementary Material for this article can be found online at: https://www.frontiersin.org/articles/10.3389/fimmu.2022.801111/full#supplementary-material

Supplementary Figure 1 | H&E staining of dorsal skin obtained post SS prime with CS peptide in PBS showing the epidermal, dermal and subdermal skin layers. **(A)** At 4h, the skin exhibited minimal histological changes post SS regardless of

adjuvant formulation. **(B)** At 24h, the SS site showed wound repair and re-epithelialization in all experimental groups.

Supplementary Figure 2 | Scoring of IHC-labeled skin obtained 24h post SS prime. Following IHC labeling of skin, the area under the SS site (outline) was examined by microscopy for cellular infiltration. The intensity of cellular infiltration was scored as: 1+, scattered positive cells; 2+, cellular staining localized to SS site; 3+, increased cellular infiltration localized to SS site; 4+ heavy cellular infiltration at SS site.

Supplementary Figure 3 | IL-22 in serum of IP-10 -/- and WT mice post SS prime. ELISA quantitation of IL-22 (pg/ml) in serum of IP-10 -/- (purple bars) as compared to WT mice (blue bars) at 4h post SS with CS peptide in PBS, Addavax, or Addavax + Resiquimod + CpG.

Supplementary Figure 4 | Anti-repeat antibody response in hyperimmunized IP-10 -/- mice. **(A)** IgG isotypes measured in CS repeat peptide ELISA using pooled hyperimmune serum (1:5120 dilution) from IP-10 -/- mice obtained 14d post the fourth SS immunization. **(B)** Kinetics of anti-CS repeat IgG antibody measured by ELISA in serum of IP-10 -/- mice collected at 14d post each of four SS immunizations (arrows). Significant difference was found after SS immunization with CS peptide in AddaVax + Resiquimod + CpG compared to AddaVax only by Mann-Whitney test post 2nd dose (*p=0.0238), post 3rd dose (**p=0.0079), and post 4th dose (**p=0.0079).

REFERENCES

1. Nussenzweig RS, vanderberg J, Most H, Orton C. Protective Immunity Produced by the Injection of X-Irradiated Sporozoites of Plasmodium Berghei. *Nature* (1967) 216(5111):160–2. doi: 10.1038/216160a0
2. Vanderberg J, Nussenzweig RS, Most H. Protective Immunity Produced by the Bite of X-Irradiated Mosquitoes Infected With Plasmodium Berghei. *J Parasitol* (1970) 56:350–1.
3. Miller RM, Woodward WE, Clyde DF, McCarthy VC. Immunization of Man Against Falciparum and Vivax Malaria by Use of Attenuated Sporozoites *. *Am J Trop Med Hyg* (1975) 24(3):397–401. doi: 10.4269/ajtmh.1975.24.397
4. Herrington D, Davis J, Nardin E, Beier M, Cortese J, Eddy H, et al. Successful Immunization of Humans With Irradiated Malaria Sporozoites: Humoral and Cellular Responses of the Protected Individuals. *Am J Trop Med Hyg* (1991) 45(5):539–47. doi: 10.4269/ajtmh.1991.45.539
5. Hoffman SL, Goh LML, Luke TC, Schneider I, Le TP, Doolan DL, et al. Protection of Humans Against Malaria by Immunization With Radiation-Attenuated Plasmodium Falciparum Sporozoites. *J Infect Dis* (2002) 185 (8):1155–64. doi: 10.1086/339409
6. Roestenberg M, McCall M, Hopman J, Wiersma J, Luty AJF, van Gemert GJ, et al. Protection Against a Malaria Challenge by Sporozoite Inoculation. *N Engl J Med* (2009) 361(5):468–77. doi: 10.1056/NEJMoa0805832
7. Nussenzweig R, Vanderberg J, Most H. Protective Immunity Produced by the Injection of X-Irradiated Sporozoites of Plasmodium Berghei. IV. Dose Response, Specificity and Humoral Immunity. *Mil Med* (1969) 134 (10):1176–82. doi: 10.1093/milmed/134.9.1176
8. Nussenzweig V, Nussenzweig RS. Rationale for the Development of an Engineered Sporozoite Malaria Vaccine. *Adv Immunol* (1989) 45:283–334. doi: 10.1016/S0065-2776(08)60695-1
9. Yoshida N, Nussenzweig R, Potocnjak P, Nussenzweig V, Aikawa M. Hybridoma Produces Protective Antibodies Directed Against the Sporozoite Stage of Malaria Parasite. *Science* (1980) 207(4426):71–3. doi: 10.1126/science.6985745
10. Hollingdale MR, Nardin EH, Tharavanij S, Schwartz AL, Nussenzweig RS. Inhibition of Entry of Plasmodium Falciparum and P. Vivax Sporozoites Into Cultured Cells; an *In Vitro* Assay of Protective Antibodies. *J Immunol* (1984) 132(2):909–13.
11. Vanderberg JP, Frevert U. Intravital Microscopy Demonstrating Antibody-Mediated Immobilisation of Plasmodium Berghei Sporozoites Injected Into Skin by Mosquitoes. *Int J Parasitol* (2004) 34(9):991–6. doi: 10.1016/j.ijpara.2004.05.005
12. Kisalu NK, Idris AH, Weidle C, Flores-Garcia Y, Flynn BJ, Sack BK, et al. A Human Monoclonal Antibody Prevents Malaria Infection and Defines a New Site of Vulnerability on Plasmodium Falciparum Circumsporozoite Protein. *Nat Med* (2019) 24(4):408–16. doi: 10.1038/nm.4512
13. Tan J, Sack BK, Oyen D, Zenklusen I, Piccoli L, Barbieri S, et al. A Public Antibody Lineage That Potently Inhibits Malaria Infection Through Dual Binding to the Circumsporozoite Protein. *Nat Med* (2018) 24(4):401–7. doi: 10.1038/nm.4513
14. Kaslow DC, Biernaux S. RTS, S: Toward a First Landmark on the Malaria Vaccine Technology Roadmap. *Vaccine* (2015) 33:7425–32. doi: 10.1016/j.vaccine.2015.09.061
15. White MT, Verity R, Griffin JT, Asante KP, Owusu-Agyei S, Greenwood B, et al. Immunogenicity of the RTS,S/AS01 Malaria Vaccine and Implications for Duration of Vaccine Efficacy: Secondary Analysis of Data From a Phase 3 Randomised Controlled Trial. *Lancet Infect Dis* (2015) 15(12):1450–8. doi: 10.1016/S1473-3099(15)00239-X
16. Regules JA, Cicatelli SB, Bennett JW, Paolino KM, Twomey PS, Moon JE, et al. Fractional Third and Fourth Dose of RTS,S/AS01 Malaria Candidate Vaccine: A Phase 2a Controlled Human Malaria Parasite Infection and Immunogenicity Study. *J Infect Dis* (2016) 214(5):762–71. doi: 10.1093/infdis/jiw237
17. Foquet L, Hermsen CC, van Gemert G-J, Van Braeckel E, Weening KE, Sauerwein R, et al. Vaccine-Induced Monoclonal Antibodies Targeting Circumsporozoite Protein Prevent Plasmodium Falciparum Infection. *J Clin Invest* (2014) 124(1):140–4. doi: 10.1172/JCI70349
18. Oyen D, Torres JL, Wille-Reece U, Ockenhouse CF, Emerling D, Glanville J, et al. Structural Basis for Antibody Recognition of the NANP Repeats in Plasmodium Falciparum Circumsporozoite Protein. *Proc Natl Acad Sci* (2017) 114(48):E10438–45. doi: 10.1073/pnas.1715812114
19. World Health Organization. *WHO Recommends Groundbreaking Malaria Vaccine for Children at Risk* . Available at: https://www.who.int/news/item/06-10-2021-who-recommends-groundbreaking-malaria-vaccine-for-children-at-risk (Accessed May 4, 2022).
20. Mitchell RA, Altszuler R, Frevert U, Nardin EH. Skin Scarification With Plasmodium Falciparum Peptide Vaccine Using Synthetic TLR Agonists as Adjuvants Elicits Malaria Sporozoite Neutralizing Immunity. *Sci Rep* (2016) 6:32575. doi: 10.1038/srep32575
21. Klinman DM. Adjuvant Activity of CpG Oligodeoxynucleotides. *Int Rev Immunol* (2006) 25(3–4):135–54. doi: 10.1080/08830180600743057
22. Tomai MA, Miller RL, Lipson KE, Kieper WC, Zarraga IE, Vasilakos JP. Resiquimod and Other Immune Response Modifiers as Vaccine Adjuvants. *Expert Rev Vaccines* (2007) 6(5):835–47. doi: 10.1586/14760584.6.5.835
23. Blander JM, Medzhitov R. Toll-Dependent Selection of Microbial Antigens for Presentation by Dendritic Cells. *Nature* (2006) 440(7085):808–12. doi: 10.1038/nature04596
24. Nardin EH, Oliveira GA, Calvo-Calle JM, Castro ZR, Nussenzweig RS, Schmeckpeper B, et al. Synthetic Malaria Peptide Vaccine Elicits High Levels of Antibodies in Vaccinees of Defined HLA Genotypes. *J Infect Dis* (2000) 182(5):1486–96. doi: 10.1086/315871
25. de Oliveira GA, Clavijo P, Nussenzweig RS, Nardin EH. Immunogenicity of an Alum-Adsorbed Synthetic Multiple-Antigen Peptide Based on B- and T-Cell Epitopes of the Plasmodium Falciparum CS Protein: Possible Vaccine Application. *Vaccine* (1994) 12(11):1012–7. doi: 10.1016/0264-410X(94)90337-9
26. O'Hagan DT. MF59 Is a Safe and Potent Vaccine Adjuvant That Enhances Protection Against Influenza Virus Infection. *Expert Rev Vaccines* (2007) 6 (5):699–710. doi: 10.1586/14760584.6.5.699
27. Tomai MA, Vasilakos JP. TLR-7 and -8 Agonists as Vaccine Adjuvants. *Expert Rev Vaccines* (2011) 10(4):405–7. doi: 10.1586/erv.11.26
28. Shirota H, Klinman DM. Recent Progress Concerning CpG DNA and Its Use as a Vaccine Adjuvant. *Expert Rev Vaccines* (2014) 13(2):299–312. doi: 10.1586/14760584.2014.863715
29. Othoro C, Johnston D, Lee R, Soverow J, Bystryn J-C, Nardin E. Enhanced Immunogenicity of Plasmodium Falciparum Peptide Vaccines Using a Topical Adjuvant Containing a Potent Synthetic Toll-Like Receptor 7 Agonist, Imiquimod. *Infect Immun* (2009) 77(2):739–48. doi: 10.1128/IAI.00974-08
30. Kumar KA, Oliveira GA, Edelman R, Nardin E, Nussenzweig V. Quantitative Plasmodium Sporozoite Neutralization Assay (TSNA). *J Immunol Methods* (2004) 292(1–2):157–64. doi: 10.1016/j.jim.2004.06.017

31. Persson C, Oliveira GA, Sultan AA, Bhanot P, Nussenzweig V, Nardin E. Cutting Edge: A New Tool to Evaluate Human Pre-Erythrocytic Malaria Vaccines: Rodent Parasites Bearing a Hybrid *Plasmodium Falciparum* Circumsporozoite Protein. *J Immunol* (2002) 169(12):6681–5. doi: 10.4049/jimmunol.169.12.6681
32. Bruña-Romero O, Hafalla JCR, González-Aseguinolaza G, Sano G, Tsuji M, Zavala F. Detection of Malaria Liver-Stages in Mice Infected Through the Bite of a Single Anopheles Mosquito Using a Highly Sensitive Real-Time PCR. *Int J Parasitol* (2001) 31(13):1499–502. doi: 10.1016/S0020-7519(01)00265-X
33. Schmidt LH, Fradkin R, Genther CS, Rossan RN, Squires W, Hughes HB. Plasmodium Cynomolgi Infections in the Rhesus Monkey. *Am J Trop Med Hyg* (1982) 31(3 Pt 2):609–703. doi: 10.4269/ajtmh.1982.31.609
34. Li Z, Gothard E, Coles MC, Ambler CA. Quantitative Methods for Measuring Repair Rates and Innate-Immune Cell Responses in Wounded Mouse Skin. *Front Immunol* (2018) 9(FEB):1–9. doi: 10.3389/fimmu.2018.00347
35. Groom JR, Richmond J, Murooka TT, Sorensen EW, Sung JH, Bankert K, et al. CXCR3 Chemokine Receptor-Ligand Interactions in the Lymph Node Optimize CD4+ T Helper 1 Cell Differentiation. *Immunity* (2012) 37(6):1091–103. doi: 10.1016/j.immuni.2012.08.016
36. Kwissa M, Nakaya HI, Oluoch H, Pulendran B. Distinct TLR Adjuvants Differentially Stimulate Systemic and Local Innate Immune Responses in Nonhuman Primates. *Blood* (2012) 119(9):2044–55. doi: 10.1182/blood-2011-10-388579
37. Moody MA, Santra S, Vandergrift NA, Sutherland LL, Gurley TC, Drinker MS, et al. Toll-Like Receptor 7/8 (TLR7/8) and TLR9 Agonists Cooperate To Enhance HIV-1 Envelope Antibody Responses in Rhesus Macaques. *J Virol* (2014) 88(6):3329–39. doi: 10.1128/JVI.03309-13
38. Dufour JH, Dziejman M, Liu MT, Leung JH, Lane TE, Luster AD. IFN-γ-Inducible Protein 10 (IP-10; CXCL10)-Deficient Mice Reveal a Role for IP-10 in Effector T Cell Generation and Trafficking. *J Immunol* (2002) 168(7):3195–204. doi: 10.4049/jimmunol.168.7.3195
39. Wang J, Shah D, Chen X, Anderson RR, Wu MX. A Micro-Sterile Inflammation Array as an Adjuvant for Influenza Vaccines. *Nat Commun* (2014) 5:4447. doi: 10.1038/ncomms5447
40. Groom JR, Luster AD. CXCR3 in T Cell Function. *Exp Cell Res* (2011) 317(5):620–31. doi: 10.1016/j.yexcr.2010.12.017
41. Krathwohl MD, Anderson JL. Chemokine CXCL10 (IP-10) is Sufficient to Trigger an Immune Response to Injected Antigens in a Mouse Model. *Vaccine* (2006) 24(15):2987–93. doi: 10.1016/j.vaccine.2005.11.032
42. Amino R, Thiberge S, Martin B, Celli S, Shorte S, Frischknecht F, et al. Quantitative Imaging of Plasmodium Transmission From Mosquito to Mammal. *Nat Med* (2006) 12(2):220–4. doi: 10.1038/nm1350
43. Mac-Daniel L, Buckwalter MR, Berthet M, Virk Y, Yui K, Albert ML, et al. Local Immune Response to Injection of Plasmodium Sporozoites Into the Skin. *J Immunol* (2014) 193(3):1246–57. doi: 10.4049/jimmunol.1302669
44. Park MK, Amichay D, Love P, Wick E, Liao F, Grinberg A, et al. The CXC Chemokine Murine Monokine Induced by IFN-γ (CXC Chemokine Ligand 9) Is Made by APCs, Targets Lymphocytes Including Activated B Cells, and Supports Antibody Responses to a Bacterial Pathogen *In Vivo*. *J Immunol* (2002) 169(3):1433–43. doi: 10.4049/jimmunol.169.3.1433
45. Rehli M. Of Mice and Men: Species Variations of Toll-Like Receptor Expression. *Trends Immunol* (2002) 23(8):375–8. doi: 10.1016/S1471-4906(02)02259-7
46. Coffman RL, Sher A, Seder RA. Vaccine Adjuvants: Putting Innate Immunity to Work. *Immunity* (2010) 33(4):492–503. doi: 10.1016/j.immuni.2010.10.002
47. Weldon WC, Martin MP, Zarnitsyn V, Wang B, Koutsonanos D, Skountzou I, et al. Microneedle Vaccination With Stabilized Recombinant Influenza Virus Hemagglutinin Induces Improved Protective Immunity. *Clin Vaccine Immunol* (2011) 18(4):647–54. doi: 10.1128/CVI.00435-10
48. Rouphael NG, Paine M, Mosley R, Henry S, McAllister DV, Kalluri H, et al. The Safety, Immunogenicity, and Acceptability of Inactivated Influenza Vaccine Delivered by Microneedle Patch (TIV-MNP 2015): A Randomised, Partly Blinded, Placebo-Controlled, Phase 1 Trial. *Lancet* (2017) 390(10095):649–58. doi: 10.1016/S0140-6736(17)30575-5

Conflict of Interest: The authors declare that the research was conducted in the absence of any commercial or financial relationships that could be construed as a potential conflict of interest.

Publisher's Note: All claims expressed in this article are solely those of the authors and do not necessarily represent those of their affiliated organizations, or those of the publisher, the editors and the reviewers. Any product that may be evaluated in this article, or claim that may be made by its manufacturer, is not guaranteed or endorsed by the publisher.

frontiers | Frontiers in Immunology

ORIGINAL RESEARCH
published: 10 June 2022
doi: 10.3389/fimmu.2022.860399

Differential Biodistribution of Adenoviral-Vectored Vaccine Following Intranasal and Endotracheal Deliveries Leads to Different Immune Outcomes

*Vidthiya Jeyanathan[1,2], Sam Afkhami[1,2], Michael R. D'Agostino[1,3], Anna Zganiacz[1,2], Xueya Feng[1,2], Matthew S. Miller[1,3], Mangalakumari Jeyanathan[1,2], Michael R. Thompson[4] and Zhou Xing[1,2]**

[1] McMaster Immunology Research Centre, M. G. DeGroote Institute for Infectious Disease Research, Hamilton, ON, Canada, [2] Department of Medicine, McMaster University, Hamilton, ON, Canada, [3] Department of Biochemistry & Biomedical Sciences, McMaster University, Hamilton, ON, Canada, [4] Department of Chemical Engineering, McMaster University, Hamilton, ON, Canada

OPEN ACCESS

Edited by:
Gabriel Pedersen,
Statens Serum Institut (SSI), Denmark

Reviewed by:
Wendy W. J. Unger,
Erasmus MC-Sophia Children's Hospital, Netherlands
Rodrigo Prado Martins,
Institut National de recherche pour l'agriculture, l'alimentation et l'environnement (INRAE), France

***Correspondence:**
Zhou Xing
xingz@mcmaster.ca

Specialty section:
This article was submitted to Vaccines and Molecular Therapeutics, a section of the journal Frontiers in Immunology

Received: 22 January 2022
Accepted: 11 May 2022
Published: 10 June 2022

Citation:
Jeyanathan V, Afkhami S, D'Agostino MR, Zganiacz A, Feng X, Miller MS, Jeyanathan M, Thompson MR and Xing Z (2022) Differential Biodistribution of Adenoviral-Vectored Vaccine Following Intranasal and Endotracheal Deliveries Leads to Different Immune Outcomes. Front. Immunol. 13:860399. doi: 10.3389/fimmu.2022.860399

Infectious diseases of the respiratory tract are one of the top causes of global morbidity and mortality with lower respiratory tract infections being the fourth leading cause of death. The respiratory mucosal (RM) route of vaccine delivery represents a promising strategy against respiratory infections. Although both intranasal and inhaled aerosol methods have been established for human application, there is a considerable knowledge gap in the relationship of vaccine biodistribution to immune efficacy in the lung. Here, by using a murine model and an adenovirus-vectored model vaccine, we have compared the intranasal and endotracheal delivery methods in their biodistribution, immunogenicity and protective efficacy. We find that compared to intranasal delivery, the deepened and widened biodistribution in the lung following endotracheal delivery is associated with much improved vaccine-mediated immunogenicity and protection against the target pathogen. Our findings thus support further development of inhaled aerosol delivery of vaccines over intranasal delivery for human application.

Keywords: respiratory mucosal immunization, intranasal, endotracheal, biodistribution, Adenovirus-vectored vaccine, Tuberculosis, mucosal immunity, T cells

INTRODUCTION

Infectious diseases of the respiratory tract are one of the top causes of global morbidity and mortality, with lower respiratory tract infections being the fourth leading cause of death worldwide in 2019 (1). In fact, the COVID-19 pandemic is a sobering example of the extent of a threat that a respiratory mucosal infection can cause to humankind (2). Vaccination is the most cost-effective public health measure to prevent or control respiratory infectious diseases. However, the vast majority of current vaccines including anti-tuberculosis (TB) BCG in human immunization program are administered *via* a parenteral route and thus, induce only limited respiratory mucosal immunity against respiratory pathogens such as *Mycobacterium tuberculosis* (*M.tb*) and

influenza (3–5). This reality calls for continuing effectors to develop respiratory mucosal vaccine strategies (3, 6). In this regard, on top of injectable flu shots, an intranasally administered live-attenuated influenza vaccine has been introduced to human immunization program as the first respiratory mucosal-deliverable vaccine in humans. Unfortunately, while this nasal flu vaccine shows high efficacy in young children, it is much less effective in adults than injectable flu shots (5, 7). This explains the reason why the injectable flu vaccine remains the top choice for seasonal flu vaccination in general populations. These facts question the suitability of intranasal vaccine delivery as a general respiratory mucosal vaccine strategy for human application. Recently, as an alternative respiratory mucosal vaccine strategy, inhaled aerosol delivery method has been developed and explored to deliver measles vaccine (8), viral-vectored TB vaccines (9, 10) and a viral-vectored COVID-19 vaccine (11) in human trials. Of importance, when parenteral intradermal or intramuscular route of vaccination was compared side-by-side with inhaled aerosol vaccination, it was found that only inhaled aerosol, but not parenteral, vaccination induced significant respiratory mucosal immunity (9, 10). Since inhaled aerosol technology bypasses the nasal passage and delivers the vaccine droplets of 2-5 μm deep into human respiratory tract (airways) (10), these clinical observations together appear to suggest that the biodistribution or the depth of respiratory vaccine delivery plays a critical role in induction of respiratory mucosal immunity. However, to firmly prove this proposition requires experimental investigation in preclinical animal models since it is very difficult to directly test it in humans.

Unfortunately, to date there has been a paucity in experimental studies to compare intranasal delivery with intratracheal/endotracheal deep-airway delivery in vaccine biodistribution, vaccine-specific mucosal immune responses, and protective efficacy. Although there are experimental studies that suggest intratracheal delivery of non-vaccine biologic agents including LPS and microbes to lead to deeper/wider biodistribution and/or manifestation of tissue inflammation, over the intranasal delivery method (12–14), other studies report the opposite observations (15, 16). To our knowledge, there are only two experimental studies where intranasal and intratracheal vaccine delivery methods were compared but these studies did not assess vaccine biodistribution and/or both mucosal T cell immunity and protective efficacy (17, 18). Therefore, there is a need to experimentally address the relationship of differential biodistribution of vaccine delivered by intranasal and intratracheal/endotracheal methods to vaccine-specific mucosal immune responses and protective efficacy. Our enhanced knowledge in this regard will help inform whether going forward, we should focus on developing inhaled aerosol deep-airway vaccine strategies over the intranasal delivery method for human application.

In the current study, using an adenovirus-vectored TB vaccine (AdHu5Ag85A) as a model vaccine, we have evaluated the biodistribution, vaccine immunogenicity and immune protective potency following a single-dose intranasal or endotracheal delivery in a murine model. We find that endotracheal delivery is superior to internasal delivery, which leads to deep lung biodistribution of vaccine, and enhanced vaccine-specific T cell responses and protective efficacy against pulmonary *M.tb* challenge. Our findings thus provide preclinical evidence to support the consideration of the deep-airway delivery method such as inhaled aerosol over the intranasal delivery for human application.

MATERIALS AND METHODS

Mice

Female BALB/c or C57BL/6 mice aged 6 to 8 weeks were sourced from Charles River Laboratories and housed in the Central Animal Facility at McMaster University. All *in vivo* work was done in compliance with guidelines from the Animal Research and Ethics Board at McMaster University and under approved animal utilization protocol (AUP #210822).

Pulmonary Delivery Methods and *in Vivo* Visualization of Deposition Sites

The impact of different pulmonary delivery methods on the deposition site of a vaccine in the lung was measured using a replication deficient adenovirus expressing luciferase (AdHu5Luc) as a distribution marker. Intranasal inoculation was performed by instilling $5x10^7$ PFU of AdHu5Luc in a total volume of 25 μL of phosphate-buffered saline solution (PBS) into the nostrils of C57BL/6 mice (12.5 μL in each nostril), as described previously (19–21). Endotracheal intubation was carried out using an intubation board set up at 45°C, an otoscope, and a 22G blunt-tip intravenous catheter, as described previously (**Figure 1A**) (22). Briefly, after anesthetizing, mice were hung by their teeth on a string attached to the intubation board allowing for easy visualization of the opening of the trachea with the otoscope (**Figure 1B**). Once the opening of the trachea was located, the catheter attached to a syringe was inserted into the trachea (**Figure 1C**). The syringe was then removed and replaced with a P200 pipette containing 100 μL water with a gap of air to confirm correct insertion into trachea (**Figure 1D**). The P200 pipette was then removed and replaced with an extended gel length pipette containing 50 μL of $5x10^7$ PFU AdHu5Luc and was allowed to be inhaled by the mouse (**Figure 1E**). Deposition of AdHu5Luc within the respiratory tract was visualized eight hours post-delivery using an *In Vivo* Imaging System (Caliper Life Sciences). For this, 15 mg/mL of D-luciferin (Caliper Life Sciences) in 25 μL was delivered intranasally as described above and fluorescence signal was visualized within 5 minutes (23). Semi-quantification of strength of fluorescence within the respiratory tract was performed using the ImageJ (Easter Greenbush, NY) image processing program.

Immunization Using Different Pulmonary Delivery Methods

To assess the consequence of different pulmonary delivery methods on the effectiveness of a vaccine, BALB/c mice were immunized with a well characterized adenoviral-vectored tuberculosis vaccine, AdHu5Ag85A, at a dose of $5x10^7$ PFU/mouse intranasally or by

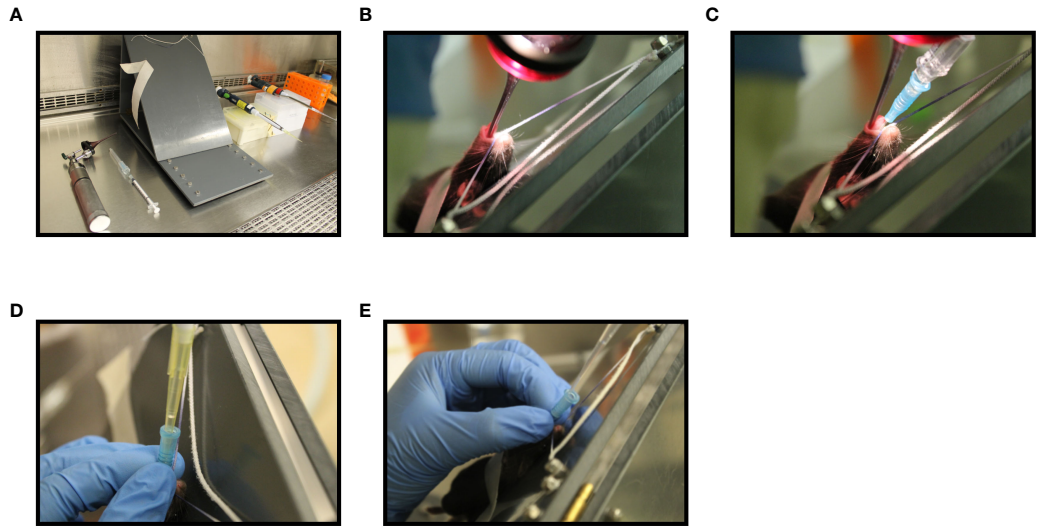

FIGURE 1 | Step-wise illustration of endotracheal delivery method (I.T). Endotracheal intubation was carried out in a C57BL/6 mouse anesthetized with 2% isoflurane and oxygen at a flow rate of 2 liters/min using an illuminated otoscope, a 22G blunt-tip intravenous catheter, a 45^0 C-angled intubation stand, a P200 pipette with P200 tip and a P200 pipette with extended length gel loading tip **(A)**. Unconscious mouse breathing at a respiration rate of 30 breaths per min was placed by hooking its upper incisor over a string attached to the intubation board. An otoscope was placed into the mouth and the vocal cord was visualized **(B)**. A 22G blunt-tip intravenous catheter attached to a syringe was then inserted into the trachea **(C)**. The syringe was then replaced with a P200 pipette attached to a p200 tip containing water and the movement of water in the tip during breathing was confirmed to affirm the insertion of catheter into the trachea **(D)**. Next, P200 pipette attached to an extended length gel-loading tip loaded with 50 µL AdHu5Luc or vaccine was inserted into the catheter and allow to inhale by the mouse **(E)**.

intubation as described above (21, 24, 25). Immunogenicity and protective efficacy were assessed four weeks post-immunization.

Bronchoalveolar Lavage and Lung Mononuclear Cell Isolation

Mice were euthanized by exsanguination. Cells in bronchoalveolar lavage and lung tissue were isolated as previously described (19–21, 26). Briefly, following exhaustive bronchoalveolar lavage (BAL), left and right lungs were collected separately and cut into small pieces and digested with collagenase type 1 (ThermoFisher Scientific Waltham, MA) at 37°C in an agitating incubator for one hour. A single-cell suspension was obtained by crushing the digested tissue through a 100 µm basket filter (BD Biosciences, San Jose, CA) and lysing the red blood cells using ACK lysis buffer. BAL was centrifuged at 6000 rpm for 3 minutes to pellet the cells. Isolated cells from BAL and the lung were resuspended in complete RPMI 1640 medium (RPMI 1640 supplemented with 10% FBS, 1% L-glutamine, and 1% penicillin/streptomycin).

Tetramer and Intracellular Cytokine Staining and Flow Cytometry

BAL and lung cells were plated at $2x10^6$ cells/mL and $20x10^6$ cells/mL, respectively, and stimulated with an Ag85a CD8 T cell-specific peptide (MPVGGQSSF) or Ag85a CD4 T cell-specific peptide (LTSELPGWLQANRHVKPTGS) at a concentration of 1 µg/well in the presence of Golgi plug (5 mg/mL brefeldin A; BD Pharmingen) for six hours in a 37°C CO_2 incubator. For tetramer immunostaining, a tetramer for the immunodominant CD8 T cell peptide (MPVGGQSSF) of Ag85A bound to the BALB/c major histocompatibility complex class I allele ($H\text{-}2L^d$ conjugated to PE fluorochrome) (NIH Tetramer Core, Atlanta, GA) was used (20). Tetramer stained and stimulated cells were then stained with T cell surface antibodies, followed by fixation/permeabilization by using Fixation/Permeabilization Solution Kit (BD Biosciences, San Jose, CA) according to the manufacturer's instructions. Cells were then stained with anti-IFN-γ-APC mAb in Perm/Wash buffer (BD Biosciences, San Jose, CA) for 30 min on ice. The monoclonal antibodies used for T cell surface markers were anti-CD3-V450, anti-CD4-APC-Cy7 and CD8-PE-Cy7. All mAbs and reagents were purchased from BD Biosciences (San Jose, CA). Immuno-stained cells were processed according to BD Biosciences instructions for flow cytometry and run on a BD LSR II flow cytometer. Data was analyzed using FlowJo (version 10.1; Tree Star, Ashland, OR).

M. Tuberculosis Preparation and Pulmonary Infection

Mtb $H_{37}Rv$ bacilli ($H_{37}RV$; ATCC 27,294) were grown in supplemented Middlebrook 7H9 broth for 14 days as described previously and stored at -70°C (20, 27). Before infection, bacilli were washed twice with PBS containing 0.05% Tween-80 and were subsequently passed 10 times through a 27-gauge needle to dislodge any clumps before *in vivo* usage. Pulmonary infection with the *Mtb* $H_{37}Rv$ strain was performed as previously described (20, 27). Briefly, anesthetized mice were intranasally infected with $1x10^4$ CFU of *Mtb* $H_{37}Rv$ in 25 µL of PBS. Dosage for infection was verified by plating 10-fold serial dilution on Middlebrook 7H10 agar plate containing Middlebrook oleic

acid-albumin-dextrose-catalase (OADC) (Invitrogen Life Technologies, Carlsbad, CA). *Mtb* H_{37}Rv burden in the lung was assessed four weeks post-infection by plating serial dilution of lung homogenates in triplicates onto Middlebrook 7H10 agar plates and incubated at 37°C for 21-28 days before enumeration.

Histological Analysis, Microscopy and Scoring

To assess the impact of different pulmonary delivery methods of vaccine on the lung histopathological changes after pulmonary *M.tb* infection, lung lobes were fixed in paraformaldehyde and subjected to hematoxylin and eosin (H&E) staining. Sections were then scored independently by two researchers blinded for the treatment groups. A scale from 1-10 was used to score the presence of granuloma, pneumonitis, and perivascular and peribronchial infiltration. Images of representative micrographs were taken on a Zeiss Axio Imager 2 Research Microscope using AxioVision digital imaging software (Carl Zeiss Microscopy GmbH, Germany).

Statistical Analysis

A two-tailed Student t test was performed for pairwise comparisons. One-way ANOVA followed by a Tukey test was performed to compare more than two groups. All analyses were performed on GraphPad Prism (Version 6, GraphPad Software, La Jolla, CA). A p value of <0.05 was considered significant.

RESULTS

Heightened Biodistribution in the Lung Following Endotracheal Inoculation Compared to Intranasal Inoculation

Intranasal instillation of 25 µL is the most widely used inoculation method for evaluation of respiratory mucosal delivered novel viral-vectored TB vaccines in mice (28, 29). To begin evaluating the impact of different respiratory route of inoculation on vaccine potency, we first studied the biodistribution of AdHu5Luc, a replication-deficient adenoviral vector expressing luciferase, in the lung as a marker of distribution. To this end, mice were inoculated with an identical dose of $5x10^7$ PFU AdHu5Luc *via* the conventional intranasal (I.N.) delivery or an endotracheal (I.T.) method (Fig.1A-E) and luciferase activity was assessed following administration of luciferin to the lung using IVIS imaging analysis. Luciferase expression was determined at eight hours post inoculation as a measure of corrected total area of fluorescence in left and right lung separately (**Figure 2A**). To define and correct autofluorescence background, PBS treated mice that received luciferin were included. Background signals were not evident in such control mice (**Figure 2B**). Overall, endotracheal delivery led to greater distribution of AdHu5Luc within the lung than intranasal delivery as indicated by much broader fluorescence intensity in both left and right lung lobes (**Figure 2C**). Of note, there was a lack of fluorescence intensity in the right lung of intranasal-inoculated animals. Indeed, upon analysis of the corrected total area of fluorescence intensity (total RFU (mean plus/minus SE) and p value), intranasal inoculation resulted in unequal biodistribution, more being deposited to the left than right lung and was variable between animals (**Figure 2D**). In contrast, biodistribution was comparable between right and left lungs following endotracheal delivery, with significantly higher deposition in the right lung than by intranasal inoculation (**Figure 2D**). These data indicate that different respiratory mucosal delivery methods result in differential biodistribution of adenoviral gene transfer vector within the lung.

Improved Vaccine-Induced Immunogenicity in the Lung Following Endotracheal Immunization Compared to Intranasal Immunization

Having demonstrated the broadened biodistribution of adenoviral vector within the lung *via* the deep respiratory delivery mediated by endotracheal inoculation, we evaluated the relationship of Ad-vectored vaccine biodistribution to vaccine immunogenicity. To this end, mice were immunized with an adenoviral-vectored TB vaccine, AdHu5Ag85A, by either I.N. or I.T. method. Mice were sacrificed four weeks post-immunization to assess antigen (Ag)-specific T cell responses (**Figure 3A**). We first assessed airway mononuclear cells from the whole lung (both left and right lungs) obtained by the bronchoalveolar lavage (BAL), with a focus on examining antigen 85A-specific CD8 T cell responses *via* CD8 T cell tetramer-immunostaining ($CD8^+Tet^+$) or intracellular cytokine-staining ($CD4^+IFN\gamma$, or $CD8^+IFN\gamma^+$) following *ex vivo* stimulation with Ag85A peptides (see gating strategy, **Supplementary Figure 1**). To define the gates and the background immunostaining, BAL cells from unimmunized mice were subjected to tetramer staining or BAL cells from immunized mice were cultured with control media (unstimulated) prior to IFNγ intracellular staining (see the top row of **Figure 3C**). Although deep respiratory delivery of the vaccine *via* I.T. inoculation induced a significant increase in total numbers of mononuclear cells in the airways compared to animals that received the vaccine *via* I.N inoculation (**Figure 3B**), comparable antigen-specific responses were induced in the BAL by either vaccine delivery method (**Figures 3C, D**).

To further evaluate the relationship between vaccine biodistribution and vaccine immunogenicity, we next assessed immune responses independently in the left and right lung tissues. Mice were vaccinated as described above, and left and right lung tissues were isolated for immune analysis (**Figure 4A**). Appropriate controls were set up to define the gates and the background immunostaining as described for BAL cells (see the top row of **Figures 4C-E**). In addition, lung tissue sections were evaluated for histological changes following these two methods of vaccination. In agreement with increased vaccine biodistribution following I.T. vaccine delivery (**Figure 2**), we observed significantly greater total cell counts in the right lung following I.T. immunization with AdHu5Ag85A, compared to I.N. delivery (**Figure 4B**). Furthermore, there were both significantly increased frequencies and absolute numbers of antigen-specific tet+ CD8 T cells (**Figures 4C, F**) and IFNγ+ CD8 (**Figures 4D, G**) and CD4 (**Figures 4E, H**) both in the left and right lungs of I.T. immunized animals than in I.N. animals.

Additionally, the increased cellular infiltration in the lung of I.T. vaccine group was due to the vaccine and was not associated

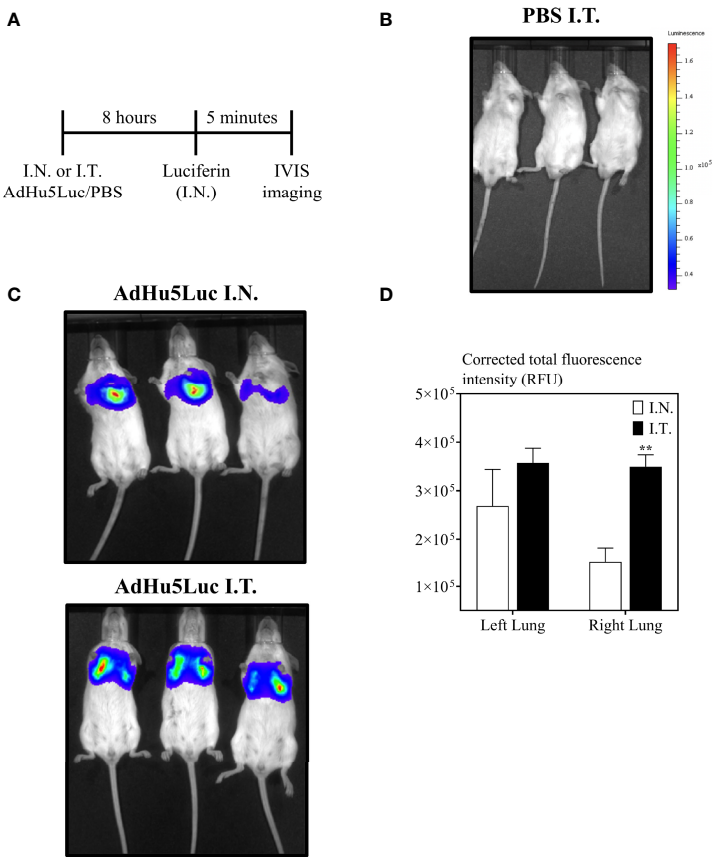

FIGURE 2 | Biodistribution of vaccine surrogate in the lung following intranasal or endotracheal inoculation. **(A)** Experimental schema. Mice were inoculated intranasally (I.N.) or endotracheally (I.T) with adenovirus-vector expressing luciferase (AdHu5Luc) or PBS. Biodistribution was visualized as a factor of light emission upon intranasal administration of luciferin. Images were obtained using an IVIS Spectrum and presented as pseudocolour images of bioluminescence in PBS **(B)** or AdHu5Luc inoculated animals **(C)**. Red represents the most intense areas of biodistribution while the blue corresponds to the weakest areas of biodistribution. Mice were imaged with an integration time of 30 sec. Three mice per treatment group is shown. **(D)** Bar graph shows corrected total fluorescence intensity measured in relative fluorescence units (RFU) and quantified using ImageJ in either right or left lung. Data is from 3 mice/group and RFU are presented as mean ± SEM. **p < 0.01.

with the procedure itself since the comparable total lung cell counts ranging 3-5 millions/lung were seen between PBS I.T.-treated and untreated naïve mice. These data together suggest that the extent of vaccine biodistribution in the lung is positively correlated with enhanced vaccine-specific immune responses within respiratory mucosal tissue compartments, which was particularly evident in both the left and right lungs.

Enhanced Protection Against Pulmonary Tuberculosis Following Endotracheal Immunization Compared to Intranasal Immunization

To examine whether improved vaccine-specific immunogenicity in the lung by broader respiratory biodistribution of AdHu5Ag85A would translate to enhanced protection against pulmonary TB, mice were immunized with AdHu5Ag85A by I.N. or I.T. delivery method (**Figure 5A**). A set of mice were left unimmunized as controls (Naïve). Four weeks after immunization, mice were challenged with virulent *M.tb*H37Rv. At four-week post-infection, mice were sacrificed. The right lung of each animal was harvested to assess mycobacterial burden by colony forming unit assay and the left lung was fixed in formalin for histopathological analysis after hematoxylin and eosin staining (**Figure 5A**). Since I.T. delivery led to significantly increased biodistribution of the vaccine primarily within the right lung over that by I.N delivery (**Figures 2B, C**), the assessment of *M.tb* bacterial burden in the right lung would more accurately address the relationship of increased vaccine biodistribution to the functional protective outcome of the vaccine. While both I.N. and I.T. immunization with AdHu5Ag85A significantly reduced the mycobacterial burden in the lung compared to the control (**Figure 5B**), I.T. immunization significantly enhanced protection as it further reduced the mycobacterial burden in the lung (~1.5 log reduction) over that by I.N. immunization (~0.8 log reduction) (**Figure 5B**).

To further examine vaccine-mediated protection, we assessed the lung immunopathology caused by *M.tb* infection. Indeed, in consistent with significantly reduced mycobacterial burden in the lung (**Figure 5B**), both I.N. and I.T. immunization markedly reduced

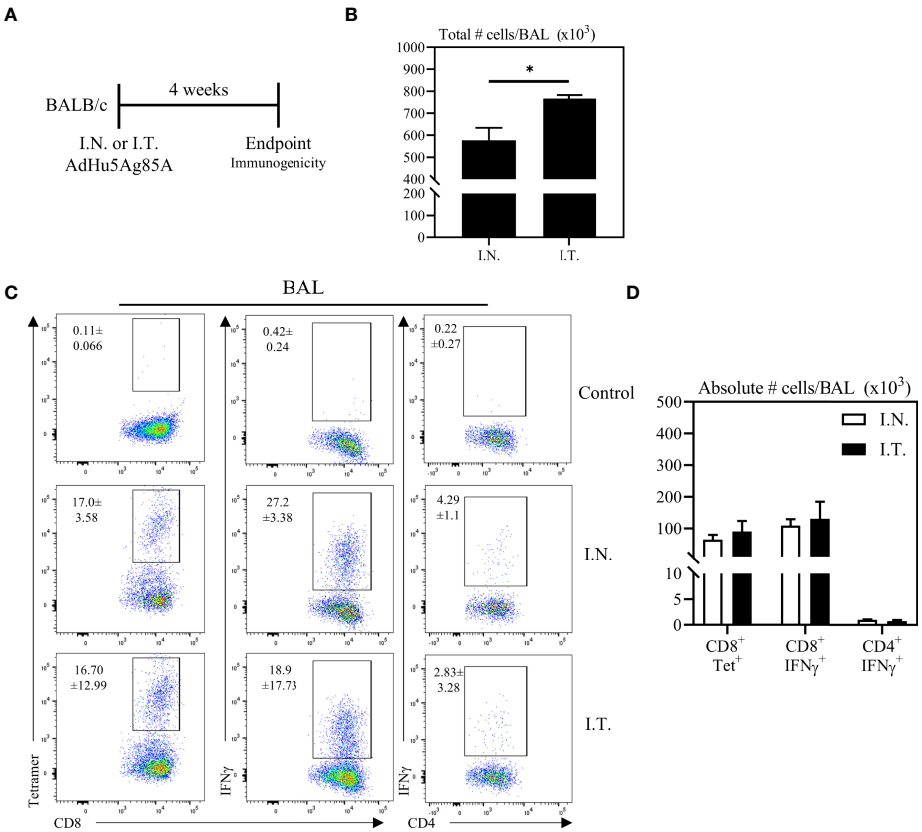

FIGURE 3 | Vaccine-specific T cell responses in the airways following endotracheal immunization compared to intranasal immunization. Experimental schema **(A)**. Mice immunized intranasally (I.N.) or endotracheally (I.T.) with AdHu5Ag85A were scarified 4 weeks post-immunization and mononuclear cells from airways were examined for vaccine-specific responses. **(B)** Bar graphs comparing total number of mononuclear cells in bronchoalveolar lavage (BAL) fluid. **(C)** Representative flow cytometric dotplots showing frequencies of Ag85A-specific CD8 T cells (CD8+tet+) determined by tetramer staining, and frequencies of IFNγ+ CD8+ and CD4+ T cells determined by intracellular cytokine staining of cells stimulated with Ag85A CD8 or CD4 T-cell specific peptides in BAL. Top row dotplots (Control) show the defining gates for tetramer population gated out of total CD8 T cells from unimmunized animal and the gates for CD8+IFNγ+ and CD4+IFNγ+ T cells out of total unstimulated CD8 and CD4 T cells from BAL of immunized mice. Numerical indicated in the dotplots represent the mean frequency of parent (CD4 or CD8 T cells) ± SEM. **(D)** Bar graphs comparing absolute number of CD8+tet+, CD8+IFNγ+, and CD4+IFNγ+ T cells in BAL of intranasal- and endotracheal-immunized mice. Absolute numbers of CD8+tetramer+, CD8+ IFN-γ+ and CD4+ IFN-γ+ shown in bar graphs were calculated based on frequency of CD3+live cells gated out of total events to exclude all non-immune cells. Data is from 3 mice/group, representative of two independent experiments and presented as mean ± SEM.*$p < 0.05$.

lung histopathology (**Figures 5C-H**). Of importance, I.T. immunization further significantly reduced lung immunopathology over that by I.N. delivery both in microscopic changes (**Figures 5C-H**) and histological scoring of relative extent of granuloma formation, pneumonitis, and inflammatory infiltration (**Figures 5I-K**). The above data together indicate that endotracheal delivery of vaccine improves protection against pulmonary TB over intranasal delivery and such improved protection is associated with collectively enhanced biodistribution of vaccine within the lung.

DISCUSSION

Respiratory mucosal (RM) immunization has been regarded as a highly appealing route of vaccination against respiratory infections given its superiority in inducing protective mucosal immunity and its advantage of being a needle-free, and thereby pain-free approach (3). Currently, several novel vaccines such as viral-vectored vaccines for TB and COVID-19 are being clinically developed for respiratory mucosal delivery (6, 9–11, 30). However, pulmonary delivery methods in humans include both intranasal and inhaled aerosol methods. Although these methods are expected to result in differential deposition sites of vaccine within the respiratory tract and subsequently, differential immune responses and protection, it is difficult to directly investigate it in humans. As a result, our understanding of the relationship of vaccine biodistribution following different methods of respiratory delivery to vaccine immunogenicity and protection has remained to be limited. In the current study, using an adenovirus-vectored TB vaccine (AdHu5Ag85A) as a model vaccine, we find that endotracheal delivery is superior to intranasal delivery in rendering wide and deep lung biodistribution of vaccine and subsequently, enhanced vaccine-specific T cell responses and protective efficacy against pulmonary *M.tb* challenge.

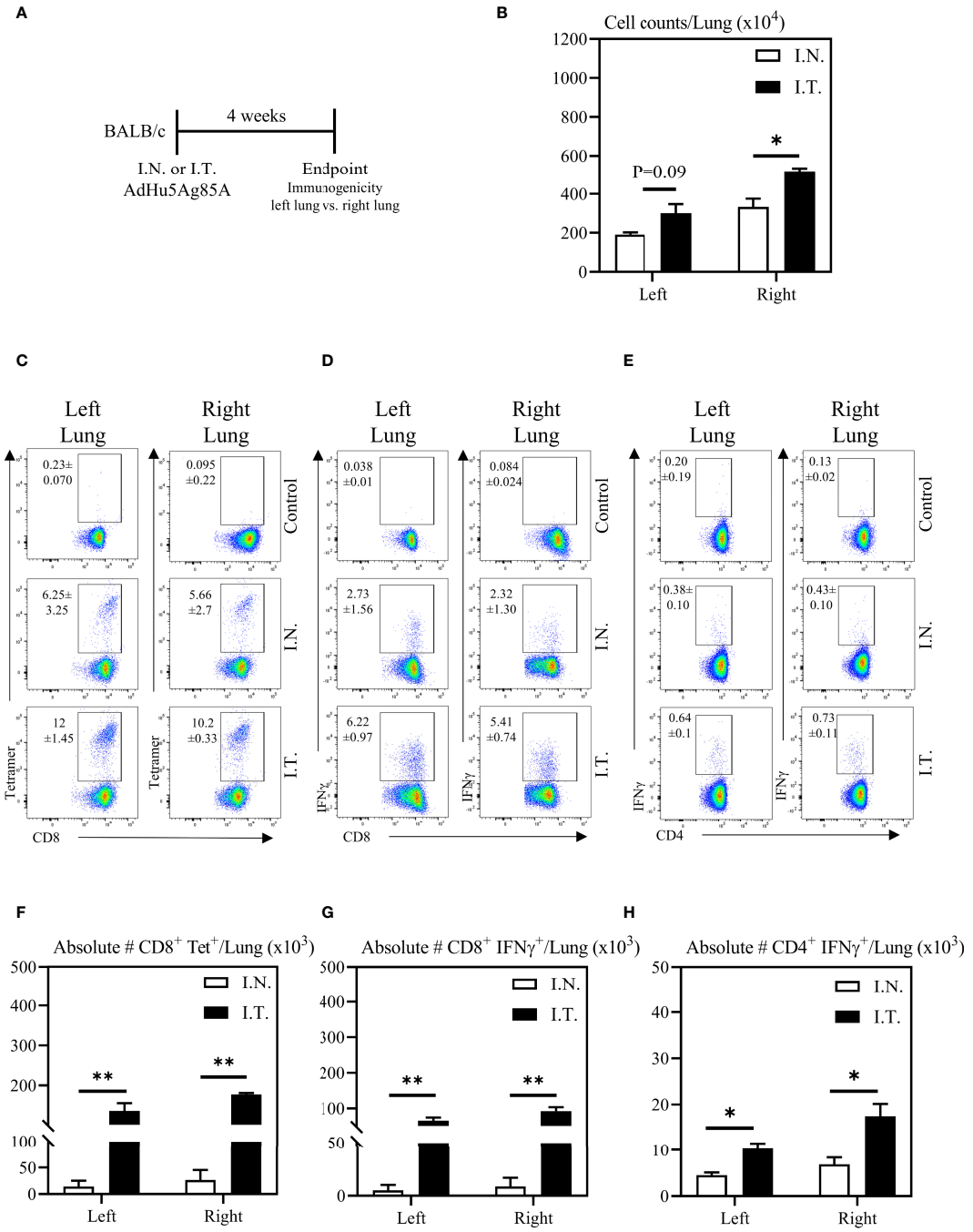

FIGURE 4 | Vaccine-specific T cell responses in the left and right lung tissues following endotracheal immunization compared to intranasal immunization. Experimental schema **(A)**. Mice immunized intranasally (I.N.) or endotracheally (I.T.) with AdHu5Ag85A were scarified 4 weeks post-immunization and mononuclear cells from left and right lung homogenates were examined for vaccine-specific responses separately. **(B)** Bar graphs comparing total numbers of mononuclear cells in left and right lung tissues. **(C–E)** Representative flow cytometric dotplots showing frequencies of Ag85A-specific CD8 T cells (CD8+tet+) determined by tetramer staining, and frequencies of IFNγ+ CD8+ and CD4+ T cells determined by intracellular cytokine staining of cells stimulated with Ag85A CD8 or CD4 T-cell specific peptides in left and right lung tissues. Top row dotplots (Control) show the defining gates for tetramer population gated out of total CD8 T cells from unimmunized animal and the gates for CD8+IFNγ+ and CD4+IFNγ+ T cells out of total unstimulated CD8 and CD4 T cells from left and right lung tissues of immunized mice. Numericals indicated in the dotplots represent the mean frequency of parent (CD4 or CD8 T cells) ± SEM. **(F–H)** Bar graphs comparing absolute numbers of CD8+ tet+, CD8+IFNγ+, and CD4+IFNγ+ T cells in left and right lung tissue of intranasal and endotracheal-immunized mice. Absolute numbers of CD8+tetramer+, CD8+ IFN-γ+ and CD4+ IFN-γ+ cells were calculated based on frequencies of CD3+live cells gated out of total events to exclude all non-immune cells. Data is from 3 mice/group, representative of two independent experiments and presented as mean ± SEM.*$p < 0.05$, **$p < 0.01$.

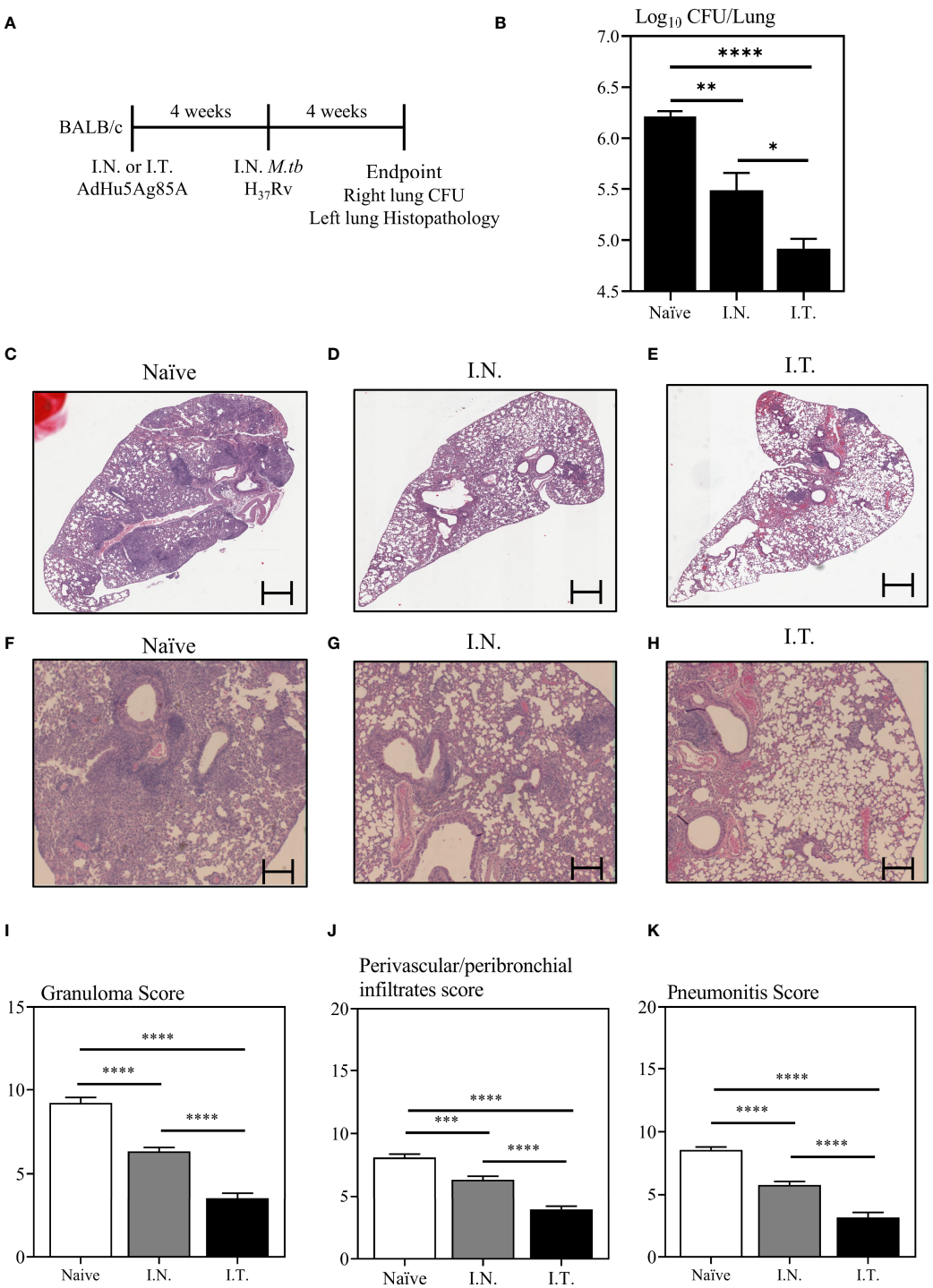

FIGURE 5 | Immune protection against pulmonary tuberculosis following endotracheal immunization compared to intranasal immunization. Experimental schema **(A)**. Mice immunized intranasally (I.N.) or endotracheally (I.T.) with AdHu5Ag85A were infected with virulent *M. tuberculosis* (Mtb) and sacrificed 4 weeks post-infection. Unimmunized mice were included as controls (Naïve). Right lung homogenates were serially diluted and plated for the assessment of mycobacterial burden (colony forming unit -CFU). **(B)** Bar graph comparing Log_{10} CFU/lung in unimmunized (naïve), or I.N. or I.T. immunized mice. Data is from n = 6 mice/group and presented as mean ± SEM. *p < 0.05; **p <0.01; ****p < 0.0001. **(C–H)** Following *M.tb* infection, lungs were processed for H&E staining and examined for immunopathological changes. Representative low-power micrographs showing overall lung architectural changes and higher-power micrographs showing granuloma, areas of pneumonitis and peribronchial/perivascular infiltrates. **(I–K)** Bar graphs comparing the semi-quantitative scoring of the extent of lung granuloma, pneumonitis and infiltration of cells in naïve, I.N. and I.T. immunized mice. Scoring was carried out on a scale of 1 to 10 and independently verified by another researcher blinded to the experimental groups. Data is from n = 6 mice/group. Data in bar graphs are presented as mean ± SEM. ***p <0.001; ****p < 0.0001.

Clinically, it was found that only inhaled aerosol, but not parenteral, vaccination induced significant respiratory mucosal immunity (9, 10). Since the inhaled aerosol technology bypasses the nasal passage, and generates and directly deposits mostly 2-5 μm size aerosol vaccine particles deep into human respiratory tract (airways) (10), these clinical observations suggest the immune efficacy by this respiratory mucosal delivery method in humans. Here for the first time, our experimental data reveals a causal relationship of relative depth and width of airway vaccine deposition to vaccine immunogenicity and protective efficacy following intranasal vs. endotracheal delivery. Our observations thus provide a potential explanation for unsatisfactory efficacy observed in human adults following intranasal delivery of flu vaccine (5, 6) and support the advantage of inhaled aerosol delivery method over intranasal delivery for human applications.

Other two previous studies that compared intranasal and intratracheal vaccine delivery did not assess vaccine biodistribution (17, 18). For instance, Minne et al. employed ovalbumin (OVA) as a surrogate and studied the influenza vaccine deposition regions in the lung by measuring OVA content in the nasal washes and lung homogenates (18). However, given that the cell tropism of a viral-vectored vaccine plays a critical role, using a surrogate that resembles the vaccine is important when evaluating biodistribution. In this regard, in our study, using a surrogate of the same viral vector as that used in the vaccine but expressing luciferase, we reliably demonstrated differential biodistribution following different methods of pulmonary delivery. Although De Swart et al. used the measles virus vaccine expressing enhanced green fluorescent protein to study the vaccine distribution, they only evaluated the bronchoalveolar cells and lung sections as a measure of vaccine distribution (17). As such they were unable to demonstrate the biodistribution.

It has now been fully established that vaccine induced CD4 and CD8 T cells residing at the respiratory mucosa plays a critical role in pulmonary immunity to pathogens by immediately encaging the pathogens at the site of infection (2, 3). Previous studies that assessed the impact of pulmonary delivery methods of vaccines on vaccine-induced immunity has shown that the delivery of vaccine to lower respiratory tract results in induction of higher titers of neutralizing antibodies (17, 18). Such knowledge cannot be generalized to induction of T cell immunity at the respiratory mucosa since the T cell responses in the lung are highly regulated to preserve the vital role of the lung, oxygen exchange. Here we show that endotracheal delivery of AdHu5Ag85A in animals yields heightened Ag-specific tetramer+ CD8+ T cells responses, IFN-γ production by CD4 and CD8 T cells in the lung and leads to enhanced protective efficacy against *M.tb* infection compared to intranasal immunization. Not only the reduction in bacterial load, but also markedly reduced histopathological damage in endotracheally immunized mice indicates that the deeper and wider biodistribution of vaccine is critical. Of note, although endotracheal delivery led to significantly greater biodistribution only in the right lung, it resulted in significantly increased antigen-specific T cell responses in both left and right lungs over those by intranasal immunization. These findings suggest that upon antigen-specific T cell priming in the local draining lymphoid tissues, similar numbers of T cells were recruited into the left and right lungs in response to the local inflammatory signals following endotracheal immunization.

Pulmonary delivery method of a vaccine for human application relies on various factors, such as vaccine formulation, *in vivo* tropism of the vaccine, and whether to target the upper or lower respiratory tract (3, 7, 8, 17). This is also reliant on the tropism of the pathogen against which the vaccine is directed to, and other parameters including duration of exposure to vaccine when delivered *via* inhalation or aerosolization, and the delivery device. In conclusion, we show that biodistribution of an adenoviral-vectored vaccine in the lung is dependent on pulmonary vaccine delivery method and that direct delivery of vaccine to deep into the respiratory tract of both lungs by endotracheal method increase the biodistribution and induce enhanced respiratory mucosal T cell immunity compared to intranasal delivery. Our study thus supports inhaled aerosol delivery over intranasal method for developing respiratory mucosal vaccine strategies for human application.

DATA AVAILABILITY STATEMENT

The raw data supporting the conclusions of this article will be made available by the authors, without undue reservation.

ETHICS STATEMENT

The animal study was reviewed and approved by The Animal Research and Ethics Board at McMaster University.

AUTHOR CONTRIBUTIONS

VJ, SA, MD'A, AZ, XF, MJ performed experiments or provided technical assistance. MT, ZX conceived the project. VJ, SA, MJ performed data analysis. VJ, MJ, ZX wrote the manuscript. All authors contributed to the article and approved the submitted version.

FUNDING

This study was supported by funds from The Canadian Institutes for Health Research and the Natural Sciences and Engineering Research Council of Canada (FDN-154316).

ACKNOWLEDGMENTS

Authors are thankful to Jane Ann Smith for her technical assistance.

SUPPLEMENTARY MATERIAL

The Supplementary Material for this article can be found online at: https://www.frontiersin.org/articles/10.3389/fimmu.2022.860399/full#supplementary-material

Supplementary Figure 1 | Dotplots depicting gating strategy used for flowcytometry data analysis of immune responses in the airways and lung tissue. Live CD3+ cells were gated after removing doublets. Debris were then gated out from Live CD3+ cells before identifying CD4+ and CD8+ T-cells for downstream gating of tetramer and IFNγ+ populations.

REFERENCES

1. World Health Organization. *WHO - The Top 10 Causes of Death*. (2018). pp. 1–7. Available at: https://www.who.int/en/news-room/fact-sheets/detail/the-top-10-causes-of-death [Accessed May 25, 2022].
2. Jeyanathan M, Afkhami S, Smaill F, Miller MS, Lichty BD, Xing Z. Immunological Considerations for COVID-19 Vaccine Strategies. *Nat Rev Immunol* (2020) 20:615–32. doi: 10.1038/s41577-020-00434-6
3. Lavelle EC, Ward RW. Mucosal Vaccines — Fortifying the Frontiers. *Nat Rev Immunol* (2021) 20:236–50. doi: 10.1038/s41577-021-00583-2
4. Jeyanathan M, Yao Y, Afkhami S, Smaill F, Xing Z. New Tuberculosis Vaccine Strategies: Taking Aim at Un-Natural Immunity. *Trends Immunol* (2018) 39:419–33. doi: 10.1016/j.it.2018.01.006
5. Osterholm MT, Kelley NS, Sommer A, Belongia EA. Efficacy and Effectiveness of Influenza Vaccines: A Systematic Review and Meta-Analysis. *Lancet Infect Dis* (2012) 12:36–44. doi: 10.1016/S1473-3099(11)70295-X
6. Alu A, Chen L, Lei H, Wei Y, Tian X, Wei X. Intranasal COVID-19 Vaccines: From Bench to Bed. *EBioMedicine* (2022) 76:103841. doi: 10.1016/j.ebiom.2022.103841
7. DiazGranados CA, Denis M, Plotkin S. Seasonal Influenza Vaccine Efficacy and its Determinants in Children and non-Elderly Adults: A Systematic Review With Meta-Analyses of Controlled Trials. *Vaccine* (2012) 31:49–57. doi: 10.1016/j.vaccine.2012.10.084
8. Low N, Bavdekar A, Jeyaseelan L, Hirve S, Ramanathan K, Andrews NJ, et al. A Randomized, Controlled Trial of an Aerosolized Vaccine Against Measles. *N Engl J Med* (2015) 372:1519–29. doi: 10.1056/NEJMoa1407417
9. Satti I, Meyer J, Harris SA, Thomas Z-RM, Griffiths K, Antrobus RD, et al. Safety and Immunogenicity of a Candidate Tuberculosis Vaccine MVA85A Delivered by Aerosol in BCG-Vaccinated Healthy Adults: A Phase 1, Double-Blind, Randomised Controlled Trial. *Lancet Infect Dis* (2014) 14:939–46. doi: 10.1016/S1473-3099(14)70845-X
10. Jeyanathan M, Fritz DK, Afkhami S, Aguirre E, Howie KJ, Zganiacz A, et al. Aerosol Delivery, But Not Intramuscular Injection, of Adenovirus-Vectored Tuberculosis Vaccine Induces Respiratory-Mucosal Immunity in Humans. *JCI Insight* (2021) 7(3). doi: 10.1172/jci.insight.155655
11. Wu S, Huang J, Zhang Z, Wu J, Zhang J, Hu H, et al. Safety, Tolerability, and Immunogenicity of an Aerosolised Adenovirus Type-5 Vector-Based COVID-19 Vaccine (Ad5-Ncov) in Adults: Preliminary Report of an Open-Label and Randomised Phase 1 Clinical Trial. *Lancet Infect Dis* (2021) 21(12):1654–64. doi: 10.1016/S1473-3099(21)00396-0
12. Kunda N, Price D, Muttil P. Respiratory Tract Deposition and Distribution Pattern of Microparticles in Mice Using Different Pulmonary Delivery Techniques. *Vaccines* (2018) 6:41. doi: 10.3390/vaccines6030041
13. Morales-Nebreda L, Chi M, Lecuona E, Chandel NS, Dada LA, Ridge K, et al. Intratracheal Administration of Influenza Virus is Superior to Intranasal Administration as a Model of Acute Lung Injury. *J Virol Methods* (2014) 209:116–20. doi: 10.1016/j.jviromet.2014.09.004
14. Santry LA, Ingrao JC, Yu DL, de Jong JG, van Lieshout LP, Wood GA, et al. AAV Vector Distribution in the Mouse Respiratory Tract Following Four Different Methods of Administration. *BMC Biotechnol* (2017) 17. doi: 10.1186/s12896-017-0365-2
15. van Erp EA, Lakerveld AJ, Mulder HL, Luytjes W, Ferwerda G, van Kasteren PB. Pathogenesis of Respiratory Syncytial Virus Infection in BALB/c Mice Differs Between Intratracheal and Intranasal Inoculation. *Viruses* (2019) 11. doi: 10.3390/v11060508
16. Khadangi F, Forgues AS, Tremblay-Pitre S, Dufour-Mailhot A, Henry C, Boucher M, et al. Intranasal Versus Intratracheal Exposure to Lipopolysaccharides in a Murine Model of Acute Respiratory Distress Syndrome. *Sci Rep* (2021) 11. doi: 10.1038/s41598-021-87462-x
17. De Swart RL, De Vries RD, Rennick LJ, Van Amerongen G, McQuaid S, Verburgh RJ, et al. Needle-Free Delivery of Measles Virus Vaccine to the Lower Respiratory Tract of Non-Human Primates Elicits Optimal Immunity and Protection. *NPJ Vaccines* (2017) 2:22. doi: 10.1038/s41541-017-0022-8
18. Minne A, Louahed J, Mehauden S, Baras B, Renauld J-C, Vanbever R. The Delivery Site of a Monovalent Influenza Vaccine Within the Respiratory Tract Impacts on the Immune Response. *Immunology* (2007) 122:316–25. doi: 10.1111/j.1365-2567.2007.02641.x
19. Yao Y, Jeyanathan M, Haddadi S, Barra NG, Vaseghi-Shanjani M, Damjanovic D, et al. Induction of Autonomous Memory Alveolar Macrophages Requires T Cell Help and Is Critical to Trained Immunity. *Cell* (2018) 175:1634–1650.e17. doi: 10.1016/j.cell.2018.09.042
20. Jeyanathan M, Thanthrige-Don N, Afkhami S, Lai R, Damjanovic D, Zganiacz A, et al. Novel Chimpanzee Adenovirus-Vectored Respiratory Mucosal Tuberculosis Vaccine: Overcoming Local Anti-Human Adenovirus Immunity for Potent TB Protection. *Mucosal Immunol* (2015) 8:1373–87. doi: 10.1038/mi.2015.29
21. Wang J, Thorson L, Stokes RW, Santosuosso M, Huygen K, Zganiacz A, et al. Single Mucosal, But Not Parenteral, Immunization With Recombinant Adenoviral-Based Vaccine Provides Potent Protection From Pulmonary Tuberculosis. *J Immunol* (2004) 173:6357–65. doi: 10.4049/jimmunol.173.10.6357
22. Cui Y, Robertson J, Maharaj S, Waldhauser L, Niu J, Wang J, et al. Oxidative Stress Contributes to the Induction and Persistence of TGF-β1 Induced Pulmonary Fibrosis. *Int J Biochem Cell Biol* (2011) 43:1122–33. doi: 10.1016/j.biocel.2011.04.005
23. Buckley SMK, Howe SJ, Rahim AA, Buning H, McIntosh J, Wong SP, et al. Luciferin Detection After Intranasal Vector Delivery is Improved by Intranasal Rather Than Intraperitoneal Luciferin Administration. *Hum Gene Ther* (2008) 19:1050–6. doi: 10.1089/hum.2008.023
24. Smaill F, Jeyanathan M, Smieja M, Medina MF, Thanthrige-Don N, Zganiacz A, et al. A Human Type 5 Adenovirus-Based Tuberculosis Vaccine Induces Robust T Cell Responses in Humans Despite Preexisting Anti-Adenovirus Immunity. *Sci Transl Med* (2013) 5. doi: 10.1126/scitranslmed.3006843
25. Jeyanathan M, Shao Z, Yu X, Harkness R, Jiang R, Li J, et al. AdHu5Ag85A Respiratory Mucosal Boost Immunization Enhances Protection Against Pulmonary Tuberculosis in BCG-Primed Non-Human Primates. *PloS One* (2015) 10:e0135009. doi: 10.1371/journal.pone.0135009
26. Jeyanathan M, Afkhami S, Khera A, Mandur T, Damjanovic D, Yao Y, et al. CXCR3 Signaling Is Required for Restricted Homing of Parenteral Tuberculosis Vaccine–Induced T Cells to Both the Lung Parenchyma and Airway. *J Immunol* (2017) 199:2555–69. doi: 10.4049/jimmunol.1700382
27. D'Agostino MR, Lai R, Afkhami S, Khera A, Yao Y, Vaseghi-Shanjani M, et al. Airway Macrophages Mediate Mucosal Vaccine–Induced Trained Innate Immunity Against Mycobacterium Tuberculosis in Early Stages of Infection. *J Immunol* (2020) 205:2750–62. doi: 10.4049/jimmunol.2000532
28. Radošević K, Wieland CW, Rodriguez A, Weverling GJ, Mintardjo R, Gillissen G, et al. Protective Immune Responses to a Recombinant Adenovirus Type 35 Tuberculosis Vaccine in Two Mouse Strains: CD4 and CD8 T-Cell Epitope Mapping and Role of Gamma Interferon. *Infect Immun* (2007) 75:4105–15. doi: 10.1128/IAI.00004-07
29. Khanna M, Rady H, Dai G, Ramsay AJ. Intranasal Boosting With MVA Encoding Secreted Mycobacterial Proteins Ag85A and ESAT-6 Generates Strong Pulmonary Immune Responses and Protection Against M. Tuberculosis in Mice Given BCG as Neonates. *Vaccine* (2021) 39:1780–7. doi: 10.1016/j.vaccine.2021.01.071
30. Afkhami S, D'Agostino MR, Zhang A, Stacey HD, Marzok A, Kang A, et al. Respiratory Mucosal Delivery of Next-Generation COVID-19 Vaccine Provides Robust Protection Against Both Ancestral and Variant Strains of SARS-CoV-2. *Cell* (2022) 185:896–915.e19. doi: 10.1016/J.CELL.2022.02.005

Conflict of Interest: The authors declare that the research was conducted in the absence of any commercial or financial relationships that could be construed as a potential conflict of interest.

frontiers | Frontiers in Immunology

ORIGINAL RESEARCH
published: 06 July 2022
doi: 10.3389/fimmu.2022.819859

Induction of Mucosal IgA–Mediated Protective Immunity Against Nontypeable *Haemophilus influenzae* Infection by a Cationic Nanogel–Based P6 Nasal Vaccine

Rika Nakahashi-Ouchida[1,2,3], Hiromi Mori[1,3], Yoshikazu Yuki[1,3,4], Shingo Umemoto[5,6], Takashi Hirano[5], Yohei Uchida[1,3], Tomonori Machita[1,3], Tomoyuki Yamanoue[1,3], Shin-ichi Sawada[7], Masashi Suzuki[5], Kohtaro Fujihashi[3,8,9], Kazunari Akiyoshi[7], Yuichi Kurono[10] and Hiroshi Kiyono[2,3,4,6,11]**

[1] Division of Mucosal Vaccines, International Research and Development Center for Mucosal Vaccines, The Institute of Medical Science, The University of Tokyo, Tokyo, Japan, [2] Division of Mucosal Immunology, IMSUT Distinguished Professor Unit, The Institute of Medical Science, The University of Tokyo, Tokyo, Japan, [3] Department of Human Mucosal Vaccinology, Chiba University Hospital, Chiba, Japan, [4] HanaVax Inc., Tokyo, Japan, [5] Faculty of Medicine, Department of Otorhinolaryngology, Head and Neck Surgery, Oita University, Oita, Japan, [6] CU-UCSD Center for Mucosal Immunology, Allergy and Vaccines (cMAV), Division of Gastroenterology, Department of Medicine, University of California, San Diego, San Diego, CA, United States, [7] Department of Polymer Chemistry, Faculty of Engineering, Kyoto University, Kyoto, Japan, [8] Division of Clinical Vaccinology, International Research and Development Center for Mucosal Vaccines, The Institute of Medical Science, The University of Tokyo, Tokyo, Japan, [9] Department of Pediatric Dentistry, The University of Alabama at Birmingham, Birmingham, AL, United States, [10] Department of Otolaryngology, Faculty of Medicine, Kagoshima University, Kagoshima, Japan, [11] Future Medicine Education and Research Organization, Mucosal Immunology and Allergy Therapeutics, Institute for Global Prominent Research, Chiba University, Chiba, Japan

OPEN ACCESS

Edited by:
Simon Daniel Van Haren, Boston Children's Hospital and Harvard Medical School, United States

Reviewed by:
Kevin Mason, Nationwide Children's Hospital, United States
Mariagrazia Pizza, GlaxoSmithKline, Italy

***Correspondence:**
Rika Nakahashi-Ouchida
ouchida@ims.u-tokyo.ac.jp
Hiroshi Kiyono
kiyono@ims.u-tokyo.ac.jp

Specialty section:
This article was submitted to Vaccines and Molecular Therapeutics, a section of the journal Frontiers in Immunology

Received: *22 November 2021*
Accepted: *31 May 2022*
Published: *06 July 2022*

Citation:
Nakahashi-Ouchida R, Mori H, Yuki Y, Umemoto S, Hirano T, Uchida Y, Machita T, Yamanoue T, Sawada S-i, Suzuki M, Fujihashi K, Akiyoshi K, Kurono Y and Kiyono H (2022) Induction of Mucosal IgA–Mediated Protective Immunity Against Nontypeable Haemophilus influenzae Infection by a Cationic Nanogel–Based P6 Nasal Vaccine. Front. Immunol. 13:819859. doi: 10.3389/fimmu.2022.819859

Nontypeable *Haemophilus influenzae* (NTHi) strains form a major group of pathogenic bacteria that colonizes the nasopharynx and causes otitis media in young children. At present, there is no licensed vaccine for NTHi. Because NTHi colonizes the upper respiratory tract and forms biofilms that cause subsequent infectious events, a nasal vaccine that induces NTHi-specific secretory IgA capable of preventing biofilm formation in the respiratory tract is desirable. Here, we developed a cationic cholesteryl pullulan–based (cCHP nanogel) nasal vaccine containing the NTHi surface antigen P6 (cCHP-P6) as a universal vaccine antigen, because P6 expression is conserved among 90% of NTHi strains. Nasal immunization of mice with cCHP-P6 effectively induced P6-specific IgA in mucosal fluids, including nasal and middle ear washes. The vaccine-induced P6-specific IgA showed direct binding to the NTHi *via* the surface P6 proteins, resulting in the inhibition of NTHi biofilm formation. cCHP-P6 nasal vaccine thus protected mice from intranasal NTHi challenge by reducing NTHi colonization of nasal tissues and eventually eliminated the bacteria. In addition, the vaccine-induced IgA bound to different NTHi clinical isolates from patients with otitis media and inhibited NTHi attachment in a three-dimensional *in vitro* model of the human nasal epithelial surface. Therefore, the cCHP-P6 nanogel nasal vaccine induced effective protection in the airway mucosa, making it a strong vaccine candidate for preventing NTHi-induced infectious diseases, such as otitis media, sinusitis, and pneumonia.

Keywords: cCHP nanogel, drug delivery system, nasal vaccine, nontypeable *Haemophilus influenzae*, mucosal IgA

INTRODUCTION

Nontypeable *Haemophilus influenzae* (NTHi) is a human-specific pathogen that mainly colonizes the upper respiratory tract and causes noninvasive infections, including otitis media, sinusitis, and pneumonia; NTHi also is associated with exacerbation of chronic obstructive pulmonary disease (1, 2). Unfortunately, no licensed vaccine specific for NTHi infections is currently available. A licensed pneumococcal vaccine containing the protein D of NTHi, PHiD-CV (*Synflorix*, GSK), has been used in the clinical setting, but it provides very limited protection against otitis media caused by NTHi infections (3–5). In addition, the introduction of pneumococcal vaccines such as PCV13 (*Prevnar*13, Pfizer Inc.) has been suggested to have led to an increase of acute otitis media and the emergence of invasive NTHi (6). Owing to the increasing number of antibiotic-resistant NTHi strains (7), the development of NTHi vaccines has become a very important issue for public health.

NTHi colonization of the upper respiratory tract is an important first step in the pathogenesis of NTHi-mediated disease; NTHi forms biofilms that promote persistence within the host environment, and this leads to increased antimicrobial resistance (8, 9). A strategy for suppressing bacterial invasion and colonization of the mucosa of the upper respiratory tract and for inhibiting biofilm formation in the airway mucosa would, therefore, be an effective way to prevent NTHi infection.

Nasal immunization efficiently induces an antigen-specific immune response on mucosal surfaces of the upper and lower respiratory tracts, as well as in the systemic compartment (10, 11). Indeed, nasal immunization with a vaccine antigen targeting the NTHi surface antigen P6 induces both antigen-specific serum IgG and mucosal secretory immunoglobulin A (SIgA), which directly recognizes and eliminates NTHi in the nasal or bronchial mucosa, thereby preventing the initiation of infections (12, 13). However, the nasal cavity has a well-developed mucosal barrier that includes cilia, mucus secretions, and tight junctions and plays an important role in host defense through innate immunity (14). Intranasally administered vaccine antigens are easily eliminated by the mucosal barrier system, making it difficult for them to induce substantial antigen-specific immune responses. Therefore, the system used to deliver the nasal vaccine needs to overcome this obstacle. Given the nature of *Haemophilus* infections, it is logical and desirable to develop nasal vaccines that effectively activate the airway mucosal immune system, where the first line of defense against NTHi infections occurs. We therefore applied our cationic cholesteryl-group-bearing pullulan (cCHP) nanogel–based nasal delivery system to the development of a nasal vaccine against NTHi.

The cCHP nanogel is a safe and effective nasal vaccine delivery vehicle that can optimally deliver vaccine antigen and stimulate the nasal mucosal immune system (15–18). Because of its cationic property, the cCHP nanogel shows persistent attachment to the surfaces of the negatively charged nasal mucosa, leading to the prolonged release of antigen to the antigen-sampling and -presenting systems of the nasal mucosa (15). The cCHP nanogel has thus been shown to effectively induce antigen-specific immune responses in both the systemic and mucosal compartments (16–18), and we therefore believe that it is an attractive and competent vehicle for delivering nasal vaccines to prevent respiratory infectious diseases, including otitis media, pneumonia, and COVID-19. Indeed, we have demonstrated that a cCHP nanogel incorporating a pneumococcal surface protein antigen (cCHP-PspA) induces PspA-specific serum IgG and SIgA in mucosal fluids in mice and nonhuman primates (16–18). These PspA-specific antibodies eliminated bacteria from lung lavage fluids, nasal washes, and the nasal passages (17). As a result, the cCHP-PspA nanogel vaccine protects against lethal or sublethal pneumococcal infections in immunized mice (17) and in mice that receive passively transferred serum from vaccinated macaques (16), as well as in pneumococcus-infected macaques (18). In addition, the vaccine antigen introduced by the cCHP nanogel did not migrate into the olfactory bulbs or brain in either murine or nonhuman primate models (16, 17); this is important evidence regarding the safety of a cCHP nanogel–based nasal vaccine delivery system.

P6 protein is a 16-kDa peptidoglycan-associated lipoprotein —one of the outer membrane proteins of NTHi—and is considered to be a potential vaccine antigen candidate for NTHi. In human studies, the amount of P6-specific SIgA correlates with the degree of inhibition of NTHi colonization of the nasopharynx and the incidence of recurrent otitis media (19, 20). Furthermore, nasal immunization of mice with P6 protein and cholera toxin, a classic and experimental mucosal adjuvant, induces P6-specific mucosal and systemic immune responses that clear NTHi from the nasal cavity after infection (21, 22). In addition, the P6 protein sequence is more than 90% conserved among NTHi strains at the nucleotide and amino acid levels, and the P6 protein is, therefore, a highly promising candidate antigen for the development of a universal NTHi vaccine (23).

Here, we investigated the quality and quantity of P6-specific immune responses, including protective efficacy, induced by nasally administered cCHP nanogel containing P6 protein (cCHP-P6). The cCHP-P6 nanogel nasal vaccine provided protective immunity against NTHi infection by inhibiting NTHi attachment to the nasal epithelial surface and preventing NTHi biofilm formation; systemic immunization did not lead to P6-specific IgA–mediated inhibition.

MATERIALS AND METHODS

Mice

Female BALB/c mice (age, 7 to 8 weeks) were purchased from SLC (Shizuoka, Japan) or Kyudo Co. Ltd. (Saga, Japan). The mice were maintained in the experimental animal facility at the Institute of Medical Science of the University of Tokyo. All experiments were conducted in accordance with the guidelines provided by the Animal Care and Use Committees of the University of Tokyo and Oita University and were approved by the Animal Committee of the Institute of Medical Science of the University of Tokyo.

P6 Antigen Construction and Recombinant Protein Purification

The P6 gene (GenBank accession no. AWP55884.1; amino acids 21–153) was synthesized by Takara Bio Inc. (Otsu, Japan). After digestion with the restriction enzymes *Nco*I and *Xho*I (Takara Bio Inc.), the gene was inserted into the pET-20b(+) vector (Novagen, Inc., Madison, WI, USA), which includes a C-terminal His tag. Rosetta2(DE3) pLysS-competent cells (Novagen, Inc.) were transformed with the P6-encoding plasmid in accordance with the manufacturer's protocol. The resultant transformant was inoculated into lysogeny broth containing 100 μg/mL ampicillin and 34 μg/mL chloramphenicol and incubated with shaking at 37°C until the OD_{600} was 0.5 to 0.8. After induction with 0.4 mM isopropyl β-D-1-thiogalactopyranoside (Wako Pure Chemical Industries, Ltd., Osaka, Japan) and incubation at 37°C for 3.5 h, the cells were harvested by centrifugation at 5000*g* for 15 min at 4°C and then resuspended in 0.025 culture volume of Tris phosphate buffer containing 6 M urea. The desired protein was dialyzed against 6 M urea/500 mM NaCl/20 mM Tris containing 10 mM imidazole. The protein was then purified by means of Ni Sepharose 6 Fast Flow affinity chromatography (GE Healthcare Bio-Sciences K.K., Tokyo, Japan) followed by gel filtration on a Sephacryl S-100 HR column; GE Healthcare Bio-Sciences K.K.) in phosphate-buffered saline (PBS) containing 6 M urea. P6 fractions were collected and dialyzed step by step against 4 M urea–PBS, 2 M urea–PBS, 1 M urea–PBS, and PBS and kept at room temperature after passage through a 0.22-μm membrane. The protein concentrations of the purified P6 were determined according to the theoretical absorbance at a wavelength of 280 nm (absorbance 0.1% = 1.054), as determined from the amino acid sequence, and calculated by using the ProtParam tool (https://web.expasy.org/cgi-bin/protparam/).

Preparation of cCHP Nanogel Vaccine and Immunization

A cationic type of nanogel (cCHP nanogel) was used for all experiments. The cCHP nanogel was synthesized as described previously (24). For the preparation of vaccine, the cCHP nanogel and recombinant P6 protein were mixed at a 1:1 molecular ratio and incubated for 1 h at 40°C. By using a *Limulus* test (Wako, Osaka, Japan), lipopolysaccharide contamination of the cCHP nanogel or recombinant P6 protein was confirmed to be less than 10 endotoxin units/mg protein. Mice were immunized intranasally with the cCHP-P6 without any adjuvant once weekly for 2 or 3 consecutive weeks (10 μg of P6 protein per immunization). Serum, nasal washes, and middle ear washes were obtained at 3, 5, 6, and 7 weeks after the first immunization. For collecting nasal wash samples, 100 μL of sterile PBS was flushed through the posterior choanae. Middle ear fluids were harvested by suspending 200 μL of sterile PBS in the middle ear (25). For systemic immunization, 20 μg of P6 protein precipitated with aluminum hydroxide was injected intramuscularly and then boosted with 10 μg of P6 in PBS at 2 and 5 weeks after the first immunization.

Bacterial Strains and Infection

All of the clinical strains of NTHi were isolated from the nasopharynx of patients with effusive otitis media at Oita University Hospital (Oita, Japan); appropriate informed consent was obtained as described previously (PMID: 9665253). In brief, a Juhn Tym-Tap fluid collection aspirator (Xomed, Jacksonville, FL, USA) was inserted into the nasopharynx through the nose, and nasopharyngeal secretions were collected by aspiration. NTHi strains were isolated from nasopharyngeal secretions, stored at –80°C, and used in a manner that did not identify personal information (Grant-in-Aid for General Scientific Research (C), no. 06671724). Before use, all of the NTHi strains were grown overnight at 37 °C on chocolate agar plates prepared by using brain heart infusion broth. The number of bacteria was calculated by using the predetermined coefficient of 1 $OD_{600} = 2 \times 10^9$ colony-forming units (cfu)/ml; cells were pelleted and then diluted in PBS.

To evaluate vaccine efficacy, mice were challenged 1 week after the last immunization. The mice underwent intranasal pretreatment with 5 μl of 5% n-acetylcysteine, and then 5 μl of 0.5% Triton X-100 to increase susceptibility to infection. A sublethal dose (1×10^8 cfu per mouse) of NTHi strain 76 diluted in 10 μL sterile PBS was then administered intranasally to each isofiurane-anesthetized mouse. Nasal washes were harvested 3 days after the sublethal challenge. For the preparation of nasal passage samples, nasal cavities were harvested 3 days after sublethal challenge, minced, and homogenized in PBS containing 1% saponin. Bacterial numbers in nasal washes or supernatant from nasal cavity homogenization were determined by counting colonies on chocolate agar plates.

Antibody Titers

The endpoint titers of anti-P6 IgG or IgA from immunized mice were determined by using enzyme-linked immunosorbent assays (ELISAs), as described previously (17). Briefly, samples of serum, nasal wash, or middle ear wash were prepared as two-fold serial dilutions and loaded into a 96-micro-well plate (Nunc MaxiSorp Immuno; Thermo Fisher Scientific, Waltham, MA, USA) coated with 1 μg/mL recombinant P6 with bovine serum albumin. Horseradish peroxidase–conjugated goat anti-mouse IgG or IgA (dilution, 1:4,000) was used as a secondary antibody. Reactions were visualized by using the TMB Microwell Peroxidase Substrate System (XPL, Gaithersburg, MD, USA). The endpoint titer was expressed as the reciprocal log2 of the last dilution that gave an OD_{450} that was at least 0.1 unit greater than that of the negative control.

IgA-Secreting Cells

Mononuclear cells were isolated from the nasal passages of immunized mice (5×10^5 cells per mouse), and the numbers of P6-specific IgA producing cells were determined by using an enzyme-linked immunospot (ELISpot) assay. Briefly, 96-micro-well plates (MultiScreen; Merck, Darmstadt, Germany) were coated with 10 μg/mL recombinant P6 and incubated overnight at 4°C. Plates were washed three times with PBS and

blocked for 1 h at 37 °C with RPMI 1640 medium supplemented with 10% fetal calf serum, 55 μM 2-mercaptoethanol, and 55 μg/ml penicillin–streptomycin. After the incubation, 2×10^5 mononuclear cells isolated from the nasal passages of mice were added to each well and cultured at 37 °C, 5% CO_2 for 6 h. Horseradish peroxidase–conjugated goat anti-mouse IgA (dilution, 1:1,000) was used as a secondary antibody. Spots were developed by adding 3-amino-9-ethylcarbazole (Merck) in 0.1 M sodium acetate buffer, pH 5.0, containing 0.05% H_2O_2 and incubating for 30 min at room temperature.

Immunohistochemistry

Nasal cavity samples for confocal microscopy were prepared as described previously (26). Briefly, the nasal cavity samples were fixed in 4% (w/v) paraformaldehyde in PBS overnight at 4 °C with rocking, followed by soaking in 30% (w/v) sucrose in PBS overnight at 4 °C with rocking. The nasal cavity samples were then embedded in Super Cryoembedding Medium (Leica Microsystems K.K., Tokyo, Japan). For immunofluorescence staining, we prepared 10-μm-thick frozen sections by using a CryoJane Tape-Transfer System (Instrumedics, St. Louis, MO) and allowing the sections to air dry. Then the sections were treated with FITC-labeled anti-P6 antibody. After several washes, the specimens were mounted in VECTASHIELD mounting medium with DAPI (Vector Laboratories, Burlingame, CA, USA) and analyzed by using an LSM 800 confocal laser-scanning microscope (Zeiss, Oberkochen, Germany).

Antibody Binding Assay

NTHi strain 76 was grown on a chocolate agar plate overnight at 37°C, and cells were collected in PBS and centrifuged at 10,000*g* for 5 min at 4°C, after which the cell pellet was diluted into FACS buffer. These NTHi cells (2×10^8 cfu) were then incubated with nasal wash (equivalent to 50 μg protein input) for 1 h at room temperature, followed by staining with biotin-conjugated anti-mouse IgA (BioLegend, San Diego, CA, USA) and allophycocyanin–streptavidin (Tonbo Biosciences, San Diego, CA, USA). Flow cytometric analysis was performed by using an Attune NxT flow cytometer (Thermo Fisher Scientific).

NTHi Adherence Assay

An *in vitro*, three-dimensional (3D) culture system reconstituted from healthy human primary airway tissue (MucilAir, Epithelix, Plan-les-Ouates, Switzerland) was used in the assay. FITC-labeled NTHi strain 76 cells (2.0×10^8 cfu) were diluted in PBS and nasal wash (equivalent to 50 μg protein input) and incubated for 1 h at 37°C. The bacteria were then washed once with PBS, diluted in antibiotic-free medium, and added to the micro-titer plates of the cell culture system, which were placed a 5% CO_2 incubator for 6 h at 37°C to allow the bacteria to adhere to the cells. Each well was then washed three times with PBS, and the cells were fixed in 4% (w/v) paraformaldehyde in PBS for 20 min at room temperature. This was followed by treatment with 0.1% Triton X-100 for permeabilization. The cells were stained with anti-β-tubulin (Merck), stained with rhodamine-conjugated anti-mouse IgG (Thermo Fisher Scientific) to visualize the cilia, mounted in VECTASHIELD mounting medium with DAPI (Vector Laboratories), and analyzed under an LSM 800 confocal laser-scanning microscope (Zeiss). By using COMSTAT2 software (27–29), we calculated the numbers of bacteria that were attached to epithelial surfaces (i.e., the biomass). This was done by determining the mean fluorescence of seven randomly selected fields of a slide image in which the FITC fluorescence signal exceeded the background fluorescence level of images obtained from 3D cultures without FITC-labeled NTHi. In addition, to deplete IgG, nasal washes were filtered through protein G Sepharose 4 Fast Flow (GE Healthcare Bio-Sciences K.K.). Residual amounts of IgG in the flowthrough samples were confirmed by using an ELISA, and the IgG-depleted samples were used at the same volumes as the crude nasal washes.

NTHi Biofilm Formation Assay

The *in vitro* biofilm assay was performed as described previously (30). Briefly, NTHi bacteria were inoculated into the wells of an eight-well chamber slide (Thermo Fisher Scientific), each of which contained nasal washes from vaccinated mice, and incubated for 40 h at 37°C, 5% CO_2. The medium in each well was changed every 12 h, and fresh nasal wash was added at each medium change. Biofilms were stained with LIVE/DEAD BacLight viability stain (Thermo Fisher Scientific) and fixed with 4% paraformaldehyde. Biofilms were visualized under a confocal microscope, and biomass values were quantified by using COMSTAT2 software (27–29).

Statistical Analysis

Statistical analysis for comparisons among groups was performed by using either a two-tailed Student's *t*-test or one-way ANOVA with a Tukey test. *P*-values less than 0.05 were considered significant.

RESULTS

Nasal Immunization With cCHP Nanogel Carrying P6 Protein Induces P6-specific Mucosal Immune Responses

Competent *Escherichia coli* cells were transformed with the P6 plasmid, and the expressed His-tagged P6 recombinant protein was purified as a single band with a molecular weight of 15.5 kDa on SDS-PAGE (**Supplementary Figure S1**). Purified recombinant P6 protein was then incubated with the cCHP nanogel at a molecular ratio of 1:1 to prepare cCHP-P6 nanogel vaccine for the immunogenicity study. SDS treatment disrupts the cCHP-P6 vaccine, and the amount of P6 antigen released from the cCHP-P6 nanogel was evaluated by SDS-PAGE. More than 96% of the P6 antigen encapsulated in the cCHP nanogel was released without degradation, thus confirming the stability of the P6 antigen in the nanogel formulation (**Supplementary Figure S2**).

We then nasally immunized one group of BALB/c mice with the cCHP-P6 nanogel vaccine once weekly for 3 consecutive weeks (**Figure 1A**). Another group of BALB/c mice received a single intramuscular injection of P6 protein precipitated with aluminum hydroxide as an adjuvant (Alum-P6), followed by an

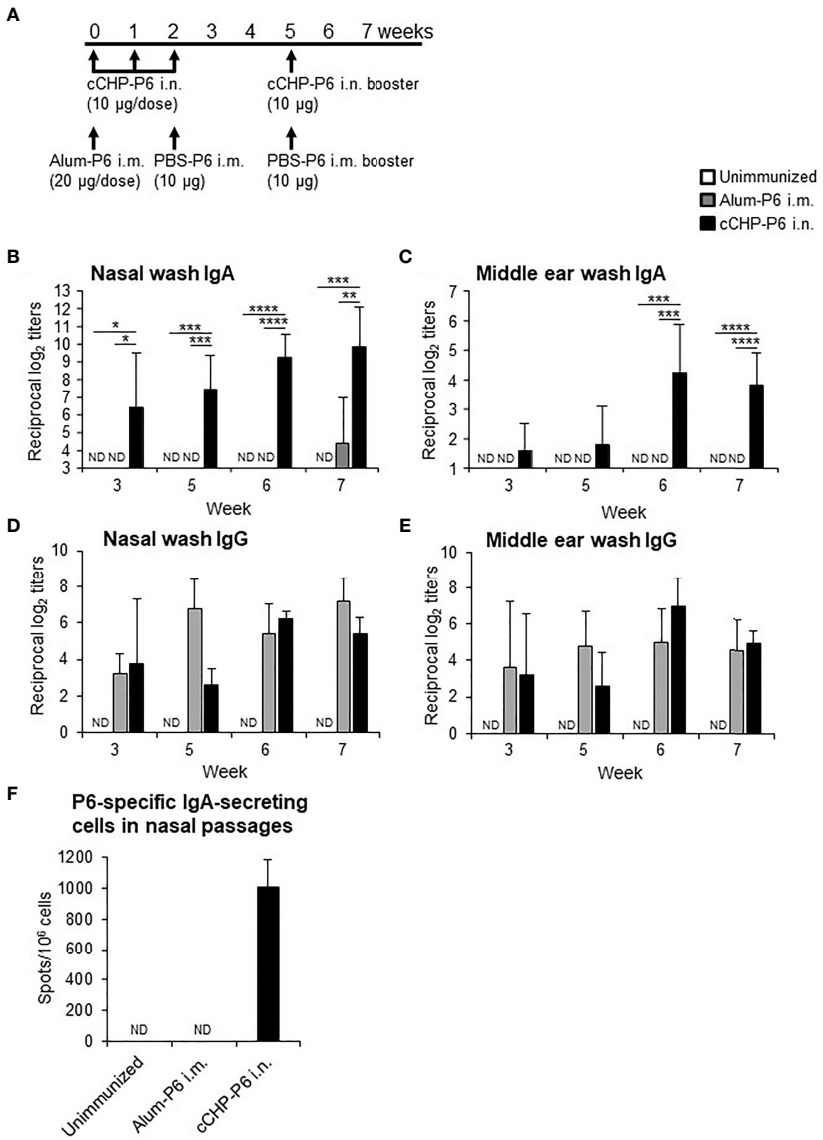

FIGURE 1 | Intranasal immunization with cCHP-P6 nanogel nasal vaccine induces P6-specific antibody responses. **(A)** Wild-type female BALB/c mice were immunized with four doses of cCHP-P6 nanogel vaccine intranasally (i.n.) or with a single dose of alum-precipitated P6 protein by intramuscular (i.m.) injection, followed by two intramuscular doses of PBS-diluted P6 protein. The control group (unimmunized) received the same volumes of PBS both intranasally and intramuscularly. **(B–E)** Levels of P6-specific IgA in nasal washes **(B)** or middle ear washes **(C)** and P6-specific IgG in nasal washes **(D)** or middle ear washes **(E)** for each immunized group (cCHP-P6, Alum-P6, or unimmunized control) were determined by ELISA. **(F)** Numbers of P6-specific IgA-secreting cells in nasal passages were analyzed by using ELISpot. Data are representative of three independent experiments, and each group consisted of seven mice. ND, not detected in undiluted samples; n.s., not significant; $^{*}P < 0.05$; $^{**}P < 0.01$; $^{***}P < 0.005$; $^{****}P < 0.001$, one-way ANOVA with *post-hoc* Tukey test. Values are means ± 1 SD.

intramuscular injection of P6 protein in PBS 2 weeks later. Mice in both groups received a booster immunization 3 weeks after the final immunization, and all animals received the same amount (40 μg) of the P6 protein. P6-specific IgA in nasal washes and middle ear washes (**Figures 1B, C**) was induced only in the mice nasally immunized with the cCHP-P6 nanogel vaccine, and the levels were strongly enhanced after booster immunization. In contrast, Alum-P6–immunized mice had undetectable levels of P6-specific IgA in both nasal and middle ear secretions (**Figures 1B, C**). However, during the primary response, higher levels of P6-specific IgG were induced in the sera of the Alum-P6 group than in the cCHP-P6 group, although comparable levels of P6-specific IgG were induced in both groups after the booster dose (**Supplementary Figure S3**). Although P6-specific IgG was detected in the nasal and middle ear washes from both cCHP-P6 nanogel-vaccine- and Alum-P6-immunized mice (**Figures 1D, E**), reflecting plasma leakage into the mucosal fluids, the titers were similar between the immunization groups, and the levels were lower

than those of the P6-specific IgA, especially in the nasal fluids. Moreover, P6-specific IgA–secreting cells were significantly more abundant in the nasal passages of the mice vaccinated with cCHP-P6 nasal vaccine but not in the nasal passages of the unimmunized controls or the mice intramuscularly immunized with Alum-P6 (**Figure 1F**).

cCHP-P6 Nanogel Nasal Vaccine Induces Antibodies That Directly Bind to NTHi

Next, we used FACS to assess whether the P6-specific antibodies induced by the cCHP-P6 nanogel vaccine directly bound to NTHi. To this end, we incubated NTHi strain 76 cells with nasal washes from mice nasally immunized with cCHP-P6 or systemically immunized with Alum-P6. The nasal washes from the cCHP-P6–immunized mice contained P6-specific IgA antibodies that bound to NTHi strain 76 (**Figure 2A**). However, the nasal washes from Alum-P6–immunized mice did not contain any IgA antibodies that bound to NTHi strain 76—similar to the fluids from the unimmunized mice (**Figure 2A**). In addition, the vaccine-induced IgA binding to NTHi cells was mediated by the P6 on the surfaces of the bacteria, because the binding was abolished when the nasal washes were preincubated with recombinant P6 protein (**Figure 2B**).

cCHP-P6 Nanogel Nasal Vaccine Suppresses NTHi Biofilm Formation

NTHi forms biofilms, which act as reservoirs of NTHi and cause infections in the upper and lower respiratory tracts (31, 32). NTHi biofilms increase resistance to antibiotics and trigger chronic and recurrent infections, including otitis media (31, 32). Because our results showed that P6-specific IgA bound effectively to the surfaces of NTHi cells (**Figure 2A**), we hypothesized that the antibody binding might physically inhibit NTHi biofilm formation. To analyze the effect of the P6-specific IgA on biofilm formation *in vitro*, NTHi strain 76 were grown in glass chamber slides for 40 h in the presence of nasal washes from mice nasally immunized with cCHP-P6. As controls, nasal washes from unimmunized or Alum-P6-immunized mice were tested also. Treatment of NTHi strain 76 cells with nasal washes from mice immunized with the cCHP-P6 nasal vaccine inhibited biofilm formation (**Figure 2C**), whereas nasal washes from Alum-P6 mice lacked inhibitory activity (**Figure 2C**). Incubation of NTHi strain 76 cells with nasal washes from the cCHP-P6 nasal vaccine group resulted in the generation of thin biofilms, and the biofilm biomass was significantly lower than that after incubation with nasal washes from Alum-P6–immunized or unimmunized control mice (**Figures 2D, E**). Because the nasal washes from the immunized group contained P6-specific IgG in addition to P6-specific IgA (**Figure 1D**), we also analyzed nasal washes from which total IgG was eliminated, to clarify the direct contribution of IgA to NTHi biofilm formation. Unlike the IgG-depleted nasal washes from Alum-P6-immunized mice, IgG-depleted nasal washes from the cCHP-P6 immunized mice decreased the biofilm biomass (**Figure 2F**). However, the inhibitory effect was slightly weaker with the IgG-depleted nasal washes from the cCHP-P6-immunized mice than with those containing IgG (**Figure 2E**), suggesting that the P6-specific IgG induced by the cCHP-P6 nasal vaccine may help to inhibit biofilm formation. Taken together, these results demonstrate that the P6-specific IgA induced by nasal immunization with cCHP-P6 reduced NTHi biofilm formation.

cCHP-P6 Nanogel Nasal Vaccine Induces NTHi Clearance and Prevents NTHi Colonization of the Nasal Cavity after Nasal Infection

To investigate the protective efficacy of the cCHP-P6 nanogel vaccine, we performed intranasal challenge experiments. Mice that had been immunized nasally with cCHP-P6 or systemically with Alum-P6, as well as unimmunized control mice, were intranasally infected with NTHi strain 76. Three days after infection, the numbers of bacteria in nasal wash fluids and nasal passages from the immunized and unimmunized control mice were determined by counting colonies on chocolate agar plates. Bacterial numbers in the nasal washes were significantly lower in the cCHP-P6–immunized mice than in the Alum-P6–immunized or unimmunized control mice (**Figure 3A**). In the nasal passages, bacterial numbers were significantly lower in the cCHP-P6-immunized mice than in the unimmunized control mice (**Figure 3B**), but the difference between cCHP-P6-immunized- and Alum-P6-immunized mice was not significant. In particular, cCHP-P6 vaccination resulted in the marked clearance of NTHi from the nasal cavity (**Figure 3A**).

Although we noted elevated levels of P6-specific IgG, including Th2-related IgG1 and IgG2b subclasses (**Supplementary Figure S3**), in the sera of Alum-P6 vaccinated mice and passive leakage of P6-specific IgG into their nasal washes (**Figures 1D, E**), the IgG was ineffective at preventing NTHi colonization of the nasal tissue and failed to clear bacteria from the nasal cavity (**Figures 3A, B**). Indeed, P6-specific IgA–secreting cells were increased in number only in the nasal passages of cCHP-P6-immunized mice at 3 days after infection (**Supplementary Figure S4**), indicating that the clearance of NTHi was mediated by the P6-specific IgA induced in the nasal mucosa. Furthermore, tissue sections taken from the nasal cavities of unimmunized mice 3 days after NTHi intranasal challenge revealed that many NTHi organisms had colonized the mucosal epithelium and subepithelial regions (**Supplementary Figure S5**). NTHi colonization was markedly lower in the mice nasally vaccinated with cCHP-P6 than in the systemically immunized and unimmunized groups. These results demonstrate that the P6-specific IgA induced in nasal wash fluids by the cCHP-P6 nanogel nasal vaccine prevents NTHi infection by reducing the number of NTHi cells in the nasal tissue.

cCHP-P6 Nanogel Nasal Vaccine–Induced IgA Binds to Different NTHi Clinical Isolates From Patients With Otitis Media

The universality of a vaccine is important for its clinical application. We incorporated the P6 protein as the vaccine antigen in our cationic nanogel (cCHP)–based nasal vaccine

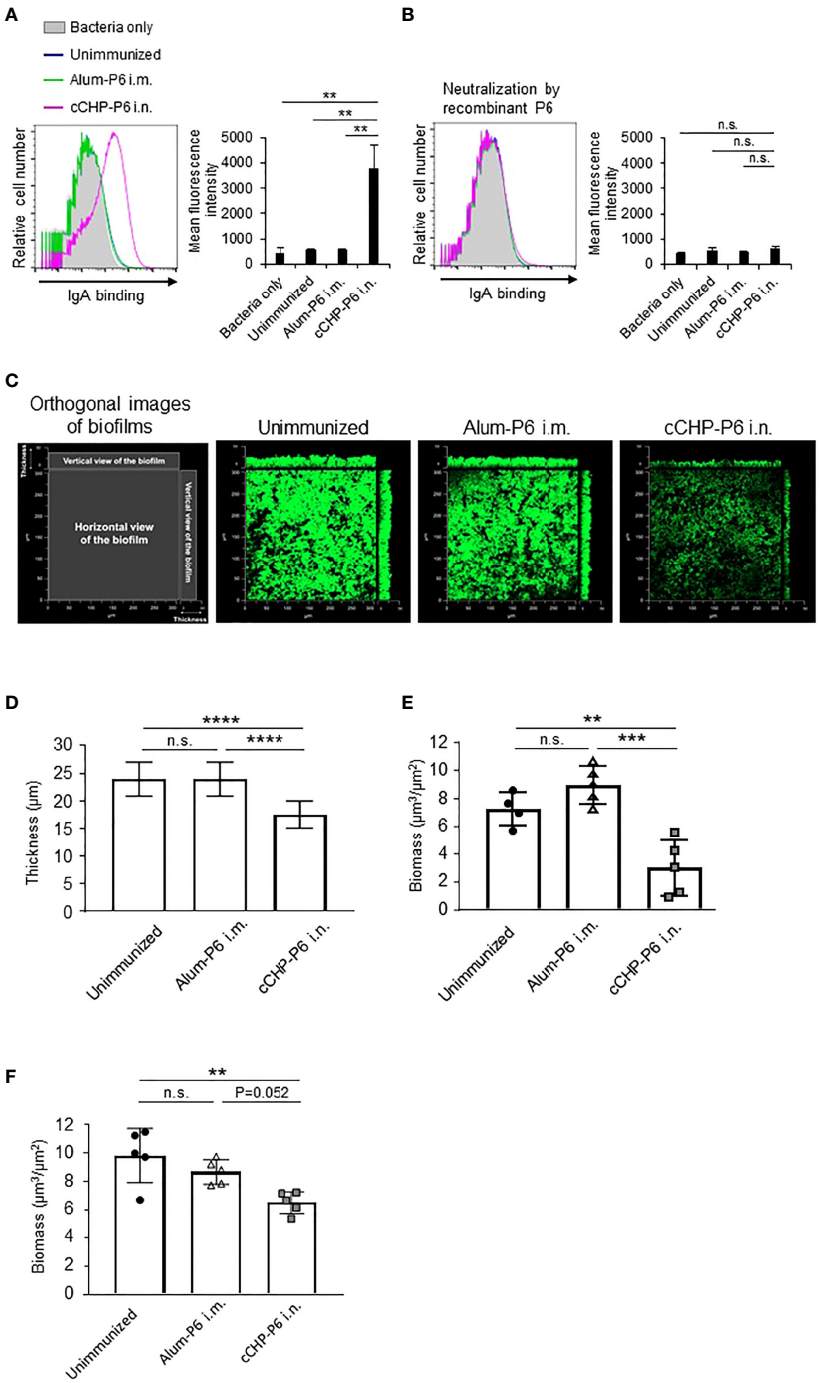

FIGURE 2 | P6-specific IgA directly binds to NTHi and inhibits biofilm formation. **(A, B)** The binding activity of P6-specific IgA in nasal washes on the surface of NTHi strain 76 **(A)** or its activity after P6 protein neutralization **(B)** was determined by FACS analysis. The mean fluorescence intensity indicates antibody binding. **(C)** NTHi biofilms grown at 37°C, 5% CO_2 for 40 h in a glass chamber slide with nasal washes of unimmunized or immunized mice. Biofilms were visualized with LIVE/DEAD BacLight viability stain and imaged with a confocal laser scanning microscope. **(D–F)** Biofilm thickness **(D)** and biomass values **(E)** treated with nasal washes or **(F)** biomass values treated with IgG-depleted nasal washes were quantified by using COMSTAT2 software. Data are representative of three independent experiments. $^{**}P < 0.01$; $^{***}P < 0.005$; $^{****}P < 0.001$; n.s., not significant; one-way ANOVA with *post-hoc* Tukey test. Values are means ± 1 SD.

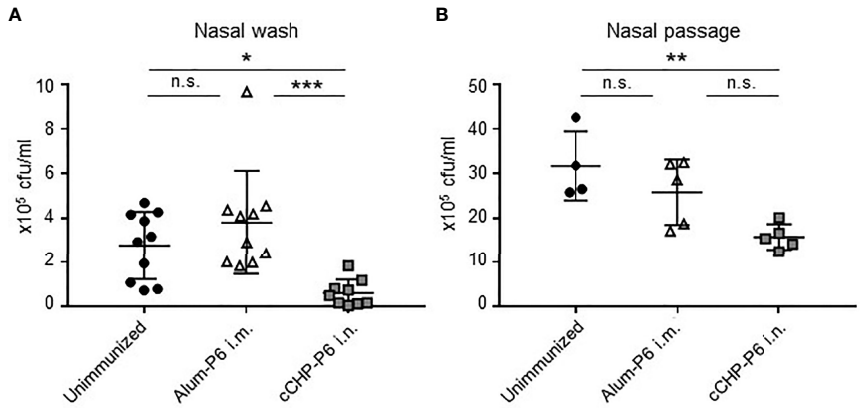

FIGURE 3 | cCHP-P6 nanogel nasal vaccine provides protective immunity against NTHi infection. **(A, B)** Bacterial clearance from the nasal cavity was determined by counting the numbers of live NTHi in nasal washes **(A)** or nasal passages **(B)**. The concentration of NTHi was expressed as colony-forming units (cfu) per milliliter of sample. Data are representative of three independent experiments, with n = 10 for Unimmunized or Alum-P6 and n = 9 for cCHP-P6 **(A)** and n = 4 for Unimmunized and n = 5 in Alum-P6 or cCHP-P6 **(B)**. *$P < 0.05$; **$P < 0.01$; ***$P < 0.005$; n.s., not significant.

for otitis media because of its high immunogenicity, high expression levels, and high conservation at the nucleotide and amino acid sequence levels among different clinical isolates of NTHi (23). To analyze the breadth of the binding activity of P6-specific IgA induced by the cCHP-P6 nanogel nasal vaccine, we used FACS to analyze NTHi clinical isolates from the nasal washes of patients with otitis media. To this end, we incubated 10 NTHi clinical isolates with nasal washes from mice nasally immunized with cCHP-P6. As observed for NTHi strain 76 (**Figure 2A**)—itself a clinical isolate from the nasopharynx of a patient with otitis media—cCHP-P6 vaccine–induced IgA clearly bound to the surfaces of all 10 NTHi clinical isolates (**Figure 4**). Therefore, the cCHP-P6 nanogel nasal vaccine induces P6-specific mucosal IgA that binds to a broad variety of NTHi isolates from patients with otitis media.

cCHP-P6 Nanogel Nasal Vaccine Inhibits NTHi Attachment to the Human Nasal Epithelial Surface

To invade the host, NTHi organisms first attach to nasal epithelial cells *via* several receptors, including platelet-activating factor receptor (8). Although the P6 protein itself does not mediate NTHi invasion, P6-specific IgA in the mucosal fluid directly binds to NTHi cells (**Figures 2A**, **4**), suggesting that the secretory antibodies enfold NTHi organisms and inhibit their attachment to mucosal epithelial cells. To test this notion and to determine whether this vaccine could be clinically useful, we investigated whether the cCHP-P6 nanogel nasal vaccine prevented NTHi attachment to human nasal epithelial cells. FITC-labeled NTHi strain 76 cells either left untreated or pretreated with nasal washes from immunized mice were co-

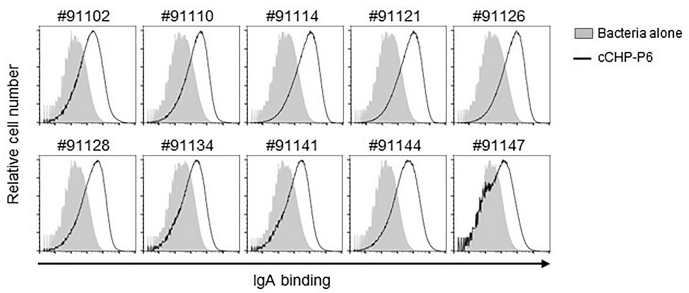

FIGURE 4 | P6-specific IgA binds to diverse NTHi clinical isolates from patients with otitis media. Nasal washes collected from mice 2 weeks after the booster immunization were incubated with 10 NTHi clinical isolates of different strains (indicated by the numbers above the graphs). Antibody binding was detected by flow cytometric analysis using a secondary antibody. Data are representative of three independent experiments.

cultured with 3D cultures of human airway epithelium, and the numbers of bacteria attached to the epithelial cells after 6 h of incubation were examined under a confocal microscope. Pretreatment with nasal washes from the cCHP-P6–nasally immunized mice significantly decreased the numbers of cells attached to epithelial cell surfaces, compared with pretreatment with nasal washes from unimmunized controls or mice intramuscularly immunized with Alum-P6 (**Figures 5A, B**). Likewise, IgG-depleted nasal washes from the cCHP-P6-immunized mice inhibited NTHi attachment to the human nasal epithelial cells (**Figures 5C, D**), indicating that P6-specific IgA, but not IgG, antibodies in nasal washes were responsible for this inhibition. These results suggest that the P6-specific IgA induced by nasal immunization with the cCHP-P6 nanogel vaccine prevents NTHi colonization of the mucosal surface by inhibiting NTHi attachment to human nasal epithelial cells.

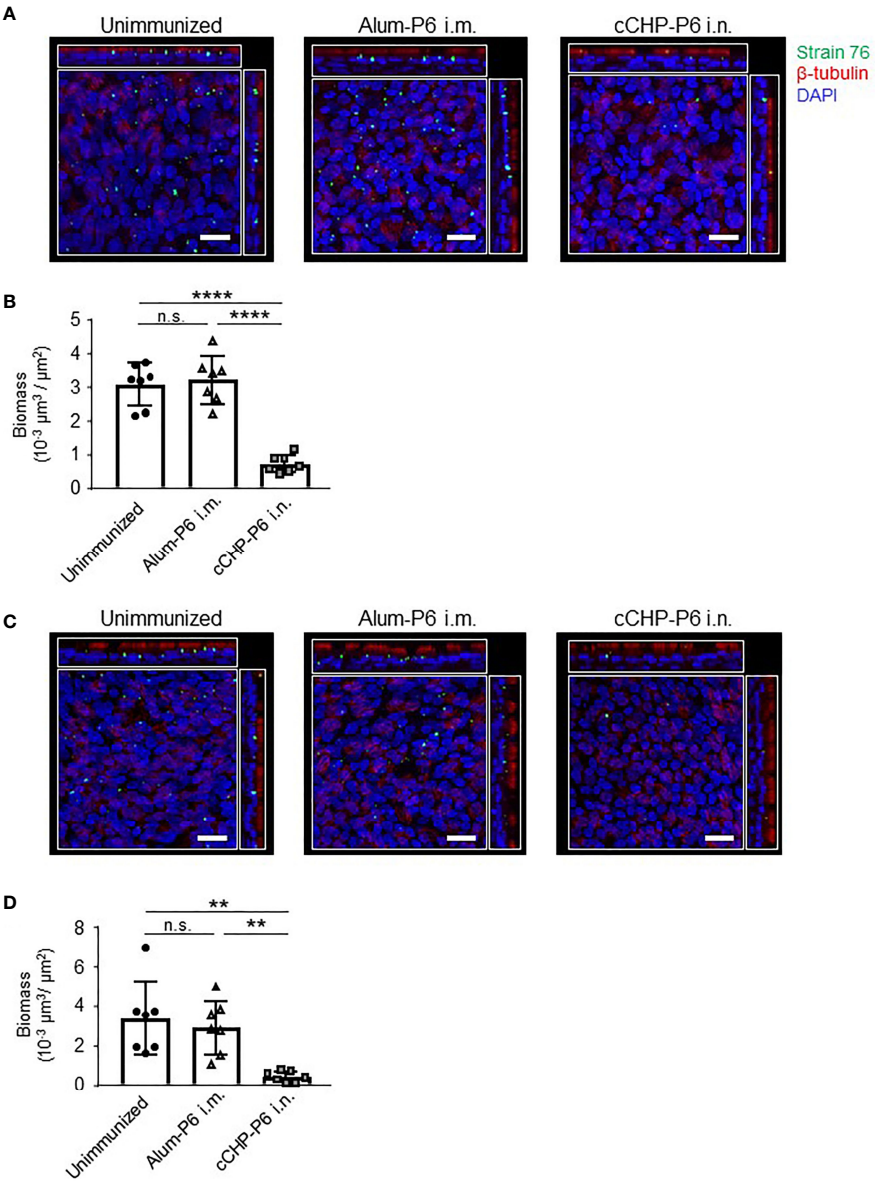

FIGURE 5 | P6-specific IgA prevents the attachment of NTHi to human nasal epithelial cells. **(A–D)** A bacterial adherence assay was performed by using FITC-labeled NTHi strain 76. NTHi were pretreated with nasal washes **(A)** or IgG-depleted nasal washes **(C)** from immunized mice and then incubated with 3D human airway epithelium cultures at 37°C, 5% CO_2 for 6 h. Epithelial cells were stained with β-tubulin (red) to visualize the cilia and with DAPI (4′,6-diamidino-2-phenylindole; blue) to visualize the nuclei. Images were obtained by confocal laser scanning microscopy. The number of NTHi organisms on the epithelial cells was determined according to the FITC signals in randomly selected fields of an image of the slide, and biomass values were quantified by using COMSTAT2 software **(B, D)**. Data are representative of three independent experiments. $^{**}P < 0.01$; $^{****}P < 0.001$; n.s., not significant. Values are means ± 1 SD.

DISCUSSION

For respiratory infections due to organisms such as NTHi, the nasal route is considered to be the most effective and logical vaccination strategy (10, 11). For example, nasal vaccination can induce both systemic and mucosal antigen-specific immune responses (12, 13). In contrast, injected vaccines effectively induce systemic antigen-specific immune responses but not mucosal immunity (33, 34). The antigen-specific SIgA produced at mucosal surfaces plays an important role in preventing invasion and colonization by pathogens at the site of infection (35). Because of these advantages of nasal vaccines, our groups have developed a cCHP-nanogel nasal vaccine delivery system and demonstrated the efficacy and safety of this system in both mice and non-human primates (16–18, 36, 37). In the present study, we developed a cCHP vehicle containing an NTHi nasal vaccine candidate antigen because a clinically desirable prophylactic vaccine for NTHi is currently unavailable. Recombinant P6 protein from NTHi is a particularly promising antigen candidate for an NTHi vaccine, because P6 has demonstrated high immunogenicity and is highly conserved among NTHi strains (23, 38, 39). We therefore incorporated P6 into cCHP and administered it intranasally to young adult mice. This resulted in the induction of high titers of P6-specific IgA and IgG in mucosal fluids and of IgG in serum (**Figures 1B–E** and **Supplementary Figure S3A**).

In our previous studies, we developed a cCHP-based pneumonia nasal vaccine, cCHP-PspA, which combined cCHP nanogel with a PspA recombinant protein that is a common surface antigen of *S. pneumoniae*. In mouse and non-human primate models, nasal immunization with cCHP-PspA effectively induced antigen-specific IgG in serum and SIgA in mucosal fluids (16–18). In addition, cCHP-PspA induced both Th2 and Th17 immune responses, which are associated with protective immunity (16–18). In our current study, cCHP nanogel combined with P6 protein similarly induced an effective Th2-type immune response supported by both IgG_1 and IgG_{2b} antigen-specific antibodies (**Supplementary Figure S3B**).

In previous studies, the induction of P6-specific IgA in mucosal secretions and serum P6-specific IgG and IgA through nasal immunization with P6 protein required co-administration of mucosal adjuvants, such as CpG oligodeoxynucleotide, alpha-GalCer, and adamantylamide dipeptide (12, 13, 40). In those studies, nasal immunization with P6 protein alone elicited minimal to no antigen-specific immune responses and thus no effective protection against NTHi (12, 13, 40). In contrast, our cCHP-P6 nanogel nasal vaccine induced P6-specific mucosal IgA and serum IgG responses in the absence of a biologically active adjuvant, and the resulting P6-specific IgG titers were comparable to those induced by the intramuscularly administered vaccine containing alum, which is an extremely potent Th2 adjuvant (**Supplementary Figure S3A**). Moreover, booster immunization further increased P6-specific mucosal IgA and serum IgG levels (**Figures 1D, E** and **Supplementary Figure S3A**).

Here, we examined the efficacy of the cCHP-P6 vaccine by challenging vaccinated mice with an intranasal sublethal dose of NTHi strain 76. More NTHi was eliminated from the nasal cavities of cCHP-P6–nasally immunized mice than of Alum-P6–intramuscularly immunized mice or unimmunized controls (**Figures 3A, B**, and **Supplementary Figure S5**). In previous investigations, the P6-specific IgG induced in mice or chinchillas that received P6 by systemic immunization or in naturally infected humans had strong bactericidal activity and contributed to host defense against NTHi infection (41–43). We demonstrated here that—in addition to this bactericidal activity of the P6-mediated immune response in the systemic compartment—the P6-specific mucosal IgA induced by our cCHP-P6 nanogel nasal vaccine helped to reduce biofilm formation (**Figures 2C–F**). In contrast, nasal washes from Alum-P6 vaccinated mice only weakly suppressed biofilm formation (**Figures 2C–F**), perhaps because of the very low levels of P6-specific IgA in their nasal fluids despite the presence of P6-specific IgG owing to plasma leakage (**Figures 1D, E**). Thus, when we examined the concentrations of P6-specific antibodies in nasal washes from intramuscularly immunized mice, the IgG levels ranged from 3 to 7 in log2-scale of reciprocal titers, whereas IgA isotype was undetectable (**Figures 1B, D**). In contrast, nasal washes from nasal cCHP-P6 immunized mice had concentrations of 3 to 9 and 3 to 6 in log2-scale reciprocal titers for P6-specific IgA and IgG isotypes, respectively (**Figures 1B, D**).

In addition to an interaction between phosphorylcholine and platelet-activating factor receptor, which is known to facilitate bacterial adhesion to the epithelium and host invasion, several adhesion factors, including Pili, HMW1/HMW2, Hap, and Hia, mediate the interaction of NTHi with host-cell extracellular matrix proteins such as laminin, fibronectin, and collagen IV to promote the aggregation of NTHi bacteria, their adherence to epithelial cells, and their entry into these cells (8). NTHi biofilms contribute to bacterial persistence and pathogenesis in the respiratory tract and pharynx, resulting in increased antibiotic resistance and chronic and recurrent otitis media (9, 44). Our current study provides evidence that P6-specific mucosal IgA reduces NTHi biofilm formation (**Figures 2C–F**).

Unlike adhesive factors such as Pili, the P6 protein is not directly involved in the adhesion of NTHi to the mucosal epithelium. Therefore, we speculate that the reduction of NTHi biofilm formation by P6-specific antibodies is due to steric hindrance caused by direct antibody binding to the surface of NTHi. Another component of the inhibition mechanism might be associated with the functional nature of P6. So far, the function of P6 protein in NTHi bacteria has not been clarified, but Pal protein—an *E. coli* homolog of P6—reportedly binds both peptidoglycan and extracellular membrane proteins and contributes to cell-wall stability (45–47). Indeed, a P6-deletion strain of NTHi proliferates more slowly than the wild-type strain, with morphological changes including increased cell size and decreased cell-wall integrity compared with those in wild-type organisms (48). Therefore, the inhibition of P6-mediated cell-wall integrity and cell growth by specific antibodies during NTHi cell division might be linked to the suppression of biofilm formation. The details of this mechanism need to be elucidated in future investigations.

Clinical reports have indicated an inverse correlation between P6-specific antibody levels and NTHi colonization of the nasopharynx or development of recurrent otitis media in children (38, 49); these findings indicate that P6 is a reasonable target for NTHi vaccination. In addition to having excellent immunogenicity, P6 is abundantly expressed in all NTHi strains, with extremely high (>90%) conservation at the nucleotide and amino acid sequence levels (23). In our hands, the 11 clinical isolates of NTHi, including strain 76, revealed high conservation, although single-amino-acid substitutions were present at three positions (**Supplementary Figure S6**). In addition, our present study showed that cCHP-P6–induced mucosal IgA directly bound to the surfaces of all 11 of the NTHi clinical isolates—each from a different patient with otitis media—without exception (**Figure 4**). In addition, through its binding activity, P6-specific mucosal IgA is supposed to capture NTHi bacteria and thus might influence the interaction between NTHi organisms and host-cell surfaces. Indeed, the P6-specific mucosal IgA induced by the cCHP-P6 nanogel nasal vaccine effectively inhibited the attachment of NTHi bacteria to primary human nasal epithelial cells in culture (**Figures 5A, B**). This inhibition is mediated by P6-specific mucosal IgA, and not by P6-specific IgG, because the inhibition was still observed when nasal washes depleted of IgG were used (**Figures 5C, D**). Moreover, nasal washes obtained after systemic (e.g., intramuscular) immunization did not prevent NTHi attachment (**Figures 5A–D**).

In conclusion, the current study demonstrated that a cCHP-nanogel nasal vaccine targeting P6 protein provides NTHi-specific protective immunity by preventing NTHi colonization of the surface of the nasal mucosa through a reduction in biofilm formation and epithelial-cell attachment of NTHi. Therefore, this cCHP-P6 nasal vaccine is a potential universal vaccine for NTHi infectious diseases, including otitis media in young children, and its ability to meet this unmet clinical need should be investigated further.

DATA AVAILABILITY STATEMENT

The original contributions presented in the study are included in the article/**Supplementary Material**. Further inquiries can be directed to the corresponding authors.

ETHICS STATEMENT

The animal study was reviewed and approved by Animal Committee of the Institute of Medical Science of the University of Tokyo.

AUTHOR CONTRIBUTIONS

RN-O, HM, and YY were responsible for study conceptualization. HM, SU, TH, YU, TM, TY, SS, KA, and YK were responsible for study methods and investigations. YU was responsible for statistical analysis. RN-O, YY, and HK were responsible for writing the manuscript. MS, KA, KF, and YK were responsible for reviewing and editing the manuscript. RN-O, YY, and HK were responsible for funding acquisition. All authors contributed to the article and approved the submitted version.

FUNDING

This research was supported by the Translational Research Program "Strategic Promotion for Practical Application of Innovative Medical Technology (TR-SPRINT)" from the Japan Agency for Medical Research and Development (AMED). The sponsor had no control over the interpretation, writing, or publication of this work.

ACKNOWLEDGMENTS

We thank Dr. Muneki Hotomi of Wakayama Medical University and Ms. Akiko Takumi, Dr. Ai Sasou, and the staff of our laboratory for their technical support and discussions.

SUPPLEMENTARY MATERIAL

The Supplementary Material for this article can be found online at: https://www.frontiersin.org/articles/10.3389/fimmu.2022.819859/full#supplementary-material

REFERENCES

1. Van Eldere J, Slack MPE, Ladhani S, Cripps AW. Non-Typeable Haemophilus Influenzae, an Under-Recognised Pathogen. *Lancet Infect Dis* (2014) 14:1281–92. doi: 10.1016/S1473-3099(14)70734-0
2. Sethi S, Murphy TF. Bacterial Infection in Chronic Obstructive Pulmonary Disease in 2000: A State-of-the-Art Review. *Clin Microbiol Rev* (2001) 14:336–63. doi: 10.1128/CMR.14.2.336-363.2001
3. Silfverdal SA, Skerlikova H, Zanova M, Papúchová D, Traskine M, Borys D, et al. Anamnestic Immune Response in 3-to 4-Year-Old Children Previously Immunized With 10-Valent Pneumococcal Nontypeable Haemophilus Influenzae Protein D Conjugate Vaccine as 2-Dose or 3-Dose Priming and a Booster Dose in the First Year of Life. *Pediatr Infect Dis J* (2011) 30:e155–63. doi: 10.1097/INF.0b013e31821feeb7
4. Van Den Bergh MR, Spijkerman J, Swinnen KM, François NA, Pascal TG, Borys D, et al. Effects of the 10-Valent Pneumococcal Nontypeable Haemophilus Influenzae Protein D-Conjugate Vaccine on Nasopharyngeal Bacterial Colonization in Young Children: A Randomized Controlled Trial. *Clin Infect Dis* (2013) 56:30–9. doi: 10.1093/cid/cis922
5. Tregnaghi MW, Sáez-Llorens X, López P, Abate H, Smith E, Pósleman A, et al. Efficacy of Pneumococcal Nontypable Haemophilus Influenzae Protein D Conjugate Vaccine (PHiD-CV) in Young Latin American Children: A Double-Blind Randomized Controlled Trial. *PLoS Med* (2014) 11:e1001657. doi: 10.1371/journal.pmed.1001657
6. Cleary D, Devine V, Morris D, Osman K, Gladstone R, Bentley S, et al. Pneumococcal Vaccine Impacts on the Population Genomics of non-Typeable Haemophilus Influenzae. *Microb Genomics* (2018) 4:e000209. doi: 10.1099/mgen.0.000209

7. Tristram S, Jacobs MR, Appelbaum PC. Antimicrobial Resistance in Haemophilus Influenzae. *Clin Microbiol Rev* (2007) 20:368–89. doi: 10.1128/CMR.00040-06
8. Duell BL, Su YC, Riesbeck K. Host–pathogen Interactions of Nontypeable Haemophilus Influenzae: From Commensal to Pathogen. *FEBS Lett* (2016) 590:3840–53. doi: 10.1002/1873-3468.12351
9. Thornton RB, Rigby PJ, Wiertsema SP, Filion P, Langlands J, Coates HL, et al. Multi-Species Bacterial Biofilm and Intracellular Infection in Otitis Media. *BMC Pediatr* (2011) 11:94. doi: 10.1186/1471-2431-11-94
10. Kiyono H, Fukuyama S. Nalt-Versus Peyer's-Patch-Mediated Mucosal Immunity. *Nat Rev Immunol* (2004) 4:699–710. doi: 10.1038/nri1439
11. Holmgren J, Czerkinsky C. Mucosal Immunity and Vaccines. *Nat Med* (2005) 11:S45. doi: 10.1038/nm1213
12. Abe N, Kodama S, Hirano T, Eto M, Suzuki M. Nasal Vaccination With CpG Oligodeoxynucleotide Induces Protective Immunity Against Nontypeable Haemophilus Influenzae in the Nasopharynx. *Laryngoscope* (2006) 116:407–12. doi: 10.1097/01.mlg.0000199740.04730.d4
13. Bertot GM, Becker PD, Guzmán CA, Grinstein S. Intranasal Vaccination With Recombinant P6 Protein and Adamantylamide Dipeptide as Mucosal Adjuvant Confers Efficient Protection Against Otitis Media and Lung Infection by Nontypeable Haemophilus Influenzae. *J Infect Dis* (2004) 189:1304–12. doi: 10.1086/382508
14. Hariri BM, Cohen NA. New Insights Into Upper Airway Innate Immunity. *Am J Rhinol Allergy* (2016) 30:319–23. doi: 10.2500/ajra.2016.30.4360
15. Nochi T, Yuki Y, Takahashi H, Sawada SI, Mejima M, Kohda T, et al. Nanogel Antigenic Protein-Delivery System for Adjuvant-Free Intranasal Vaccines. *Nat Mater* (2010) 9:572–8. doi: 10.1038/nmat2784
16. Fukuyama Y, Yuki Y, Katakai Y, Harada N, Takahashi H, Takeda S, et al. Nanogel-Based Pneumococcal Surface Protein A Nasal Vaccine Induces microRNA-Associated Th17 Cell Responses With Neutralizing Antibodies Against Streptococcus Pneumoniae in Macaques. *Mucosal Immunol* (2015) 8:1144–53. doi: 10.1038/mi.2015.5
17. Gyu Kong I, Sato A, Yuki Y, Nochi T, Takahashi H, Sawada S, et al. Nanogel-Based Pspa Intranasal Vaccine Prevents Invasive Disease and Nasal Colonization by Streptococcus Pneumoniae. *Infect Immun* (2013) 81:1625–34. doi: 10.1128/IAI.00240-13
18. Nakahashi-Ouchida R, Uchida Y, Yuki Y, Katakai Y, Yamanoue T, Ogawa H, et al. A Nanogel-Based Trivalent PspA Nasal Vaccine Protects Macaques From Intratracheal Challenge With Pneumococci. *Vaccine* (2021) 39:3353–64. doi: 10.1016/J.VACCINE.2021.04.069
19. Harabuchi Y, Faden H, Yamanaka N, Duffy L, Wolf J, Krystofik D. Human Milk Secretory IgA Antibody to Nontypeable Haemophilus Influenzae: Possible Protective Effects Against Nasopharyngeal Colonization. *J Pediatr* (1994) 124:193–8. doi: 10.1016/S0022-3476(94)70302-7
20. Nasopharyngeal Colonization With Nontypeable Haemophilus Influenzae And Recurrent Otitis Media (Accessed March 4, 2020).
21. Hotomi M, Saito T, Yamanaka N. Specific Mucosal Immunity and Enhanced Nasopharyngeal Clearance of Nontypeable Haemophilus Influenzae After Intranasal Immunization With Outer Membrane Protein P6 and Cholera Toxin. *Vaccine* (1998) 16:1950–6. doi: 10.1016/S0264-410X(98)00122-4
22. Sabirov A, Kodama S, Sabirova N, Mogi G, Suzuki M. Intranasal Immunization With Outer Membrane Protein P6 and Cholera Toxin Induces Specific Sinus Mucosal Immunity and Enhances Sinus Clearance of Nontypeable Haemophilus Influenzae. *Vaccine* (2004) 22:3112–21. doi: 10.1016/j.vaccine.2004.01.066
23. De Chiara M, Hood D, Muzzi A, Pickard DJ, Perkins T, Pizza M, et al. Genome Sequencing of Disease and Carriage Isolates of Nontypeable Haemophilus Influenzae Identifies Discrete Population Structure. *Proc Natl Acad Sci USA* (2014) 111:5439–44. doi: 10.1073/pnas.1403353111
24. Ayame H, Morimoto N, Akiyoshi K. Self-Assembled Cationic Nanogels for Intracellular Protein Delivery. *Bioconjug Chem* (2008) 19:882–90. doi: 10.1021/bc700422s
25. Hirano T, Kodama S, Kawano T, Suzuki M. Accumulation of Regulatory T Cells and Chronic Inflammation in the Middle Ear in a Mouse Model of Chronic Otitis Media With Effusion Induced by Combined Eustachian Tube Blockage and Nontypeable Haemophilus Influenzae Infection. *Infect Immun* (2015) 84:356–64. doi: 10.1128/IAI.01128-15
26. Kim D-Y, Sato A, Fukuyama S, Sagara H, Nagatake T, Kong IG, et al. The Airway Antigen Sampling System: Respiratory M Cells as an Alternative Gateway for Inhaled Antigens. *J Immunol* (2011) 186:4253–62. doi: 10.4049/jimmunol.0903794
27. Heydorn A, Nielsen AT, Hentzer M, Sternberg C, Givskov M, Ersboll BK, et al. Quantification of Biofilm Structures by the Novel Computer Program COMSTAT. *Microbiology* (2000) 146:2395–407. doi: 10.1099/00221287-146-10-2395
28. Vorregaard M. *Comstat2-A Modern 3D Image Analysis Environment for Biofilms*. Available at: www.imm.dtu.dk (Accessed July 14, 2020).
29. *Comstat 2*. Available at: http://www.comstat.dk/ (Accessed July 14, 2020).
30. Mokrzan EM, Ward MO, Bakaletz LO. Type IV Pilus Expression is Upregulated in Nontypeable Haemophilus Influenzae Biofilms Formed at the Temperature of the Human Nasopharynx. *J Bacteriol* (2016) 198:2619–30. doi: 10.1128/JB.01022-15
31. Novotny LA, Brockman KL, Mokrzan EM, Jurcisek JA, Bakaletz LO. Biofilm Biology and Vaccine Strategies for Otitis Media Due to Nontypeable Haemophilus Influenzae. *J Pediatr Infect Dis* (2019) 14:69. doi: 10.1055/S-0038-1660818
32. Weeks JR, Staples KJ, Spalluto CM, Watson A, Wilkinson TMA. The Role of Non-Typeable Haemophilus Influenzae Biofilms in Chronic Obstructive Pulmonary Disease. *Front Cell Infect Microbiol* (2021) 11. doi: 10.3389/FCIMB.2021.720742
33. Brandtzaeg P. Function of Mucosa-Associated Lymphoid Tissue in Antibody Formation. *Immunol Invest* (2010) 39:303–55. doi: 10.3109/08820131003680369
34. Suzuki H, Watari A, Hashimoto E, Yonemitsu M, Kiyono H, Yagi K, et al. C-Terminal Clostridium Perfringens Enterotoxin-Mediated Antigen Delivery for Nasal Pneumococcal Vaccine. *PLos One* (2015) 10:e0126352. doi: 10.1371/journal.pone.0126352
35. Kraehenbuhl JP, Neutra MR. Molecular and Cellular Basis of Immune Protection of Mucosal Surfaces. *Physiol Rev* (1992) 72:853–79. doi: 10.1152/physrev.1992.72.4.853
36. Yuki Y, Nochi T, Kong IG, Takahashi H, Sawada S, Akiyoshi K, et al. Nanogel-Based Antigen-Delivery System for Nasal Vaccines. *Biotechnol Genet Eng Rev* (2013) 29:61–72. doi: 10.1080/02648725.2013.801226
37. Nakahashi-Ouchida R, Yuki Y, Kiyono H. Development of a Nanogel-Based Nasal Vaccine as a Novel Antigen Delivery System. *Expert Rev Vaccines* (2017) 16:1231–40. doi: 10.1080/14760584.2017.1395702
38. Kaur R, Casey JR, Pichichero ME. Serum Antibody Response to Three non-Typeable Haemophilus Influenzae Outer Membrane Proteins During Acute Otitis Media and Nasopharyngeal Colonization in Otitis Prone and non-Otitis Prone Children. *Vaccine* (2011) 29:1023–8. doi: 10.1016/j.vaccine.2010.11.055
39. Khan MN, Kaur R, Pichichero ME. Bactericidal Antibody Response Against P6, Protein D, and OMP26 of Nontypeable Haemophilus Influenzae After Acute Otitis Media in Otitis-Prone Children. *FEMS Immunol Med Microbiol* (2012) 65:439–47. doi: 10.1111/j.1574-695X.2012.00967.x
40. Noda K, Kodama S, Umemoto S, Nomi N, Hirano T, Suzuki M. Th17 Cells Contribute to Nontypeable Haemophilus Influenzae-Specific Protective Immunity Induced by Nasal Vaccination With P6 Outer Membrane Protein and α-Galactosylceramide. *Microbiol Immunol* (2011) 55:574–81. doi: 10.1111/j.1348-0421.2011.00352.x
41. DeMaria TF, Murwin DM, Leake ER. Immunization With Outer Membrane Protein P6 From Nontypeable Haemophilus Influenzae Induces Bactericidal Antibody and Affords Protection in the Chinchilla Model of Otitis Media (1996) (Accessed March 5, 2020).
42. Murphy TF, Bartos LC, Rice PA, Nelson MB, Dudas KC, Apicella MA. Identification of a 16,600-Dalton Outer Membrane Protein on Nontypeable Haemophilus Influenzae as a Target for Human Serum Bactericidal Antibody. *J Clin Invest* (1986) 78:1020–7. doi: 10.1172/JCI112656
43. Pichichero ME, Kaur R, Casey JR, Sabirov A, Khan MN, Almudevar A. Antibody Response to Haemophilus Influenzae Outer Membrane Protein D, P6, and OMP26 After Nasopharyngeal Colonization and Acute Otitis Media in Children. *Vaccine* (2010) 28:7184–92. doi: 10.1016/j.vaccine.2010.08.063
44. Starner TD, Zhang N, Kim GH, Apicella MA, McCray PB. Haemophilus Influenzae Forms Biofilms on Airway Epithelia: Implications in Cystic

Fibrosis. *Am J Respir Crit Care Med* (2006) 174:213–20. doi: 10.1164/rccm.200509-1459OC
45. Nelson MB, Murphy TF, van Keulen H, Rekosh D, Apicella MA. Studies on P6, an Important Outer-Membrane Protein Antigen of Haemophilus Influenzae. *Rev Infect Dis* (1988) 10(Suppl 2):S331–6. doi: 10.1093/cid/10.Supplement_2.S331
46. Bogdan JA, Apicella MA. Mapping of a Surface-Exposed, Conformational Epitope of the P6 Protein of Haemophilus Influenzae. *Infect Immun* (1995) 63:4395. doi: 10.1128/iai.63.11.4395-4401.1995
47. Godlewska R, Wiśniewska K, Pietras Z, Jagusztyn-Krynicka EK. Peptidoglycan-Associated Lipoprotein (Pal) of Gram-Negative Bacteria: Function, Structure, Role in Pathogenesis and Potential Application in Immunoprophylaxis: Minireview. *FEMS Microbiol Lett* (2009) 298:1–11. doi: 10.1111/j.1574-6968.2009.01659.x
48. Murphy TF, Kirkham C, Lesse AJ. Construction of a Mutant and Characterization of the Role of the Vaccine Antigen P6 in Outer Membrane Integrity of Nontypeable Haemophilus Influenzae. *Infect Immun* (2006) 74:5169–76. doi: 10.1128/IAI.00692-06
49. Yamanaka N, Faden H. Antibody Response to Outer Membraneprotein of Nontypeable Haemophilus Influenzae in Otitis-Prone Children. *J Pediatr* (1993) 122:212–8. doi: 10.1016/S0022-3476(06)80115-0

Conflict of Interest: YY and HK are directors and founders of HanaVax Inc. RN-O, S-IS, KA, and YK are scientific advisors of HanaVax Inc.

The remaining authors declare that the research was conducted in the absence of any commercial or financial relationships that could be construed as a potential conflict of interest.

frontiers | Frontiers in Immunology

TYPE Original Research
PUBLISHED 28 July 2022
DOI 10.3389/fimmu.2022.894277

OPEN ACCESS

EDITED BY
Ali M. Harandi,
University of Gothenburg, Sweden

REVIEWED BY
Chris von Csefalvay,
Starschema Inc., United States
Nan Huo,
Mayo Clinic, United States

*CORRESPONDENCE
Maria Elena Romero-Ibarguengoitia
MROMEROI@novaservicios.com.mx
Maria Rescigno
maria.rescigno@hunimed.eu

SPECIALTY SECTION
This article was submitted to Vaccines and Molecular Therapeutics, a section of the journal Frontiers in Immunology

RECEIVED 11 March 2022
ACCEPTED 29 June 2022
PUBLISHED 28 July 2022

CITATION
Romero-Ibarguengoitia ME, González-Cantú Á, Pozzi C, Levi R, Mollura M, Sarti R, Sanz-Sánchez MÁ, Rivera-Salinas D, Hernández-Ruíz YG, Armendariz-Vázquez AG, Del Rio-Parra GF, Barco-Flores IA, González-Facio R, Azzolini E, Barbieri R, de Azevedo Dias AR, Henriques Guimarães Júnior M, Bastos-Borges A, Acciardi C, Paez-Bo G, Teixeira MM and Rescigno M (2022) Analysis of immunization time, amplitude, and adverse events of seven different vaccines against SARS-CoV-2 across four different countries.
Front. Immunol. 13:894277.
doi: 10.3389/fimmu.2022.894277

Analysis of immunization time, amplitude, and adverse events of seven different vaccines against SARS-CoV-2 across four different countries

Maria Elena Romero-Ibarguengoitia[1,2]*, Arnulfo González-Cantú[1,2], Chiara Pozzi[3], Riccardo Levi[3,4], Maximiliano Mollura[5], Riccardo Sarti[3,4], Miguel Ángel Sanz-Sánchez[1,2], Diego Rivera-Salinas[1,2], Yodira Guadalupe Hernández-Ruíz[1,2], Ana Gabriela Armendariz-Vázquez[1,2], Gerardo Francisco Del Rio-Parra[1,2], Irene Antonieta Barco-Flores[1], Rosalinda González-Facio[1], Elena Azzolini[3,4], Riccardo Barbieri[5], Alessandro Rodrigo de Azevedo Dias[6], Milton Henriques Guimarães Júnior[7], Alessandra Bastos-Borges[7], Cecilia Acciardi[8], Graciela Paez-Bo[9], Mauro Martins Teixeira[10] and Maria Rescigno[3,4]*

[1]Research Department, Hospital Clínica Nova de Monterrey, San Nicolás de los Garza, Nuevo Leon, Mexico, [2]Vicerrectoría de Ciencias de la Salud, Escuela de Medicina, Universidad de Monterrey, San Pedro Garza García, Mexico, [3]Instituti di Ricovero e Cura a Carattere Scientifico (IRCCS) Humanitas Research Hospital, Milan, Italy, [4]Department of Biomedical Sciences, Humanitas University, Milan, Italy, [5]Department of Electronic, Information and Bioengineering, Politecnico di Milano, Milan, Italy, [6]Health Department, Ternium Brazil, Rio de Janeiro, Brazil, [7]Research Department, Fundação São Francisco Xavier, Ipatinga, Brazil, [8]Health Secretary, Unidad Hospitalaria San José, Campana, Argentina, [9]Laboratory Department, Hospital Interzonal General de Agudos San Felipe, San Nicolás de los Arroyos, Argentina, [10]Biochemistry and Immunology Department, ICB, Universidade Federal de Minas Gerais, Belo Horizonte, Brazil

Background: Scarce information exists in relation to the comparison of seroconversion and adverse events following immunization (AEFI) with different SARS-CoV-2 vaccines. Our aim was to correlate the magnitude of the antibody response to vaccination with previous clinical conditions and AEFI.

Methods: A multicentric comparative study where SARS-CoV-2 spike 1-2 IgG antibodies IgG titers were measured at baseline, 21-28 days after the first and second dose (when applicable) of the following vaccines: BNT162b2 mRNA, mRNA-1273, Gam-COVID-Vac, Coronavac, ChAdOx1-S, Ad5-nCoV and Ad26.COV2. Mixed model and Poisson generalized linear models were performed.

Results: We recruited 1867 individuals [52 (SD 16.8) years old, 52% men]. All vaccines enhanced anti-S1 and anti-S2 IgG antibodies over time ($p<0.01$). The highest increase after the first and second dose was observed in mRNA-1273 ($p<0.001$). There was an effect of previous SARS-CoV-2 infection; and an interaction of age with previous SARS-CoV-2 infection, Gam-COVID-Vac and ChAdOx1-S ($p<0.01$). There was a negative correlation of Severe or Systemic AEFI (AEs) of naïve SARS-CoV-2 subjects with age and sex ($p<0.001$); a positive interaction between the delta of antibodies with Gam-COVID-Vac ($p=0.002$). Coronavac, Gam-COVID-Vac and ChAdOx1-S had less AEs compared to BNT162b ($p<0.01$). mRNA-1273 had the highest number of AEFIs. The delta of the antibodies showed an association with AEFIs in previously infected individuals ($p<0.001$).

Conclusions: The magnitude of seroconversion is predicted by age, vaccine type and SARS-CoV-2 exposure. AEs are correlated with age, sex, and vaccine type. The delta of the antibody response only correlates with AEs in patients previously exposed to SARS-CoV-2.

Registration number: ClinicalTrials.gov, identifier NCT05228912.

KEYWORDS

COVID-19, SARS-CoV-2, immunization, vaccines, seroconversion

Introduction

Covid-19 is a pneumonia-like disease caused by a coronavirus, named SARS-CoV-2. It is highly contagious, and the World Health Organization declared it in 2020 as a pandemic (1). SARS-CoV-2 caused COVID-19 that has a wide range of clinical presentations, from asymptomatic disease to severe acute respiratory distress syndrome and death (2). SARS-CoV-2 utilizes its surface spike glycoprotein to enter host cells. Each unit of the spike trimer contains an S1 and S2 subunit, with the N-terminal S1 subunit binding to the cellular angiotensin-converting enzyme 2 (ACE2) receptor through an internal receptor-binding domain (RBD) (3).

To prevent SARS-CoV-2 infection, 113 vaccines are being tested in human clinical trials, and 44 have reached the final step of testing (4). Based on the mechanism of action, vaccines can be clustered in four groups: 1) mRNA vaccines, for example, BNT162b2 mRNA and mRNA-1273. They use genetically engineered modified RNA to produce the spike protein that safely prompts an immune response safely. 2) Viral vector (adenovirus) vaccines, for example, ChAdOx1-S, Ad26.COV2, Ad5-nCoV, and Gam-COVID-Vac. They use a virus that has been genetically engineered so that it cannot cause disease but produces coronavirus proteins to safely generate an immune response. 3) Inactivated virus vaccines, for example, Coronavac, use a form of the virus that has been inactivated or weakened, so it does not cause disease but still generates an immune response. 4) Protein subunits vaccines, for example, NVX-CoV2373. It is a protein-based vaccine that uses harmless fragments of proteins or protein shells that mimic the SARS-CoV-2 to safely generate an immune response (5).

Currently BNT162b2 mRNA, mRNA-1273, ChAdOx1-S, Ad26.COV2, Ad5-nCoV, Gam-COVID-Vac, Coronavac, have been administered to people across 587 countries (4). However, no studies have compared using the same assay and time frame the effectiveness of seroconversion and incidence of adverse events in response to vaccines in different countries in the same study.

This study aimed to correlate the magnitude of the antibody response after the first and second dose (if applicable) between BNT162b2 mRNA, mRNA-1273, ChAdOx1-S, Ad26.COV2, Ad5-nCoV, Gam-COVID-Vac, and Coronavac by measuring SARS-CoV-2 spike 1-2 IgG antibodies, using the same standardized assay, with previous clinical conditions and assessing systemic and severe adverse events (AEs).

Abbreviations: (AEFI), Adverse events following immunization; (AEs), Severe adverse events.

Materials and methods

This was a multicentric observational study of volunteers who received an approved complete scheme of BNT162b2 mRNA, mRNA-1273, ChAdOx1-S, Ad26.COV2, Ad5-nCoV, Gam-COVID-Vac, or Coronavac COVID-19 vaccine during 2021 in five hospital centers (Hospital Clinica Nova, Humanitas Clinical and Research Center, Fundacion San Francisco Xavier, Ternium Health Center in Rio, Hospital Municipal San Jose, Hospital Interzonal de Agudos San Felipe) from four different countries: Mexico, Italy, Brazil and Argentina. This study followed STROBE guidelines (6). The study was approved by each local Institutional Review Board and conducted per the Code of Ethics of the World Medical Association (Declaration of Helsinki) for experiments that involve humans.

The inclusion criteria were volunteers of both genders, any age, who consented to participate, planned to conclude the immunization regimen of any vaccine, and agreed to be followed up for the duration of the study. The following vaccines were available: BNT162b2 mRNA, mRNA-1273, ChAdOx1-S, Ad26.COV2, Ad5-nCoV, Gam-COVID-Vac, or Coronavac. The exclusion criteria were to have received any SARS-CoV-2 vaccine prior to study entry.

Each country's Health System defined the available vaccines, the schedule, and dose assignation. On the vaccination day, the research team invited any subject who planned to receive any vaccine scheme, explained the project and asked to sign the informed consent. Inclusion-exclusion criteria were applied, and a plasma sample was collected. The baseline sample was taken before receiving the first dose of any SARS-CoV-2 vaccine (T0). The second (T1) and third samples (T2) were taken after 21 days (+/- 7 days) of the first and second dose, respectively.

At each visit, participants had to answer a questionnaire. The basal questionnaire aimed at obtaining patients' medical history and previous SARS-CoV-2 infections. The questionnaires applied after the first and second dose of vaccines aimed at recognizing adverse events following immunization (AEFI) (7) and identifying a potential SARS-CoV-2 infection after receiving any vaccine dose. SARS-CoV-2 infection was also monitored by the epidemiology team through PCR testing, which informed the research team of any new infection.

Primary outcome, IgG determination

Our primary outcome was to correlate the magnitude of the antibody response to vaccination with previous clinical conditions and AEs . To determine the amount of specific anti-S1 and anti-S2 IgG antibodies against SARS-CoV-2 in plasma samples, the laboratory personnel used a chemiluminescence immunoassay (CLIA) developed by DiaSorin, which had a sensitivity of 97.4% (95% CI, 86.8-99.5) and a specificity of 98.5% (95% CI, 97.5-99.2). The results were reported as follows: <12.0 AU/ml was considered negative, 12.0 to 15.0 AU/ml was indeterminate, and > 15 AU/ml was positive. This kit is comparable with other commercial kits and has been used elsewhere (8–11).

The variables we analyzed were age, sex, personal medical history (for example, the presence of type 2 diabetes, hypertension, obstructive pulmonary disease, any heart condition, obesity, cancer, liver steatosis, any autoimmune disease), and confirmed SARS-CoV-2 (through nasal swab or serologic tests such as IgG determination). The following AEs were considered of particular interest: fever (>37.5°C), adenopathy, diffuse rash, edema, facial paralysis, orthostatic hypotension, headache, arthralgia, myalgia, nausea, vomit, and diarrhea. Anti-S1 and anti-S2 IgG antibodies against SARS-CoV-2 were measured at baseline, 21-28 days post-first dose (S1), and 21-28 days post-second dose if applicable.

Statistical methods

The researchers reviewed the quality control and the anonymization of the database. Normality assumption was evaluated with the Shapiro-Wilk test or Kolmogorov. Descriptive statistics such as mean, standard deviation, median, interquartile range, frequencies, and percentages were computed. Kruskal-Wallis test with Dunn's multiple comparisons test was performed for IgG comparisons. We performed a mixed model where the dependent variable was the delta of the antibodies. The personal variability and time were constructed as a random effect, whereas each type of vaccine, age, history of SARS-CoV-2, and the interaction of each vaccine with age were fixed effects. BNT162b mRNA was the reference vaccine group. For the analysis of AEs, the study population was divided into two separate cohorts by stratifying according to the history of SARS-CoV-2 infection (1050 Naïve SARS-CoV-2 subjects and 471 SARS-CoV-2 history subjects). Poisson generalized linear models (PGLM) were performed on both cohorts with the counts of AEs events after the second dose as the outcome variables. Included regressors were age, sex, body mass index, 1,000 AU/mL variation of IgG levels after the second dose compared to the baseline IgG levels, type of vaccine and the interactions between vaccines and IgG level variation. BNT162b mRNA was the reference vaccine group Missing completely at random values were analyzed through complete case analysis since missing antibody levels were less than 5% and we considered it incorrect to impute any AEFI. A sample size of 1870 patients was calculated, according to the primary aim, by using a mixed model formula with an alpha of 0.05, power of 90%, the effect size of 0.15, and k=7. The statistical programs used were R v.4.0.3 and Python v. 3.8.3. The analyses were two-tailed. A p-value less than 0.05 was statistically significant.

10.3389/fimmu.2022.894277

Results

A total of 1867 patients were recruited from all countries: 1352 from Mexico, 42 from Italy, 260 from Brazil, and 213 from Argentina. The most frequent vaccine used was ChAdOx1-S in 666 subjects, Coronavac in 582, BNT162b2 mRNA in 289, Gam-COVID-Vac in 213, mRNA-1273 in 65, Ad26.COV2 in 31, and Ad5-nCoV in 19. The mean (SD) age was 52 (16.8) years, being statistically different across vaccine groups ($p<0.05$) as some vaccines were proposed to a particular age group. Fifty-two % of subjects were men, 559 (30%) had obesity, and 501 (26.8%) had hypertension. Table 1 shows the medical history of patients divided by vaccine type.

History of SARS-CoV-2

Positive history of SARS-CoV-2 infection was considered if the volunteer had a confirmatory swab or IgG positive serological test at baseline. Additionally, we considered a positive SARS-CoV-2 history if specific anti-S1 and anti-S2 IgG antibodies against SARS-CoV-2 in plasma samples were > 15 AU/ml at baseline. We had a total of 627 positive cases before vaccination, of which 165 (24.8%) received ChAdOx1-S, 246 (42.2%) Coronavac, 107 (37.1%) BNT162b2 mRNA, 55 (25.8%) Gam-COVID-Vac, 31 (47.6%) mRNA-1273, 18 (58%) Ad26.COV2, and 5 (26%) Ad5-nCoV.

Antibody titers

All vaccines showed significant anti-S1 and anti-S2 IgG antibody changes with significant differences across vaccines and depending on SARS-CoV-2 history. In naïve patients, the highest increase [Median (IQR) AU/ml] after the first dose was observed in mRNA-1273 [175.5 (76.7)], then BNT162b mRNA [78.1 (55)], and Ad5-nCoV [43.4(55.9)]. In subjects previously exposed to SARS-CoV-2, the highest increase after the first dose

TABLE 1 General characteristics and medical history.

	BNT162b2 mRNA (%)	mRNA-1273 (%)	Gam-COVID-Vac (%)	Coronavac (%)	ChAdOx1-S (%)	Ad5-nCoV (%)	Ad26.COV2 (%)	p-value
Total	289	65	200	582	666	19	31	
Obesity	54 (18.6)	11 (16.9)	44 (22)	188 (32.3)	248 (37.2)	8 (42.1)	6 (19.3)	<0.001
Smoker	37 (12.8)	10 (15.3)	27 (13.5)	60 (10.3)	38 (5.7)	2 (10.5)	2 (6.4)	0.001
Hypertension	36 (12.4)	2 (3)	77 (38.5)	116 (19.9)	265 (39.7)	3 (15.7)	2 (6.4)	<0.001
Dyslipidemia	27 (9.3)	3 (4.6)	55 (27.5)	76 (13.5)	150 (22.5)	1 (5.2)	1 (3.2)	<0.001
Type2 Diabetes	13 (4.4)	1 (1.5)	32 (16)	78 (13.4)	164 (24.6)	0	0	<0.001
Asthma	9 (3.1)	3 (4.6)	6 (3)	13 (2.3)	17 (2.5)	0	0	0.79
Other autoimmune disease such as thyroiditis or psoriasis	9 (3.1)	0	4 (2)	29 (4.9)	60 (9)	1 (5.2)	1 (3.2)	<0.001
Rheumatoid arthritis	7 (2.4)	1 (1.5)	16 (8)	11 (1.8)	56 (8.4)	0	1 (3.2)	<0.001
Surgery in the last year	6 (2)	0	6 (3)	26 (4.4)	45 (6.7)	3 (15)	1 (3.2)	0.002
Previous Cancer	5 (1.7)	1 (1.5)	1 (0.5)	5 (0.8)	29 (4.3)	0	0	0.001
NAFLD	4 (1.3)	0	7 (3.5)	27 (4.6)	21 (3.1)	2 (10.5)	0	0.042
Immunosuppressive treatment	4 (1.3)	0	3 (1.5)	6 (1)	11 (1.6)	0	0	0.86
Other liver disease	3 (1)	0	10 (5)	10 (1.7)	10 (1.5)	0	0	0.02
End stage renal disease	2 (0.7)	0	2 (1)	3 (0.5)	11 (1.6)	0	0	0.44
Pregnancy	2 (0.7)	1 (1.5)	0	3 (0.5)	0	1 (5.2)	0	0.005
Cirrhosis	2 (0.7)	0	0	2 (0.3)	4 (0.6)	0	0	0.88
Pulmonar Obstructive Chronic Disease	1 (0.3)	0	3 (1.5)	4 (0.6)	8 (1.2)	0	0	0.68
Coronary heart disease	1 (0.3)	0	15 (7.5)	3 (0.5)	23 (3.4)	0	0	<0.001
Gout	1 (0.3)	0	10 (5)	19 (3.2)	27 (4.05)	0	0	0.02
Active Cancer	0	0	1 (0.5)	1 (0.17)	10 (1.5)	0	0	0.054
Atrial Fibrilation	0	0	13 (6.5)	6 (1)	36 (5.4)	0	0	0.001
Congestive heart failure	0	0	18 (9)	1 (0.2)	12 (1.8)	0	0	0.001
Stroke	0	0	2 (1)	1 (0.2)	13 (1.9)	0	0	0.01
Trasplant	0	0	0	3 (0.5)	5 (0.7)	0	0	0.63
Pregnancy	2	1	0	3 (0.5)	0	1 (5.2)	0	0.05

Table 1 shows the medical history and comparison between vaccine groups, $p<0.05$ was considered statistically significant.

10.3389/fimmu.2022.894277

was observed in mRNA-1273 [5920(4705)], then BNT162b mRNA [2500(3080)], and ChAdOx1-S [1025(2489)].

In naïve patients, the highest increase [Median (IQR) AU/ml] after the second dose (T2) was observed in mRNA-1273 [1875 (1190)], then BNT162b mRNA [998 (1241)], and Gam-COVID-Vac [501 (55.9)], whereas in SARS-CoV-2 previously exposed subjects the highest increase after the second dose was observed in mRNA-1273 [4950 (3060)], then Gam-COVID-Vac [3620 (5356)], and BNT162b mRNA [2630 (2672.5)]. Figure 1, Supplementary Figure S1 show the change in antibody levels through time, classified by vaccine type. Table 2 shows the antibody levels classified by vaccine type.

The mixed model that showed a positive effect of SARS-CoV-2 previous infection (B=767.468, p<0.001), a positive interaction of age with previous SARS-CoV-2 infection (B=13.03, p=0.003), and an interaction of Gam-COVID-Vac and ChAdOx1-S with age (B=46.5, p<0.001; B=20.5; p=0.006). With respect to BNT162b mRNA, mRNA-1273 showed a higher change in antibody titers, while all the other vaccines had less change (p<0.01). We computed sex in the model, but there was no significant correlation, so we eliminated it from the final model. These results are shown in Table 3 and Figure 2.

Adverse events following immunization

At least one AEFI was observed after the first dose in 71% of respondents receiving BNT162b2 mRNA, in 93% with mRNA-1273, 38% with Gam-COVID-Vac, 42% with Coronavac, 51% with ChAdOx1-S, 74% with Ad5-nCoV, and 81% with Ad26.COV2. After the second dose, 65%, 88%, 23%, 33%, and 23% of the respondents experienced at least one AEFI after receiving BNT162b2 mRNA, mRNA-1273, Gam-COVID-Vac, Coronavac, and ChAdOx1-S, respectively. For each vaccine, the majority of the adverse events occurred during the first 24 hrs after injection, either after the first or the second dose. Patients receiving BNT162b2

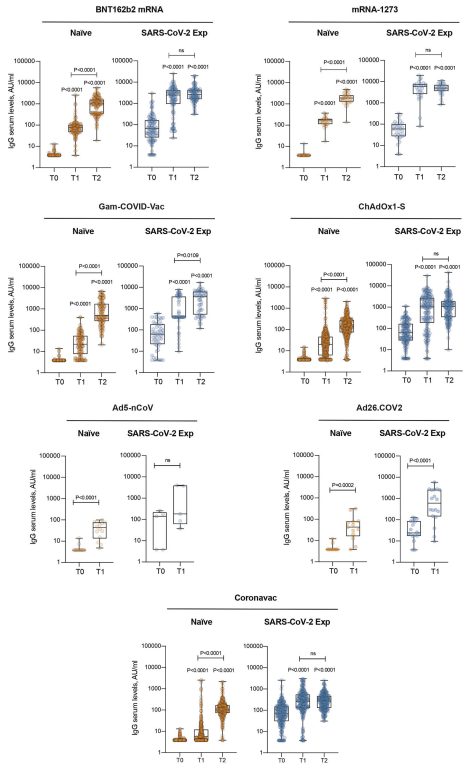

FIGURE 1
IgG antibody levels by vaccine. IgG antibody response was measured in serum of naïve and SARS-CoV-2 previously exposed (SARS-CoV-2 Exp) subjects at different time points (T0, T1 and T2) and vaccinated with different vaccine types. Samples ≥ 15 AU/mL were considered positive. Log scale on y axis. The box plots show the interquartile range, the horizontal lines show the median values, and the whiskers indicate the minimum-to-maximum range. Each dot corresponds to an individual subject. P-values were determined using 2-tailed Kruskal-Wallis test with Dunn's multiple comparisons test. P-values refer to baseline (T0) when there are no connecting lines. ns, not significant.

TABLE 2 Antibody differences between vaccine types.

	SARS CoV-2 Naïve							
Vaccine Median (IQR)	**BNT162b2 mRNA (n=289)**	**mRNA-1273 (n=65)**	**Gam-COVID-Vac (n=213)**	**Coronavac (n=582)**	**ChAdOx1-S (n=666)**	**Ad5-nCoV Cansino (n=19)**	**Ad26.COV2 (n=31)**	**p-value**
Basal	3.8 (0)	3.8 (26.6)	3.8 (0)	3.8(0.9)	3.8 (0)	3.8 (0)	3.8 (13.5)	p<0.005
After First Dose	78.1 (55.0)	175.5 (76.7)	22.1 (44.5)	5.59 (8.0)	19.9 (39.6)	43.45 (55.9)	42.6 (57.5)	p<0.001
After Second Dose	998 (1241.0)	1875 (1190.0)	501 (1453.7)	109 (97.6)	140.5 (199.5)	NA	NA	p<0.001
	SARS CoV-2 Positive							
Basal	66.9 (130.8)	59.3 (67.9)	59.8 (157.3)	72.4 (119.0)	61.9 (134.8)	141.0 (175.2)	24 (66.7)	p<0.001
After First dose	2500.0 (3080.0)	5920.0 (4705.0)	400.0 (3252.0)	264.5 (422.7)	1025.0 (2489.0)	182.0 (3734.6)	606.5 (23.69.0)	p<0.001
After Second Dose	2630.0 (2672.5)	4950.0 (3060)	3620 (5356)	279(337)	1020 (1538)	NA	NA	p<0.001

BNT162b2 mRNA, mRNA-1273 and Gam-COVID-Vac showed higher antibody levels after first and second dose.
*Kruskal-Wallis test was performed for comparison, p<0.05 was considered statistically significant. NA, does not apply.

TABLE 3 Mixed model of antibody changes.

	Estimate	Std. Error	95% CI	t value	p-value
(Intercept)	1909.02	345.73	1271.81 – 2546.23	5.52	<0.001
Age	-19.40	6.79	-32.6 7– -6.11	-2.855	0.004
SARS CoV2 previous infection	767.46	231.84	314.45 – 1220.31	3.31	0.001
mRNA-1273	1855.79	501.63	876.08 – 2836.04	3.69	<0.001
Gam-COVID-Vac	-2768.04	482.86	-3711.06 – -1824.4	-5.73	<0.001
Coronavac	-2184.03	430.93	-3025.82– -1342.09	-5.06	<0.001
ChAdOx1-S	-1808.26	361.77	-2514.69 – -1101.2	-4.99	<0.001
Ad5-nCoV	-2710.10	1542.89	-5727.76 – 304.30	-1.75	0.079
Ad26.COV2	-791.46	1291.27	-3317.21 – 1731.09	-0.613	0.54
Age*mRNA-1273	-20.82	15.95	-52 – 10.34	-1.3	0.192
Age*Gam-COVID-Vac	46.57	9.15	28.69 – 64.44	5.09	<0.001
Age*Coronavac	16.78	9.44	-1.67 – 35.22	1.77	0.076
Age*ChAdOx1-S	20.51	7.46	5.92 – 35.08	2.749	0.006
Age*Ad5-nCoV	44.44	35.86	-25.68 – 114.54	1.23	0.215
Age*Ad26.COV2	-4.24	32.52	-67.82 – 59.33	-0.13	0.896
Age*COVID-19 infection	13.03	4.44	4.35 – 21.71	2.93	0.003

Mixed model. The dependent variable is the delta of antibodies. Time and personal variability are random effects. Reference group BNT162b2 mRNA. Previous exposure to SARS-CoV-2 were related to a higher antibody change. Older subjects that received Gam-COVID-Vac or ChAdOx1-S had higher antibody change.
* means "interaction", i.e. the product of the variables.

mRNA, mRNA-1273, Gam-COVID-Vac, Coronavac, ChAdOx1-S, Ad5-nCoV, and Ad26.COV2 subjectively qualified the AEFI after the first dose as "very mild" or "mild" in 85%, 80%, 95%, 84%, 67%, 93%, and 57% of cases, respectively. The AEFI after the second dose were qualified as "very mild" or "mild" by 82%, 49%, 98%, 89%, and 76% of patients receiving BNT162b2 mRNA, mRNA-1273, Gam-COVID-Vac, Coronavac, and ChAdOx1-S respectively. Finally, 49% of patients receiving mRNA-1273 qualified for their adverse events after the second dose as "moderate". Figure 3 shows the percentages of AEs per vaccine.

AEs were evaluated by using PGLM. The model for naïve SARS-CoV-2 subjects showed a negative association of the count of adverse

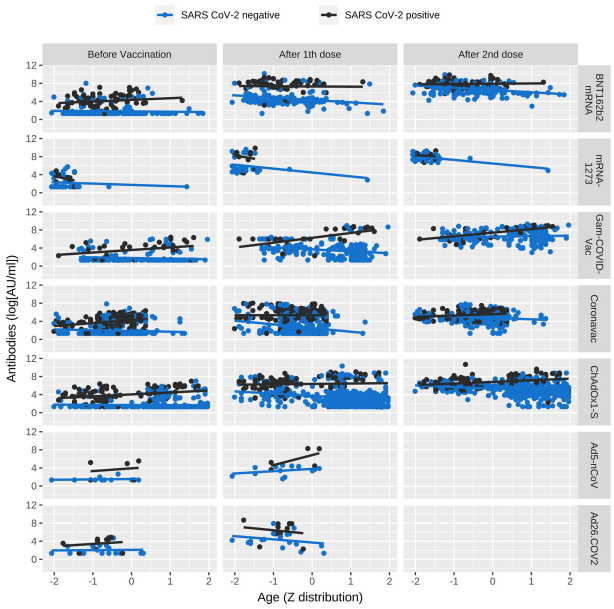

FIGURE 2
Antibody titers classified by age type of vaccine and Time. Figure shows change in antibody concentration through age, divided SARS-CoV-2 history, and vaccine type. Antibodies are expressed in logarithm and age has a Z distribution.

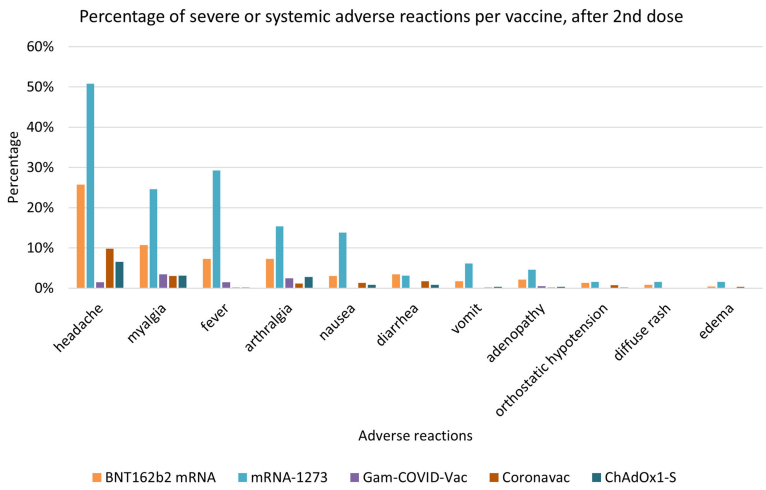

FIGURE 3
Percentage of systemic or severe adverse events after the second dose, stratified by vaccine. The graph shows the frequency of appearance of each systemic or severe adverse event across the considered vaccine groups.

events with age (B=-0.0327, p<0.001) and sex (B=-0.8145, p<0.001). A negative effect with respect to BNT162b mRNA was observed for Gam-COVID-Vac (B=-1.8582, p<0.001), Coronavac (B=-0.5736, p=0.047) and ChAdOx1-S (B=-0.7871, p=0.006). Finally, a positive interaction was found between the delta of antibodies due to vaccination and Gam-COVID-Vac (B=0.5604, p=0.002).

The model for subjects previously exposed to SARS-CoV-2 showed a negative association of the count of adverse events with age (B=-0.0190, p=0.013) and sex (B=-1.0042, p<0.001). The delta of the antibodies showed a positive association with the count of adverse events (B=0.1018, p<0.001). A positive effect with respect to BNT162b mRNA was observed for Gam-COVID-Vac (B=1.2737, p=0.038), whereas a negative effect was observed for Coronavac (B=-1.1304, p<0.001). Negative interactions were also found between the delta of antibodies due to vaccination and the vaccines Gam-COVID-Vac (B=-8.5758, p<0.001) and ChAdOx1-S (B=-1.2386, p=0.013). See Tables 4, 5 and Figure 4 for details.

SARS-CoV-2 infection

Subjects were followed up to 28 days after the second dose administration. Between the first and second dose, one (0.34%)

TABLE 4 Number of systemic or severe adverse events following vaccination in SARS-CoV-2 Naïve subjects.

	β	e^{β}	95% CI	p-value
Intercept	0.73	2.08	0.95-4.57	0.066
Age	-0.03	0.96	0.95-0.97	<0.001
Sex (M)	-0.81	0.44	0.33-0.58	<0.001
Body Mass Index	0.015	1.01	0.99-1.03	0.175
Delta IgG	-0.21	0.80	0.60-1.06	0.128
mRNA-1273	0.46	1.59	0.71-3.54	0.255
Gam-COVID-Vac	-1.85	0.15	0.06-0.35	<0.001
Coronavac	-0.57	0.56	0.31-0.99	0.047
ChAdOx1-S	-0.78	0.45	0.25-0.79	0.006
Delta IgG*mRNA-1273	0.13	1.14	0.78-1.68	0.479
Delta IgG*Gam-COVID-Vac	0.56	1.75	1.22-2.49	0.002
Delta IgG*Coronavac	-1.63	0.19	0.01-2.39	0.201
Delta IgG*ChAdOx1-S	0.97	2.64	0.93-7.44	0.066

Poisson Generalized Linear Model regression. The reference group is BNT162b2 mRNA. Women and young individuals developed more severe or systemic AEFI (AEs). There was no effect of Body Mass Index. In the naïve SARS-CoV-2 cohort, the vaccines Gam-COVID-Vac, Coronavac and ChAdOx1-S were related to fewer AEs after the second dose than BNT162b mRNA. However, for naïve SARS-CoV-2 patients who received Gam-COVID-Vac, higher antibody levels after the second dose were related to a greater number of AEs.
* means "interaction", i.e. the product of the variables.

TABLE 5 Number of systemic or severe adverse events following vaccination in SARS-CoV-2 previously exposed subjects. .

	β	e^{β}	95% CI	p-value
Intercept	0.45	1.57	0.66-3.71	0.297
Age	-0.01	0.98	0.96-0.99	0.013
Sex (M)	-1.00	0.36	0.25-0.51	<0.001
Body Mass Index	0.004	1.00	0.97-1.03	0.776
Delta IgG	0.10	1.10	1.05-1.16	<0.001
mRNA-1273	0.23	1.26	0.48-3.31	0.628
Gam-COVID-Vac	1.27	3.57	1.07-11.89	0.038
Coronavac	-1.13	0.32	0.18-0.57	<0.001
ChAdOx1-S	-0.18	0.82	0.40-1.67	0.597
Delta IgG*mRNA-1273	-0.001	0.99	0.86-1.15	0.982
Delta IgG*Gam-COVID-Vac	-8.57	0.0001	0.00016-0.00022	<0.001
Delta IgG*Coronavac	0.19	1.22	0.52-2.84	0.644
Delta IgG*ChAdOx1-S	-1.23	0.28	0.10-0.76	0.013

Poisson Generalized Linear Model regression. Reference group is BNT162b2 mRNA. Women and young individuals developed more severe or systemic AEFI (AEs). There was no effect of Body Mass Index. In subjects previously exposed to SARS-CoV-2, those receiving Gam-COVID-Vac showed a greater number of AEs compared to BNT162b mRNA, while subjects receiving Coronavac showed significantly fewer events when compared to BNT162b mRNA.
* means "interaction", i.e. the product of the variables.

patient with BNT162b2 mRNA, 0 with mRNA-1273, 1 (0.46%) with Gam-COVID-Vac, 3 (0.51%) with Coronavac, 4 (0.6%) with ChAdOx1-S, 2 (10%) with Ad5-nCoV and 1 (3%) with Ad26.COV2 got the SARS-CoV-2 infection. After the second dose, 4 (1.3%) with BNT162b2 mRNA, 1 (1.5%) with mRNA-1273, 0 with Gam-COVID-Vac, 18 (3%) with Coronavac, and 11 (1.6%) with ChAdOx1-S became infected with SARS-CoV-2 ($p<0.01$).

Discussion

This multicenter study compared the 21-28 day seroconversion, the AEFI after first and second doses, and the associated predictors of AEs of seven of the most common vaccines used worldwide: BNT162b2 mRNA, mRNA-1273, Gam-COVID-Vac, Coronavac, ChAdOx1-S, Ad5-nCoV, and Ad26.COV2 (4).

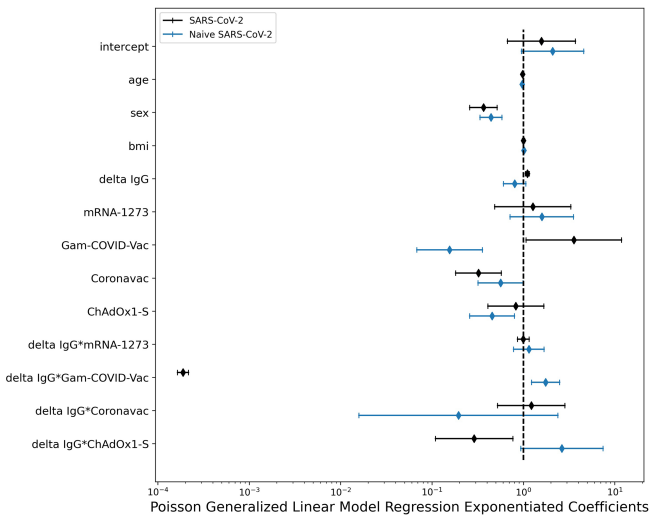

FIGURE 4
Forest plot for the GLM Poisson model coefficients stratified by SARS-CoV-2 history. Women and young individuals developed more severe or systemic AEFI (AEs). There was no effect of Body Mass Index. In the naïve SARS-CoV-2 cohort, the vaccines Gam-COVID-Vac, Coronavac and ChAdOx1-S were related to fewer AEs after the second dose than BNT162b mRNA. However, for naïve SARS-CoV-2 patients who received Gam-COVID-Vac, higher antibody levels after the second dose were related to a greater number of AEs. In people previously exposed to SARS-CoV-2, those receiving Gam-COVID-Vac showed a greater number of AEs compared to BNT162b mRNA, while subjects receiving Coronavac showed significantly fewer events when compared to BNT162b mRNA.

All vaccines showed immunogenicity and seroconversion after the complete vaccination scheme. The greatest change in antibody levels occurred with mRNA-1273, followed by BNT162b2 mRNA and Gam-COVID-Vac. Previous studies have shown a greater change in antibody titers for mRNA vector vaccines. This type of vaccines delivers the genetic information for the antigen, and vaccinated individuals synthesize antigens in the host cells (12–14).

Our study found that the previous history of SARS-CoV-2 was related to an increase in change in antibody levels as confirmed elsewhere (12). SARS-CoV-2 infection induces a robust humoral and cellular immune response. IgM, IgA, and IgG can be detected in the blood 5–15 days following symptom onset or a positive reverse transcriptase polymerase chain reaction (RT-PCR) test. Both binding and neutralizing antibody titers rise faster and reach a higher peak in patients with more severe COVID-19. SARS-CoV-2 vaccines result in early production of serum IgA, IgM, and IgG antibodies, and also induce long-lasting memory B- and T-cell responses (15). It seems that the presence of previous SARS-Cov-2 synergizes with all the vaccines tested in this study and offers a boost in antibody levels. This is a logical finding as the infection would be the first contact with the antigen and vaccination the second encounter with relevant antigens.

Previous studies found that persons aged 65-80 years and above have significantly lower peak of anti-S and neutralizing antibody titers following vaccination than those less than 65 years (16–18). We confirmed this result in our mixed model for most of the vaccines except for patients who had previous SARS-CoV-2 infection and received Gam-COVID or ChAdOx1-S, where we found higher antibody levels. There is limited literature to which to compare this finding; however, the study of Logunov et al. that tested the efficacy of Gam-COVID Vac reported a higher increase of anti-SARS-CoV-2 IgG levels in the group of 18-30 years and no particular change in other age groups (19); but they excluded patients with previous SARS-CoV-2 infection, so these results are not comparable. Whatever the explanation for this finding, it is interesting to note that older individual may benefit from vaccinating with adenoviral vector vaccines, such as Gam-COVID or ChAdOx1-S. However, in the study conducted by Ramasamy et al., similar antibody titers were seen 28 days after the boost vaccination of ChAdOx1 across all groups, regardless of age or vaccine dose (20). Therefore, it is difficult to take firm conclusions regarding the preferential use of this vaccine in older age groups.

Increasing age has been associated with decreased likelihood of seroconversion but higher peak antibody titers among those who do seroconvert after SARS-CoV-2 infection (21). Also, both binding and neutralizing antibody titers rise faster and reach a higher peak in patients with more severe COVID-19 (21–23). It is possible that older patients in our group of the study had a more severe disease during SARS-CoV-2 infection and that they developed higher antibody titers, as it has been reported that patients aged higher than 60 can develop this condition (11, 24). So higher antibodies in the elderly may simply reflect the likelihood of previous more severe SARS-CoV2 disease.

We also found that except for the Gam-COVID Vac, in the other vaccines requiring two doses, the first dose was sufficient to induce maximal antibody levels in subjects with a history of SARS-CoV-2, as previously shown for the BNT162b2 mRNA vaccine (9, 25–29)

For most patients, at least one AEFI occurred with all types of vaccines during the first 24 hrs. after injection, and most of them qualified the symptoms as “very mild” or “mild” both after the first and second dose, except for mRNA-1273 for which nearly half of the volunteers reported moderate symptoms after the second dose as reported previously (19, 20, 28, 30–34).

Our models showed a higher risk for women and young people to experience AEs. A real-world study that reported AEFI of patients receiving BNT162b2 mRNA, mRNA-1273, or Ad26COV2 in one or two doses (35), an independent studies conducted with Gam-COVID also confirmed this result (33, 36). The study of Ramasamy et al. on ChAdOx1 showed more adverse events in the group of 18-55 years old (20). The study conducted by Scott A et al. showed that severe adverse events (grade 5) were more frequent in women with Ad5-nCoV (32).

On one hand, for the Naïve SARS-CoV-2 cohort, the vaccines Gam-COVID-Vac, Coronavac, and ChAdOx1-S were related to fewer AEs after the second dose than BNT162b mRNA, and to the best of our knowledge, there are no studies that compare AEs across these types of vaccines. Also, the delta of antibodies was related to AEs after the second dose in Gam-COVID-Vac. As previously published, mRNA-1273 had higher AEFIs when compared to BNT162b2 mRN (37).

On the other hand, for subjects previously exposed to SARS-CoV-2, those receiving Gam-COVID-Vac showed a greater number of AEs than BNT162b mRNA, while subjects receiving Coronavac showed significantly fewer events when compared to BNT162b mRNA. In general, an increase in the antibody levels was related to an increase in the number of AEFIs, but for people receiving Gam-COVID-Vac or ChAdOx1-S, greater changes in antibody levels corresponded to fewer AEs. This last result should be taken with caution due to the limited number of patients falling in the category. To the best of our knowledge, this has not been previously shown. The study conducted by Sung Hee-Lim et al. that compared the antibody response with adverse events in patients vaccinated with BNT162b mRNA or ChAdOx1-S reported no association with antibody change and adverse events; however, patients previously infected with SARS-CoV-2 were excluded (38).

Interactions between age and vaccines were included for two main reasons: first, we decided to include in the model the

vaccination strategies performed by the different countries that administered different vaccines according to age to correct for this possible confounding effect.

Second, our results show that with respect to BNT162b2 mRNA vaccine (where age showed a negative correlation with AEs), any other vaccines with a significant coefficient > 19.403 (e.g. Gam-COVID-Vac, ChAdOx1-S) will be correlated with AEs but with a positive correlation instead of a negative one like for BNT162b2 mRNA. Therefore, in comparison with BNT162B2 a higher level of antibodies in those who receive Gam-COVID-Vac, ChAdOx1-S or Coronavac are related to less AEs.

This study shows a low rate of infection in all vaccine groups. However, the highest rate of SARS-CoV-2 infection in this follow-up period was for the one-dose vaccines Ad5-nCoV and Ad26.COV2. Also, Coronavac had a high rate of infection. It is important to consider that the patients were followed for a short period.

As a limitation of our study, we recognize that we had a small sample size in some vaccine groups such as Ad5-nCoV; however, to the best of our knowledge, there is no other study where this type of vaccine has been compared to other types of vaccines in a real-world setting. Even though there was a standardization between countries in relation to AEFI definition and the method for registration of these events, there can be cultural differences that can affect the likelihood of the degree of reporting and registration of an AEFI event. Also, the personal sense of seeking for help and vaccination differs among participants and across health systems. In the future it will be of interest to follow the IgG titers for a longer period and to evaluate the effect of heterologous combinations of these vaccines.

In conclusion, this comparative study of vaccine types shows positive immunogenicity and seroconversion of BNT162b2 mRNA, mRNA-1273, Gam-COVID-Vac, Coronavac, ChAdOx1-S, Ad5-nCoV, and Ad26.COV2. The highest IgG response was for the mRNA vector vaccines and the lower for the inactivated vaccine. Women and young individuals developed more AEs. In the naïve SARS-CoV-2 cohort, the vaccines Gam-COVID-Vac, Coronavac, and ChAdOx1-S were related to fewer AEs after the second dose of BNT162b mRNA. For patients who received Gam-COVID-Vac, higher antibody levels after the second dose were related to a greater number of AEs. In people previously exposed to SARS-CoV-2, those receiving Gam-COVID-Vac showed a greater number of AEs than BNT162b mRNA, while subjects receiving Coronavac showed significantly fewer events when compared to BNT162b mRNA. In general, an increase in antibody levels was related to AEs.

Data availability statement

The raw data supporting the conclusions of this article will be made available by the authors, upon reasonable request.

Ethics statement

This study was approved by the local Institutional Review Board of each institution (Universidad de Monterrey, Humanitas Clinical and Research Center, Fundação São Francisco Xavier, Ternium Health Center in Rio, Hospital Municipal San Jose, Hospital Interzonal de Agudos San Felipea) and conducted per the Code of Ethics of the World Medical Association (Declaration of Helsinki) for experiments that involve humans.The patients/participants provided their written informed consent to participate in this study.

Author contributions

Conceptualization: MR-I, MR, MT, MS-S, and EA. Formal analysis: MR-I, MR, MT, MS-S, AG-C, CP, RL, RS, MM, and RB. Investigation: MR-I, AG-C, MR, MT, MS-S, CP, RL, RS, RB, MM, DR-S, YH-R, AA-V, GD-P, IB-F, RG-F, EA, AA, MH-G, AB-B, CA, GP-B, MT, and MR. Resources: MR, MT, and MS-S. Writing – original draft: MR-I, AG-C, CP, MM, RS, RL, RB, MS-S, EA, DR-S, YH-R, AA-V, GD-P, IB-F, RG-F, EA, AA, MH-G, AB-B, CA, GP-B, MT, MR. Writing – review and editing: MR-I, AG-C, CP, MM, RS, RL, RB, MS-S, EA, DR-S, YH-R, AA-V, GD-P, IB-F, RG-F, EA, AA, MH-G, AB-B, CA, GP-B, MT, MR. Project administration: MR, MT, MS-S. Supervision: MR-I, MT, MR, and MS-S. Funding acquisition: MT, MR, and MS-S. All authors contributed to the article and approved the submitted version.

Funding

This research was conducted using private funding from Techint Group of Companies. The funders had no role in study design, data collection, analysis, and decision to publish.

Acknowledgments

We thank Erika Bienek (Techint Group Community Relations Director), Walter Bruno (Humanitas Communications Director), Cesar Bueno (Fundación São Francisco Xavier President), Mario Galli (Techint Group Communications Director), Pablo Sturiale (Apsot Director) for their support of the work and discussions.

Conflict of interest

The authors declare that the research was conducted in the absence of any commercial or financial relationships that could be construed as a potential conflict of interest.

Publisher's note

Supplementary material

The Supplementary Material for this article can be found online at: https://www.frontiersin.org/articles/10.3389/fimmu.2022.894277/full#supplementary-material.

References

1. WHO. *Director-general's opening remarks at the media briefing on COVID-19 - 11 March 2020*. Available at: https://www.who.int/dg/speeches/detail/who-director-general-s-opening-remarks-at-the-media-briefing-on-covid-19—11-march-2020 (Accessed April 19, 2020).

2. Kannan S, Shaik Syed Ali P, Sheeza A, Hemalatha K. COVID-19 (Novel coronavirus 2019) – Recent trends. *Eur Rev Med Pharmacol Sci* (2020) 24:2006–11. doi: 10.26355/eurrev_202002_20378

3. Kumar S, Nyodu R, Maurya VK, Saxena SK. "Morphology, genome organization, replication, and pathogenesis of severe acute respiratory syndrome coronavirus 2 (SARS-CoV-2).,". In: SK Saxena, editor. *Coronavirus disease 2019 (COVID-19). medical virology: From pathogenesis to disease control*. Singapore: Springer Singapore (2020). p. 23–31. doi: 10.1007/978-981-15-4814-7_3

4. *Covid-19 vaccine tracker: Latest updates - the New York times* . Available at: https://www.nytimes.com/interactive/2020/science/coronavirus-vaccine-tracker.html (Accessed January 11, 2022).

5. Mascellino MT, Di Timoteo F, De Angelis M, Oliva A. Overview of the main anti-SARS-CoV-2 vaccines: Mechanism of action, efficacy and safety. *IDR* (2021) 14:3459–76. doi: 10.2147/IDR.S315727

6. von Elm E, Altman DG, Egger M, Pocock SJ, Gøtzsche PC, Vandenbroucke JP. STROBE initiative. the strengthening the reporting of observational studies in epidemiology (STROBE) statement: Guidelines for reporting observational studies. *Ann Intern Med* (2007) 147:573–7. doi: 10.7326/0003-4819-147-8-200710160-00010

7. Chen M, Yuan Y, Zhou Y, Deng Z, Zhao J, Feng F, et al. Safety of SARS-CoV-2 vaccines: Aa systematic review and meta-analysis of randomized controlled trials. *Infect Dis Poverty* (2021) 10:94. doi: 10.1186/s40249-021-00878-5

8. Bonelli F, Sarasini A, Zierold C, Calleri M, Bonetti A, Vismara C, et al. Clinical and analytical performance of an automated serological test that identifies S1/S2-neutralizing IgG in COVID-19 patients semiquantitatively. *J Clin Microbiol* (2020) 58:1-10. doi: 10.1128/JCM.01224-20

9. Levi R, Azzolini E, Pozzi C, Ubaldi L, Lagioia M, Mantovani A, et al. One dose of SARS-CoV-2 vaccine exponentially increases antibodies in individuals who have recovered from symptomatic COVID-19. *J Clin Invest* (2021) 131:e149154. doi: 10.1172/JCI149154

10. Levi R, Ubaldi L, Pozzi C, Angelotti G, Sandri MT, Azzolini E, et al. The antibody response to SARS-CoV-2 infection persists over at least 8 months in symptomatic patients. *Commun Med* (2021) 1:32. doi: 10.1038/s43856-021-00032-0

11. Sandri MT, Azzolini E, Torri V, Carloni S, Pozzi C, Salvatici M, et al. SARS-CoV-2 serology in 4000 health care and administrative staff across seven sites in Lombardy, Italy. *Sci Rep* (2021) 11:12312. doi: 10.1038/s41598-021-91773-4

12. Szczepanek J, Skorupa M, Goroncy A, Jarkiewicz-Tretyn J, Wypych A, Sandomierz D, et al. Anti-SARS-CoV-2 IgG against the s protein: A comparison of BNT162b2, mRNA-1273, ChAdOx1 nCoV-2019 and Ad26.COV2.S vaccines. *Vaccines* (2022) 10:99. doi: 10.3390/vaccines10010099

13. Lau O, Vadlamudi NK. Immunogenicity and safety of the COVID-19 vaccines compared with control in healthy adults: A qualitative and systematic review. *Value Health* (2021) 25:S1098301521017344. doi: 10.1016/j.jval.2021.09.003

14. Rotshild V, Hirsh-Raccah B, Miskin I, Muszkat M, Matok I. Comparing the clinical efficacy of COVID-19 vaccines: A systematic review and network meta-analysis. *Sci Rep* (2021) 11:22777. doi: 10.1038/s41598-021-02321-z

15. Sokal A, Barba-Spaeth G, Fernández I, Broketa M, Azzaoui I, de la Selle A, et al. mRNA vaccination of naive and COVID-19-recovered individuals elicits potent memory b cells that recognize SARS-CoV-2 variants. *Immunity* (2021) 54:2893–2907.e5. doi: 10.1016/j.immuni.2021.09.011

16. Canaday DH, Carias L, Oyebanji OA, Keresztesy D, Wilk D, Payne M, et al. Reduced BNT162b2 messenger RNA vaccine response in severe acute respiratory syndrome coronavirus 2 (SARS-CoV-2)–naive nursing home residents. *Clin Infect Dis* (2021) 73:2112–5. doi: 10.1093/cid/ciab447

17. Weinberger B. Vaccines and vaccination against SARS-CoV-2: Considerations for the older population. *Vaccines* (2021) 9:1435. doi: 10.3390/vaccines9121435

18. Zhu F-C, Guan X-H, Li Y-H, Huang J-Y, Jiang T, Hou L-H, et al. Immunogenicity and safety of a recombinant adenovirus type-5-vectored COVID-19 vaccine in healthy adults aged 18 years or older: Aa randomised, double-blind, placebo-controlled, phase 2 trial. *Lancet* (2020) 396:479–88. doi: 10.1016/S0140-6736(20)31605-6

19. Logunov DY, Dolzhikova IV, Shcheblyakov DV, Tukhvatulin AI, Zubkova OV, Dzharullaeva AS, et al. Safety and efficacy of an rAd26 and rAd5 vector-based heterologous prime-boost COVID-19 vaccine: An interim analysis of a randomised controlled phase 3 trial in Russia. *Lancet* (2021) 397:671–81. doi: 10.1016/S0140-6736(21)00234-8

20. Ramasamy MN, Minassian AM, Ewer KJ, Flaxman AL, Folegatti PM, Owens DR, et al. Safety and immunogenicity of ChAdOx1 nCoV-19 vaccine administered in a prime-boost regimen in young and old adults (COV002): A single-blind, randomised, controlled, phase 2/3 trial. *Lancet* (2020) 396:1979–93. doi: 10.1016/S0140-6736(20)32466-1

21. Gudbjartsson DF, Norddahl GL, Melsted P, Gunnarsdottir K, Holm H, Eythorsson E, et al. Humoral immune response to SARS-CoV-2 in Iceland. *N Engl J Med* (2020) 383:1724–34. doi: 10.1056/NEJMoa2026116

22. Röltgen K, Powell AE, Wirz OF, Stevens BA, Hogan CA, Najeeb J, et al. Defining the features and duration of antibody responses to SARS-CoV-2 infection associated with disease severity and outcome. *Sci Immunol* (2020) 5:eabe0240. doi: 10.1126/sciimmunol.abe0240

23. Rose R, Neumann F, Grobe O, Lorentz T, Fickenscher H, Krumbholz A. Humoral immune response after different SARS-CoV-2 vaccination regimens. *BMC Med* (2022) 25(20):31. doi: 10.1186/s12916-021-02231-x

24. Cannistraci CV, Valsecchi MG, Capua I. Age-sex population adjusted analysis of disease severity in epidemics as a tool to devise public health policies for COVID-19. *Sci Rep* (2021) 11:11787. doi: 10.1038/s41598-021-89615-4

25. Krammer F, Srivastava Kthe PARIS team, , Simon V. Robust spike antibody responses and increased reactogenicity in seropositive individuals after a single dose of SARS-CoV-2 mRNA vaccine. *[preprint]. Allergy Immunol* (2021). doi: 10.1101/2021.01.29.21250653

26. Krammer F, Srivastava K, Alshammary H, Amoako AA, Awawda MH, Beach KF, et al. Antibody responses in seropositive persons after a single dose of SARS-CoV-2 mRNA vaccine. *N Engl J Med* (2021) 384:1372–4. doi: 10.1056/NEJMc2101667

27. Saadat S, Rikhtegaran Tehrani Z, Logue J, Newman M, Frieman MB, Harris AD, et al. Binding and neutralization antibody titers after a single vaccine dose in health care workers previously infected with SARS-CoV-2. *JAMA* (2021) 325:1467–9. doi: 10.1001/jama.2021.3341

28. Sadoff J, Gray G, Vandebosch A, Cárdenas V, Shukarev G, Grinsztejn B, et al. Safety and efficacy of single-dose Ad26.COV2.S vaccine against covid-19. *N Engl J Med* (2021) 384:2187–201. doi: 10.1056/NEJMoa2101544

29. Samanovic MI, Cornelius AR, Gray-Gaillard SL, Allen JR, Karmacharya T, Wilson JP, et al. Robust immune responses after one dose of BNT162b2 mRNA vaccine dose in SARS-CoV-2 experienced individuals. [preprint]. *Infect Dis (except HIV/AIDS)* (2021). doi: 10.1101/2021.02.07.21251311

30. Polack FP, Thomas SJ, Kitchin N, Absalon J, Gurtman A, Lockhart S, et al. Safety and efficacy of the BNT162b2 mRNA covid-19 vaccine. *N Engl J Med* (2020) 383:2603–15. doi: 10.1056/NEJMoa2034577

31. Baden LR, El Sahly HM, Essink B, Kotloff K, Frey S, Novak R, et al. Efficacy and safety of the mRNA-1273 SARS-CoV-2 vaccine. *N Engl J Med* (2021) 384:403–16. doi: 10.1056/NEJMoa2035389

32. Halperin SA, Ye L, MacKinnon-Cameron D, Smith B, Cahn PE, Ruiz-Palacios GM, et al. Final efficacy analysis, interim safety analysis, and immunogenicity of a single dose of recombinant novel coronavirus vaccine (adenovirus type 5 vector) in adults 18 years and older: an international, multicentre, randomised, double-blinded, placebo-controlled phase 3 trial. *Lancet* (2022) 399:237–48. doi: 10.1016/S0140-6736(21)02753-7

33. Jarynowski A, Semenov A, Kamiński M, Belik V. Mild adverse events of Sputnik V vaccine in Russia: Social media content analysis of telegram *via* deep learning. *J Med Internet Res* (2021) 23:e30529. doi: 10.2196/30529

34. Halder A, Imamura H, Condon S, Boroughs K, Nilsson SC, Anderson T, et al. Pfizer/BioNtech BNT162b2: adverse events and insights from an Australian mass vaccination clinic for COVID-19. *Intern Med J* (2022) 52:121–4. doi: 10.1111/imj.15623

35. Beatty AL, Peyser ND, Butcher XE, Cocohoba JM, Lin F, Olgin JE, et al. Analysis of COVID-19 vaccine type and adverse effects following vaccination. *JAMA Netw Open* (2021) 4:e2140364. doi: 10.1001/jamanetworkopen.2021.40364

36. Babamahmoodi F, Saeedi M, Alizadeh-Navaei R, Hedayatizadeh-Omran A, Mousavi SA, Ovaise G, et al. Side effects and immunogenicity following administration of the Sputnik V COVID-19 vaccine in health care workers in Iran. *Sci Rep* (2021) 11:21464. doi: 10.1038/s41598-021-00963-7

37. Meo SA, Bukhari IA, Akram J, Meo AS, Klonoff DC. COVID-19 vaccines: comparison of biological, pharmacological characteristics and adverse effects of Pfizer/BioNTech and moderna vaccines. *Eur Rev Med Pharmacol Sci* (2021) 25:1663–9. doi: 10.26355/eurrev_202102_24877

38. Lim S-H, Choi S-H, Kim B, Kim J-Y, Ji Y-S, Kim S-H, et al. Serum antibody response comparison and adverse reaction analysis in healthcare workers vaccinated with the BNT162b2 or ChAdOx1 COVID-19 vaccine. *Vaccines* (2021) 9:1379. doi: 10.3390/vaccines9121379

frontiers | Frontiers in Immunology

TYPE Original Research
PUBLISHED 03 August 2022
DOI 10.3389/fimmu.2022.904415

OPEN ACCESS

EDITED BY
Gabriel Pedersen,
Statens Serum Institut (SSI), Denmark

REVIEWED BY
Mustafa Akkoyunlu,
United States Food and Drug Administration, United States
JoséFrancisco Muñoz-Valle,
University of Guadalajara, Mexico

*CORRESPONDENCE
Stefania P. Bjarnarson
stefbja@landspitali.is

SPECIALTY SECTION
This article was submitted to Vaccines and Molecular Therapeutics, a section of the journal Frontiers in Immunology

RECEIVED 25 March 2022
ACCEPTED 07 July 2022
PUBLISHED 03 August 2022

CITATION
Aradottir Pind AA, Thorsdottir S, Magnusdottir GJ, Meinke A, Del Giudice G, Jonsdottir I and Bjarnarson SP (2022) A Comparative Study of Adjuvants Effects on Neonatal Plasma cell survival niche in bone marrow and persistence of humoral immune responses.
Front. Immunol. 13:904415.
doi: 10.3389/fimmu.2022.904415

A comparative study of adjuvants effects on neonatal plasma cell survival niche in bone marrow and persistence of humoral immune responses

Audur Anna Aradottir Pind[1,2], Sigrun Thorsdottir[1], Gudbjorg Julia Magnusdottir[1,2], Andreas Meinke[3], Giuseppe Del Giudice[4], Ingileif Jonsdottir[1,2] and Stefania P. Bjarnarson[1,2]*

[1]Department of Immunology, Landspitali, The National University Hospital of Iceland, Reykjavik, Iceland, [2]Faculty of Medicine, School of Health Sciences, University of Iceland, Reykjavik, Iceland, [3]Valneva Austria GmbH, Vienna, Austria, [4]GSK Vaccines, Siena, Italy

The neonatal immune system is distinct from the immune system of older individuals rendering neonates vulnerable to infections and poor responders to vaccination. Adjuvants can be used as tools to enhance immune responses to co-administered antigens. Antibody (Ab) persistence is mediated by long-lived plasma cells that reside in specialized survival niches in the bone marrow, and transient Ab responses in early life have been associated with decreased survival of plasma cells, possibly due to lack of survival factors. Various cells can secrete these factors and which cells are the main producers is still up for debate, especially in early life where this has not been fully addressed. The receptor BCMA and its ligand APRIL have been shown to be important in the maintenance of plasma cells and Abs. Herein, we assessed age-dependent maturation of a broad range of bone marrow accessory cells and their expression of the survival factors APRIL and IL-6. Furthermore, we performed a comparative analysis of the potential of 5 different adjuvants; LT-K63, mmCT, MF59, IC31 and alum, to enhance expression of survival factors and BCMA following immunization of neonatal mice with tetanus toxoid (TT) vaccine. We found that APRIL expression was reduced in the bone marrow of young mice whereas IL-6 expression was higher. Eosinophils, macrophages, megakaryocytes, monocytes and lymphocytes were important secretors of survival factors in early life but undefined cells also constituted a large fraction of secretors. Immunization and adjuvants enhanced APRIL expression but decreased IL-6 expression in bone marrow cells early after immunization. Furthermore, neonatal immunization with adjuvants enhanced the proportion of plasmablasts and plasma cells that expressed BCMA both in spleen and bone marrow. Enhanced BCMA expression correlated with enhanced vaccine-specific humoral responses, even though the effect of alum on BCMA was less pronounced than those of the other adjuvants at later time points. We propose that low APRIL expression in bone marrow as well as low BCMA

expression of plasmablasts/plasma cells in early life together cause transient Ab responses and could represent targets to be triggered by vaccine adjuvants to induce persistent humoral immune responses in this age group.

KEYWORDS

neonatal vaccination, adjuvant, comparative study, a proliferation inducing ligand (APRIL, TNFSF13), IL-6, B cell maturation antigen (BCMA, TNFRSF17), plasma cell survival niche

Introduction

The neonatal immune system is immature leaving neonates particularly vulnerable to infection and poor responders to vaccination. Low and transient antibody (Ab) responses following infection or vaccination in this age group have been associated with limited germinal center activation and decreased survival of plasma cells (1). In germinal centers, activated B cells undergo clonal expansion, affinity maturation, class switch recombination and can differentiate into memory B cells or plasmablasts that secrete Abs (2). Subsequently, plasmablasts can migrate to the bone marrow where they differentiate to long-lived plasma cells and persist (3). It has been reported that in neonatal mice that of the few plasmablasts formed in germinal centers, most of them home efficiently to the bone marrow but cannot persist due to lack of a proliferation inducing ligand (APRIL) (4), a critical survival factor for plasma cells. B cell maturation antigen (BCMA) is a high affinity receptor for APRIL whereas transmembrane activator calcium modulator and cyclophilin ligand interactor (TACI) binds APRIL with lower affinity (reviewed in (5)). TACI-deficient mice have diminished numbers of plasma cells, both in spleen and bone marrow (6) whereas BCMA-deficient mice display a drastic reduction in numbers of bone marrow plasma cells (7–9), leaving plasma cells in secondary lymphoid organs unaffected (8, 10) suggesting that BCMA is essential for survival of long-lived plasma cells in the bone marrow whereas TACI may be more important for the induction and survival of plasma cells in secondary lymphoid organs (reviewed in (11)).

A large fraction of vaccine candidates undergoing clinical development are made of highly purified recombinant protein or peptide antigens. This has driven the need for adjuvants as key components in modern vaccines since purified protein vaccines are rarely immunogenic (12). Adjuvants are immune-stimulating agents that can enhance and modulate responses to antigens and can be used as tools to enhance responsiveness to vaccines in vulnerable populations such as young infants (13). However, alum is the only adjuvant licensed for use in the pediatric population with the exception of MF59 and AS03 that have been licensed for use in seasonal and pandemic influenza vaccines (14). Thus, there is an unmet need for novel adjuvants and elucidation of their and other established adjuvants' mechanisms of action in order to identify adjuvants active in early life and optimize vaccination responses in the pediatric population.

We evaluated effects of four adjuvants to overcome limitations of neonatal immunity and induce potent and persistent immune responses following neonatal immunization with the protein vaccine tetanus toxoid (TT) and compared with the previously established effect of LT-K63 (15). The adjuvants assessed are of various categories and have been reported to employ different mechanisms of action. We assessed effects of two toxin-based adjuvants, LT-K63, a mutant of *E.coli* heat labile enterotoxin and mmCT, a multiple mutant of cholera toxin (CT) derived from *V.cholarae*. MF59 is a squalene-based oil-in-water emulsion and has been licensed for use in children from 6 months of age (14). IC31 is a TLR9 agonist combined with an antimicrobial peptide (16) and lastly alum, the most widely used adjuvant that has been licensed in several paediatric vaccines. Table 1 lists the adjuvants assessed herein and their main properties on adult and neonatal immune responses. We have previously compared the effects of the selected adjuvants with another vaccine, a pneumococcal conjugate Pnc1-TT, where we found that LT-K63, mmCT, MF59, and IC31, but not alum, enhanced germinal center formation and follicular dendritic cell maturation in neonatal mice which was associated with enhanced and prolonged persistence of vaccine-specific antibody-secreting cells (ASCs) and Abs up to 9 weeks after immunization (19, 20). However, alum only transiently enhanced vaccine-specific ASCs in bone marrow and serum Abs up to week 6 (20). Ab persistence is mediated by long-lived plasma cells that reside in specialized survival niches in the bone marrow (34) and their survival was recently shown to be dependent on direct contacts with stromal cells as well as APRIL : BCMA binding (35). In line with that, we demonstrated that LT-K63 enhanced early APRIL expression by bone marrow accessory cells, particularly by eosinophils, macrophages and megakaryocytes after immunization of neonatal mice with Pnc1-TT (15). Additionally, a higher

TABLE 1 Adjuvants assessed and their reported immune profiles.

Adjuvant	Composition	Immune profile	Early life immune profile
LT-K63	Toxin-based - mutant of LT	Th1 (17)	Th1/Th2 (18), Abs, FDCs, GCs (19), TNF-R and ligands (15), persistent ASC and Abs (19, 20)
mmCT	Toxin-based – mutant of CT	Th17 (21), IgA and IgG Abs (22, 23)	FDCs, GCs, persistent ASC and Abs (20)
MF59®	Squalene-based oil-in-water emulsion	Mixed Th1/Th2 (24) or Th2 and Abs (25)	Tfh (26), FDCs, GCs, persistent ASC and Abs (20)
IC31®	$KLKL_5KLK$ antimicrobial peptide with a synthetic TLR-9 agonist ODN1a	Mixed Th1/Th2 (16) or Th1 and Abs (27)	Mixed Th1/Th2 (28) or Th1 (29), Tfh cell (30), FDC, GC, persistent ASC and Abs (20)
Alum	Inorganic insoluble aluminum salts (aluminum hydroxide)	Th2 and Abs (31, 32)	Th2 and Abs (33)

LT, E.coli heat-labile enterotoxin; CT, Cholera toxin; FDC, follicular dendritic cell; GC, germinal center; TNF-R, tumor necrosis factor receptor; ASC, antibody-secreting cell; Abs, antibodies; Tfh, T follicular helper cell; TLR, Toll-like receptor.

proportion of plasmablasts and plasma cells of neonatal mice immunized with Pnc1-TT with LT-K63 expressed BCMA (15). Therefore, we wanted to explore whether the difference we previously observed (20) in the persistence of humoral immune responses induced by the selected adjuvants could be explained by their different effects on expression of plasma cell survival factors by bone marrow accessory cells and BCMA expression of plasmablasts/plasma cells up to this 6 week time point, where LT-K63 is used as a positive control. Furthermore, we assessed how the observed effects related to germinal center activation and induction of humoral immune responses. Prior to assessing the effects of neonatal immunization and adjuvants, we investigated age-dependent maturation of accessory cells of the plasma cell survival niche and their expression of survival factors APRIL and IL-6, for the first time to our best knowledge.

Materials and methods

Mice

Adult NMRI mice were purchased from Taconic (Skansved, Denmark) and adapted for a minimum of one week after arrival before initiation experiments. For breeding of neonatal mice, two adult female mice were put in the cage of one adult male mouse for two weeks. Female mice were then separated from the male and kept in separate breeding cages which were checked daily for new births and the pups stayed with the mother until weaning at the age of 4 weeks. Mice were housed under standardized conditions at the vivarium facility Arctic Las (Reykjavík, Iceland) with regulated daylight, humidity and temperature and kept in micro-isolator cages where they had free access to commercial pelleted food and water. All experiments were carried out in accordance with Act No. 55/2013 on animal welfare and regulations 460/2017 on protection of animals used for scientific research. The protocol was approved by the Experimental Animal Committee of Iceland (license no. 2015-10-01).

Vaccine, adjuvants, and immunization

Purified tetanus toxoid (TT) was purchased from Statens Serum Institute (Copenhagen, Denmark). LT-K63 (36) and MF59 (37) were produced and purified by Novartis Vaccines & Diagnostics (now GSK vaccines, Siena, Italy). mmCT was provided by Jan Holmgren, Michael Lebens and Manuela Terrinoni, from the Department of Microbiology and Immunology, Gothenburg University and was produced as described (22). IC31 was produced by Intercell AG, (now Valneva Austria GmbH, Vienna, Austria) as described (16). Aluminum hydroxide (Alhydrogel) was purchased from Brenntag Biosector A/S (Ballerup, Denmark). Neonatal (7 days old) mice were immunized with either vaccine alone, vaccine with adjuvant or saline as unimmunized controls. Mice were immunized subcutaneously (s.c.) at the base of the tail with 2 µg (0.8 limit of floculation, Lf) of purified TT (Statens Serum Institute) alone or mixed with the adjuvants LT-K63 (5 µg/mouse), mmCT (2 µg/mouse), MF59 (50% of injected volume/mouse), IC31 (50 nmol KLK and 2 nmol ODN1a/mouse) or alum (0.48% aluminum hydroxide per 1 µg of protein/mouse) in 50 µl of saline, or with 50 µl of saline alone as a control.

Blood sampling

For blood collection, mice were bled from the tail vein and serum was prepared by centrifugation at 2400 rpm for 10 minutes at room temperature and stored at –20°C until use.

Measurements of TT-specific antibodies in mouse sera

Measurement of TT-specific IgG antibodies was done using the following protocol. Microtiter plates (MaxiSorp) were coated with 5.0 µg/ml purified TT (Sanofi Pasteur) in 0.10 M carbonate buffer (pH 9.6) and incubated overnight at 4°C. Plates were washed 3

times with PBS containing 0.05% Tween 20 (v/v) (PBS-Tween20, Sigma) and then blocked with PBS-Tween20 containing 1% bovine serum albumin (BSA) for 1 hour at room temperature. Plates were washed as before and samples and standard were serially diluted (three-fold dilutions) and incubated in duplicates on TT-coated plates for 2 h at room temperature. The plates were washed as before and specific antibodies were detected with horseradish peroxidase (HRP)-conjugated goat anti-mouse antibody (Southern Biotechnology Associates Inc., Birmingham, AL, USA) diluted in PBS-Tween20 for 2 h at room temperature. As before the plates were washed and development of the enzyme reaction was performed by adding 100 µl of 3,3′,5,5′-tetramethylbenzidine peroxidase (TMB) substrate (Kirkegaard & Perry Laboratories, Gaithersburg, MD, USA) into each well for approximately 15 min and the reaction was stopped with 100 µl of 0.18 M H_2SO_4. The absorbance was read at 450 nm in a Titertek Multiscan Plus MK II spectrophotometer (ICN Flow Laboratories, Irvine, UK). Results were calculated from standard curves constructed by serial dilutions of a reference serum pool from hyperimmunized adult mice. The titers of the reference serum pool corresponded to the inverse serum dilution giving an optical density of 1.0, which has been assigned 100 ELISA units per ml (EU/ml). Results were expressed as mean log EU/ml ± standard deviation (SD).

Measurements of TT-specific antibody-secreting cells in spleen and bone marrow

TT-specific ASC were enumerated by ELISPOT, as previously described (15, 19, 20, 38). MultiScreen High protein binding immobilon-P membrane plates (Millipore Corporation, Bedford, MA) were coated with 10 µg/ml TT overnight at 37°C, blocked with complete RPMI 1640 (Life Technologies BRL, Life Technologies, Paisley, U.K.). Duplicates of cells from spleen and bone marrow in four three-fold dilutions starting with 1×10^7 cells in 100 µL in complete RPMI 1640 per well were incubated for 5 hours at 37°C, washed and incubated with ALP-goat anti-mouse IgG (Southern Biotechnology Associates) overnight at 4°C, and developed by 5-bromo-4-chloro-3-indolylphosphate and NBT in AP development buffer (Bio-Rad Labs, Hercules, CA). The number of spots, each representing a cell secreting TT-specific IgG antibodies, was counted with ELISPOT reader ImmunoSpot® S6 ULTIMATE using ImmunoSpot® SOFTWARE (Cellular Technology Limited (CTL) Europe, Bonn, Germany).

Immunofluorescent staining of tissue sections

Spleens were frozen in Tissue-Tek OCT (Sakura, Zouterwoude, the Netherlands) and cut into 7 µm cryosections at 2 levels, starting 1,750 µm into the tissue and separated by 210 µm, fixed in acetone for 10 minutes, and stored at −70°C. Two sections per spleen (one from each level) were stained with fluorescent labeled IgM-FITC (BD Pharmingen) to visualize follicles, and biotinylated peanut agglutinin (PNA)-bio (Vector Laboratories, Burlingame, CA) to label dark-zone B cells, to visualize active GC reaction. Primary antibodies were incubated at room temperature for 30 minutes. The sections were then washed in PBS for 2 × 5 minutes prior to incubation with APC Streptavidin (BD Biosciences, Stockholm, Sweden) at room temperature for another 30 minutes and sections washed again as before. DAPI (Invitrogen, Eugene, OR) was used for nuclear counterstaining and incubated for the last 10 minutes of the later staining step. The sections were photographed with a digital camera (AXIOCAM; Zeiss) in a microscope (Zeiss) equipped with x10 and x40 objectives and AxioImaging Software (Birkerod, Denmark) for light and three-color immunofluorescence. Areas of PNA-positive staining were measured from all pictures using the AxioImaging Software.

Immunofluorescence staining and flow cytometry

Spleens and bone marrow were collected 4, 8, 14 and 42 days after immunization for flow cytometry analysis using the following protocol as described (15). Single-cell suspensions from spleen and bone marrow were prepared and cells were washed and incubated (30 minutes on ice) in PBS with 0.5% BSA (Sigma) with 4 mmol/L EDTA (Sigma) with fluorochrome-labeled antibodies to B220, CD21, CD23, BAFF-R, CD138, Gr-1 (all from BD Biosciences), APRIL, CD11c, CD11b, CD200R3 (all from Biolegend), CD41, Siglec-F, F4/80 (all from eBioScience/Thermo Fisher) and BCMA (R&D Systems). Fc block (BD Biosciences), rat serum and mouse serum (2.7% each) was added to the staining mix to minimize unspecific binding. The stained cells were analyzed using Navios cytometer (Beckman Coulter, Brea, CA, USA) where recorded events were 400,000, and the generated data were analyzed by Kaluza® analysis software (version 2.1 from Beckman Coulter) where dead cells and doublets were excluded prior to analysis.

Statistical analysis

Mann-Whitney U test was used for comparison between groups and correlation was assessed using Spearman rank-order correlation applying a significance threshold of $p<0.05$ for both tests. All statistical analyses were carried out using Graphpad Prism 9.03 (GraphPad Software, La Jolla, CA).

Results

Limitations in APRIL, but not IL-6 expression in early life

Before assessing the effects of neonatal immunization and adjuvants on bone marrow accessory cells and their expression of survival factors, we investigated their age-dependent maturation at steady state in 1-, 2-, 3-week-old and adult mice. In this study, we analyzed a broader range of accessory cell types than we had done previously (15). Eosinophils were defined as Gr-1^{int}F4/80^{+}CD11b^{+}Siglec-F^{+}SSC^{high}, macrophages as Gr-1^{+}F4/80^{+}CD11b^{+}Siglec-F^{int}SSC^{int}, megakaryocytes as CD41^{+}F4/80^{-}CD11c^{-}Gr-1^{-}FSC^{high}, monocytes as Gr-1^{int}F4/80^{+}CD11b^{+}Siglec-F^{-}SSC^{low}, basophils as CD200R3^{+}F4/80$^{-/int}$Gr-1$^{-/int}$, neutrophils as Gr-1^{+}F4/80^{-}CD11b^{+} and dendritic cells as CD11c^{+}CD200R^{-}Siglec-F^{-} FSC^{low}SSC^{low} (Supplementary Figure 1). We found that APRIL expression by bone marrow cells was limited in early life as previously shown (4) and that it had not reached adult levels at 3 weeks of age (Figure 1A). Frequency and total number of eosinophils, megakaryocytes, monocytes and neutrophils were reduced in young mice and had not reached adult levels at 3 weeks of age (Supplementary Figures 2A, C, D, F, G). Macrophages and lymphocytes were limited in 1-2 week old mice, but reached adult levels at 3 weeks of age (Supplementary Figures 2B, E). When assessing APRIL expression of accessory cells we found that frequency and number of APRIL^{+} cells; eosinophils, macrophages, megakaryocytes, monocytes and lymphocytes was reduced in young mice and had not reached adult levels at 3 weeks of age (Figures 1B–F). Undefined APRIL^{+} cells, i.e. APRIL^{+} cells that did not fall into any of our flow cytometry gates, constituted for over 60% in 1 week old mice (Figure 1G). This high proportion of undefined cells among APRIL^{+} cells decreased with increasing age, and around 10% of APRIL^{+} cells remained undefined in adult mice (Figure 1G). Neutrophils, dendritic cells and basophils expressed very low levels of APRIL, constituting less than 1% of APRIL^{+} cells both in young or adult mice (data not shown).

In contrast to APRIL expression, IL-6 expression seemed to be higher in 1- and 2-week-old-mice than in adult mice, as they had increased frequency of IL-6^{+} cells. However, the total numbers of IL-6^{+} cells in 1- and 2-week-old-mice was still lower than in adult mice (Figure 2A). Frequency of IL-6^{+}cells; macrophages, monocytes, lymphocytes and neutrophils, was higher in young mice than in adults (Figures 2C, E, F, G),

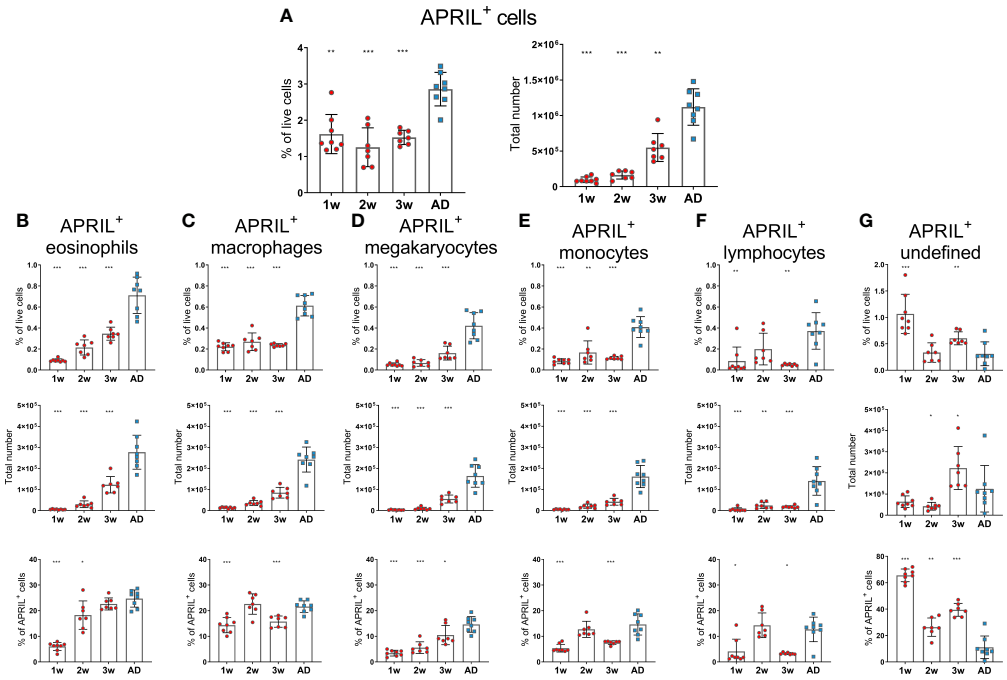

FIGURE 1
APRIL expression of bone marrow cells is limited in early life. Frequency and total number of APRIL^{+} cells **(A)** and frequency, total number and proportion out of total APRIL^{+} cells for APRIL^{+} eosinophils **(B)**, APRIL^{+} macrophages **(C)**, APRIL^{+} megakaryocytes **(D)**, APRIL^{+} monocytes **(E)**, APRIL^{+}lymphcoytes **(F)** and undefined APRIL^{+} cells **(G)** in bone marrow assessed by flow cytometry in 1-, 2-, 3-week-old and adult (AD) mice. Each red circle and blue square represents one mouse and results are demonstrated as means ± SD. Mann Whitney U test was used for statistical comparison where values from 1-, 2- or 3-week-old-mice were compared to adult mice and *p ≤ 0.05, **p ≤ 0.01, ***p ≤ 0.001.

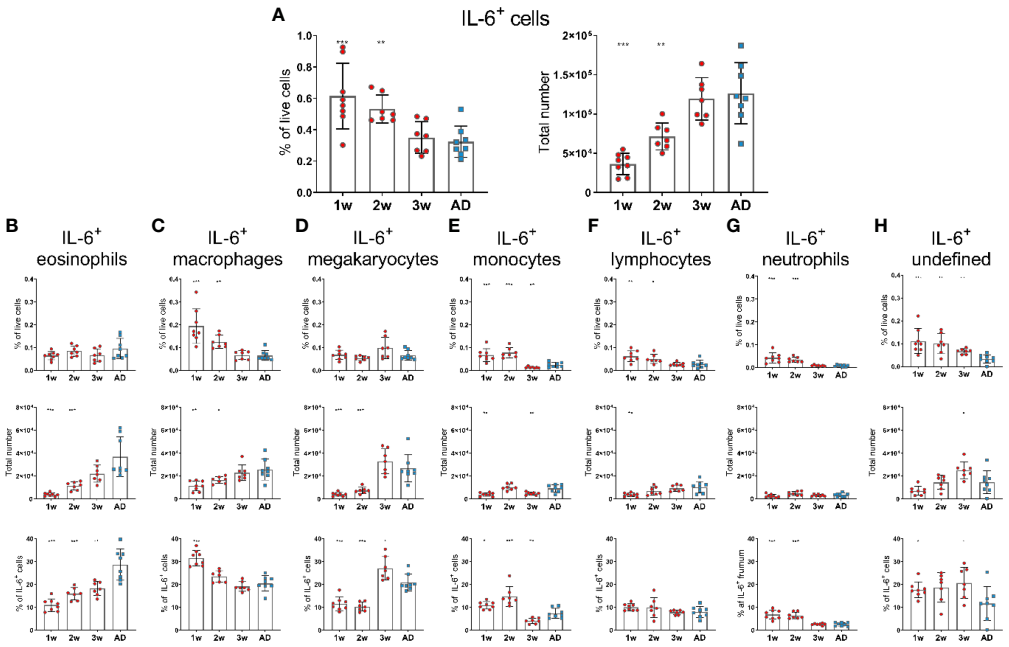

FIGURE 2
IL-6 expression of bone marrow cells is enhanced in early life. Frequency and total number of IL-6$^+$ cells **(A)** and frequency, total number and proportion out of total IL-6$^+$ cells for IL-6$^+$eosinophils **(B)**, IL-6$^+$ macrophages **(C)**, IL-6$^+$ megakaryocytes **(D)**, IL-6$^+$ monocytes **(E)**, IL-6$^+$ lymphocytes **(F)**, IL-6$^+$ neutrophils **(G)** and undefined IL-6$^+$ cells **(H)** in bone marrow assessed by flow cytometry in 1-, 2-, 3-week-old and adult (AD) mice. Each red circle and blue square represents one mouse and results are demonstrated as means ± SD. Mann Whitney U test was used for statistical comparison where values from 1-, 2- or 3-week-oldmice were compared to adult mice and *p ≤ 0.05, **p ≤ 0.01, ***p ≤ 0.001.

whereas no difference was observed for eosinophils and megakaryocytes (Figures 2B, D). Undefined cells constituted for around 20% of IL-6$^+$ cells in 1-, 2- and 3-week-old mice but had dropped down to 10% in adult mice (Figure 2H). Dendritic cells and basophils expressed very low levels of IL-6 and together constituted for less than 1% of IL-6$^+$ cells, both in young and adult mice (data not shown).

Taken together, these data demonstrate that APRIL expression was limited in bone marrow at least up to 3 weeks of age whereas IL-6 expression was higher in 1-2-week-old than adult mice. Various accessory cells contributed to the production of these survival factors and undefined cells were more prominent at early age.

Neonatal immunization and adjuvants enhance APRIL expression of bone marrow cells and BCMA expression of plasmablasts/plasma cells

We have previously demonstrated that neonatal immunization with Pnc1-TT+LT-K63 enhanced APRIL expression of bone marrow cells early after immunization which associated with enhanced persistence of vaccine-specific humoral immune responses (15). We therefore wanted to address if the adjuvants tested also mediated their adjuvanticity through a similar mechanism. Thus, neonatal mice (7 days old) were immunized s.c. at base of tail with TT w/wo the adjuvants LT-K63, mmCT, MF59, IC31 or alum or injected with saline as controls. Immunization with TT alone enhanced both frequency and total numbers of APRIL$^+$ cells in bone marrow when compared with saline-injected mice 4, 8 and 14 days after immunization (Figures 3A, B and Supplementary Table 1). Additionally, all the adjuvants assessed further enhanced APRIL$^+$ cells in bone marrow, however with different kinetics (Figures 3A, B). LT-K63, IC31 and alum enhanced frequency and total number of APRIL$^+$ cells 4 days after immunization, where the effect of LT-K63 was most pronounced. mmCT enhanced frequency and total number of APRIL$^+$ cells 8 days after immunization and lastly, MF59 enhanced frequency of APRIL$^+$ cells in bone marrow 14 days after immunization. Eosinophils, macrophages, monocytes and lymphocytes constituted considerable fractions of APRIL$^+$ cells, but undefined cells were generally still the most abundant (Figure 3C and Supplementary Table 2). Of note, lymphocytes accounted for a large proportion of APRIL$^+$ cells at the peak of its expression for each adjuvant (Figure 3 and Supplementary Table 2).

When assessing the effect of immunization and adjuvants on the kinetics of accessory cell populations, we found that LT-K63, MF59, IC31 and alum enhanced megakaryocytes in bone marrow 4 days after immunization (Supplementary Figure 3C).

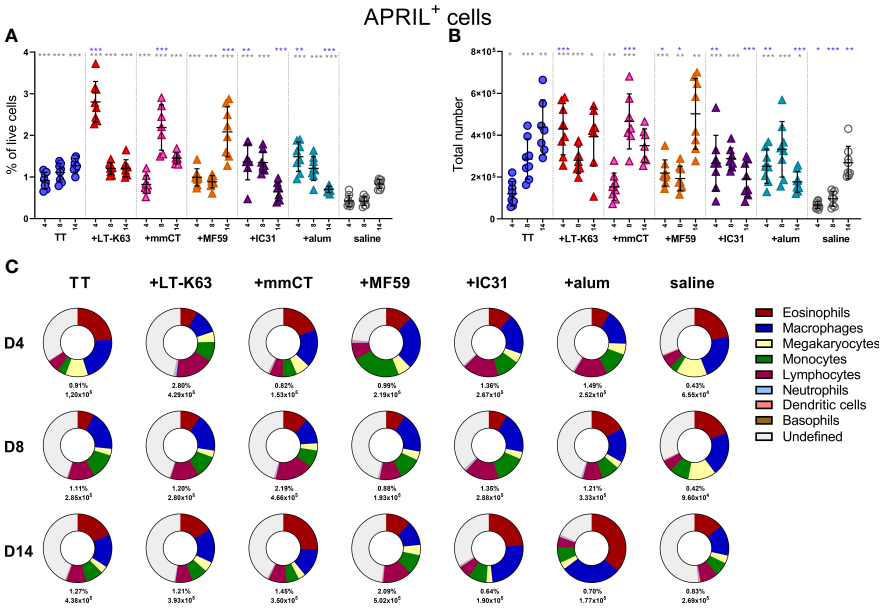

FIGURE 3
Neonatal immunization and adjuvants enhance APRIL expression in bone marrow cells. Frequency **(A)** and total numbers **(B)** of APRIL$^+$ cells in bone marrow and mean distribution of APRIL$^+$ cell types, mean frequencies and total numbers of APRIL$^+$ cells for each group and time point **(C)** 4, 8 and 14 days after neonatal immunization with TT (blue circle) w/wo adjuvants LT-K63 (red triangle), mmCT (pink triangle), MF59 (orange triangle), IC31 (purple triangle), alum (turquoise triangle) or saline-injected mice (light grey circles) as controls. Each symbol represents one mouse and results are shown as means ± SD in 8 mice per group per time point (except n=7 for TT group on day 14 and n=7 for TT+mmCT group on days 8 and 14). For statistical evaluation Mann–Whitney U-test was used. Blue stars represent p values after comparison of TT group to adjuvant groups and grey stars represent comparisons of all the groups to saline group. *p ≤ 0.05, **p ≤ 0.01, ***p ≤ 0.001.

Additionally, mmCT, MF59 and IC31 enhanced monocytes (Supplementary Figure 3D) and neutrophils (Supplementary Figure 3G) early after immunization, where neutrophils accounted for up to 30% of bone marrow cells in the TT +mmCT group 4 days after immunization (Supplementary Figure 3G). The kinetics of different APRIL$^+$ accessory cells and undefined APRIL$^+$ cells in bone marrow following immunization with TT w/wo adjuvants or saline are depicted in Supplementary Figures 4A–F.

It was recently reported that both stromal cell contact and binding of APRIL to BCMA is required for plasma cell survival (35). Since APRIL expression was enhanced by bone marrow cells early after immunization we next assessed BCMA expression of bone marrow plasmablasts/plasma cells at these early time points. Like we had observed before (15), we found that CD138 expression was lower in neonatal than adult mice so two populations of plasmablasts/plasma cells were assessed. Firstly, we defined B220$^+$CD138$^+$ cells as pre-plasmablasts/plasmablasts (prePB/PB), containing both pre-plasmablasts and plasmablasts (4, 39) and secondly B220$^{+/-}$CD138^{high} cells were defined as plasmablasts/plasma cells (PB/PC), containing both plasmablasts and plasma cells (39, 40). Immunization with TT alone subtly enhanced the proportion of bone marrow plasmablasts/plasma cells at these early time points (Figures 4A, B). Most of the adjuvants further enhanced plasmablasts/plasma cells but with different kinetics, where the effects of LT-K63 and IC31 were most pronounced (Figures 4A, B and Supplementary Figures 5A, B). Likewise, immunization with TT alone transiently enhanced the proportion of plasmablasts/plasma cells that expressed BCMA, whereas inclusion of each of the adjuvants further enhanced their proportion that persisted up to 14 days after immunization (Figures 4C, D). Of note, the immunization and adjuvant effects on the PB/PC subset were more pronounced as a much higher proportion of this subset was BCMA$^+$ than of the prePB/PB subset in all immunization groups (Figures 4C, D).

Taken together, immunization and adjuvants enhanced both APRIL expression by accessory cells and BCMA expression of plasmablasts/plasma cells in bone marrow at early time points after immunization but the effects were more pronounced when adjuvants were included.

Neonatal immunization and adjuvants decrease IL-6 expression by bone marrow cells

Since we found that immunization and adjuvants enhanced APRIL$^+$ cells in bone marrow early after immunization we were

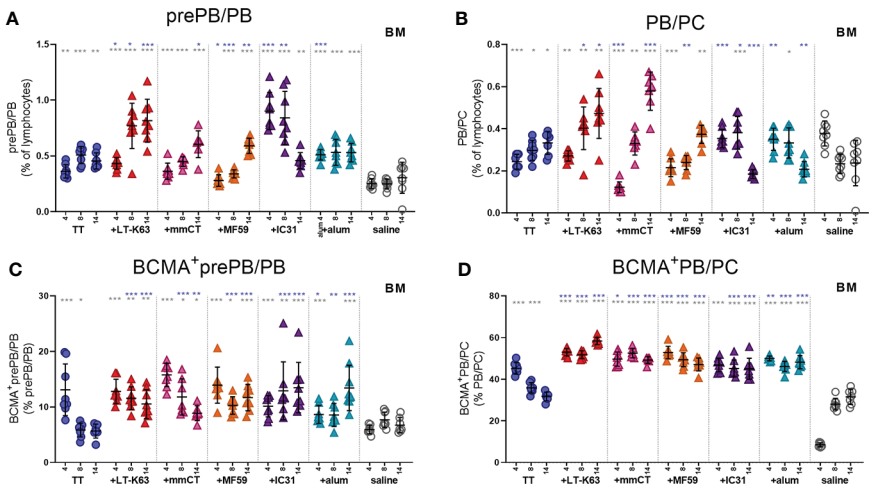

FIGURE 4
Neonatal immunization and adjuvants enhance early BCMA expression of plasmablasts/plasma cells in bone marrow. Frequency **(A, B)** and proportional BCMA expression **(C, D)** of B220^{+}CD138^{+}prePB/PB **(A, C)** and B220$^{+/-}$CD138^{high} PB/PC **(B, D)** in bone marrow 4, 8 and 14 days after neonatal immunization with TT (blue circles) w/wo adjuvants LT-K63 (red triangle), mmCT (pink triangle), MF59 (orange triangle), IC31 (purple triangle), alum (turquoise triangle) or saline-injected mice (light grey circles) as controls. Each symbol represents one mouse and results are shown as means ± SD in 8 mice per group per time point (except n=7 for TT group on day 14 and n=7 for TT+mmCT group on days 8 and 14). For statistical evaluation Mann–Whitney U-test was used. Blue stars represent p values after comparison of TT group to adjuvant groups and grey stars represent comparisons of all the groups to saline group. *p ≤ 0.05, **p ≤ 0.01, ***p ≤ 0.001.

curious to know if the same effects would be observed for IL-6^{+} cells, considering that like APRIL, IL-6 has been linked to prolonged plasma cell survival (41–43). On the contrary, immunization with TT alone decreased IL-6^{+} cells in the bone marrow 8 days after immunization and including adjuvants in the immunization accelerated this decrease (Figure 5A, B and Supplementary Table 3). As for APRIL^{+} cells, eosinophils, macrophages and lymphocytes all constituted a considerable fraction of IL-6^{+} cells, but megakaryocytes and undefined cells were also abundant (Figure 5C and Supplementary Table 4). The kinetics of different IL-6^{+} accessory cells and undefined IL-6^{+} cells in bone marrow following immunization are depicted in Supplementary Figure 6A–G.

Enhanced BCMA expression of splenic plasmablasts and plasma cells by adjuvants correlates with enhanced TT-specific antibody-secreting cells in spleen and serum antibodies 2 weeks after immunization

Next we wanted to assess if immunization and adjuvants mediated similar effects on splenic plasmablasts/plasma cells and their BCMA expression like we observed for bone marrow and if these effects could be connected to enhanced induction of vaccine-specific humoral responses.

Thus, neonatal mice were immunized as before and spleens harvested at various time points after immunization. We found that immunization with TT alone did not increase plasmablasts/plasma cells nor enhance their BCMA expression (Figures 6A, B, Supplementary Figures 7A, B and Supplementary Table 6). On the contrary, including adjuvants in the immunization enhanced both prePB/PB and PB/PC in spleen at early time points and the proportion BCMA^{+} cells (Figures 6A, B, Supplementary Figure 7A, B, Supplementary Table 6).

In response to a protein antigen, activated B cells can enter germinal center reactions where class switching, affinity maturation and differentiation into memory B cells or plasmablasts/plasma cells occurs (44). Germinal centers are generally attenuated in human infants (45–47), but some adjuvants have been shown to overcome limitations and induce potent germinal centers in early life murine models (19, 20, 30). We had previously demonstrated that the adjuvants LT-K63, mmCT, MF59 and IC31 enhanced germinal center induction after neonatal immunization with a pneumococcal conjugate vaccine (Pnc1-TT). In order to assess if the adjuvants would have similar effects on germinal center induction with a purified protein, TT vaccine, spleens were obtained 8 and 14 days after immunization of neonatal mice. We found that mmCT enhanced germinal center induction 8 and 14 days after immunization (Figure 6C, Supplementary Figure 7D) and LT-K63 and IC31 only at day 14 (Figure 6C). On the contrary, neither MF59 nor alum enhanced germinal center induction after neonatal immunization with TT.

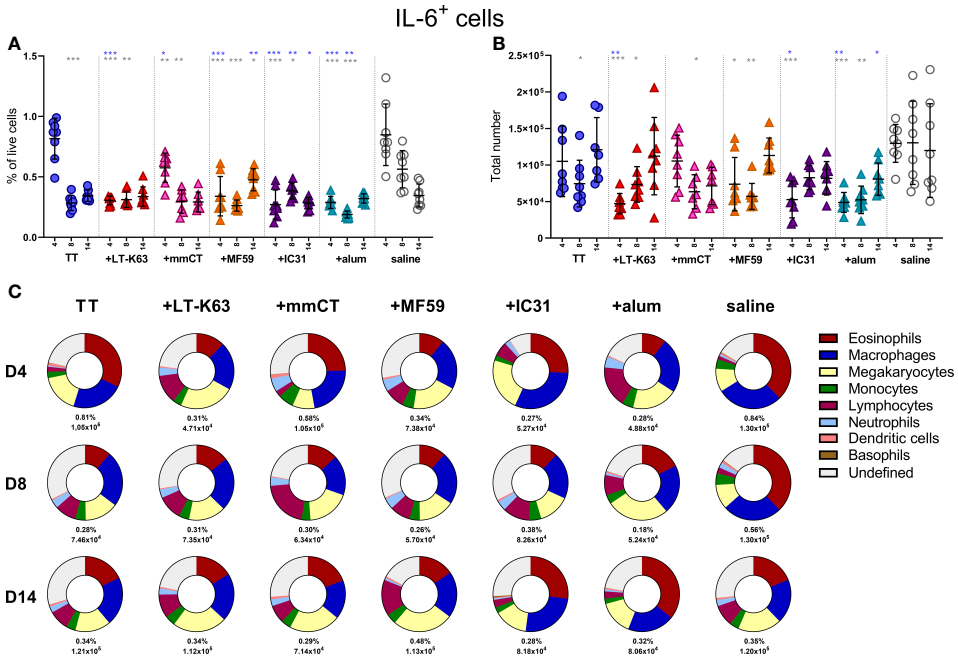

FIGURE 5
Neonatal immunization and adjuvants decrease IL-6 expression in bone marrow cells. Frequency **(A)** and total numbers **(B)** of IL-6$^+$ cells in bone marrow and mean distribution of IL-6$^+$ cell types, mean frequencies and total numbers of IL-6$^+$ cells for each group and time point **(C)** 4, 8 and 14 days following neonatal immunization with TT (blue circle) w/wo adjuvants LT-K63 (red triangle), mmCT (pink triangle), MF59 (orange triangle), IC31 (purple triangle), alum (turquoise triangle) or saline-injected mice (light grey circles) as controls. Each symbol represents one mouse and results are shown as means ± SD in 8 mice per group per time point (except n=7 for TT group on day 14 and n=7 for TT+mmCT group on days 8 and 14). For statistical evaluation Mann–Whitney U-test was used. Blue stars represent p values after comparison of TT group to adjuvant groups and grey stars represent comparisons of all the groups to saline group. *p ≤ 0.05, **p ≤ 0.01, ***p ≤ 0.001.

However, all adjuvants enhanced TT-specific IgG$^+$ASCs in spleen (Figure 6D, left) and TT-specific IgG Abs in serum (Figure 6D, right) 14 days after immunization. Of note, the adjuvants mmCT, MF59 and IC31 additionally enhanced TT-specific ASC in bone marrow already at this same time point. Furthermore, the adjuvants LT-K63, mmCT and MF59 prolonged the induction in spleen since TT-specific IgG$^+$ ASC were still enhanced 6 weeks after immunization (Supplementary Figure 7C). To assess if there was any association between BCMA expression of plasmablasts/plasma cells and vaccine-specific responses we analyzed the correlation between proportional BCMA expression of the two plasmablast/plasma cell populations and TT-specific ASC and Abs 14 days after immunization. A significant correlation was found between proportional BCMA expression of prePB/PB and TT-specific ASC (Figure 6E) and Abs (Figure 6F) and also between proportional BCMA expression of PB/PC and TT-specific ASC (Figure 6G) but not Abs (Figure 6H).

Taken together, all the adjuvants enhanced BCMA expression by plasmablasts and plasma cells in spleen, which correlated with enhanced vaccine-specific humoral immune responses. However, only LT-K63, mmCT and IC31 enhanced GC induction.

Enhanced BCMA expression of bone marrow plasmablasts and plasma cells by adjuvants correlates with vaccine-specific humoral immune responses 6 weeks after immunization

Lastly, we wanted to explore if enhanced APRIL expression by bone marrow cells early after immunization and increased BCMA expression of plasmablasts/plasma cells by adjuvants were associated with enhanced persistence of vaccine-specific humoral immune responses. We were also curious to know if BCMA expression by plasmablasts/plasma cells induced by adjuvants persisted after immunization. Thus, we assessed the frequency and total numbers of plasmablasts/plasma cells and TT-specific ASC in bone marrow and TT-specific serum Abs 6 weeks after immunization. At this time point, we did not detect much effect of immunization and adjuvants on the frequency and BCMA expression of prePB/PB in bone marrow (Figure 7A, Supplementary Table 5). However, PB/PC of mice immunized as neonates with each of the adjuvants were more frequently BCMA$^+$ than PB/PC of mice immunized with vaccine alone or saline-injected mice (Figure 7B). Of note, even though neonatal immunization with TT+alum enhanced BCMA expression by

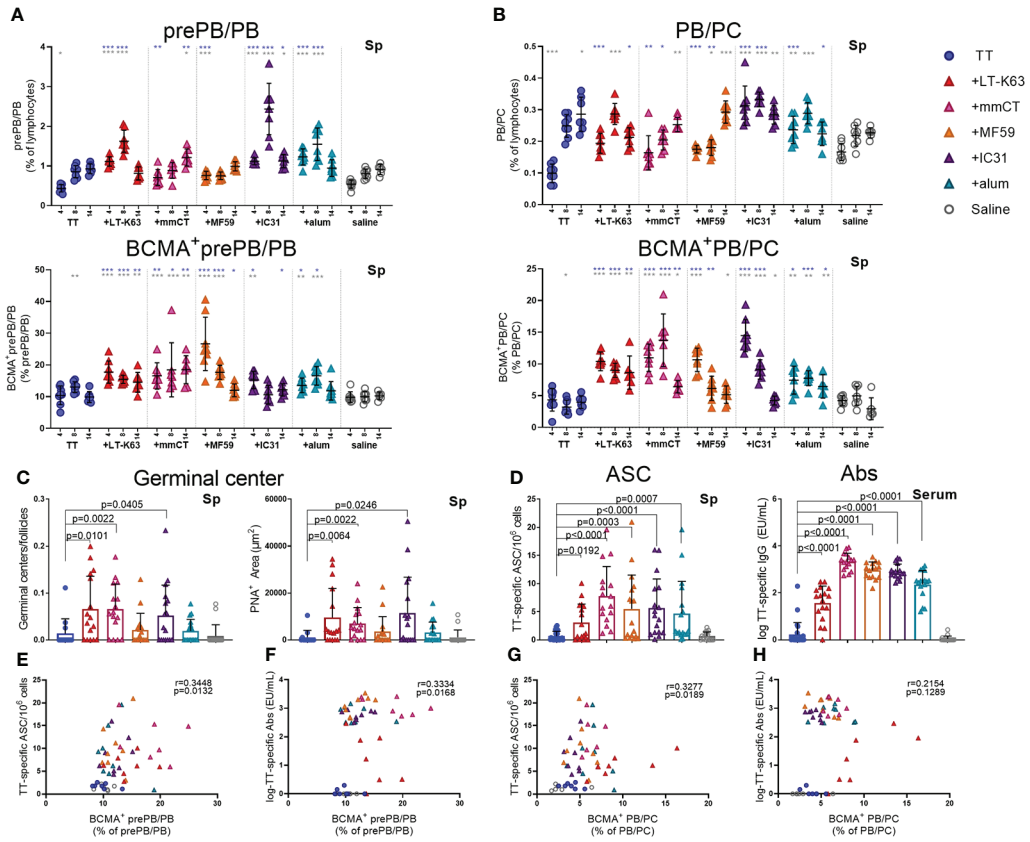

FIGURE 6
Adjuvants enhance BCMA expression of plasmablasts/plasma cells in spleen correlating with enhanced TT-specific antibody-secreting cells and antibodies. Frequency and BCMA expression of B220^{+}CD138^{+}prePB/PB **(A)** and B220$^{+/-}$CD138^{high} PB/PC **(B)** in spleen 4, 8 and 14 days after neonatal immunization with TT (blue circles) w/wo adjuvants LT-K63 (red triangle), mmCT (pink triangle), MF59 (orange triangle), IC31 (purple triangle), alum (turquoise triangle) or saline-injected mice (light grey circles) as controls. Germinal center activation determined by fluorescent staining of spleen sections with PNA and anti-IgM 14 days after immunization of neonatal mice. PNA/IgM ratio represents activated GCs in relation to total number of follicles (**C**, left panel) and PNA^{+} area represents total area of positive PNA staining per section (**C** right panel). TT-specific antibody-secreting cells (ASC) in spleen (**D**, left panel) and TT-specific IgG serum antibodies (**D**, right panel) 14 days after immunization. Each symbol represents one mouse and results are shown as means ± SD in 8 mice per group per time point (except n=7 for TT group on day 14 and n=7 for TT+mmCT group on days 8 and 14). Results for germinal center induction **(C)**, ASCs and Abs **(D)** are pooled from two independent experiments. For statistical evaluation Mann–Whitney U-test was used. Blue stars represent p values after comparison of TT group to adjuvant groups and grey stars represent comparisons of all the groups to saline group. *p ≤ 0.05, **p ≤ 0.01, ***p ≤ 0.001. In C-H, p values are visible on the figures. Spearman correlation plots for evaluation of association between BCMA^{+}prePB/PB frequency and TT-specific ASC **(E)** or TT-specific IgG Abs **(F)** or BCMA^{+} PB/PC frequency and TT-specific ASC **(G)** or TT-specific IgG Abs **(H)** 14 days after immunization.

PB/PC to a higher degree than immunization with TT alone at this time point, LT-K63 (p=0.0121), mmCT (p=0.0016), MF59 (p=0.0002) and IC31 (p=0.0002) were superior to alum in inducing persistent enhanced BCMA expression. All of the adjuvants enhanced TT-specific ASC in bone marrow and serum Abs at this time point (Figure 7C). Again, mmCT (p=0.0003 for ASC and p=0.0008 for Abs) and MF59 (p=0.0014 for ASC and p=0.0415 for Abs) were superior to alum in enhancing vaccine-specific ASC and Abs. To explore if there was any association between BCMA expression of plasmablasts/plasma cells in bone marrow and vaccine-specific responses, we assessed the correlation between proportional BCMA expression of the two plasmablast/plasma cell populations and TT-specific ASC in bone marrow and serum Abs 6 weeks after immunization. A significant correlation was observed between proportional BCMA expression of prePB/PB and TT-specific Abs (Figure 7E) but not ASC (Figure 7D) and also between proportional BCMA expression of PB/PC and TT-specific ASC (Figure 7F) and Abs (Figure 7G). Interestingly, mice immunized with the adjuvants LT-K63, mmCT, MF59 and IC31 grouped together in the correlation plot while alum-immunized mice rather grouped with mice immunized with TT alone (Figure 7G).

To summarize, immunization with adjuvants induced a higher proportion of PB/PC to express BCMA which persisted up to 6 weeks, although these effects were significantly less

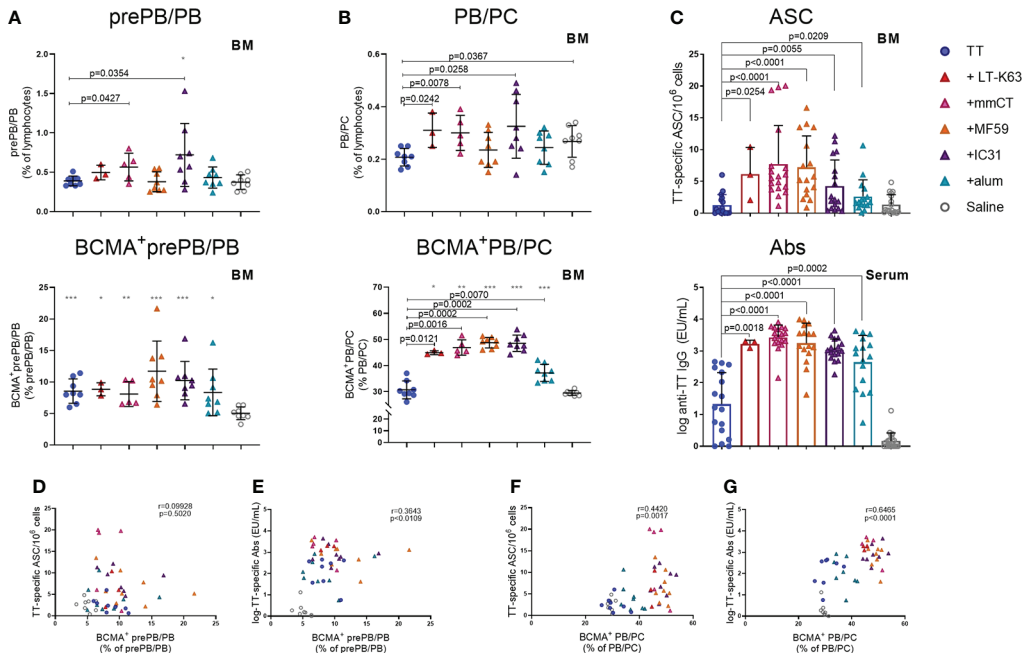

FIGURE 7
Adjuvants enhance BCMA expression of plasmablasts/plasma cells correlating with enhanced vaccine-specific humoral responses 6 weeks after immunization. Frequency (upper panels) and proportional BCMA expression (lower panels) of B220^{+}CD138^{+}prePB/PB **(A)** and B220$^{+/-}$CD138^{high} PB/PC **(B)**, TT-specific antibody-secreting cells (ASC) in bone marrow (**C**, upper panel) and TT-specific IgG serum antibodies (Abs) (**C**, lower panel) 6 weeks after neonatal immunization with TT (blue circles) w/wo adjuvants LT-K63 (red triangle), mmCT (pink triangle), MF59 (orange triangle), IC31 (purple triangle), alum (turquoise triangle) or saline-injected mice (light grey circles) as controls. Spearman correlation plots for evaluation of association between BCMA^{+}prePB/PB frequency and TT-specific ASC **(D)** or TT-specific IgG Abs **(E)** or BCMA^{+} PB/PC frequency and TT-specific ASC **(F)** or TT-specific IgG Abs **(G)** 6 weeks after immunization. Each symbol represents one mouse and results are shown as means ± SD in 8 mice per group (except n=3 for TT+LT-K63 group n=5 for TT+mmCT group). Results for ASC and Abs **(C)** are pooled from two independent experiments. For statistical evaluation Mann–Whitney U-test was used. P values from comparisons between TT group and adjuvants groups are visible on the figures whereas grey stars represent comparisons of all groups to saline group. *p ≤ 0.05, **p ≤ 0.01, ***p ≤ 0.001.

pronounced for alum. This enhanced BCMA expression correlated with persistent vaccine-specific humoral immune responses.

Discussion

It has previously been reported from experiments using mouse models that the majority of plasmablasts emerging from germinal centers after neonatal and infant immunization efficiently migrates to the bone marrow (48). However, poor APRIL expression by bone marrow stromal cells (4) was associated with reduced persistence and enhanced apoptosis of plasmablasts (48). This lack of survival signals in neonatal bone marrow could therefore explain transient Ab responses reported in this age group (1), since Ab persistence is mediated by long-lived plasma cells that reside in specialized survival niches in the bone marrow (34). APRIL can be expressed by stromal cells but can additionally be expressed by various hematopoietic cells, also termed accessory cells, in the bone marrow (49, 50). For the first time in a neonatal mouse model we performed a comparative analysis of different adjuvants on APRIL expression by accessory cells in the bone marrow. Before assessing effects of immunization and different adjuvants, we wanted to assess, also for the first time, age-dependent maturation of bone marrow accessory cells and their expression of the plasma cell survival factors APRIL and IL-6 at steady state. We found that APRIL was poorly expressed by early life accessory cells, but this was not the case for IL-6. Furthermore, neonatal immunization, in particular with adjuvants, enhanced APRIL expression by accessory cells but decreased their IL-6 expression. This is in line with what we previously showed for LT-K63, when administered with a pneumococcal conjugate vaccine (15) (and unpublished data).

Importantly, all five adjuvants assessed herein enhanced APRIL expression in bone marrow but the extent and kinetics of this APRIL enhancement differed between adjuvants. Early increase in APRIL following immunization was not expected since plasma cell influx to the bone marrow after immunization usually remains low until after more than 3 weeks (19). However, soluble APRIL can be bound by heparan sulphate proteoglycans (51, 52) in the bone marrow and APRIL bound to proteoglycan has been found to be superior to soluble APRIL in

activation of B cells (52, 53). In line with that, APRIL-rich niches with plasma cells have been found in human mucosa where heparan sulphate proteoglycans retained neutrophil-derived APRIL (54). Furthermore, mice deficient in glucuronyl C5-epimerase, an enzyme that controls heparan sulphate chain flexibility affecting ligand binding, failed to respond to APRIL-mediated survival signals resulting in reduced plasma cells and Ab levels (55), emphasizing the importance of heparan sulphate proteoglycans in plasma cell survival.

It must be noted that the effects of adjuvants on APRIL expression was less pronounced than we had previously reported when neonatal mice were immunized with Pnc1-TT with LT-K63 (15). However, there were some fundamental differences between the sets of experiments described herein and the experiments previously published (15). In the previous study T cells, B cells, NK cells, dendritic cells, mast cells and basophils were depleted from the bone marrow cell suspension prior to analysing APRIL expression and accessory cells. Therefore, the cells that have potential of APRIL expression might have been more concentrated in the earlier study. Additionally, the depletion protocol might have stimulated the cells to some extent. Finally, the cells were analysed in a different flow cytometer and thus inevitably with different settings.

It was surprising that immunization and adjuvants decreased IL-6 expression by bone marrow cells since IL-6 has been identified as a plasma cell survival factor (41–43). Nonetheless, other data from mice suggest that IL-6 seems to only be required for induction but not maintenance of plasma cells *in vivo* (56). Additionally, blocking of IL-6R using tocilizumab has not been shown to affect serum IgG Ab levels of patients (57). Of note, co-injection of adult mice with IL-6 and a pneumococcal conjugate vaccine enhanced T follicular helper (Tfh) cells and T follicular regulatory (Tfr) cells that was associated with improved Ab responses. On the contrary, the same immunization protocol in neonatal mice reduced the expansion of Tfh cells but increased Tfr cells that led to limited Ab responses. This could be explained by enhanced expression of IL-6R by neonatal compared with adult Tfr cells and decreased IL-6R expression of neonatal Tfh cells compared with adult Tfh cells (58). This suggests that even though IL-6 can be beneficial for induction of immune responses in adult setting it could have opposite effects in a neonatal setting.

How the adjuvants induce their effects on cells of the bone marrow is still unclear. We find it unlikely that the adjuvants reach the bone marrow to directly activate cells there, although we cannot exclude that possibility. A more plausible explanation would be that they induce influx of immune cells to site of injection, and through the engagement of pattern recognition receptors or other receptors lead to activation and secretion of pro-inflammatory cytokines and chemokines that in turn enhances hematopoiesis and activation of cells in the bone marrow. During infection or inflammation, hematopoietic stem cells respond to inflammatory stimuli by emergency myelopoiesis (59). Interestingly, enhanced IL-6 was recently found to be involved in age-associated hematopoietic decline (60). Therefore, decreased IL-6 expression in bone marrow cells early after immunization, which was more pronounced with the inclusion of adjuvants, could be a sign of enhanced hematopoiesis (Figure 5A).

A large fraction of both APRIL$^+$ cells and IL-6$^+$ cells in bone marrow remained undefined, i.e. didn't fall into any of our assigned cell population gates. These cells accounted for more than 60% of APRIL$^+$ cells in 1 week old mice but decreased with increasing age. Thus, they may represent precursor cells and therefore lack efficient expression of cell-identifying surface markers. Interestingly, bone marrow neutrophil precursors have been shown to express APRIL in adult mice (61). Another explanation may be that some other cell types that were not assessed herein expressed plasma cell survival factors to a higher degree in younger than adult mice. Like before (15), eosinophils, macrophages and megakaryocytes constituted a big part of APRIL$^+$ cells in bone marrow but herein we additionally found that monocytes and lymphocytes were frequently APRIL$^+$. Likewise, eosinophils, macrophages, megakaryocytes and lymphocytes constituted a big fraction of IL-6$^+$ cells.

BCMA is predominantly expressed by GC B cells, memory B cells and plasma cells (5) and has been shown to be needed for survival of long-lived plasma cells in the bone marrow, as BCMA-deficiency in mice drastically reduced numbers of bone marrow plasma cells (7–9), leaving plasma cells in secondary lymphoid organs unaffected (8, 10). Following differentiation of B cells into plasmablasts in secondary lymphoid organs they can relocate to the bone marrow, and it has been demonstrated that plasmablasts sufficiently migrate to the early life bone marrow compartments following neonatal immunization (48). Like we had previously found for LT-K63 (15) when administered with a pneumococcal conjugate vaccine, immunization with TT, and in particular when adjuvants were included, enhanced BCMA expression of plasmablasts/plasma cells, both in spleen and bone marrow. This enhanced BCMA expression of the PB/PC subset induced by adjuvants was still observed 6 weeks after immunization. Enhanced BCMA expression of plasma cells may render them more fit for prolonged survival, enabling binding of APRIL. BCMA expression of plasmablasts/plasma cells correlated with vaccine-specific ASCs, early in spleen and later in bone marrow, and with serum Abs. The correlation was generally weaker in the spleen and the best correlation was observed between proportional BCMA expression of PB/PC subset with TT-specific Abs 6 weeks after immunization. This indicates a strong association between BCMA expression and Abs at later time points after immunization, fitting well with previous publications demonstrating that BCMA is essential for long-lived plasma cells (8).

In our previous work (20) we demonstrated that LT-K63, mmCT, MF59 and IC31 but not alum accelerated maturation of follicular dendritic cells and enhanced germinal center induction

when they were administered to neonatal mice with a pneumococcal conjugate vaccine, Pnc1-TT. Herein, only LT-K63, mmCT and IC31 enhanced germinal center induction, but MF59 and alum did not. Even though MF59 and alum did not enhance germinal center formation, both adjuvants induced enhanced TT-specific IgG^+ ASC in spleen and IgG serum Abs at 2 and 6 weeks after immunization, compared with TT alone. Of interest, MF59 could enhance IgG Abs following immunization of CD4 knockout mice or CD4-depleted mice after immunization with a TD influenza virus split vaccine (62) suggesting that a CD4-independent pathway bypassing GC induction can be an alternative mechanism for MF59. It might be that the timepoints assessed were suboptimal for assessing GC induction following immunization with TT, since vaccine adjuvants have been shown to differently affect kinetics of germinal center responses (63), or it could be that these adjuvants trigger more extra-follicular responses. However, the adjuvanticity of MF59 has been shown to be mediated through enhanced Tfh cells and in turn enhanced germinal center induction, but MF59 was unable to activate Tfh cells following neonatal immunization with HA (26).

We have also previously shown that a single immunization of neonatal mice with Pnc1-TT with the adjuvants LT-K63, mmCT, MF59 and IC31, but not alum, was sufficient to induce vaccine-specific ASCs in bone marrow and serum Abs that persisted above protective levels against pneumococcal bacteremia and lung infection 9 weeks after immunization (20). On the contrary, alum only transiently enhanced vaccine-specific ASCs in bone marrow and serum Abs up to week 6 (20). In this study, all the adjuvants induced higher levels of IgG Abs than TT alone. Of interest, bone marrow PB/PC of mice immunized with TT+alum were less frequently $BCMA^+$ 6 weeks after immunization than PB/PC of mice immunized with any of the other adjuvants assessed herein and may therefore be less fit for prolonged survival as was observed in previous studies (20, 64).

It was surprising that adjuvants with previously established different mechanisms of action (Table 1) all induced similar responses in our model, i.e. enhanced APRIL and BCMA expression, although with different kinetics and magnitudes and decreased IL-6 expression, that associated with enhanced humoral immune responses. It still remains unknown through which mechanisms this enhanced APRIL and BCMA expression and decreased IL-6 expression is mediated and likely they differ between adjuvants, and will be studied in more detail in future experiments. Nonetheless, a significant correlation of BCMA expression among plasmablasts/plasma cells and serum Abs 6 weeks after immunization suggests that upregulation of BCMA on plasmablasts/plasma cells is an important step in rendering these cells more fit for prolonged survival and induction of persistent Ab responses after neonatal immunization. In line with that, mice immunized with LT-K63, mmCT, MF59 and IC31 clearly grouped together on this correlation plot whereas mice immunized with alum grouped with mice immunized with TT alone (Figure 7G), revealing differences between alum and the other adjuvants that could explain more transient responses induced by alum as previously reported by us and others (20, 64).

To summarize, we found that APRIL expression was limited in young mice whereas IL-6 expression was higher in younger than adult mice. We identified eosinophils, macrophages, megakaryocytes, monocytes and lymphocytes as important secretors of survival factors in early life but undefined cells also constituted a large fraction of secretors. Neonatal immunization and adjuvants enhanced APRIL expression but decreased IL-6 expression in bone marrow cells early after immunization. Moreover, immunization and adjuvants enhanced proportions of plasmablasts/plasma cells that expressed BCMA early in spleen and later in bone marrow, and this enhanced BCMA expression significantly correlated with enhanced vaccine-specific humoral responses. It must be noted that alum's effect on BCMA expression was less pronounced at later time points than the effects of the other adjuvants which could explain previous reports of transient humoral immune responses induced by alum (20, 64). We demonstrate that not only APRIL is limited in early life, but also BCMA expression of plasmablasts/plasma cells and that enhanced BCMA expression induced by adjuvants correlated with enhanced persistence of vaccine-specific humoral immune responses, offering an explanation for transient Ab responses in early life. These results together with our previously published data (20) warrant further investigations of the adjuvants mmCT, MF59 and IC31 for use in early life vaccinology.

Data availability statement

The raw data supporting the conclusions of this article will be made available by the authors, without undue reservation.

Ethics statement

The animal study was carried out in accordance with Act No. 55/2013 on animal welfare and regulations 460/2017 on protection of animals used for scientific research. The protocol was reviewed and approved by Experimental Animal Committee of Iceland, MAST, Austurvegur 64, 800 Selfoss, Iceland (license no. 2015-10-01).

Author contributions

AP, IJ, and SB conceived and designed the study, interpreted the results and wrote the manuscript. IJ and SB supervised the study. AP, GM, ST, and SB performed the experiments. AP and

SB analyzed the data. AM and GD provided material and expertise. All authors contributed to and approved the final version of the manuscript.

Funding

AP was a recipient of a doctoral study grant from the University of Iceland Research Fund (2015-18). This study was financially supported by grants from the Icelandic Research Fund (130675051-53), The University of Iceland Research Fund (2018-20) and the Landspitali Science Fund (A-2017-068, A-2017-069, A-2018-076, A-2018-077, A-2019-084).

Acknowledgments

We thank Professor Jan Holmgren, MD, PhD, Michael Lebens, PhD and Manuela Terrinoni at the Department of Microbiology and Immunology at University of Gothenburg, for providing the adjuvant mmCT and Professor Jan Holmgren for his expert advice. Part of the work presented in this paper was presented as a poster at the 50th Anniversary Meeting of the Scandinavian Society for Immunology, Aarhus, October 19th-22nd 2021 and in an oral presentation on the 48th Annual Meeting of the Scandinavian Society for Immunology, Reykjavík, June 12th-15th 2022.

Conflict of interest

GD is a previous employee and holds shares in the GSK group of companies. AM is an employee of Valneva Austria GmbH.

The remaining authors declare that the research was conducted in the absence of any commercial or financial relationships that could be construed as a potential conflict of interest.

Publisher's note

Supplementary material

The Supplementary Material for this article can be found online at: https://www.frontiersin.org/articles/10.3389/fimmu.2022.904415/full#supplementary-material

References

1. Siegrist CA, Aspinall R. B-cell responses to vaccination at the extremes of age. *Nat Rev Immunol* (2009) 9:185–94. doi: 10.1038/nri2508

2. Huang C. Germinal center reaction. *Adv Exp Med Biol* (2020) 1254:47–53. doi: 10.1007/978-981-15-3532-1_4

3. Radbruch A, Muehlinghaus G, Luger EO, Inamine A, Smith KG, Dorner T, et al. Competence and competition: The challenge of becoming a long-lived plasma cell. *Nat Rev Immunol* (2006) 6:741–50. doi: 10.1038/nri1886

4. Belnoue E, Pihlgren M, McGaha TL, Tougne C, Rochat AF Bossen C, et al. APRIL is critical for plasmablast survival in the bone marrow and poorly expressed by early-life bone marrow stromal cells. *Blood* (2008) 111:2755–64. doi: 10.1182/blood-2007-09-110858

5. Dostert C, Grusdat M, Letellier E, Brenner D. The TNF family of ligands and receptors: Communication modules in the immune system and beyond. *Physiol Rev* (2019) 99:115–60. doi: 10.1152/physrev.00045.2017

6. Ou X, Xu S, Lam K-P. Deficiency in TNFRSF13B (TACI) expands T-follicular helper and germinal center b cells *via* increased ICOS-ligand expression but impairs plasma cell survival. *Proc Natl Acad Sci* (2012) 109:15401–6. doi: 10.1073/pnas.1200386109

7. Peperzak V, Vikstrom I, Walker J, Glaser SP, LePage M, Coquery CM, et al. Mcl-1 is essential for the survival of plasma cells. *Nat Immunol* (2013) 14:290–7. doi: 10.1038/ni.2527

8. O'Connor BP, Raman VS, Erickson LD, Cook WJ, Weaver LK, Ahonen C, et al. BCMA is essential for the survival of long-lived bone marrow plasma cells. *J Exp Med* (2004) 199:91–8. doi: 10.1084/jem.20031330

9. Benson MJ, Dillon SR, Castigli E, Geha RS, Xu S, Lam KP, et al. Cutting edge: the dependence of plasma cells and independence of memory b cells on BAFF and APRIL. *J Immunol (Baltimore Md 1950)* (2008) 180:3655–9. doi: 10.4049/jimmunol.180.6.3655

10. Xu S, Lam KP. B-cell maturation protein, which binds the tumor necrosis factor family members BAFF and APRIL, is dispensable for humoral immune responses. *Mol Cell Biol* (2001) 21:4067–74. doi: 10.1128/mcb.21.12.4067-4074.2001

11. Cornelis R, Chang HD, Radbruch A. Keeping up with the stress of antibody production: BAFF and APRIL maintain memory plasma cells. *Curr Opin Immunol* (2021) 71:97–102. doi: 10.1016/j.coi.2021.06.012

12. Del Giudice G, Rappuoli R, Didierlaurent AM. Correlates of adjuvanticity: A review on adjuvants in licensed vaccines. *Semin Immunol* (2018) 39:14–21. doi: 10.1016/j.smim.2018.05.001

13. Nanishi E, Dowling DJ, Levy O. Toward precision adjuvants: optimizing science and safety. *Curr Opin Pediatr* (2020) 32:125–38. doi: 10.1097/mop.0000000000000868

14. Wilkins AL, Kazmin D, Napolitani G, Clutterbuck EA, Pulendra B, Siegrist CA, et al. AS03- and MF59-adjuvanted influenza vaccines in children. *Front Immunol* (2017) 8:1760. doi: 10.3389/fimmu.2017.01760

15. Aradottir Pind AA, Molina Estupiñan JL, Magnusdottir GJ, Del Giudice G, Jonsdottir I, Bjarnarson SP, et al. LT-K63 enhances b cell activation and survival factors in neonatal mice that translates into long-lived humoral immunity. *Front Immunol* (2020) 11:527310. doi: 10.3389/fimmu.2020.527310

16. Schellack C, Prinz K, Egyed A, Fritz JH, Wittmann B, Ginzler M, et al. IC31, a novel adjuvant signaling *via* TLR9, induces potent cellular and humoral immune responses. *Vaccine* (2006) 24:5461–72. doi: 10.1016/j.vaccine.2006.03.071

17. Ryan EJ, McNeela E, Pizza M, Rappuoli R, O'Neill L, Mills KH, et al. Modulation of innate and acquired immune responses by escherichia coli heat-labile toxin: Distinct pro- and anti-inflammatory effects of the nontoxic AB complex and the enzyme activity. *J Immunol (Baltimore Md 1950)* (2000) 165:5750–9. doi: 10.4049/jimmunol.165.10.5750

18. Olafsdottir TA, Hannesdottir SG, Giudice GD, Trannoy E, Jonsdottir I. Effects of LT-K63 and CpG2006 on phenotype and function of murine neonatal lymphoid cells. *Scandinavian J Immunol* (2007) 66:426–34. doi: 10.1111/j.1365-3083.2007.01970.x

19. Bjarnarson SP, Adarna BC, Benonisson H, Del Giudice G, Jonsdottir I. The adjuvant LT-K63 can restore delayed maturation of follicular dendritic cells and poor persistence of both protein- and polysaccharide-specific antibody-secreting cells in neonatal mice. *J Immunol (Baltimore Md 1950)* (2012) 189:1265–73. doi: 10.4049/jimmunol.1200761

20. Aradottir Pind AA, Dubik M, Thorsdottir S, Meinke A, Harandi AM Holmgren J, et al. Adjuvants enhance the induction of germinal center and antibody secreting cells in spleen and their persistence in bone marrow of neonatal mice. *Front Immunol* (2019) 10:2214. doi: 10.3389/fimmu.2019.02214

21. Larena M, Holmgren J, Lebens M, Terrinoni M, Lundgren A. Cholera toxin, and the related nontoxic adjuvants mmCT and dmLT, promote human Th17 responses *via* cyclic AMP-protein kinase a and inflammasome-dependent IL-1 signaling. *J Immunol (Baltimore Md 1950)* (2015) 194:3829–39. doi: 10.4049/jimmunol.1401633

22. Lebens M, Terrinoni M, Karlsson SL, Larena M, Gustafsson-Hedberg T, Kallgard S, et al. Construction and preclinical evaluation of mmCT, a novel mutant cholera toxin adjuvant that can be efficiently produced in genetically manipulated vibrio cholerae. *Vaccine* (2016) 34:2121–8. doi: 10.1016/j.vaccine.2016.03.002

23. Terrinoni M, Holmgren J, Lebens M, Larena M. Requirement for cyclic AMP/Protein kinase a-dependent canonical NFkappaB signaling in the adjuvant action of cholera toxin and its non-toxic derivative mmCT. *Front Immunol* (2019) 10:269. doi: 10.3389/fimmu.2019.00269

24. Vono M, Taccone M, Caccin P, Gallotta M, Donvito G, Falzoni S, et al. The adjuvant MF59 induces ATP release from muscle that potentiates response to vaccination. *Proc Natl Acad Sci USA* (2013) 110:21095–100. doi: 10.1073/pnas.1319784110

25. Podda A, Del Giudice G. MF59-adjuvanted vaccines: increased immunogenicity with an optimal safety profile. *Expert Rev Vaccines* (2003) 2:197–203. doi: 10.1586/14760584.2.2.197

26. Mastelic Gavillet B, Eberhardt CS, Auderset F, Castellino F, Seubert A, Tregoning JS, et al. MF59 mediates its b cell adjuvanticity by promoting T follicular helper cells and thus germinal center responses in adult and early life. *J Immunol (Baltimore Md 1950)* (2015) 194:4836–45. doi: 10.4049/jimmunol.1402071

27. Knudsen NP, et al. Different human vaccine adjuvants promote distinct antigen-independent immunological signatures tailored to different pathogens. *Sci Rep* (2016) 6:19570. doi: 10.1038/srep19570

28. Olafsdottir TA, Lingnau K, Nagy E, Jonsdottir I. Novel protein-based pneumococcal vaccines administered with the Th1-promoting adjuvant IC31 induce protective immunity against pneumococcal disease in neonatal mice. *Infection Immun* (2012) 80:461–8. doi: 10.1128/iai.05801-11

29. Kamath AT, Rochat AF, Valenti MP, Agger EM, Lingnau K, Andersen P, et al. Adult-like anti-mycobacterial T cell and *in vivo* dendritic cell responses following neonatal immunization with Ag85B-ESAT-6 in the IC31 adjuvant. *PLoS One* (2008) 3:e3683. doi: 10.1371/journal.pone.0003683

30. Vono M, Eberhardt CS, Mohr E, Auderset F, Christensen D, Schmolke M, et al. Overcoming the neonatal limitations of inducing germinal centers through liposome-based adjuvants including c-type lectin agonists trehalose dibehenate or curdlan. *Front Immunol* (2018) 9:381. doi: 10.3389/fimmu.2018.00381

31. Brewer JM, Conacher M, Hunter CA, Mohrs M, Brombacher F Alexander J, et al. Aluminium hydroxide adjuvant initiates strong antigen-specific Th2 responses in the absence of IL-4- or IL-13-mediated signaling. *J Immunol (Baltimore Md 1950)* (1999) 163:6448–54.

32. Grun JL, Maurer PH. Different T helper cell subsets elicited in mice utilizing two different adjuvant vehicles: The role of endogenous interleukin 1 in proliferative responses. *Cell Immunol* (1989) 121:134–45. doi: 10.1016/0008-8749(89)90011-7

33. Dowling DJ, Levy O. Pediatric vaccine adjuvants: Components of the modern vaccinologist's toolbox. *Pediatr Infect Dis J* (2015) 34:1395–8. doi: 10.1097/inf.0000000000000893

34. Chang HD, Tokoyoda K, Radbruch A. Immunological memories of the bone marrow. *Immunol Rev* (2018) 283:86–98. doi: 10.1111/imr.12656

35. Cornelis R, Hahne S, Taddeo A, Petkau G, Malko D, Durek P, et al. Stromal cell-contact dependent PI3K and APRIL induced NF-κB signaling prevent mitochondrial- and ER stress induced death of memory plasma cells. *Cell Rep* (2020) 32:107982. doi: 10.1016/j.celrep.2020.107982

36. Giuliani MM, Del Giudice G, Giannelli V, Dougan G, Douce G, Rappuoli R, et al. Mucosal adjuvanticity and immunogenicity of LTR72, a novel mutant of escherichia coli heat-labile enterotoxin with partial knockout of ADP-ribosyltransferase activity. *J Exp Med* (1998) 187:1123–32. doi: 10.1084/jem.187.7.1123

37. O'Hagan DT, Ott GS, Nest GV, Rappuoli R, Giudice GD. The history of MF59((R)) adjuvant: A phoenix that arose from the ashes. *Expert Rev Vaccines* (2013) 12:13–30. doi: 10.1586/erv.12.140

38. Bjarnarson SP, Benonisson H, Del Giudice G, Jonsdottir I. Pneumococcal polysaccharide abrogates conjugate-induced germinal center reaction and depletes antibody secreting cell pool, causing hyporesponsiveness. *PloS One* (2013) 8: e72588. doi: 10.1371/journal.pone.0072588

39. Wilmore JR, Jones DD, Allman D. Protocol for improved resolution of plasma cell subpopulations by flow cytometry. *Eur J Immunol* (2017) 47:1386–8. doi: 10.1002/eji.201746944

40. Pracht K, Meinzinger J, Daum P, Schulz SR, Reimer D, Hauke M, et al. A new staining protocol for detection of murine antibody-secreting plasma cell subsets by flow cytometry. *Eur J Immunol* (2017) 47:1389–92. doi: 10.1002/eji.201747019

41. Chu VT, Berek C. Immunization induces activation of bone marrow eosinophils required for plasma cell survival. *Eur J Immunol* (2012) 42:130–7. doi: 10.1002/eji.201141953

42. Rodriguez Gomez M, Talke Y, Goebel N, Hermann F, Reich B, Mack M, et al. Basophils support the survival of plasma cells in mice. *J Immunol (Baltimore Md 1950)* (2010) 185:7180–5. doi: 10.4049/jimmunol.1002319

43. Gabler J, Wittmann J, Porstner M, Renz H, Jäck HM, Abram M, et al. Contribution of microRNA 24-3p and Erk1/2 to interleukin-6-mediated plasma cell survival. *Eur J Immunol* (2013) 43:3028–37. doi: 10.1002/eji.201243271

44. Young C, Brink R. The unique biology of germinal center b cells. *Immunity* (2021) 54:1652–64. doi: 10.1016/j.immuni.2021.07.015

45. Kruschinski C, Zidan M, Debertin AS, von Hörsten S, Pabst R. Age-dependent development of the splenic marginal zone in human infants is associated with different causes of death. *Hum Pathol* (2004) 35:113–21. doi: 10.1016/s0046-8177(03)00422-2

46. Timens W, Boes A, Rozeboom-Uiterwijk T, Poppema S. Immaturity of the human splenic marginal zone in infancy. Possible contribution to the deficient infant immune response. *J Immunol* (1989) 143:3200–6.

47. Zandvoort A, Lodewijk ME, de Boer NK, Dammers PM, Kroese FG, Timens W, et al. CD27 expression in the human splenic marginal zone: The infant marginal zone is populated by naive b cells. *Tissue Antigens* (2001) 58:234–42. doi: 10.1034/j.1399-0039.2001.580403.x

48. Pihlgren M, Friedli M, Tougne C, Rochat AF, Lambert PH, Siegrist CA, et al. Reduced ability of neonatal and early-life bone marrow stromal cells to support plasmablast survival. *J Immunol (Baltimore Md 1950)* (2006) 176:165–72. doi: 10.4049/jimmunol.176.1.165

49. Chang HD, Radbruch A. Maintenance of quiescent immune memory in the bone marrow. *Eur J Immunol* (2021) 51:1592–601. doi: 10.1002/eji.202049012

50. Zehentmeier S, Roth K, Cseresnyes Z, Sercan O, Horn K, Niesner RA, et al. Static and dynamic components synergize to form a stable survival niche for bone marrow plasma cells. *Eur J Immunol* (2014) 44:2306–17. doi: 10.1002/eji.201344313

51. Hendriks J, Planelles L, de Jong-Odding J, Hardenberg G, Pals ST, Hahne M, et al. Heparan sulfate proteoglycan binding promotes APRIL-induced tumor cell proliferation. *Cell Death differentiation* (2005) 12:637–48. doi: 10.1038/sj.cdd.4401647

52. Ingold K, Zumsteg A, Tardivel A, Huard B, Steiner QG, Cachero TG, et al. Identification of proteoglycans as the APRIL-specific binding partners. *J Exp Med* (2005) 201:1375–83. doi: 10.1084/jem.20042309

53. Kimberley FC, van Bostelen L, Cameron K, Hardenberg G, Marquart JA, Hahne M, et al. The proteoglycan (heparan sulfate proteoglycan) binding domain of APRIL serves as a platform for ligand multimerization and cross-linking. *FASEB J Off Publ Fed Am Societies Exp Biol* (2009) 23:1584–95. doi: 10.1096/fj.08-124669

54. Huard B, McKee T, Bosshard C, Durual S, Matthes T, Myit S, et al. APRIL secreted by neutrophils binds to heparan sulfate proteoglycans to create plasma cell niches in human mucosa. *J Clin Invest* (2008) 118:2887–95. doi: 10.1172/jci33760

55. Reijmers RM, Groen RW, Kuil A, Weijer K, Kimberley FC, Medema JP, et al. Disruption of heparan sulfate proteoglycan conformation perturbs b-cell maturation and APRIL-mediated plasma cell survival. *Blood* (2011) 117:6162–71. doi: 10.1182/blood-2010-12-325522

56. Cassese G, Arce S, Hauser AE, Lehnert K, Moewes B, Mostarac M, et al. Plasma cell survival is mediated by synergistic effects of cytokines and adhesion-dependent signals. *J Immunol (Baltimore Md 1950)* (2003) 171:1684–90. doi: 10.4049/jimmunol.171.4.1684

57. Roll P, Muhammad KSchumann M, Kleinart S, Einsele H, Dorner , et al. *In vivo* effects of the anti-interleukin-6 receptor inhibitor tocilizumab on the b cell compartment. *Arthritis rheumatism* (2011) 63:1255–64. doi: 10.1002/art.30242

58. Yang J, Sakai J, Siddiqui S, Lee RC, Ireland DDC, Verthelyi D, et al. IL-6 impairs vaccine responses in neonatal mice. *Front Immunol* (2018) 9:3049. doi: 10.3389/fimmu.2018.03049

59. Mitroulis I, Kalafati L, Bornhäuser M, Hajishengallis G, Chavakis T. Regulation of the bone marrow niche by inflammation. *Front Immunol* (2020) 11:1540. doi: 10.3389/fimmu.2020.01540

60. Valletta S, Thomas A, Meng Y, Ren X, Drissen R, Sengül H, et al. Micro-environmental sensing by bone marrow stroma identifies IL-6 and TGFβ1 as regulators of hematopoietic ageing. *Nat Commun* (2020) 11:4075. doi: 10.1038/s41467-020-17942-7

61. Belnoue E, Tougne C, Rochat AF, Lambert PH, Pinschewer DD, Siegrist CA, et al. Homing and adhesion patterns determine the cellular composition of the bone marrow plasma cell niche. *J Immunol (Baltimore Md 1950)* (2012) 188:1283–91. doi: 10.4049/jimmunol.1103169

62. Ko EJ, Lee YT, Kim KH, Jung YJ, Lee Y, Denning TL, et al. Effects of MF59 adjuvant on induction of isotype-switched IgG antibodies and protection after immunization with T-dependent influenza virus vaccine in the absence of CD4+ T cells. *J Virol* (2016) 90:6976–88. doi: 10.1128/jvi.00339-16

63. Pedersen GK, Wørzner K, Andersen P, Christensen D. Vaccine adjuvants differentially affect kinetics of antibody and germinal center responses. *Front Immunol* (2020) 11:579761. doi: 10.3389/fimmu.2020.579761

64. Pihlgren M, Tougne C, Schallert N, Bozzotti P, Lambert PH, Siegrist CA, et al. CpG-motifs enhance initial and sustained primary tetanus-specific antibody secreting cell responses in spleen and bone marrow, but are more effective in adult than in neonatal mice. *Vaccine* (2003) 21:2492–9. doi: 10.1016/S0264-410X(03)00052-5

Frontiers in Immunology

Explores novel approaches and diagnoses to treat immune disorders.

The official journal of the International Union of Immunological Societies (IUIS) and the most cited in its field, leading the way for research across basic, translational and clinical immunology.

Discover the latest Research Topics

See more →

Frontiers

Avenue du Tribunal-Fédéral 34
1005 Lausanne, Switzerland
frontiersin.org

Contact us

+41 (0)21 510 17 00
frontiersin.org/about/contact